U.S. DEPARTMENT OF COMMERCE
National Technical Information Service
PB80-101512

Air Pollution: Proceedings of the Eighth International Technical Meeting on Air Pollution Modeling and Its Application, Held at Louvain-La-Neuve, Belgium on 20-23 September, 1977

NATO Committee on the Challenges of Modern Society, Brussels (Belgium)

1977

PB80-101512

COMMITTEE ON THE CHALLENGES OF MODERN SOCIETY

NATO CDSM

OTAN CCMS

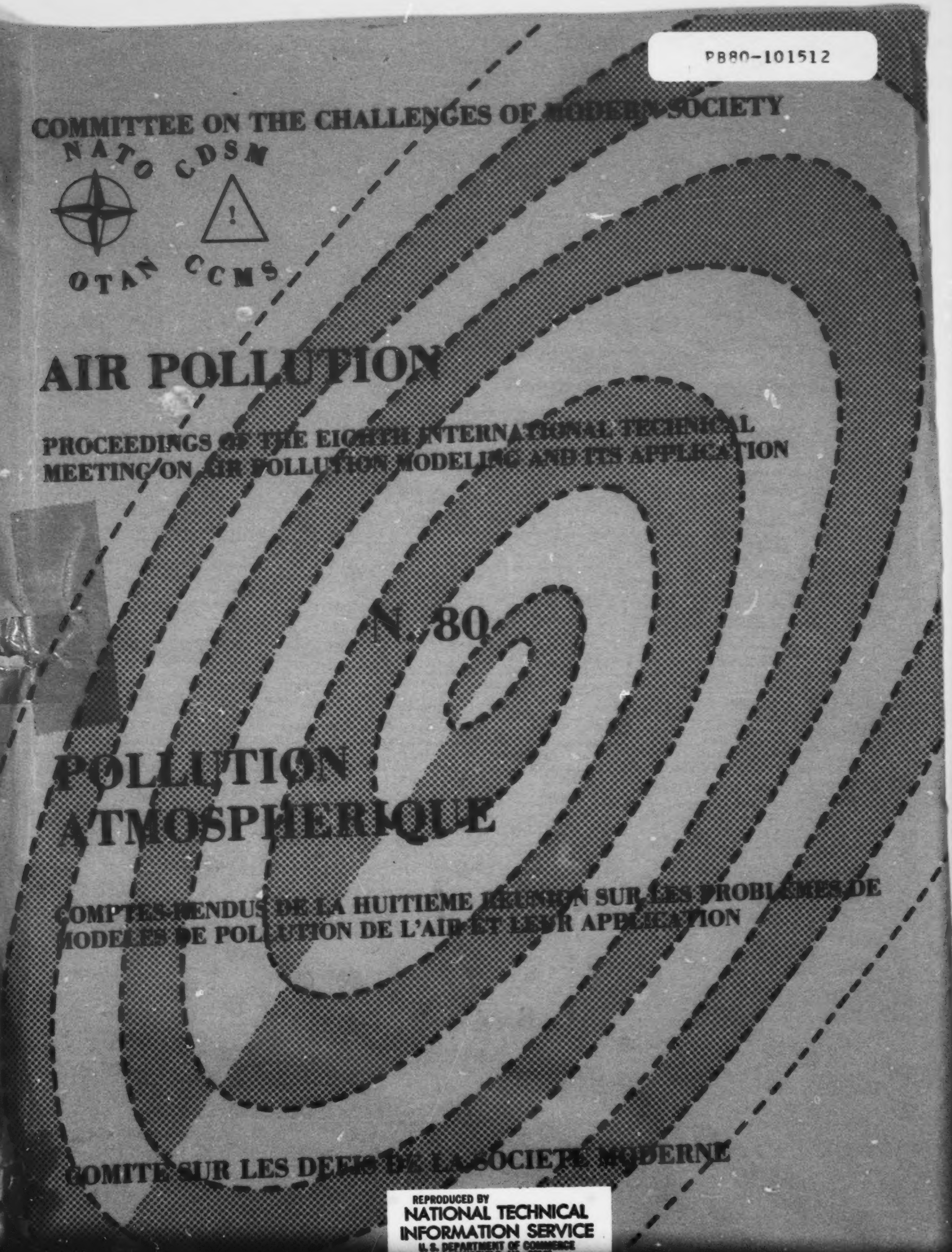

AIR POLLUTION

PROCEEDINGS OF THE EIGHTH INTERNATIONAL TECHNICAL MEETING ON AIR POLLUTION MODELING AND ITS APPLICATION

N. 80

POLLUTION ATMOSPHERIQUE

COMPTES-RENDUS DE LA HUITIEME REUNION SUR LES PROBLEMES DE MODELES DE POLLUTION DE L'AIR ET LEUR APPLICATION

COMITE SUR LES DEFIS DE LA SOCIETE MODERNE

REPRODUCED BY
NATIONAL TECHNICAL
INFORMATION SERVICE
U.S. DEPARTMENT OF COMMERCE
SPRINGFIELD, VA. 22161

TECHNICAL REPORT DATA

(Please read Instructions on the reverse before completing)

1. REPORT NO. CCMS Report No. 80	2.	3. RECIPIENT'S ACCESSION NO. PB80-101 512
4. TITLE AND SUBTITLE Air Pollution		5. REPORT DATE Sept. 20-23, 1977
		6. PERFORMING ORGANIZATION CODE
7. AUTHOR(S)		8. PERFORMING ORGANIZATION REPORT NO.
9. PERFORMING ORGANIZATION NAME AND ADDRESS Proceedings of the Eighth International Technical Meeting on Air Pollution Modeling and Its Application		10. PROGRAM ELEMENT NO.
		11. CONTRACT/GRANT NO.
12. SPONSORING AGENCY NAME AND ADDRESS North Atlantic Treaty Organization Committee on the Challenges of Modern Society		13. TYPE OF REPORT AND PERIOD COVERED
		14. SPONSORING AGENCY CODE

15. SUPPLEMENTARY NOTES

16. ABSTRACT

This study focuses attention on air quality simulation modeling and it tries to provide information exchange on modeling and closely related topics.

17. KEY WORDS AND DOCUMENT ANALYSIS

a. DESCRIPTORS	b. IDENTIFIERS/OPEN ENDED TERMS	c. COSATI Field/Group

18. DISTRIBUTION STATEMENT	19. SECURITY CLASS *(This Report)*	21. NO. OF PAGES 763
	20. SECURITY CLASS *(This page)*	22. PRICE $2150-A01

EPA Form 2220-1 (9-73)

PROCEEDINGS OF THE EIGHTH INTERNATIONAL TECHNICAL MEETING ON AIR POLLUTION MODELING AND ITS APPLICATION

20 - 23 September 1977

LOUVAIN - LA - NEUVE
BELGIUM

A Report of the Air Pollution Pilot Study
NATO Committee on the Challenges to Modern Society
1977

PREFACE

One major aim of the NATO/CCMS Air Pollution Pilot Study on Assessment Methodology and Modeling is to bring together the users and developers of air quality simulation models. Modeling continues to attract widespread attention and plays an important role in the development and application of air quality management systems. The modeling techniques are rapidly advancing and the diversity of the applications of models has made it desirable to provide an opportunity for an information exchange on modeling and closely related topics.

With these objectives in mind, the participation at the Eighth International Technical Meeting on Air Pollution Modeling and its application extended far beyond the regular membership countries. It included experts from Austria (2), Belgium (22), Canada (2), Denmark (1), France (6), Federal Republic of Germany (13), Greece (1), Italy (11), Libye (2), Luxemburg (1), The Netherlands (8), Norway (1), United Kingdom (3), United States (12), and Switzerland (1).

Nine topics were discussed: comparison of different diffusion models, consideration of transformation processes of air pollutants in models, guidelines for the application of air quality simulation models in the NATO community, quantitative application of models to the development of control strategy, estimation of combined effects of emissions from several large stacks, trans-national air quality modeling, modeling in complex terrain, novel approaches in air quality modeling, and influence and choice of meteorological inputs.

Exceptionally fine facilities were made available for the meeting. Special thanks are due to the Institut de l'Astronomie et de Géophysique, Université Catholique de Louvain and to Dr. A. Berger and his staff.

The present document contains the papers submitted together with the reports of the several rapporteurs to the different sessions of the meeting, summarizing the discussions which followed the presentations.

I would like to take the opportunity to thank all authors and rapporteurs for having submitted their presentations and reports so promptly.

Erich Weber

Erich Weber, Chairman
Federal Ministry of the Interior
Bonn, Germany

CONTENTS

Page:

CHAPTER I

QUANTITATIVE APPLICATION OF MODELS TO THE DEVELOPMENT OF CONTROL STRATEGY 1

1. Some practical examples of the impact of individual sources upon the cumulative frequency distributions of the daily SO_2-concentrations in an urban industrial area.
(J.G. Kretzschmar, G. de Baere, J. Vandervee, D. Cosemans, I. Mertens) 2

2. A source finding algorithm: A novel approach for relating air quality data to dispersion models
(R. J. Yamartino, Jr.) 24

3. Dual analysis in air pollution modeling
(Y. Jacquart) 38

4. A unit construction system of dispersion models for air quality management
(B. Gutsche, D. Jost, Ch. Ludwig) 55

5. Development of an air pollution index
(A. Joukoff) 81

6. Forecasting the air pollution potential by means of a multiple regression model
(L. van der Auwera) 98

7. A purely statistical approach to the warning, alarm and emergency problem
(J. P. Orfeuil) 122

8. Univariate stochastic models and real time predictors of daily SO_2 pollution in Milan
(G. Finzi, G. Fronza, A Spirito) 152

9. Rapporteur's Summary Report: W. B. Johnson 166

CHAPTER II

COMPARISON OF DIFFERENT DIFFUSION MODELS 168

10. A methodology for the comparison of air quality simulation models
(K. L. Brubacker, A. E. Smith, D. M. Rote).......... 169

Page:

11. Comparative Study of four mathematical air dispersion models for a new urban industrial complex at Sines, Portugal
(Richard Porter, John Christiansen, José F. Conseicao, Leonel D. Canelas) 184

12. Application of the ATDL simple urban dispersion model to Frankfurt, West Germany
(Steven R. Hanna, Frankling A. Gifford, Jr.) 202

13. Comparison of dispersion calculations with measurements in the Cologne area
(L. Kropp) 218

14. Rapporteur's Summary Report: B. Sivertsen 230

CHAPTER III

GUIDELINES FOR THE APPLICATION OF AIR QUALITY SIMULATION MODELS IN THE NATO COMMUNITY.............................. 235

15. Influence of meteorological data on the dispersion calculation results
(L. Kropp, W. Bahmann) 236

16. Experience with UNAMAP
(D. B. Turner, A. D. Busse) 248

17. Air pollution studies in Canada
(F. H. Fanaki, M. Kwizak).......................... 266

18. The development of a guideline on air quality modeling by the US Environmental Protection Agency
(Herschel H. Slater, Joseph A. Tikvart).............. 310

19. Rapporteur's Summary Report: J. G. Kretzschmar 318

CHAPTER IV

INFLUENCE AND CHOICE OF METEOROLOGICAL INPUTS 321

20. Simulation of daily temperatures for environmental modeling
(R. Santangelo, R. Cecchi, M. Marseguerra, S. Morelli, S. Pugnaghi) 322

Page:

21. The dispersion of pollutants over a water surface (F. T. M. Nieuwstadt) 337

22. A procedure for computing vertical wind profiles in the planetary boundary layer (Jacob Padro) 360

23. Rapporteur's Summary Report: C. A. Velds 375

24. Assessment of stability categories as meteorological input of air pollution modeling (A. Longhetto, P. Bacci, L. Bristore, G. Elisei, L. Santomauro) 379

25. New technics of estimation of dispersion coefficients - Generalization of the diffusivity concept - (A. Saab, J. P. Granier) 393

26. Comparison between inversion observation and modeling (G. Schayes) 418

27. Rapporteur's Summary Report: D. B. Turner 425

CHAPTER V

CONSIDERATIONS OF TRANSFORMATION PROCESSES OF AIR POLLUTANTS IN MODELS 427

28. Project Mistt: Plume modeling of the dispersion, transformation and ground removal of SO_2 over the B-mesoscale range (25 - 250 km) (N. V. Gillani, R. B. Husar) 428

29. An improved source depletion model for deposition from a GAUSSian plume (J. Giebel) 481

30. On the dispersion of chemically reacting pollutants (K. H. Müller) 498

31. Rapporteur's Summary Report: St. R. Hanna 519

Page:

CHAPTER VI

MODELING IN COMPLEX TERRAIN 521

32. The Austrian Alps air pollution study
(W. Kofler) 522

33. Microscale Atmospheric model
(J. Vanderborght) 539

34. Calculation of carbon monoxide caused by traffic
(M. Schorling) 559

CHAPTER VII

NOVEL APPROACHES IN AIR MODELING........................ 581

35. Air pollution studies using planetary boundary layer and K-models
(E. Runca, R. D. Bornstein) 582

36. Calculation of atmospheric pollutants dispersion by the computer program XPIC for instationary and inhomogeneous conditions
(H. Schultz, E. Voelz, C. D. Wüneke) 596

37. A K-analytical model, including calm wind situations
(A. Berger, Cl. Demuth,
Y. Jacquart, G. Schayes) 610

38. Rapporteur's Summary Report: R. A. Porter 631

CHAPTER VIII

TRANSNATIONAL AIR QUALITY MODELING 634

39. Pseudospectral dispersion modeling
(R. Berkowicz, L. P. Prahm) 635

40. Long-term regional distributions and transfrontier exchanges of airborne sulfur pollution in Europe

(W. B. Johnson) 658

Page:

41. Transnational air quality:
The case for the stratosphere
(J. B. Knox, M. H. Dickerson, R. Lange,
K. R. Peterson) 688

42. Rapporteur's Summary Report: K. L. Brubacker 703

CHAPTER IX

ESTIMATING THE COMBINED EFFECTS OF EMISSIONS FROM SEVERAL LARGE STACKS

ESTIMATING THE COMBINED EFFECTS OF EMISSIONS FROM SEVERAL LARGE STACKS 707

43. Modeling of combined effects of emission from
multiple sources.
(D. Anfossi, G. Bonino, F. Bossa
R. Richiardone) 708

44. Aerodynamic effects of natural draught cooling
towers on the local low level air pollution
(K. Fischer, H. Ruscheweyh) 720

Agenda.. 735
Attendees 745

PROCEEDINGS OF THE EIGHTH INTERNATIONAL TECHNICAL MEETING ON AIR POLLUTION MODELING AND ITS APPLICATION

20 - 23 September 1977

LOUVAIN - LA - NEUVE
BELGIUM

A Report of the Air Pollution Pilot Study
NATO Committee on the Challenges to Modern Society
1977

X

8th NATO/CCMS INTERNATIONAL TECHNICAL MEETING ON AIR POLLUTION MODELING

TOPIC 1

QUANTITATIVE APPLICATION OF MODELS TO THE DEVELOPMENT OF CONTROL STRATEGY

(AIR QUALITY MANAGEMENT SYSTEM)

8th International Technical Meeting
on Air Pollution Modeling and its Application

SOME PRACTICAL EXAMPLES OF THE IMPACT OF INDIVIDUAL SOURCES UPON THE CUMULATIVE FREQUENCY DISTRIBUTIONS OF THE DAILY SO_2-CONCENTRATIONS IN AN URBAN AND INDUSTRIAL AREA*

J.G. KRETZSCHMAR, G. COSEMANS, G. DE BAERE
I. MERTENS AND J. VANDERVEE
Nuclear Energy Centre, Mol, Belgium

September 20 - 23, 1977
Louvain-la-Neuve
BELGIUM

---

*Part of this work was carried out within the framework of the National Research and Development Program on the Environment, Interministerial Commission for Science Policy, Belgium

INTRODUCTION

For a given pollutant most Air Quality Standards specify an average level over a given period (e.g. arithmetic- or geometric mean for one year), as well as certain short term levels not to be exceeded at all,or not to be exceeded more than a predetermined number of times during that same period (e.g. 95- or 98-percentile of the distribution of the daily averages during that year). The evaluation of the impact of the emission of new or existing sources,as a function of specifications of this kind,requires a statistical study based on complete frequency distributions of the ground level concentrations in an important number of points in the region under investigation. The same is true for urban planning or industrial zoning, where for a given (measured) situation certain measures of sanitation have to be taken in the near future, in order to improve the air quality or to prevent further degradation. Due to the important economical,financial, social and well-being implications in general, such a planning has to be based on an objective comparative study between different alternatives.

The Belgian Nuclear Energy Centre, facing those problems in the nuclear field, even long before the non-radioactive pollutants became a worldwide problem, therefore developed the so-called Immission Frequency Distribution Model (IFDM) in order to have a versatile tool for studying air pollution impact problems. The model has been extensively described in previous publications, as well as to its structure and possibilities [4,5], as to its validation [2]. The main properties of the model are : multiple-source bi-Gaussian approach, based on hourly observations of windspeed, wind direction and atmospheric stability, using yearly emission averages for the industrial point sources and hourly data for space heating emissions. The latter are based on total yearly fuel consumption, hourly average outside temperature, average windspeed and amount of sunshine. Although whatever plume rise formula and dispersion parameter scheme could be used in the model, the results of this paper have been obtained by applying the second plume rise formula of Stümke [7] and the dispersion coefficients of the S.C.K./C.E.N. as determined by Bultynck et al. [8].

Up to now the IFDM has been practically applied in Belgium on many different cases. The optimal chimney height, or the consequences of the choice of a specific chimney height for the air pollution in a given zone,have been studied for power plants, nuclear as well as thermal, for refineries, chemical plants and cokes production units. The model was also involved in the NATO - CCMS pilot study on the Frankfurt common SO_2-data base [3].

The present paper equally deals with a model user's problem namely, what is the specific SO_2 contribution of three existing industrial SO_2 sources to the overall SO_2 pollution in a complex industrial and urban zone, and what are the net results of two quite different sanitation strategies.

PROBLEM DESCRIPTION

The region of Antwerpen, one of the biggest Belgian cities and industrial zones, as well as one of the most important European harbours, is given on Figure 1a. Of the approximately 150 important SO_2-point sources in that region (Figures 3a and b), three specific chimneys, marked as "studied sources" on Figure 1a, are under investigation. Some preliminary (rule of thumb) calculations showed that the main influence of those sources could be expected within a zone of approximately 100 km^2 around the sources. The final choice of the test zone was also influenced by the fact that one wanted to have in that same zone a maximum number of monitoring stations, where valid concentrations for the period under investigation were available. With the specific choice given on Figure 1a ten such stations of the Belgian Sulphur-Smoke Network [1] are available for the validation of the actual calculations. More details of this test zone and the position of the monitoring stations,as well as the studied sources and the meteorological tower, are given on Figure 1b.

The yearly emission rate of the industrial sources were obtained from the Stadslaboratorium of Antwerpen, in cooperation with the local industries. The emission due to space heating (area sources) was obtained from total fuel and coal consumption and a degree-hour system described in [4]. The SO_2-emission densities, total, area sources and point sources, for the period April 1972 - September 1972 (summer 1972) are represented on Figure 2. Hourly meteorological data came from the local meteorological tower (N.V. Vinçotte and S.C.K./C.E.N.).

The specific questions to be answered in this study are : what is the impact of the three studied SO_2-point sources upon the actual SO_2-levels and what would be the impact if those three sources would be replaced by one new chimney, which height is based on the Belgian Royal Decree of 8 August 1975, specifying the required chimney heights for new combustion installations.

CALCULATION OF THE ACTUAL SO_2-SITUATION AND VALIDATION

As impact studies could have quite important implications as well for the industrial zoning and urban planning in general as for individual industrial sources, it is obvious that the model user must acquire confidence in his model. As far as this is possible he therefore always starts his impact study with a simulation of the actual or past situation, in order to validate his model and be aware of the possibilities and shortcomings of the latter. It must be emphasized that most of the time the extent and detail of such a study will be determined predominantly by the quantity and quality of the available input data (emission, meteorology and measured immission).

For the present study the summer period of 1972 (April - September) has been used as reference period. As mentioned before complete cumulative frequency distributions of the daily SO_2-averages during that period have been calculated for each of the 132 grid points of a test zone of 110 km^2. The calculated arithmetic or seasonal averages are represented in the upper part of Figure 3a. The test zone, together with the greater Antwerp region is represented in the lower part of the same figure, while the middle part gives the height and the position of the industrial point sources which were taken into account for the calculations. SO_2-emission densities for the latter as well as for the space heating sources are given on Figure 2. Analogous information for the 95-percentiles of the daily SO_2-averages is given on Figure 3b. Those figures show that the highest average and extreme levels occur in the industrial zone around the docks. For the average levels (Figure 3a) there is also a net increase in the centre of the town of Antwerpen.

The actual SO_2-situation becomes even clearer when the spatial distribution of the grid points exceeding certain Air Quality Standards is represented. This is dono on Figure 4 for the following Air Quality Standards : arithmetic average $\bar{x}$ = 100 µg SO_2/m^3, 95-percentile of the daily averages $x_{.95,24h}$ = 300 µg SO_2/m^3 and maximum daily average $x_{max,24h}$ = 500 µg SO_2/m^3. The latter is based on the fact that the Belgian Law (Royal Decree of 8/8/1975 [6]) forces the important industrial sources to switch to fuels with low sulphur content as soon as the daily SO_2-average becomes larger than 500 µg SO_2/m^3.

Figure 5 illustrates the goodness of fit between the calculated and measured values for $\bar{x}$ and $x_{.95,24h}$ in the ten ZR-monitoring stations [1] in the testzone or on the borders of this zone. Relative differences are within the range 10 % to 20 %. More elaborated examples of the validation procedure and the possibilities of the model are given in [2], as well as in the practical demonstration on the Frankfurt pilot study [3].

IMPACT OF THE MAXIMUM MEASURE OF SANITATION

The evaluation of the impact of new or existing sources of a specific pollutant upon the existing levels in a given region requires the following steps in the IFDM-calculations :

- based on known emission and meteorological data the *past or actual immission situation* is calculated in a representative number of grid points in the region. The size and the number of the meshes is determined by the total surface and the complexity of the region under investigation. For a specified period (one season, one year...) the pollution in a given point is completely specified by the cumulative frequency distribution of the individual levels measured as averages over a given averaging time (t_{av} = 1h, 1 day,...) ;

- in specific points of the region, where measured immission data for the same period and with the same averaging time are available, the cumulative frequency distributions, or certain specific statistical parameters, for the measured and the calculated pollution situation are compared (*validation* of the model) as explained before ;

- if the result of the validation is satisfactory, *the new situation is calculated* by using the same meteorological and emission data as before (same period) but taking into account the new source(s) or the change(s) in some of the existing sources ;

- *comparison* between the corresponding results for *the new and the existing* situation, or *the new situation and air quality standards*, determines the impact of the changes. These comparisons are done on an absolute as well as a relative basis.

The maximum possible measure of sanitation for a specific source is quite clearly the complete elimination of that source. The difference between the actual situation and the situation that is obtained if the maximum measure of sanitation would be applied on the source under investigation, also gives the contribution of that source to the actual pollution. Before doing more computations, this is a step which has to be done, in order to appreciate if for that source, it is worthwhile to take any measure of sanitation at all.

Figures 6a and b (middle part) illustrate the absolute ($\Delta_1\bar{x}$) and relative ($\delta_1\bar{x}$) changes in the average SO_2-levels in all the grid points if the three sources, represented in the lower part of the same figures, are eliminated. The absolute and relative changes are defined as follows : $\Delta_1\bar{x}$ is the difference between the average situation for the summer period 1972 calculated with all the SO_2-sources, exclusive the three studied sources, and the calculated actual situation with all the sources, this means inclusive the studied ones (Figures 2 and 3a). $\delta_1\bar{x}$ equals 100 $\Delta_1\bar{x}$ divided by the actual situation, inclusive the three sources (Figure 3a). As such $|\delta_1\bar{x}|$ is the percentage decrease due to the elimination of the studied sources. It is obvious that the largest decreases occur in the vicinity of the sources. The southwest-northeast axis is related to the predominance of southwesterly and northeasterly winds in that region.

Figures 7a and b (middle part) give the same information for the 95-percentiles of the daily averages. The definition of $\Delta_1 x_{.95,24h}$ and $\delta_1 x_{.95,24h}$ is analogous with the definition for $\Delta_1\bar{x}$ and $\delta_1\bar{x}$. For the changes in the 95-percentiles it is seen that the maximum changes are $\simeq$ 50 µg SO_2/m^3 and $\simeq$ 15 % respectively. Both are linked to the southwest-northeast axis. The first one occurs at $\simeq$ 1,5 km, the second at $\simeq$ 2,5 km of the three sources. There is almost no influence in the highly populated areas.

IMPACT OF A NEW CHIMNEY BASED ON THE BELGIAN CHIMNEY HEIGHT REGULATIONS [6]

Once one knows the contribution of a specific source, and once one has decided to take sanitation measures, it is necessary to appreciate the possible effects of such measures. As an example we replaced the three sources, studied in the previous example, by means of a single chimney through which the combined emissions have to take place. The chimney height of this new stack is determined by means of the formula given in the Belgian Royal Decree of 8 August 1975 [6] namely

$$h_g = \sqrt{3400\,Q\,\sqrt[3]{\frac{1}{R\Delta T}}} \qquad \text{meter (1)}$$

with
h_g : the minimum required stack height (m) ;
Q : SO_2-emission rate in kg/h ;
R : total gas flow in m^3/h ;
ΔT : temperature difference between stack exit temperature and ambient temperature.

The IFDM calculations were repeated then for the same region and meteorological period with all the SO_2-sources, inclusive the new stack instead of the three existing stacks. For each grid point the difference between the new situation (one stack) and the actual situation (three stacks) was calculated for the seasonal average $\bar{x}$ as well as for the 95-percentile of the daily averages $x_{.95,24h}$ in that summer 1972. Those differences are given as $\Delta_2\bar{x}$ and $\delta_2\bar{x}$ on Figures 6a and b (upper part) and as $\Delta_2\ x_{.95,24h}$ and $\delta_2\ x_{.95,24h}$ on Figures 7a and b (upper part) respectively.

From those figures it is clearly seen that the new and higher stack decreases the SO_2-pollution in the vicinity of the existing three stacks but increases the SO_2-pollution outside a region of $\approx$ 25 km^2 around the studied sources. This is not surprising as the new chimney is higher, while the total SO_2-emission rate did not change. Although the increases of the SO_2-levels in certain densely populated urban areas around the industrial zone of Antwerpen is not at all dramatic, it remains a fact that one has to be careful with certain measures of sanitation. It is also obvious that a mathematical model is the only reasonable tool to do such impact studies in regions where urban and industrial areas are so closely spaced.

CONCLUSIONS

It has been shown that the Immission Frequency Distribution Model is a versatile and reliable tool to simulate the *actual air pollution situation* in an important number of points in a region with complex source characteristics. With this *validated* model it is possible to study the *contribution* of *existing sources* as well as the *impact of whatever change* in the source configuration, or in the characteristics of a single source or a group of sources. As the model calculates complete cumulative frequency distributions of short term averages during a given period.there exists a *link* between the output of the model and the majority of existing *air quality standards*.

The specific examples given for three existing sources in the region of Antwerpen also showed how careful one has to be with certain *measures of sanitation*. A unique chimney height regulation could lead to an increase of the SO_2-pollution in certain urban areas, especially when urban and industrial zones are closely spaced, as this is mostly the case in Belgium. Different Air Quality Standards for industrial, urban, agricultural and recreational zones together with emission standards is a possible option to avoid this.

Whatever strategy one wants to follow, prognoses will have to be made and mathematical models are by far the best possible means at the moment.

REFERENCES

[1] **A. DEROUANE et al.**
Luchtverontreiniging door zwaveloxyde en rook in België van 1 april 1972 tot 31 maart 1973.
KMI-Brussel, Publicaties serie A, nr. 88, 1975.

[2] **J.G. KRETZSCHMAR, G. DE BAERE and J. VANDERVEE**
Validation of the Immission Frequency Distribution Model in the Region of Antwerpen, Belgium.
Proc.7th International Technical Meeting on Air Pollution Modeling and its Application, NATO-CCMS, Nr. 51(1976), pp. 235-270.

[3] **NATO MODELING PANEL**
Practical Demonstration of Urban Air Quality Simulation Models.
Techn. Doc. M.P. 1.5/1977 (first draft), Umweltbundesamt, Berlin 1977.

[4] **J.G. KRETZSCHMAR et al.**
IFDM. The Immission Frequency Distribution Model, Workgroup Mathematical Models, S.C.K./C.E.N., Mol, Belgium, March 1977.

[5] **J.G. KRETZSCHMAR, G. DE BAERE and J. VANDERVEE**
The Immission Frequency Distribution Model of the S.C.K./C.E.N., Mol, Belgium.
Proceedings of the IFIP Working Conference on Modeling and Simulation of Land, Air and Water Resources Systems, Gent, 30 August - 2 September 1977.

[6] **ROYAL DECREE OF 8 AUGUST 1975**
Koninklijk Besluit betreffende het voorkomen van luchtverontreiniging door zwaveloxyden en stofdeeltjes afkomstig van industriële verbrandingsinstallaties.
Belgisch Staatsblad van 2 oktober 1975, pp 12171 - 12180.

[7] **H. STÜMKE**
Vorschlag einer empirischen Formel für die Schörnsteinüberhöhung.
Staub, Bd. 23, No. 12, 1963.

[8] **H. BULTYNCK and L. MALET**
Evaluation of atmospheric dilution factors for effluents diffused from an elevated continuous point source.
Tellus XXIV, No. 5., 1972.

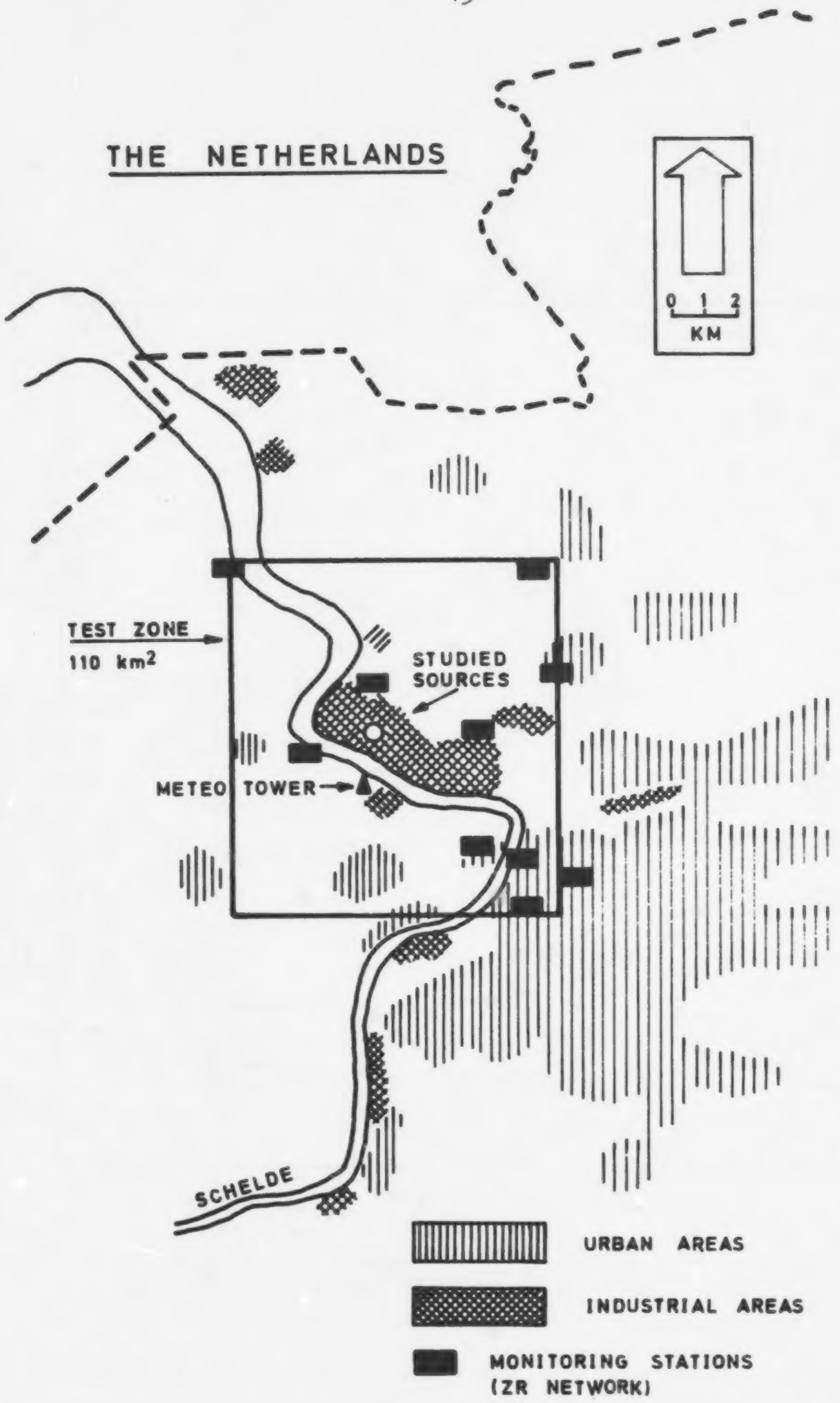
THE NETHERLANDS
0 1 2
KM
TEST ZONE
110 km²
STUDIED SOURCES
METEO TOWER
SCHELDE
URBAN AREAS
INDUSTRIAL AREAS
MONITORING STATIONS (ZR NETWORK)

Figure 1a : Lay-out of the area and sources under investigation.

Reproduced from
best available copy.

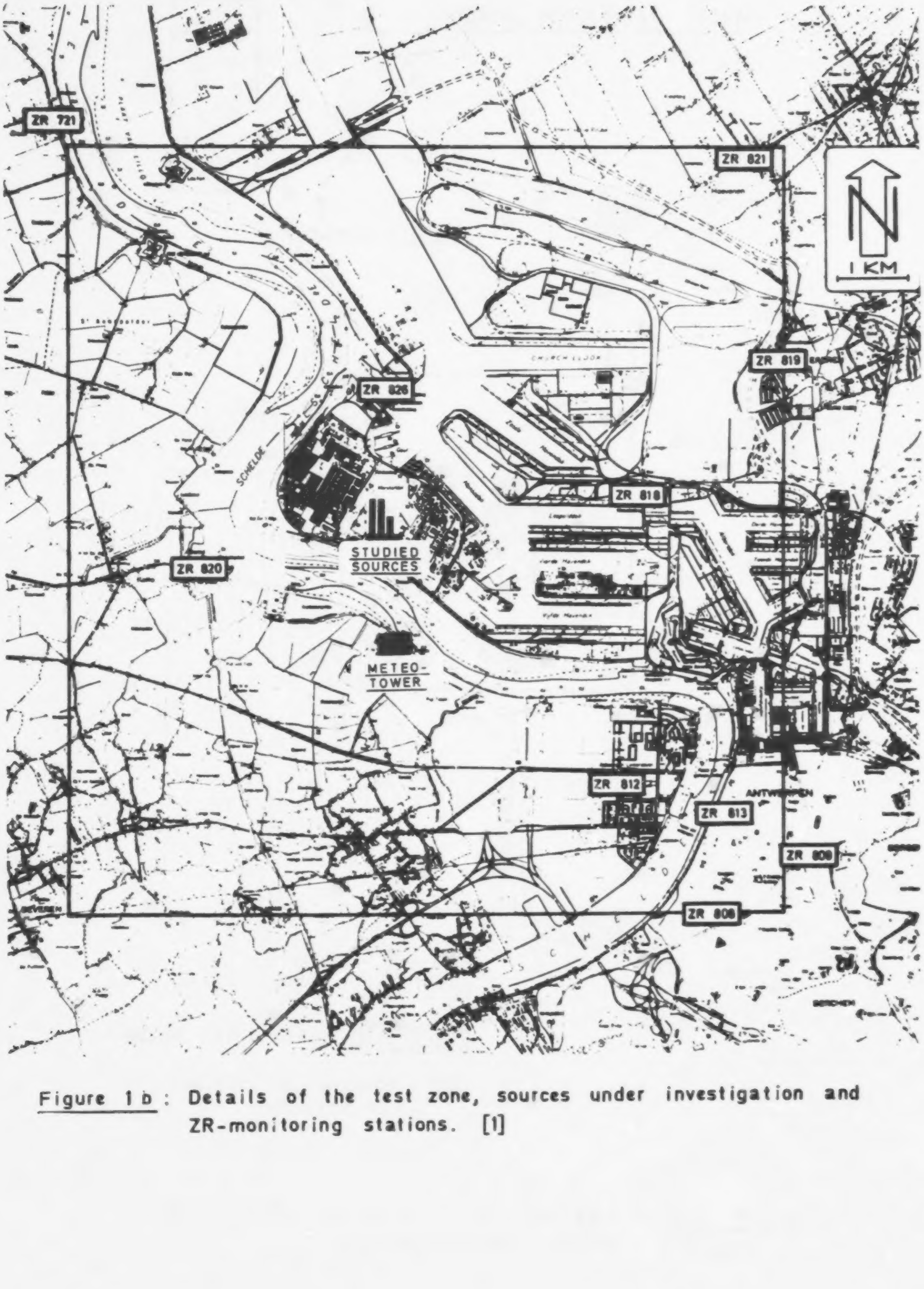
ZR 721
ZR 821
N
1 KM
ZR 819
ZR 826
SCHELDE
ZR 818
STUDIED SOURCES
ZR 820
METEO-TOWER
ZR 812
ANTWERPEN
ZR 813
ZR 809
ZR 808

Figure 1b : Details of the test zone, sources under investigation and ZR-monitoring stations. [1]

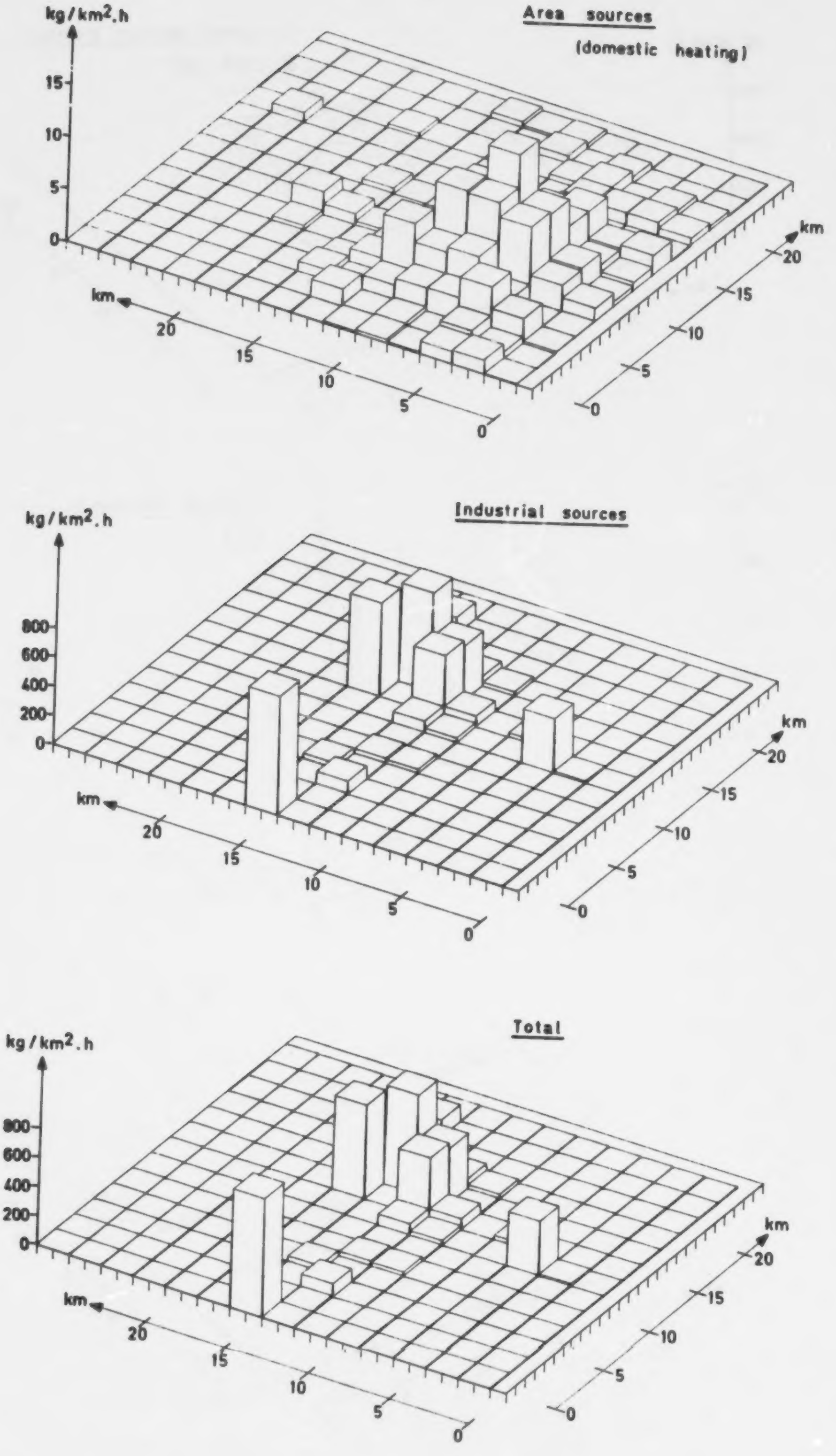

Figure 2. SO_2-emission density for industrial and domestic sources during the summer period 1972 (April-September 72).

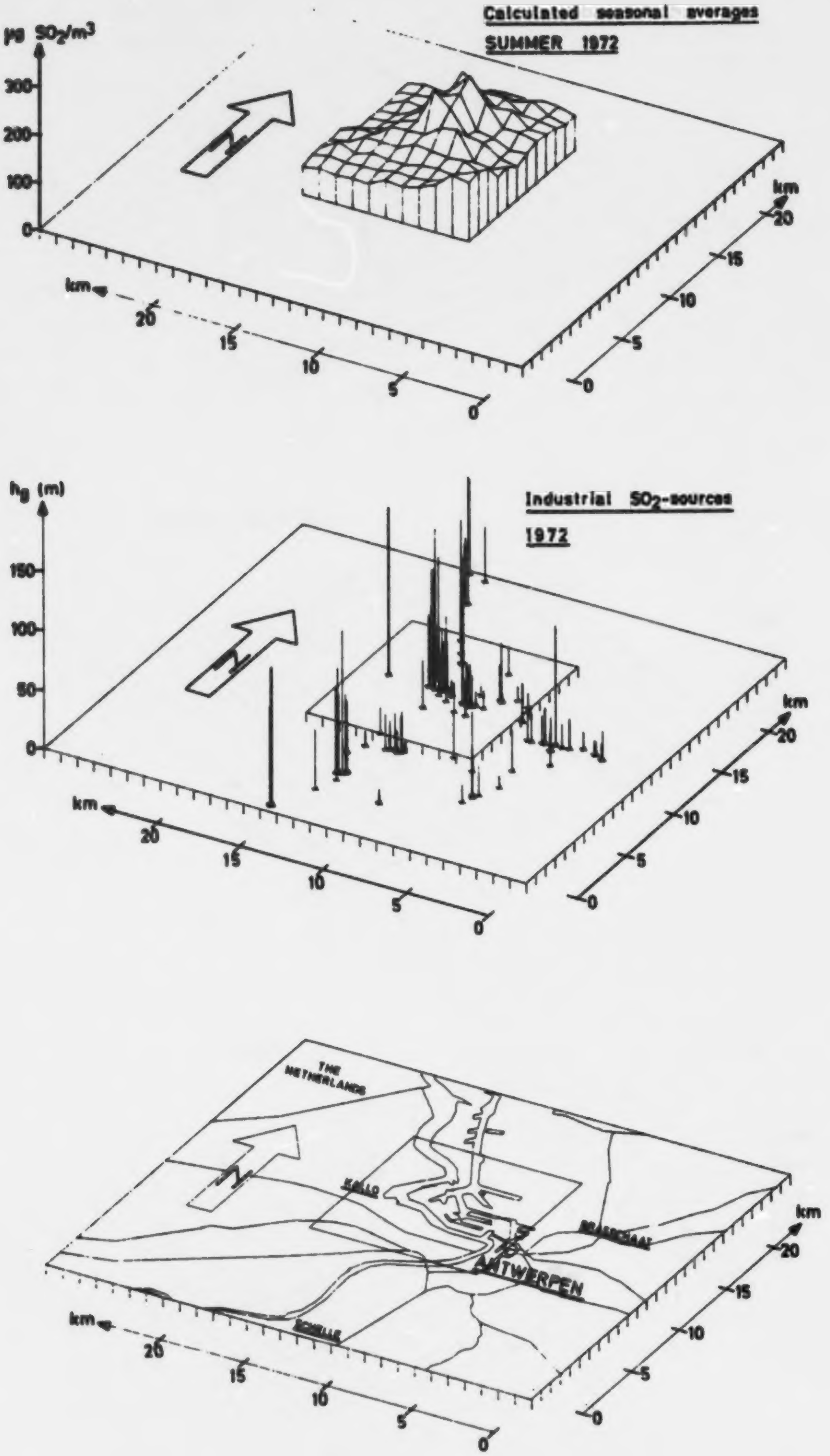

Figure 3a. Calculated actual $\bar{\bar{X}}$.

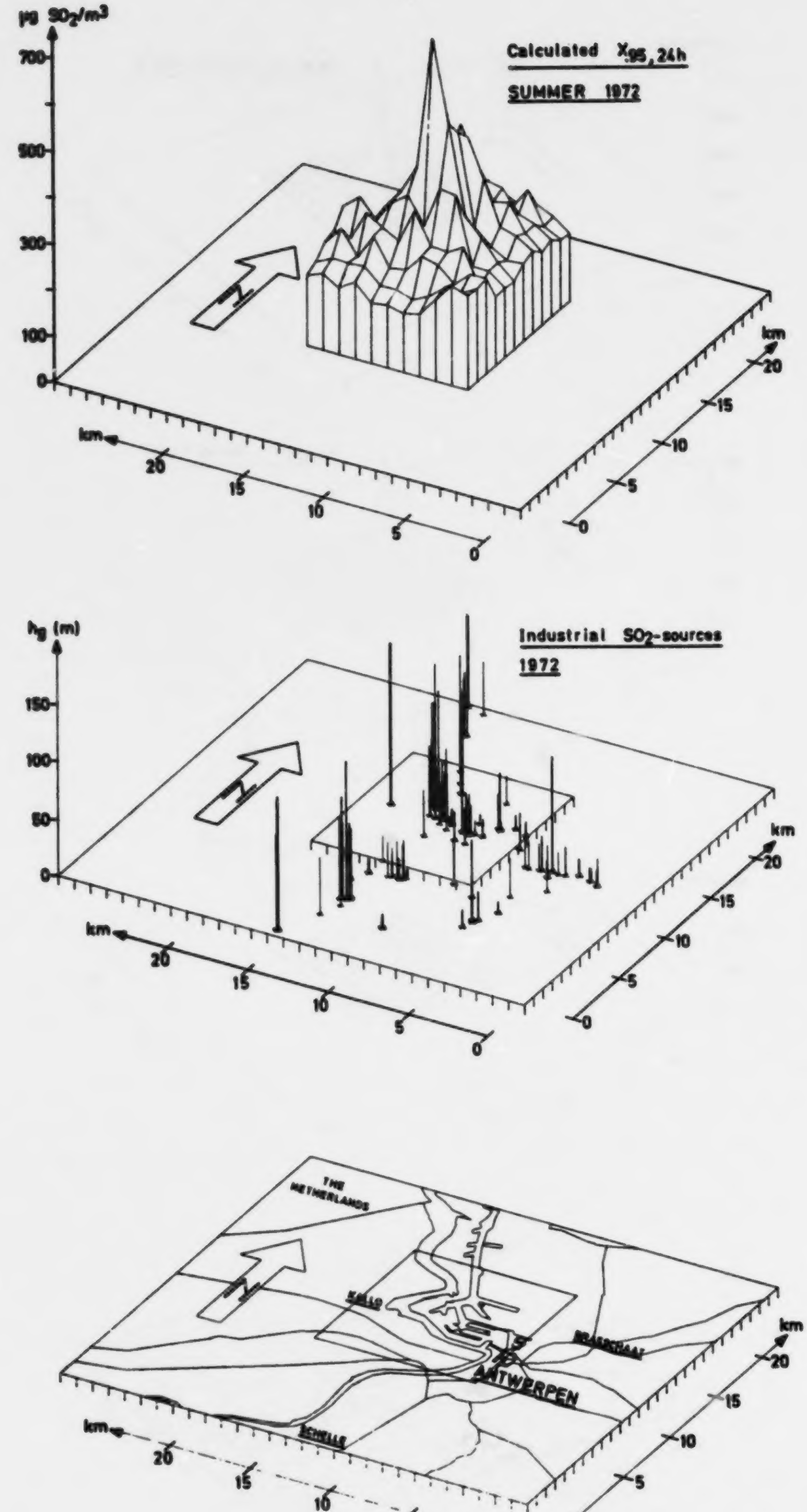

Figure 3b. Calculated actual $X_{95,24h}$.

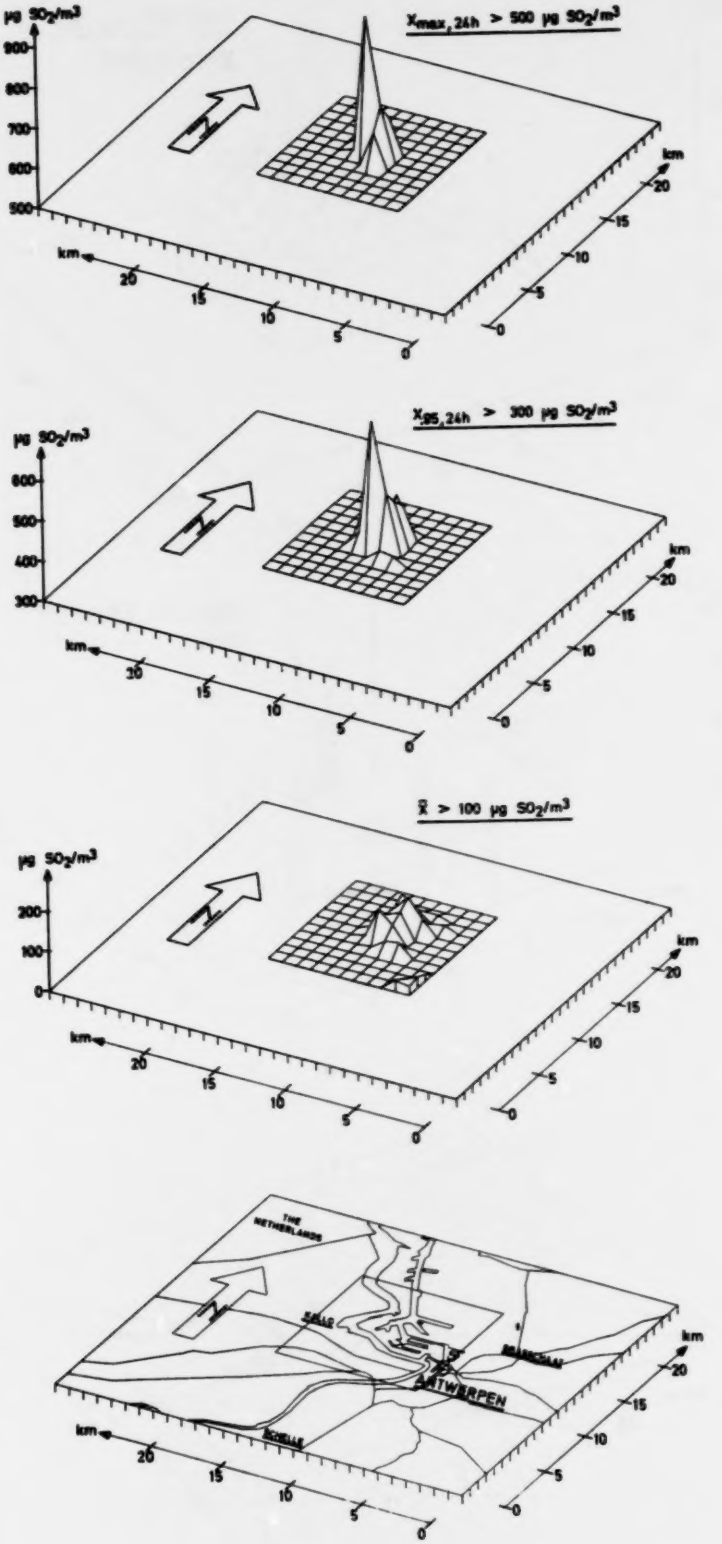

Figure 4. Subregions where certain SO_2 Air Quality Standards are violated.

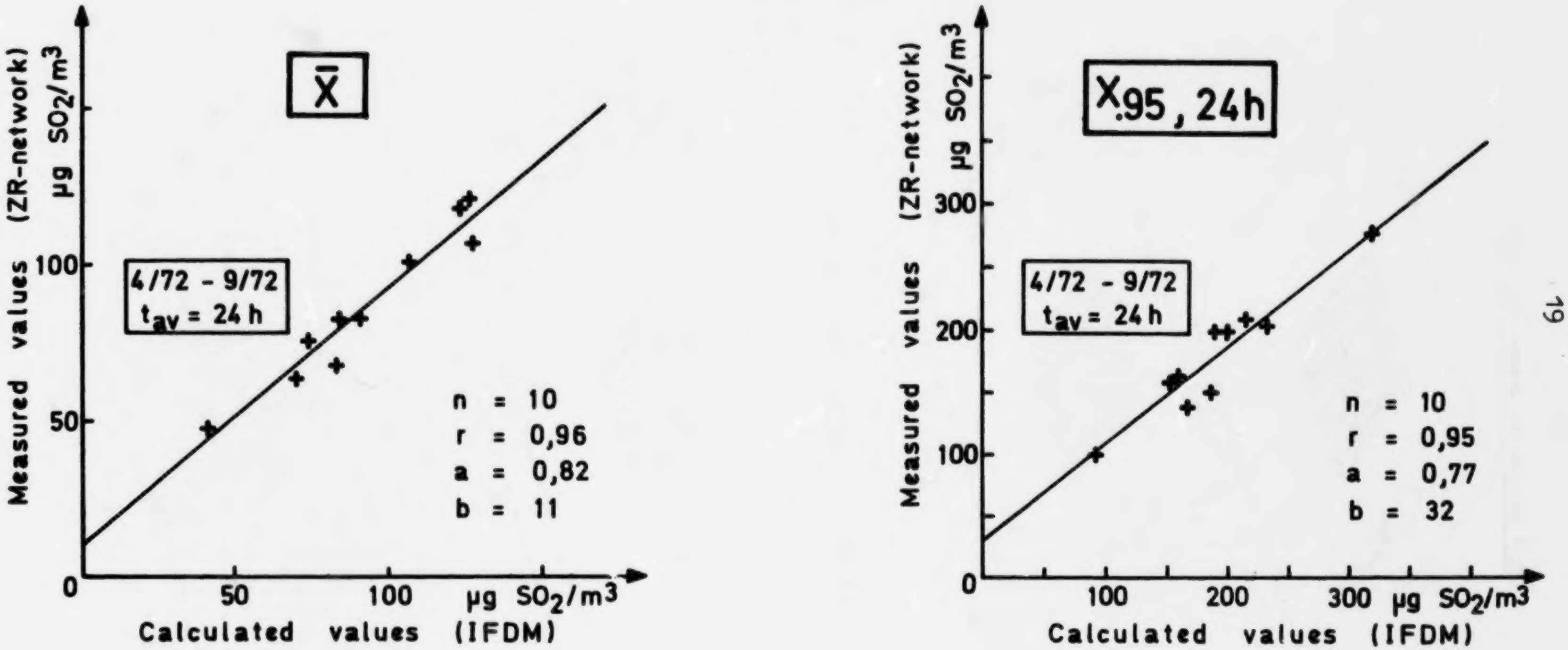

Figure 5 : Correlation between calculated and measured averages and 95-percentiles in ten monitoring stations of the national ZR-network (IHE-KMI).

Δ_2 $\bar{X}$ with the new chimney (RD 8/8/75)

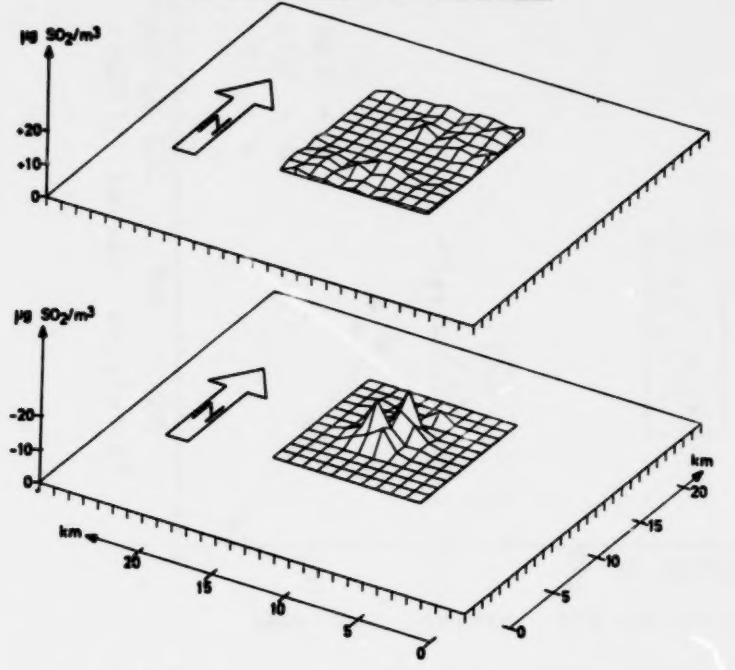

Δ_1 $\bar{X}$ with the elimination of the three SO_2-sources

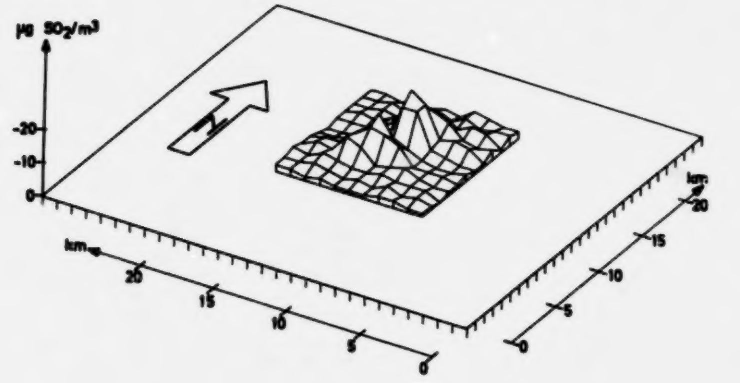

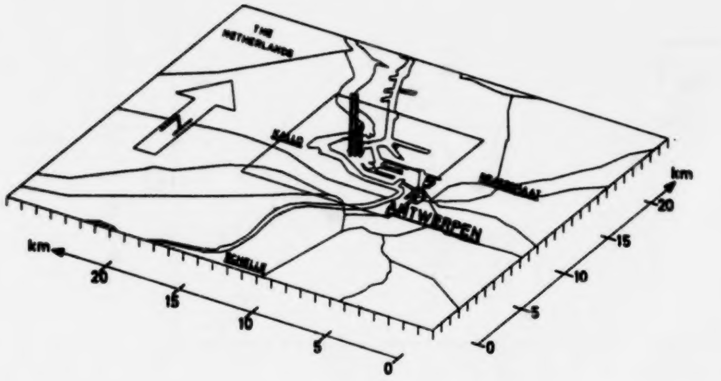
THE NETHERLANDS
KALLO
ANTWERPEN
SCHELDE
km
20
15
10
5
0
km
20
15
10
5
0

Figure 6a. Absolute influence of two possible measures of sanitation upon the average SO_2-levels.

$\delta_2\ \bar{X}$ with the new chimney (RD 8/8/75)

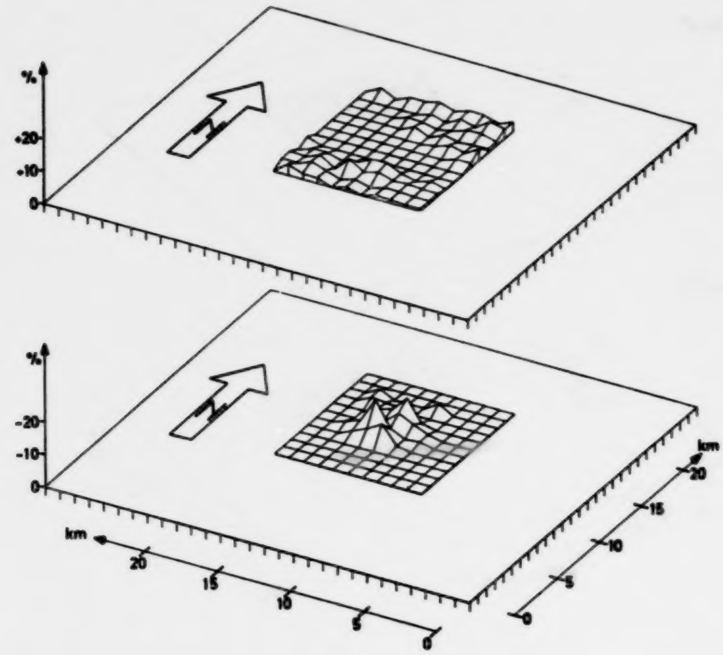

$\delta_1\ \bar{X}$ with the elimination of the three SO_2-sources

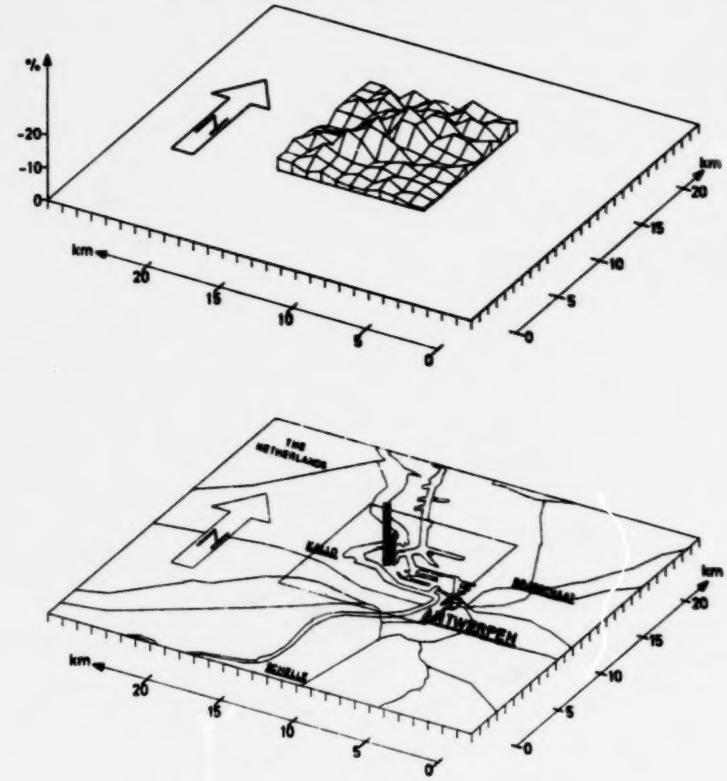

Figure 6b. Relative influence of two possible measures of sanitation upon the average SO_2-levels.

$\Delta_2\ X_{95,24h}$ with the new chimney (RD 8/8/75)

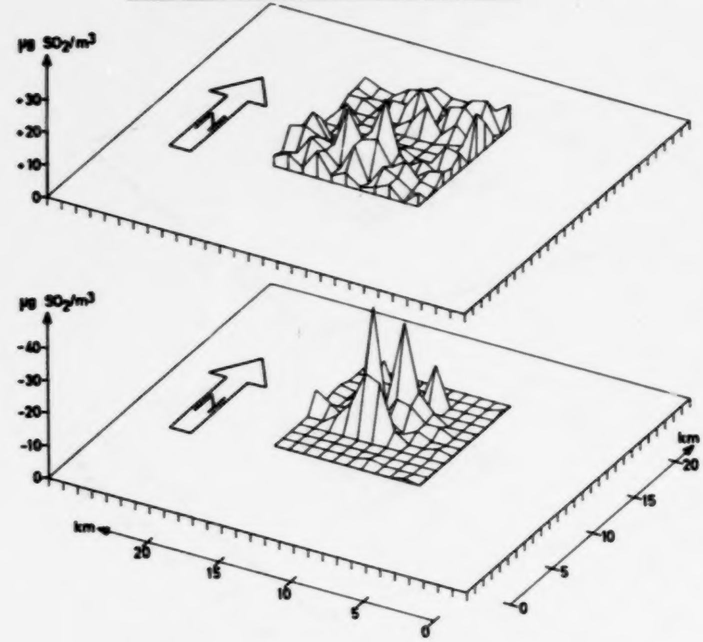

$\Delta_1\ X_{95,24h}$ with the elimination of the three SO$_2$-sources

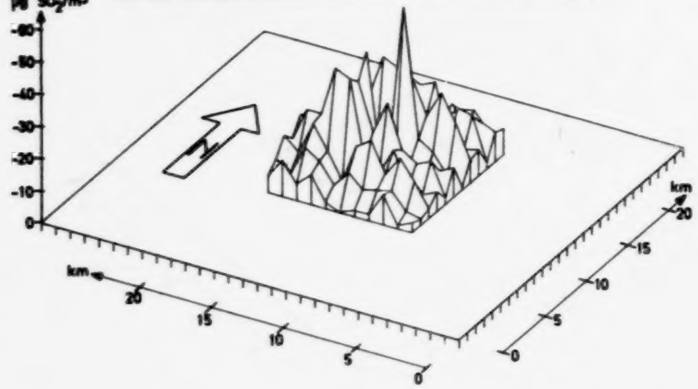

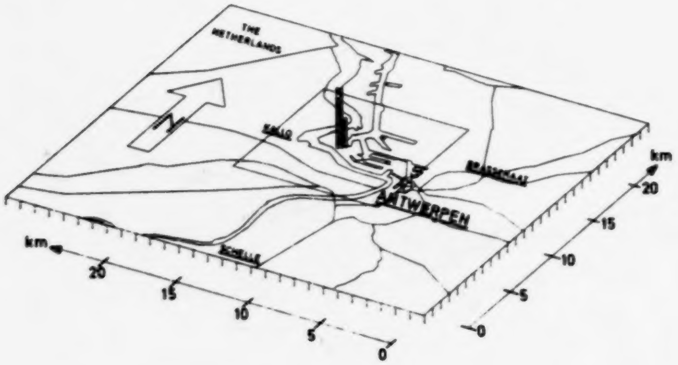
THE NETHERLANDS
BRASSCHAAT
ANTWERPEN
SCHELLE
km
20
15
10
5
0
km
20
15
10
5
0

Figure 7a. Absolute influence of two possible measures of sanitation upon the 95-percentiles of the daily SO$_2$-averages.

$\delta_2\ \chi_{95,24h}$ with the new chimney (RD 8/8/75)

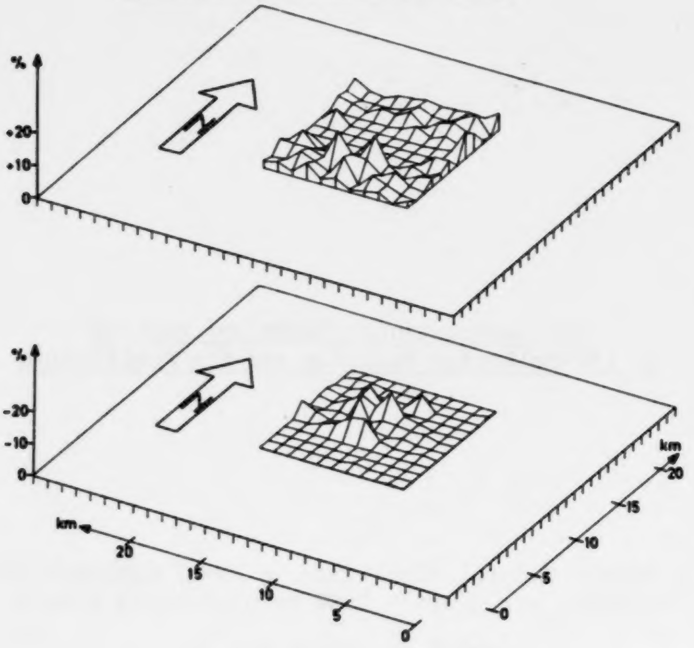

$\delta_1\ \chi_{95,24h}$ with the elimination of the three SO_2-sources

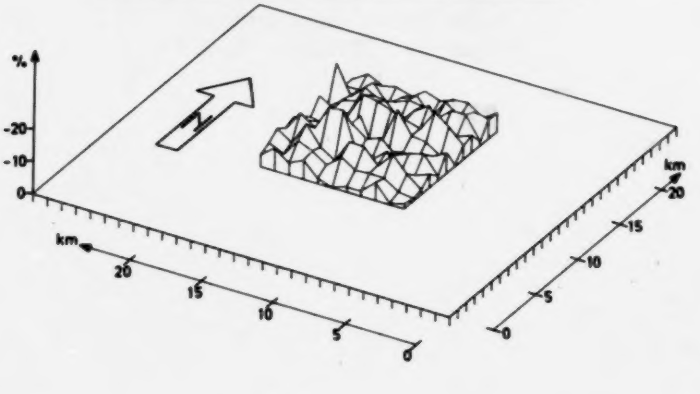

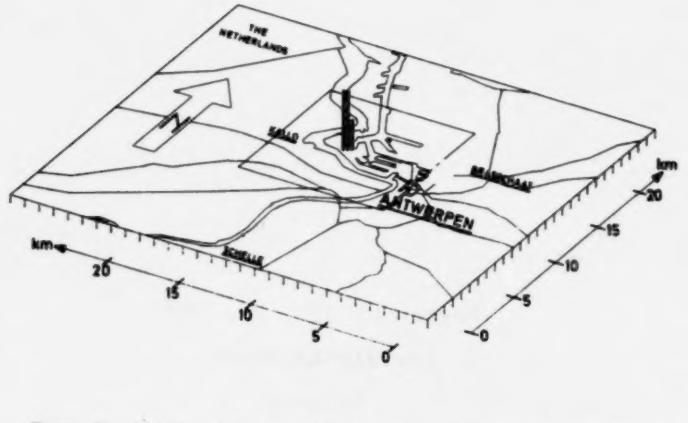
THE NETHERLANDS
KALLO
ANTWERPEN
SCHELDE
km
20
15
10
5
0
km
20
15
10
5
0

Figure 7b. Relative influence of two possible measures of sanitation upon the 95-percentiles of the daily SO_2-averages.

8th International Technical Meeting on Air Pollution Modeling and its Application

A Source Finding Algorithm: A Novel Approach for Relating Air Quality Data to Dispersion Models

Robert J. Yamartino, Jr.

Energy and Environmental Systems Division
Argonne National Laboratory
9700 South Cass Avenue
Argonne, Illinois 60439

September 20 - 23, 1977

Louvain-La-Neuve

Belgium

A Source Finding Algorithm: A Novel Approach for Relating Air Quality Data to Dispersion Models

Introduction

The increasing number and complexity of air quality monitoring networks in operation throughout the world, coupled with the greatly incresed quantity of data such networks generate, suggests the need for innovative data analysis techniques. The urgency of this need was echoed in the U.S. CEQ's Sixth Annual Report[1] where they pointed out that:

a) "The numbers, locations, and methods of measurement must be scientifically consistent and adequate to provide valid and useful data."

b) "The data must be handled and used effectively to provide the needed information."

c) "It will be necessary to develop better guidelines for more standardized siting of monitoring stations..."

Many analysis tools (such as the use of frequency and cumulative frequency distributions, time series analysis, and factor analysis), while well suited for understanding the significance of data from a single receptor, become somewhat unwieldy when applied to data from a network of receptors. Ideally, one might hope that the data from an n-station array would result in more, and not less, information than obtainable from n stations considered individually.

In the present paper, we develop a technique for relating the aerometric data obtained from a monitoring network under a wide range of meteorological conditions to the spatial distribution and strengths of emissions sources via the use of existing air quality dispersion algorithms. The approach may be envisioned, quite literally, as the running of an air quality dispersion model "in reverse" with the result being, in essence, the n-receptor, two-dimensional, generalization of the well known "pollution rose." This ability to generate an effective emission density map from observational aerometric and meteorological data has potential applications which include:

a) an independent means of checking source inventories and determining source culpability,

b) the ability to locate inadvertent leaks of hazardous effluents into the atmosphere, and

c) as an enforcement tool for air pollution regulatory agencies.

Perhaps its most immediate impact, however, will be in graphically imparting the notion of an aerometric monitoring network as a "pollution source telescope." Development of a formalism for quantifying the "resolving power" of such a receptor network then emerges as a badly needed ingredient if receptor networks are to be designed to optimally match the spatial extent and emission complexity of the region being studied.

Model Development

Air quality dispersion models are most often concerned with the determination of pollutant concentrations at a receptor given known source strengths and locations. Assuming steady state conditions have been achieved, the concentration, C_{kt}, at the k^{th} receptor during the t^{th} time interval can be expressed as

$$C_{kt} = \sum_j R_{jkt} Q_j \ ,$$

where Q_j is the time independent strength of the j^{th} source and R_{jkt} is the transport coupling coefficient between the j^{th} source and k^{th} receptor for the meteorological conditions existent during the t^{th} time interval. The solution of the simple inverse problem $Q_j = \sum_k R^{-1}_{jkt} C_{kt}$ is not of particular interest as a unique solution might exist only if the number of receptors, K, equalled the number of source candidates, J. A more reasonable problem would consist of determining the set of Q_j values leading to the minimization of the quantity χ^2, defined as

$$\chi^2 = \sum_{t,k} \frac{\left[C_{kt} - \sum_{i=1}^{J} R_{ikt}\, Q_i\right]^2}{(\Delta C_{kt})^2}, \tag{1}$$

where ΔC_{kt} is the uncertainty in C_{kt}, i is a dummy index, and a summation over both t and k is required. This problem generally will lead to a unique set of J source strengths provided the number of measurements M (nominally KT, where T is the number of time periods of data available) exceeds J, and secondly, that the sources Q_j of interest actually couple to the data in hand (i.e., $R_{jkt} \neq 0$ for all j and some k,t). Given these conditions, one may write down the set of J equations generated by the relations $\frac{\partial\chi^2}{\partial Q_j} = 0$. These equations are of the form

$$\sum_j A_{ij}\, Q_j = B_i$$

$$\text{where} \quad A_{ij} \equiv \sum_{t,k} \frac{R_{ikt}\, R_{jkt}}{(\Delta C_{kt})^2}$$

$$\text{and} \quad B_i \equiv \sum_{t,k} \frac{C_{kt}\, R_{ikt}}{(\Delta C_{kt})^2} \tag{2}$$

and, upon obtaining the inverse A^{-1} of the symmetric matrix A, one arrives at the solution

$$Q_j = \sum_i A^{-1}_{ji}\, B_i \tag{3}$$

This route is quite acceptable provided the number of candidate source locations J is small (e.g., J < 100); however, if nothing is known about the source locations and, instead, an array of point or area sources is conjectured to exist on an X-Y grid of size n x m, then the dimension of the matrix A requiring inversion will be (n x m) by (n x m). Thus, for example, the reasonable choice of a 50 x 50 grid leads to the required inversion of a rather unreasonable 2500 x 2500 matrix and to a minimum of 2500 concentration measurements!*

A more rational approach might consist of the following two-step procedure:

(i) develop a procedure, utilizing the data, to determine the most likely locations of the most significant sources.**

(ii) given this greatly reduced number of source candidates, solve the problem as per equation (3).

We now turn the development of the procedure alluded to in (i).

Consider first a somewhat altered and less general form of equation (1) given by the expression

$$\chi^2 = \sum_{t,k} [\ln C_{kt} - \ln Q_j R_{jkt}]^2$$

This definition of χ^2 implies

a) the concentrations at the k^{th} receptor are lognormally distributed in time,

b) the measurement errors, ΔC_{kt}, are simple percentage errors (i.e., $\Delta C_{kt} \propto C_{kt}$), and

c) the entire concentration at a given receptor k during a given time interval t is attributed to the influence of a single source Q_j.

Ignoring the fact that the third assumption may be often quite unreasonable, we continue development of the formalism. Since the source of interest, j, may differ for each term t,k in the sum, one may include explicit summation over j in the expression

---

*Though not pursued in this paper, it may be reasonable to proceed iteratively from a coarse grid to a fine grid, removing unlikely source candidates after each iteration and thereby holding the dimensionality of A within tractable bounds.

It should also be noted that the solution given by equation (3) does not constrain all Q_j to be positive. Should such "sink" terms (i.e., $Q_j < 0$) be considered unacceptable, they may be excluded by the addition of a penalty function (e.g., $\sum_{j=1}^{J} \frac{e^{-aQ_j}}{a}$ where a >> 1) to the right hand side of equation (1). Unfortunately, such penalty functions usually cause the problem to become non-linear and thus considerably more difficult to solve.

**An ambiguity arises here in the sense that for a particular data set the strongest sources may not be the most significant in terms of observed concentrations at the receptors.

$$\chi^2 = \sum_{j=1}^{J} \chi_j^2 \text{ , where} \tag{4}$$

$$\chi_j^2 \equiv \frac{n_j}{N_j} \sum_{\substack{k,t \\ R_{jkt} \neq 0}} [\ln C_{kt} - \ln(Q_j \, R_{jkt})]^2 \tag{5}$$

and where N_j is the number of cases for which $R_{jkt} \neq 0$ and n_j is the number of cases for which the j^{th} source is actually the assumed sole contributor. Other than noting the sum rule, $\sum_{j=1}^{J} n_j = M$, the individual n_j appear to be some unknown, meteorology dependent function of the source strengths and positions relative to the receptor network geometry. Rearrangement of the ln terms in equation (5) and the subsidiary definitions, $q_{jkt} \equiv \ln(C_{kt}/R_{jkt})$ and $\overline{q}_j \equiv \ln Q_j$, enables one to rewrite equation (4) as

$$\chi^2 = \sum_{j=1}^{J} n_j \, \sigma_j^2 \tag{6}$$

where $\sigma_j^2 \equiv \frac{1}{N_j} \sum_{\substack{k,t \\ R_{jkt} \neq 0}} (q_{jkt} - \overline{q}_j)^2$ *

and σ_j is simply the standard deviation of the logarithm of the source strength about its expectation value $\overline{q}_j$. Though the unknown characteristics of n_j have blocked efforts at obtaining an exact solution to the minimization of χ^2 as expressed by equation (6), preliminary empirical investigations suggest that a search in the X-Y plane for local maxima of the function $f_j \equiv \frac{N_j - 1}{\sigma_j^2}$ serves to determine the locations of the most significant sources (i.e., those sources

---

*In practice, the unbiased estimator, $\sigma_j^u = \left(\frac{N_j}{N_j - 1}\right)^{1/2} \sigma_j$, was used; however, the difference is generally insignificant.

which give the most significant reductions in χ^2, as given by the exact formulation of equation (1) but subject to the additional condition, $\Delta C_{kt} \propto C_{kt}$). It also appears that the magnitude of f_{j*} at the position, $j*$, of the local maxima is strongly correlated with the net reduction of χ^2 realized by inclusion of a source at location $j*$. At present, the role of locations for which f_j is large and yet not a local maximum remains somewhat unclear. Though inclusion of these locations also leads to some improvement in χ^2, it is not clear that the overall confidence level, $\Gamma\left(\frac{M-J}{2}, \frac{\chi^2}{2}\right) / \Gamma\left(\frac{M-J}{2}\right)$, does not also drop. The ideal situation is, of course, achieved when the number of sources included, J, maximizes the confidence level.

Model Application

The Data Bases

The model has been applied to two distinct, yet highly related, data sets pertaining to a network of 18 CO monitors at Williams Air Force Base, Arizona. The network, set up to assess the feasibility and desirability of a more extensive study, produced hourly average CO concentrations for 37 hours of finite wind speed, daytime operation spanning a two week period. Accompanying the experimental data base was a companion set of calculated concentrations (henceforth referred to as the theoretical data base) computed by means of the ANL/USAF developed Air Quality Assessment Model (AQAM),[2] which basically operates by applying the Gaussian plume formalism to the complex inventory of point, line, and area sources encountered at an airbase or airport. Figure 1 shows the airbase boundary, principal aircraft parking areas, taxiways, and runways, as well as the locations of the 18 CO monitors.

Computation of R_{jkt}

The coupling coefficients, R_{jkt}, were also computed via the Gaussian plume formalism; however, due to the a priori unknown nature of the sources,

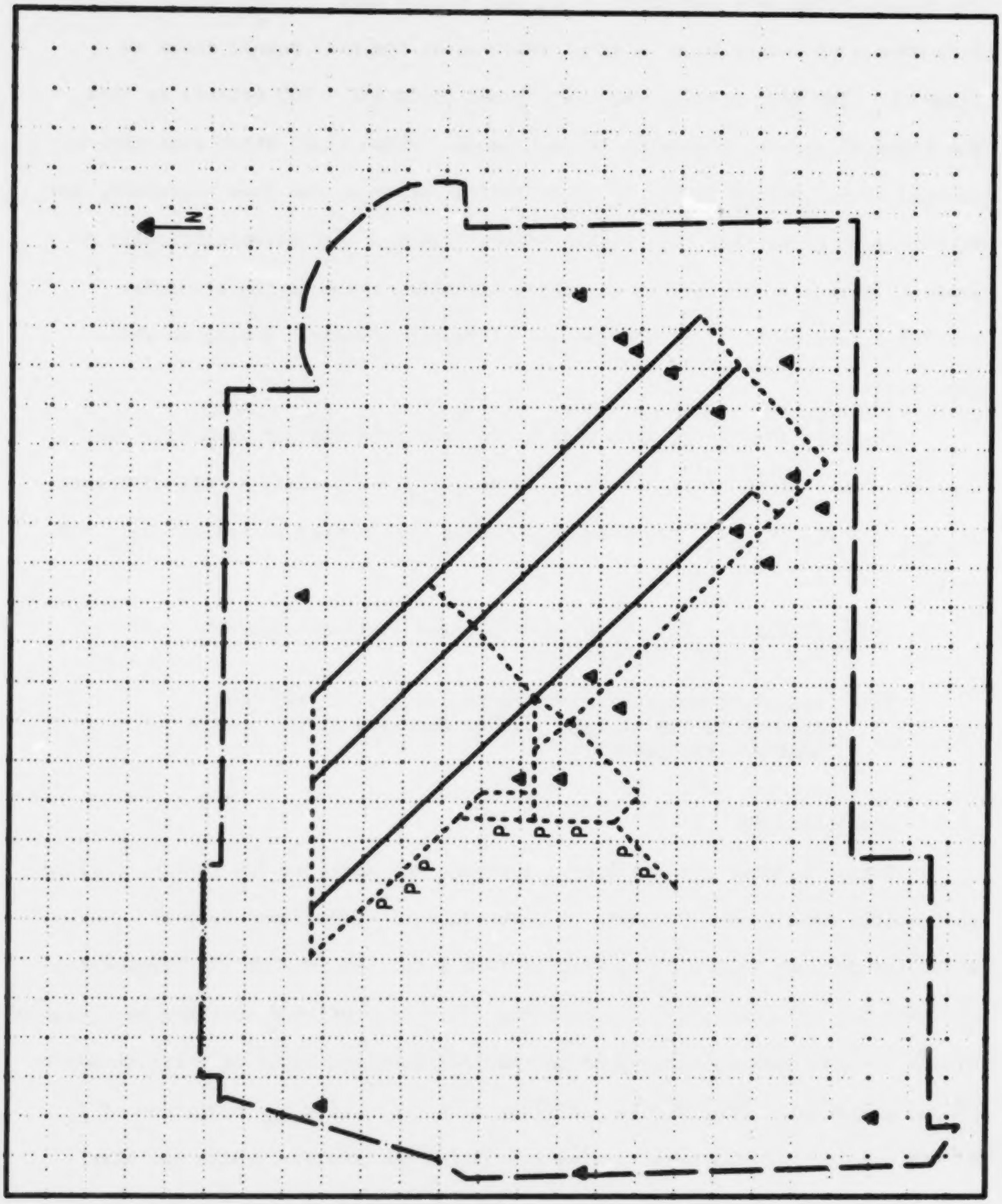

Figure 1. Map of Williams AFB, Arizona showing runways (————), taxiways (-----), aircraft parking areas (P), CO monitoring sites (Δ), and airbase boundary (——·——). The computational grid (......) is also displayed.

the calculations were performed as if each source were a ground-level, square, area source of length ΔX on a side, centered on the mesh points shown in Figure 1. The mesh spacing was also chosen as ΔX ($\Delta X = 200$ meters) so that the array of source candidates is contiguous. Plume rise, which also must be assumed to be unknown in any "source-finding" program, has been neglected, and it should be noted that this highly source oriented, yet meteorologically dependent, parameter represents the major stumbling block in the otherwise trivial extension of this two-dimensional "source-finding" theory to three dimensions.

The only departures from well known prescriptions[3] for computing the coupling coefficient arise because allowing $R_{jkt} \to 0$ results in the divergence of $q_{jkt} = \ln(C_{kt}/R_{jkt})$. Two rules which were implemented to prevent $R_{jkt} \to 0$ were:

(i) situations for which the crosswind distance exceeded $2.15\ \sigma_y$ were ignored, and

(ii) receptors embedded within a source (i.e., $j=k$) were assumed to lie at least $0.3\ \Delta X$ downwind of the upwind edge of that source.

Model Results

Figure 2 shows the results of applying the model to the AQAM determined, theoretical data base. Contours of a conveniently normalized form of f_j are shown for integer values of f_j ranging from 1 to a maximum of 11. Evaluation of the exact solution, given by equation (3), has confirmed that the most significant on-base sources correspond to the locations indicated as relative maxima by the contours of Fig. 2. In addition, it appears that the magnitude of f_j at the position of the local maxima correlates qualitatively with the magnitude of the reduction in χ^2 realized by the inclusion of that location as a source. Interpretation of those regions where f_j is large and yet not at a local maxima is somewhat unclear. How rapid a rise in f_j should one expect on approaching a point source versus a diffuse area source? Clearly this

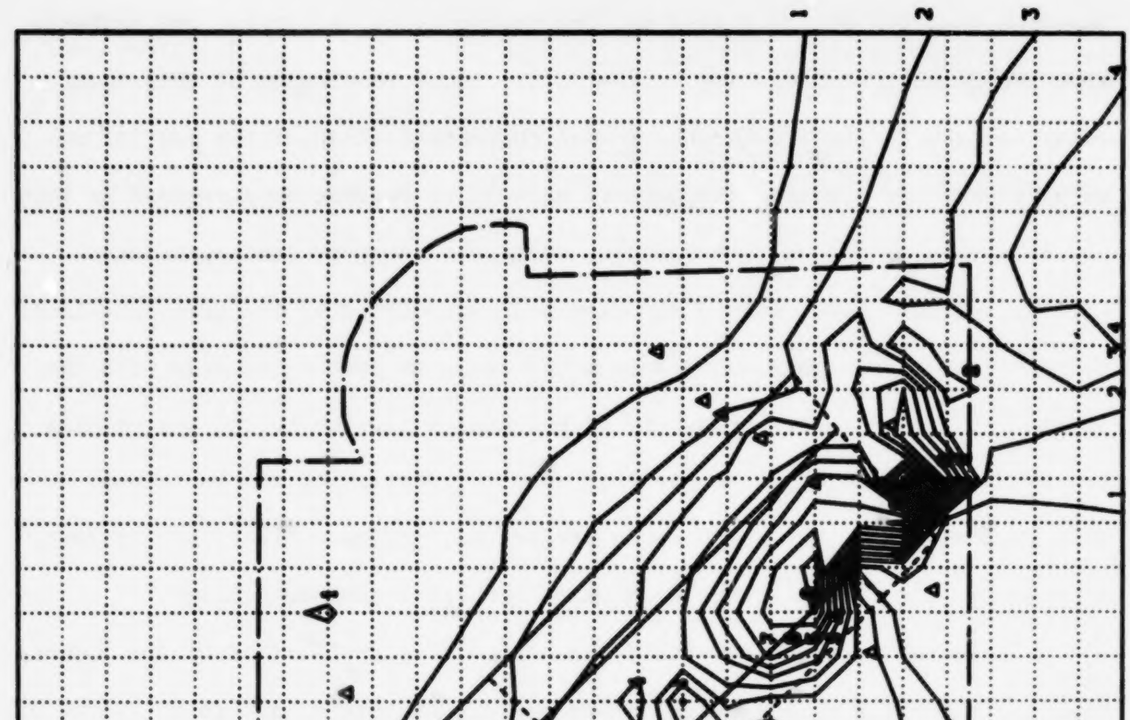

Figure 2. Contours of the normalized form of f_j resulting from model application to the AQAM determined, theoretical CO concentration data base.

question involves the grid size ΔX, the proximity of receptors, and probably also the quantity and quality of the data. Thus, resolution of this issue seems certain to require further formal characterization of the spatial resolving power of a monitoring network as well as further applications of this new technique to data sets possessing different receptor configurations. Finally, we note that, within the resolution permitted by the grid, the locations of the most significant sources are found to correspond well with the regions of high aircraft emissions (i.e., engine startup in the jet parking areas and engine idle in the aircraft queuing portions of the taxiways). This is reassuring, but by no means unexpected, as these highly significant sources are also input to the AQAM which generated this data base.

Results of the considerably less definitive application of the "source finding" technique to the actual experimental data are displayed in Figure 3. The inability to resolve any clear on-base sources is due in part to the fact that aircraft and airbase sources are estimated to contribute only 10-25 percent of the hourly-average CO signal measured at these receptors; the rest is due to background CO levels which were assumed non-existent in the AQAM theoretical data set. A second factor contributing to the reduced source resolving power is the presence of experimental measurement errors. This factor, absent from the theoretical data set, can only act to blur the source resolving power of a monitoring network.

Summary and Conclusions

A formalism has been developed for utilizing data obtained from an air quality monitoring network to determine the locations and strengths of those sources contributing most significantly to the observed concentrations. Though the problem may be solved exactly for the case of J source candidates via the inversion of a J x J matrix, this approach becomes unmanageable in situations

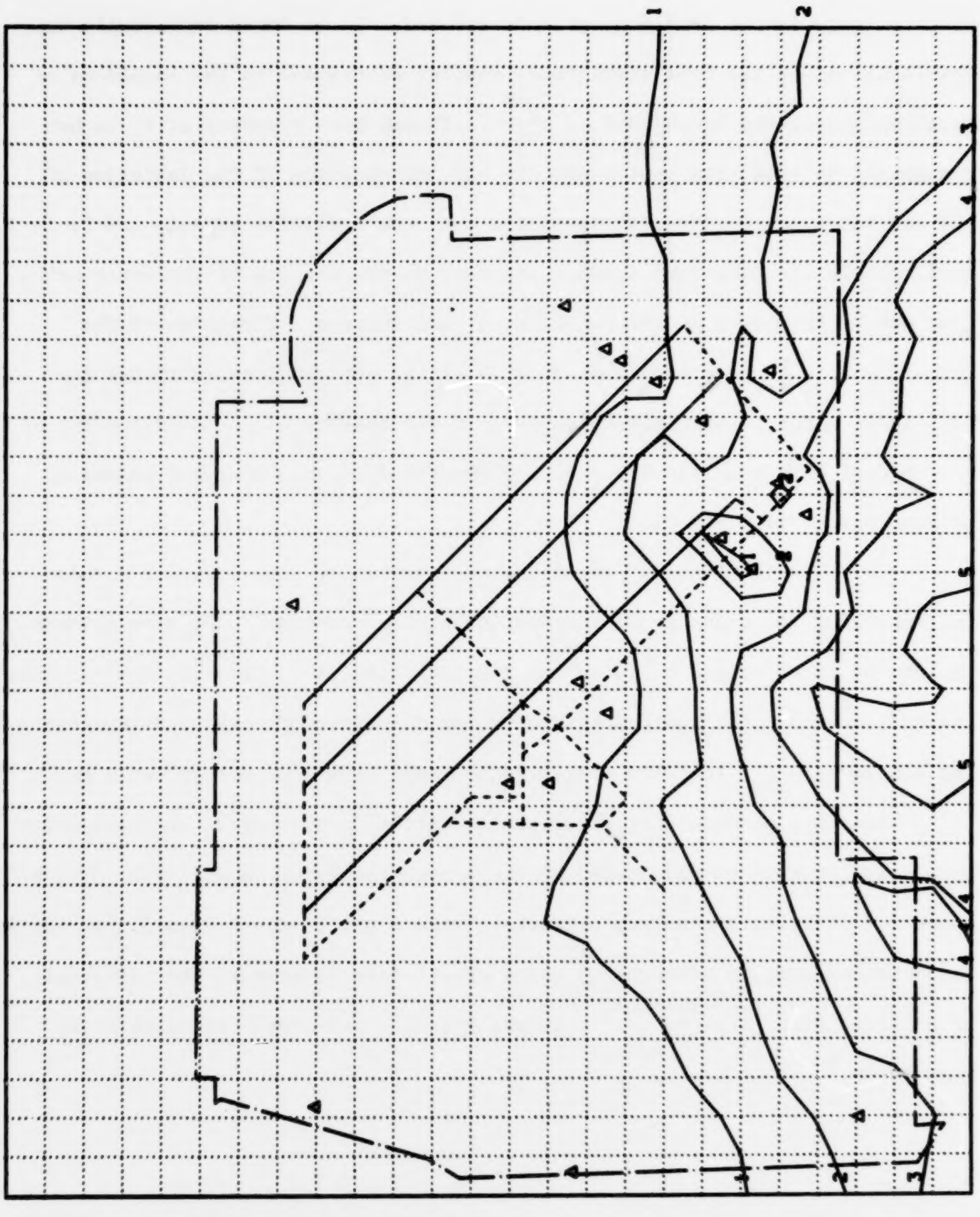

Figure 3. Contours of the normalized form of f_j resulting from model application to the experimental CO concentration data base. The pattern shown is thought to result from the combination of high background CO levels and the predominance of southerly winds.

where a large source candidate grid is assumed. It is found empirically that the locations of the most significant sources correspond to the locations of local maxima in the function $f_j \equiv \frac{N_j-1}{\sigma_j^2}$. Though this property of f_j is not rigorously derived, its equivalence to the minimization of the deviation of the estimated source strength about its mean has intuitive appeal, and it is confirmed in the described application both by the results of the exact solution and by the known locations of the actual sources. Extension of the formalism to a three-dimensional grid should be straightforward though its usefulness might be strongly questioned in the absence of an understanding of how to deal with specifically source dependent (and thus a priori unknown) phenomena such as plume rise.

This "source finding" formalism may eventually also serve as a tool for improving the understanding of pollutant transport and diffusion through the use of experimental pollutant monitoring data. The rationale here is that the more accurate the representation of the dispersion process via the coupling constants R_{jkt}, the more realistic the resulting source "map" will be.

Finally, we note that these preliminary efforts suggest that attention should be focussed on understanding the source resolving capabilities of proposed and existing monitoring networks. This might be accomplished numerically for existing complex networks by using actual data to compute the classical resolution, $\Delta r \equiv \left[2\Big/\left(\frac{\partial^2\chi^2}{\partial r^2}\right)\right]^{1/2}$, or analytically for simple receptor array geometries.

Acknowledgments

This work was supported in part by the U.S. Air Force Civil Engineering Center, Tyndall AFB, Florida and by the Federal Aviation Administration. I would like to thank Mr. David Lamich for his computer graphics assistance.

References

1. Council on Environmental Quality, The Sixth Annual Report of the Council on Environmental Quality, U.S. Government Printing Office, Washington, D.C., December 1975.

2. Rote, M., and L.E. Wangen, A Generalized Air Quality Assessment Model for Air Force Operations - Technical Report, AFWL-TR-74-304, February 1975.

3. Turner, D.B., Workbook of Atmospheric Dispersion Estimates, U.S. Department of Health, Educations, and Welfare, 1970.

38

8th International Technical Meeting on
Air Pollution Modeling and its Application.

DUAL ANALYSIS IN AIR POLLUTION MODELLING

Y. JACQUART

Institut d'Astronomie et de Géophysique
Université Catholique de Louvain
Chemin du cyclotron, 2

B-1348 LOUVAIN-LA-NEUVE
BELGIUM

September 20-23, 1977
Louvain-la-Neuve
Belgium.

1. BACKGROUND OF THE MODEL.

Meteorological variables (which particular definition considered in this study shall be given in the next section) measured at a station close to Louvain-la-Neuve and SO_2 immission variables measured at five stations around Louvain-la-Neuve are considered. In this area, the paper-factory of Mont-Saint-Guibert is a dominant point-source of SO_2 (fig. 1) (Ronneau, 1976). The synchronisation of the observations is described in the next section.

Each variable can be considered as a point in the space of the observations. The i^e coordinate of this point is the value of the variable at the i^e observation. In the same way, each observation can be considered as a point in the space of the variables. Thus, in each space, a cloud of points has been built. Each cloud holds his principal factors, i.e. his principal inertial axis if a mass is attributed at each point, and a metric is choosen for the space. In a preliminary application, a metric has been defined in such a way that greater is the correlation between two variables, nearer are the two corresponding points in the space of the observations and greater is the covariance between two observations, nearer are the two corresponding points in the space of the variables. It can be demonstrated (Schifflers, 1975) that each factor of one space corresponds to a factor of the other space : there is a real duality which justifies the appellation "Dual analysis".

The matrix being choosen, the cosine between an observation and a factor is defined and also the cosine between a variable and a factor. For any two factors, five cartesian diagrams are drawn as outputs of the "Dualan program". In one diagram, the coordinates of each variable are proportional to the cosine between the variable and the two factors (fig. 1.a, 1.b and 1.c). In the other diagrams the coordinates of each observation are proportional to the cosine between the observation and the two factors; these four diagrams are related to the four seasons (fig. 3.a to 3.d are some examples).

2. DESCRIPTION OF THE INPUTS AND NOTATION OF THE VARIABLES.

The period analysed is january 1, 1970 to may 31, 1974, which means 1613 days. Unfortunately no more than 488 days have complete datas.

An observation is defined, in this study, as a vector of which 105 components (5 for pollution, 96+2+2 for meteorology) are the following measurements made during one day (table 1) :

A Five pollution variables noted 01, 02, 03, 04, 05 :
a pollution variable is defined as being formed by the daily concentration at five stations.

B Twelve meteorological parameters observed eight times a day (indice 1 characterizes 3.00, indice 2 6.00 ... indice 8 24.00).

- R1 ... R8 : dew point;
- N1 ... N8 : nebulosity;
- F1 ... F8 : windspeed;
- V1 ... V8 : visibility;
- P1 ... P8 : atmospheric pression;
- T1 ... T8 : temperature;
- C1 ... C8 : ceiling;
- Z1 ... Z8 : water vapor pressure;
- A1 ... A8 : solar radiation (Holsworth, 1974);
- S1 ... S8 : altitude of the sun;
- K1 ... K8 : atmospheric stability (Holzworth, 1974);
- H1 ... H8 : relative humidity.

Thus, these twelve parameters lead us with 12 x 6 = 96 variables.

C Other meteorological variables.

- PA, PP : rain recorded twice a day;
- TN, TX : minimal and maximal temperature in a day.

The variables are apparent in the figures 2.a, 2.b and 2.c as described in section 1.

3. NOTATION IN THE OBSERVATIONS.

The observations are apparent in the figures 3.a, 3.b, 3.c, 3.d and 3.e as described in section 1. Each observation is designated only by his month : 1 for the observations of january to 9 for september, A for october, B for november, C for december.

4. OUTPUT ANALYSIS.

A First factor.

The first factor shows an opposition between the summer observations, on the left side (fig. 3.a), and the winter observations, on the right side (fig. 3.b). Thus, the first factor represents the seasonal cycle. Because of the duality, the variables reaching their maximum values in summer are on the left side in fig. 2.a (e.g. T1, ... T8) and the variables reaching their maximum values in winter are on the right side (e.g. H3, ... H8).

Let us consider figure 2.a (factors 6 and 1).

A.1 Meteorological variables.

Are greater in summertime : temperature (T), dew point (R), water vapor pressure (Z), altitude of the sun (S).
Nights are relatively fresh in summer (T1, T2, T8, T7 are less on the left side than T3, T4, T6, T5 and TN is on the right hand side of TX). The tendency is not so great for : ceiling (C), nocturnal stability (K1, K7, K8), visibility (V), diurnal radiation (A2, ..., A6).

Are greater in wintertime : diurnal humidity (H7, H8, H2, H1), nebulosity (N), windspeed (F), atmospheric pression (P).

The rain is not significantly more important in winter than in summer : PA and PP are near the y-axis.

In this figure, factor 1 plays also an interesting role. Indeed, a relative opposition between night and day is apparent for three parameters : visibility (V), humidity (H) and windspeed (F).
Mainly during the day, the humidity is greater in winter than in summer. Mainly during the night, the windspeed is greater in winter than in summer. Mainly during the day, the visibility is greater in summer than in winter. For the stability, the opposition is much more absolute : K1, K7, K8 are on the summer side and K2, ... K6

are on the winter side.

A.2 Pollution variables

There is an opposition between station 2 (02 on the summer side) and station 4 (04 on the winter side). This opposition could be explained by the winddirection : the north-east wind would have been more frequent or more polluting in summer time than in winter time and the south-west wind more frequent or more polluting in winter than in summer, station 2 being located south-west of the paper-mill and station 4 being located in the east-north-east sector (fig. 1). In a future application the winddirection will be introduced in such a way that this hypothesis will definitively be corroborated or invalidated.

Moreover, at stations 1 and 4, far away from the factory, the pollution due to domestic heating is becoming to be more significant as compared to the paper-mill point source. This could explain that the pollution at these stations is greater in winter (04 and 01 on the winter side), while the pollution at stations 3 and 5 is the same in winter and in summer.

B Other factors.

Factors 2 and 3 show oppositions into meteorological parameters (fig. 2.b) independantly of the seasons (fig. 3.c and 3.d). These factors show a situation of high pollution at station 4 and mainly at station 1 : 01 is far away from the center. Stations 4 and 1 being far away from the paper-mill, it could be a situation of high background pollution.

Factors 4 and 5 take into account the variations of the meteorological parameters during the day : there is definitely an opposition between N1 and N8, between C1 and C8, ... (fig. 2.c). Nevertheless, the pollution seems to be independant of these variations (01, 02, 03, 04, 05 being not scattered in the direction β of figure 2.c).

Factor 6 modifies the tendencies of factors 2 and 3. With factor 1, it sets an opposition between night and day (fig. 2.a).

More details about factors 2 to 6 are given in (Jacquart, 1977).

Each of the remaining factors explains not more than 2% of the total variance. They are not considered.

5. CONCLUSIONS AND FUTURE PROSPECTS.

The first six principal factors explain more than 70% of the total variance of the 100 meteorological variables. They explain only 27% of the pollution at station 1, 20% at station 4 and 7% at the other stations. As possible explanations, it must be noted :

1. The daily observation (as defined in section 2), begins at 3.00 while immission pollution is daily recorded beginning at 9.00. In a future application, the meteorological observation first considered will have to be the 9.00 one.
2. The winddirection has not been considered.
3. The number of pollutant variables (5) is small comparatively to the number of meteorological variables (100).
4. Emission variations through time would also be usefull.

As soon as we will be able to get a better explanation of the variance of the observed pollution variables by the meteorological ones, we plan to use as pollution variables the difference between observed and computed values obtained from a mathematical diffusion model. We expect that this will lead to determine eventually which meteorological variables the model do not take into account adequately or which have to be introduced in the model. Maybe the existence of some sequences of meteorological situations is also important, e.g. a high diurnal instability following a high nocturnal stability or a period of steady well oriented wind following a period of calm wind.

OBSERVATIONS VARIABLES		January 01 ... 1970	... May 31 1974
5 pollution variables	01		
	02		
	03		
	04		
	05		
12 Meteorological parameters $\underbrace{12 \times 8}_{96}$ Meteorological variables	R1		
	⋮		
	R8		
	N1		
	⋮		
	N8		
	F1		
	⋮		
	F8	MATRIX OF DATAS	
	⋮		
	H1		
	⋮		
	H8		
4 Meteorological variables	PA		
	PP		
	TN		
	TX		
total : 105 variables			

TABLE 1

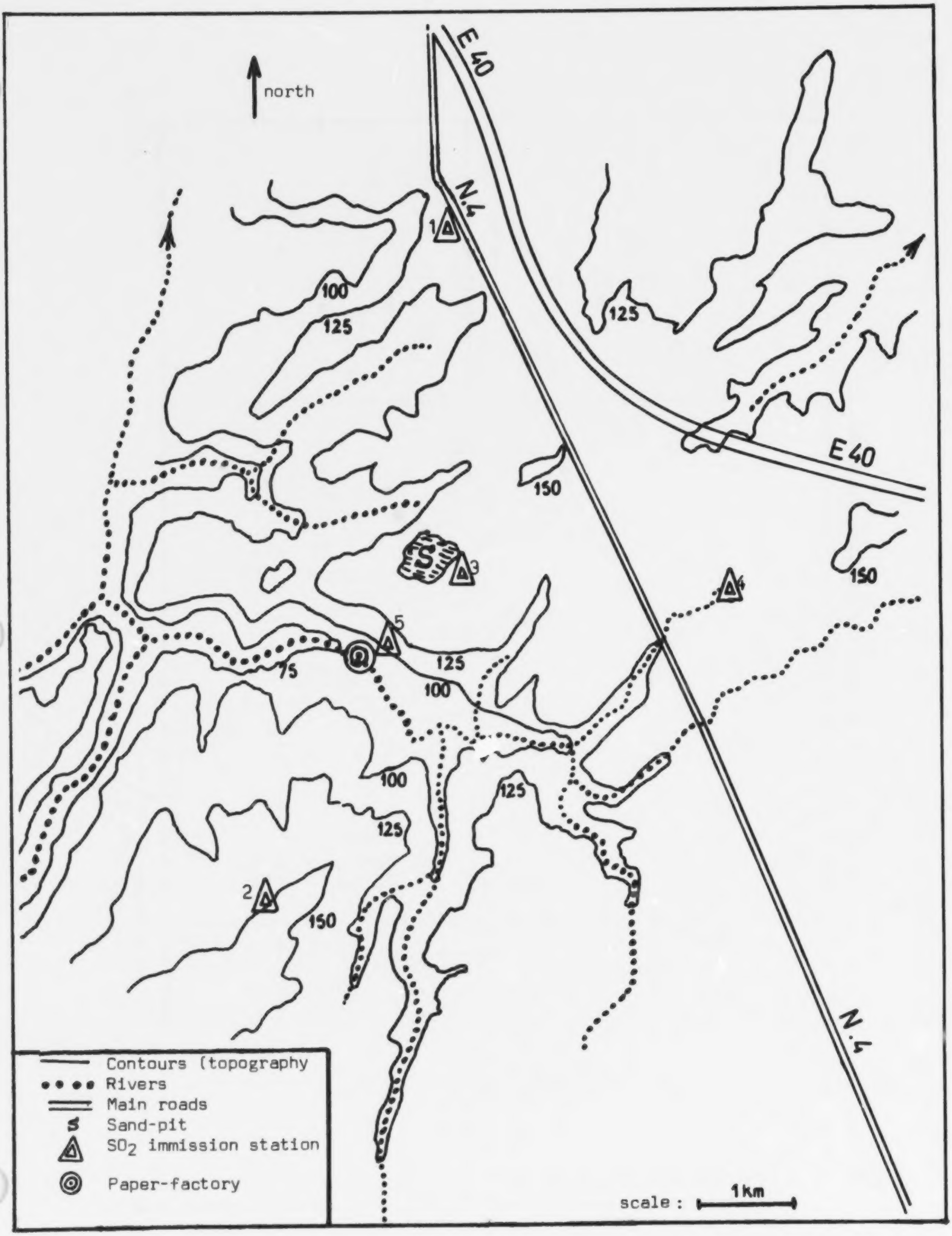
north
E 40
N.4
E 40
N.4
1
2
3
4
5
S
75
100
125
150
Contours (topography
Rivers
Main roads
Sand-pit
SO2 immission station
Paper-factory
scale :
1 km

FIGURE 1 : Map of the studied country.

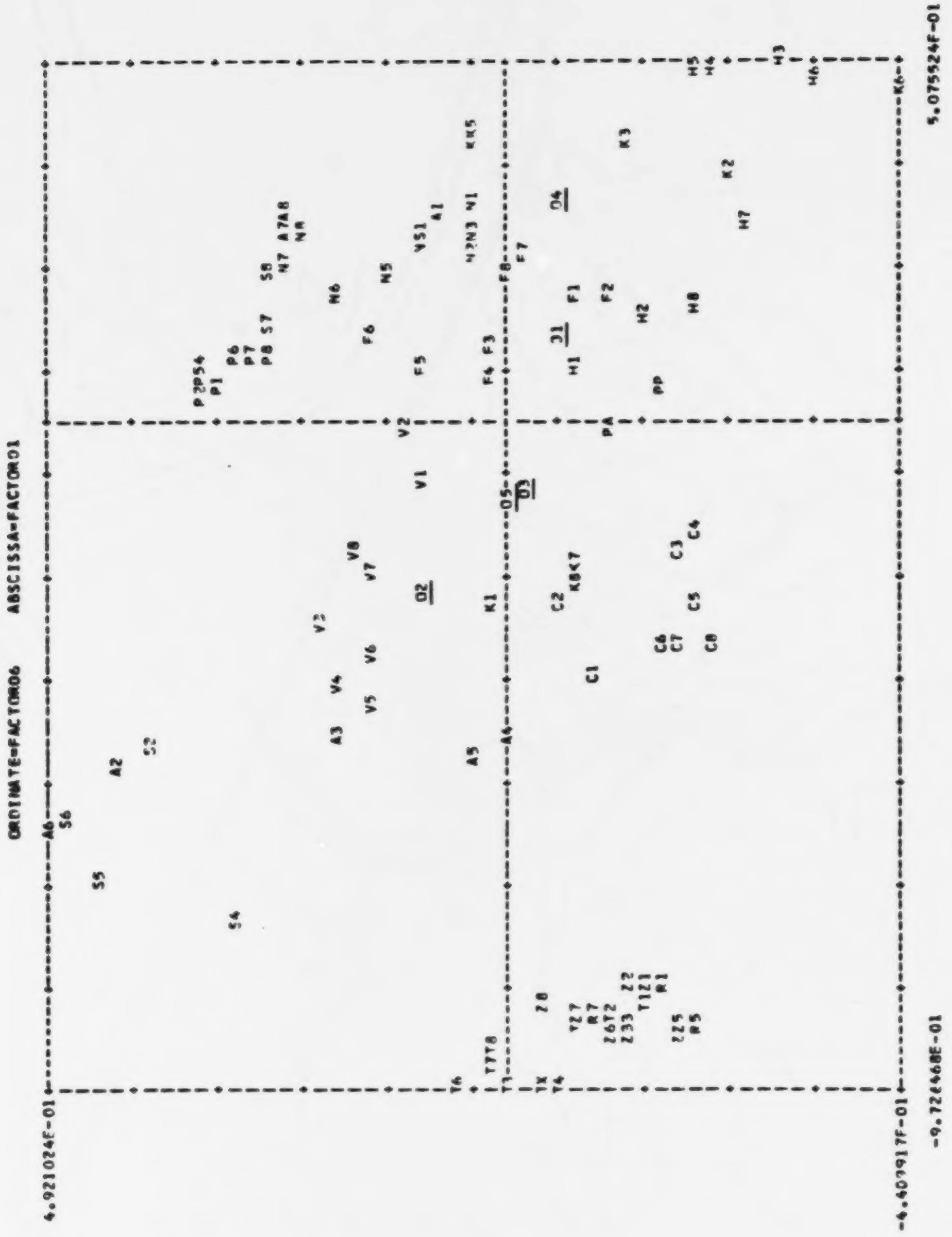

FIGURE 2a : Clusters and distances for variables projected on the plane determined by factors 1 and 6. Pollution variables have been underlined. The variables reaching their maximum values in summer are on the left side and the variables reaching their maximum values in winter are on the right side.

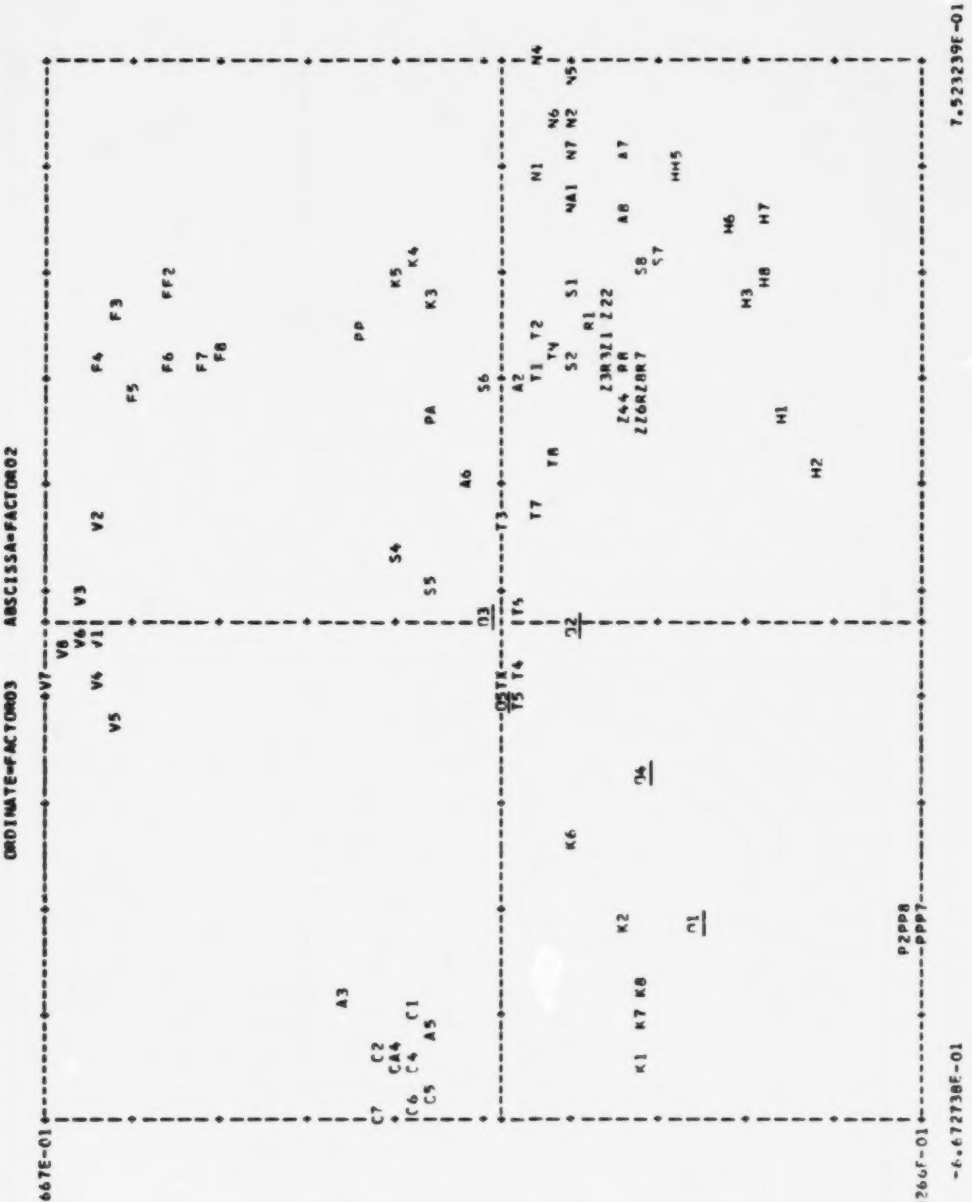

FIGURE 2b : Clusters and distances for variables projected on the plane determined by factors 2 and 3. Pollution variables have been underlined.

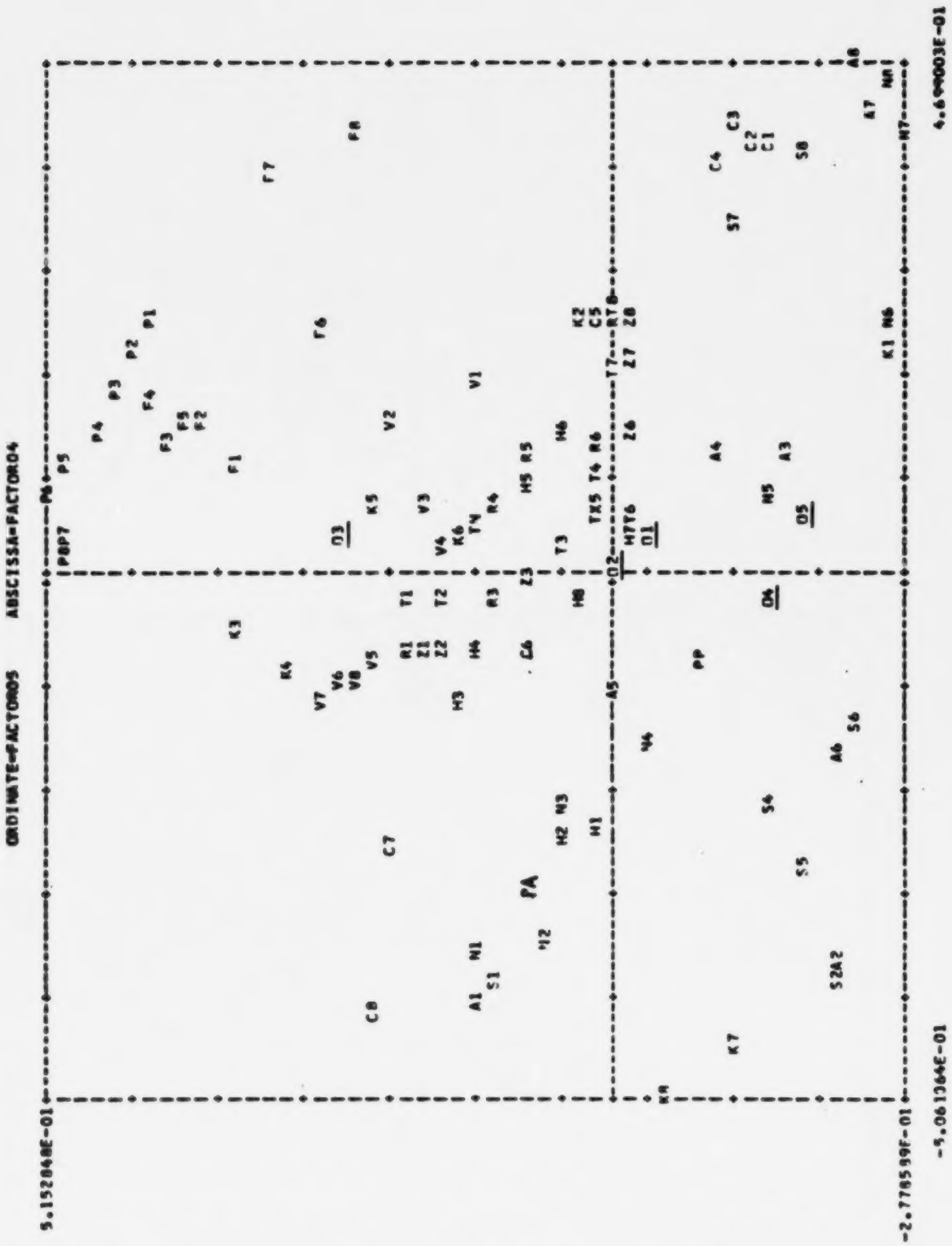

FIGURE 2c : Clusters and distances for variables projected on the plane determined by factors 4 and 5. Pollution variables have been underlined. Factors 4 and 5 show clearly oppositions between variations of meteorological parameters during a day.

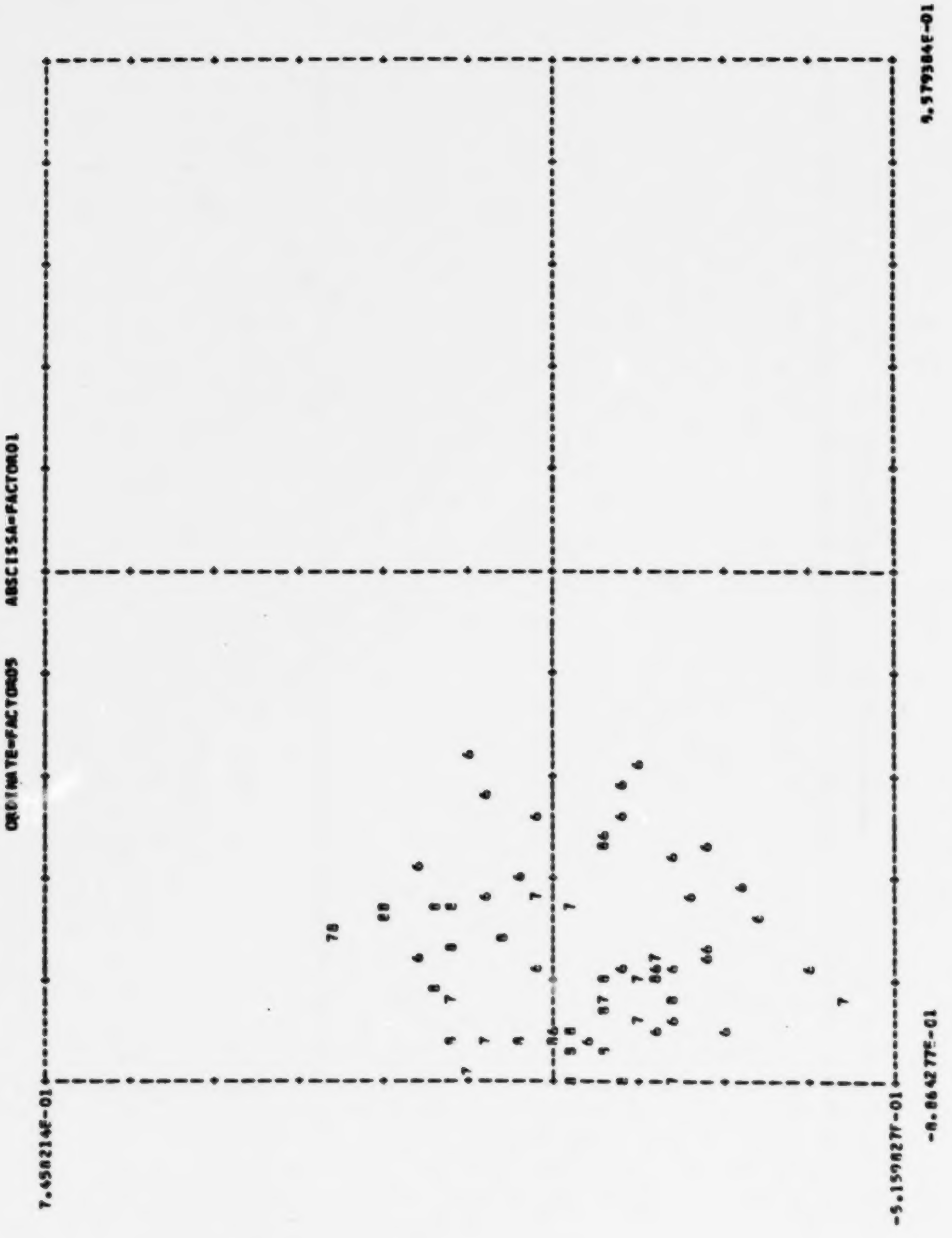

FIGURE 3a : Clusters and distances for summer observations, labelled by their month and projected on the plane determined by factors 1 and 5. The left side of factor 1 is obviously the summer side.

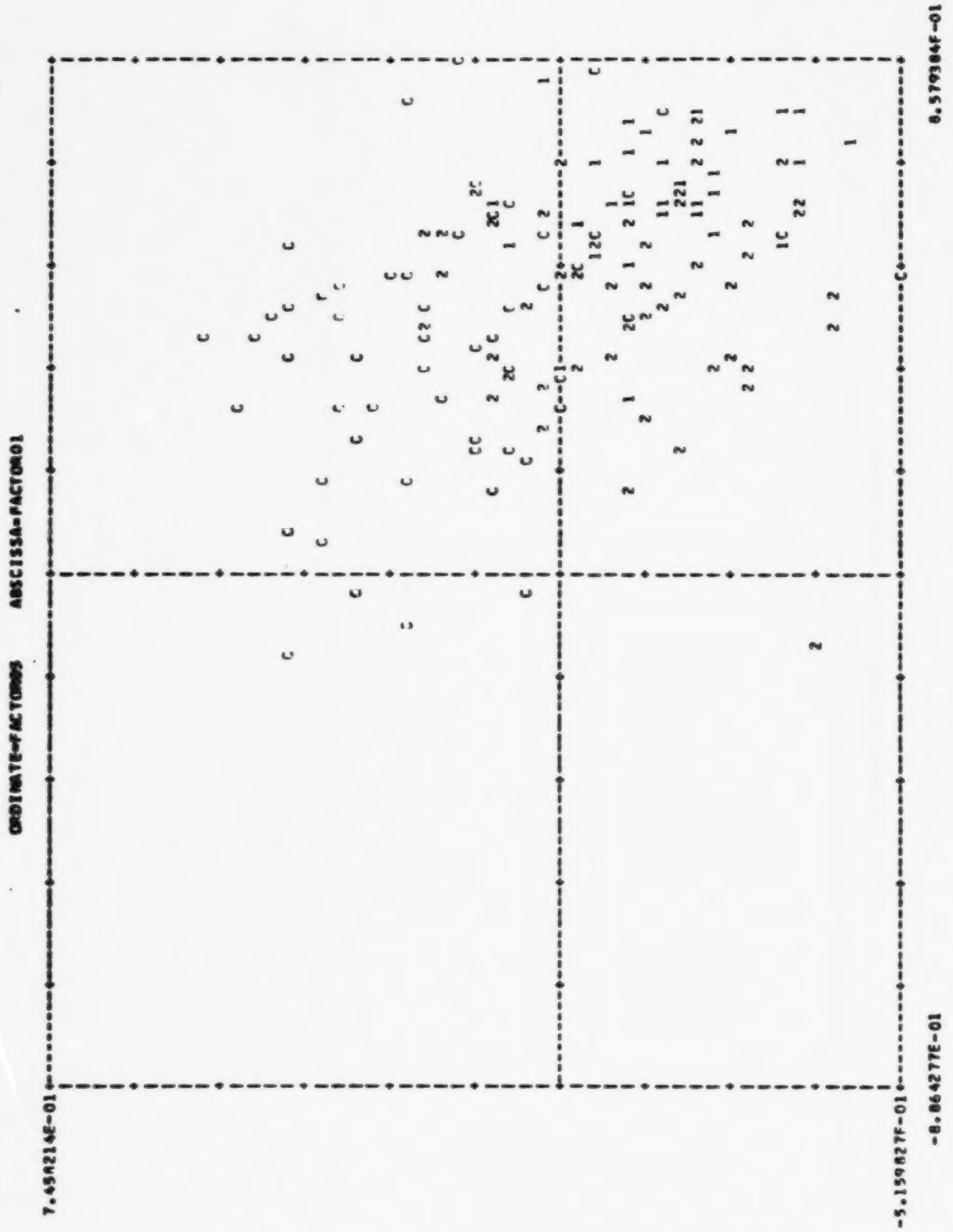

FIGURE 3.b : Clusters and distances for winter observations, labelled by their month and projected on the plane determined by factors 1 and 5. The right side of factor 1 is obviously the winter side.

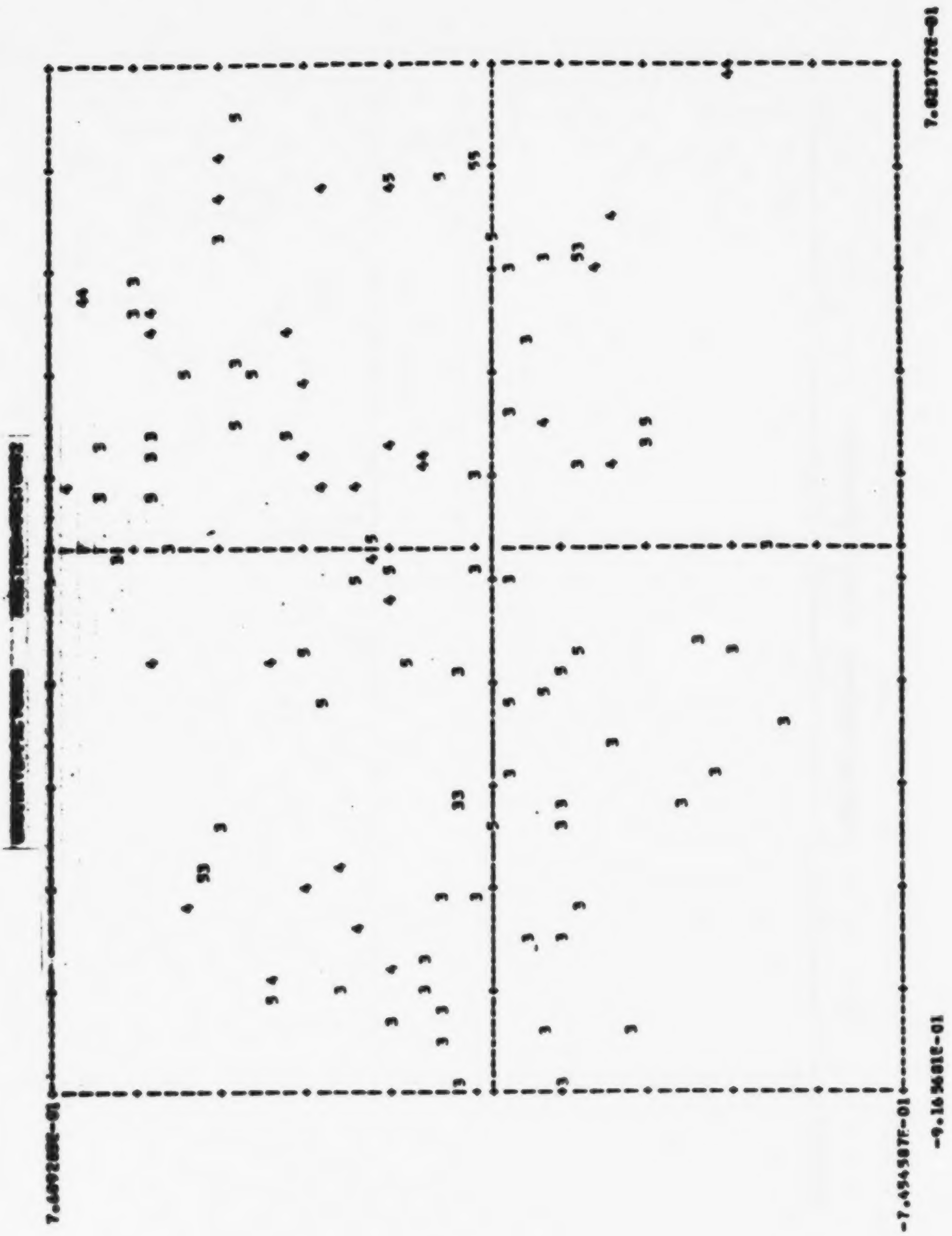

FIGURE 3.c : Clusters and distances for spring observations, labelled by their month and projected on the plane determined by factors 2 and 3.

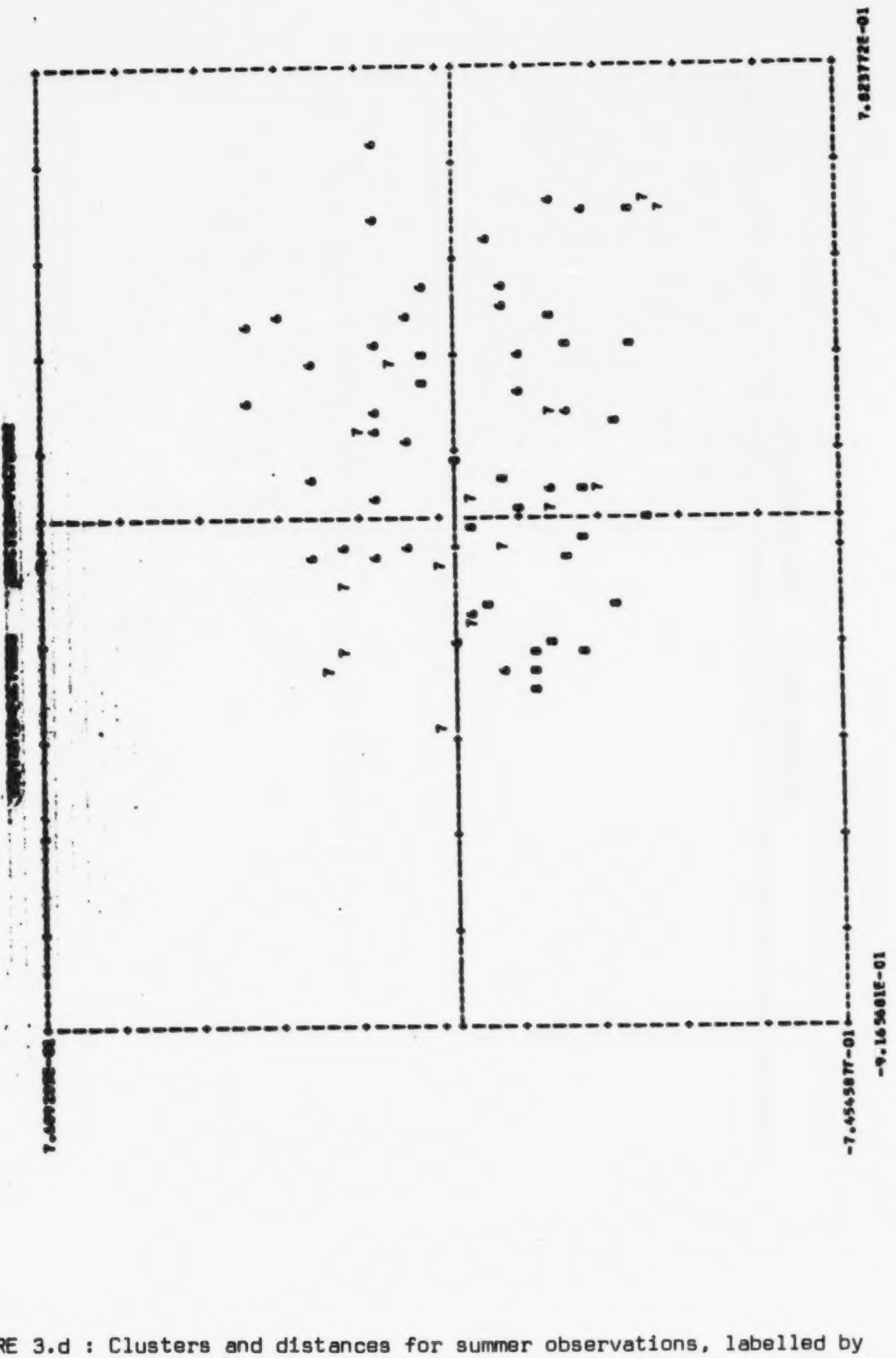

FIGURE 3.d : Clusters and distances for summer observations, labelled by their month and projected on the plane determined by factors 2 and 3. Factors 2 and 3 are not significantly dependant of the season.

REFERENCES

1. I.R.M. - R.V.A. "Observations synoptiques - bulletin mensuel".

2. I.R.M. - I.H.E. "Bulletin mensuel de pollution atmosphérique".

3. D.H. Anderson, A.M. Daeninck and E. Schifflers, Dualan, U.C.L. Centre de Calcul, report n°13 (1975).

4. G.C. Holzworth, "Climatological aspects of the composition and pollution of the atmosphere". World Meteorological Organization, n° 939, Genève (1974).

5. P. Dagnelie, "L'analyse statistique à plusieurs variables". Les presses Agronomiques de Gembloux (1975).

6. L. Lebart ET J.P. Fénelon, "Statistique et informatique appliquées" Dunod, Paris, (1971).

7. J.P.Benzecri, "L'analyse des données", Dunod, Paris.

8. Y. Jacquart, "Analyse duale : technique de calibration des modèles". Programme National R-D environnement, projet air,Progress Report AL/4.1 - 1977, Dept. for Science Policy, Brussels, 8 rue de la Science.

9. C. Ronneau, "Emissions de dioxyde de soufre par l'usine de pâte à papier de Mont-Saint-Guibert". Personal Communication (1976), Louvain-la-Neuve, 2 chemin du cyclotron.

ACKNOWLEDGEMENT

I wish to thank Dr. A. Berger who kindly read this manuscript and offered helpful suggestions. I would like also to aknowledge Dr. Cl. Demuth and Dr. G. Schayes for stimulating discussions.

This study is part of the Air Project of the Belgian National Programme on the Environnement sponsered by the Ministry of Scientific Policy.
The author wishes to express his gratitude for the financial assistance with the aid of which the work was carried out.

I thank M. E. Schifflers for his advices and effective asistance.

8th International Technical Meeting on
Air Pollution Modeling and its Application

A UNIT CONSTRUCTION SYSTEM OF DISPERSION MODELS FOR AIR QUALITY MANAGEMENT

B. GUTSCHE D. JOST
Umweltbundesamt, Bismarckplatz 1
D - looo Berlin 33, West-Germany

Ch. LUDWIG
Free University of Berlin, Thielallee 5o
D - looo Berlin 33, West - Germany

September 2o-23, 1977
Louvaine-La-Neuve
Belgium

Contents

1. Introduction
2. Standardization of GAUSSian plume models
3. Application of other model types
    3.1 Finite-difference models
    3.2 Particle-in Cell-Method on Monte-Carlo-Basis
4. Combination of different scale models for traffic emissions as a simple example for a unit construction system of dispersion models
5. Conclusions

1. Introduction

The three basic questions to be answered by an air quality management system have been formulated by SLATER (1) in 1974:

1. How does one characterize the air quality distribution?
2. How is the air quality distribution related to the emission distribution?
3. How may the emission distribution be altered to attain the air quality standards?

and he continues, that, to answer these questions, considerable dependence is placed on the results of air quality models. But, so he said, the 'perfect model' is yet to be devised.

This was the point, we looked around and asked: What could be the requirements of an ideal air quality management system with regard to such a perfect model? And: What could be - on the basis of these demands - the structure of a perfect model?

These requirements of an air quality management system enclose among others (Table 1).

- long-term air quality studies for even and topographic terrain (for licensing procedures and clean air plans);
- short-term predictions for case studies and for an analysis of episodes;
- short-term predictions for the analysis of causes by iterative comparison with concentration measurements;
- simulation of weak-wind weather situations when air circulation is poor for smog warning plans and licensing procedures in areas with frequent weak wind situations;
- calculation of the dispersion of automobile emissions in streets;

- inclusion of physical, chemical and photochemical reactions into dispersion calculations;
- describing the spreading of heavy gases.

To analyse advantages and limits of applicability of different model types with regard to these requirements of an air quality management system, we set (Table 1) our subjective assessment of the stage of development of the different model types against these requirements.

Though such a diagram reflects to a high degree a subjective view, some general aspects may be emphasized:

- not all the model types are applicable to all types of questions;
- the different model types appear to have specific advantages, but also specific disadvantages with respect to particular questions;
- the demands of different model types with respect to extent and accuracy of input-data are extremely different;
- the different model types require extremely different computer-time and-core;
- the stage of development of models is individually different; but there seem to be some possibilities in novel approaches, the consequences of which cannot yet be fully recognized;
- the range of applicability of various model types cannot be extended arbitrarity; the model assumptions limit the applicability in such a sense that it cannot be expected to receive satisfying answers for all questions cited above.

The consequence of these statements will be, that it does not seem advisable to propose a single 'perfect model'. It will be appropriate to have a spectrum of different air quality simulation models, each of which being able to yield problem-specific answers to a given question. That is: there is a need not for 'one perfect model' for air quality management, but for a unit construction system of different models being reconciled with one another by use of sensitivity analyses. On the basis of such a procedure a closed system of models for air quality management may be obtained.

To these theoretical demands some administrative specifications have to be added: such a system

- must be as simple and practicable and easy to handle as possible,
- has to give clear and definite solutions,
- and must as far as possible reflect the stand of current knowledge.

The second point, clear and definite solutions, requires a standardization and harmonization of each model by itself and of the whole unit construction system.

A glance at Table 1 shows that at now GAUSSian plume models seem to us to be the only ones being suitable for standardization at the moment. Of the three administrative specifications they fulfill the first one, that they are simple, practicable and easy to handle, and with respect to the second one, they will yield definite solutions if there will exist a standardized GAUSSian plume model. Thus, they will be for a long time the principle item of a unit construction system of dispersion models; and other model types will give supplementary information for critical examination and assessment of problems which cannot be solved by GAUSSian plume models due to the limitations being inherent in the model assumptions.

2. Standardization of GAUSSian plume-models

The main efforts to be undertaken in standardization of GAUSSian plume-models have determined the activities of the Modeling

Panel of the NATO/CCMS Pilot Study Air Pollution. They can be summarized as follows (3):

(I) World-wide registration and examination of the variety of applied and validated GAUSSian plume-models;

(II) Comparative model calculations of all these GAUSSian plume-models using an identical set of input data and prescribed model output;

(III) Evaluation of sensitivity analyses of all these models;

(IV) Clarification and determination of those output data which can be predicted by a standardized GAUSSian plume-model with sufficient accuracy.

(V) Determination of the exact limitations of the applicability of GAUSSian plume-models.

Basic material for the first three steps will be summarized in Technical Documents by the Modeling Panel.

At this place we only want to demonstrate the necessity of these investigations by arbitrarily picking out one point of interest: the choice of adequate dispersion parameters.

Fig. 1 shows the effect of using various sets of dispersion parameters (4). Due to greater roughness the Jülich dispersion parameters are considerably larger than those determined at the Brookhaven National Laboratory by SINGER and SMITH. As a consequence the position of maximum concentration comes closer to the source's position with considerably higher concentration values. This effect can even clearly be seen in the field of the annual mean ground-level concentrations due to singular emittents with calculated concentrations being about 50 % higher in the vicinity of an industrial area (south west region); left numbers indicating values which have been calculated using the Jülich data, right numbers using SINGER and SMITH's data. The differences, however, are much more pronounced in the resulting cumulative frequency distribution for a receptor-site in this area (Fig. 2).

Because the effect of the choice of an adequate system of dispersion parameters can already be seen in a multiple-source system it is clear that the differences and, thus, the uncertainties for a licensing procedure, are much more pronounced for a single-source system.

Furthermore, with respect to step (IV) of our standardization procedure, the comparison of Fig.1 and Fig. 2 demonstrates, that at best the annual mean concentration value seems to be a quantity which can be predicted by a GAUSSian plume-model with sufficient accuracy at present.

3. Application of other model types

The restrictive presuppositions of the GAUSSian plume formula makes necessary the development and the application of other models to find solutions for the problems listed in Table 1.

From the variety of model types, also listed in Table 1, integrated GAUSSian puff-models, quasi-analytical solutions, and multiple box-models are already discussed in the literature for a long time. Their advantages and disadvantages need not be repeated at this place. Concerning the spectral and pseudo-spectral method we want to refer to CHRISTENSEN and PRAHM (5) who have first applied this method, developed by ELIASSEN, MACHENHAUER and RASMUSSEN for numerical weather prediction, to air quality simulation.

In the following we want to present some first preliminary results of the application of a grid-model and a stochastic model,

3.1 Finite-difference models

Since a long time already one has viewed upon finite-difference models as one of the most promising methods in numerical weather prediction and air quality simulation, and the success of multiple-source models like those by SHIR and SHIEH or by RUNCA has confirmed the ability of such models to predict the air pollution simulation under complex conditions.

On the other hand, the remarks just made concerning the differences between multiple-source and single-source models, i. e. the quasi-statistical smeering-out effects of multiple-source superpositions, have caused us to examine carefully the deficiencies of finite-difference methods with respect to air quality simulation. Besides stability of the numerical scheme, concentration calculations impose three additional conditions to the numerical treatment

- mass conservation,
- positiveness,
- and, if possible, far-reaching suppression of numerical pseudo-diffusion.

Problems with these conditions are especially to be expected in regions of strong concentration gradients near singular emittents.

We want to show this by using RUNCA's modeling technique (6): a fractional step scheme, simulating the advective step by use of CARLSON's method and the diffusive step by help of the CRANK-NICHOLSON procedure, an implicit method of fourth order (Table 2) (after (7)).

Fig. 3 clearly demonstrates the necessity of a problem-specific choice of the parameter in $\bar{u}\Delta t/\Delta x$ to avoid numerical pseudo-diffusion in treating the advective term. This problem will be of special importance, if one tries to extend RUNCA's method to situations with pronounced horizontal and vertical inhomogeneities of the meteorological field. This is the subject of a current research project sponsored by the Federal Environmental Agency of the Federal Republic of Germany.

Fig. 4 demonstrates in a comparison of a GAUSSian plume solution with a numerical fractional step solution of the diffusion equation (CARLSON-scheme for the advective step and CRANK-NICHOLSON method for the diffusion step), that under extreme conditions the finite-difference method may yield values strongly deviating from the GAUSSian pume solution, sometimes even negative concentration values.

This is not a vote against finite-difference methods, just the opposite: this is a call for further investigations to find finite-difference methods fulfilling the requirement of air quality simulation problems: mass conservation, positiveness, and small numerical pseudo-diffusion. Investigations in this direction are now initiated in West-Germany.

3.2 Particle-in-Call-method on Monte-Carlo-Basis

To avoid just these difficulties of mass conservation, maintaining positiveness and suppression of pseudo-diffusion we have developed a particle-in-cell-method on Monte-Carlo-Basis. The continuous mass concentration field is represented by a finite set of discrete mass points,each of which being located in the center of mass being represented by it. These finite mass points fulfill a random walk, the transition probabilities of which being characterized by the EINSTEIN - KOLMOGOROFF-equation and by additional assumptions defining the physical nature of the stochastic process. The corresponding residence probability of a particle at place (i, j) after N "jumps" (Fig. 5) in a two-dimensional random walk is given in Table 3 (8). Here, p, q, r, and s indicate the transition probabilities in positive and negative y- and 7-direction, respectively.

Standing against the advantages of this model approach - absolute positiveness, mass conservation and no numerical pseudo-diffusion - are the disadvantages: extremely high computer core and -time to realize a sufficient accuracy, because the gain in accuracy is proportional only to the square root of the particle number.

Another advantage of this method is the fact, that it is very easy to incorporate physical, chemical and photochemical process into the transition probabilities describing the transmission process though the required computation times are increasing exponentially. First test runs (9) yield reasonable results for the numerical simulation of a photochemical-smog-situation.

4. Combination of different scale models for traffic emissions as a simple example for a unit construction system of dispersion models

In the following we want to present calculations with a possible combination of different scale models for automative emissions. Such a procedure characterizes first steps into the direction of a unit construction system for different dispersion model.

Urban air pollution planning of automative emission has to consider two different scales (Table 4):

- the local ambient air quality situation in the micro-scale to which a person is exposed on the pavement of a street canyon,
- the urban background concentration which is object of urban and regional planning activities.

These two scales are characterized by extremely different meteorological conditions (Table 4):

- the unsteady, inhomogeneous flow-field within the street canyon,
- the nearly steady and homogeneous flow in the urban scale.

The unit construction system of dispersion models has to take these differing features into consideration when it claims to be a suitable system to answer the questions cited above.

With the help of a particle-in-cell-method on Monte-Carlo-Basis, as described in the last chapter, we simulated the temporal development of the micro-scale dispersion of automative emissions within the street canyon. Figs. 6 and 7 mark the concentration distribution in a street canyon with orthogonal urban-scale-flow of 2.5 m/s roof-top-velocity and a helical circulation within the street canyon after 80 and 300 seconds. The situation turns out to be stationary after about 600 seconds of physical time with a "street output" of about 2 ppm.

This "street output" has been used as "model input" into a GAUSSian urban scale model,

with the help of which the urban scale dispersion of automotive emissions has been calculated for the vicinity of a street crossing (Fig. 8).

The "street emissions" have been simulated by virtual point sources in roof-top level of the street.

The combination of these two different-scale models seem to give answers for both indicated questions

- the local concentration distribution within the street canyon
- and the urban background concentration.

This simple example shall demonstrate, that it is necessary and possible to use a combination of different model types reconciled to one another to find a comprehensive instrument for air quality management.

5. Conclusions

It was the intention of this paper to give a small but necessary contribution to a formulation of the possible rôle of dispersion models in an air quality management system and to present a simple example for a possible realization of such procedure.

LITERATURE

/1/ SLATER, H.: Applications of air quality models by EPA; Proc. 5th Meeting of the NATO/CCMS Expert Panel on Air Pollution Modeling Roskilde; June, 4 - 6, 1974

/2/ GUTSCHE, B., LUDWIG, Ch.: Anwendung von Ausbreitungsmodellen als Instrumente der Luftgüteplanung in: Lufthygienisch-Meteorologische Modelluntersuchungen in der Region Untermain, Regionale Planungsgemeinschaft Untermain, Frankfurt 1977 (to be published)

/3/ JOST, D., GUTSCHE, B.: International trends in standardization of air pollution modeling and its application; 4th International Clean Air Congress, Tokyo; May, 16 - 20, 1977

/4/ STERN, R., B. GUTSCHE, B. TIMM: Calculation of the ambient air quality situation using the NATO/CCMS common data base for the Test-City; Berlin 1977

/5/ CHRISTENSEN, D., PRAHM, L. P.: A pseudospectral model for dispersion of atmospheric pollutants J. Appl. Met. 15 (1976), 1284 - 1294

/6/ RUNCA, E.: An efficient air quality K-model Proc. 7th International Technical Meeting on Air Pollution Modeling and its Application, Airlie House; Sept. 7 - 10, 1976

/7/ STERN, R., GUTSCHE, B., KEPP, W.: Überprüfung numerischer Verfahren als Grundlage für die Entwicklung eines Ausbreitungsmodells für windschwache Wetterlagen 2nd contribution of the model group of the research project "Untersuchung der Schadstoffausbreitung bei windschwachen Wetterlagen als Grundlage für Ausbreitungsrechnungen", Regionale Planungsgemeinschaft Untermain, Frankfurt 1977, (in preparation)

/8/ GUTSCHE, B.: Monte-Carlo-Simulation der Ausbreitung von Autoabgasen in Straßenschluchten (in preparation)

/9/ LUDWIG, Ch.: Einbau photochemischer Reaktionen in ein Diffusionsmodel (in preparation) short version in Interim Report of the "Forschungsprojektschwerpunkt: Aero- und hydrodynamische Prozesse der Ausbreitung von Beimengungen", Free University of Berlin, 1975.

Applicability / Type of model	Long-term air quality studies for even terrain (licensing procedure; clean air plan)	Long-term air quality studies for topographic terrain (licensing procedure under consideration of topography)	Short-term predictions (case studies; analysis of episodes)	Short-term predictions (analysis of causes by iterative comparison with concentration measurements)	Weak-wind weather situations when air circulation is poor (smog warning plans; licensing procedures for areas with frequent weak-wind situations)	Dispersion of automobile emissions in street canyons	Inclusion of chemical and photochemical reactions (smog warning plan; clean air plan)	Inclusion of sedimentation (e.g. dispersion of particles; clean air plan)	Dispersion of heavy gases (e.g. explosive mixtures; ventilation effect of fresh air streams for regional planning)
GAUSSian plume-model	4	-	2	2	-	-	(2)	(2)	-
Integrated GAUSSian puff-model + quasi-analytical models	2	2	2	0	2	-	(0)	(0)	-
Multiple box-models	2	1	3	1	2	2	2	2	0
Grid-models	1	0	2	0	2	2	1	0	0
Spectral and pseudospectral models	0	0	1	0	0	-	0	0	0
Stochastic models	0	0	1	0	1	1	1	0	0

Table 1: Stage of development of different types of urban air quality simulation models with respect to given scope of application

Key:

0	Application is possible in principle
1	Subject of research
2	Has been applied in individual cases
3	Generally tested
4	Suitable for standardization for administration purposes
-	Not applicable
( )	Applicable under use of simplifying additional assumptions

Diffusion Equation:

$$\frac{\partial c}{\partial t} + \mathbb{V} \cdot \nabla c = \frac{\partial}{\partial x}\left(K_x \frac{\partial c}{\partial x}\right) + \frac{\partial}{\partial y}\left(K_y \frac{\partial c}{\partial y}\right) + \frac{\partial}{\partial z}\left(K_z \frac{\partial c}{\partial z}\right) + \text{Sinks} + \text{sources}$$

Boundary Conditions

$K_z \frac{\partial c}{\partial z} = 0$ for $z = 0$ and for $z = H_I(t)$ (inversion height)

Initial Condition:

$c\,(x,y,z;0) = 0$

Advection equation: $\frac{\partial c}{\partial t} + \mathbb{V} \cdot \nabla c = 0$ solved using the CARLSON-scheme

Diffusion equation: $\frac{\partial c}{\partial t} - \frac{\partial}{\partial x}\left(K_x \frac{\partial c}{\partial x}\right) - \frac{\partial}{\partial y}\left(K_y \frac{\partial c}{\partial y}\right) - \frac{\partial}{\partial z}\left(K_z \frac{\partial c}{\partial z}\right) = 0$ solved using the CRANK-NICHOLSON-scheme

$$\frac{C_i^{t+\Delta t} - C_i^{t}}{\Delta t} = \frac{2}{\Delta x_i \,(\Delta x_i + \Delta x_{i-1})} \left\{ \theta \cdot D\left[C_i^{t+\Delta t}\right] + (1-\theta) \cdot D\left[C_i^{t}\right] \right\}$$

$$D\left[C_i\right] = \frac{\Delta x_i}{\Delta x_{i-1}} K_{x_{i-1/2}} C_{i-1} - \left(\frac{\Delta x_i}{\Delta x_{i-1}} K_{x_{i-1/2}} + K_{x_{i+1/2}}\right) C_i + K_{x_{i+1/2}} C_{i+1}$$

Table 2: RUNCA's fractional step method for solving the diffusion equation.

$$W (N | i,j) = p^{\frac{|i| + i}{2}} q^{\frac{|i| + i}{2}} r^{\frac{|j| + j}{2}} s^{\frac{|j| - j}{2}} \times$$

$$\times \sum_{\delta=0}^{\frac{N - |i| - |j|}{2}} \binom{N}{N - |j| - \delta} \binom{N - |j| - \delta}{\frac{N - |i| - |j|}{2}} \binom{\frac{N - |i| - |j|}{2}}{\delta} \times$$

$$\times \quad (pq)^{\frac{N - |i| - j}{2} - \delta} (rs)^{\delta}$$

$$\text{for} \quad \frac{1}{2} (N - |i| - |j|) \in \mathbb{N} \cup \{0\}$$

$W (N | i, j) = 0$ elsewhere

Table 3: Residence probability $W (N | i, j)$ of a particle at the place (i, j) after N jumps in a two-dimensional MARKOV-process

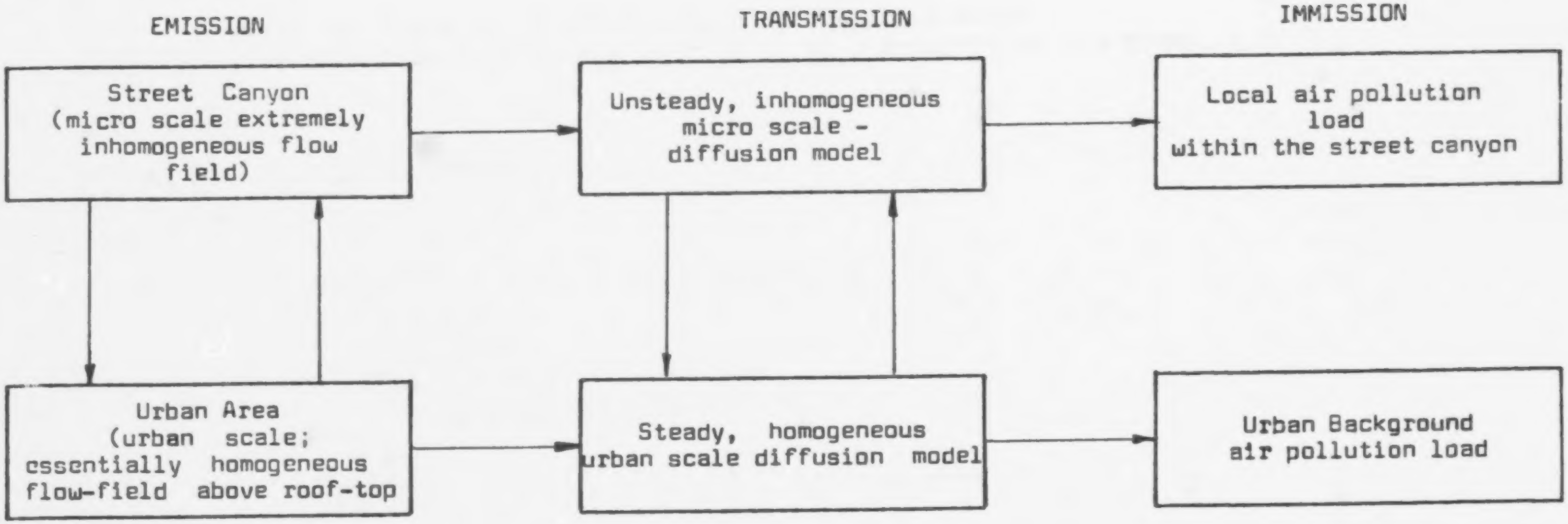
EMISSION
TRANSMISSION
IMMISSION
Street Canyon (micro scale extremely inhomogeneous flow field)
Unsteady, inhomogeneous micro scale - diffusion model
Local air pollution load within the street canyon
Urban Area (urban scale; essentially homogeneous flow-field above roof-top
Steady, homogeneous urban scale diffusion model
Urban Background air pollution load

Table 4: Connexion of different scale diffusion models in the case of traffic emissions' dispersion

Reproduced from best available copy.

SO_2-Ausbreitungsrechnung

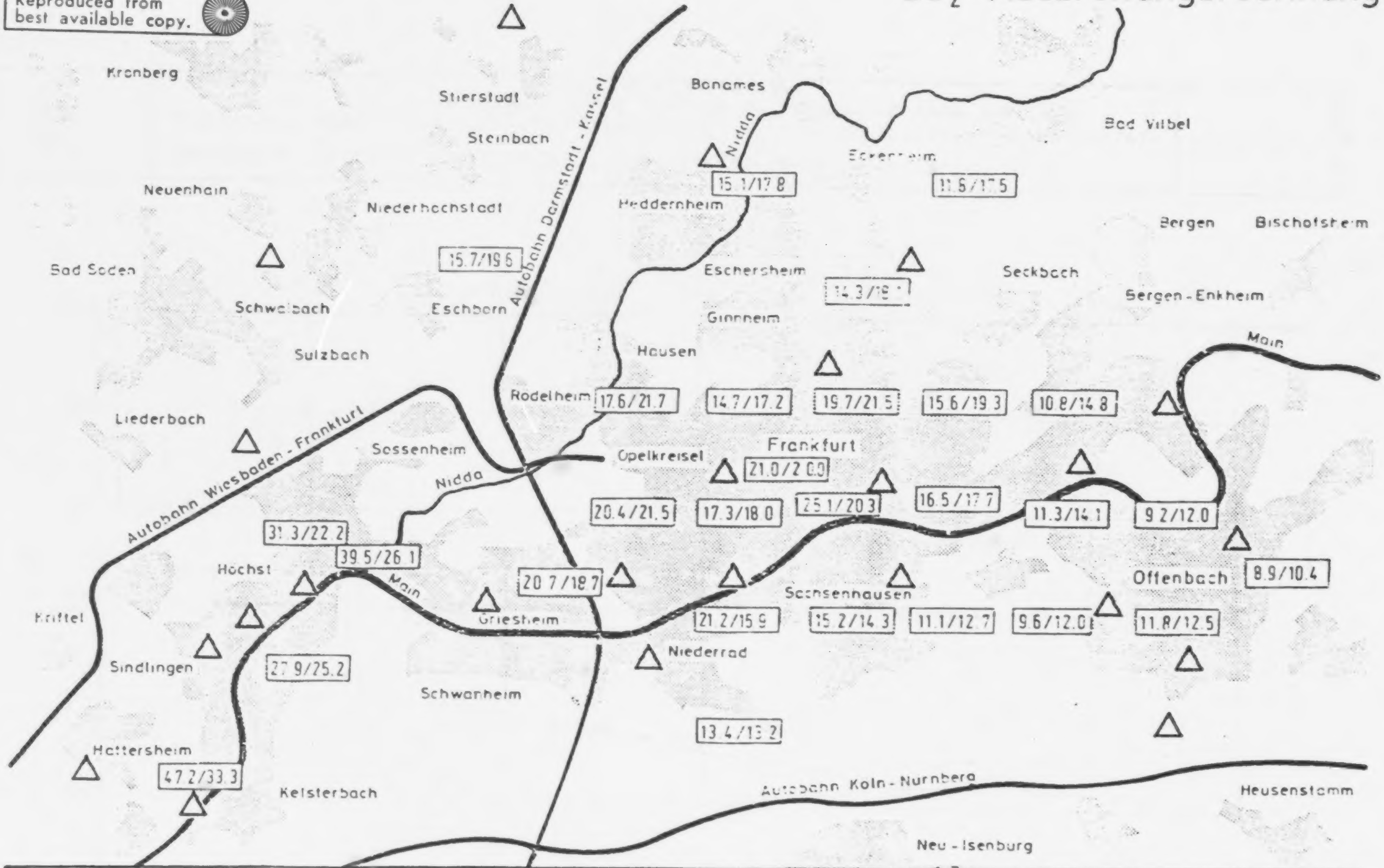

Kronberg
Stierstadt
Steinbach
Bonames
Bad Vilbel
Neuenhain
Niederhochstadt
Heddernheim
Eckenheim
15.1/17.8
11.6/17.5
Bergen
Bischofsheim
Bad Soden
15.7/19.6
Eschersheim
14.3/18.1
Seckbach
Bergen-Enkheim
Schwalbach
Eschborn
Ginnheim
Sulzbach
Hausen
Main
Rodelheim
17.6/21.7
14.7/17.2
19.7/21.5
15.6/19.3
10.8/14.8
Liederbach
Frankfurt
Sossenheim
Opelkreisel
21.0/20.0
Nidda
20.4/21.5
17.3/18.0
25.1/20.3
16.5/17.7
11.3/14.1
9.2/12.0
31.3/22.2
39.5/26.1
Höchst
20.7/18.7
Offenbach
8.9/10.4
Main
Sachsenhausen
Kriftel
Griesheim
21.2/15.9
15.2/14.3
11.1/12.7
9.6/12.0
11.8/12.5
Sindlingen
27.9/25.2
Niederrad
Schwanheim
13.4/13.2
Hattersheim
47.2/33.3
Kelsterbach
Autobahn Koln-Nurnberg
Heusenstamm
Neu-Isenburg
Autobahn Darmstadt-Kassel
Autobahn Wiesbaden-Frankfurt

UBA
1977

Calculated annual mean SO_2-ground level concentrations ($\mu g/m^3$) due to big singular emittents; left number: using dispersion parameters from the Jülich experiments
right number: using SINGER and SMITH's dispersion parameters
triangles: position of some of the biggest singular emittents.

Fig. 1

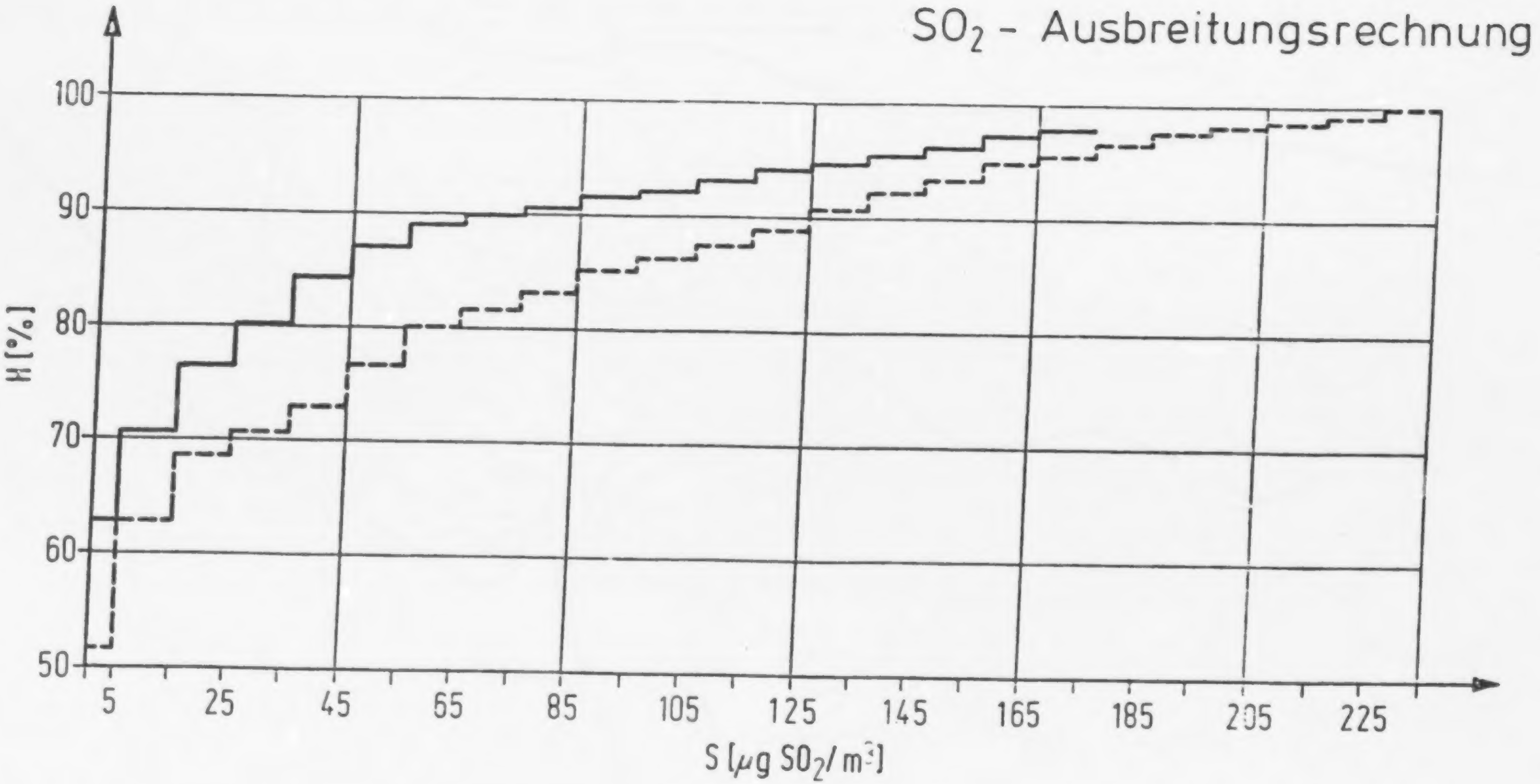

UBA 1977	Cumulative frequency distribution for a receptor-site in the vicinity of an industrial area. upper curve: using SINGER and SMITH's dispersion parameters lower curve: using dispersion parameters from the Jülich experiments	Fig. 2

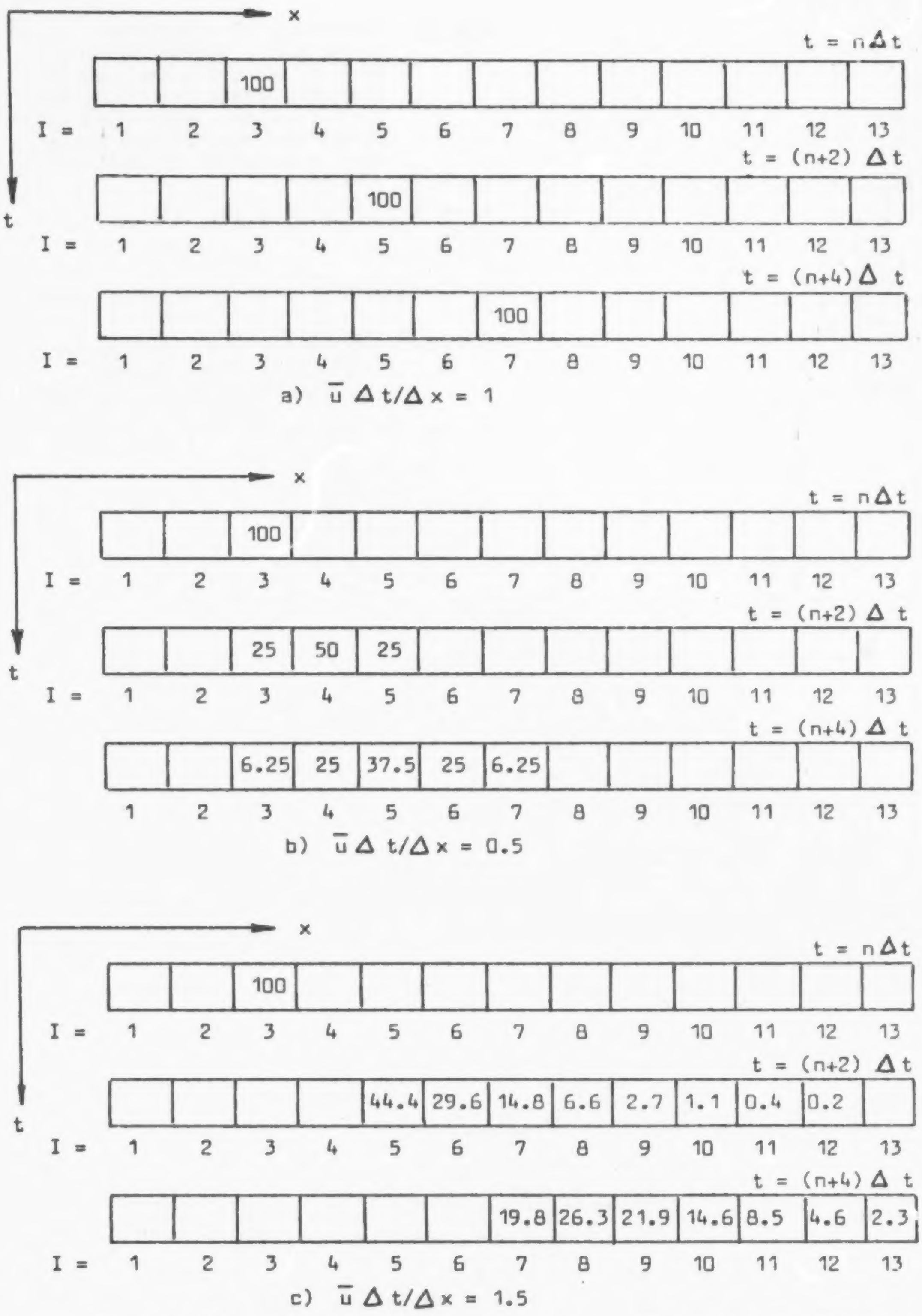

t	I = 1	2	3	4	5	6	7	8	9	10	11	12	13
$t = n\Delta t$			100										
$t = (n+2)\Delta t$					100								
$t = (n+4)\Delta t$							100						

a) $\bar{u}\Delta t/\Delta x = 1$

t	I = 1	2	3	4	5	6	7	8	9	10	11	12	13
$t = n\Delta t$			100										
$t = (n+2)\Delta t$			25	50	25								
$t = (n+4)\Delta t$			6.25	25	37.5	25	6.25						

b) $\bar{u}\Delta t/\Delta x = 0.5$

t	I = 1	2	3	4	5	6	7	8	9	10	11	12	13
$t = n\Delta t$			100										
$t = (n+2)\Delta t$					44.4	29.6	14.8	6.6	2.7	1.1	0.4	0.2	
$t = (n+4)\Delta t$							19.8	26.3	21.9	14.6	8.5	4.6	2.3

c) $\bar{u}\Delta t/\Delta x = 1.5$

Fig. 3: One-dimensional advection of mass 100 using the CARLSON-scheme with different values for the factor $\bar{u}\Delta t/\Delta x$. A mass of 100 (arbitrary units) has been injected into the field at the position I = 3 at time $t = n\Delta t$.

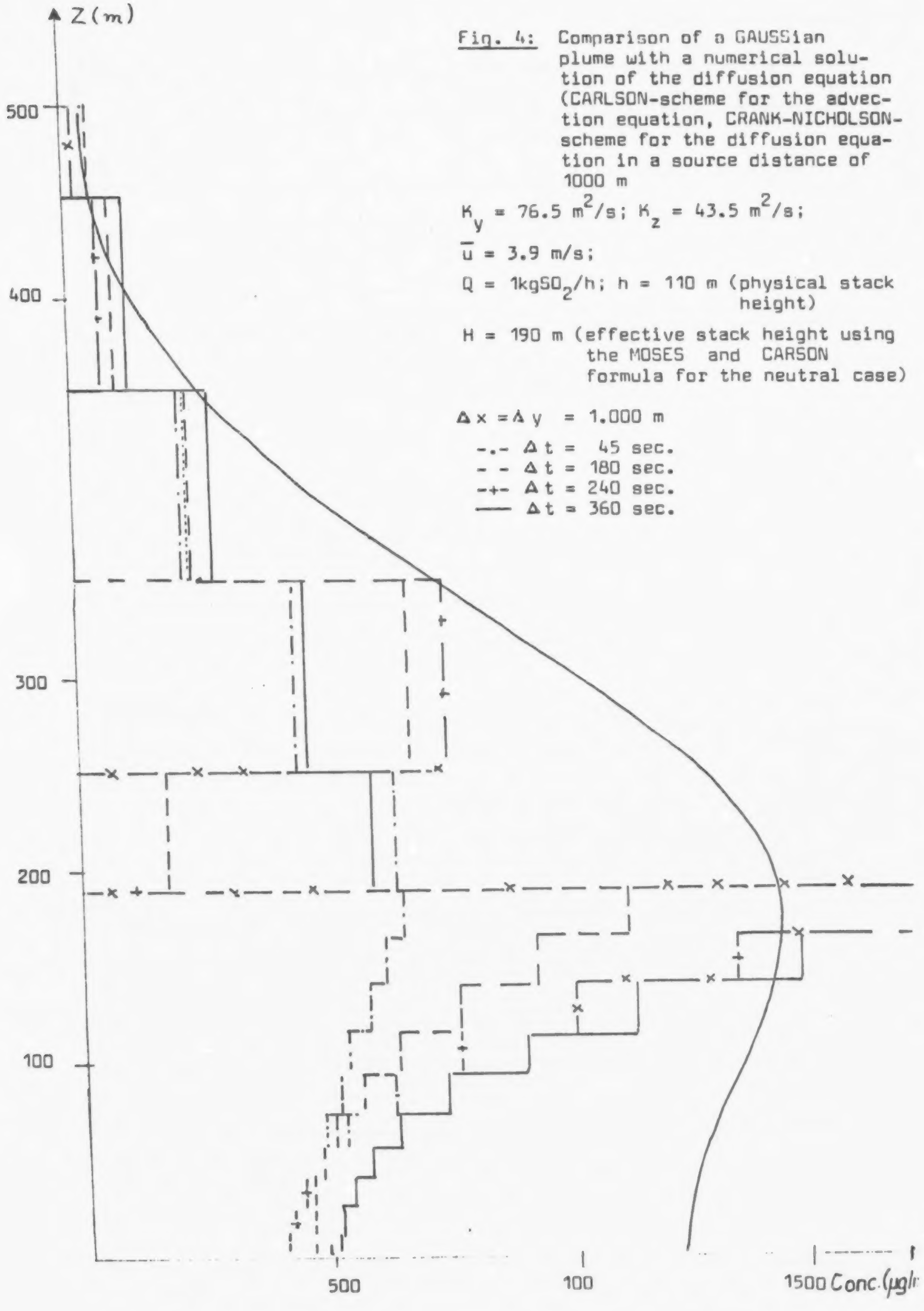

Fig. 4: Comparison of a GAUSSian plume with a numerical solution of the diffusion equation (CARLSON-scheme for the advection equation, CRANK-NICHOLSON-scheme for the diffusion equation in a source distance of 1000 m

$K_y = 76.5\ m^2/s$; $K_z = 43.5\ m^2/s$;

$\overline{u} = 3.9\ m/s$;

$Q = 1 kg SO_2/h$; h = 110 m (physical stack height)

H = 190 m (effective stack height using the MOSES and CARSON formula for the neutral case)

$\Delta x = \Delta y = 1.000\ m$

-.- Δt = 45 sec.
- - Δt = 180 sec.
-+- Δt = 240 sec.
—— Δt = 360 sec.

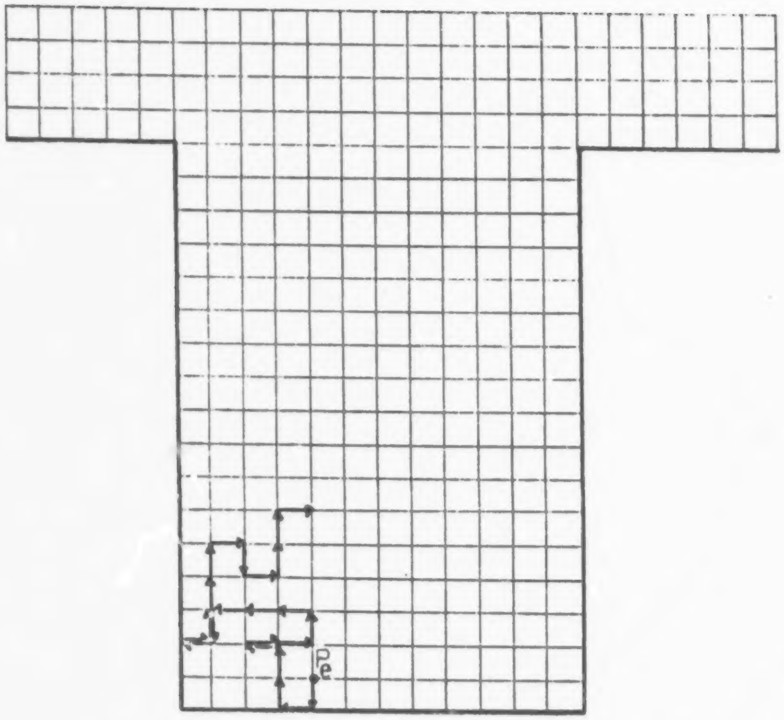

Fig. 5: Example for the random walk of a particle which has been emitted at position P_e within a street canyon

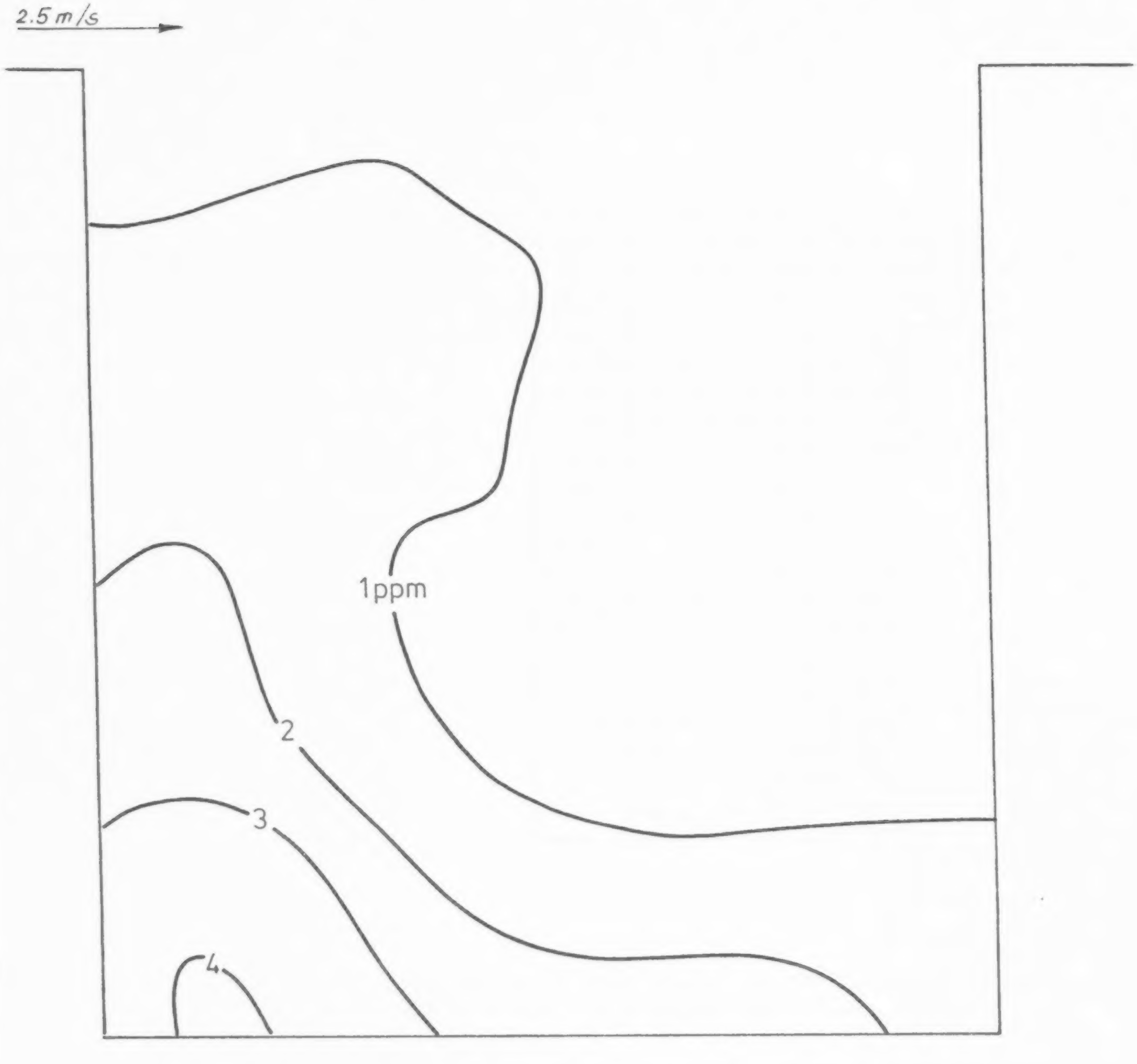

Fig. 6: Two-dimensional CO-concentration field within a street canyon (width: 21 m; height: 21 m) after t = 80 sec.
Flow field orthogonal to the street canyon with a roof-top-velocity of 2.5 m/s; constant exchange-coefficient of 3 m^2/s.

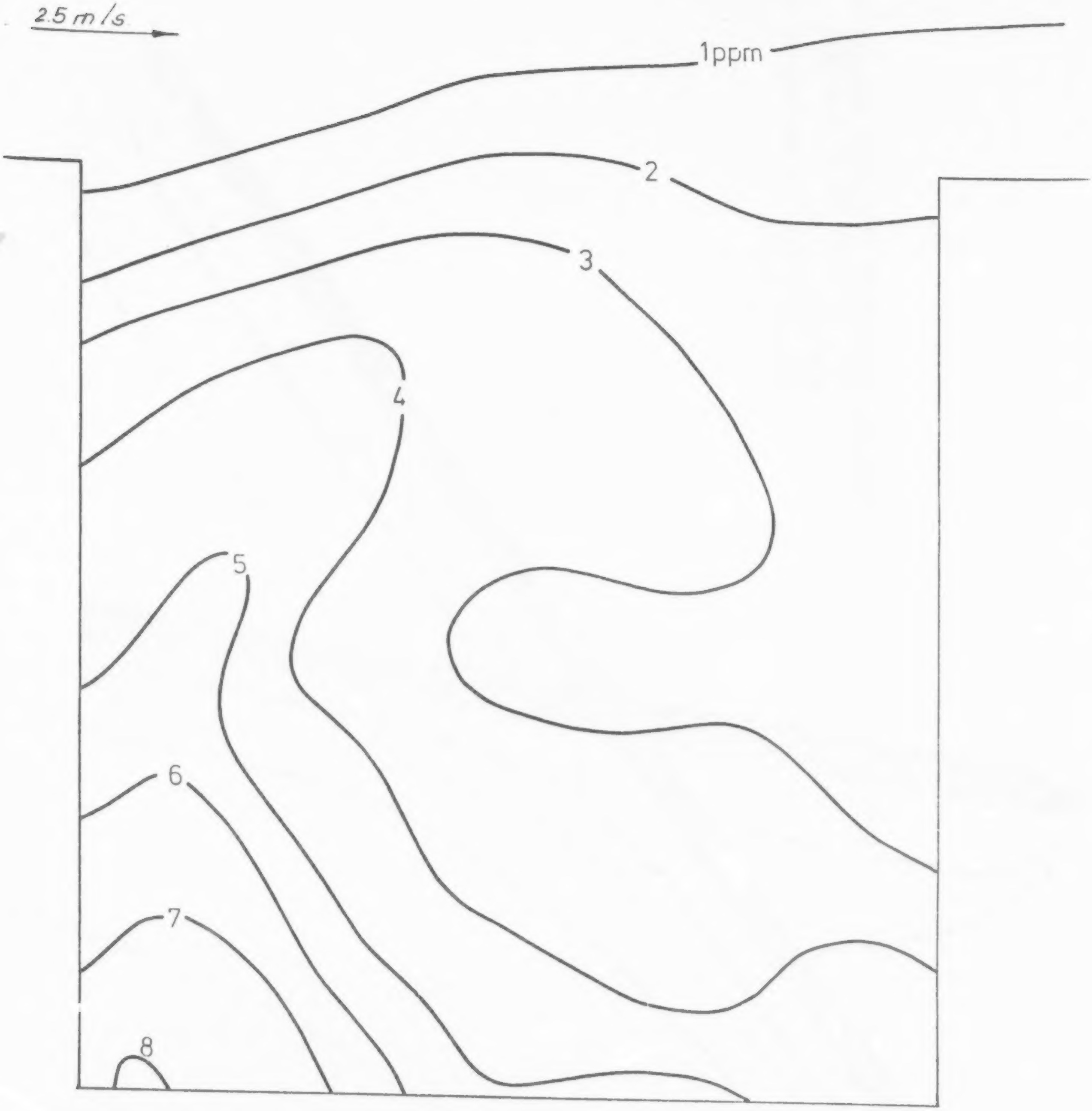

Fig. 7: Two-dimensional CO-concentration field within a street canyon (width: 21 m; height: 21 m) after t = 300 sec.
Flow field orthogonal to the street canyon with a roof-top-velocity of 2.5 m/s;
constant exchange-coefficient of 3 m^2/s.

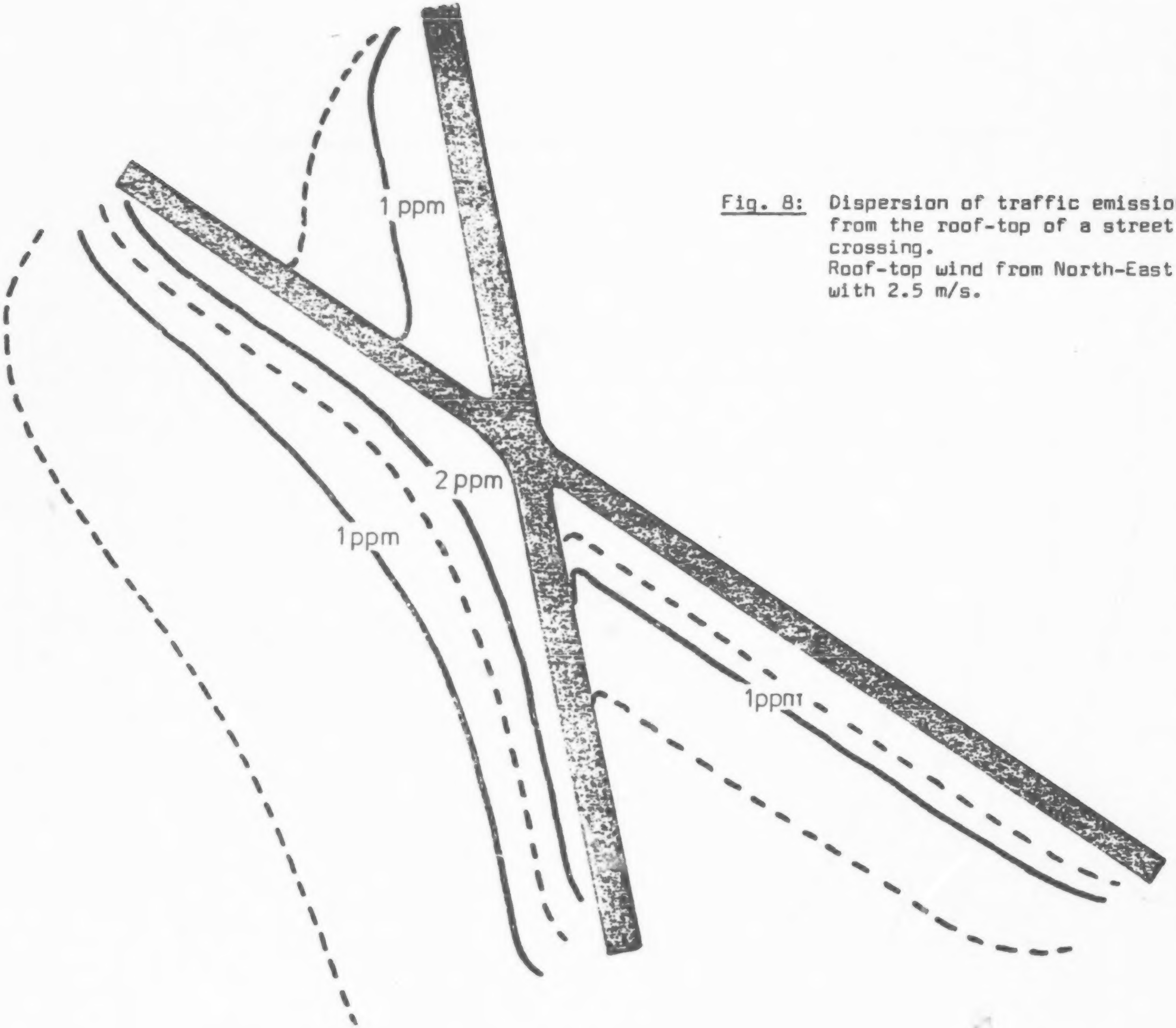
1 ppm
2 ppm
1ppm
1ppm

Fig. 8: Dispersion of traffic emissions from the roof-top of a street crossing.
Roof-top wind from North-East with 2.5 m/s.

8th International Technical Meeting
on Air Pollution Modeling and its Application

DEVELOPMENT OF AN AIR POLLUTION INDEX

by

A. JOUKOFF

ROYAL METEOROLOGICAL INSTITUTE
OF BELGIUM

September 20 - 23, 1977
Louvain-La-Neuve
Belgium

DEVELOPMENT OF AN AIR POLLUTION INDEX

In the context of the National Data Processiong Centre of the belgian telemetric network for air quality monitoring, an air quality index, based on urban mean concentration is defined.
This index has two purposes :

1. air quality appreciation in the five great urban areas to be covered by the automatic network (Antwerp, Brussels, Charleroi, Ghent and Liège) ;
2. short term forecasting (24 hours) of the air quality from meteorological parameters.

1. URBAN MEAN DEFINITION

Urban mean concentration M is defined from concentration observations X_i at the n measuring stations situated within the considered urban area. In a first step, we use 24-hours integrations as measured by the SO_2-particulates network [1], [2] 30-minutes averages will be used as soon as the automatic network becomes operational, in such a way as it has been defined for the alert-strategy.
By definition :

$$M = \frac{1}{\sum a_i} \sum_{i=1}^{n} a_i X_i$$

the weighting factors $a_i = X_i^{50} / X_i^{98}$ are calculated from the 50th and 98th percentiles of the concentration distribution observed at each station in the past (reference period : 1968-1973 [3]), from each of the three considered periods : heating period B (November to March), non-heating period D (June to September) and intermitted heating period C (April, May and October). Such weighting factors are used to diminish the influence of less representative measuring stations, showing great time variations in the observed concentrations (variations probably due to the vicinity of major sources).

Urban means distributions have been calculated for each year (april to march) from 1968 to 1976, for the three periods (B, C and D) and for each of the two measured pollutants (SO_2 and particulates). Figures 1 to 5 show the evolution of the 50th, 90th and 98th percentiles in the 5 belgian greatest urban areas. Diminishing is striking, especially for the winter period. Such a trend is probably due to the extension of natural gas use for domestic heating and also to the reglementation of the sulfur contents of fuels. Relative mildness of the winters beginning from 1971-1972, has perhaps contributed to this trend (fig. 6) [4]. Urban means distributions have also been determined separately for the weekdays M_o and for the sundays and holidays M_f. Table 1 gives ratios M_f/M_o of the 50th, 90th and 98th percentiles of the urban means distributions for the period april 1971 to march 1976, for periods B and D (period C is more difficult to interpret).

TABLE 1. - RATIOS M_f/M_o Urban means April 1971-March 1976

Area	Per.	Particulates			SO_2		
		M_f^{50}/M_o^{50}	M_f^{90}/M_o^{90}	M_f^{98}/M_o^{98}	M_f^{50}/M_o^{50}	M_f^{90}/M_o^{90}	M_f^{98}/M_o^{98}
Antwerp	B	0.571	0.759	0.991	1.011	1.150	1.211
	D	0.571	0.565	0.542	0.771	0.783	0.782
Brussels	B	0.718	0.789	0.878	1.006	1.127	1.172
	D	0.654	0.634	0.647	0.901	0.818	0.750
Charleroi	B	1.024	0.962	0.818	0.992	1.091	1.133
	D	0.613	0.596	0.600	0.818	0.818	0.825
Ghent	B	1.062	0.985	0.843	1.039	0.981	0.904
	D	0.619	0.583	0.553	0.856	0.856	0.859
Liège	B	1.029	0.914	0.739	0.993	1.099	1.143
	D	0.870	0.744	0.651	0.859	0.856	0.854

One can see that during winter, sunday values usually are higher than weekdays ones ($M_f/M_o > 1$) at least for some percentiles, except for Antwerp and Brussels for particulates.
At the contrary, during summer, sunday urban means always remain below the weekdays values ($M_f/M_o < 1$). One can interpret these differences by the dominant role of domestic heating during winter and of industry during summer.

2. APPRECIATION INDEX

Appreciation index is defined from the urban mean M

$$I = M/M_{98}$$

M_{98} being the 98th percentile of the urban mean distribution for the considered period.

Using such an index presents some advantages :

1. seasonal variation is strongly diminished, enabling easier comparisons ;
2. indexes from the five great belgian urban areas are directly comparable ;
3. "technical episode" is defined in a very straight-forward way : $I \geq 1$.

Moreover, this definition can easily be modified to give a sanitary index by substituing the 98th percentile M_{98} by some immission standard M_s. A sanitary episode ($I = M/M_s \geq 1$) is more adequate to the use by authorities charged to keep protection measures.

Previsional index, based on appreciation index, is established by correlation with meteorological parameters. Two levels of index forecasting are planned for routine use in the future national data processing centre of the belgian automatic network for air quality monitoring :

1. air quality class forecasting ;
2. air pollution level forecasting by means of a regression formula.

Appreciation index can be used for broadcasting purposes ; in this case a scale with various qualificatives must be introduced in order to avoid too technical definitions.

3. AIR QUALITY CLASS FORECASTING

A first approach to air quality forecasting is to predict an air pollution class, based on the appreciation index [5]. One can define three classes :

1.	$I \geq 0.8$	very strong pollution
2.	$0.5 \leq I < 0.8$	moderately strong pollution
3.	$I < 0.5$	weak pollution

To establish this simple model, one computes, for each class i the arithmetic mean $\bar{x}_{ij}$ and the dispersion σ^2_{ij} of each of the considered parameters x_j $(j=1, 2, \ldots n_p)$, and this for each period, as defined in § 1,

$$\bar{x}_{ij} = \frac{1}{n_i} \sum_{n_i} x_j$$

n_i = number of observations of class i during the considered period

$$\sigma^2_{ij} = \frac{1}{n_i - 1} \left[\sum_{n_i} x_j^2 - \frac{1}{n_i} \left(\sum_{n_i} x_j \right)^2 \right].$$

The predicted meteorological situation being characterized by values p_j of parameters, one computes the three quantities (or "distances")

$$d_i^2 = \sum_{j=1}^{n_p} \frac{(p_j - \bar{x}_{ij})^2}{\sigma_{ij}^2} \quad , \quad (i = 1, 2, 3) ;$$

minimum d_i^2 determines the forecasted air quality class i.

During the first tests of the method, the following parameters have been tried :

T_{min} : minimum temperature (acts on heating sources) ;

RR : total precipitation during 24 h ;

dd : wind direction (mean on 24 h) ;

ff_a : wind speed (arithmetic mean on 24 h) ;

h_m : mixing height (weightened mean of mixing height of preceding day at 12 UT and of the considered day at 0 and 12 UT) ;

ven = $ff_a^{\alpha} h_m^{\beta}$: ventilation factor, with $\alpha = 0.5$ and $\beta = 0.2$ [6].

per : persistance factor of wind direction (ratio of vectorial to arithmetic means of wind speed) ;

I_{j-1} : appreciation index of air pollution for the preceding day.

This method has been tested on SO_2 measurements in Antwerp (period : april 1968 - march 1974) ; results are shown in table 2 : first with M_{98}, $\bar{x}_{ij}$ and σ^2_{ij} for each considered year (parameter significance test), then with M_{98}, $\bar{x}_{ij}$ and σ^2_{ij} from preceding year (forecasting capability test). In addition to correct results, we have introduced a tolerance of 0.1 on class limits (e.g. class 1 prediction with observed index I = 0.7 is considered as "correct") : results are strongly improved.

One weakness of the method is the tendence to predict too much high pollution occurence. However, for future use in the national data processing centre, this will not be very troublesome because alerts only become effective from the moment that warning levels of air pollution are reached.

TABLE 2.- AIR QUALITY CLASS FORECASTING (%)

Parameters									Heating period					Year	
n	T_{min}	RR	dd	per	ff_a	h_m	ven	I_{j-1}	Class 1	Class 1 (tol)	wa	total	total (tol)	total	total (tol)
M_{98}, $\bar{x}_{ij}$ and σ^2_{ij} for the considered year															
8	x	x	x	x	x	x	x	x	75.0	90.0	51.6	71.6	88.1	68.05	86.95
7		x	x	x	x	x	x	x	76.3	91.3	56.4	70.6	86.7	67.50	86.03
7	x		x	x	x	x	x	x	77.5	91.3	53.4	69.7	87.2	66.82	85.94
7	x	x		x	x	x	x	x	75.0	90.0	54.6	70.8	87.2	66.45	85.17
7	x	x	x		x	x	x	x	75.0	88.8	50.4	71.8	88.1	68.14	86.81
7	x	x	x	x		x	x	x	77.5	91.3	59.5	68.6	85.9	66.64	85.67
7	x	x	x	x	x		x	x	75.0	88.8	52.0	72.0	88.5	67.96	87.36
7	x	x	x	x	x	x		x	68.8	83.8	53.8	69.2	87.8	67.50	87.04
7	x	x	x	x	x	x	x		72.5	88.8	50.9	70.3	87.2	64.35	83.48
6	x	x	x		x	x		x	76.3	86.3	47.4	71.3	88.8	67.91	87.49
6	x	x	x		x		x	x	76.3	87.5	49.6	72.6	88.8	67.73	87.31
5	x	x	x				x	x	77.5	92.5	54.4	70.6	87.8	67.28	87.17
M_{98}, $\bar{x}_{ij}$ and σ^2_{ij} from preceding year (forecasting)															
7	x	x	x		x	x	x	x	69.7	89.4	44.6	72.1	89.6	63.03	83.73

tol : 0.10 tolerance on class limits
wa : wrong alerts.

4. AIR POLLUTION LEVEL FORECASTING

In order to forecast numerical values for the index, I_j linear regression coefficients a_j and b_j have been calculated for each period B, C and D and each previsional parameter x_j.

$$I_j = a_j + b_j x_j$$

on basis of meteorological parameters and appreciation index observed in Antwerp (april 1968 - march 1974). Table 3 gives correlation coefficients between calculated and observed values of the index, standard errors and percentage of success within a tolerance of 0.15 on the values.

A mean I of the index prediction I_j has also been calculated

$$I = \frac{1}{\sum |r_j|} \sum_{j=1}^{n} |r_j| I_j$$

using correlation coefficients r_j as weighting factors in order to account for the actual importance of the parameters x_j. Last column of table 3 gives results for a "mean" index. A rather high correlation of 0.75 is observed during the heating period. During this period, the most important parameters are T_{min} (domestic heating), ventilation factor and preceding day index. During the non-heating periods, the only important parameter is the preceding day index, showing the dominant role of persistance.

As test of the forecasting capability of these simple linear regression, formulas derived from observation of one year were applied to meteorological observations of the next year ; this represents the operational possibility for such a method (doing this, one suppose that emissions do not change significantly from one year to the next). Results are shown in the second part of table 3.

As one can expect, regression formulas tend to miss extreme pollution situations (very high as well as very low values), but gives very good results for index values ranging from 0.4 to 0.7.

5. CONCLUDING REMARKS

Two different methods to forecast air quality in an urban area have been presented in this paper, giving two levels of forecasting : class and index value. Class prediction by means of "distance" calculations in a parameter space tends to overpredict the occurence of high pollution levels ; but in pratical use in the National Data Processing Centre (NDPC) of the belgian telemetric network, this weakness is of little importance, as alerts only become effective after observational confirmation. At the other hand, regression formulas tend to underpredict dangerous levels but are well suited for mean values prediction. So, simultaneous use of the two methods is planned for operation in the NDPC.

It must be noted that, in pratical use, only meteorological forecastings will be available, so the efficiency of both methods to forecast air quality is strongly dependent on the reliability of the meteorological forecasting. During the tests, only meteorological observations have been used.

TABLE 3.- LINEAR REGRESSION-FORECASTING (Antwerp)

	PARAMETERS							
	T_{min}	RR	dd	ff_a	h_m	ven	I_{j-1}	Mean
a) VERIFICATION (values for the considered year)								
PERIOD B (907 obs.)								
Correlation coef.	0.563	0.387	0.296	0.622	0.495	0.684	0.667	0.750
Standard error	0.165	0.185	0.191	0.157	0.174	0.146	0.149	0.143
Correct (± 0.15)%	69.46	67.25	64.28	73.87	68.47	75.85	75.52	79.71
PERIOD C (552 obs.)								
Correlation coef.	0.346	0.363	0.239	0.507	0.445	0.578	0.644	0.681
Standard error	0.180	0.179	0.186	0.165	0.172	0.156	0.147	0.151
Correct (± 0.15) %	62.14	61.59	62.32	65.58	63.59	68.12	73.37	72.28
PERIOD D (732 obs.)								
Correlation coef.	0.371	0.213	0.242	0.403	0.267	0.407	0.613	0.646
Standard error	0.173	0.182	0.181	0.171	0.180	0.170	0.147	0.154
Correct (± 0.15)%	66.12	64.07	66.26	64.21	64.21	65.98	74.59	72.54
b) FORECASTING (values from preceding year)								
PERIOD B (756 obs.)								
Correlation coef.	0.571	0.448	0.404	0.641	0.487	0.677	0.719	0.764
Standard error	0.185	0.202	0.208	0.174	0.197	0.166	0.157	0.161
Correct (± 0.15) %	69.58	61.38	61.11	70.77	64.55	72.62	76.98	77.38
PERIOD C (459 obs.)								
Correlation coef.	0.271	0.263	0.110	0.444	0.167	0.513	0.637	0.606
Standard error	0.191	0.194	0.198	0.179	0.205	0.175	0.153	0.162
Correct (± 0.15)%	58.61	58.17	57.95	62.75	58.03	63.62	72.77	67.32
PERIOD D (610 obs.)								
Correlation coef.	0.191	0.084	0.097	0.305	0.380	0.311	0.616	0.570
Standard error	0.206	0.208	0.207	0.198	0.187	0.198	0.163	0.178
Correct (± 0.15)%	58.36	57.87	57.21	60.33	60.35	58.85	72.30	64.92

REFERENCES

1. Monthly bulletin "Pollution Atmosphérique", edited by IRM from january 1968 to december 1974 and by IHE from january 1975.

2. "La pollution atmosphérique par les oxydes de soufre et la fumée en Belgique", I.R.M., Publications série A n° 74 (1971), n° 78 (1972), n° 88 (1975) and n° 92 (1975).

3. L.M. MALET, A. JOUKOFF, L. VAN DER AUWERA, H. de SADELEER "Distribution des concentrations journalières du dioxyde de soufre et des fumées dans l'atmosphère d'après les données du réseau belge pour la période janvier 1968 à mars 1973", I.R.M., publications série A n°95 (1976).

4. Monthly bulletin "Observations climatologiques" edited by I.R.M.

5. M.E. BERLYAND
"Present topics in atmospheric diffusion and air pollution" (in russian) chapt 12, Leningrad 1975.

6. H. BULTYNCK and F. BOSMANS
Fiche 4.2.2. "Verband tussen de dagelijkse gemiddelde concentratie SO_2 in een stad en enkele meteorologische parameters" (work document) 1976.

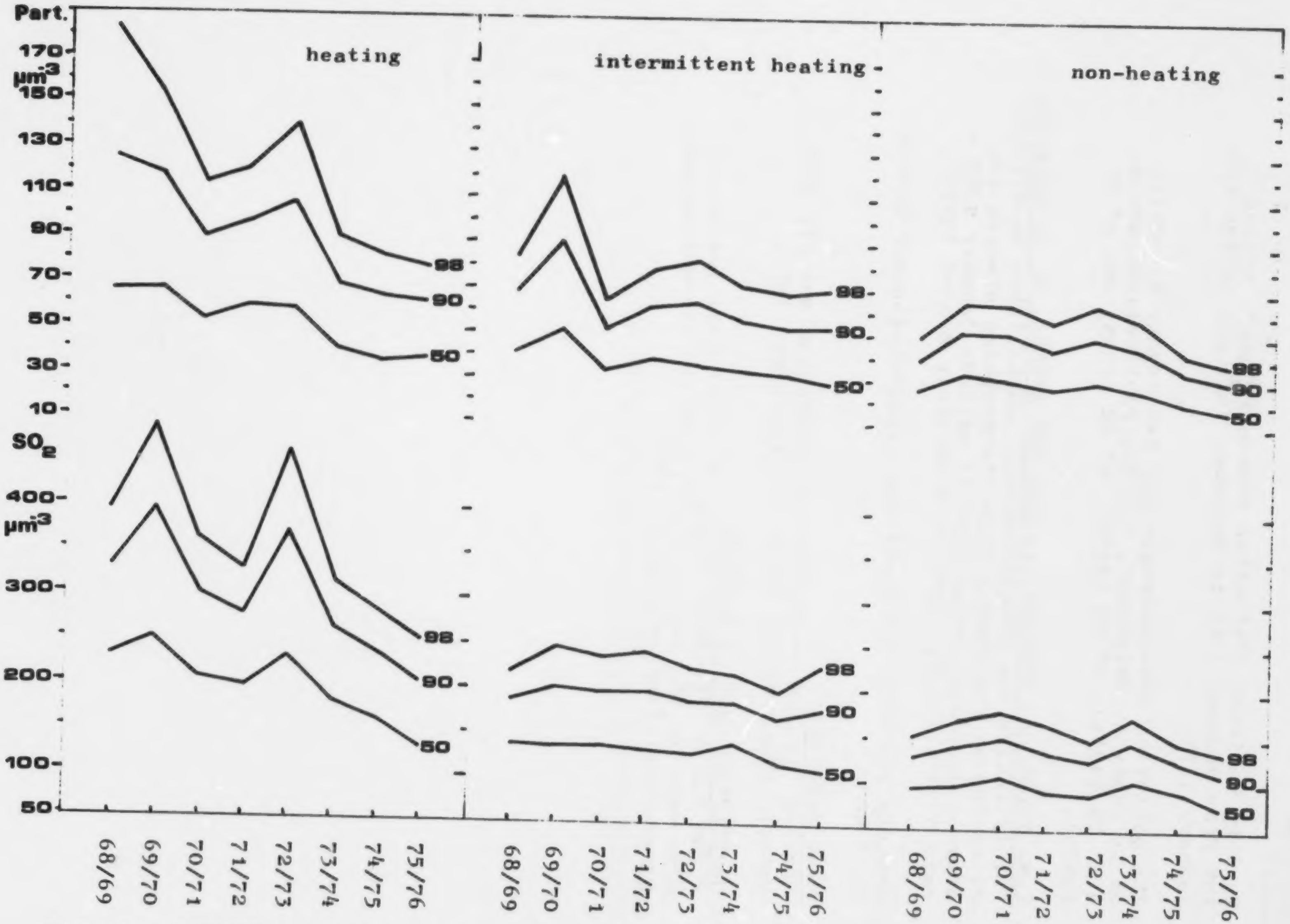

Fig. 1.- ANTWERP : Urban mean distributions (50, 90 and 98th percentiles)

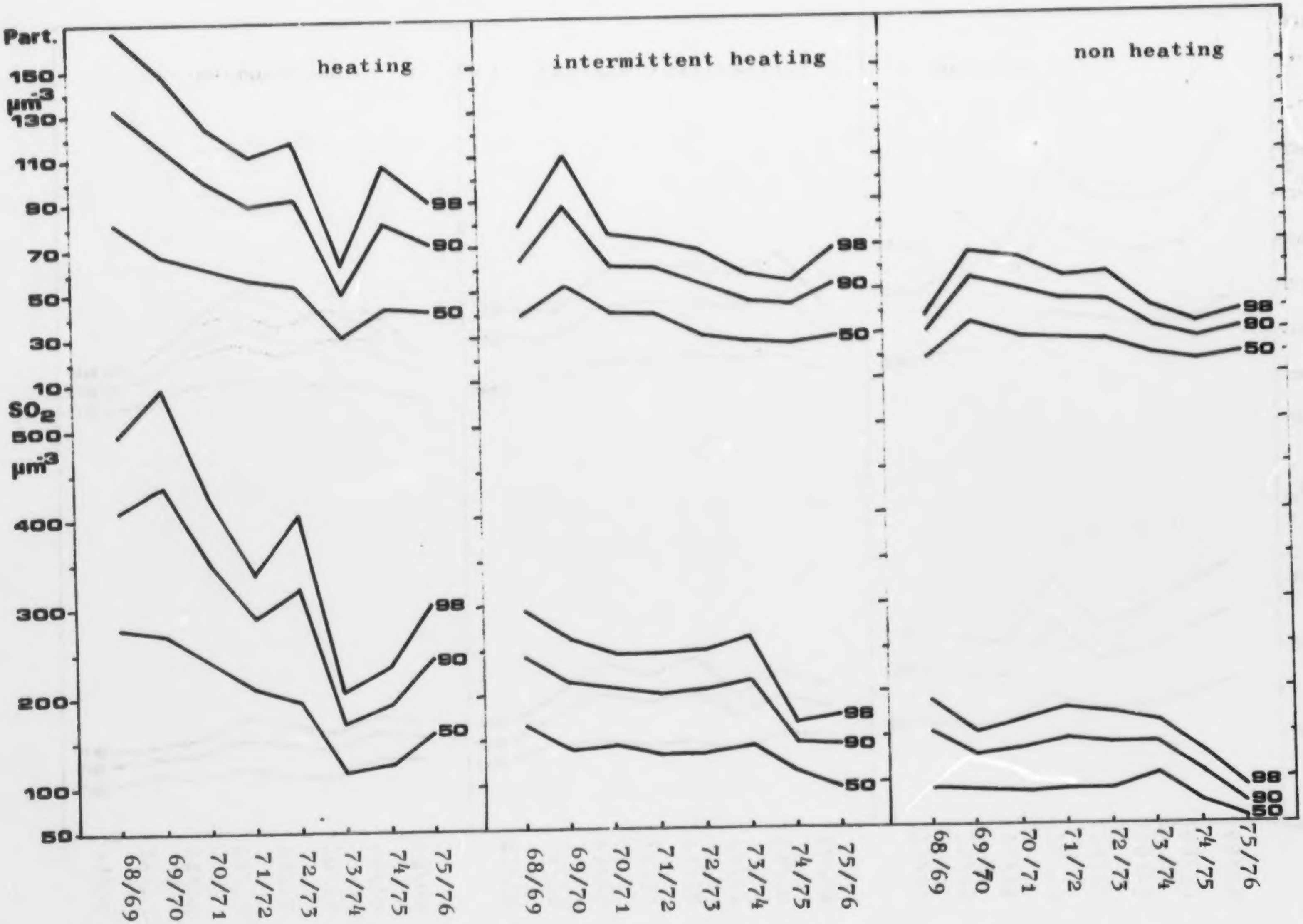

Fig.2.- BRUSSELS : Urban mean distributions

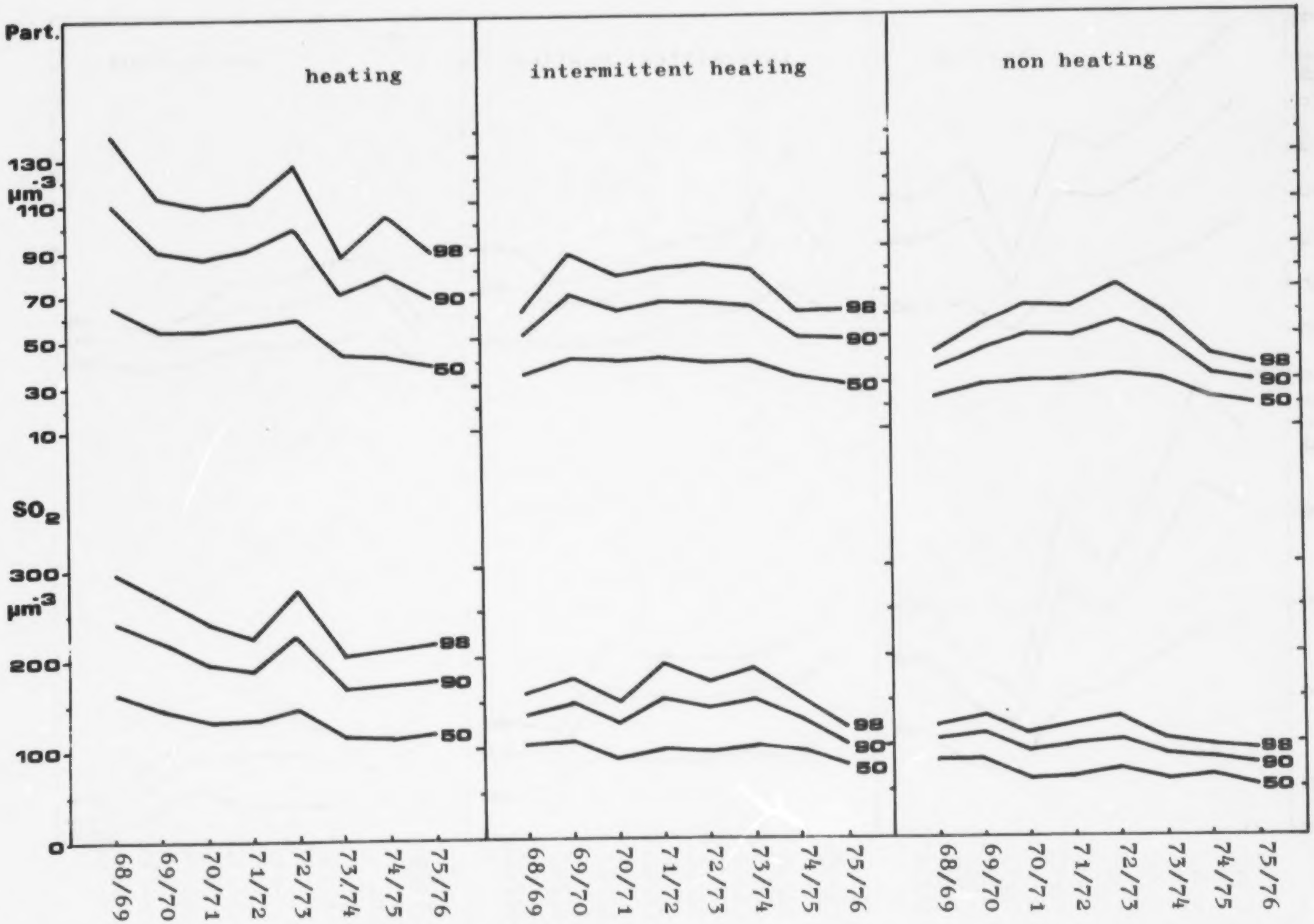

Fig. 3.- CHARLEROI : Urban mean distributions

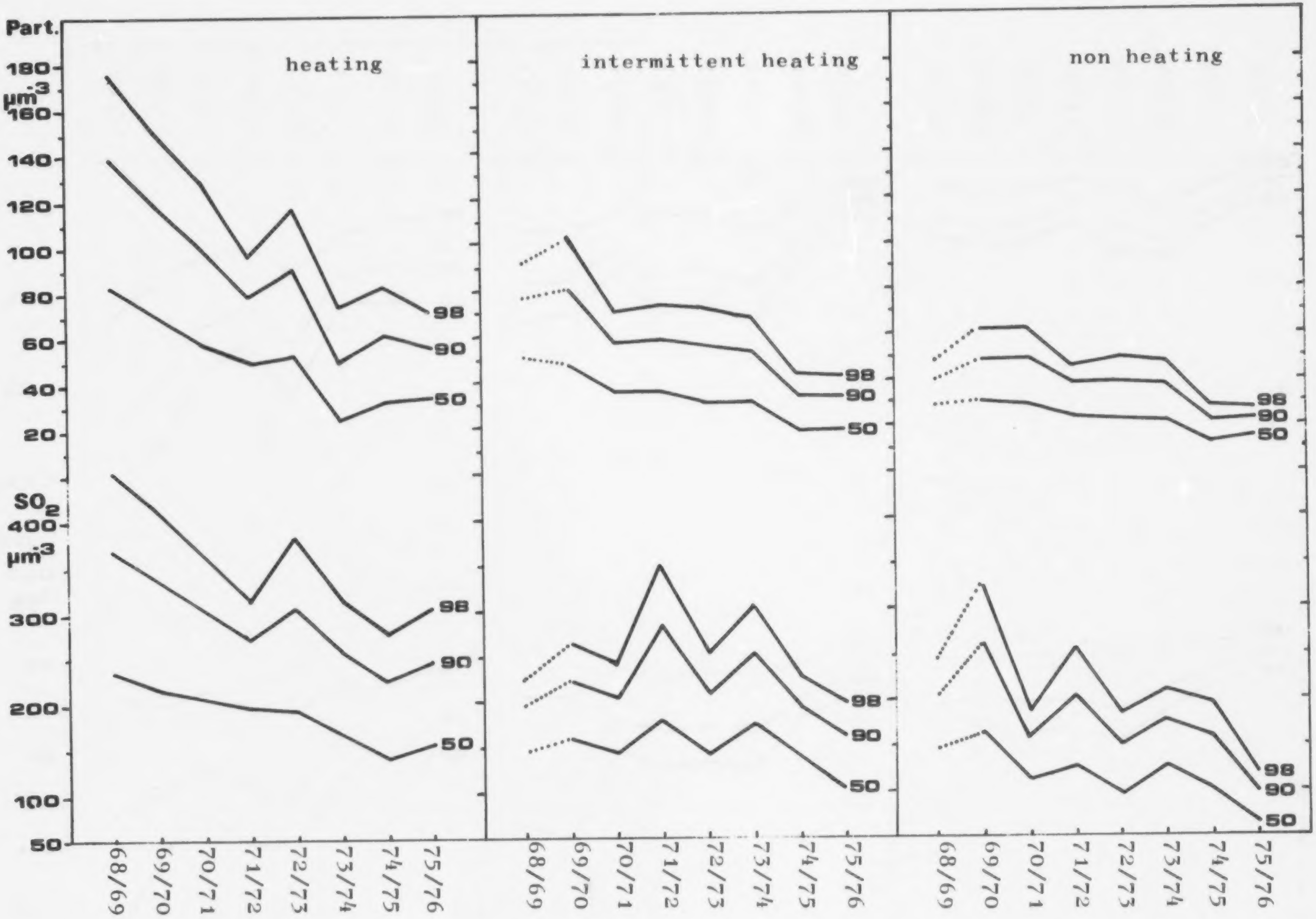

Fig. 4.- GHENT : Urban mean distributions

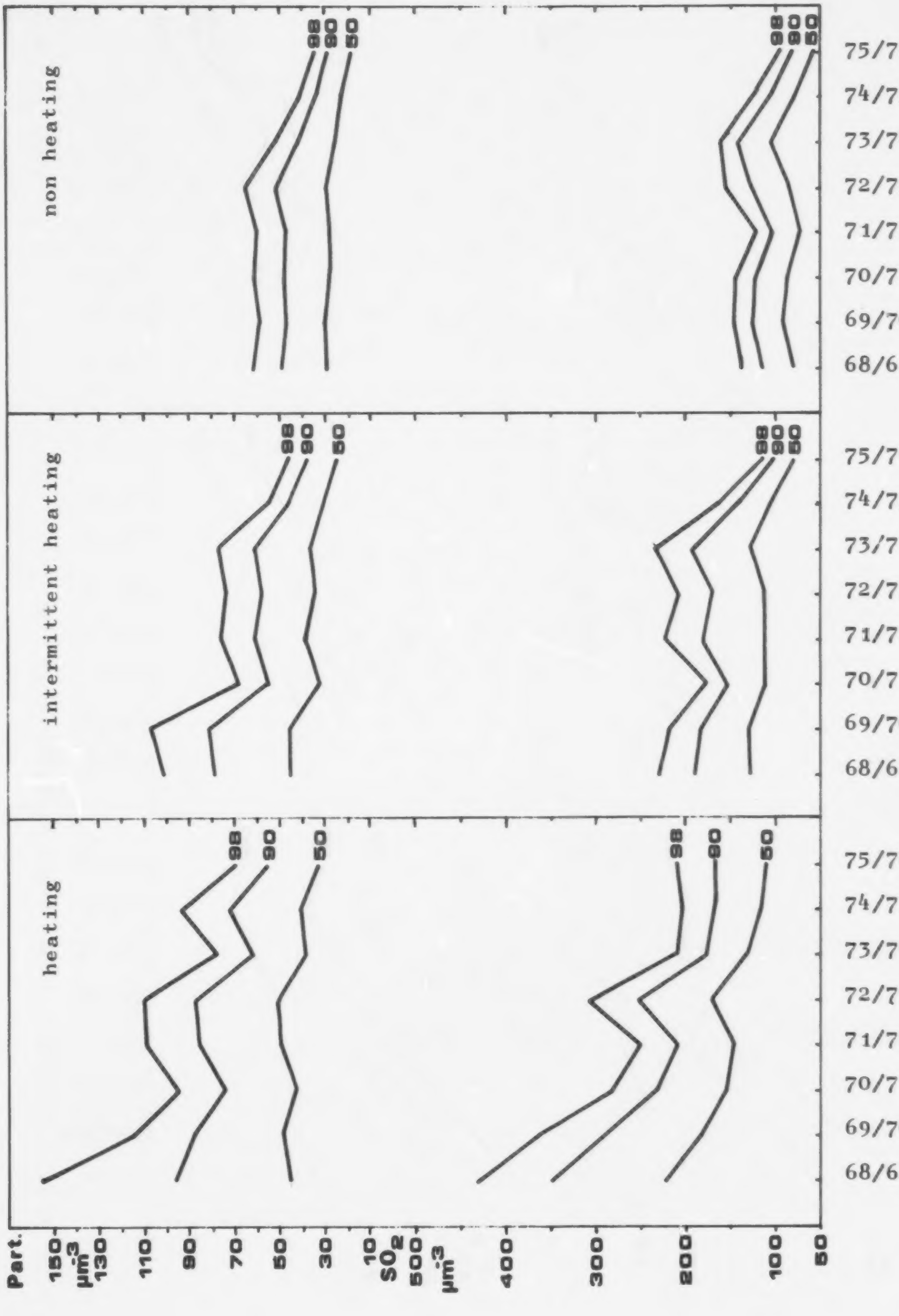

Fig. 5.- LIEGE : Urban mean distributions

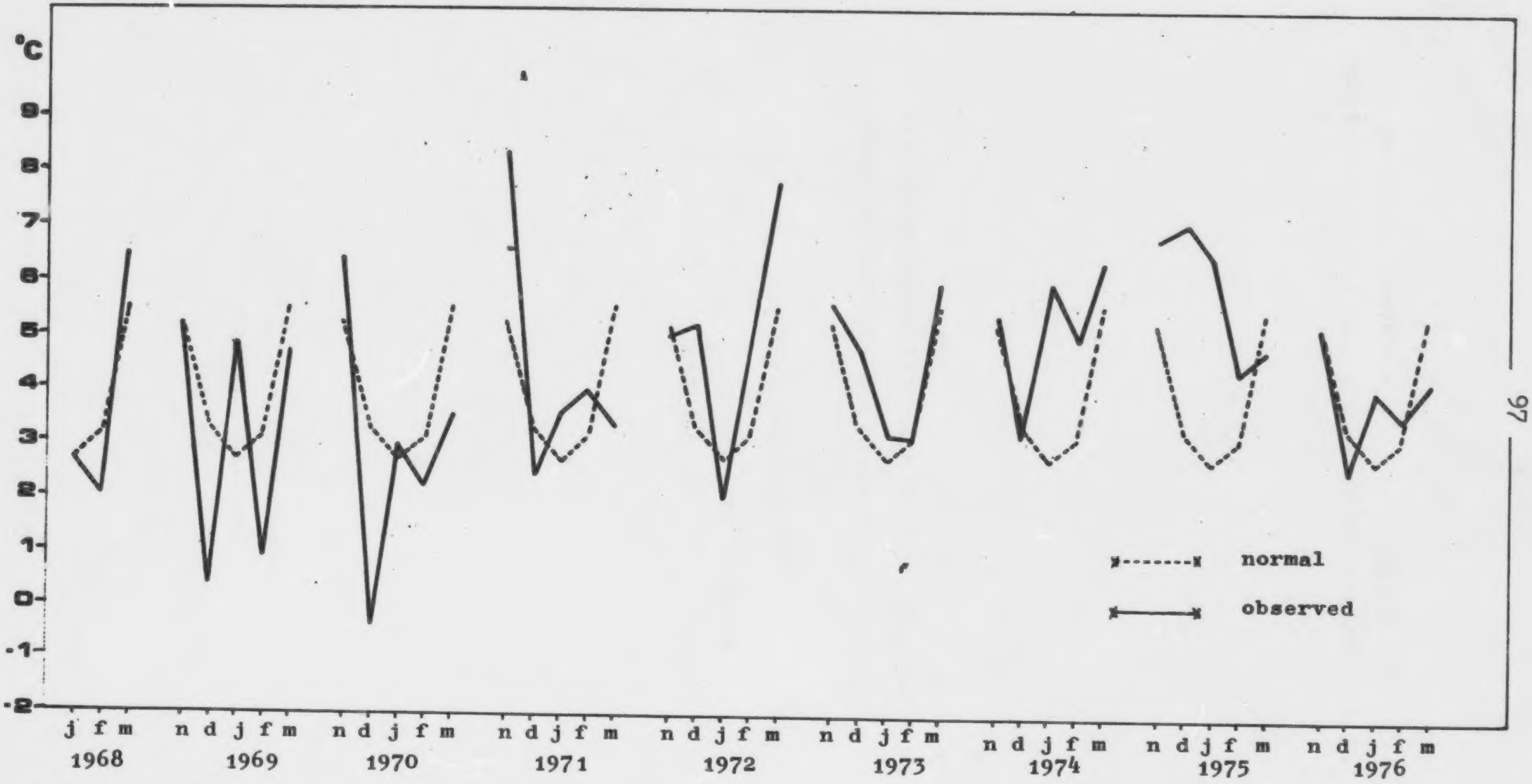

Fig. 6.- UCCLE : Mean temperature during heating months

8th International Technical Meeting
On Air Pollution Modeling and its Application

FORECASTING THE AIR POLLUTION POTENTIAL BY MEANS OF A MULTIPLE REGRESSION MODEL

by
L. VAN DER AUWERA

ROYAL METEOROLOGICAL INSTITUTE
OF BELGIUM

September 20 - 23, 1977
Louvain-La-Neuve
Belgium

FORECASTING THE AIR POLLUTION POTENTIAL BY MEANS OF A MULTIPLE REGRESSION MODEL

1. INTRODUCTION

Owing to the fact that Belgium will soon have in its principal urban and industrial agglomerations an automatic system to control the air quality, the Royal Meteorological Institute has been given the task to issue pollution forecasts.
In order to meet this requirement, a model based on multiple regression techniques is being set up.

The model uses both meteorological and pollution parameters ; it has been applied to the ANTWERP area with , as first objective, the prediction of the daily mean values of the sulphur dioxyde concentration at each of the measuring station sites.
When the automatic network will supply halfhourly means in a continuous and permanent manner, the model will be duly adapted.

2. THE MULTIPLE REGRESSION MODEL

Multiple regression analysis is mainly a curve fitting problem. The proposed model has the form :

$$y = a_o + \sum_{i=1}^{k} a_i x_i \qquad (1)$$

where y = the dependent variable = SO_2 daily mean concentrations ;
x_i = the independent variables ;
a_o, a_i = the regression coefficients ;
$k = 4$ = number of independent variables.

The regression coefficients can only be calculated if one has at his disposal a sufficient number of preexisting simultaneous values of the dependent and independent variables observed in comparable conditions.

The physical input in the model results from the choice of the independent variables and the form in which they are introduced in the above relation (1).

3. DATA INPUT

In order to evaluate the regression coefficients in relation (1) the meteorological and pollution data used have been those of the winter period ; i.e. the daily means observed between the 1st of October and the 31st of March each year from the 1st of October 1968 to the 31st of December 1973, for the 25 stations dissiminated in the Antwerp area.

Owing to the fact that the measuring method is not fiable for very low and very high SO_2 concentrations, values outside the range 50 to 1000 $\mu g.m^{-3}$ have been discarded.

Further, the dependent variable has been multiplied by a factor taking into account the weekly variation of the intensity namely of the domestic sources. This factor is the ratio of the mean value for a particular day and station to the overall mean for all days of the week.

4. CHOICE OF THE INDEPENDENT VARIABLES

The meteorological parameters used in the model as independent variables are not necessarily directly observed. Some have to be computed. This way of doing may seem to complicate the model. However a pragmatic analysis was applied to derive the parameters accepted as independent variables. Only those having a good partial correlation with the sulphur dioxyde concentrations were retained.

This also means that in the future, other parameters can be used or that already accepted parameters will be used in a different form.

In the present work, the following parameters were accepted as the most suitable independent variables.

4.1. VENTILATION VARIABLE

This is probably the most important variable to explain the variations of the air pollution data ; it allows for horizontal diffusion. It is a combination of windspeed and mixing height in the form :

$$x_1 = \frac{10^3}{ff_v^{0.5} \cdot H^{0.2}}$$

where ff_v = amplitude of the mean vector wind ;
H = mean mixing height.

Mixing height is an important parameter ; its determination was made by the HOLZWORTH's method using the soundings at noon and midnight of the Uccle aerological station near Brussels.

Minimum values for H were imposed :

at night $H_1 \geq 100$ m
at noon $H_2 \geq 200$ m

and the final value was computed using the relation :

$$H = 0.75\ H_2 + 0.25\ H_1$$

4.2. PRODUCTION FACTOR

The meteorological parameter that is probably best correlated with the production of sulphur dioxyde is a kind of temperature. Many types of temperatures were tried to find the best results. The pseudo-adiabatic wet bulb temperature was retained.

This temperature is related to humidity and its good correlation with SO_2 concentration can be explained by the fact that it is a kind of sensible temperature. Its daily mean value was calculated from the individual wet bulb temperatures taken at the synoptic station of Deurne-Antwerp. These temperatures were calculated using the following relation :

$$-x_2 = T_w = T - \frac{(r_w(p,T_w) - r).L_v(T_w)}{c_p + r . c_{pv}}$$

with T,p : synoptic temperature and pressure ;

T_w : the wet bulb temperature ;

L_v : the latent heat of water ;

c_p (c_{pv}): specific heat of air (water vapor) at constant pressure ;

$r(r_w)$: (saturated) mixing ratio at p and T (T_w).

4.3. STABILITY FACTOR

Vertical diffusion, governed by stability, is also a very important parameter in air pollution problems. Many stability parameters can be used. A single value representing the stability for a whole day may however be very doubtful. Therefore it is very difficult to find a variable explaining the variance of the dependent variable due to this kind of atmospheric property. Finally a value based on atmospheric pressure was retained ; nevertheless it shows the worst correlated variable with air pollution concentrations and it is certainly not the better choice. This variable is calculated using the relation :

$$x_4 = (\overline{p}_{atm} - \overline{p}) + T.s_p$$

where $\overline{p}_{atm}$ = the mean atmospheric pressure ;

$\overline{p}$ = 1013.2 mb

s_p^2 = the variance of 8 synoptic measurements of the atmospheric pressure.

The value T should give information about the trend of the atmospheric pressure during the day of interest. It is calculated in the following way :

$$\begin{array}{lll} p(t) > p(t-3h) & & T = T+0.5 \\ p(t) < p(t-3h) & & T = T-0.5 \\ p(t) > \overline{p} + 10\ mb & & T = T+0.5 \\ p(t) < \overline{p} - 10\ mb & & T = T-0.5 \end{array}$$

with the limitations that

$$(-15 \leq T.s_p \leq 15)\ mb$$
$$(-15 \leq \overline{p}_{atm} - p \leq 15)\ mb$$

Calculated in this way the independent variable x_4 should be positively correlated with stability.

4.4. PERSISTANCE FACTOR

The fourth independent variable can be taken as the concentration of the preceding day. This is the only nonmeteorological parameter, although it implicity contains all the meteorological information of the preceding days.

It follows that :

$$x_3 = y(t-1)$$

5. CLASSES :

To take into account the position of sources relative to the receptors, the regression coefficients in relation (1) are calculated separately for 24 sectors of wind directions, 15° wide, the first one being centered on the north.

Further, special attention is given to very low ventilation situations by defining a 25th class occurring when

$$ff_a.H \leq 450\ m^2.\ s^{-1}$$

whatever the wind direction may be.

6. SOLUTION OF THE EQUATION

For each class and for each station, the same linear multiple regression expression of the form (1) is solved by the method of least squares.

Each time this is done with a variable number of equations, the independent variables are not always equally important. Therefore as a first step, they are rearranged in order of decreasing partial correlation with the dependent variable.

The model is then solved with all independent variables (i.e. four) taken into account and the multiple correlation coefficient calculated. The value

$$F_1 = \frac{R_r^2}{1-R_r^2}\,\frac{n-r-1}{r}$$

with R_r^2 = the multiple correlation of the model with r independent variables ;

n = the number of equations

r = 4

follows an F-distribution with (r, n-r-1) degrees of freedom under the null hypothesis that all regression coefficients are zero. This hypothesis will be rejected at a significance level α = 0.2.

Two possibilities arise :

a) the null-hypothesis may be rejected. In this case only those independent variables are sought which explain a significant part of the variance of the dependent variable. These are found after calculating the value :

$$F_2 = \frac{R_r^2 - R_k^2}{1 - R_r^2}\,\frac{n-r-1}{r-k}$$

which follows an F-distribution with (r-k , n-r-1) degrees of freedom under the null-hypothesis that the last (r-k) variables are zero.

As long as :

$$F_2 \geqslant F_{0.80} (r-k, n-r-1)$$

this hypothesis is rejected, which means that still more variables from the last (r-k) are significantly different from zero.

b) The null-hypothesis may not be rejected. In this case the expression (1) is in fact unsufficient. Nevertheless in such a case, those variables are taken as different from zero which are larger than their corresponding error.

7. FITTING A CURVE TO THE REGRESSION COEFFICIENTS

For each station, 125 regression coefficients, zero or not, are calculated. From these 120 = 24x5 are winddirection dependent and each set of 24 coefficients corresponds to the same independent variable. A polynomial fit has been carried out to set a value of this particular coefficient immediately from winddirection. Otherwise, there would be an abrupt change in the used value when winddirection turned from one sector to the next. The proposed polynomial has the form :

$$a_{ij} = b_{oi} + \sum_{k=1}^{m} b_{ki} T_k (x_j) + \varepsilon_j$$

where a_{ij} = one of the 24 regressioncoefficients a_i ;
T_k = TSCHEBYSHEFF polynomial of order k ;
b_o, b_k = second set of regression coefficients, to be calculated ;
m = order of the highest polynomial, to be calculated ;
x_j = the variable corresponding to a winddirection of 15 (j-1) degrees ;
ε_j = residue, distributed N $(0, \sigma^2)$.

The only purpose of this polynomial is to fit the data a_{ij} sufficiently well. Therefore the order m of the highest polynomial results from the requirement that :

$$\rho(a_i, \hat{a}_i) \geq 0.95$$

so that at least 90 percent of the variance is explained.

Results of the application of this is shown in figure 1.

9. FORECASTING

In fact, quite a lot of regression coefficients have to be calculated. Nevertheless, once they are computed, an estimate for the air pollution level at each station becomes possible, when a value for :

- winddirection ;
- windspeed and mixing height ;
- wet bulb temperature ;
- atmospheric situation ;
- the air pollution level of the preceding day

is known or predicted.

The first action however is to decide whether a situation with a poor ventilation will not be present. In that case an estimate for each station can be found immediately from the first set of winddirection independent regression coefficients for the respective stations. If not, with the estimate or knowledge of the winddirection and the respective regression values for the TSCHEBYSHEFF polynomials, a value of the first set of regression coefficients can be derived, one for each variable and an estimate for a_o. Then the procedure is the same as above.

The calculated concentration is afterwards corrected twice : first by multiplying with the factor that takes account of the day of the week, second by keeping the forecasted concentrations between the limits $\mu \pm 1.65\,\sigma$ where these are respectively the mean and standard deviation from the concentration data used in a given sector. Further, the lower limit of all calculated concentrations is subjectively fixed at 50 $\mu g/m^3$.

10. RESULTS

The success of the model can be found by comparing calculated with measured values for a period that was not used to derive the regression coefficients. The results can be judged twofold : first one can look to the calculated results for a particular station to find those which give the better confidence and second, one can compare the forecasted situation with the really observed concentrations. Both types of results are given in tables and figures.

They are neither extremely good, nor very bad. They are certainly not worse than the results reported from models that are much more complicated. It must however be possible to improve the predicted values, by regularly recalculating the model constants with more and also more recent measurements, because during the period 1968-1973 the sulphur dioxyde concentrations show a considerable decrease.

Tabel 1 shows the output for a particular station. The successive columns contain : the sector, the number of days in that sector, minimum value for the forecasts, maximum value for the forecasts, a_o, a_1, a_2, a_3, a_4, the significance level of the expression, the multiple correlation coefficient and the root mean square error, defined as :

$$RMSE = \left[\frac{1}{N-1} \sum_{k=1}^{N} (\chi_i^{cal} - \chi_i^{meas.})^2\right]^{1/2}$$

Below, the information of the polynomial fit can be found. Table 2 shows the output for one week of forecasts.

For each day is printed :

First line :
- number of forecasted days
- date
- day of the week (monday = 1)
- value for x_1 variable
- idem x_2
- idem x_4
- winddirection sector
- number of forecasted values (stations)
- correlation between forecasted and measured values
- mean error between forecasted and measured values
- correlation between measured values of the day and the preceding day ;
- mean error when concentrations of preceding day were taken as predictions for the following day.

Four second lines contain in order per station :
- station number
- calculated value
- measured value.

It should be noted that the calculated values of station 826 are never considered in the calculations because of the abnormal character of this station.

Table 3 gives the final result for each station separately. Some stations seem to deserve much more confidence than others. Nevertheless high correlations are not found. The persistence model, which takes simply the measured value of today as the forecasted value for tomorrow, is worse for 21 stations on 25.

What also must be remembered is that these values depend strongly on the length of the period that is predicted.

Figures 1 to 7 show some results of the calculations. Most important are the predicted situations for the whole urban area as shown in fig. 6 and fig. 7. Here the stations are indicated. Full lines represent the calculated situation and dashed lines the real situation for the same day. The individual values from this figure can be found in table 2.

11. CONCLUSION

Theidea of a model that predicts the daily mean air pollution level for an urban area is described. It is based on some simple linear regression techniques. That simplicity is the most important argument in favour of such a model. The results are certainly satisfactory as in air pollution studies very good results are still more ore less utopian.

Needed is a large amount of available data and the regression coefficients must and can regularly be recomputed with more recent measurements. The success of the model is directly dependent on the reliability of the input data and calculated regression coefficients have no absolute significance. They are only the results of the measurements and the model that is proposed.

Only meteorology and air pollution winter data are necessary. The only fundamental parameters are sufficiently described above. This does not mean that no other meteorological parameters were tried. Nevertheless they are, in this kind of model, not significant. Among them :
- the minimum night-time temperature
- a mean daily temperature
- precipitation : amount and intensity
- the amount of sunshine
- cloudiness
- relative humidity, etc.

Of course, the most important remark is that all the predictions for the air pollution concentrations must be made from forecasts for the meteorological input and not with measured values as it was done here. As with all other types of model the results will strongly depend on the predicted values of the parameters introduced and will only be as good as those forecasts.

REFERENCES

1. ANDERSON, R.L., BANCROFT, T.A. : Statistical theory in research (1952)

2. BENARIE M., et al : Emploi des regressions multiples pour la definition du niveau de fond de la pollution urbaine et pour sa prevision a court terme (1972) Pollution atmosphérique n°53.

3. BRANDT, S. : Statistical and computational Methods in Data Analysis (1973), North Holland Publ. Comp.

4. BULTYNCK, H. : Verband tussen de dagelijkse gemiddelde concentratie SO_2 in een stad en enkele meteorologische parameters (1976).

5. DICKSON, R.R. : Meteorological factors affecting Particulate Air Pollution of a city (1960) Bull of Am. Meteor. Soc. n°8.

6. KENDALL, M.G. : The advanced theory of statistics (1946) Vol. 1, Griffin & Co.

7. O.M.M. : Tables météorologiques internationales (1966)

8. SINGER, I. : Steadiness of the wind (1967) Journ. of Appl. Meteor. 6

TABLE 1.-

```
                          CALCULATIONS FOR STATION NR 804
                          ********************************
                                                          0.255    0.0      0.074   0.699   46.2
SECTOR  1     14  *  124.9  311.6   11.031   3.098   5.464   0.0     -1.822   0.013   0.786   44.8
SECTOR  2     17  *   93.2  308.8   -9.273   4.441   3.292   0.0     -1.806   0.020   0.757   60.0
SECTOR  3     33  *   50.0  322.3  -34.873   4.808   8.661   0.0      0.0     0.084   0.660   60.1
SECTOR  4     43  *   53.3  311.9  -34.683   4.432   7.594   0.358   -2.360   0.004   0.656   75.0
SECTOR  5     60  *   58.1  374.5   67.186   1.789   4.317   0.511    0.0     0.164   0.709   71.3
SECTOR  6     72  *   77.5  406.4  144.587   0.0     8.049   0.578    0.0     0.162   0.709   64.6
SECTOR  7     71  *  108.1  406.1  141.900   0.0     7.372   0.0      0.0     0.045   0.557   75.7
SECTOR  8     43  *  115.0  408.5  114.080   2.952  11.096   0.283    0.0     0.037   0.547   59.1
SECTOR  9     33  *   74.9  320.5  162.131   0.0     5.015   0.285    0.0     0.034   0.739   40.3
SECTOR 10     51  *   99.2  290.2   88.677   1.213   7.531   0.216    0.0     0.021   0.687   38.8
SECTOR 11     47  *  115.2  285.9  110.578   1.223   7.271   0.0      1.054   0.036   0.708   41.7
SECTOR 12     62  *  119.6  309.5  165.874   1.732   8.175   0.0      1.846   0.084   0.761   45.5
SECTOR 13     80  *  102.3  329.0  183.998   1.776   8.668   0.186    0.0     0.082   0.726   48.3
SECTOR 14     97  *   96.9  324.9   47.624   3.074   5.560   0.192    0.0     0.124   0.740   44.4
SECTOR 15    119  *   84.6  299.8   57.641   2.648   5.385   0.237    0.0     0.110   0.724   51.2
SECTOR 16    120  *   78.3  320.0   10.745   3.388   3.218   0.212    0.0     0.150   0.761   47.3
SECTOR 17    120  *   93.5  331.3   30.880   3.555   4.924   0.167    1.272   0.083   0.804   38.1
SECTOR 18    116  *  100.6  308.1   74.019   3.293   8.534   0.196    1.678   0.021   0.768   41.7
SECTOR 19     74  *   99.5  308.2   76.807   2.995   8.923   0.239    1.632   0.003   0.720   43.1
SECTOR 20     40  *  102.5  296.7   93.144   1.953   8.586   0.234    1.361   0.003   0.753   54.7
SECTOR 21     28  *   96.6  349.8  142.247   1.628  14.081   0.302    1.772   0.007   0.745   61.7
SECTOR 22     22  *   88.4  363.2  136.737   1.575  21.121   0.0      0.780   0.046   0.789   39.4
SECTOR 23     12  *   81.4  261.8  109.545   2.713  16.294   0.247    1.229   0.135   0.769   54.1
SECTOR 24     12  *   86.2  308.6   27.860   2.734   9.400   0.333    0.0     0.020   0.733  101.6
SECTOR 25     37  *   88.3  560.4  -77.163   3.714  10.034
POLYNOMIAL FIT FOR REGRESSION COEFFICIENT NR 1
           N PARAM. = 14  CORRELATION = 0.951  F(13,11) =  7.99  SIGN. LEVEL = 0.76E-03  ESTIMATED ERROR =  28.90
POLYNOMIAL FIT FOR REGRESSION COEFFICIENT NR 2
           N PARAM. = 16  CORRELATION = 0.961  F(15, 9) =  7.29  SIGN. LEVEL = 0.25E-02  ESTIMATED ERROR =   0.51
POLYNOMIAL FIT FOR REGRESSION COEFFICIENT NR 3
           N PARAM. = 14  CORRELATION = 0.952  F(13,11) =  8.18  SIGN. LEVEL = 0.69E-03  ESTIMATED ERROR =   1.84
POLYNOMIAL FIT FOR REGRESSION COEFFICIENT NR 4
           N PARAM. = 19  CORRELATION = 0.951  F(18, 6) =  3.13  SIGN. LEVEL = 0.82E-01  ESTIMATED ERROR =   0.08
POLYNOMIAL FIT FOR REGRESSION COEFFICIENT NR 5
           N PARAM. = 15  CORRELATION = 0.974  F(14,10) = 13.32  SIGN. LEVEL = 0.16E-03  ESTIMATED ERROR =   0.21
```

TABLE 2.-

```
69 74070.   1        79.0      -4.5   5.655     9  *   22     0.636   57.77    0.718   35.03
*801  265. 163. *802  200. 183. *803  125. 167. *804 -999.-999. *805  237. 181. *806  234. 205. *807  128. 148.
*808  209. 240. *809  254. 215. *810  219. 210. *811  253. 220. *812  158. 192. *813  245. 247. *814  317. 214.
*815 -999.-999. *816  298. 190. *817  207. 173. *818  192. 170. *819  173. 135. *820  142. 123. *821  189.  70.
*822  115.  86. *823  190. 108. *824   74. 103. *826   78.  57. *
70 74071.   2        47.5      -5.0   3.253    13  *   22     0.874   71.62    0.915   67.88
*801  163. 259. *802  161. 265. *803  144. 180. *804 -999.-999. *805  180. 236. *806  173. 252. *807  155. 189.
*808  199. 292. *809  212. 307. *810  208. 322. *811  173. 281. *812  170. 224. *813  231. 300. *814  243. 362.
*815 -999.-999. *816  204. 265. *817  213. 265. *818  180. 214. *819  140. 165. *820   96. 124. *821  148. 103.
*822  128. 108. *823  168. 152. *824  115. 114. *826  228.  66. *
71 74072.   3       107.7      -2.8   0.456    14  *   21     0.694  138.36    0.882   60.74
*801  244. 162. *802  287. 189. *803  233. 201. *804 -999.-999. *805  326. 165. *806  299. 214. *807  250. 173.
*808  414. 189. *809  362. 267. *810  450. 219. *811  329. 215. *812  286. 170. *813  420. 242. *814  418. 268.
*815 -999.-999. *816  310. 205. *817  398. 201. *818  281.-999. *819  292. 167. *820  108. 130. *821  275. 122.
*822  253.  86. *823  250. 144. *824  207. 136. *826  193.  91. *
72 74073.   4        60.4      -3.5   2.626    19  *   21     0.930   26.99    0.849   31.90
*801  190. 154. *802  187. 181. *803  144. 159. *804 -999. 329. *805  151. 181. *806  232. 210. *807  194. 212.
*808  198. 194. *809  281. 261. *810  258. 237. *811  221. 214. *812  118. 133. *813  233. 203. *814  303. 233.
*815 -999.-999. *816  246. 244. *817  226. 258. *818 -999.-999. *819  143. 153. *820   50. 100. *821  117. 138.
*822   79.  71. *823   92.  95. *824   93.  73. *826  117.  42. *
73 74074.   5        45.3      -2.7 -18.026    13  *   22     0.714   26.22    0.707   67.14
*801  107. 135. *802   91. 129. *803   90.  98. *804  186. 191. *805  128. 112. *806  111. 143. *807  123. 146.
*808  126. 127. *809  165. 172. *810  144. 144. *811  125. 144. *812  115. 128. *813  165. 149. *814  169. 194.
*815 -999.-999. *816  157. 127. *817  148. 196. *818 -999.-999. *819  116. 121. *820   79. 112. *821  119. 149.
*822   92. 122. *823  127.  96. *824   86. 136. *826  198. 100. *
74 74075.   6        36.4      -6.9 -12.054    17  *   22     0.839   17.25    0.710   54.38
*801   89.  83. *802   80.  70. *803   91.  63. *804  138. 120. *805   80. 103. *806  110. 114. *807   99.  95.
*808   65.  72. *809  124. 129. *810  102. 104. *811   96.  80. *812   50.  53. *813   84. 115. *814  139. 154.
*815 -999.-999. *816   96.  51. *817  108. 107. *818 -999.-999. *819   83. 110. *820   50.  58. *821  138. 149.
*822   69.  73. *823   50.  44. *824   58.  61. *826  105.  34. *
75 74076.   7        43.6      -7.2 -14.390    16  *   22     0.753   20.57    0.690   27.33
*801   90.  76. *802   81.  55. *803   60.  56. *804  125. 125. *805   80.  85. *806  108.  79. *807   80.  64.
*808   79.  70. *809  111. 101. *810  111. 103. *811  100.  70. *812   62.  63. *813   86. 132. *814  137. 149.
*815 -999.-999. *816   71.  51. *817  122.  89. *818 -999.-999. *819   78.  59. *820   50.  47. *821   97.  59.
*822   61.  73. *823   54.  60. *824   50.  53. *826   83.  67. *
```

Reproduced from
best available copy.

TABLE 3.-

nr.Stat.	Number of Forecast. days	Regression model		Persistence model	
		Correlat.	RMSE	Correlat.	RMSE
801	74	0.372	68.33	0.249	67.87
802	89	0.677	49.08	0.524	57.07
803	89	0.540	55.41	0.519	49.88
804	72	0.387	79.69	0.449	82.46
805	89	0.569	47.39	0.360	50.69
806	89	0.658	50.36	0.431	59.36
807	82	0.596	43.59	0.433	53.46
808	80	0.646	71.28	0.708	62.31
809	89	0.721	51.34	0.530	57.65
810	89	0.631	64.83	0.431	71.25
811	57	0.408	74.91	0.613	55.00
812	89	0.705	44.19	0.454	53.53
813	89	0.576	62.76	0.442	63.68
814	89	0.523	66.46	0.382	66.90
815	49	0.539	70.29	0.565	66.89
816	71	0.609	57.24	0.370	71.20
817	77	0.543	69.71	0.305	85.44
818	71	0.733	37.67	0.421	57.80
819	75	0.594	42.21	0.497	44.75
820	89	0.679	46.57	0.606	41.05
821	72	0.353	53.67	0.137	132.88
822	89	0.459	44.50	0.100	61.62
823	73	0.645	40.26	0.414	52.90
824	39	0.562	35.49	0.129	54.33
826	88	0.591	93.42	0.558	101.63

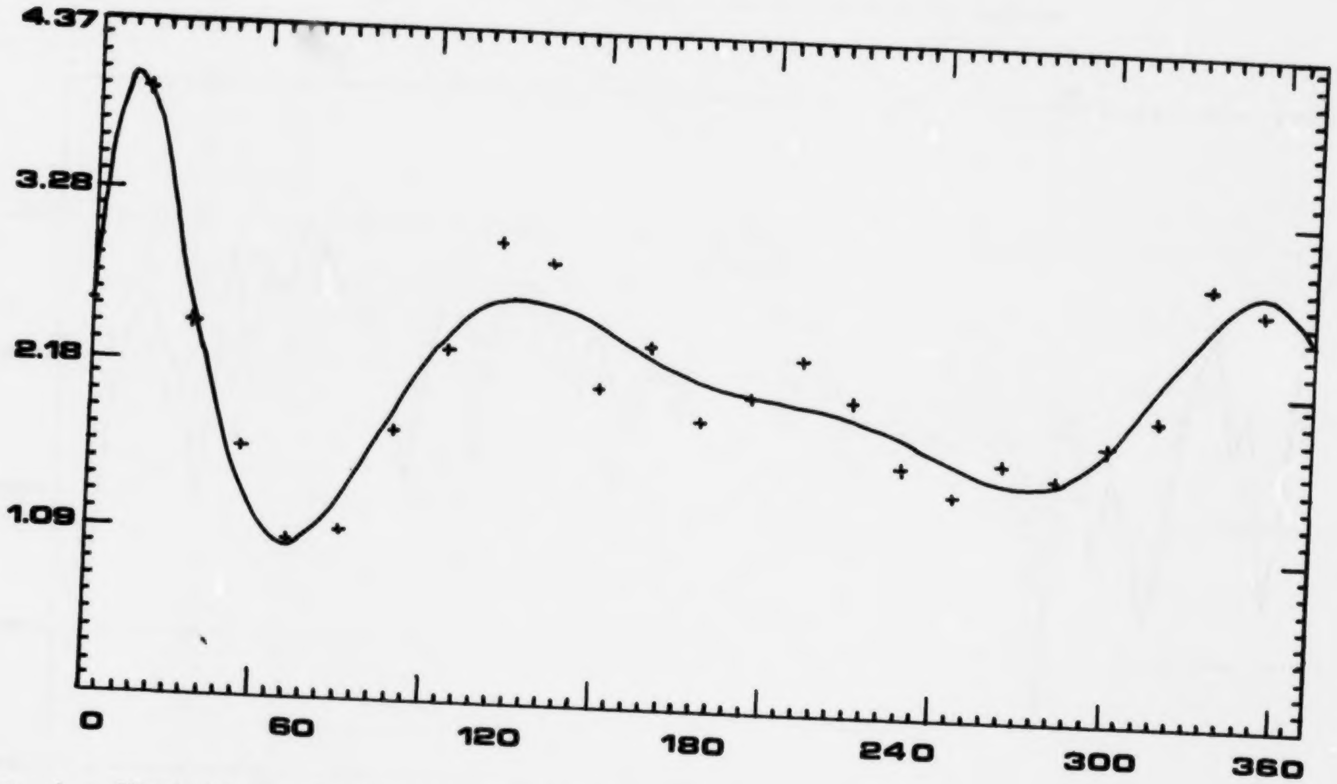

Fig. 1.- Variation of regresscoefficient a_1 as a function of winddirection for a given station.

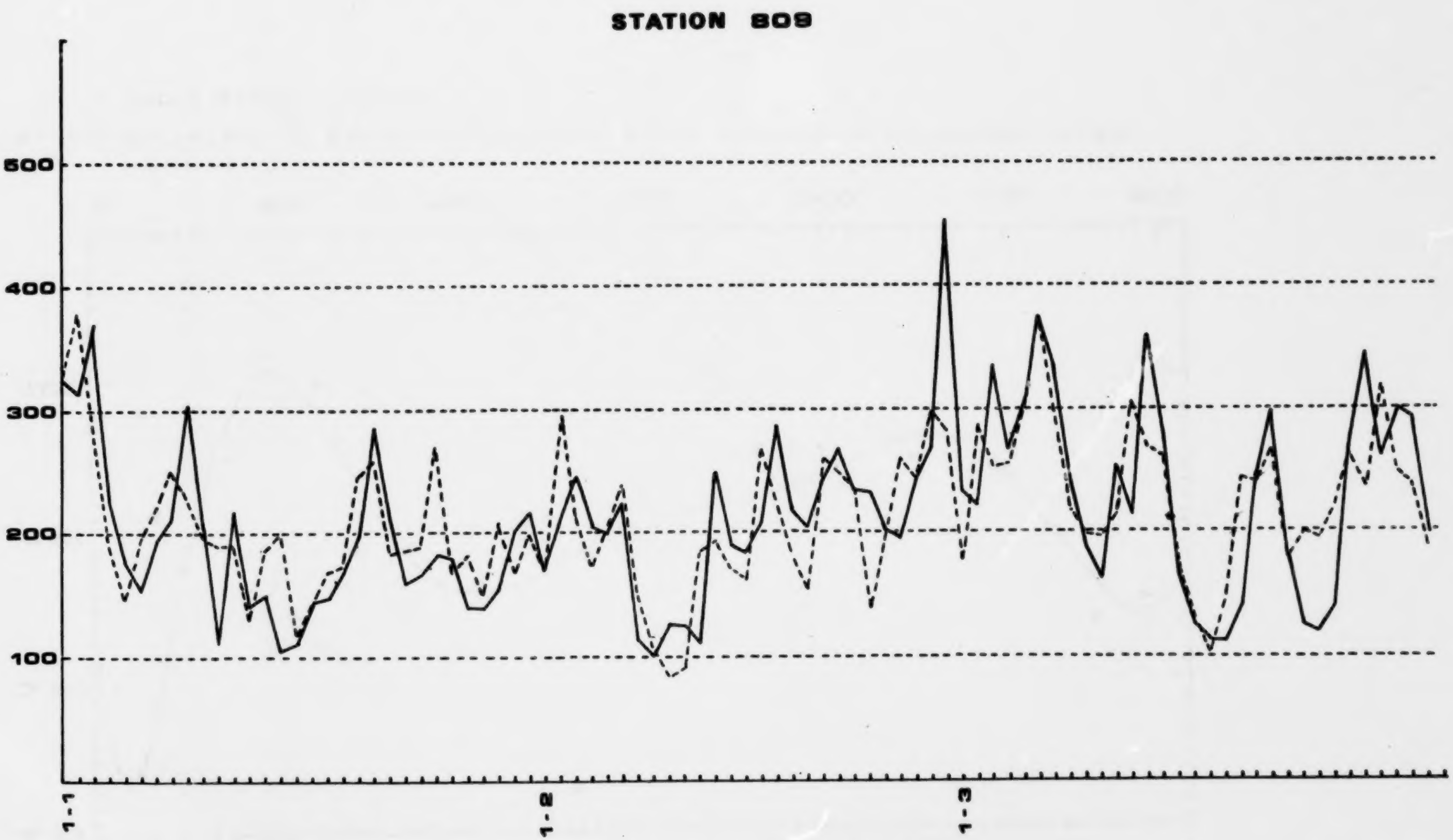

Fig. 2.- Time series of predicted and measured values.

——— predicted

------ measured

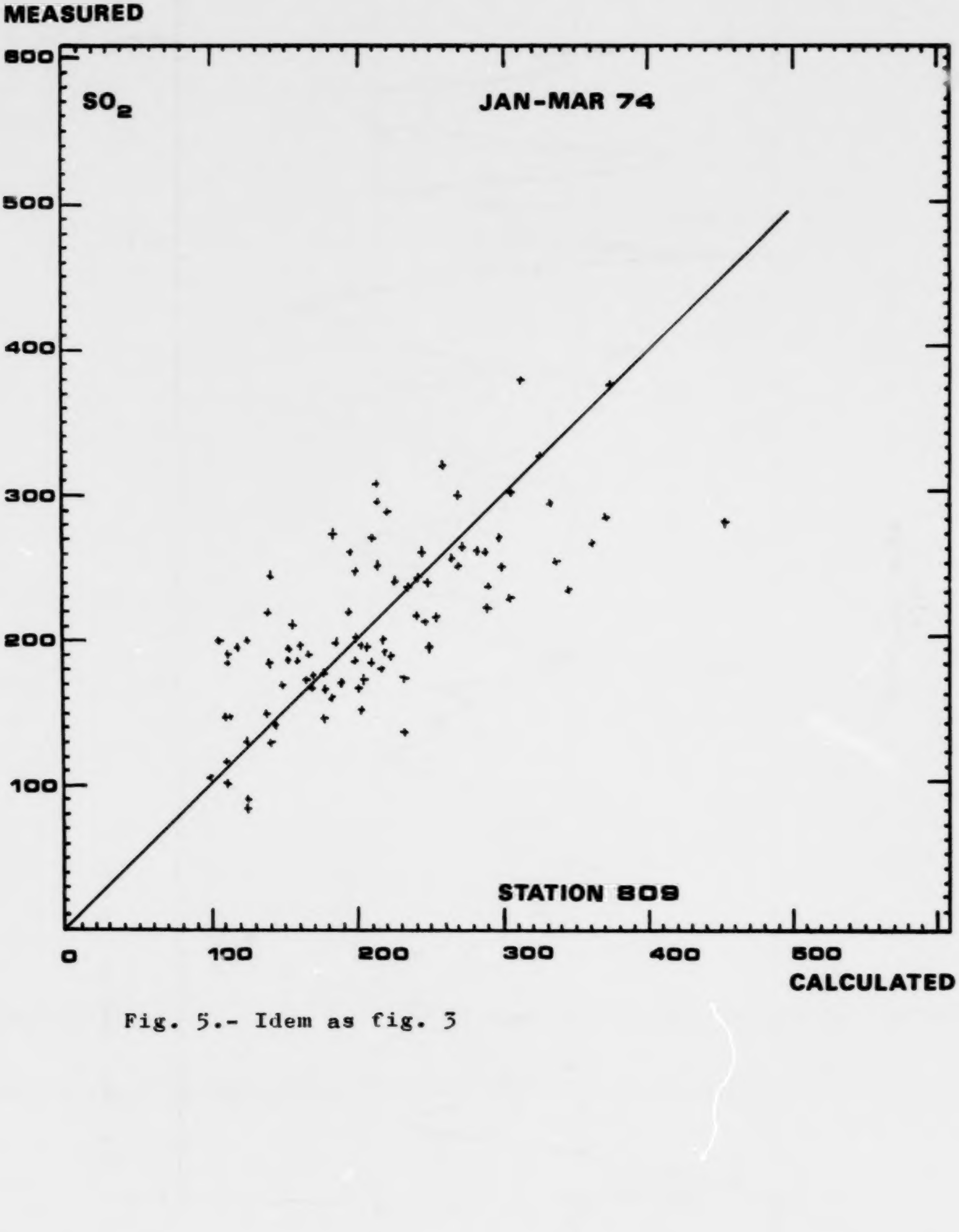

Fig. 5.- Idem as fig. 3

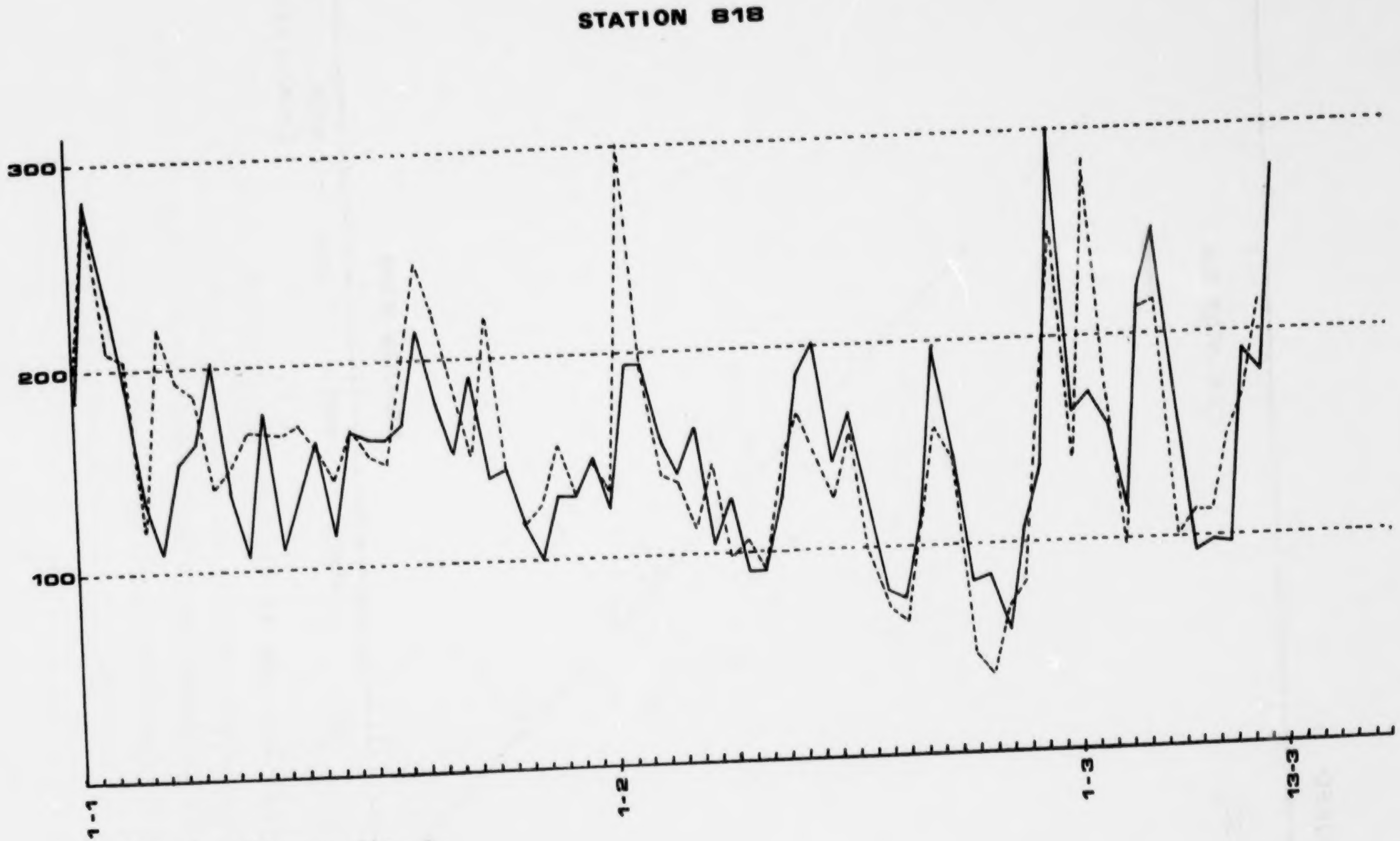

Fig. 4.- idem as fig. 2.

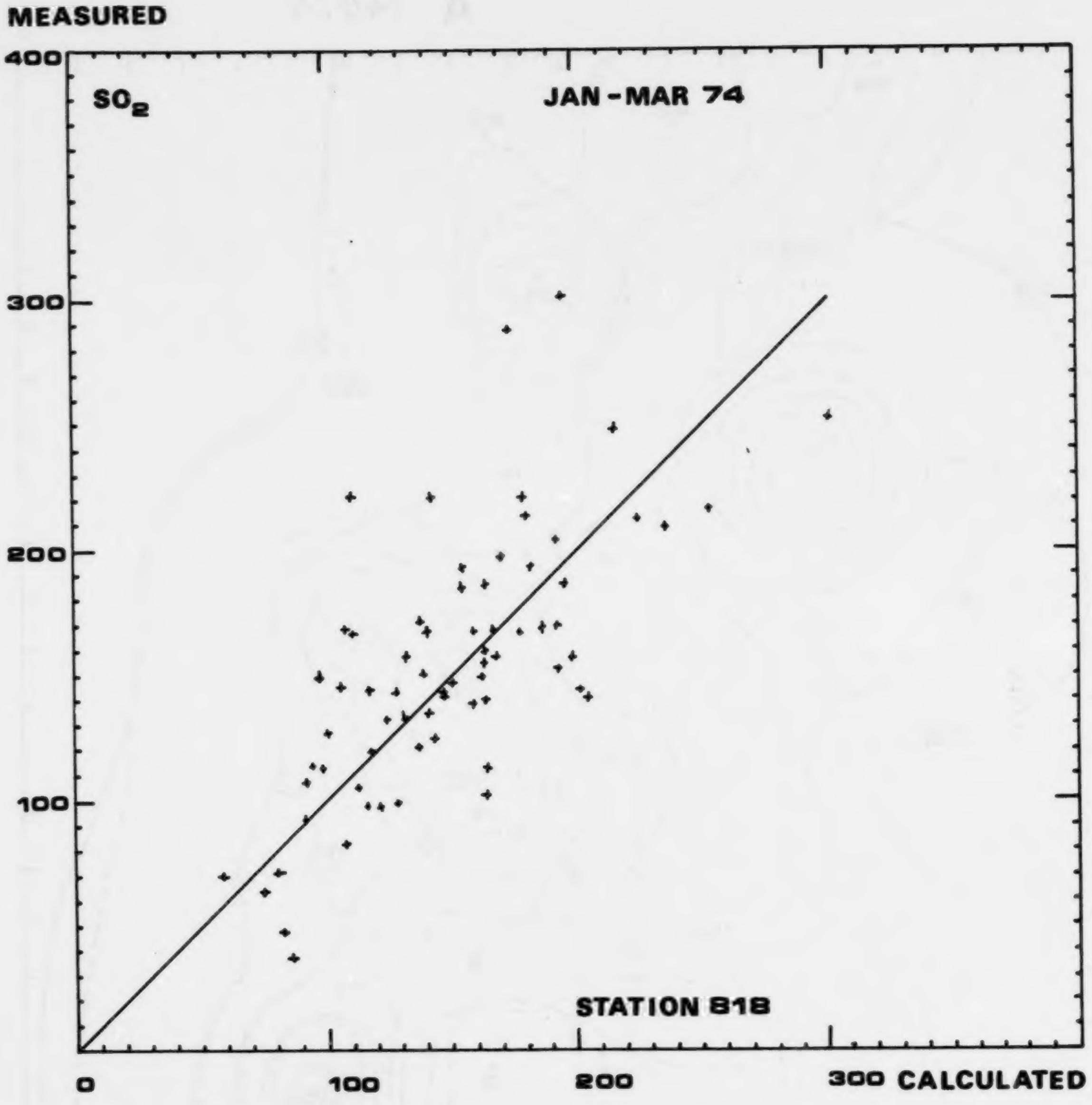

Fig. 3.- 3 month measured versus calculated values.

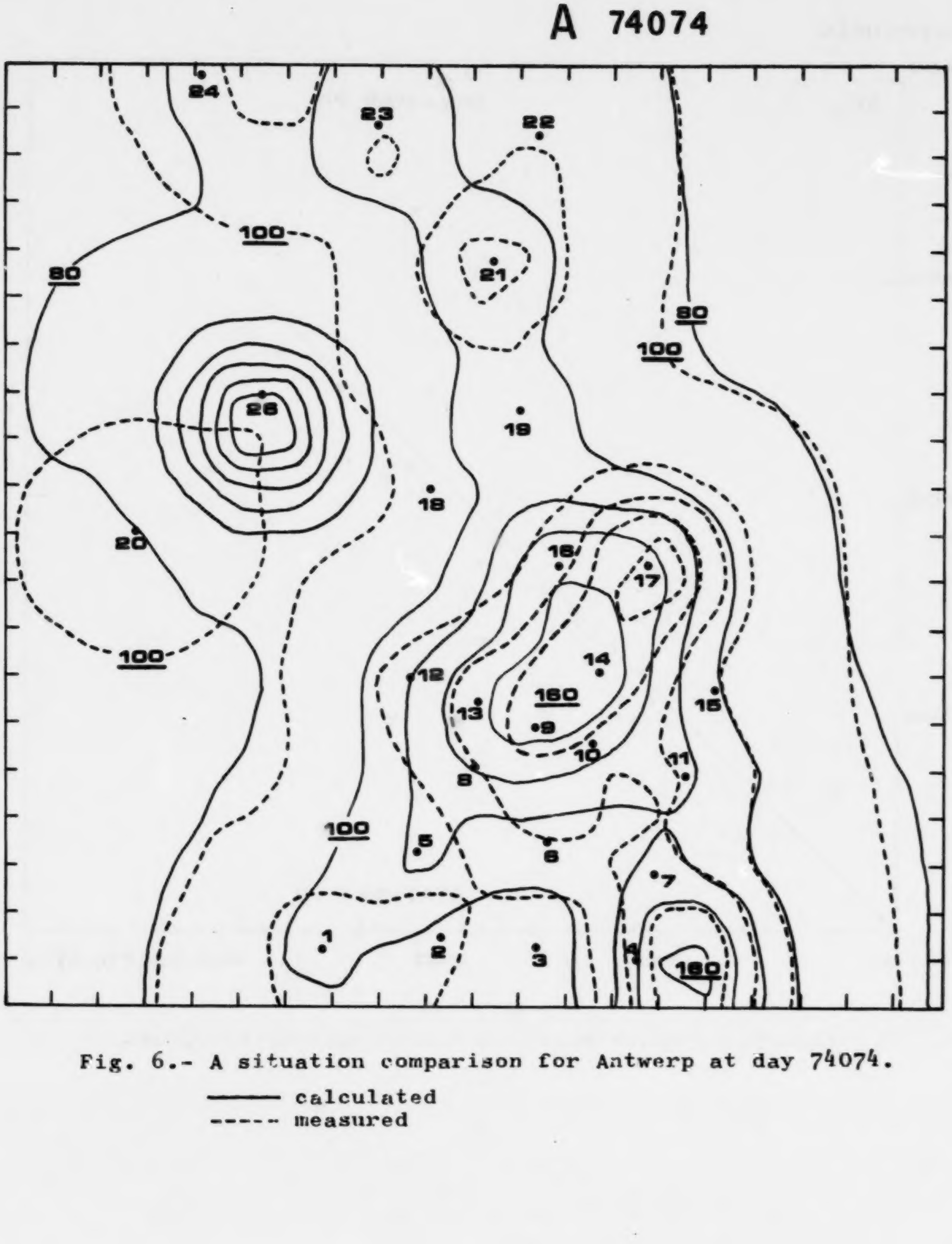
A 74074
24
23
22
100
80
21
80
100
26
19
18
20
100
16
17
14
12
160
13
15
9
10
11
8
100
5
6
7
1
2
3
4
160

Fig. 6.- A situation comparison for Antwerp at day 74074.
——— calculated
----- measured

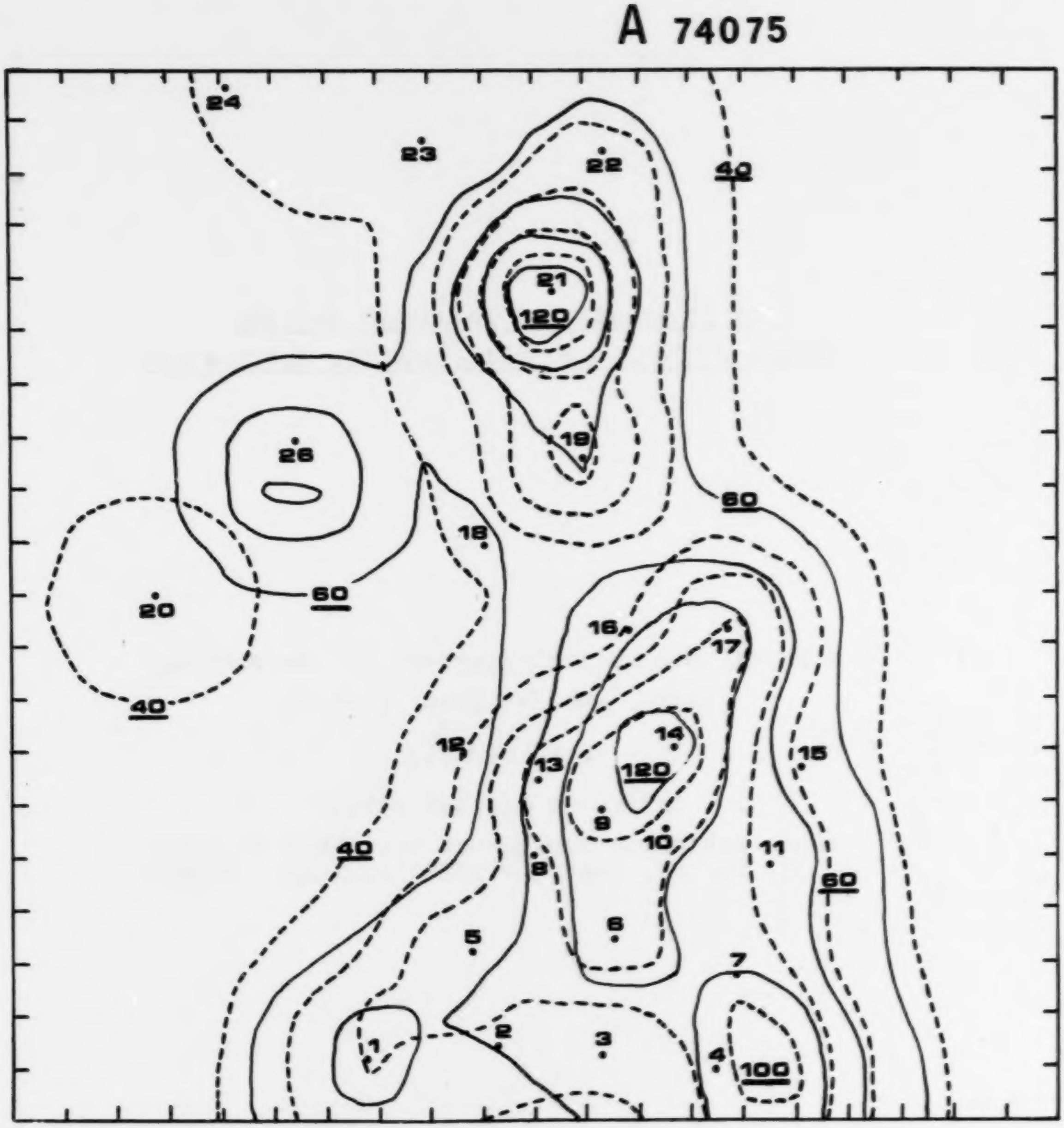
A 74075
24
23
22
40
21
120
19
26
60
18
20
60
40
16
17
14
12
13
120
15
9
10
11
40
8
60
5
6
7
1
2
3
4
100

Fig. 7.- Same as fig. 6 but for day A 74075

8th International Technical Meeting on Air Pollution Modeling and its Application

A Purely Statistical Approach to the Warning, Alarm, and Emergency Problem

J.P. ORFEUIL

Centre de Géostatistique

Ecole Nationale Supérieure des Mines de Paris
35, rue St. Honoré - FONTAINEBLEAU - FRANCE

September 20 - 23, 1977
Louvain-la-Neuve
Belgium

A PURELY STATISTICAL APPROACH TO THE WARNING, ALARM, AND EMERGENCY PROBLEM

When studying air pollution, we have to distinguish two kinds of problems :

- The study of the impact on the environment of a new power plant, of a new factory, of new regulations about the emissions of cars; boilers, a.s.o... In this case, we need a physical model, simulating the air diffusion under several conditions, and giving outputs (air quality) as complex functions of the inputs (emissions, meteorology).
- The routine control of the air quality of a specific area. In this case, we need algorithms relating the near past to a short-dated future; we especially need to predict whether some levels considered as severe (warning) or critical (alarm of emergency) will be exceeded or not. This prediction must be performed with available routine data (levels of pollution at some points, wind, temperature, pressure) excluding expensive measurements (mixing depth, vertical profile of winds, a.s.o...). Here, physical models are irrelevant, because of the lack of some crucial data. On the other hand, a statistical approach is always possible : it only requires a relevant analysis of the relationships between available data and a precise formulation of the problem to be solved. The domain of application of this approach will increase in the near future with the developments of networks controlling industrial or urban areas.

In this paper, we present a method for solving the alarm problem (parts I, II, III and Appendix) and a case study (part IV).

I - DESCRIPTION OF THE PROBLEM.

Several Time-Series are available and must be used for prediction :

- METEOROLOGICAL SERIES

They can be measured either at one point or at several locations. Some of the measurements are real values (Temperature, Pressure). Some are vector values (Wind), some are scales (Cloudiness). We have to extract from these partially redundant informations synthetic variables which are well related to the diffusion or the accumulation of pollutants.

- EMISSIONS DATA

are seldom available with a good accuracy at any given time (except sometimes in the case of an isolated source). Generally, only raw estimations during large periods can be performed. We shall not take them into account for predictions on the scale of an hour.

- AIR POLLUTION LEVELS

Let us denote $L_{ix}(t)$ the level of the i^{th} pollutant at location x and time t. Our aim is the prediction of the distribution of $L_{ix}(t+h)$, given all the past data. In other words, we want to estimate a function f defined as follows :

$$f(\ell) \begin{cases} = 1 & \text{iff} \quad L_{ix}(t+h) \geq \ell \\ = 0 & \text{iff} \quad L_{ix}(t+h) < \ell \end{cases}$$

In the following, we shall call the function f the thresholding function.

II - MAIN DIFFICULTIES OF THE STATISTICAL ANALYSIS

Some are specifically related to the complexity of the phenomenon to be analyzed. The others are related to the aim itself : the introduction of threshold leads us to a typical non-linear problem.

II-1 - A great lot of different variables interfere, so that multivariate techniques are needed. Moreover, the complexity of the interactions between meteorological variables and pollution makes linear analysis of relationships irrelevant. A non-linear method, the Correspondance Analysis (BENZECRI, 1966 [1] , [11]) will be used. We outline it in Appendix I^{I}.

II-2 - A priori, we cannot assume stationarity (even in a weak sense) neither in space nor in time.

For spatial variations, we shall use an optimal geostatistical method called Non-Stationary Kriging. Theory : MATHERON, 1967 [7], [8]. Computer package BLUEPACK : DELFINER, CHILES, DELHOMME, 1974 [3]) for interpolation, mapping, contouring, and optimal location problems.

For time variation, it may be necessary to separate regular trends (slow evolution or periodic effects) and local residuals. Fortunately, this structural analysis is generally easy because we know the main features of the time evolution : a mean variation during the day due to combined effects of solar and human activity, and homogeneity during the week except for Saturday and Sunday in urban areas. Anyway, we shall assume in the following that the series of pollutants can be regarded as the sum of a regular trend and a stationary effect. Actually in many cases (continuous working power plants or factories) the series are stationary so that no decomposition is required.

II-3 - The problem of the thresholding function is undoubtedly the most difficult for statistical theory. The estimation of the function $f(\ell)$ introduced in I is theoretically possible by way of Conditional Expectation Theory. Unfortunately, the required statistical inference (a (n+1) dimensions distribution if n is the number of predictors) is practically impossible when n is greater than 3 or 4. It is the reason why MATHERON proposed in 1973 a Simple Substitute for Conditional Expectation, named Disjunctive Kriging (D.K. for short. [9], [10]). This method - which permits non-linear prediction, only requires the statistical inference of the bivariate laws, whatever the number of predictors is. This method, outlined in Appendix I, will be out basic tool for threshold analysis. The case study will show that D.K. may be very efficient and supply us with very accurate predictions.

III - THE PRACTICAL SCHEME OF THE PREDICTION

We summarize here the different phases of the computation of the time model, as they are performed by the ALERTE Package, setting aside the spatial interpolation and mapping problems performed by BLUEPACK. The parameters of the model are computed on the available data of a week or a month and periodically updated (Computation time : from one to six minutes on IBM 370-165 or CII Iris 80). Then the model can be used in real time on a mini-computer for predictions during the following days or months.

III-1 - FIRST PHASE : STRUCTURAL ANALYSIS OF THE SERIES OF POLLUTANTS.

III-1-1 - TIME EVOLUTION.

We compute the autocorrelation functions to measure the degree of time dependence of the series, and the periodograms to decide whether it is worth considering periodic trends or not. According to the result of the decision, we shall work either on raw data, or on the residuals from the optimal fit.

III-1-2 - CHARACTERISTICS OF THE A PRIORI DISPERSION.

For all the problems of thresholding, a very precise description of the distribution laws is required : the mean and variance are really not at all sufficient. We must first define clearly the scale of the time-averaging : we have to select different scales and consider for example the mean values over a quarter of an hour, an hour, four hours. As an example, we see on Fig. 2 bis that the threshold $\ell = 180\ \mu g/m^3$ is exceeded one time out of ten for the quarter of an hour means, and only one time out of thirty for four hours means. More, the shape of the distribution is not always preserved through changes of scale : the quarter of an hour and hourly mean look like lognormal distribution. However, the four hours means seem to follow a bimodal distribution! This is a case where LARSEN's permanence law ([5], [6]) is not applicable. We prefer - and in fact data compell us to do so - to model precisely each distribution in terms of transformation methods called Anamorphosis in [9] which is the main reference in the domain).

It can be shown that any variable X with an increasing continuous cumulative distribution F is the transform of a normalized Gaussian Y (cumulative distribution G) by an increasing function A, whose expression is given by :

$$X = A(Y) \quad ; \quad A = F^{-1}\, G$$
$$Y = A^{-1}(X); \quad A^{-1} = G^{-1}\, F$$

For example, a lognormal distribution is the result of the exponentiation of a gaussian :

$$X \text{ lognormal} \Leftrightarrow \begin{cases} X = A(Y) = e^{m+\sigma Y} \\ Y = A^{-1}(X) = \dfrac{\operatorname{Log} X - m}{\sigma} \end{cases}$$

Very efficient numerical methods have been developped to compute A from the experimental histogram, expand it upon a suitable basis of polynomials (see Appendix I), and to associate to each experimental value X_t the corresponding value Y_t of a normalized Gaussian variable. So, for all the pollutants and all the chosen scales of time averaging, we can substitute new series to experimental time series, all with the same normalized distribution.

III-2 - SECOND PHASE : THE TREATMENT OF THE METEOROLOGICAL INFORMATION.

We have to take all the available meteorological data into account, but we cannot use a physical model because we generally lack some major informations : height of mixing depths, vertical profile of wind, diffusivity coefficients for example. So, the relations between meteorology and pollution must be inferred from the data themselves. To achieve this, we use a kind of nonlinear Canonical Analysis named Correspondance Analysis (outlined in Appendix II). Denote (M_i, i = 1, m) the set of meteorological variables

$$F = \sum_{i=1}^{i=m} f_i(M_i)$$

a sum of non-linear functions of these variables, $G = g(P)$ a function of the level of the pollutant P to be predicted. Correspondence Analysis finds the pair (F_1, G_1) which is the most correlated, afterwards the pair (F_2, G_2) satisfying the same optimum under the condition that G_1 and G_2 are uncorrelated, and so on by iterations.

This method gives us an ordered set of non-linear functions F_i of the meteorology (called factors) which are of major influence on the pollution distribution. Then the effective value of each time of these functions is computed. Afterwards, Gaussian series are associated by transformation techniques in exactly the same way as before.

III-3 - THIRD PHASE : A SUMMARY OF D.K.'s OPERATIONS

Let us denote by $Y^{ij}(t)$ the Gaussian series associated with the i^{th} pollutant for the j^{th} averaging scale, $GM^{m}(t)$ the Gaussian series associated with the m^{th} meteorological factor, $X(t+\tau)$ the pollution level to be predicted and $Y(t+\tau)$ its associated Gaussian image.

The main features of D.K. (outlined in Appendix I) are the following ones :

- In order to perform the non-linear estimation of any function $h(X(t+\tau))$, it is only necessary to predict all the elements $H_n(Y(t+\tau))$ of a suitable orthogonal basis of polynomials. The best estimator for $f(X(t+\tau))$ is obtained by substituting in the expansion $\left(f(X(t+\tau)) = \sum_{n\geq 0} f_n H_n(Y(t+\tau))\right)$ the best estimator H_n^* of the basic functions $H_n(Y(t+\tau))$.
- Denote $F_n(t)$ the vector space generated by the family $(H_n(Y^{ij}(\tau)), H_n(GM^{m}(\tau)), \tau \leq t)$. If all the bivariate distributions are Gaussian (it is easy to check this from the data), then the spaces $F_n(t)$ and $F_m(t)$ are orthogonal as long as n is not equal to m. It follows that the general prediction space $F(t)$ generated by $\bigcup_{n\geq 0} F_n(t)$ is the direct sum $\bigoplus_{n\geq 0} F_n(t)$, that the optimal predictor H_n^* of $H_n(Y(t+\tau))$ belongs to $F_n(t)$ and is obtained by linear regression on $F_n(t)$.

- For usual functions, and particularly for thresholding functions, an expansion limited to order 10 is generally largely sufficient to obtain a good precision. So, in practice, we have two main operations to perform : the expansion of the function $f(X(t+\tau))$ on the orthogonal basis $(H_n(Y(t+\tau))$ and the estimation of a maximum of ten regression systems. To prevent these from being too large, we keep only the data of a period T preceding t and select the most efficient predictors by stepwise-type techniques. The required statistical inference is reduced to the estimation of a maximum of ten low-order correlation matrices.

IV - A CASE STUDY.

The following data come from a zone located around a power plant and a chemical factory, each of them working continuously. Available meteorological data are wind, temperature, hygrometry, pressure, cloudiness, and PASQUILL stability class. All the measurements are performed at the same location, every quarter of an hour during four days. We want to predict whether the levels of NO_x will be greater than 140 $\mu g/m^3$ (resp. SO_2 greater than 140 $\mu g/m^3$) during the hour following the moment of the prediction. We shall briefly outline the structural analysis and stress the practical results.

IV-1 - STRUCTURAL ANALYSIS OF POLLUTANTS' TIME SERIES

- Autocorrelation functions are plotted on Figure 1. For a lag of one hour, the correlation is .73 for NO_x , .48 for SO_2. The correlations vanish around five hours for NO_x, four for SO_2. The time evolution is more regular for NO_x than for SO_2. The correlations remain near zero for great lags : we may assume that the series are well modeled by a stationary time process. However, we prefer to make sure that there are no periodic trends : to achieve this, we compute the optimal coefficients A(P), B(P), C(P) of the fit :

$$X(t) = A(P) \cos \left(\frac{2\pi\, t}{P}\right) + B(P) \sin \left(\frac{2\pi\, t}{P}\right) + C(P)$$

The indicator R^2 (ratio of the explained variance by a fit of period P) over the total variance, never exceeds .12, whatever

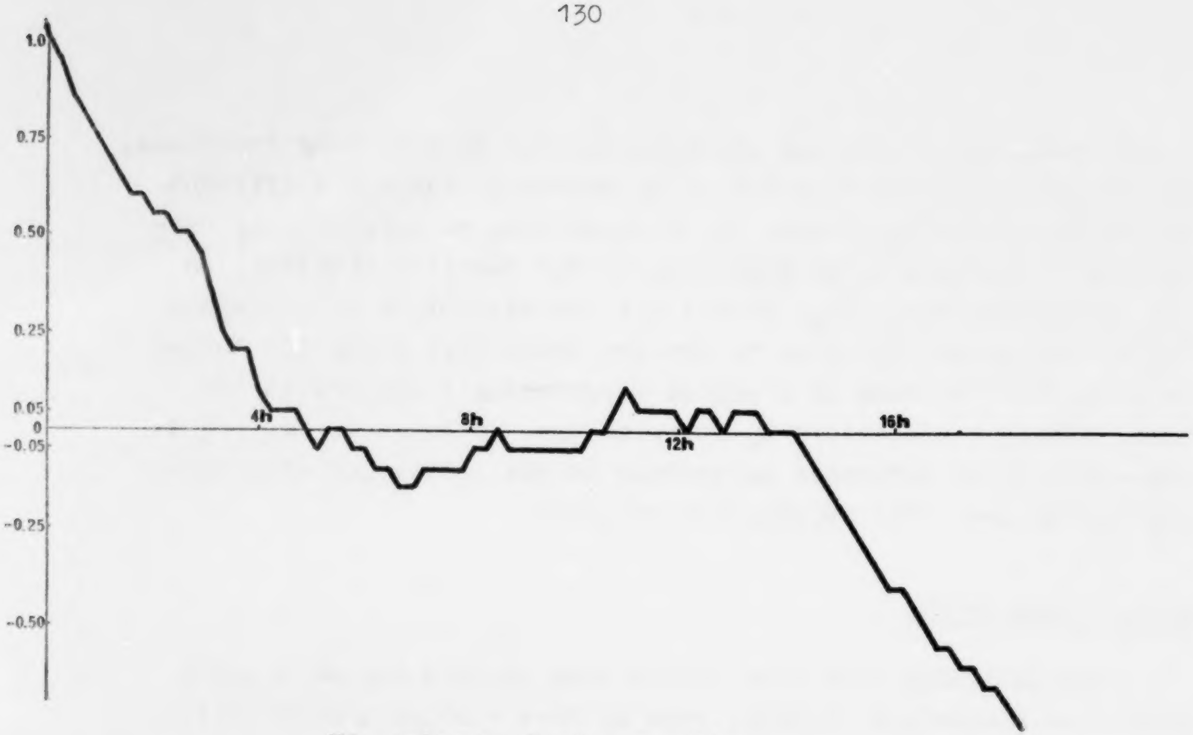

NO_x Autocorrelation Function

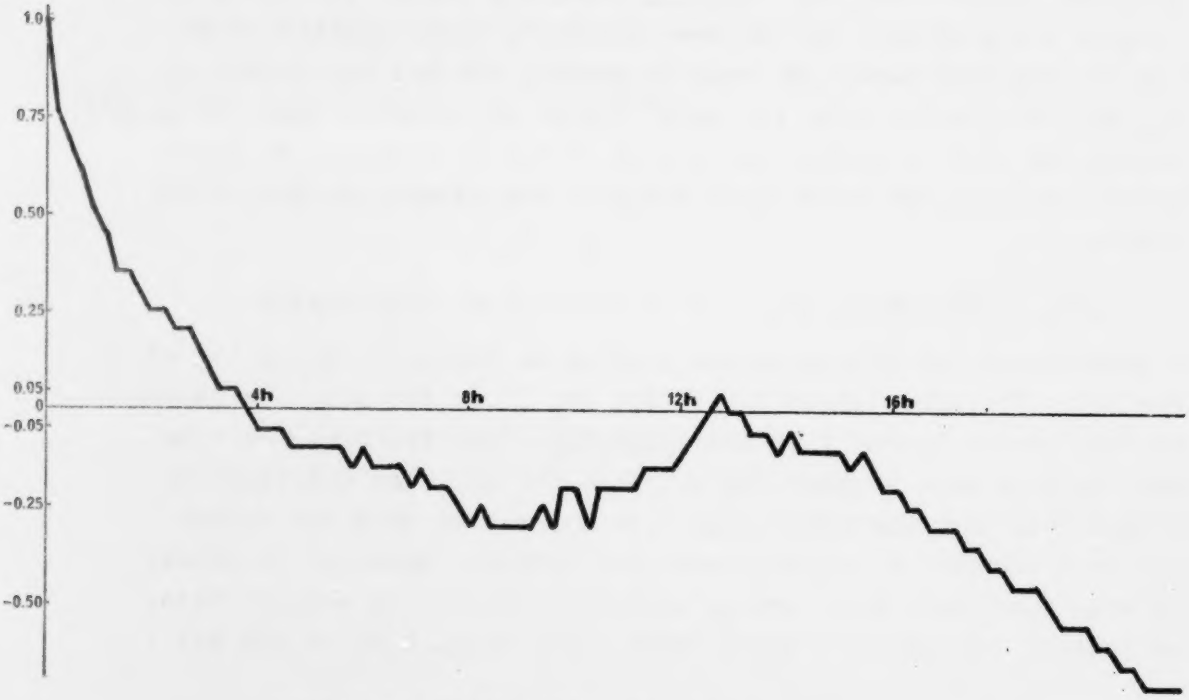

Acidity Autocorrelation Function

Figure 1

Figure 2 - NO_x Histograms

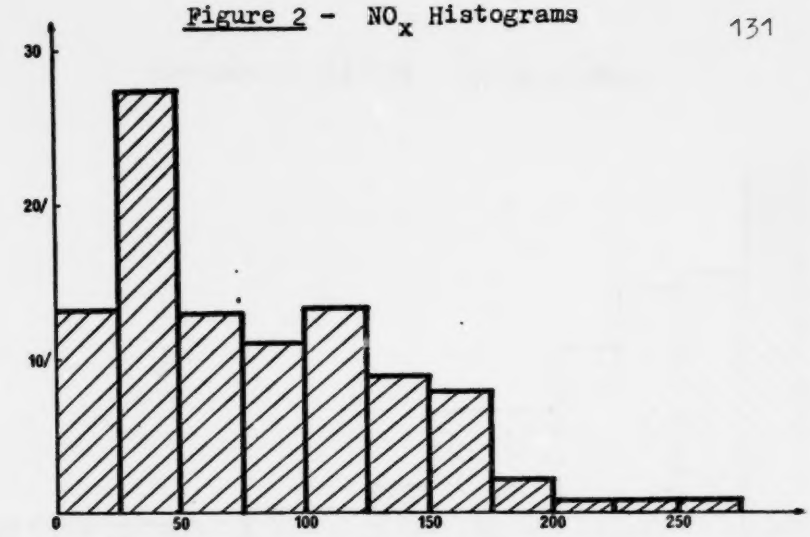

Instantaneous Rates

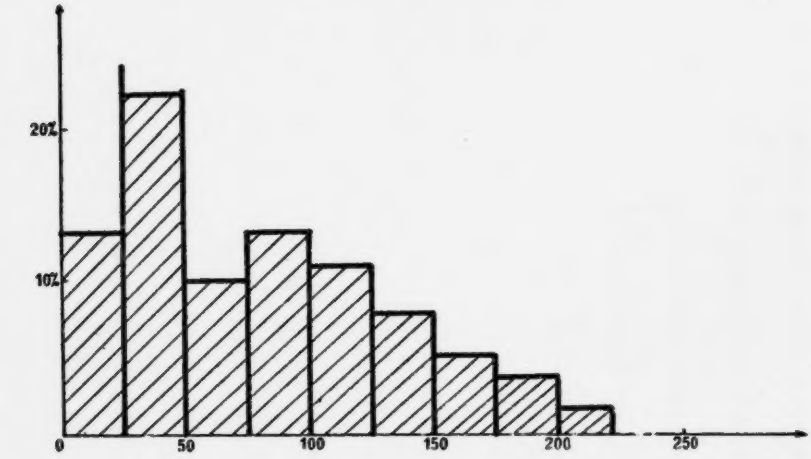

Hourly Rates

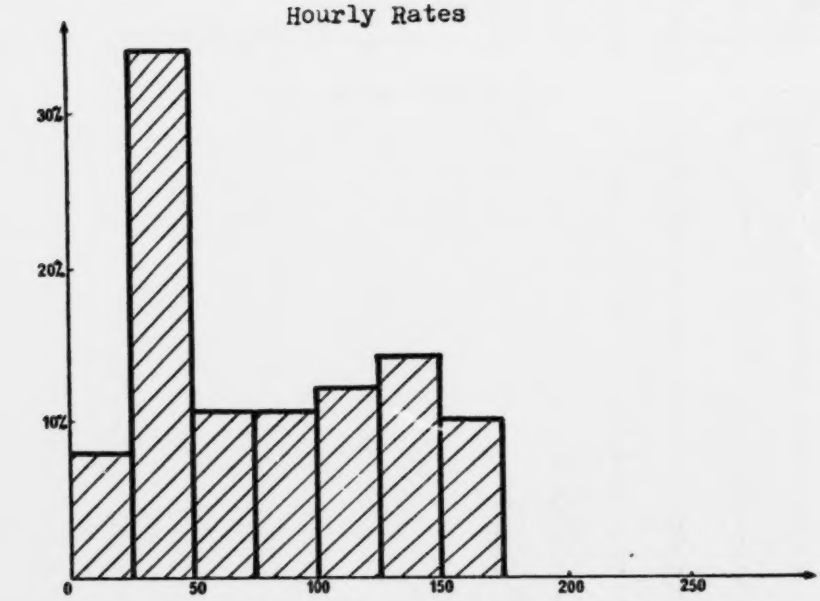

Four Hours Rates

Figure 2-bis - Acidity Histograms

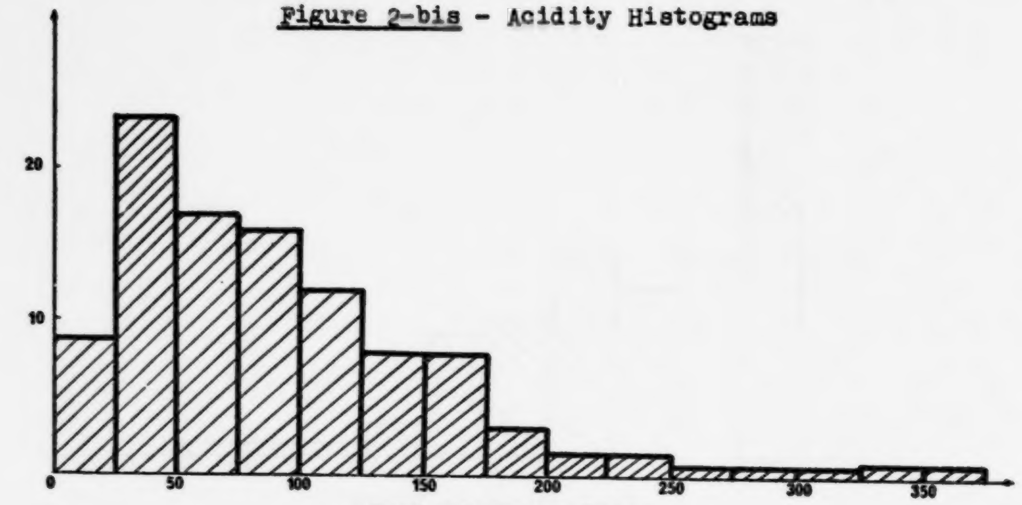

Instantaneous Rates

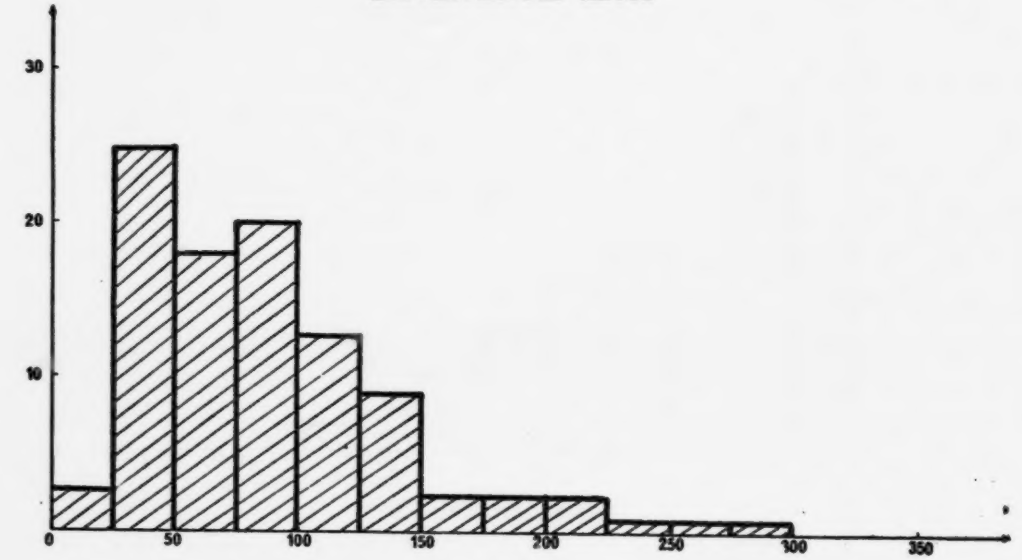

Hourly Rates

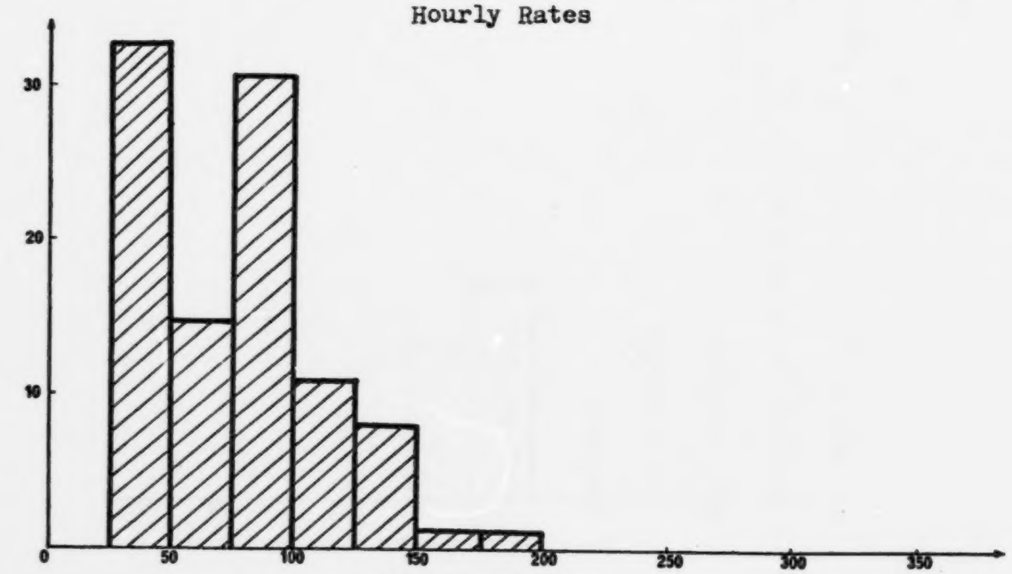

Four Hour Rates

may be. So, the stationary hypothesis holds.

- Histograms are plotted on Figure 2. For the two pollutants, a lognormal fit would be realistic for instantaneous data, but would become inaccurate for hourly or four-hour averaged data. Besides, these visual remarks are corroborated by the shape and the analytic expansion of the Gaussian transformation, which becomes very different from an exponential as the length of time averaging increases.

- Cross correlations between the two series are asymetric. Inside a lag of six hours, correlations decrease from .6 to .5 when SO_2 follows NO_x, and from .6 to .3 when NO_x follows SO_2.

IV-2 - RELATIONSHIPS BETWEEN METEOROLOGICAL DATA AND POLLUTION LEVELS.

These relations are similar for NO_x and SO_2. So we limit the presentation to the results concerning NO_x. The main explicative variables are wind, temperature and prèssure. The plottings on Figure 3 give the evolution of NO_x with these variables. Except for the wind speed, the evolutions are not linear at all, so that a simple correlation analysis would fail. A very synthetic descriptive output - the simultaneous representation of the first two pairs (φ^I, φ^J) of factors (see Appendix II) is given on Figure 4. We may interpret it as follow : meteorological conditions are settled down round pollution levels which generally follow them. Let us take some examples.

- In these data, a level lower than 60 $\mu g/m^3$ often occurs when the wind speed is greater than 3 m/s, when pressure is around 990 mb, and when temperature is greater than 3° C. On the contrary, when it freezes, when pressure exceeds 1005 mb, when there is no wind, the pollution levels may exceed 130 $\mu g/m^3$. Medium levels are obtained for a very low pressure, for medium wind and especially when hygrometry is between 90 and 95. A lower hygrometry generally leads to higher levels, a greater one to lower levels. Let us stress the fact that these conclusions hold for that particular area during four days of winter : they do not claim to be general.

Now, given meteorological conditions, we can set a corresponding "meteorological point" by taking the center of gravity

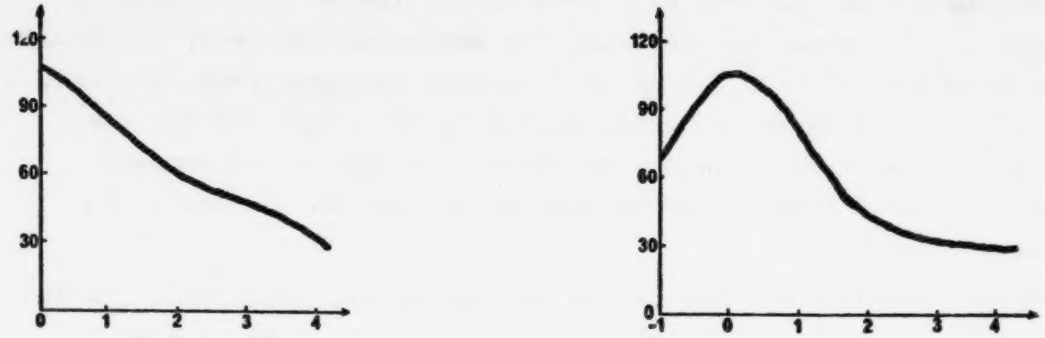

Wind Velocity

Radial Wind Component

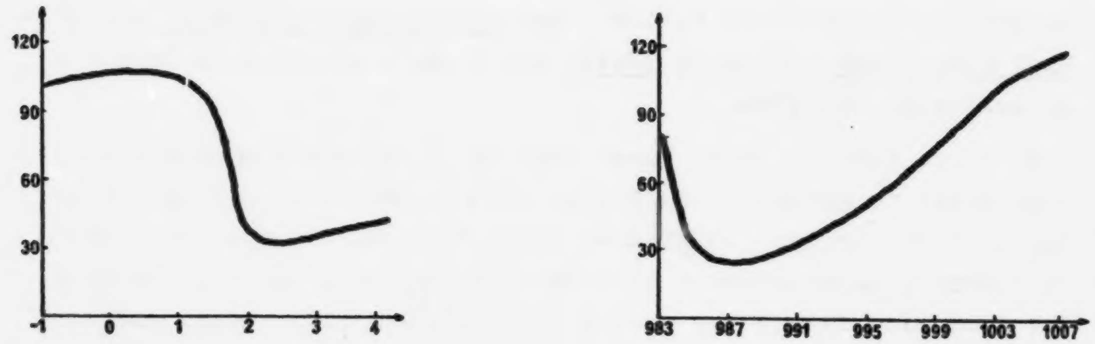

Temperature

Pressure

Figure 3 - Evolution of NO_x with major meteorological variables.

Figure 4 - First Factorial Plan

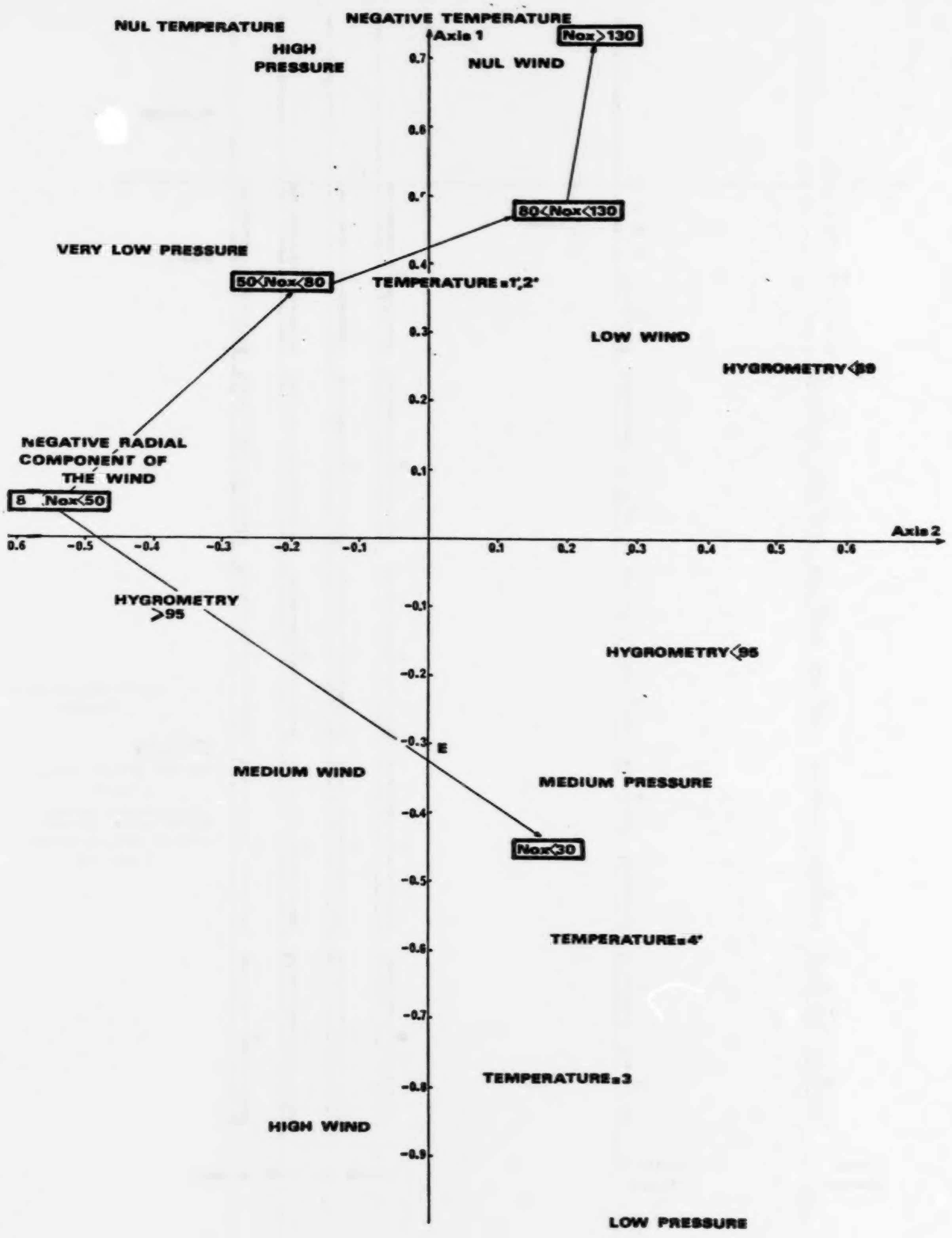

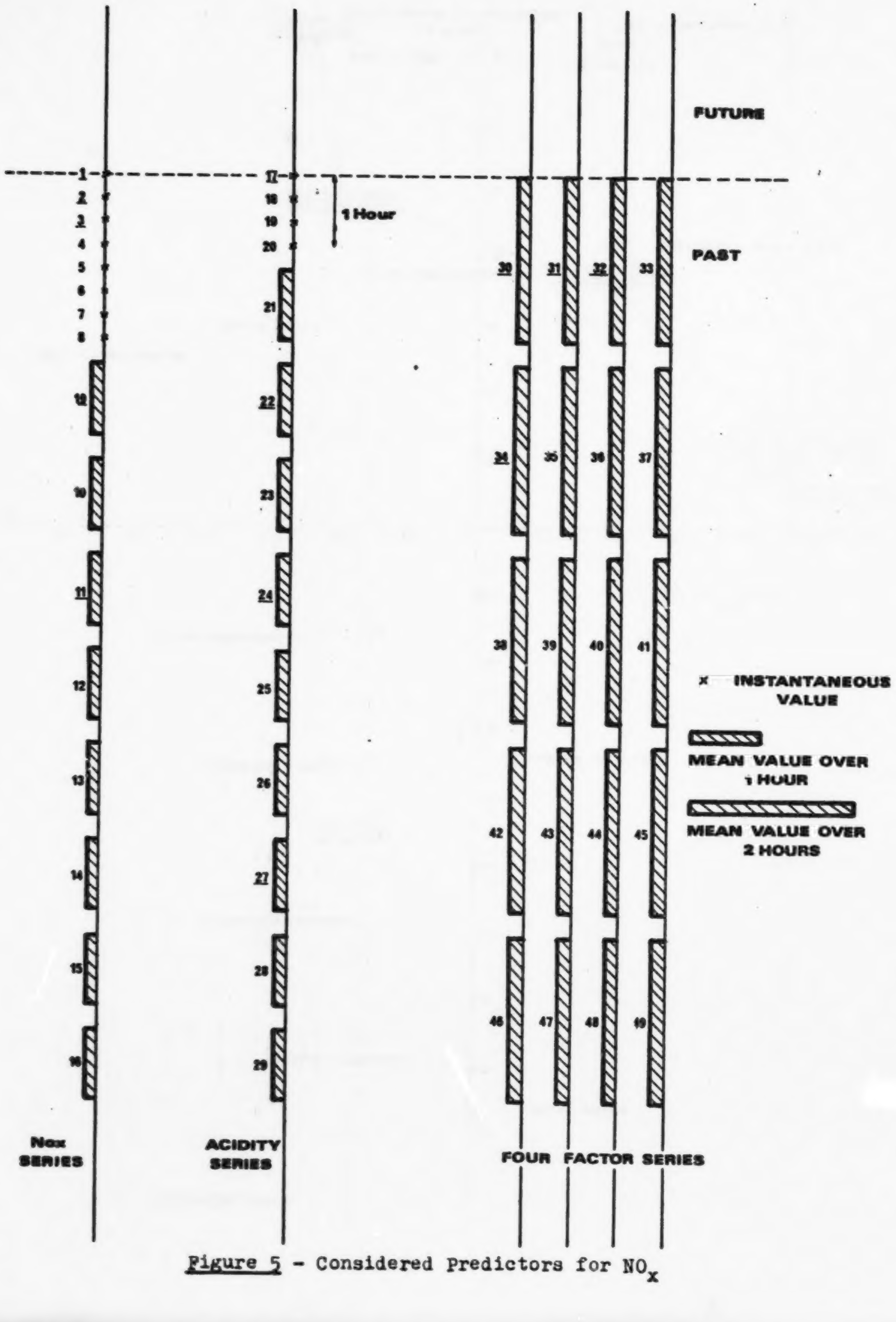
FUTURE
PAST
1 Hour
1
2
3
4
5
6
7
8
9
10
11
12
13
14
15
16
17
18
19
20
21
22
23
24
25
26
27
28
29
30
31
32
33
34
35
36
37
38
39
40
41
42
43
44
45
46
47
48
49
x INSTANTANEOUS VALUE
MEAN VALUE OVER 1 HOUR
MEAN VALUE OVER 2 HOURS
Nox SERIES
ACIDITY SERIES
FOUR FACTOR SERIES

Figure 5 - Considered Predictors for NO_x

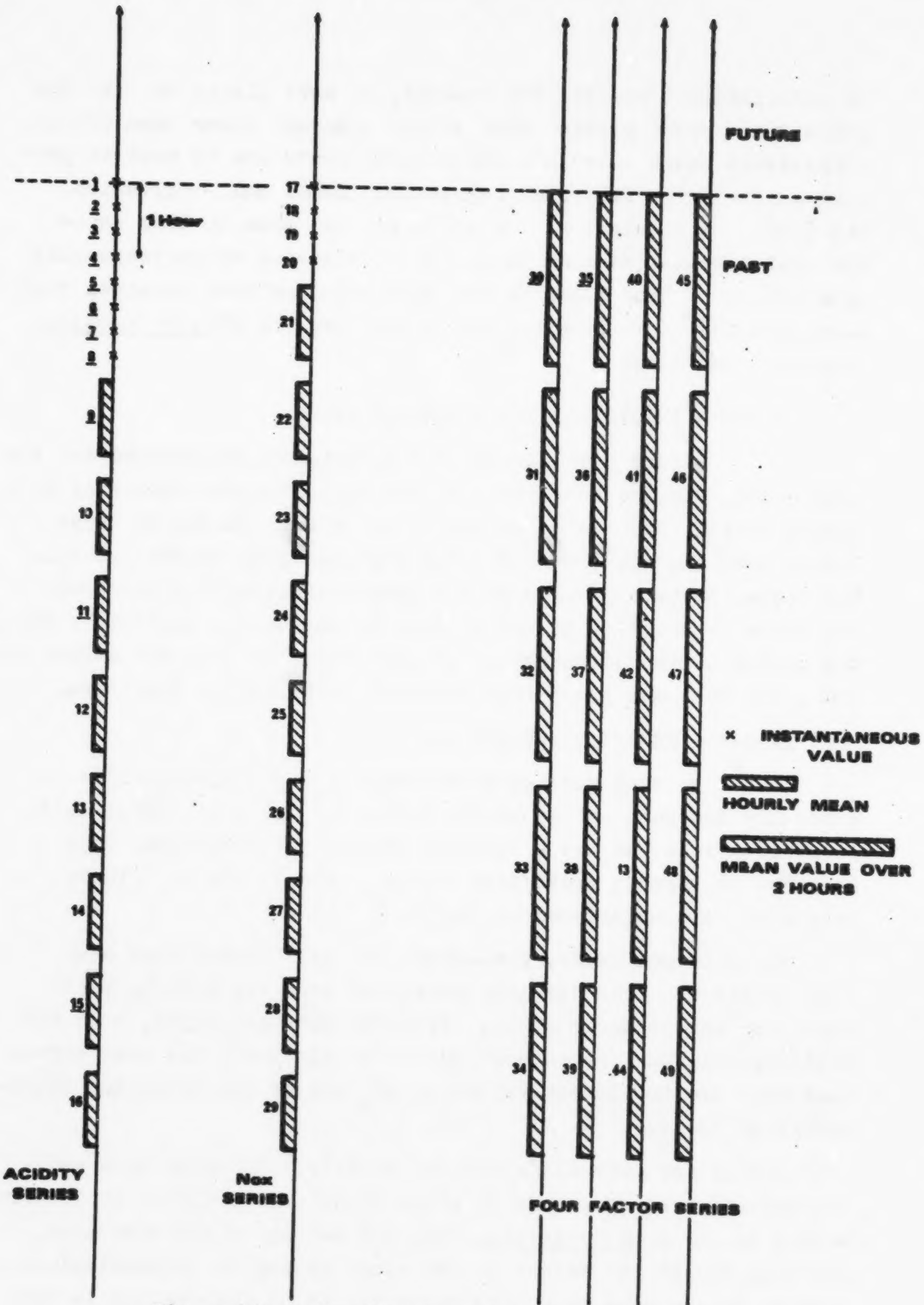
FUTURE
PAST
1 Hour
1
2
3
4
5
6
7
8
9
10
11
12
13
14
15
16
17
18
19
20
21
22
23
24
25
26
27
28
29
30
31
32
33
34
35
36
37
38
39
40
41
42
13
44
45
46
47
48
49
ACIDITY SERIES
Nox SERIES
FOUR FACTOR SERIES
× INSTANTANEOUS VALUE
HOURLY MEAN
MEAN VALUE OVER 2 HOURS

__Fig. 5 bis__ - Considered Predictors for Acidity of the different events. For example, we have placed in E the point "wind speed greater than 4 m/s, pressure lower than 987 mb, temperature equal to 1° C". These settlements can be used to perform a non-linear factorial regression (named Ball-regression, see [12]), or simulation). We shall not use them in this sense, but just compute, at each time, the coordinates of corresponding meteorological conditions on the main axis. We have retained four axes, and the corresponding time series are the factor functions presented in III-2.

IV-3-1 - PREDICTORS UNDER CONSIDERATION

Figure 5 summarizes the information considered for the prediction. For the near past, we use instantaneous values of pollution levels. For the older past, we use mean values of these levels over one hour. We limit the explored past to the previous ten hours. We have previously averaged meteorological data over two hours : according to the scheme, we may use 16 predictors from the series of the pollutant to be predicted, 13 from the series of the other one, and 4 × 5 from meteorological factor functions.

IV-3-2 - SELECTED PREDICTORS

We thus have 49 predictors at our disposal. This is generally too much and we prefer to select the most useful ones. To achieve this, we use a STEPWISE-REGRESSION technique. This leads us to keep 13 predictors for NO_x, and 17 for SO_2 (these predictors are underlined on Figure 5).

For Nitrogen Oxyds, predictors are well distributed over time (seven are from the near past, six from the further past) and according to their nature (five for Nitrogen Oxyds, four for acidity, and four for meteorological conditions). The most important ones are the latest values of NO_x and of the first two meteorological factors.

Things are very different for acidity : the near past and the acidity series are now of prime importance : eleven predictors belong to the Acidity Series, fourteen belong to the near past, and only two of the selected predictors belong to Meteorological series. We are here in a case where the total information is synthetized by the near past of the Time Series itself.

IV-3-3 - EVALUATION OF THE STATISTICAL MODEL

We now compare the ALERTE-predicted values P_{t_i} to the real ones R_{t_i}.

- For the levels, the usual criterion is the variance of the estimation.

$$V = \frac{1}{N} \sum_{i=1}^{i=N} (R_{t_i} - P_{t_i})^2$$

We have to compare the estimation variance with those obtained from simpler statistical models. Let us define :

- VAP : A priori variance : the estimator is the mean value M of the series.
- VM : MARKOV hypothesis variance : the estimator is the latest known value of the pollutant.
- VPP : Pseudo-permanence hypothesis variance : the estimator is an optimal combination of the mean value M and of the latest known value.
- VAT : Autoregressive model variance : the estimator is an optimal combination of the previous ten known values. Table 1 summarizes all these variances :

	VAP	VM	VPP	VAT	V
NO_x	4288	2123	1969	1686	840
SO_2	3842	3248	3084	1754	1305

It appears clearly that D.K. estimators are more precise than all the others. The average error is 29 $\mu g/m^3$ for NO_x , 36 $\mu g/m^3$ for SO_2 (against 41 $\mu g/m^3$ and 42 $\mu g/m^3$ for the autoregressive model). The benefits of using D.K. are greater for NO_x - because meteorological data are valuable - than for SO_2 (where meteorological data are useless).

But these estimations are not our main purpose. Over all; we want to be able to predict whether the future level will be greater than a given threshold or not. We have chosen a threshold equal to

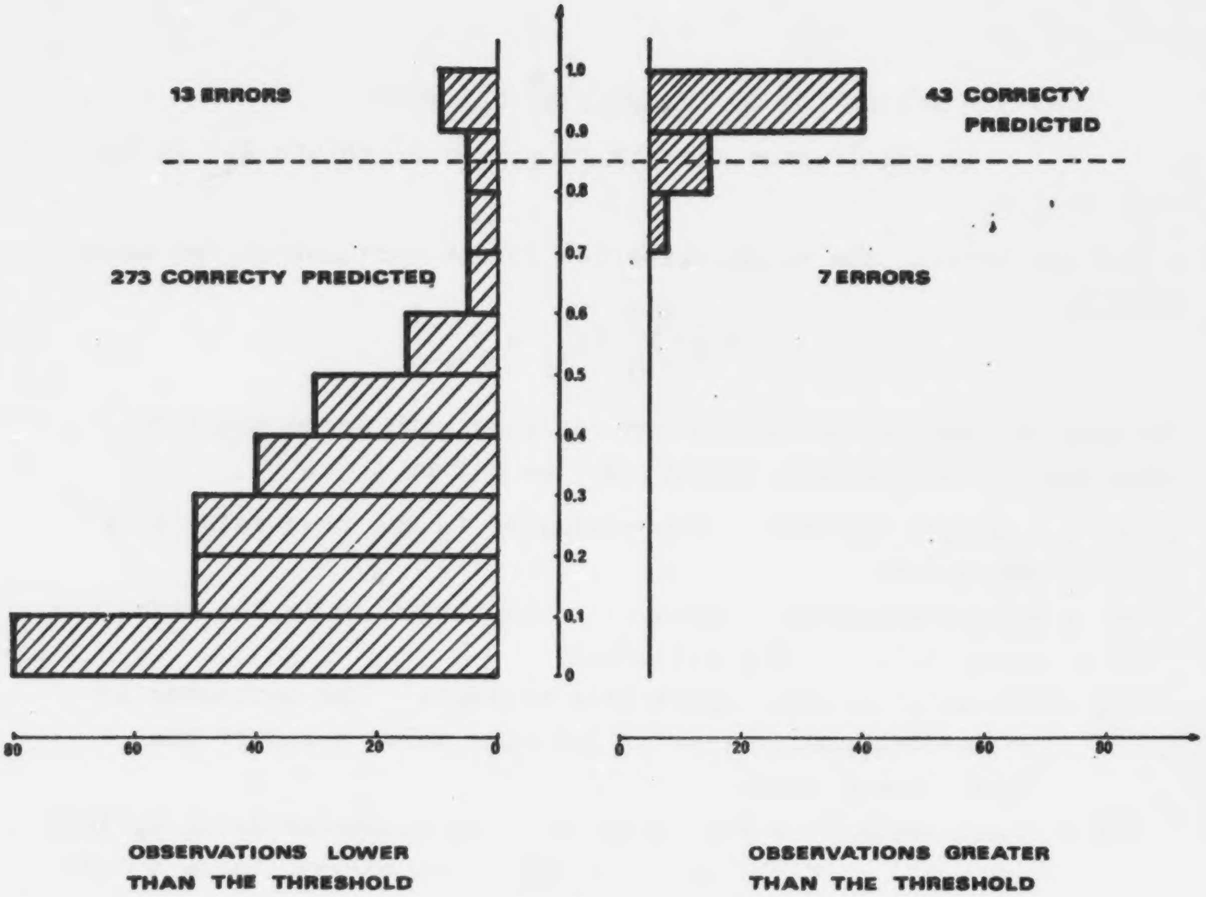

NITROGEN OXYDS

IN THIS CASE THE DISCRIMINATION IS EXCELLENT

RATE OF ERROR : 5.9 %

Figure 6

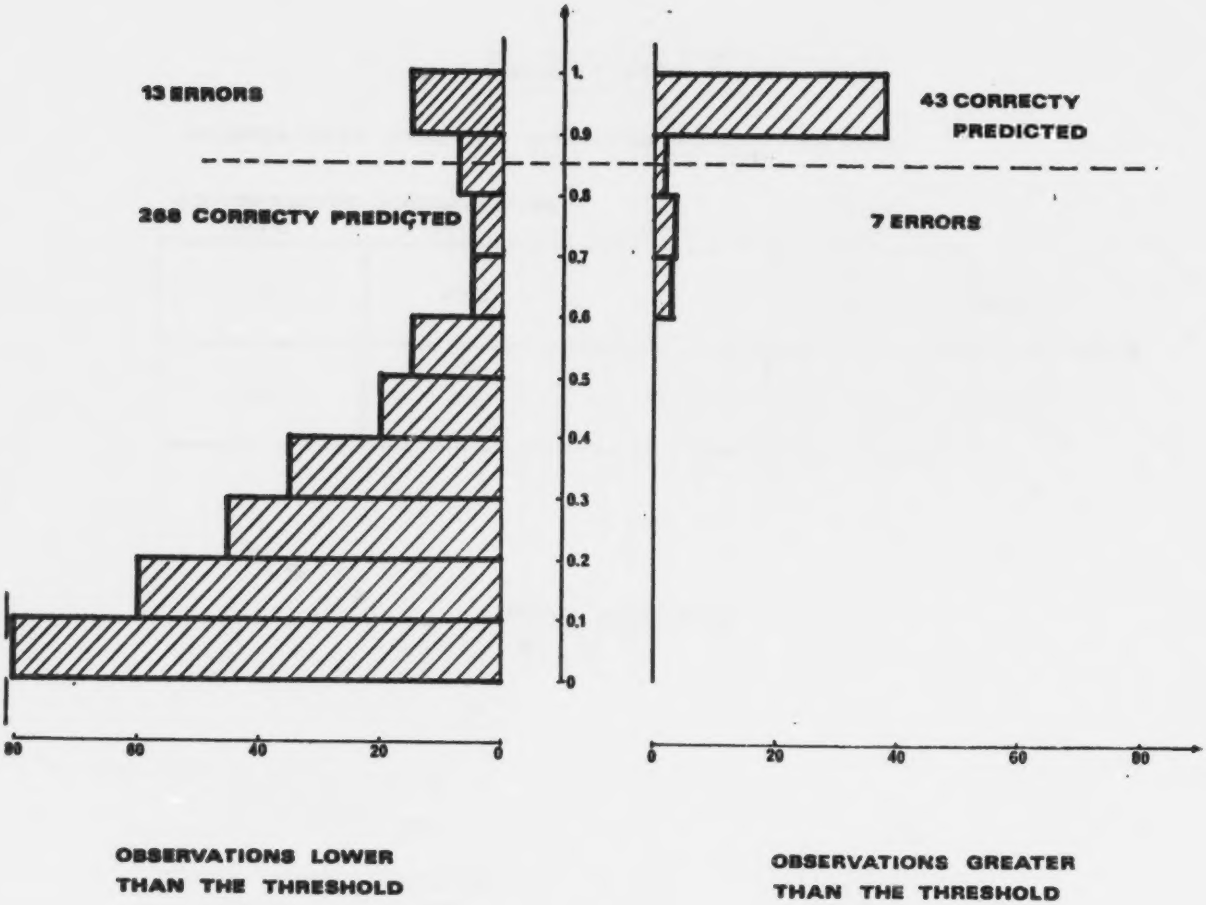

ACIDITY

IN THIS CASE THE DISCRIMINATION IS GOOD

RATE OF ERRORS : 7.4%

Figure 6 bis

NEXT HOUR PREDICTIONS

A COMPARAISON BETWEEN D.K. AND PERMANENCE

		D.K. <140	D.K. >140	PERMANENCE <140	PERMANENCE >140
REALITY	<140	273	13	257	2
	>140	7	43	25	25

NITROGEN OXYDS

		D.K. <140	D.K. >140	PERMANENCE <140	PERMANENCE >140
REALITY	<140	268	18	237	49
	>140	7	43	22	28

ACIDITY

TABLE 7

140 $\mu g/m^3$ for NO_x , 140 $\mu g/m^3$ for SO_2 . DK allows the estimation of the function, which is zero if the level is lower than the chosen threshold, one if the level is greater. D.K. estimators run from zero to one. The higher the estimator, the higher is the risk of exceeding the level. On Figure 6, we have separated the cases where the real, future value (unknown at the time of the prediction) is lower than the threshold from the others. We know that the threshold is exceeded (either for NO_x or SO_2) 15% of the time. So the decision rule is the following : define x so that (o,x) contains 85% of the estimated values. We decide that there is no risk if the predictor p^* belongs to (o,x), and we decide on a "warning" if p^* belongs to (x,1). The results of the estimation for the following hour are summarized in Table 7, and for the hour after in Table 8. We fail in our estimation in two cases : either we predict problems and there is no problem, or we predict a normal situation and the threshold is exceeded. Over 336 predictions, we have failed 20 times for NO_x, 25 times for SO_2 for the next hour prediction, so that the error rates are respectively 5.9% and 7.4%. If we just assume a permanence rule (the next hour level will be greater than the threshold if and only if the latest one was greater), the error rates are respectively 16% and 21% ! For the hour after, D.K. rates are 8.4% and 13.1% (against 24% and 33%).

So the use of elaborated statistical methods permits us to reduce in great proportions the mistakes in our previsions.

V - CONCLUSION

D.K. and the ALERTE package may be good tools for supplying us with efficient short-term predictions, even when physical, chemical and meteorological phenomenae are not well known in the studied area. The reduction of the error rates in Alarm decisions will be of prime importance when a great number of networks are running. We do hope that efficient, fast, and automatic statistical methods will contribute to achieve this purpose.

APPENDIX I : DISJUNCTIVE KRIGING

A-I-1 - THEORETICAL BACKGROUND : HILBERT SPACES GENERATED BY RANDOM VARIABLES AND CLOSED SUBSETS.

Denote (X_i, i = 1,p) as the set of real-valued predictors considered as random variables, X a variable to be predicted, $F(dx_1, dx_2, \dots dx_p, dx)$ as the associated (n+1) distribution law, $F^*_p(dx_1, dx_2, dx_p)$, $F_{ij}(dx_i\ dx_j)$ $F_i(dx_i)$ as the marginal laws associated with the unknown variable and one predictor, and finally F(dx) as the marginal law associated with the unknown variable.

Let us now define some Hilbert spaces built upon $(X_1, X_2, \dots X_n, X)$ with the norm of mathematical expectations : the scalar product $< X_i\ X_j >$ is $E(X_i\ X_j) = \int x_i\ x_j\ F_{ij}(dx_i\ dx_j)$.

- H (resp. H_p)* : general Hilbert space associated with all the measurable square integrable functions :

$$H = \left\{ f(X_1, X_2, \dots X_p, X) \mid E(f^2) < \infty \right\}$$

$$H_p = \left\{ f_p(X_1, X_2, \dots X_p) \mid E(f_p^2) < \infty \right\}$$

- D (resp. D_p) : Disjunctive Hilbert space defined as follows :

$$D = \left\{ f(X) + \sum_{i=1}^{i=p} f_i(X_i) \mid E\ f^2 < \infty\ ,\ \forall\ i\ E\ f_i^2 < \infty \right\}$$

$$D_p = \left\{ \sum_{i=1}^{i=p} f_i(X_i) \mid \forall\ i\ \ E\ f_i^2 < \infty \right\}$$

- L (resp. L_p) : linear Hilbert space generated by linear combinations.

$$L = \left\{ \Sigma\ a_i\ X_i + d\ X \right\}$$

$$L_p = \left\{ \Sigma\ a_i\ X_i \right\}$$

Clearly, L (resp. L_p) is included in D (resp. D_p) which is included in H (resp. H_p), and any p indexed space is included and topologically closed in the non-indexed corresponding space. So the problems of optimal estimation are solved by orthogonal projection in the framework of HILBERT's geometrical theory. Let us relate these spaces to well-known statistical methods :

---

* - In the following, p stands for predictors.

- The Regression Domain (Multivariate Regression, Autoregressive processes, BOX and JENKINS' ARIMA models, MATHERON's Simple Kriging) is related to projections from L (or a part of L) upon L_p. For the estimators to be efficient, both the underlying structure and the nature of the problem must be linear. The only prerequisite is the estimation of a covariance matrix : statistical inference is very simple.

- The Conditional Expectation Domain refers to projections from H upon H_p. It is theoretically the best way for building optimal estimators. But the prerequisite (knowledge of the joint distribution of (p+1) variables) is beyond the reach of a serious statistical inference, as soon as p is greater than 3. The attempts to go around this difficulty in the framework of H space - by assuming that the joint distribution is Gaussian or lognormal for example - are generally arbitrary, simply because we cannot test the hypothesis on available data. In fact, the space H_p is really too large and too rich for us to expect good estimations.

On the contrary, the spaces D and D_p enjoy good properties : they enable us to carry out non-linear estimations in reasonable conditions for statistical inference.

A-I-2 - DISJUNCTIVE KRIGING : THE THEORETICAL POINT OF VIEW.

We want to predict f(X) when $(X_1, X_2, \dots X_p)$ are given. We look for the estimator in the class of disjunctive estimators

$$f^* = \sum_{j=1}^{j=p} f_j(X_j)$$

The optimal one satisfies the orthogonality condition :

$$f(X) - f^* \perp D_p(X_1, \dots X_p) \qquad (1)$$

As $D_p(X_1, X_2, \dots X_p)$ is generated by $\cup D_j(X_j)$, it is sufficient to impose :

(1') $$\forall i \quad f(X) - f^* \perp D_i(X_i)$$.

Numerically we obtain :

(1") $$\forall i, \forall h(X_i) \in D_i(X_i) :$$

$$\int f(x)\, h(x_i)\, F_i\,(dx, dx_i) = \sum_j \int f_j(x_j)\, h(x_i)\, F_{ij}\,(dx_i, dx_j)$$

Clearly, this system takes into account only bivariate laws, which are accessible to statistical inference. However, we should have some trouble solving this integral system just as it is ! In such cases, the natural mathematical process is spectral decomposition of complex spaces into much simpler ones.

A-I-3 - A SPECTRAL DECOMPOSITION ASSOCIATED WITH ISOFACTOR SCHEMES.

Let (Y_0, Y_1, Y_2, Y_p) be a set of random variables satisfying the two conditions :

(2) - All of them admit the same distribution : $\forall i \quad F_i(dy) = F(dy)$

(3) - The bivariate laws admit the decomposition :

$$F_{ij}(dy_i\; dy_j) = F(dy_i)\, F(dy_j) \sum_{k\geq 0} T_{ij}^{(k)}\, H_k(y_i)\, h_k(y_j)$$

where, for all i, $H_k(Y_i)$ is an orthogonal basis of the space $D(Y_i)$. Several such bases are well known ; for example :

- HERMITE POLYNOMIALS ASSOCIATED WITH GAUSSIAN KERNELS

Definition : $$H_n(y)\, e^{-y^2/2} = \frac{d^n}{dy^n}\, e^{-y^2/2}$$

Recurrence : $H_0(y) = 1$; $H_1(y) = -\, y$; $H_{n+1}(y) = -y\, H_n(y) - n\, H_{n-1}(y)$

- LAGUERRE POLYNOMIALS ASSOCIATED WITH GAMMA KERNELS

Definition : $$L_n(y)(-1)^n\, n!\; y^{\alpha-1}\, e^{-y} = \frac{d^n}{dy^n}\, y^{n+\alpha-1}\, e^{-y}$$

- LEGENDRE POLYNOMIALS are associated with uniform laws.

A set of variables satisfying (2) and (3) is called an isofactor scheme.

Denote D (resp. D_p) the disjunctive space associated with $(Y_o, Y_1, \ldots Y_p)$ (resp. $Y_1 \ldots Y_p$) and, for each k, D^k (resp. D_p^k) the space generated by the family $(H_k(Y_o), H_k(Y_1), \ldots H_k(Y_p))$ (resp. $H_k(Y_1), H_k(Y_2), \ldots H_k(Y_p)$).

It follows from (3) :

$$\forall\, k \neq k' \quad D^k \perp D^{k'} \quad ; \quad D_p^k \perp D_p^{k'}$$

$$D = \oplus\, D^k \quad ; \quad D_p = \oplus\, D_p^k$$

(where the symbol $\oplus$ denotes the direct sum of the spaces).

A-1-4 - THE GENERAL CASE FOR DISJUNCTIVE KRIGING : TRANSFORMATION TECHNIQUES.

We use transformation techniques (see III-1-2) to reduce a general D.K. problem to an isofactor D.K. problem. To the experimental set of variables $(X_o, X_1, \ldots X_p)$, we associate, by a set of appropriate one-to-one transformations A_o, a set of variables $(Y_o, Y_1, \ldots Y_p)$ admitting the same distribution $F_i = F$. Then we look for a close isofactor model, that is, we compute the experimental family $T_{ij}^{(k)}$ and fit it to a known model. For our study, we used a Gaussian Kernel with Hermite polynomials. If we denote ρ_{ij} the correlation between Y_i and Y_j, we chose the model $T_{ij}^{(k)} = \rho_{ij}^k$, corresponding to the hypothesis that all the bivariate laws are Gaussian. All the results are computed on the new variable Y_o and are extended to X_o through the transformation $X_o = A_o(Y_o)$ and its expansion $\sum_n A_o^{(n)} H_n(Y_o)$ upon the Hermite basis.

Denote $E(X|Y)$ the Conditional Expectation of X, given Y : clearly, from (3) :

$$E(H_k(Y_i)|Y_i) = T_{ij}^k\, H_k(Y_j)$$

So the spaces D^k are stable under the operation of conditional expectation. Under these conditions, the D.K. system is very easy to solve : we want to estimate $g(Y_o)$, using the information $(Y_1, Y_2, \ldots Y_p)$.

- We expand $g(Y_o)$ on the orthogonal basis :

$$g(Y_o) = \sum_k g^{(k)} H_k(Y_o)$$

- $H_k(Y_o)$ is orthogonal to any space $D_p^{k'}$ for $k' \neq k$. So the orthogonal projection of $H_k(Y)$ upon D_p belongs to D_p^k. Then the optimal estimator H_k^* is a linear combination $\sum_i \lambda_k^i H_k(Y_i)$ satisfying :

$$H_k(Y_o) - H_k^* \perp D_p^k$$

Explicitly :

$$\boxed{\forall\, i \quad \sum T_{ij}^{(k)} \lambda_k^j = T_{oi}^{(k)}}$$

This is an ordinary regression system.

- The D.K. estimation of $g(Y_o)$ is given by :

$$g(Y_o) = \sum g^{(k)} H_k^*$$

REMARK

For all the usual laws, the series $(T_{ij}^{(k)}, k = 0 \rightarrow \infty)$ vanish quickly to zero, so that we have to solve only very few systems (generally five or six, sometimes ten). When the appropriate number of systems is solved, we may estimate any function $g(Y_o)$, and especially the thresholding functions, the value of which is 0 if Y is lower than s, 1 if Y is greater.

APPENDIX II : CORRESPONDENCE ANALYSIS

A-II-1 - THE MATHEMATICAL PROBLEM AND ITS SOLUTION.

Let $(f_{ij})_{\substack{i\in I\\ j\in J}}$ be a bivariate discrete distribution.on a set I × J. Denote $f_{i.} = \sum_j f_{ij}$ and $f._j = \sum_i f_{ij}$ the corresponding marginal laws. We want to find a pair of functions (φ^I on the first set, ψ^J on the second one) whose correlation is maximum. For example, the first set can be associated with the levels of Nitrogen Oxides, the second one to measures of temperature, and f_{ij} is the probability that the pollutant belongs to an interval $B_i = (b_i, b_{i+1})$ and that, simultaneously, temperature belongs to $A_j = (a_j, a_{j+1})$. Mathematical analogy with canonical analysis is very strong, as the analytic formulation of the problem is :

Find ψ^I, ψ^J so that

(1) $< \varphi^I, \psi^J > = \sum_{i,j} f_{ij} \varphi^I \psi^J$ is maximum under the conditions

$$\|\varphi^I\|^2 = 1 \quad : \quad \sum f_{i.} (\varphi^i)^2 = 1 \tag{2}$$

$$\|\varphi^J\|^2 = 1 \quad : \quad \sum_j f_{.j} (\psi^j)^2 = 1 \tag{3}$$

LAGRANGE's formalism leads us to solve simultaneously :

$$\forall\ j : \sum_i f_{ij} \varphi^i = a\, f_{.j} \psi^j \tag{4}$$

$$\forall\ i : \sum_j f_{ij} \varphi^j = b\, f_{i.} \varphi^i \tag{5}$$

Because of conditions (2) and (3), we have :

$$a = b = \text{Max} < \varphi^I, \psi^J >$$

We obtain the sought-for functions φ (resp. ψ) by extracting ψ from (4) (resp. φ from (5)) and reporting in (5) (resp. (4)) :

$$\forall\ j \quad : \sum_{ij'} \frac{f_{ij}\, f_{ij'}}{f_i\, f_j} \psi^{j'} = a^2 \psi^j$$

$$\forall\, i \;:\; \sum_{ji'} \frac{f_{ij}\, f_{i'j}}{f_i\, f_j}\, \varphi^{i'} = a^2\, \varphi^{i}$$

The pairs (a,φ) and (a,ψ) are eigenvalues and eigenvectors of two corresponding square matrices. The i^{th} solution of the problem is the triplet $(a\varphi,\psi)$ associated with the i^{th} eigenvalue (in decreasing order).

A-II-2 - THE EXTENSION OF THE METHOD AND APPLICATION TO THE POLLUTION PROBLEM.

It is easy to extend correspondence analysis to a family of bivariate distributions $(f_{IJ_1}, f_{IJ_2},\ldots f_{IJ_n})$ where the first set is always the same. For us, I will always be a set associated with pollution levels. The family of the second sets will represent all the available meteorological data. In this way, we may extract from the meteorological information the part which really influences pollution levels : this part is synthetized by the first two, three, four or more factors ψ^J.

BIBLIOGRAPHY

[1] BENZECRI - L'Analyse des Données, Tome 2 - Dunod, Paris, 1973

[2] BLOOMFIELD - Fourier analysis of Time Series - Wiley and Sons, New York, 1976

[3] DELFINER, CHILES, DELHOMME - Presentation du Programme BLUEPACK - Internal Report, Centre de Géostatistique.

[4] DUMAY - Etude de l'influence du phénomène météorologique sur la pollution par analyse des correspondances. Internal Report - Centre de Géostatistique.

[5] LARSEN - Calculating air quality and its control. 1965 APCA XV, 12.

[6] LARSEN - A new mathematical model of air pollutant concentration. 1969 AOCA XIX-1.

[7] MATHERON - The theory of intrinsic random functions. 1972.

[8] MATHERON - La Théorie des Variables Régionalisées et ses Applications. Cahier C.M.M. N° 5, 1971.

[9] MATHERON - A simple substitute for conditional expectation : the disjunctive kriging. NATO A.S.I. "Geostat 75" Rome, 1975.

[10] MATHERON - The transfer functions and their estimation. NATO A.S.I. "Geostat 75", Rome, 1975.

[11] ORFEUIL - L'Analyse des Données.- Internal Report, Centre de Géostatistique.

[12] ORFEUIL - Etude, mise en Oeuvre et test d'un modèle de prédiction à court terme de pollution atmosphérique. Internal report, Centre de Géostatistique

[13] ORFEUIL - Etude par analyse des données de la structure de la haute atmosphère terrestre. Thèse de Doctorat, Paris, 1976.

[14] ORFEUIL - Géostatistique et Analyse des Données. NATO A.S.I. "Geostat 75", Rome, 1975.

152

8th International Technical Meeting on
Air Pollution Modeling and its Application

UNIVARIATE STOCHASTIC MODELS AND REAL TIME PREDICTORS OF DAILY SO_2 POLLUTION IN MILAN

by

G.FINZI, G.FRONZA, A.SPIRITO

Istituto di Elettrotecnica ed Elettronica - Centro Teoria
Teoria dei Sistemi CNR - Politecnico di Milano, Milan, Italy

September 20-23, 1977
Louvaine-La-Neuve
Belgium

1. INTRODUCTION

In order to fit time series of pollutant concentrations, a certain number of stochastic models of the ARIMA (AutoRegressive Integrated Moving Average) type have been proposed in the literature [1] - [4]. In accordance with the techniques illustrated in [5], such models can be suitably used for real time forecast, namely for predicting future concentration levels on the basis of the data recorded up to the present.

The ARIMA type representations can be considered as simplified mathematical descriptions of the pollution phenomenon, if compared with another class of stochastic models [6]-[8]. Specifically, such models are derived by turning the numerical solution of the advection-diffusion partial differential equations (the Carlson-Crank-Nicholson scheme, for example) into a set of stochastic relationships via the addition of an error term (noise), accounting for all the inaccuracies of the representation (mainly due to the uncertainties in the evaluation of the diffusion parameters, meteorological variables, emission and boundary conditions). The predictors, derived from this second class of models through Kalman filtering techniques, exhibit a higher degree of reliability than the ARIMA ones, though they require a much heavier computational effort.

Actually, a comparison in terms of forecast efficiency is not fully significant, since the required information, i.e. the predictor input is not the same in the two cases.

First, in [1]-[4] the exploitation of the available data is not complete. In fact, the concentration sequences in the monitoring stations are considered as separate time series (in practice, as independent stochastic processes) and correspondingly the forecasts are made separately, thus losing all the information supplied by the cross correlations. An alternative approach obviously consists of setting up a multivariate ARIMA model and predictor of the vector of concentrations in all the stations. Or, if only an overall description of the pollution phenomenon is required, it is again possible to deal with a univariate stochastic model by considering a weighted spatial average of the station measurements (as done in the present analysis).

Another basic difference between the two above mentioned classes of predictors is due to the circumstance that no physical factor (meteorology adn emission) is used as input in [1]-[4]. This causes the pronounced filtering effect usually exhibited by the ARIMA predictors, namely their unprecise forecast of rapidly increasing pollution peaks.

The possibility of improving the performance of ARIMA predictors by introducing meteorological inputs such as wind speed and direction has already been recognized in [9]-[10], where SO_2 concentrations in a region around a power plant in the Po Valley and in the city of Venice are respectively considered.

A similar analysis is carried out in the present paper with respect to SO_2 pollution in central Milan. Instead of wind speed and direction, here temperature and atmospheric stability "categories" are separately introduced into an AR(1) (autoregressive of order 1) model of the daily dosage area product or DAP. The DAP is proportional to the integral of the dosage over a certain region [11] and hence is an overall index, which simultaneously takes into account the pollution level, the duration of pollution events and the spatial extension of the pollution phenomenon. The method used for estimating the DAP from the point measurements supplied by ten monitoring stations is illustrated in Section 2. Different stochastic models of daily DAP are described in Section 3 together with the forecast performances of the corresponding predictors.

2. ESTIMATION OF THE DAP FROM THE STATION MEASUREMENTS

This paper considers SO_2 pollution in the central Milan area, denoted by $\mathcal{R}$ in Fig. 1, where also the locations of the ten monitoring stations are shown.

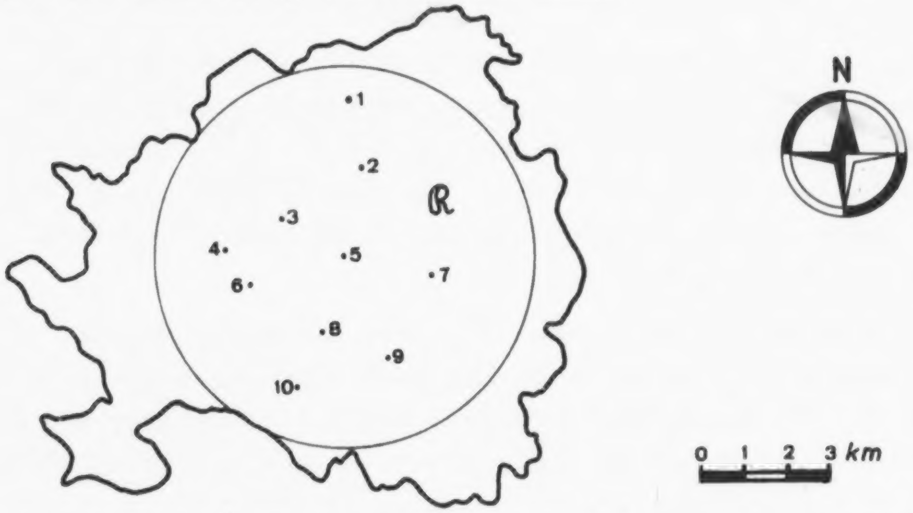

Fig. 1 Area $\mathcal{R}$ under consideration and monitoring stations.

The k-th day DAP over the region $\mathcal{R}$ is defined as

$$DAP(k) = \frac{1}{A.T} \int_{\mathcal{R}} dxdy \int_{(k-1)T}^{kT} c(x,y,t)dt \qquad k=1,2,... \qquad (1)$$

where

T = 1 day

$c(x,y,t)$ = pollutant concentration at point (x,y) at the instant t.

A = area of $\mathcal{R}$.

Alternatively, if the k-th day dosage

$$D(x,y,k) = \frac{1}{T} \int_{(k-1)T}^{kT} c(x,y,t)\,dt$$

is introduced, eq. (1) can be written as

$$DAP(k) = \frac{1}{A} \int_{\mathcal{R}} D(x,y,k)\ dxdy \qquad (2)$$

For each k, an estimation of the integral in eq. (2) must be carried out on the basis of the available concentration data, namely the set of the dosages $\left\{D_i(k)\right\}_{i=1}^{10}$ recorded in the monitoring stations. Such estimation can be made by means of the polygons method, which simply consists of the following procedure.

i) Divide $\mathcal{R}$ in ten subregions $\mathcal{R}_i$. The subregion $\mathcal{R}_i$ is defined as the locus of points in $\mathcal{R}$ for which the i-th station is the nearest station. Hence the boundary of $\mathcal{R}_i$ in the interior of $\mathcal{R}$ turns out to have a polygonal form.

ii) Compute the integral in eq. (2) by the approximation $D(x,y,k) \simeq D_i(k)$ for all $(x,y) \in \mathcal{R}_i$. Thus, if A_i denotes the area of $\mathcal{R}_i$, the DAP turns out to be a linear combination of the measurements in the monitoring stations :

$$DAP\ (k) \simeq \frac{1}{A} \sum_{i=1}^{10} A_i D_i(k)\ .$$

The above estimation procedure has been applied to the winter daily dosage data, corresponding to the periods October 15th 1975 - March 31st 1976 and January 24th 1977 - March 31st 1977. So a time series $\{\widetilde{DAP}(k)\}_{k=1}^{236}$ of estimated DAPs has been obtained. In order to check its reliability, the series has been compared with the one resulting from a different procedure. Precisely, the DAP estimation method described in [9] and based on the use of polynomial interpolating curves has been applied to the dosage data. The most important characteristics of the resulting series, namely its statistical parameters, haven't turned out to be significantly different from the ones previously obtained.

3. DAILY DAP MODELS AND PREDICTORS

The time series of 236 estimated DAPs, mentioned in the previous section, corresponds to periods which belong to the domestic heating season and can be approximately considered as homogeneous from the meteorological viewpoint . Hence it is reasonable to assume that $\{\widetilde{DAP}(k)\}_{k=1}^{236}$ is a (partial) realization of a stationary stochastic process $\{DAP(k)\}_k$. Such process has been identified through the following steps. (here only the 169 DAP data corresponding to the period October 15th 1975. March 31st 1976 have been taken into account, the remaining data have been used only for testing the predictor, as specified below).

a) By applying to the Kolmogorov - Smirnov test, the distribution of the process has turned out to be lognormal at more than 25% significance level. Hence $\{y(k)\}_k$, where

$$y(k) = \ln DAP(k), \tag{3}$$

has been considered as a normal process. Its (estimated) mean and standard deviation have respectively turned out to be $\mu_y = -1.823$, $\sigma_y = 0.564$.

b) The standardized normal process $\left\{x(k)\right\}_k$, where

$$x(k) = [y(k) - \mu_y] / \sigma_y , \qquad (4)$$

has been considered (its correlogram, namely its estimated autocorrelation function $r(\tau)$, is shown in Fig. 2) and three ARMA (=stationary ARIMA) models have been regarded to as possible representations of such process. Precisely, the AR(1), AR(2) and ARMA (1,1) model have been separately assumed and their parameters have been estimated.

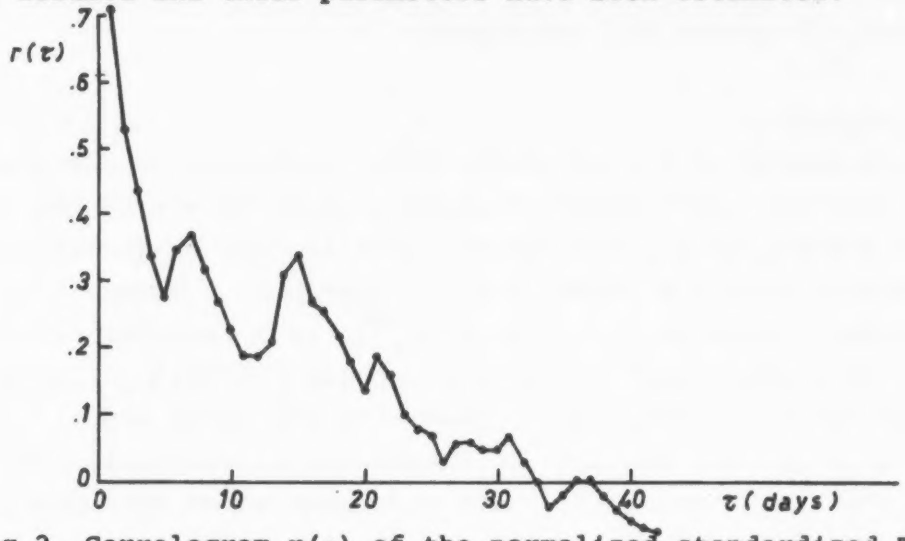

Fig.2 Correlogram $r(\tau)$ of the normalized standardized DAP process

c) The three models have been compared on the basis of the cumulative periodogram test [5]. The best fitting has turned out to be the one given by the AR(1) representation

$$x(k) = \phi x(k-1) + \varepsilon(k) \qquad (5)$$

where $\phi = 0.713$ and $\{\varepsilon(k)\}_k$ is a purely random process (white noise) with zero mean and standard deviation $\sigma_\varepsilon = \left[1-\phi^2\right]^{1/2} = 0.701$.

The predictor, derived by the overall model (3)-(5) simply consists of setting $\varepsilon(k)$ in eq. (5) to its expected value, namely zero. Precisely, the forecast of the k-th day DAP, made at the end of the (k-1)-th day, is given by the relationships

$$\hat{x}(k) = \phi\, x(k-1) \qquad (6)$$

$$\hat{DAP}(k) = \exp\left[\mu_y + \sigma_y \hat{x}(k)\right] \qquad (7)$$

where $\hat{}$ denotes a forecast value and $x(k-1)$ in eq. (6) must be regarded to as a datum, obtained via eqs. (3), (4) from the (k-1)-th DAP datum.

The predictor (6),(7) has been tested in correspondence with both the some period used for estimating the parameters of the model (3)-(5) and the remaining period (the overall result is shown in Fig. 3 , where the pairs "actual DAP-predicted DAP" are reported).

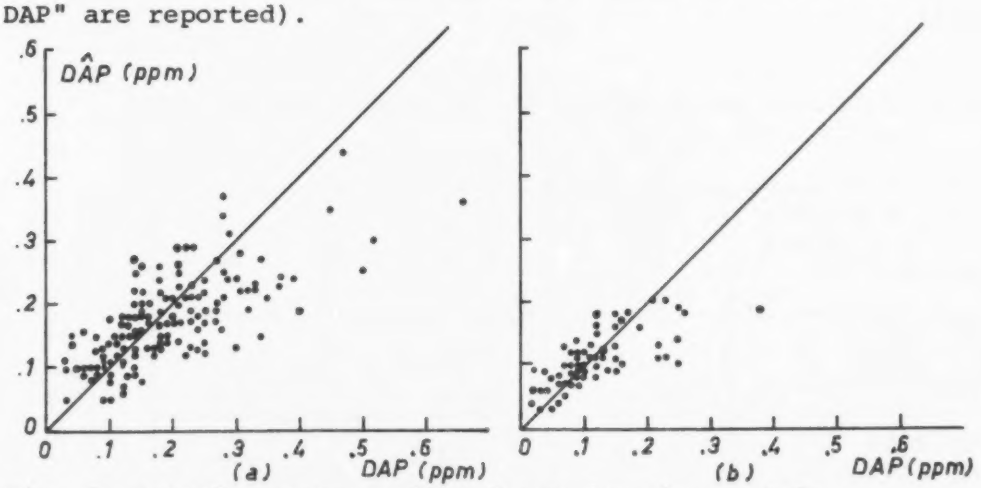

Fig. 3. Actual versus predicted DAP for the periods a) Oct.15th,75 - Mar. 31st 76; b) Jan. 24th, 77 Mar. 31st, 77

The forecast bias (=difference between the mean of the predicted DAP and the DAP mean $\mu = 0.188$) has turned out to be negligible. The performance of the predictor has been measured by three indexes:

I) The correlation θ between actual and predicted DAP.

II) The ratio σ_ε/μ between the standard deviation of the forecast error (equal to σ_ε, since there is no error bias) and the DAP mean.

III) The standard deviation σ_e of the forecast error during "episodes" (an episode has been defined as a period of days characterized by DAP (k) > $\mu + \sigma$ where σ = is the DAP standard deviation).

The results are reported in Table 1, where one of the σ_e is missing, since the corresponding number of "episode days" was not significant. Clearly, the performance does not significantly change when turning from the period used for estimating the parameters of the model (3)-(5) ("winter" 1975/76) to the other period (in "winter" 1976/77). This guarantees that the model (3)-(5) exhibits a satisfactory degree of reliability.

Table 1. Forecast performance of the predictor with no meteorological input

Forecast index / period	θ	$\frac{\sigma_\varepsilon}{\mu}$	σ_e
Oct.15th. 75 Mar.31st. 76	0.71	0.37	0.14
Jan.24th. 77 Mar.31st. 77	0.70	0.40	---

In order to improve the forecast performance, meteorological inputs have been introduced in the form of "categories" into the model (3)-(5).

A) The average daily temperature $T(k)$ has first been taken into account and its range has been subdivided into four regions, respectively corresponding to :
$T(k) \leq 1.6^{\circ}C$, $1.6^{\circ}C < T(k) \leq 4.5^{\circ}C$, $4.5^{\circ}C < T(k) \leq 10^{\circ}C$, $10^{\circ}C < T(k)$. So, four temperature categories have been defined. If $c(k)$ denotes the k-th day category, the following modifications have been introduced into eqs. (4)-(5):

$$x'(k) = \left[y(k) - \mu_y(c(k-1))\right] / \sigma_y\,(c(k-1)) \qquad (4')$$

$$x'(k) = \emptyset\,(c(k-1))x'(k-1) + \varepsilon'(k) \qquad (5')$$

Namely, the k-th day DAP (recall that $y(k) = \ln DAP(k)$) has been made to depend upon the temperature category of the previous day. As shown in Table 2, first row, the performance of the predictor derived from the model (3), (4'), (5') exhibits a satisfactory improvement with respect to the forecast supplied by eqs. (6), (7).

Table 2. Forecast performances of the predictors with meteorological inputs.

Forecast index / Meteorological input	ϑ	$\frac{\sigma_\varepsilon}{\mu}$	σ_e
$c(k-1)$	0.74	0.36	0.079
$c(k)$	0.72	0.37	0.070
$s(k)$	0.71	0.37	0.080

The second row of Table 2 accounts for the quality of another predictor, corresponding to the following modifications of eqs. (4), (5) :

$$x''(k) = \left[y(k) - \mu_y(c(k))\right] / \sigma_s(c(k)) \qquad (4'')$$

$$x''(k) = \emptyset\ (c(k))\ x''(k-1) + \varepsilon''(k) \qquad (5'')$$

Here, the k-th day DAP is made to depend upon the k-th day instead of the (k-1)-th day temperature category. The prediction is slightly worse and this might be due to the time lag between the occurrence of a certain temperature and the subsequent variation of the emission.

Moreover, note that c(k-1) is an available datum at the beginning of the k-th day, but c(k) is not. Hence, while the first row of Table 3 gives on actual predictor performance, the second row must be rather regarded to as an upper bound, corresponding to the ideal case of a priori knowledge (i.e. perfect forecast) of the k-the day temperature category.

B) For each day of the above mentioned period, two vertical temperature profiles, recorded at 0 a.m. and at 12 a.m. respectively, were available. Thus it has been possible to define four gross daily stability categories: α (inversion condition neither at 0 a.m. nor at 12 a.m.), β (inversion only at 0 a.m.), γ (inversion only at 12 a.m.), δ (inversion both at 0 a.m. and at 12 a.m.). Hence the following relationships of the type (4), (5)

$$x'''(k) = \left[y(k) - \mu_y(s(k))\right] / \sigma_y(s(k))$$

$$x'''(k) = \emptyset(s(k))\ x'''(k-1) + \varepsilon'''(k),$$

where s(k) is the k-th day stability category, have been considered together with the corresponding predictor. The forecast performance is shown in Table 2, third row. As in the case of the predictor derived by (3), (4"), (5"), the result must be regarded to as an upper bound, since s(k) is not available at the beginning of the k-th day.

4. CONCLUDING REMARKS

Simple stochastic models and predictors of an overall pollution index, the dosage area product, have been tested in this paper on Milan SO_2 concentration data. An improvement in the forecast quality has been obtained by separately introducing meteorological inputs such as temperature and stability categories. Statistical confidence requirements, namely the shortness of the available record hasn't allowed to take into account two meteorological variables simultaneously.

Both the daily average and the maximum wind speed exhibit relatively small flutuations around their (low) mean values and shouldn't be able to account for a significant percent of the present forecast inaccuracies. Also the daily pattern of wind directions is rather constant in winter and shouldn't play a relevant role in the dynamics of the daily DAP. Moreover, the area under consideration exhibits a certain radial symmetry with respect to the emissions, so that the integral of the daily dosage over such area shouldn't be significantly affected by the pattern of hourly wind directions.

In general, the performance of the predictors illustrated in the previous section seems satisfactory and is anyway better than the result supplied by a similar analysis in other cases [9], [10]. Clearly, a higher forecast quality should be obtained, if shorter unit time intervals (twelve hours , for instance) were considered.

REFERENCES

[1] P.H. MERZ, L.Y. PAINTER and P.R. RYASON: Aerometric data analysis. Time series analysis and forecast and an atmospheric smog diagram. *Atmosph. Envir.* 6, 319-342 (1972).

[2] G.M. McCOLLISTER and J.R. WILSON: Linear stochastic models for forecasting daily maxima and hourly concentrations of air pollutants. *Atmosph. Envir*. 9, 417-423 (1975).

[3] D.P. CHOCK, T.R. TERRELL and S.B. LEVITT: Time-series analysis of Riverside, California air quality data. *Atmosph*. Envir. 9, 978-989 (1975).

[4] G.C. TIAO, G.E.P. BOX and HAMMING: A statistical analysis of the Los Angeles ambient carbon monoxide data 1955-1972. *JACPA* 25, 1129-36, (1975).

[5] G.E.P. BOX and G.M. JENKINS: *Time Series Analysis, Forecasting and Control*. Holden-Day, San Francisco (1970).

[6] A.A. DESALU, L.A. GOULD and F.C. SCHWEPPE: Dynamic estimation of air pollution. *IEEE Trans. on Autom. Contr.* AC-19, 904-910 (1974).

[7] Y. SAWARAGI and S. IKEDA (eds.): Proceedings of the Symposium on : *Modelling for the Control and Prediction of Air Pollution*. Kyoto (Japan) (1974).

[8] S.G. BANKOFF and E.L. HANZEVACK: The adaptive-filtering transport model for prediction and control of pollutant concentration in an urban airshed. *Atmosph. Envir.*, 9, 793-808(1975).

[9] G.FINZI, G. FRONZA and S. RINALDI: Stochastic modelling and forecasting of the dosage area product. *Atmosph. Envir.* (to appear).

[10] G. FINZI, G. FRONZA, S. RINALDI and P. ZANNETTI: Modelling and forecast of the dosage population product in Venice. Proceed. of the IFAC Symposium on Envir. Syst. Planning, Design and Control, Kyoto (Japan), August 1977.

[11] S. DUCKWORTH and E. KUPCHANKO : Air analysis: the standard Dosage Area Product. JAPCA 17, 379-383, (1967)

ACKNOWLEDGMENT

The authors thank Dr. Gualdi and Dr. Tebaldi of the Laboratorio Provinciale Igiene e Profilassi, Milan for their collaboration and useful criticism.

Rapporteur's Summary Report:
Prepared by: W. B. Johnson
Papers covered by: Jost/Gutsche
Joukoff
Orfeuil
Finzi /Fronza

Paper: A unit construction system of dispersion models for air quality management, B. Gutsche, D. Jost

Question: Schorling	Did you investigate the relationship between concentrations and emissions from traffic in street canyon?
Answer: Jost	In the theoretical model exercises , we used an arbitrary value for the traffic emissions; of course, there is a linear relationship between CO concentrations and environs.
Question: Fischer	In using diffusion coefficients in models I think one must be careful that there is a match between the surface roughness (Z_o) value at the site where the coefficients were derived and the Z_o value at the site where the model is applied. For example, Z_o at Jülich is about 1.8 m, while that at Brookhaven (Smith-Singer coefficients) is about 1.0 m.
Answer: Jost	Of course, you are right, and this may be the reason why the Jülich diffusion coefficients are larger.

Paper: Development of an air pollution index

Question: Godart	I believe that in such an analysis one must choose the parameters very carefully. For example, wet bulb temperature is very good because it is representative of air mass type. Also, I believe that solar radiation (or, possibly, an index related to amount of cloud cover) would be a good parameter. Have you tried this?
Answer: Joukoff	Yes, it was tried but found not to work as well as the other parameters that were discussed.
Question: Williams	What range of values did you get for the various partial regression correlation coefficients?
Answer: Joukoff	The mean of these values was about 0.4

Paper: A purely statistical approach to the warning, alarm and emergency problem, J.P. Orfeuil

Question:	Slater	I would just like to comment that the success of much statistical methods depends very critically upon the quality of the available input data.
Answer:	Orfeuil	I agree!
Question:	Runca	Could you give us some details on the data interpolation technique that you used?
Answer:	Orfeuil	This aspect of the work is rather theoretical, and for details the paper should be consulted. However, in general, the method searcher for minimum variance (optimal weight).

Paper: Univariate stochastic models and real time predictors of daily SO_2 pollution in Milano, G. Finzi, G. Fronza

Question:	Kretzschmar	In our work in Antwerp, we improved our correlation significantly by including air temperature (T), as you did. We found that T worked better than the wind speed in our regression analysis.
Answer:	Fronza	Yes, T works well; it seems to be highly correlated with pollutant levels.
Question:	Slater	I have a brief comment. I am happy to see that the meteorological variables do have some influence on pollutant concentrations! Of course, the effects are not large (over the long term) for a receptor near an urban center, because the wind direction (for a symmetrical city) becomes irrelevant, and the wind speed changes in your analysis are small.
Answer:	Fronza	Yes, I agree with your comment.

8th NATO/CCMS INTERNATIONAL TECHNICAL MEETING ON AIR POLLUTION MODELING

TOPIC 2

COMPARISON OF DIFFERENT DIFFUSION MODELS

8th International Technical Meeting on Air Pollution Modeling and its Application

A Methodology for the Comparison of Air Quality Simulation Models*

K. L. Brubaker, A. E. Smith, and D. M. Rote

Energy and Environmental Systems Division
Argonne National Laboratory
Argonne, Illinois 60439
U.S.A.

September 20-23, 1977

Louvain-La-Neuve
Belgium

---

*This work was sponsored by the Office of Air Quality Planning and Standards, U.S. Environmental Protection Agency, under Interagency Agreement EPA-IAG-D6-0013.

INTRODUCTION

During a series of workshops given in the United States on air quality maintenance planning, the issue of model evaluation frequently arose. State air pollution control officials often carry out air quality computations using a wide variety of modeling approaches. Before employing a particular model, state officials need to have reasonable assurance that the model used will be acceptable to the federal reviewers. It is also desirable for the various EPA Regional Offices to use a consistent methodology for determining model acceptability. In particular, it would be useful to be able to compare a given model with one which, by virtue of its extensive use within the federal EPA, has achieved the status of acceptability.

The present paper describes a methodology satisfying these needs. The methodology involves the qualitative comparison of the technical approaches used by two models. It is based on an application-specific approach and is intended for use by people who are not themselves modeling experts, although it is assumed that expert advice is available if needed. The user is required to make judgements based upon the specific application of interest.

The methodology described in this paper enables the user to determine the relative technical validity of two air quality models. This determination involves the consideration of the manner in which basic phenomena governing atmospheric pollutant concentrations are described and formulated as well as the manner in which these formulations are translated into an algorithm with which to make numerical concentration estimates. In practice, other considerations are also involved in the selection of an appropriate model for a given application and in the evaluation of the results. These other considerations include the availability of appropriate meteorological and emission data, and the manpower and computational resources required to implement the model. These factors must clearly be taken into account in selecting a model for use. The accuracy and representativeness of the input data would also need to be assessed in evaluating the results. The methodology described herein does not address these issues.

The evaluation of a model clearly must depend on the nature of the application. In applying the methodology, the user must determine in which of 256 different application classes the application of interest belongs.

In order to provide a uniform standard for comparison, a reference model is associated with each application class. The specific reference models which were chosen are models which are widely used in the United States for air quality management purposes and are familiar to most workers in the field. These reference models are not intended as recommendations but simply as bench marks for comparison purposes. The user may either compare a given model to the appropriate reference model or may compare two models, neither of which is a reference model. The approach emphasizes simulation models. Statistical and rollback models are treated separately.

The complete methodology has been presented in a workbook (in preparation) and forms are provided in the workbook for documenting each step in the comparison.

OVERVIEW OF THE PROCEDURE

The procedure for the comparison of air quality simulation models is summarized in Fig. 1. The user first classifies the application of interest in terms of pollutant characteristics, averaging time, source characteristics, and transport characteristics as shown in the Application Tree, Fig. 2. A numerical index corresponding to the user's particular application is constructed for reference purposes. An appropriate reference model is associated with each value of this index. The technical comparison is then carried out either between the reference model and the user's model or between the two models which the user desires to compare. To facilitate this comparison, twelve major factors determining atmospheric pollutant concentrations have been identified and are presented schematically in Fig. 3. These factors are called "application elements." The relative level of detail with which the two models treat each of these application elements is determined by the user on an element-by-element basis. The result of each comparison is a judgement on the part of the user that the treatment of that element by one model is better than, comparable to or worse than the treatment used by the other model. These twelve individual comparisons comprise part of the information needed to make an overall technical comparison of the two models. In addition, the importance of each element to the application must also be determined. This is accomplished by assigning a qualitative importance rating to each element for each application. Each importance rating consists of one of the following words: critical, high, medium, low, irrelevant.

A complete list of importance ratings for each application is provided in the workbook. The element-by-element comparisons and the corresponding importance ratings together form the basis for an overall comparative evaluation of the two models.

DETAILED DESCRIPTION OF THE METHODOLOGY

As mentioned above, the first step in the methodology is to classify the application of interest using the Application Tree shown in Fig. 2. In each of the four major categories, the user follows the tree, choosing the branch which best describes the situation to be modeled. Guidelines are provided in the workbook to aid the user in making appropriate choices at each branch point. Each branch ends in a single digit number which classifies the given application within that major category. The numbers corresponding to the four major categories are combined to form a four-digit "application index." This index is used to identify the appropriate reference model and set of importance ratings.

There are 256 different application indices resulting from this tree. Additional categories could have been introduced, but in order to keep the total number of applications manageable, the number had to be restricted. The categories finally chosen reflect the most significant factors in characterizing applications from the point of view of atmospheric transport and dispersion. Furthermore, these categories allow consideration of a wide variety of modeling approaches.

After the application has been classified, the appropriate reference model may be identified from a table in the workbook. Other information needed when treatments of the application elements are determined or compared is also recorded at this point. Each model is classified according to the general modeling approach adopted (numerical or semiempirical) and according to its treatment of the time dependence of pollutant concentrations (steady-state, dynamic, sequential, or climatological). The appropriate classification for all reference models is provided in the workbook. In addition, a quick check of the compatibility of each model with the application is made. This check, which need not be made for the reference model, determines if all physical and chemical processes of interest are treated in both models and if both provide the desired output. If either model fails to satisfy both checks, that model is not compatible with the user's specific application. Generally, reference models can be used as standards of comparison even when they are not strictly compatible with the application of interest. Finally, the working equations used by each model are documented. The equations used by the reference models are given in the workbook.

The final preliminary step is to review the importance ratings for the application of interest. A complete table of importance ratings, in which each element is rated as having either high, medium, or low importance to the particular application is given in the workbook. Based on unique knowledge of the specific situation, the user may modify these ratings. An element of extreme importance can be designated critical. A critical element is given extraordinary weight in making the overall evaluation. An element representing a physical or chemical process having no effect whatever on ambient pollutant concentrations in the particular application may be designated irrelevant and is given no weight in making the overall evaluation.

The user must now determine for each model the treatment of each application element which is not rated irrelevant. As illustrated in Fig. 3, these application elements represent the physical and chemical processes governing the concentrations of atmospheric pollutants. Again, the choice of these elements was a compromise between a manageable number and the number required to describe the relevant phenomena in full detail. The workbook provides guidelines for determining the treatment of each element by a given model. Tables of possible treatments arranged according to their relative level of detail are also provided. Appendices give detailed descriptions of the physical processes represented by each element and of the possible methods of treating each element in a model. Additional tables provide descriptions of the treatments used by the reference models. For each element, the user describes the treatment used by each model along with the importance rating for that element on a form provided for that purpose. Then, the two treatments are compared based on their relative levels of detail, taking into consideration the extent to which a detailed, sophisticated treatment is required in the application of interest. The user's model may treat a particular element at a level of detail that is technically better than, comparable to, or worse than the level of detail used in the reference model. In making these comparisons, the tables of ranked treatments are consulted. In difficult cases, the technical material in the appendices may also be referred to for guidance.

To arrive at an overall evaluation, the user first examines the comparisons for those elements which are of high importance. Based on the relative number of comparisons in the better, comparable, and worse categories, an initial comparative evaluation is made. In ambiguous cases, the user may go back over the descriptions of the treatments and review them in more detail in light of the situation to be modeled. Next, the elements of medium importance are examined to see whether the initial comparison should be retained or modified. Since these elements are of lesser individual importance to the application, they are each given correspondingly less weight and the evaluation depends primarily on the elements of high importance. In determining the relative weights to be assigned to the elements of high importance and the elements of medium importance, the number of elements in each category must also be considered. Elements of low importance are considered only in especially ambiguous cases. Irrelevant elements are never considered. If a critical element has been designated, it is considered first and the initial evaluation is based upon that element alone.

ILLUSTRATIVE EXAMPLE

As an example of the use of the methodology, assume that a regulatory agency has received a permit application for a power plant. The application relies on concentration estimates calculated with the Best Estimator for Simulated Transport (BEST) model for the maximum 24-hour sulfur dioxide (SO_2) concentration due to the proposed plant. This particular concentration is of interest in the United States due to the existence of a 24-hour air quality standard for sulfur dioxide. The plant is to be situated on level terrain and the major interest is in the area near the plant where the maximum ground level concentration is likely to occur.

Chemical transformation of SO_2 between source and receptor is judged to be negligible but for illustrative purposes dry deposition will be considered significant. The agency needs to determine whether the concentration estimates obtained from BEST are acceptable. It does this by determining if the BEST model is of at least comparable technical validity when compared to the reference model given in the workbook for the application of interest.

First, the application is classified according to the scheme shown in Fig. 2 using the guidelines provided for its use. The pollutant (SO_2) would be characterized as "PRIMARY." Dry deposition is a "PHYSICAL" removal process. Thus, the final branch in the pollutant characteristics category is number 3. According to the text, averaging times of 24 hours of less are classified "SHORT-TERM" so that branch number 2 under averaging time is chosen. Similarly, branches 1 and 3 are chosen in the categories of source characteristics and transport characteristics, respectively. The application index is thus determined to be 3213 and this index is used to identify the XCETER* model as the reference model for this class of applications.

These models would then be classified, the working equations documented, and the compatibility of BEST with the application checked. BEST is a numerical/dynamic model. A table in the workbook indicates that XCETER is a semiempirical/sequential (steady-state) model. All this information is entered on forms provided in the workbook.

Next the importance ratings for application 3213 are checked and any modifications necessary in view of the particular situation to be modeled or the user's special interests would be made.

The information on the twelve application elements would then be consulted. Based on this information, the treatment of each element by BEST would be determined and described in writing on a form along with the treatment by XCETER as provided in the workbook. Then the two treatments would be compared and the treatment by BEST rated as "better" than, "comparable" to, or "worse" than the treatment by XCETER. In making this comparison, the discussions of treatments and the tables of treatments in terms of relative level of detail would be consulted. (In the interests of brevity, only four application elements will be considered in this example: emission rate, plume rise, vertical dispersion, and dry deposition). To illustrate: BEST is a model which treats dry deposition by the appropriate specification of the boundary condition at the ground. XCETER, according to tables in the workbook, treats dry deposition as an exponential decay process. In the tables of treatments of dry deposition, treating dry deposition in terms of the boundary condition at the ground is rated as substantially more detailed and hence of greater technical validity than treating it by exponential decay. Hence, BEST is

---

*Both BEST and XCETER are fictitious models, used here for illustrative purposes.

"better" than XCETER in its treatment of dry deposition. The text also indicates that dry deposition is of "MEDIUM" importance in application 3213. Similarly, the treatments of the other elements are compared and rated. The results are summarized in Fig. 4.

To perform the overall technical evaluation, the comparative evaluations and importance ratings of each element are examined and combined. The work is conveniently organized on a form like that shown in Fig. 5. First, the highly important elements should be considered. BEST treats two such elements better and one worse than XCETER. This situation is clearly somewhat ambiguous. In practice, a careful review of the elements involved and their importance in the specific situation of interest would be called for. If such a review failed to give additional insight, an initial comparative rating of BETTER would be entered as in this example. Turning next to the element of medium importance, this initial rating would be confirmed by finding the treatment by BEST to be better than that of XCETER. Since there would be no reason to revise the original rating, BETTER would be enetered as the appropriate rating after considering the elements of medium importance. The low elements, if any, would be ignored, because the comparison is unambiguous at this point. The final comparative evaluation would be that BEST is better than XCETER. This should be interpreted as meaning that BEST is of higher technical validity than XCETER for this particular application.

The reviewer would thus have a basis for accepting the concentration estimates based on BEST because, at least qualitatively, it does a better technical job than a model widely used in such circumstances. It may happen, of course, that some element, say plume rise, has been judged critical to the particular application. In such a case, the methodology would allow the reviewer to rate the importance of plume rise as "CRITICAL" and to reject BEST, because its treatment of the critical element is worse than that of the reference model.

Summary

A recently developed, user-oriented methodology for comparing air quality simulation models is briefly described. The methodology constitutes a comprehensive framework for comparing models from an application-specific point of view in terms of the technical aspects of the modeling problem.

The methodology involves an examination of model treatments of those basic phenomena which govern the ambient concentration of atmospheric pollutants. Possible model treatments of these basic elements are ranked in a manner which allows the user to compare qualitatively the treatments used by two different models. A scheme is provided for combining these individual comparisons into an overall comparative evaluation.

A more detailed description of the methodology and examples of its application to selected models will be available in a workbook now in preparation under contract to the U.S. Environmental Protection Agency. This methodology provides a uniform basis for model comparison and should also serve as a benchmark for future model comparison techniques.

Fig. 1. Procedure for the Comparison of Air Quality Simulation Models.

Fig. 2. Application Tree

Fig. 3. Application Elements

Fig. 4. Evaluation Form - Treatments of Elements

Fig. 5. Evaluation Form - Technical Comparison

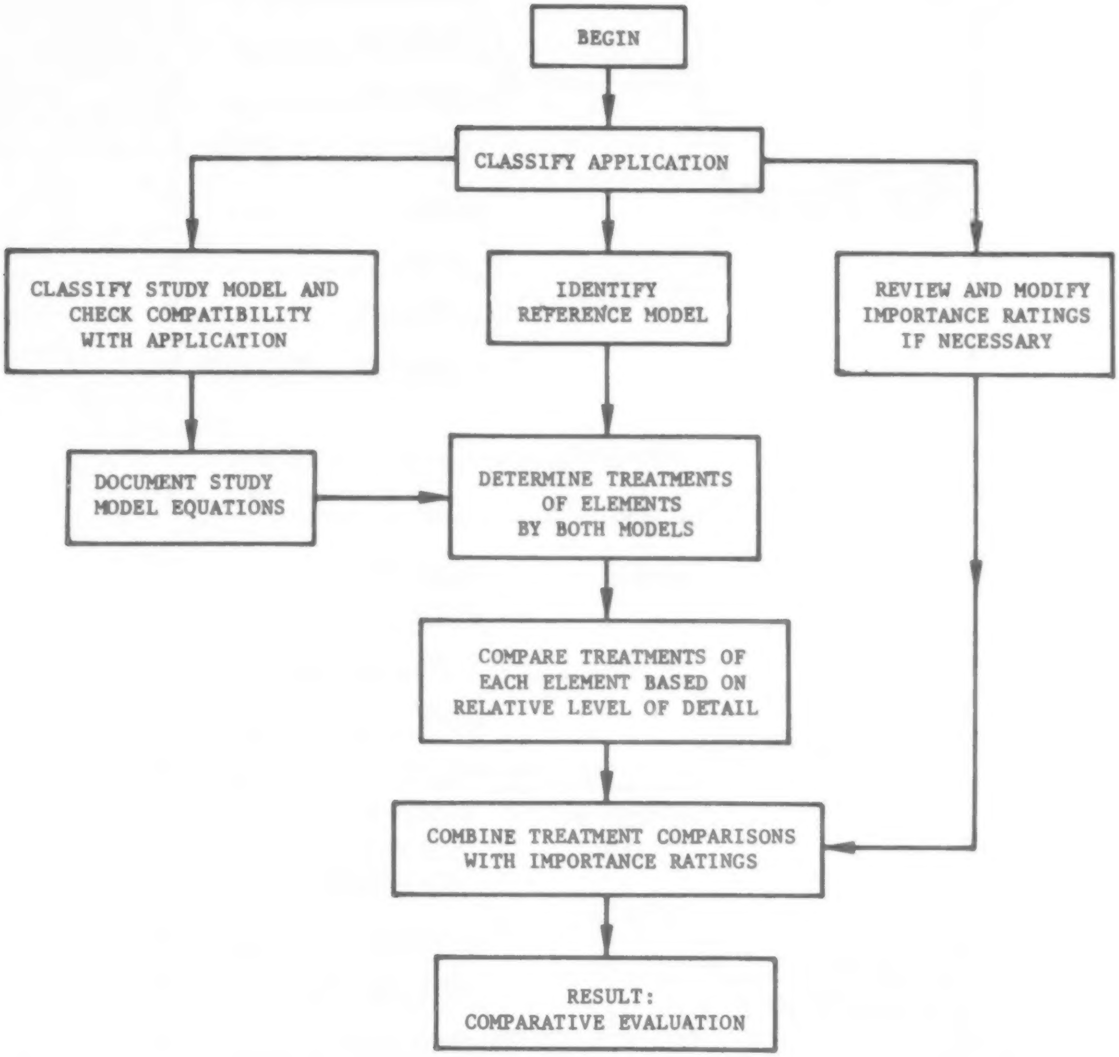
BEGIN
CLASSIFY APPLICATION
CLASSIFY STUDY MODEL AND CHECK COMPATIBILITY WITH APPLICATION
IDENTIFY REFERENCE MODEL
REVIEW AND MODIFY IMPORTANCE RATINGS IF NECESSARY
DOCUMENT STUDY MODEL EQUATIONS
DETERMINE TREATMENTS OF ELEMENTS BY BOTH MODELS
COMPARE TREATMENTS OF EACH ELEMENT BASED ON RELATIVE LEVEL OF DETAIL
COMBINE TREATMENT COMPARISONS WITH IMPORTANCE RATINGS
RESULT: COMPARATIVE EVALUATION

Fig. 1. Procedure for the Comparison of Air Quality Simulation Models

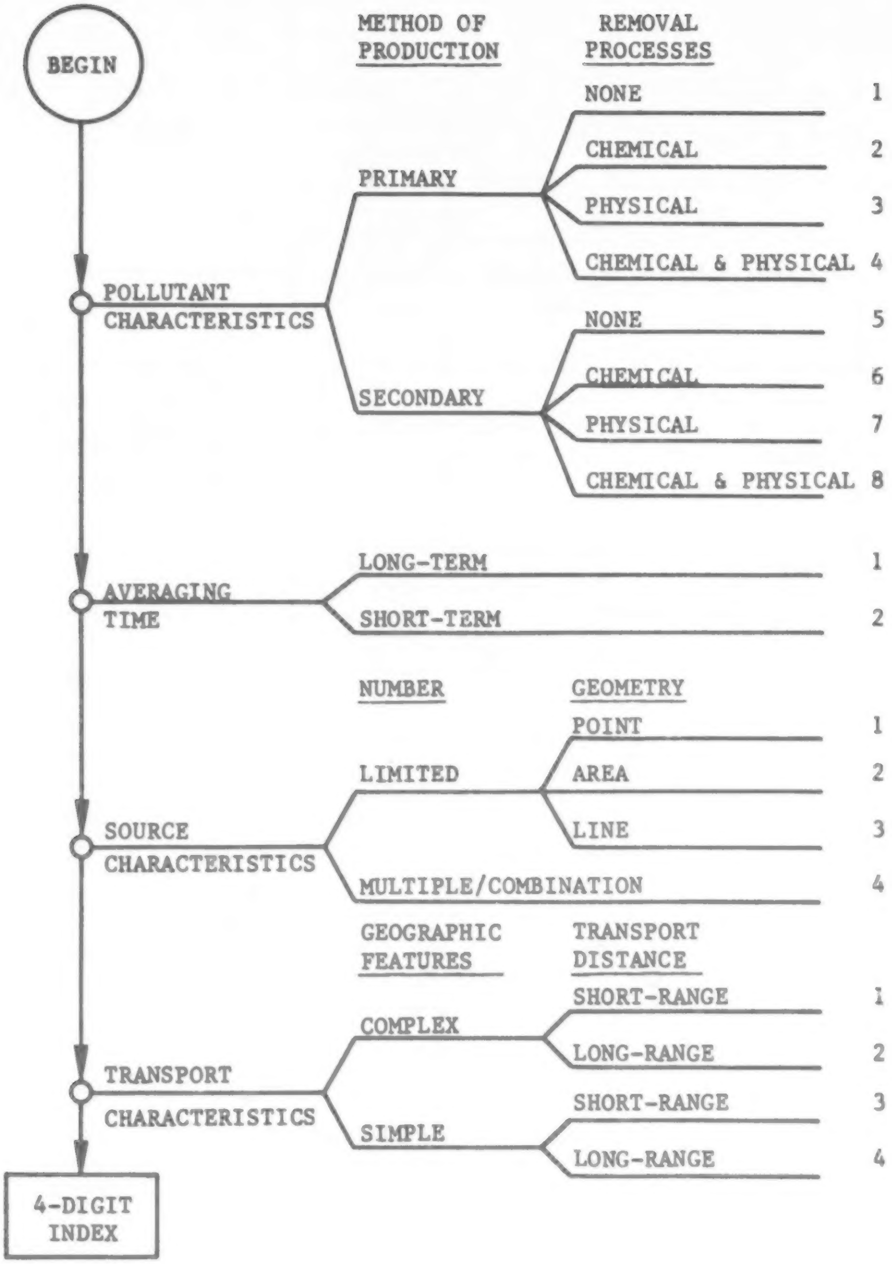
BEGIN
METHOD OF PRODUCTION
REMOVAL PROCESSES
POLLUTANT CHARACTERISTICS
PRIMARY
NONE 1
CHEMICAL 2
PHYSICAL 3
CHEMICAL & PHYSICAL 4
SECONDARY
NONE 5
CHEMICAL 6
PHYSICAL 7
CHEMICAL & PHYSICAL 8
AVERAGING TIME
LONG-TERM 1
SHORT-TERM 2
NUMBER
GEOMETRY
SOURCE CHARACTERISTICS
LIMITED
POINT 1
AREA 2
LINE 3
MULTIPLE/COMBINATION 4
GEOGRAPHIC FEATURES
TRANSPORT DISTANCE
TRANSPORT CHARACTERISTICS
COMPLEX
SHORT-RANGE 1
LONG-RANGE 2
SIMPLE
SHORT-RANGE 3
LONG-RANGE 4
4-DIGIT INDEX

Fig. 2. Application Tree

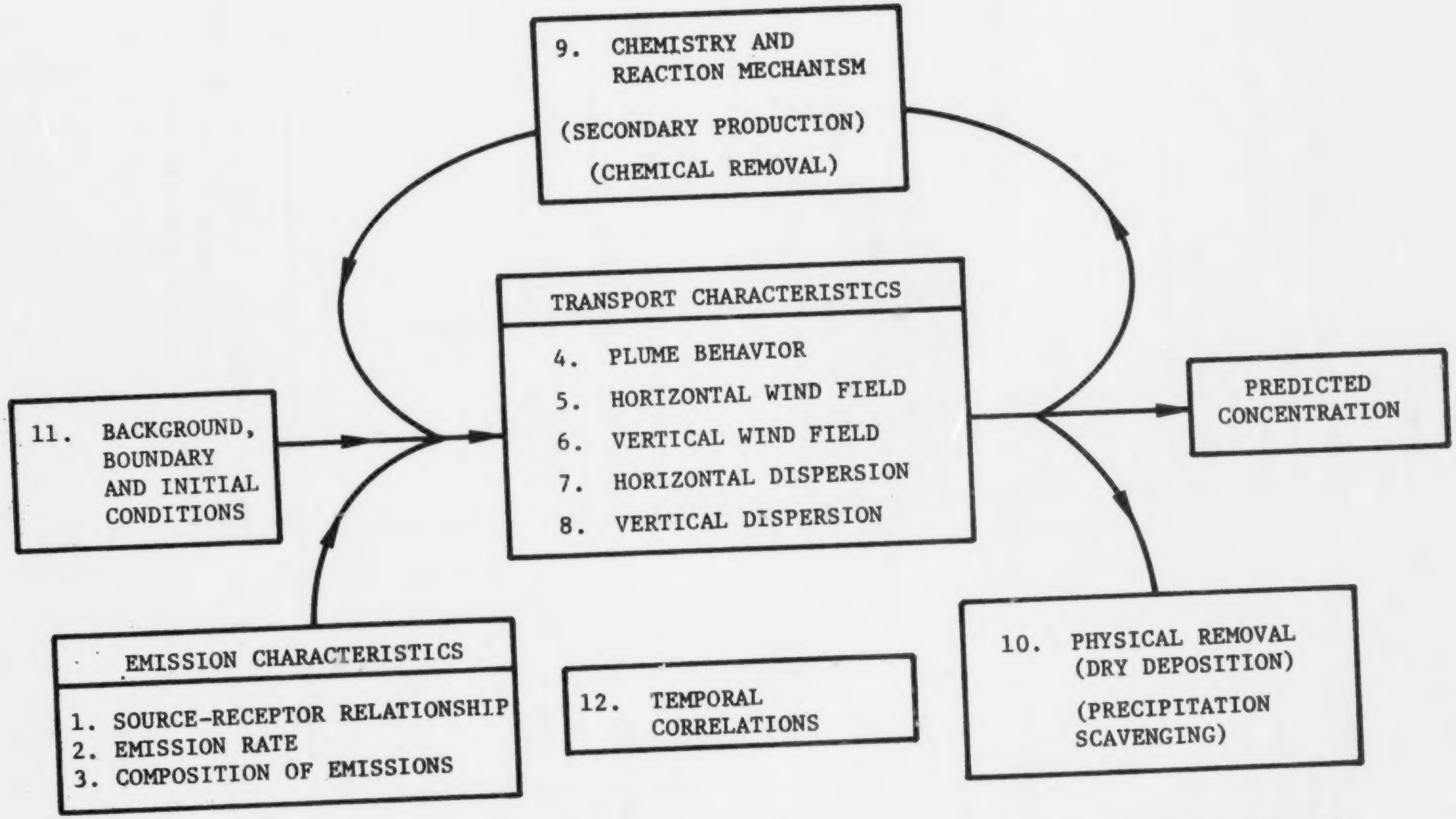
9. CHEMISTRY AND REACTION MECHANISM
(SECONDARY PRODUCTION)
(CHEMICAL REMOVAL)
TRANSPORT CHARACTERISTICS
4. PLUME BEHAVIOR
5. HORIZONTAL WIND FIELD
6. VERTICAL WIND FIELD
7. HORIZONTAL DISPERSION
8. VERTICAL DISPERSION
11. BACKGROUND, BOUNDARY AND INITIAL CONDITIONS
PREDICTED CONCENTRATION
EMISSION CHARACTERISTICS
1. SOURCE-RECEPTOR RELATIONSHIP
2. EMISSION RATE
3. COMPOSITION OF EMISSIONS
12. TEMPORAL CORRELATIONS
10. PHYSICAL REMOVAL (DRY DEPOSITION)
(PRECIPITATION SCAVENGING)

Note: Temporal correlations relate the time variations of all the other application elements.

Fig. 3. Application Elements

EVALUATION FORM

Treatment of Elements

Application Index: 3213

Application Element: Dry deposition	Application Element: Vertical dispersion
Reference Model: XCETER Treatment: Exponential decay. Single, constant user-supplied halflife.	Reference Model: XCETER Treatment: Semiempirical/sequential (steady-state). Gaussian plume. Seven stability classes. Surface roughness effects ignored.
Study Model: BEST Importance Rating: MEDIUM Comparative Evaluation: BETTER Treatment: As a boundary condition at the ground. Removal rate depends on ground-level concentration and constant user-input dry deposition velocity.	Study Model: BEST Importance Rating: HIGH Comparative Evaluation: BETTER Treatment: Numerical/dynamic. Eddy diffusivity a function of height, time, and surface roughness. Functional form correct near ground.
Application Element: Plume rise	Application Element: Emission rate
Reference Model: XCETER Treatment: Briggs' (1971) final plume rise formulas; plume rise not treated as a function of downwind distance. If plume rise exceeds mixing height, concentrations further downwind assumed equal to zero.	Reference Model: XCETER Treatment: Arbitrary average emission rate for each source. No temporal variation allowed.
Study Model: BEST Importance Rating: HIGH Comparative Evaluation: WORSE Treatment: Single user-input value of product (wind speed)x(plume rise) used to calculate plume rise. Effect of mixing height ignored.	Study Model: BEST Importance Rating: HIGH Comparative Evaluation: BETTER Treatment: User-input hourly emission rates.

Fig. 4. Evaluation Form - Treatments of Elements

EVALUATION FORM

Technical Comparison

Application Index: 3213 Reference Model: XCETER Study Model: BEST

Importance Rating of Application Elements	Number of Treatments					Comparative Rating of Study Model
	Total	BETTER	COMPARABLE	WORSE		
CRITICAL	0	—	—	--		---
HIGH	3	2	0	1		BETTER
MEDIUM	1	1	0	0		BETTER
LOW[a]	0	0	0	0		
IRRELEVANT	____	XXX	XXX	XXX	COMPARATIVE EVALUATION	BETTER
Total	4					

---

[a] Used only in ambiguous cases.

Fig. 5. Evaluation Form -- Technical Comparison

8th International Technical Meeting on
Air Pollution Modeling and its Application

Comparative Study of Four Mathematical Air Dispersion Models for a New Urban Industrial Complex at Sines, Portugal

José F. Conceic ao and Leonel D. Canelas
Gabinete Area Sines, Divisao Controle Ambiente, Lisboa, Portugal

and

Richard Porter and John Christiansen
University of Texas and Dallas and Texas Air Control Board
United States of America

September 2o-23, 1977
Louvaine-La-Neuve
Belgium

1. INTRODUCTION

Taking advantage of the unique geographical position of Portugal between the Middle East producers of oil and North Europe, the Portuguese Government through Gabinete da Area de Sines (GAS), has been coordinating construction of one of the largest urban-industrial complexes in the world. Estimated investment for the complex is 5 billion dollars. The site of the proposed complex is near Sines, Portugal, a small fishing village approximately 150 kilometers (90 miles) south of Lisbon (Figure 1). This complex is scheduled to include an oil refinery, a petrochemical complex, an integrated steel mill, a pyrite processing plant, a fertilizer complex, and a new town of about 60,000 people. Basic to the complex is construction of one of the largest harbors in the world, capable of receiving super tankers of 500,000 DWT.

The complex is situated near one of the largest pyrite ore resources in Europe. These pyrites, together with the sulfur and iron, include substantial amounts of copper, zinc, lead, silver and gold. The Portuguese Government is in the final phase of selection of hydrometallurgical processes to use the sulfur for production of sulfuric acid, the iron as purple ore to the steel mill, with substantial recovery of nonferrous metals. In addition to the sulfuric acid plant, the fertilizer complex will include production of ammonia, urea, and various fertilizer components (Table 1).

Presently the harbor is 90 percent complete, the refinery 80 percent complete, and the petrochemical complex is starting with construction of an ethylene and polyethylene plants. The new town is about 20 percent complete.

2. STRATEGY FOR AIR POLLUTION CONTROL

In 1971 when the Portuguese Government decided on the construction of this huge complex 90 miles south of Lisbon, the now-called Sines Area was the small fishing village of Sines, and was surrounded by large agricultural areas. Practically no industrial developments existed in those days and the demographic density was very low. Under these conditions and since no major impacts of other areas have been reported, the Sines Area could be classified as a virgin area from the point of view of air pollution.

FIGURE 1

REGIONAL MAP OF PROPOSED SINES INDUSTRIAL COMPLEX

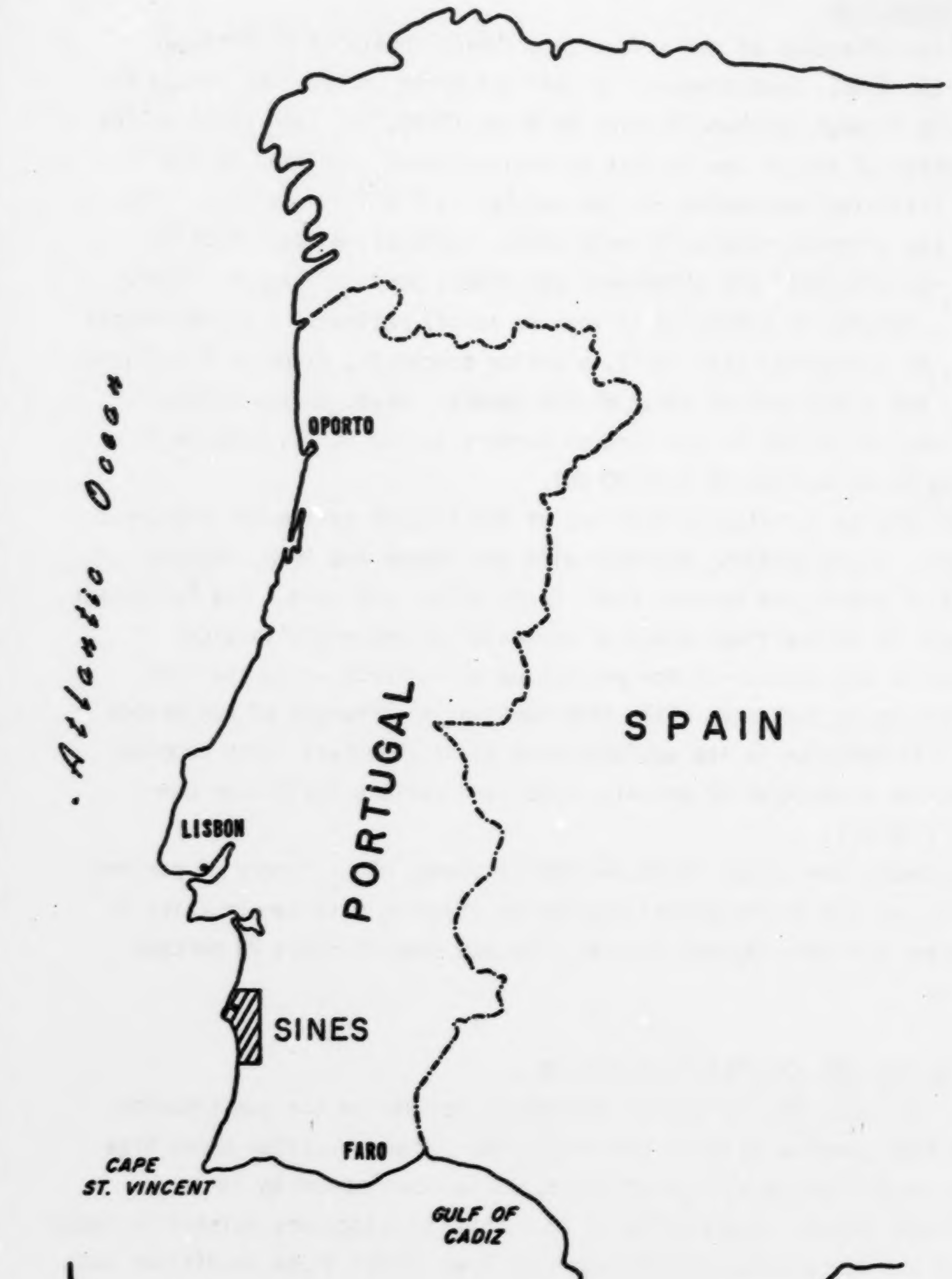
Atlantic Ocean
OPORTO
LISBON
PORTUGAL
SPAIN
SINES
CAPE ST. VINCENT
FARO
GULF OF CADIZ
STRAIT OF GIBRALTAR
N
0
50
100 KM

TABLE 1

COMPONENTS OF THE INDUSTRIAL COMPLEX AT SINES, PORTUGAL

	Capacities (TON/Year)
Petroleum Refinery	10,000,000
Petrochemical Complex	
Steam Cracker of Ethylene	300,000
HDPE	80,000
LDPE	120,000
Polypropylene	50,000
VCM	150,000
PVC	55,000
Styrene	150,000
Polystyrene	25,000
ACN	48,000
SBR	50,000
Steel Mill	1,500,000
Pyrite Complex	
Hydrometallurgy	247,500
Treatment of Residues	700,000
Fertilizer Complex	
Sulfuric Acid	825,000
Urea	300,000
Ammonia	500,000
Phosphoric Acid	200,000
MAP	350,000
Fertilizer Compounds	250,000

Gabinete da Area de Sines, through its Department of Environmental Control (Divisao Controle Ambiente) attempted since the very beginning to take advantage of this rather unusual situation to develop a detailed and carefully planned set of actions in order to preserve the environment with reasonable costs for the Government and industries to be installed.

We assumed, looking at some bad foreign experiences, that it was significantly less expensive to plan carefully and install better process technologies rather than try to correct ecological distortions after the start-up of plants. For economical reasons it was decided to export low sulfur content fuel and use 3.5 percent sulfur content fuel oil throughout the complex. Natural gas was not available.

After careful economic studies were done, we concluded that it was less expensive to use tall stacks for dispersion of pollutants and reject modern equipment to remove pollutants at source which are more expensive and not technically proved today. In these conditions the establishment of ambient air standards and the early use of mathematical dispersion models were the fundamental tools to our unique approach: the scientific calculations of the necessary heights of stacks to guarantee the air quality standards desired in the Area.

In our case the key output of dispersion models will be the stack height values which are communicated in advance to the industries to be installed in the Sines Area.

Together with the intensive modeling activities discussed in this paper, it should be mentioned briefly that to complement these actions a network of ambient air monitoring control has been operating since 1973, and will provide data for calibration purposes.

Technological approaches have been and will continue to be used, such as floating roof tanks and sulfur recovery Claus Units.

The new town was located north of the complex to avoid reception of air pollution since prevailing winds are from the north. A green area of about 10,000 acres located between the new town and the industrial complex was reserved for recreational purposes and as a green belt between the new town and the complex.

Three primary air contaminants were considered by Divisao Controle Ambiente, based on the natural characteristics of the Sines Area and the recommendations of the World Health Organization. Air quality standards were accepted for three averaging periods - 30 minutes, 24 hours, and annual (Table 2). Figure 2 shows the locations of the various plants in

TABLE 2

AMBIENT AIR QUALITY STANDARDS FOR SINES, PORTUGAL

Pollutant	Absolute Maximum Concentration ($\mu g/m^3$)	Averaging Time
SO_2	1126	30 min.
	250	24 hr.
	60	Annual
NO_x (as NO_2)	500	30 min.
	250	24 hr.
	100	Annual
Particulates	500	30 min.
	150	24 hr.
	40	Annual

FIGURE 2

LOCATION OF THE PLANTS AT SINES COMPLEX

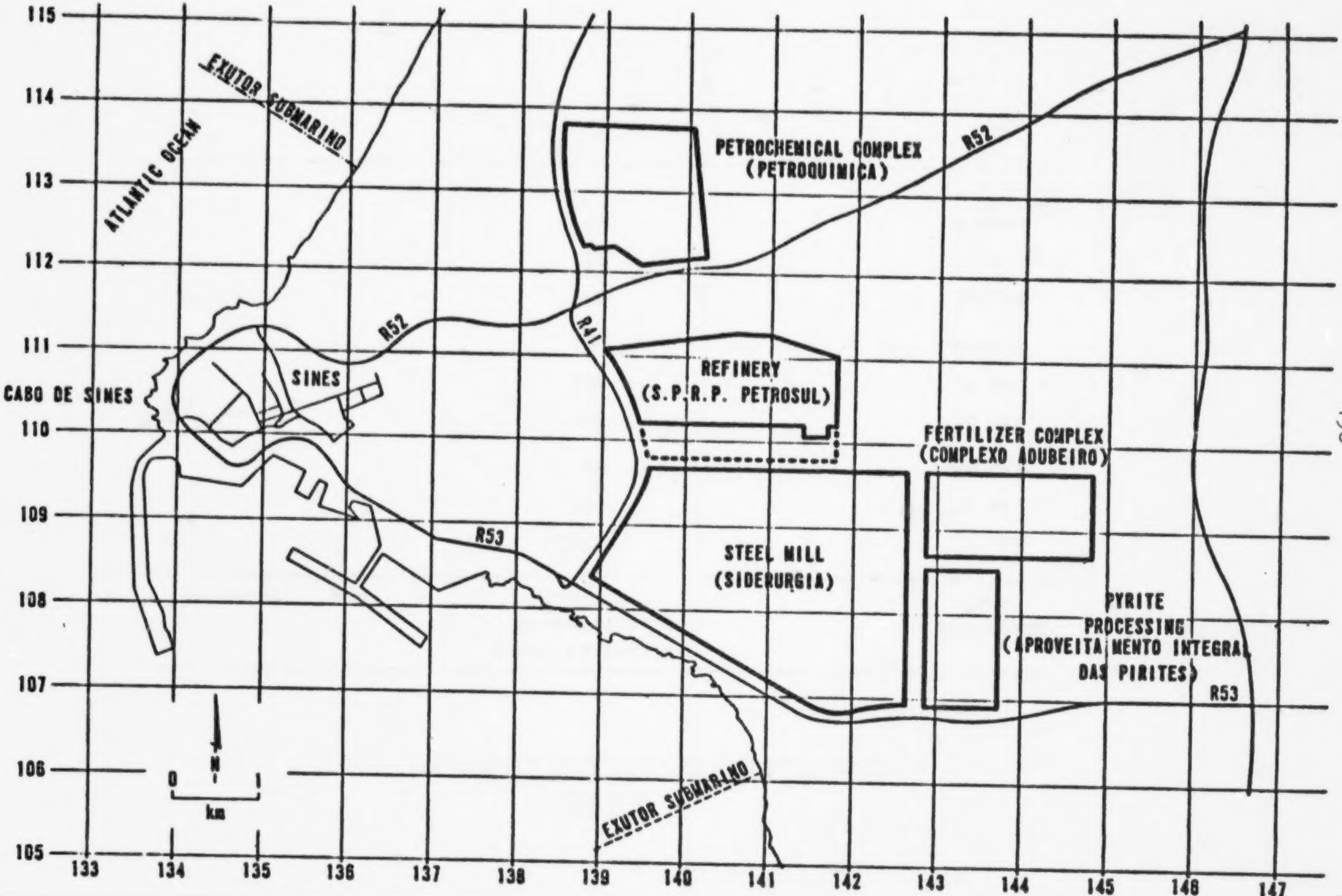

115
114
113
112
111
110
109
108
107
106
105
133
134
135
136
137
138
139
140
141
142
143
144
145
146
147
EXUTOR SUBMARINO
ATLANTIC OCEAN
CABO DE SINES
SINES
R52
R41
R53
PETROCHEMICAL COMPLEX (PETROQUIMICA)
REFINERY (S.P.R.P. PETROSUL)
FERTILIZER COMPLEX (COMPLEXO ADUBEIRO)
STEEL MILL (SIDERURGIA)
PYRITE PROCESSING (APROVEITAMENTO INTEGRAL DAS PIRITES)
N
0
1
km
EXUTOR SUBMARINO

the complex.

3. METHODOLOGY

The refinery was the first plant to be constructed in the area and its power plant will burn approximately 20% of total fuel consumed in the area. An initial approach used by Divisao Controle Ambiente was the decision to give them 20% of total value of standards and using the Briggs and Sutton equations in these conditions a stack height value of 233 meters (765 feet) was established. This stack has now been constructed. With the continuous growing of the complex as scheduled and because concentration due to multiple point sources had to be evaluated a complete inventory of air emissions of all the complex had to be prepared. For this purpose together with the information furnished by industries we used extensively the emissions factors adopted by the United States Environmental Protection Agency to calculate SO_2, NO_X, and particulate matter emissions (1).

To complement the input necessary for the models some physical stack parameters and other technological variables not mentioned in EPA Reports were obtained from comparable facilities in operation or proposed in the United States.

The major pollutant of concern is SO_2 with significant emissions derived from the consumption of 3.5 percent sulfur fuel oil throughout the complex. In cases where industries could not provide data, the fuel oil consumption was proportioned among the various processes on a percentage basis using consumptions from typical American facilities.

Fuel oil consumption within the pyrite processing facilities was limited to the ustulation (roasting processes). Within the fertilizer complex the only significant processes producing SO_2 were the two sulfuric acid plants. Particulate emissions resulted from both fuel oil consumption and process emissions and again were calculated with EPA approved emission factors. Since emission factors are strongly dependent upon efficiency of recovery of technology used for steel mills, we selected devices with about 90% recovery efficiency. Table 3 summarizes the emission inventory for all the complex.

Climatological data necessary for mathematical models came from surface observations already done by Divisao Controle do Ambiente. This data was compared with a complete listing of STAR Program from Lisbon and

TABLE 3

EMISSION INVENTORY OF INDUSTRIAL PROCESSES AT SINES, PORTUGAL

Source Description	SO_2 Emissions (g/sec)	Particulates Emissions (g/sec)
Refinery		
Power Plant	1331.4	92.0
Petrochemical Complex		
Power Plant	1295.9	89.0
Polyethylene (HD)	0.0	1.9
Polyethylene (LD)	0.0	1.0
Polypropylene	0.0	2.38
ACN Incinerator	39.0	1.39
VCM	39.0	1.39
Styrene	101.19	3.61
PVC	0.0	0.28
Polystyrene	0.0	0.11
Integrated Steel Mill		
Blast Furnace	0.0	95.1
Coking	264.8	70.3
Steelmaking	0.0	388.1
Sintering	305.1	130.8
Others 1	50.7	1.9
Others 2	50.7	1.9
Pyrite Processing	710.10	49.0
Fertilizer Complex		
Ammonia	865.4	60.0
Urea	58.6	12.4
Sulfuric Acid I	58.5	0.0
Sulfuric Acid II	58.5	0.0
Mono-Ammonia phosphate	0.0	2.85

Faro, the two nearest airports. Surface observations from Lisbon STAR were considered applicable to the Sines Area and used in all models applied. Table 4 summarized STAR data of Lisbon applicable to Sines.

In modeling Sines Complex various combinations of meteorological conditions, emission sources and stack heights had to be considered, the last ones mainly because various hypotheses of processes to be used were not yet decided.

As mentioned before the key aspect of models application was to determine the stack heights which allow sufficient dispersion to keep relatively clean air levels in stringent accordance with standards. Nevertheless, for well known mathematical reasons the models run giving concentrations for established stack heights.

We used various stack height values as a first approach and computed the concentrations. It was considered a good basis of work to use average stack heights from plants already existing of similar capacities, shown in Table 5. To calculate ground level impact from emissions of SO_2, NO_X, and particulate matter, two dispersion models were used. The United States Environmental Protection Agency's "Air Quality Display Model" (AQDM)(2) estimated long-term annual average concentrations. For short-term (30 minutes and 24 hours) concentrations, a modified version of EPA's multiple point source diffusion model PTMTP was used (APMAX) (3). Since the details were published already by Conceicao and Canelas (4,5), we include only a table for comparison purposes with the models applied in the third phase. In this phase we applied the Texas Air Control Board "Texas Episodic Model" (T.E.M.) (6) for short-term concentrations of SO_2 and particulates, and the Texas Air Control Board "Texas Climatological Model" (T.C.M.) (7) to estimate long-term concentrations for SO_2 and particulates also.

The main reasons for the application of these recent models are that they seem to present some advantages over the AQDM and APMAX. These advantages were described in a paper presented at the last C.C.M.S.-N.A.T.O. 1976 Meetings in Virginia by Porter and Christiansen (8).

RESULTS

Typical results of the computer runs of T.E.M. and T.C.M. are shown in Table 6. The predicted maximum annual average SO_2 and particulates concentrations are below the standards adopted by Divisao Controle Ambiente

TABLE 4

FREQUENCY DISTRIBUTION OF METEOROLOGICAL DATA - LISBON, PORTUGAL

(percent)

	Wind Speed (km/hr)								Stability Class					
Direction	0-6	7-12	13-19	20-30	31-38	>38	Total	Average WS (km/hr)	A	B	C	D	E	F
N	1.0	4.8	7.6	8.6	2.7	0.3	25.1	20.4	0.1	0.9	3.1	13.8	4.0	3.2
NNE	0.5	1.9	1.0	0.6	0.1	*	4.1	13.7	0.1	0.3	0.8	1.1	0.6	1.3
NE	0.7	2.7	1.6	0.4	*	*	5.4	12.6	*	0.3	0.9	1.3	1.1	1.8
ENE	0.9	3.8	2.7	0.7	*	*	8.1	12.8	0.1	0.7	1.8	2.4	1.4	1.6
E	0.9	3.1	1.2	0.3	*	*	5.6	11.3	0.3	1.0	1.2	1.7	0.6	0.9
ESE	0.3	0.9	0.2	0.1	*	*	1.4	10.0	0.1	0.3	0.2	0.5	0.2	0.2
SE	0.1	0.4	0.2	0.1	*	*	0.8	12.8	*	0.1	0.1	0.4	0.1	0.1
SSE	0.2	0.6	0.3	0.2	*	*	1.3	13.1	*	0.1	0.2	0.7	0.2	0.1
S	0.2	0.8	0.7	0.5	0.2	*	2.4	17.2	*	0.6	0.1	1.7	0.3	0.1
SSW	0.1	0.4	0.5	0.5	0.2	0.1	1.7	20.7			0.1	1.3	0.2	0.1
SW	0.2	0.6	0.8	1.0	0.3	0.1	3.0	21.1	*	*	0.1	2.4	0.3	0.2
WSW	0.4	1.4	1.8	1.7	0.4	0.1	5.7	18.5	*	0.1	0.3	3.9	0.7	0.5
W	0.8	2.8	2.2	1.7	0.4	0.1	8.1	16.5	*	0.2	0.6	4.4	1.4	1.3
WNW	0.5	1.9	1.6	1.1	0.2	*	5.3	15.9	*	0.1	0.4	2.6	1.1	1.0
NW	0.4	1.9	2.3	1.8	0.3	0.1	6.7	17.6	*	0.1	0.6	3.5	1.3	1.0
NNW	0.5	2.5	4.7	5.9	1.5	0.2	15.2	20.7	*	0.4	1.3	9.6	2.5	1.4
Total	7.7	30.4	29.4	25.1	6.3	1.1		16.8						
A	0.4	0.5	*	*	*	*	0.9							
B	1.5	2.5	0.7	*	*	*	4.8							
C	0.8	4.6	5.2	1.2	0.2	*	12.0							
D	1.0	5.7	13.6	23.9	6.2	1.0	51.3							
E	*	6.0	10.0	*	*	*	16.0							
F	4.0	11.0	*	*	*	*	15.0							

*Less than 0.05%

TABLE 5

DESIRED VALUES FOR STACK HEIGHTS OF SINES INDUSTRIAL COMPLEX

Source Description	Ht. (M)	Diam. (M)	Vel. (M/S)	Temp. (K)
Refinery				
Power Plant	233.00	8.000	25.00	544.15
Petrochemical Complex				
Power Plant	150.00	7.900	25.00	448.15
Polyethylene HD	45.70	.600	15.20	366.45
Polyethylene LD	45.70	.600	15.20	366.45
Polypropylene	45.70	.600	15.20	366.45
ACN Incinerator	30.50	3.700	15.20	424.85
VCM	61.00	3.700	15.20	477.55
Styrene	61.00	3.700	15.20	449.85
PVC	61.00	3.700	15.20	449.85
Polystyrene	61.00	3.700	15.20	449.85
Integrated Steel Mill				
Blast Furnace	45.70	2.600	10.70	450.15
Coking	68.60	2.700	10.70	394.15
Steelmaking	61.00	3.100	10.70	422.15
Sintering	91.50	1.800	10.70	422.15
Others 1	53.40	1.800	10.70	366.45
Others 2	53.40	1.800	10.70	366.45
Pyrite Processing	91.40	3.700	10.70	449.85
Fertilizer Complex				
Ammonia	100.00	3.100	15.20	783.15
Urea	30.50	3.100	15.20	448.15
Sulfuric Acid I	45.70	3.100	9.10	344.15
Sulfuric Acid II	47.50	3.100	9.10	344.15
Mono-Ammonia Phosphate	30.50	3.100	15.20	448.15

TABLE 6

PREDICTED CONCENTRATIONS AT SINES, PORTUGAL

Averaging Period	Maximum Concentration µg/m³		Associated Meteorology				
			Wind				
	SO_2	Particulates	Direc.	Speed m/sec	Stability	Mixing Depth (meters)	Penetration Factor
30 Minutes	457	256	N	2.46	A	500	2
	612	193	NNW	2.46	A	500	2
	468	164	N	2.46	A	500	3
	616	200	NNW	2.46	A	500	3
	316	232	N	2.46	A	1,000	2
	566	174	NNW	2.46	A	1,000	2
	421	305	N	1.50	A	1,000	3
	316	232	N	2.46	A	1,000	3
	566	174	NNW	2.46	A	1,000	3
	316	230	N	2.46	A	1,500	3
	1,225	509	N	1.50	B	300	3
	806	319	N	1.50	B	400	3
	477	271	N	1.50	B	600	3
	378	253	N	4.47	B	400	3
	308	250	N	4.47	B	600	3
	308	248	N	4.47	B	1,500	3
	225	215	N	9.61	C	600	3
	278	214	NNW	2.46	E	500	2
	207	150	NNW	4.47	E	500	2
	269	214	NNW	2.46	E	10,000	2
	207	150	NNW	4.47	E	10,000	2
	155	193	NNW	1.50	F	500	2
	140	151	NNW	2.46	F	500	2
	155	193	NNW	1.50	F	10,000	2
	140	151	NNW	2.46	F	10,000	2
24 Hours	161	104	NNW	*	*	*	2
	141	86	NNW	*	*	*	2
Annual	43	17					

*Several wind speeds, stabilities, and mixing heights were used in 24-hour scenarios.

for the Sines area. When all facilities are operating, theoretically short-term maximum calculated will not exceed the 30-minute or 24-hour standards unless very slightly even under a rather unusual inversion we simulated at 300 meters.

Although the T.E.M. and T.C.M. were run for a couple of months after AQDM and APMAX and in some cases using different stack heights, some runs in exactly the same conditions were done. The values of SO_2 concentrations can be compared in Table 7 for one-half hour periods. The annual results were:

	T.C.M.	AQDM
Annual SO_2	43 $\mu g/m^3$	49 $\mu g/m^3$
Annual Particulates	17 $\mu g/m^3$	26 $\mu g/m^3$

TABLE 7

COMPARISON OF SO_2 CONCENTRATIONS

Pol-lutant	Period of Time	Stability Class	Wind Velocity (m/s)	Direction	Mixing Height* m	Penetr. Factor	T.E.M.	APMAX (PTMTP)**
SO_2	1/2 Hour	A	2.46 m/s	N	500 "	2	457	959
"	"	"	"	"	" "	3	468	959
"	"	"	"	"	1000 "	2	316	598
"	"	"	"	"	" "	3	316	598
"	"	"	"	NNW	500 "	2	612	884
"	"	"	"	"	" "	3	616	884
"	"	"	"	NNW	1000 "	2	566	578
"	"	"	"	"	" "	3	566	578

*Mixing height in meters

**Concentration in $\mu g/m^3$

Other runs showed us that T.E.M. gives a lower value of concentration using 400 m of mixing depth compared with the result of APMAX for 500 m mixing depth.

							T.E.M.	APMAX
SO_2	1/2 Hour	B	4.47	N	400	3	378	-
"	"	"	"	"	500	-	-	483

CONCLUSIONS

The efforts of Divisao Controle Ambiente since 1973 now increased with the application of T.E.M. and T.C.M. models to the Sines urban-industrial complex showed that for all the runs no violation of standards is observed if stack heights indicated in Table 5.were constructed. The approach followed by Divisao Controle Ambiente using stacks for dispersion and care in planning seem to be successful to get the stringent standards of the Area, with reasonable costs. Results for the annual concentrations of SO_2 at the Sines Complex were similar with the application of AQDM or T.C.M. shown on page 14.

Both the T.E.M. and the modified P.T.M.T.P. APMAX computer models use the bivariate Gaussian plume hypothesis for prediction of short-term concentrations. Due to several differences in the meteorological assumptions made in the two models, however, APMAX predicts systematically higher concentrations than T.E.M. for estimated 30-minute worst case conditions.

Both models consider the effect of varying the sampling time on predicted concentration levels, and the increase of wind speed with height in the surface layer. In APMAX, these effects are independent of atmospheric stability, while in T.E.M., they are rather strongly dependent on stability class. In particular, predicted maximum concentration decreases more rapidly with increasing sampling time in unstable air than in stable air. In the Sines Complex, where most of the SO_2 is to be emitted from tall stacks, predicted worst case maximum concentrations occur under unstable (classes A or B) conditions. Under such conditions, T.E.M.'s stability-dependent sampling time correction will reduce predicted concentrations by a greater amount than the corresponding correction in APMAX.

In all situations, the modified APMAX program employs a Briggs plume rise formula intended for thermal buoyancy-dominated plumes under stable conditions. T.E.M. uses an ensemble of six Briggs (9) equations, choosing the appropriate equation on the basis of atmospheric stability and the dominant influence on plume rise (buoyancy or momentum). Since concentration predictions are extremely sensitive to effective source height, it is expected that the more sophisticated plume rise treatment in T.E.M. is another contributor to the discrepancies between T.E.M. and APMAX predictions. Other T.E.M. features such as first-order pollutant decay, the ability of sufficiently energetic plumes to escape the mixing layer, and the capability to change meteorological parameters every hour or three hours in a 24-hour simulation are also expected to have an effect.

The authors consider the T.E.M. predictions to more closely represent the future air quality of the Sines Area than do the APMAX results.

Under these conditions Table 5 with the decided values of stack heights constitutes an unusual point of great planning value and has the probable guarantee of a good air quality for the population of the Sines Area with reasonable costs for the Portuguese Government and the involved industries.

BIBLIOGRAPHY

(1) Compilation of Air Pollution Emission Factors - AP-42, United States Environmental Protection Agency, April, 1975.

(2) United States Environmental Protection Agency, "Air Quality Display Model," Publication PB 189184, November, 1969.

(3) Engineering-Science, Inc., "Users Guide for the APMAX Computer Program,"

(4) Canelas, L., and Conceicao, J., High, D., and March, S., "Planning for Industrial Development in Portugal," Air Pollution Control Association Annual Meeting, 1977, Toronto, Canada.

(5) Canelas, L., Conceicao, J., High, D., and Marsh, S., "Air Quality Assessment of Proposed Urban-Industrial Complex, Sines, Portugal," Report to Gabinete da Area de Sines, Portuguese Government.

(6) Christiansen, J.H., "Users' Guide to the Texas Episodic Model," Texas Air Control Board, 1976.

(7) Christiansen, J.H., and Porter, R.A., "Users' Guide to the Texas Climatological Model," Texas Air Control Board, 1976.

(8) Porter, R.A., and Christiansen, J.H., "Two Efficient Gaussian Plume Models Developed at the Texas Air Control Board," Proceedings of the Seventh NATO/CCMS International Meeting on Air Pollution Modeling, Airlie, Virginia, 1976.

(9) Briggs, G.A., Plume Rise, U.S. Atomic Energy Commission, Division of Technical Information, Oak Ridge, Tennessee, 1969.

(10) Stern, A., "Air Pollution," Volumes I, II, III, Academic Press, New York, 1976.

8th International Technical Meeting on
Air Pollution Modeling and its Application

APPLICATION OF THE ATDL SIMPLE URBAN DISPERSION MODEL TO FRANKFURT, WEST GERMANY

Steven R. HANNA
and
Franklin A. GIFFORD, Jr.

Air Resources Atmospheric Turbulence and Diffusion Laboratory
National Oceanic and Atmospheric Administration
Oak Ridge, Tennessee 3783o

September 2o-23, 1977
Louvaine-La-Neuve
Belgium

1. Introduction

We were asked to apply the ATDL urban dispersion model to predict SO_2 concentrations in Frankfurt, West Germany, as part of the Practical Demonstration of Urban Air Quality Simulation Models, in the NATO/CCMS Air Pollution Pilot Study. The input data were supplied in Report N6 by the NATO Committee on the Challenges of Modern Society. The time period of interest is August 1971 to July 1972. Annual average SO_2 concentrations and frequency distributions at six locations were requested, as well as a template for average annual concentrations over the entire Frankfurt region. Measured concentrations at the six stations and results of the applications of other models will be released by the NATO committee at some later date.

In this application, we attempted to stress the simple aspects of the model, in order to provide a more extreme basis for comparison with other models. Our experience has shown that in most applications the simplest model works as well as or better than much more complex models. The simplest version of the ATDL model is

$$\chi = CQ/U \qquad (1)$$

where χ is concentration in $\mu g/m^3$, C is a dimensionless parameter, Q is area source emissions in $\mu g/m^2$ sec, and U is wind speed in m/s (Gifford and Hanna, 1970 and Hanna, 1971). The parameter C, which is a function mostly of stability, is predicted theoretically to have values of 50, 200, and 600 during unstable, neutral, and stable conditions, respectively. The neutral value is also assumed to apply to averages over time periods of one day or greater. Recently Hanna (1977) verified the theoretical predictions of the diurnal variation of C, using observations of carbon monoxide emissions and concentrations and wind speeds at many stations in the eastern U.S. Gifford and Hanna (1973) calculated the ratio $\chi U/Q = C$ for several cities and found that the annual average C for suspended particles agreed with the theoretical prediction. However the observed C equaled 50 for SO_2 and 700 for CO. We reason that the measured C is low for SO_2 because of removal processes and the fact that SO_2 sources tend to be elevated. Likewise, the measured C is high for CO because of the tendency to locate CO monitors right next to busy highways.

A slightly more complex version of the ATDL model was also applied to the Frankfurt data. In this version (Gifford and Hanna, 1970 and Hanna, 1973) advection from upwind grid squares is accounted for in the formula:

$$\chi = \sqrt{2/\pi}((\Delta X/2)^{1-b}/\xi aU(1-b))[Q_o + \sum_{i=1}^{N} Q_i((2i+1)^{1-b}-(2i-1)^{1-b})] , \quad (2)$$

where ΔX is the grid size and N is the number of grid squares between the receptor and the upwind edge of the city. The factors a and b appear in the relation

$$\sigma_z = ax^b \qquad (x \text{ and } \sigma_z \text{ in meters}) \qquad (3)$$

For average or neutral conditions, it is assumed that $a = .15$ and $b = .75$. A 16 point wind direction rose is used in conjunction with equation (2). Concentrations due to large point sources are calculated separately using the Gaussian plume formula and Briggs'(1969) plume rise formulas.

When applied to annual average emissions and wind speeds, the simple model does not yield a frequency distribution of hourly pollution concentrations. It is possible to generate such a distribution by applying the model hour by hour for a year. But in keeping with our emphasis on simplicity, in this exercise the frequency distribution in Frankfurt is assumed to be similar to those reported by Larsen (1971) for eight U.S. cities. His data show that the cumulative frequencies of hourly SO_2 concentrations in urban areas fall along a straight line when plotted on log-normal graph paper. Agreement with the straight line is best for points within two standard deviations of the geometric mean. The average slope of the line, given by the ratio (16 percent concentration)/(50 percent concentration), equals 2.22. Knowing the geometric mean concentration, the distribution can be estimated by drawing a straight line on log-normal graph paper.

2. Input data

In report N6 it is stated that the average annual wind speed in Frankfurt is 2 m/s. The wind direction frequency distribution, used in the more complex version of the simple model, is given in Table 1.

Table 1

Wind Direction Frequencies for Frankfurt

Direction	Fraction	Direction	Fraction
N	.081	S	.030
NNE	.148	SSW	.107
NE	.081	SW	.194
ENE	.032	WSW	.094
E	.030	W	.054
ESE	.027	WNW	.032
SE	.022	NW	.027
SSE	.013	NNW	.028

Stabilities are assumed to be similar to those in previous studies; i.e., the average C = 50 for SO_2.

Area source emissions are given in 0.5 km grid squares in report N6. In our application, the published area source emissions are averaged over 4 km grid squares, since we have found that the best correlation between pollutant concentrations and emissions within a surrounding area A occur when A is about 10 km^2. The area source emissions used in this analysis are summarized in Figure 1, where the x-y coordinate system is the same as that used in report N6. Point source emissions are not listed here because their contribution to the total concentration was found to be slight when compared to the area sources.

3. Results of Application of Simpler Model

Calculations of ground level SO_2 concentrations due to a few of the largest point sources were made using the Gaussian plume formula, leading to the conclusion that the contribution due to point sources is usually less than 5 $\mu g/m^3$. Consequently point sources are neglected in this model application.

The contribution to ground level SO_2 concentrations due to Frankfurt area sources is obtained by multiplying the emissions listed in Figure 1 by C/U, or 25 sec/m. Because of the strong industrialization of the western Germany region in which Frankfurt is located, a background must also be included. Best agreement with the magnitude of observed SO_2 concentrations is obtained by assuming a background of 40 $\mu g/m^3$. Predicted SO_2 concentrations for each grid square are given in Figure 2 and isopleths based on these values are given in Figure 3. The six stations for which predictions are made are also shown on the figures. All but station 3 are located near the center of grid squares, and the concentration can be assumed to be equal to that listed in the grid square. The concentration at station 3 is assumed to be given by the average of the four surrounding grid squares. The predicted concentrations are listed in Table 2 along with the predictions of other models. The observed concentrations are best estimates interpolated from data in the N6 report.

Table 2

Model Predictions and Observations of Annual SO_2 Concentration in Frankfurt

Station	Observed $\chi(\mu g/m^3)$	ATDL Simpler Model χ	ATDL More Complex χ	(a) CDM χ	(a) CDM36 χ	(b) Texas χ	(c) Neth. χ	(d) SCAM χ
1	95	97	88	68	71	123	79	72
2	96	125	111	59	60	97	65	57
3	93	116	104	71	76	111	88	75
4	62	67	65	50	53	85	70	47
5	77	54	59	29	30	23	45	21
6	68	70	78	35	37	51	42	38
Correlation between observed and predicted		.83	.80	.70	.68	.61	.56	.67

(a) Turner (1976)
(b) Christiansen and Porter (1976)
(c) Nieuwstadt and Engeldal (1976)
(d) Irwin (1976)

The other model predictions are taken from reports sent to us during the past few months by some of the other research groups participating in the model comparison. The ATDL "more complex" model predictions will be discussed in the next section. The correlations listed in the table show that the simpler ATDL model produces the best correlation ($r = .83$) between observed and predicted concentrations.

Predicted frequency distributions of hourly SO_2 concentrations for the six stations are given in Figure 4. These are based on Larsen's (1971) findings that urban distributions are log-normal and that the ratio of the 16 percent to the 50 percent concentation averages 2.22 for eight U.S. cities. For a log-normal distribution the geometric mean equals the arithmetic mean (given in Table 2) divided by $\exp(0.5\ \ln^2 2.22)$. The curves in Figure 3 are truncated at ± two standard deviations because of uncertainties in the extreme values.

4. Results of Application of More Complex Model

The more complex model described by equation (2) accounts for advection from upwind grid squares. Also, individual calculations of contributions due to 51 point sources with source strength greater than 5 kg/hr are made. The computer program listed by Hanna (1973) was used to make these calculations, using a grid size of 4 km, a mean wind speed of 2 m/s, and the wind direction frequency distribution in Table 1. A background SO_2 concentration of 40 $\mu g/m^3$ is assumed, as before. The predicted concentrations at each grid square are given in Figure 5, where the number in parentheses is the contribution due to point sources. It is seen that the contribution due to point sources is nearly always a small fraction of that due to area sources, especially in the areas with higher concentrations. The predicted concentrations for the six monitoring stations are listed in Table 2, giving a correlation of .80 between observations and predictions. It is interesting that the simpler model gives the best correlation for these data, although the slight difference is statistically insignificant. We find that this happens consistently, whenever the simple model is compared with more complex models using new sets of urban pollution data. A comprehensive comparison of our model with many others was given by Gifford (1973) at the 4th meeting of the NATO/CCMS group.

5. Conclusions

The average annual SO_2 concentrations predicted by the simple ATDL urban dispersion model are listed in Table 2. The correlation between the predictions and interpolated observations is .83. The template for annual SO_2 concentrations is given in Figure 3, which is directly proportional to the area source emissions template in Figure 1. Point sources were determined to be unimportant in these calculations. Cumulative frequency distributions of hourly SO_2 concentrations are given in Figure 4, based on the assumptions of a log-normal distribution with a slope determined by SO_2 data from U.S. cities.

6. Acknowledgements

Much of the Frankfurt data was relayed to us by Bruce Turner and John Irwin of the U.S.E.P.A. This research was conducted under an agreement between the National Oceanic and Atmospheric Administration and the Energy Research and Development Administration.

REFERENCES

Briggs, G. A., 1969: *Plume Rise*, AEC Critical Rev. Series, TID-25075, 81 pp.

Christiansen, J. H. and R. A. Porter, 1976: Predictions of Annual Sulfur Dioxide Concentrations for Frankfurt Main, Federal Republic of Germany. Texas Air Control Board, Austin, Texas, 28 pp.

Gifford, F. A., 1973: The simple ATDL urban air pollution model, proceedings of 4th Meeting of NATO/CCMS Panel on Modeling, 17 pp.

Gifford, F. A. and S. R. Hanna, 1970: Urban Air Pollution Modeling, presented at 11 Dec. 1970 meeting of the Int. Union of Air Poll. Prev. Assoc., Washington, 17 pp, proceedings published by Nat. Air Poll. Cont. Assoc.

Gifford, F. A. and S. R. Hanna, 1973: Modeling urban air pollution. *Atmos. Environ*., *7*, 131-136.

Hanna, S. R., 1971: A simple method of calculating dispersion from urban area sources. *J. Air Poll. Cont. Assoc*., *21*, 774-777.

Hanna, S. R., 1973: Description of ATDL Computer Model for Dispersion from Multiple Sources. *Industrial Air Pollution* Control, Ann Arbor Science, Ann Arbor, MI, 23-32.

Hanna, S. R., 1977: A stability correction term for a simple urban dispersion model. Proceedings of AMS Conference on Applications of Air Pollution Meteorology, Salt Lake City, 28 Nov. - 2 Dec. Available from Am. Meteorol. Soc., 45 Beacon St., Boston, MA.

Irwin, J. S., 1976: The Application of the SCAM (Sampled Chronological Air Quality Model) to the NATO Common Data Base for Frankfurt. U.S. EPA, Research Triangle Park, NC, 27711, 12 pp.

Larsen, R. I., 1971: A Mathematical Model for Relating Air Quality Measurements to Air Quality Standards, EPA Office of Air Programs, Research Triangle Park, NC, Publ. No. AP-89, vii + 56 pp.

NATO Committee on the Challenges of Modern Society, 1974: Air Pollution, Appendix C - Assessment of Air Quality in Frankfurt, Federal Republic of Germany, Report N6, Air Poll. Tech. Inf. Center, Office of Air & Waste Management, U.S. EPA, Research Triangle Park, NC, 27711, 238 pp.

Nieuwstadt, F. T. M. and C. A. Engeldal, 1976: Application of the Recommended National Air Pollution Model of the Netherlands to the NATO Common Data Base for the Frankfurt Area. Wetenschappelijk Rapport W. R. 76-17, De Bilt, 12 pp.

Turner, D. B., 1976: The Application of the CDM (Climatological Dispersion Model) to the NATO Common Data Base for Frankfurt, U.S. EPA, Research Triangle Park, NC, 27711, 9 pp.

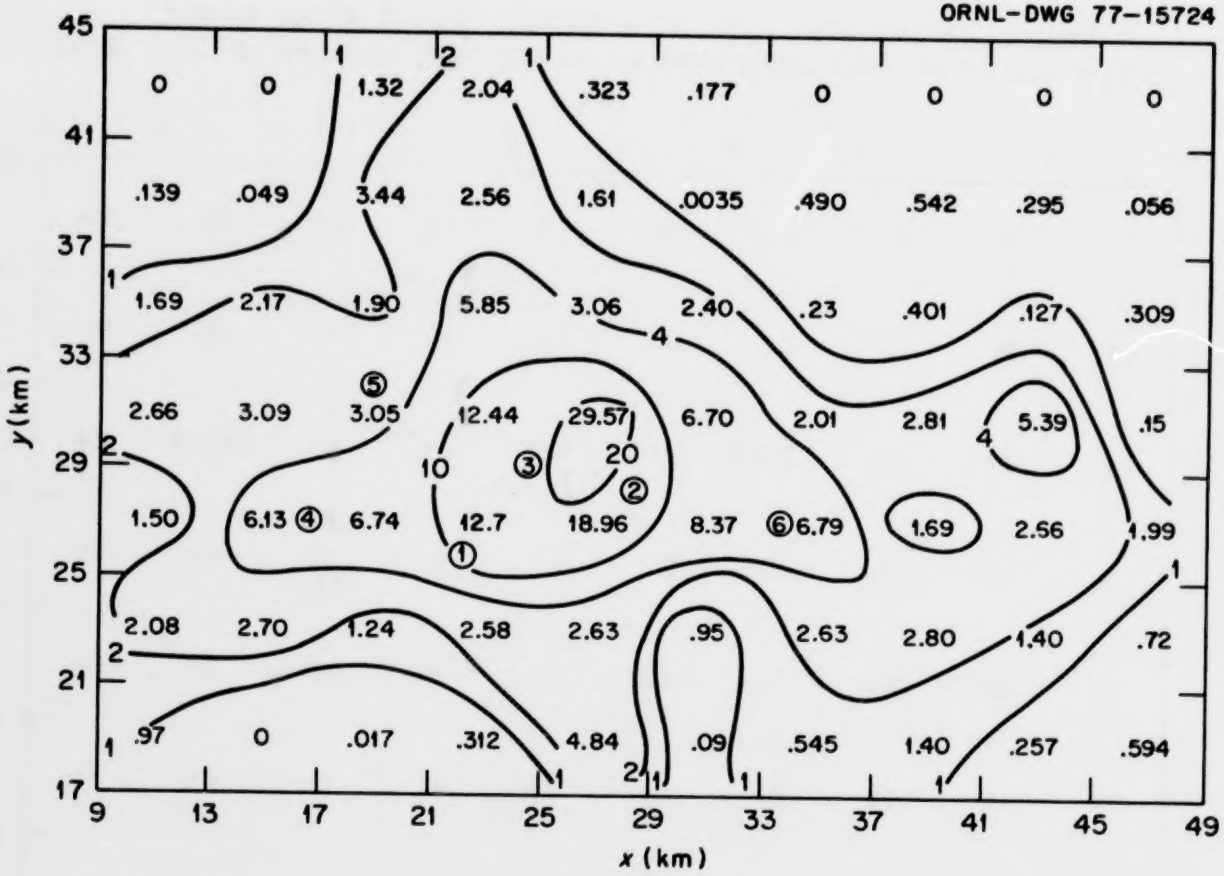
ORNL-DWG 77-15724
y(km)
x (km)
45
41
37
33
29
25
21
17
9
13
17
21
25
29
33
37
41
45
49
0 0 1.32 2.04 .323 .177 0 0 0 0
.139 .049 3.44 2.56 1.61 .0035 .490 .542 .295 .056
1.69 2.17 1.90 5.85 3.06 2.40 .23 .401 .127 .309
2.66 3.09 3.05 12.44 29.57 6.70 2.01 2.81 5.39 .15
1.50 6.13 6.74 12.7 18.96 8.37 6.79 1.69 2.56 1.99
2.08 2.70 1.24 2.58 2.63 .95 2.63 2.80 1.40 .72
.97 0 .017 .312 4.84 .09 .545 1.40 .257 .594
①
②
③
④
⑤
⑥
1
2
4
10
20

Fig. 1: Area Source Emissions in $\mu g/m^2$ sec. Monitoring Station Locations are Circled.

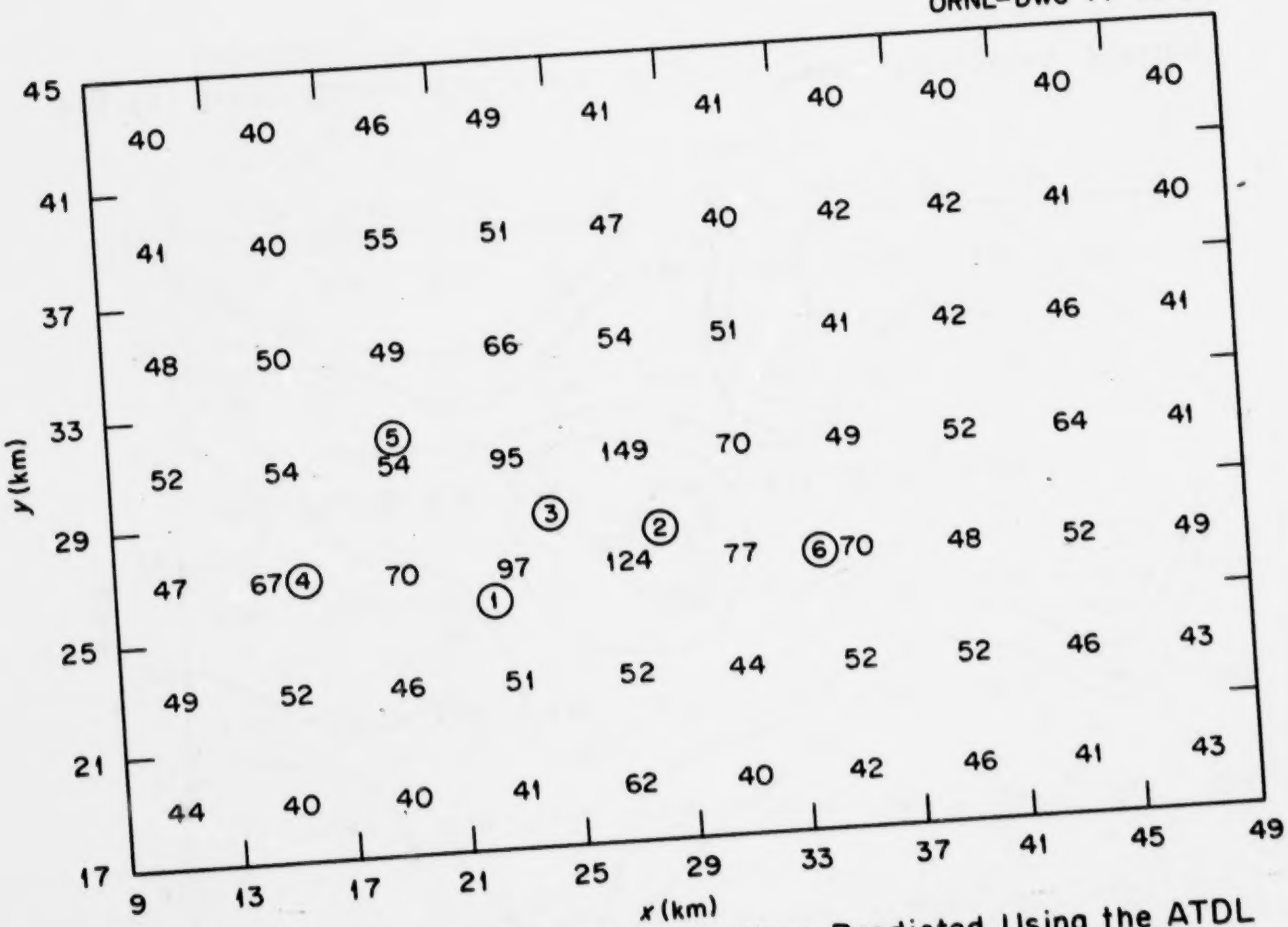
ORNL-DWG 77-15725

Fig. 2. Annual Average SO_2 Concentrations Predicted Using the ATDL Simple Model χ = Background + 50 Q/U. Monitoring Station Locations are Circled.

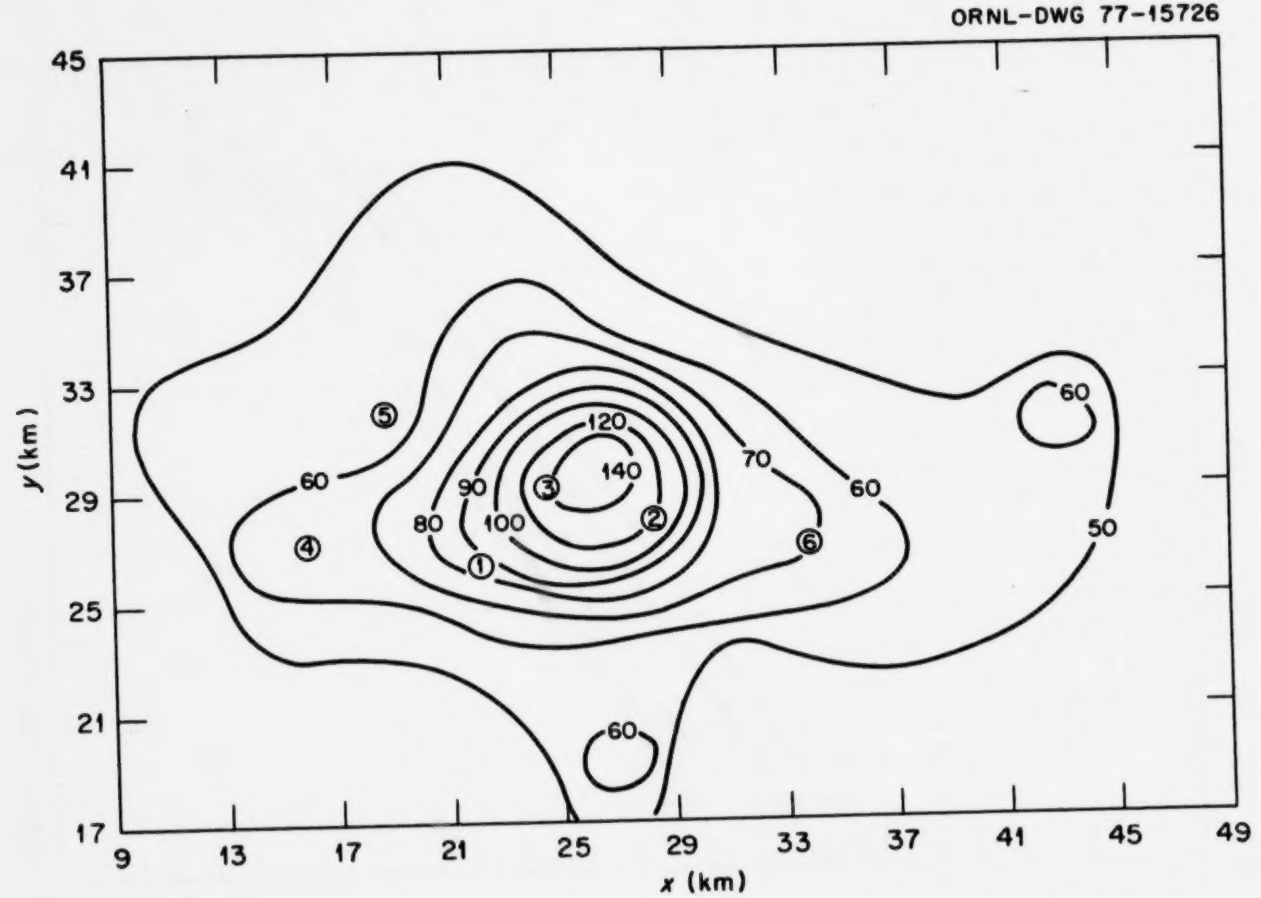

Fig. 3: Isopleths of Annual Average SO_2 Concentrations, Drawn from the Data in Figure 2. Monitoring Station Locations are Circled.

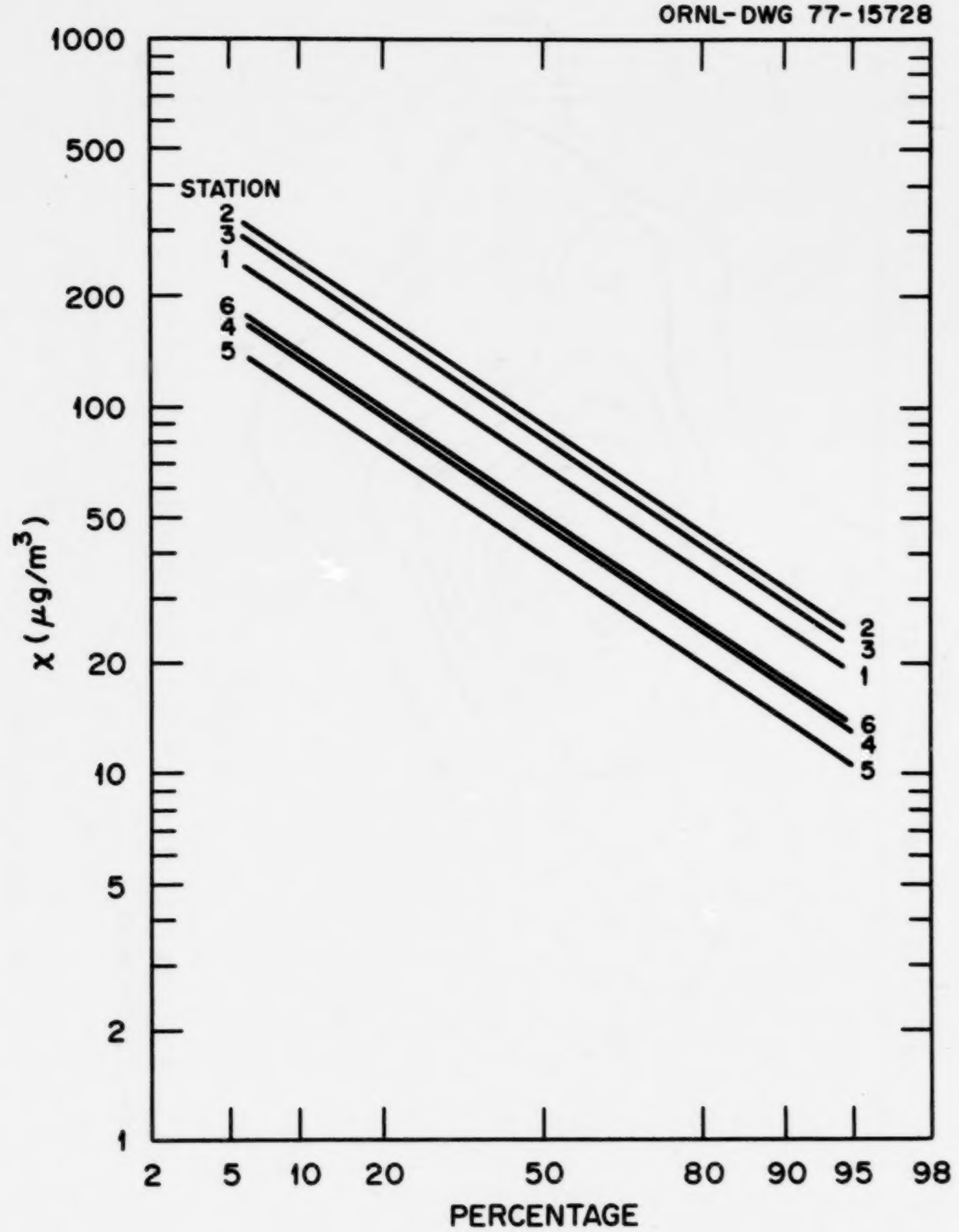

Fig. 4. Frequency of 1hr SO_2 Concentration Equal to or in Excess of Stated Values. Frankfurt, West Germany, 1971 - 1972.

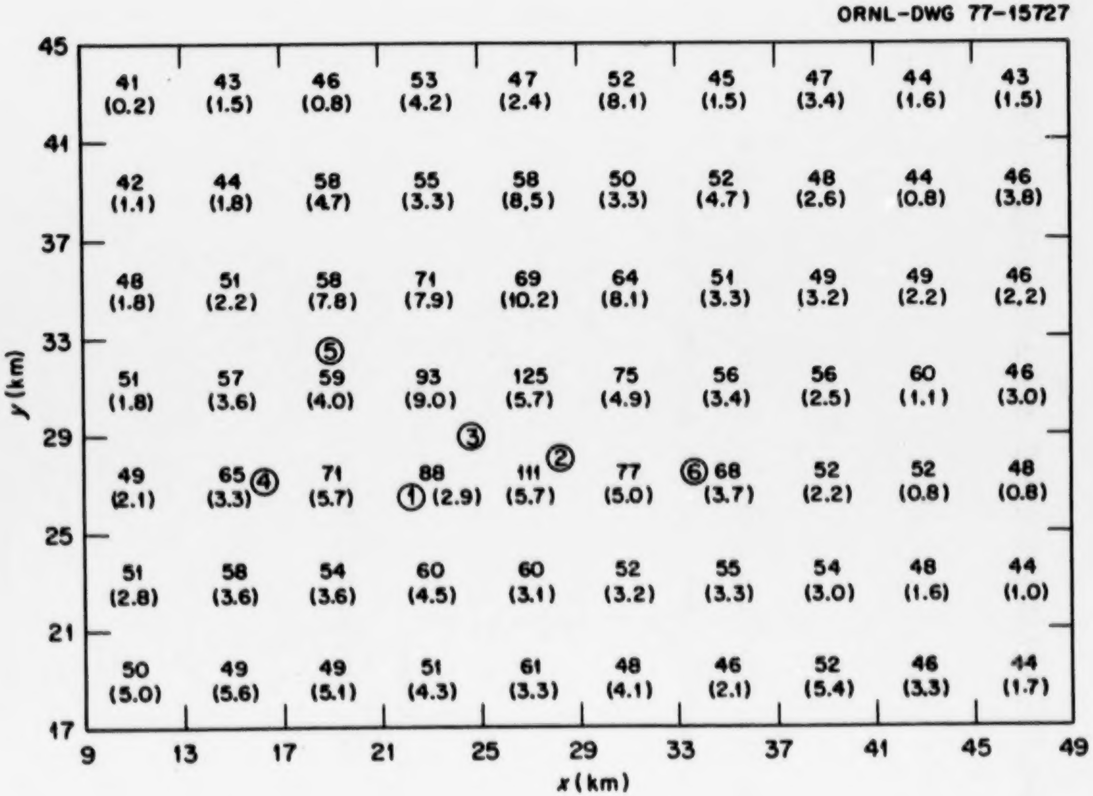

FIG. 5: Annual Average SO_2 Concentrations Predicted Using the ATDL Computer Model (Based on Equation (2) for Area Sources and the Gaussian Plume Formula for Point Sources). Numbers in Parentheses are the Point Source Contributions. Monitoring Station Locations are Circled.

8th International Technical Meeting

on Air Pollution Modeling and its Application

Comparison of Dispersion Calculations with Measurements in the Cologne Area

L. Kropp

TÜV Rheinland, Köln, FRG

September 20 - 23, 1977

Louvain-La-Neuve

Belgium

Comparison of Dispersion Calculations with Measurements in the Cologne Area

Dr. L. Kropp, TÜV Rheinland, Köln, FRG

Introduction

Dispersion calculations are performed e.g. within air quality forecasts

- during the licensing procedures of new or expanding plants or
- to decide upon measures to reduce air pollution load within clean air plans.

For the first task the aim is to prevent air pollution before plant erection. The second application shall help reduce already existing air pollution load. In this case an as good as possible model should be available while in the former application the idea is the calculation "pro environment".

Model used

The model is of gaussian plume type. The dispersion parameters are those of McElroy/Pooler and Singer/Smith for low (less than 100 m) and high (more than 100 m) sources, respectively, as cited in [1]. The plume rise is calculated following Moses and Carson's formula for neutral conditions [2]. All SO_2 emissions of industry and domestic heating as well as small trade industries in the Cologne region were taken into account. Smaller emissions are fed together to area sources with a standardized plume rise.

The meteorologic joint frequency distribution of wind speed, direction and turbulence class of Cologne is used. A five years observation with Turner's stability classification was introduced.

Measurements

Ambient air quality of SO_2 was measured in a grid system with a mash size of 1 x 1 km by the LIS (Landesanstalt für Immissionsschutz = state institution to control air quality) in Northrhine-Westphalia.

The published data [3] are annual mean values and 95-percentiles (concentrations not exceeded during 95 percent of the time) of 1975. The data correspond to the load within a square kilometer each.

Calculations

The calculated data derived from the comprehensive emissions inventory of 1974 represent the expected air quality in the center of the same square kilometer as defined for the measurements.

Results

Measured and calculated data are compared by

- plotting their absolute values for several cross sections through the Cologne region as indicated in fig. 1.+)

+) A first comparison was presented by Schmitt at the IUAPPA-Congress in Japan [4]

- forming the ratios between calculated and measured values for each mash and drawing the frequency distributions for the total area and parts of it, respectively (see fig. 1 indicated by N, C and S).

Annual mean values

Fig. 2 displays measured and calculated annual mean SO_2 data for 5 sections from West to East. The bar inserted in the display of section III indicates a factor of 1.5 for the ratio. In general deviations are smaller than this factor of 1.5. The exception (large deviations) in the eastern part of section I is due to industry in this part of the region that has not been taken into regard for the calculations.

Fig. 3 presents the annual mean values for 3 more sections:

- sections VI and VII are oriented form North to South and
- section VIII form NW to SE.

The deviations are generally in the order of 1.5 or less.

The overall evaluation of the deviations can be seen from fig. 4. It presents the frequency of the ratio between calculated and measured annual mean SO_2 values for each grid point:

T stands for the total ensemble of data in the region,
N represents the data for the northern part only (ref. to fig. 1),
S is for the southern part only (as indicated in fig. 1),
C includes the data of the central (city) part.

The sum frequency distributions of measured and calculated data are given as insert in fig. 4, respectively.
Annual mean calculations are - averaged over the total ensemble - about 10 % higher than the measured data. About 70 % of all calculated data are between 0.8 and 1.5 times the measured data. Corresponding results can be derived for the different parts of the region from fig. 4. It is to be seen that the calculation seems to be better for the northern industrial part than for the southern industrial one or the central parts.

95 - percentiles

The corresponding results for the 95-percentiles (during 95 % of the time the indicated concentrations are not exceeded) of SO_2 are displayed in figs. 5 to 7. The calculated values are generally higher than the measured ones. The comparison for sections I, II and VIII show a better agreement than for section III to VII. For better valuation a factor of 2 as deviation is drawn as a bar in the displays of section III and V.
From fig. 7 an average deviation of about 1.9 for the data of the whole area can be derived with about 70 % of all ratios lying between 1.3 and 2.5. The agreement is also better in the northern industrial area (curve N) and less in the central (C) or southern industrial (S) parts. The sum frequencies of calculated and measured 95-percentiles are displayed as inserts.

Conclusion

The comparison of calculated and measured SO_2 data in the Cologne area show that for a region of more than 500 km² and introducing the comprehensive inventory though no model calibration was performed

- calculations of annual mean values fit the measured data by a factor of approx. 1.1 ± 0.3 and

- calculations of 95-percentiles fit the measured data by a factor of approx. 1.9 ± 0.6.

It therefore can be derived that even higher percentiles will be overestimated more with a lager scattering assuming that the measured data be correct.

Unfortunately no comparison could be made for hydrocarbons or other measured components because of missing calculations.

Acknowledgement

Thanks are due to the Ministry of Labour, Health and Social Affairs of Northrhine-Westphalia for the permission to use the calculations performed during the preparation of the Clean Air Plan for Cologne [3].

References

[1] Regulations for the licensing of Refineries and Petrochemical Plants. RdErl. MAGS III B 4/III B 6 - 8856.4 (III Nr. 13/1975) v. 14.4.1975

[2] Moses, H. and Kraimer, M. R.: Plume rise determination JAPCA 22 (1972) 621

[3] Clean Air Plan for the Cologne Region ed. and publ. by Minister of Labour, Health and Social Affairs of Northrhine-Westphalia, Germany (1976)

[4] Schmitt, O.A.
A Standardized Dispersion Model for Judging Permissibility of Air Pollution Industrial Facilities in the Fed. Rep. of Germany. Paper presented at 4 th Clean Air Congress May 1977. Tokyo, Japan

Figure caption

Fig. 1	Area under investigation (Cologne)
Fig. 2	Average concentrations calculated and measured for 5 W - E sections
Fig. 3	Average concentrations calculated and measured for 3 more sections
Fig. 4	Frequency distribution of ratios between calculaed and measured values (averages)
Fig. 5	95 percentiles calculated and measured for 5 W - E sections
Fig. 6	95 percentiles calculated and measured for 3 more sections
Fig. 7	Frequency distribution of ratios between calculated and measured 95 percentiles

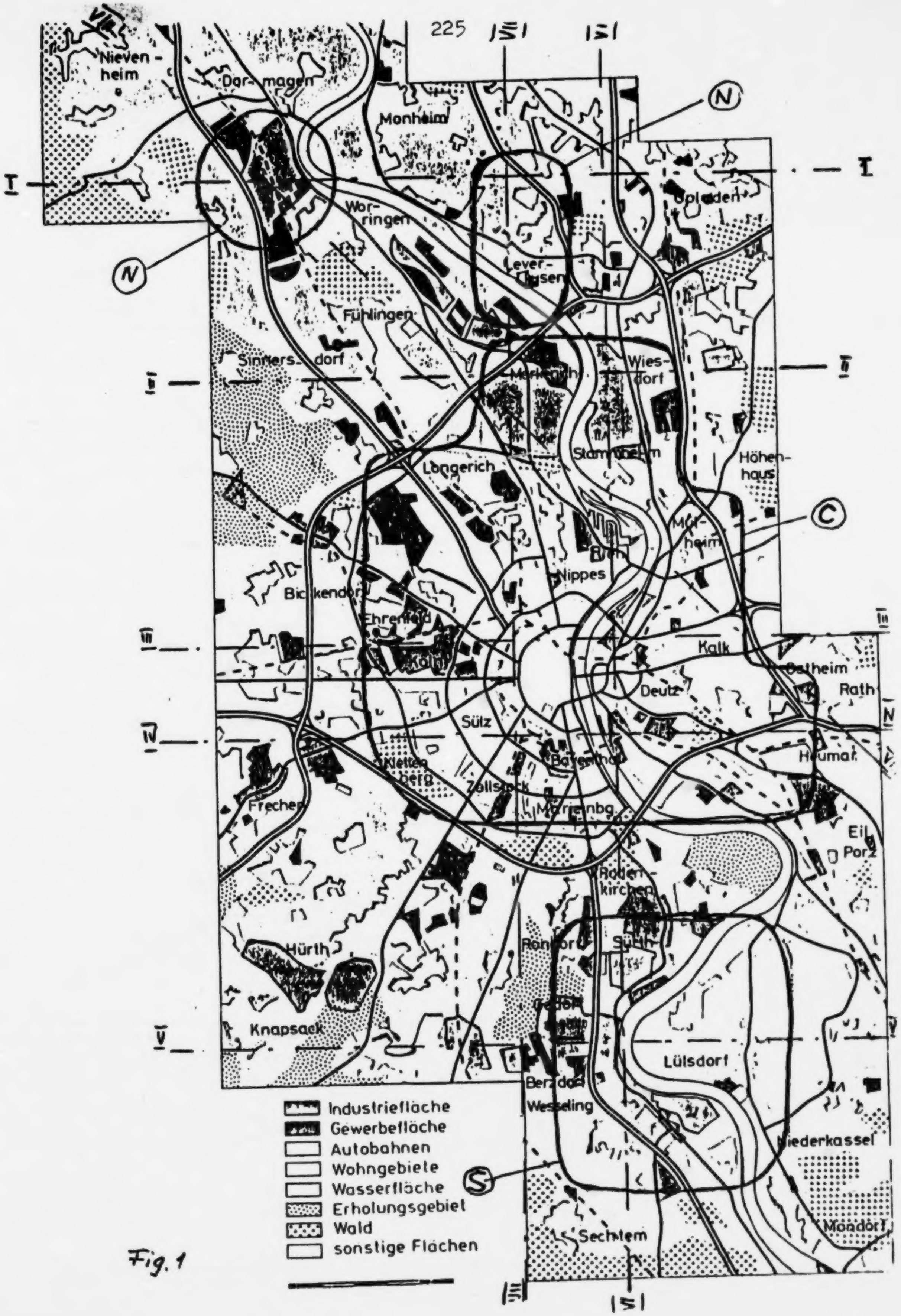

|S|
|S|
Nieven-heim
Dor-magen
Monheim
N
I
I
Opladen
Wor-ringen
N
Lever-kusen
Fühlingen
Sinners-dorf
Merkenich
Wies-dorf
II
II
Stammheim
Höhen-haus
Longerich
C
Mül-heim
Nippes
Bickendorf
Ehrenfeld
Köln
III
III
Kalk
Ostheim
Rath
Deutz
Sülz
IV
IV
Bayenthal
Heumar
Klettenberg
Zollstock
Frechen
Marienbg.
Eil
Porz
Roden-kirchen
Hürth
Rondorf
Sürth
Godorf
Knapsack
V
V
Lülsdorf
Berzdorf
Wesseling
Niederkassel
S
Sechtem
Mondorf
|S|
|S|
Industriefläche
Gewerbefläche
Autobahnen
Wohngebiete
Wasserfläche
Erholungsgebiet
Wald
sonstige Flächen

Fig. 1

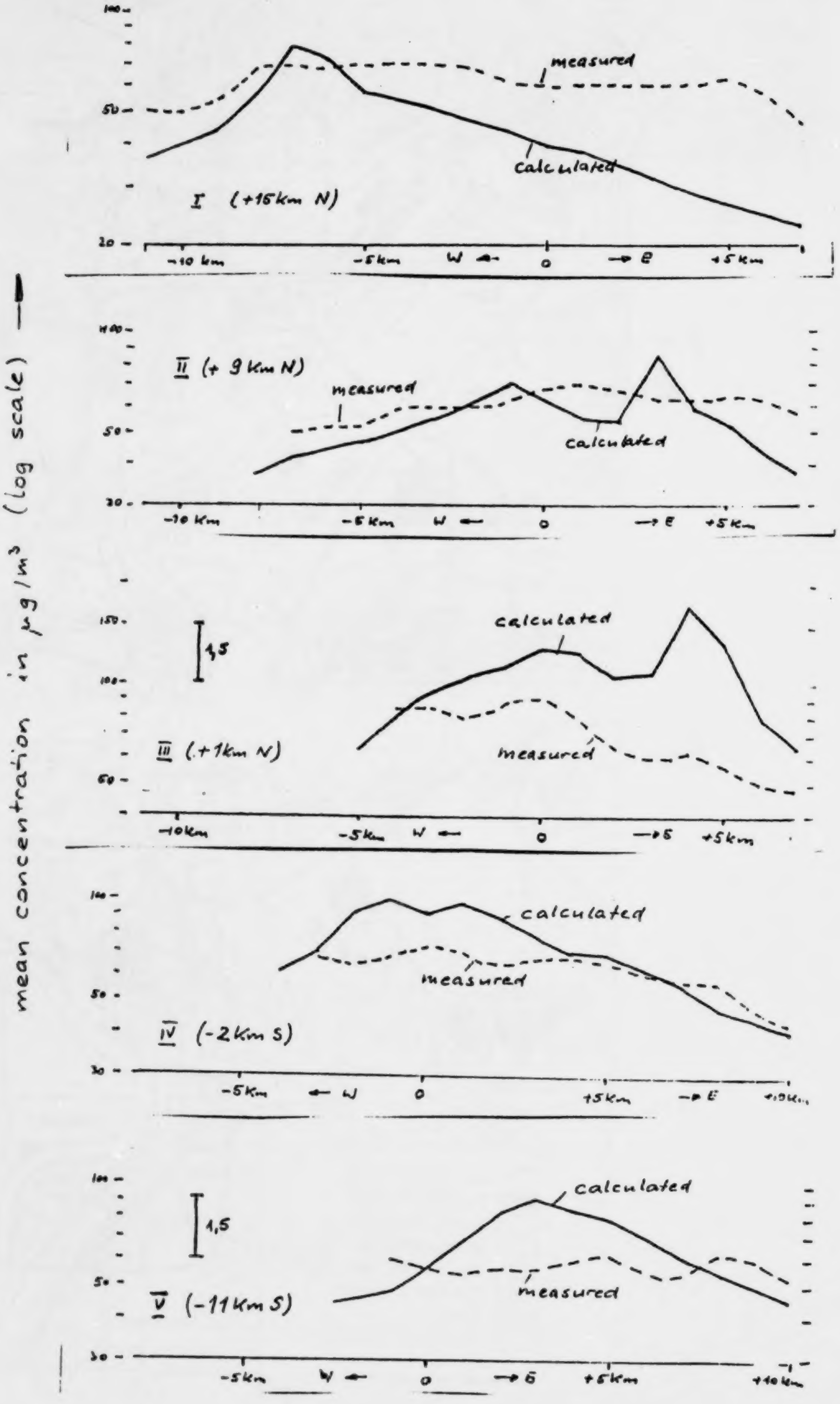
mean concentration in µg/m³ (log scale)
I (+15km N)
measured
calculated
100
50
20
-10 km
-5km
W
0
E
+5km
II (+ 9 Km N)
measured
calculated
100
50
30
-10 Km
-5 Km
W
0
E
+5 Km
III (+1km N)
calculated
measured
1,5
150
100
50
-10km
-5km
W
0
E
+5km
IV (-2Km S)
calculated
measured
100
50
30
-5Km
W
0
+5Km
E
+10Km
V (-11Km S)
calculated
measured
1,5
100
50
30
-5Km
W
0
E
+5Km
+10Km

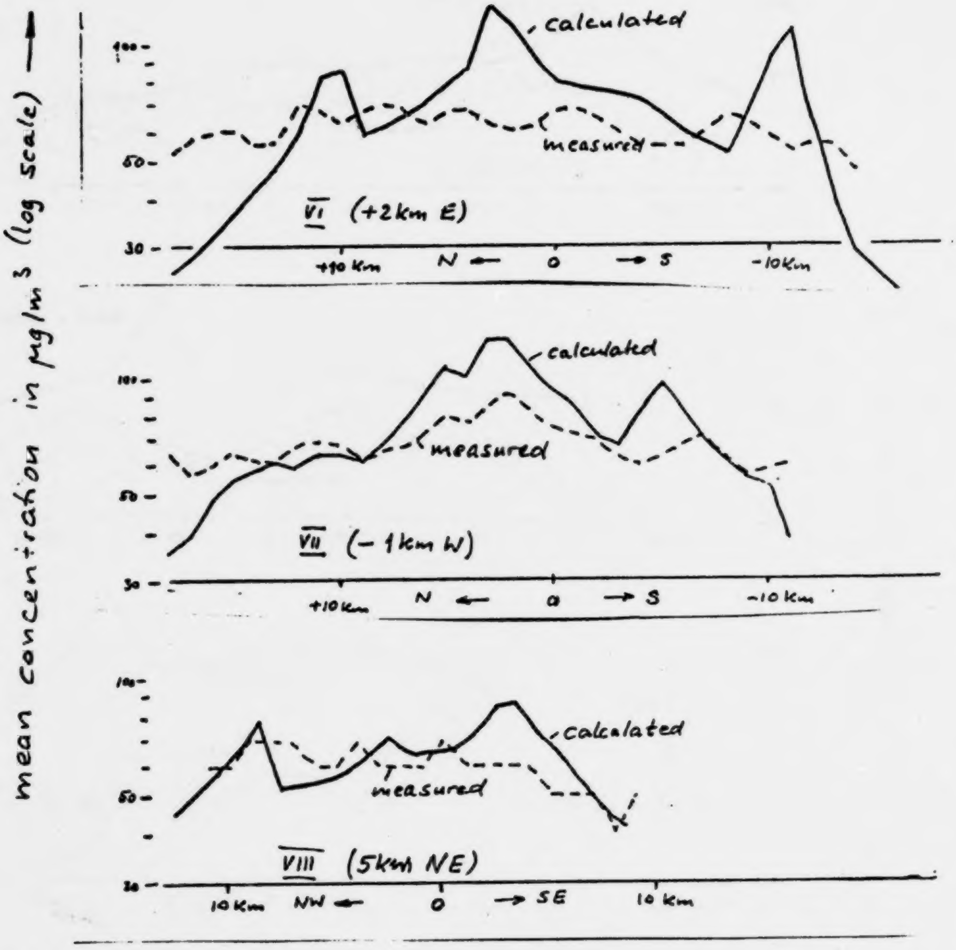
mean concentration in µg/m³ (log scale)
100
50
30
calculated
measured
VI (+2km E)
+10 Km
N
0
S
-10 Km
calculated
measured
VII (-1km W)
+10 Km
N
0
S
-10 Km
calculated
measured
VIII (5km NE)
10 Km
NW
0
SE
10 Km

Fig. 3.

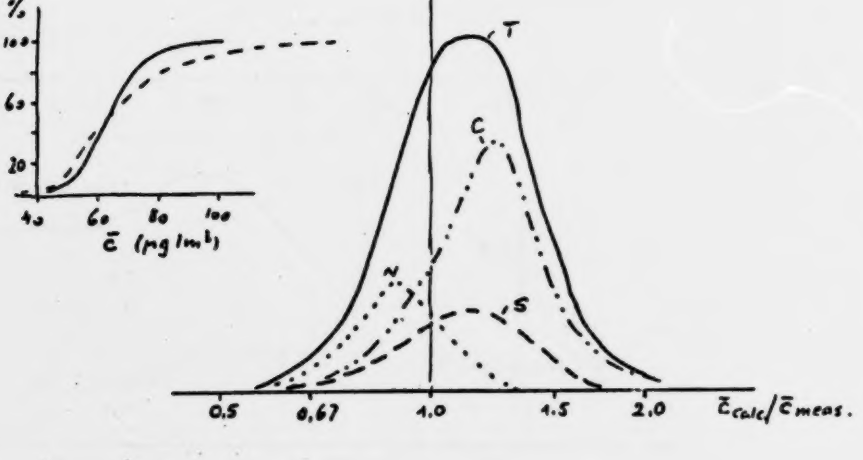
%
100
60
20
40
60
80
100
c̄ (µg/m³)
T
C
N
S
0,5
0,67
1,0
1,5
2,0
c̄calc/c̄meas.

Fig. 4.

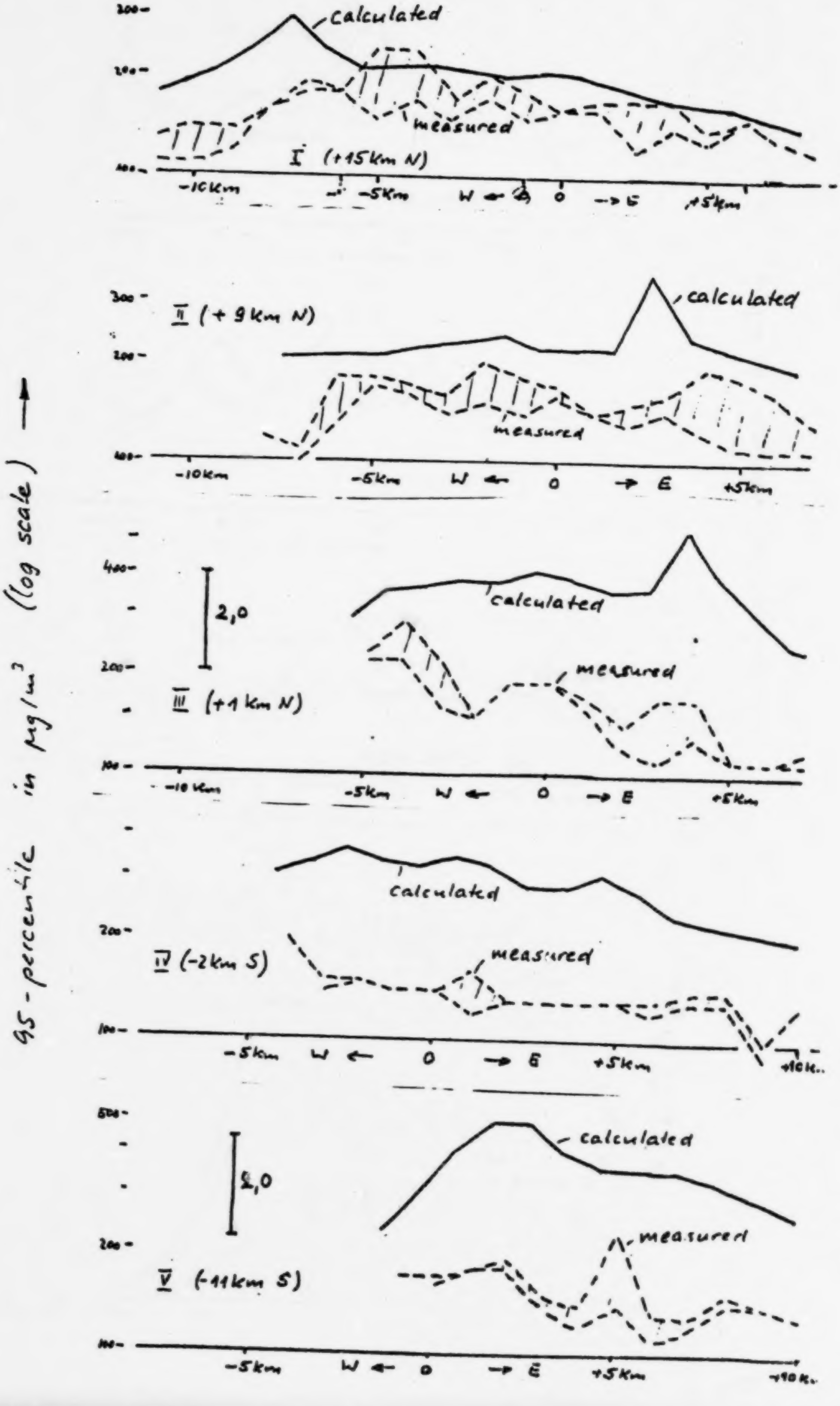
95-percentile in µg/m³ (log scale) →
calculated
measured
I (+15km N)
200
100
-10km
-5km
W ← 0 → E
+5km
II (+9km N)
300
200
100
calculated
measured
-10km
-5km
W ← 0 → E
+5km
400
200
100
2,0
calculated
measured
III (+1km N)
-10km
-5km
W ← 0 → E
+5km
calculated
200
measured
IV (-2km S)
100
-5km
W ← 0 → E
+5km
+10km
500
2,0
calculated
200
measured
V (-11km S)
100
-5km
W ← 0 → E
+5km
+10km

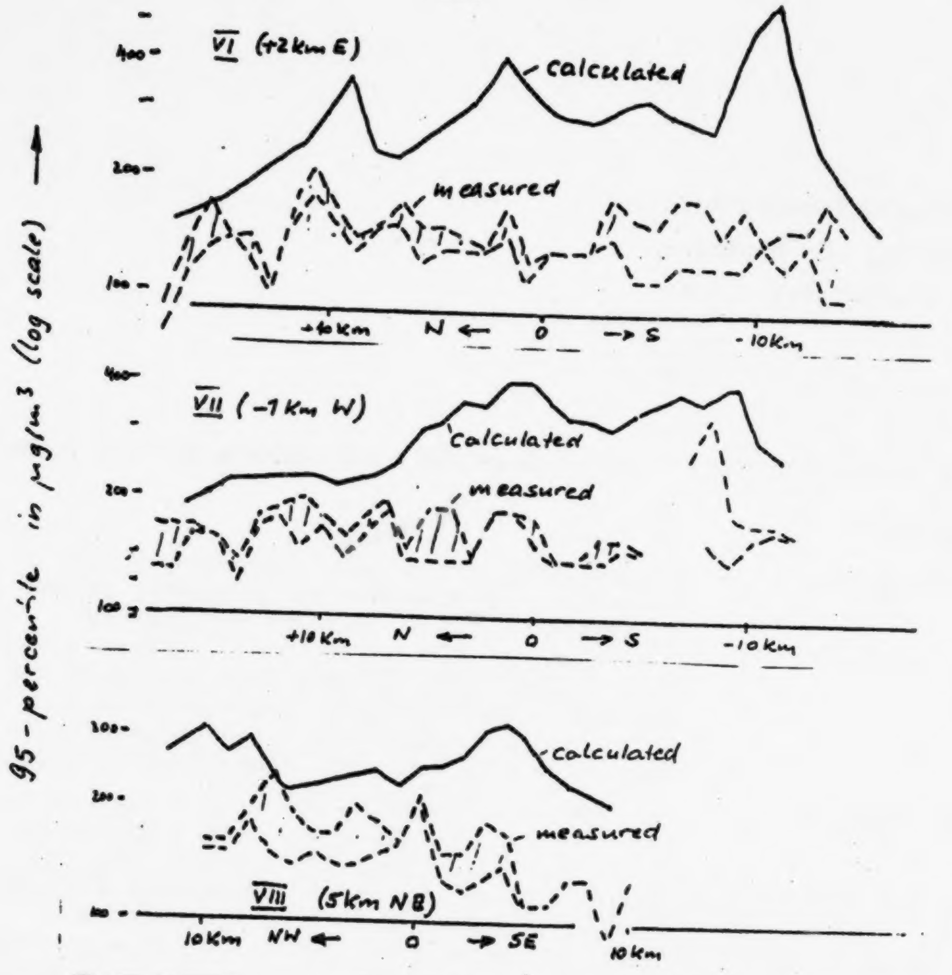
95-percentile in µg/m³ (log scale) →
400
200
100
VI (+2km E)
calculated
measured
+10km N ← 0 → S -10km
400
VII (-1km W)
calculated
measured
200
100
+10km N ← 0 → S -10km
300
200
calculated
measured
100
VIII (5km NE)
10km NW ← 0 → SE 10km

Fig. 6

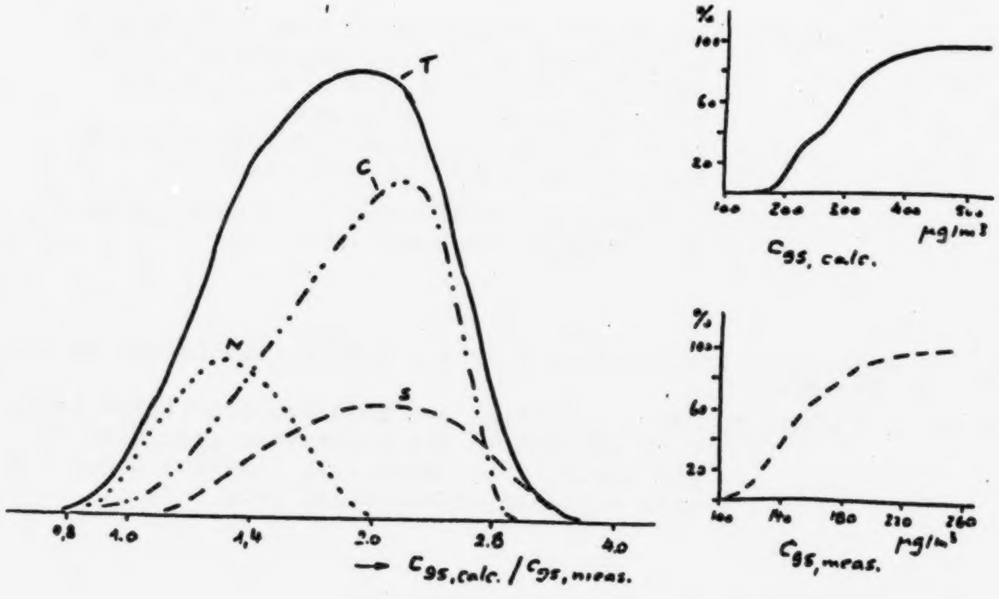
T
C
N
S
0.8
1.0
1.4
2.0
2.8
4.0
→ C95,calc. / C95,meas.
%
100
60
20
100
200
300
400
500
µg/m³
C95, calc.
%
100
60
20
100
140
180
220
260
µg/m³
C95,meas.

Rapporteur's Summary Report:

Prepared by: B. Sivertsen

Papers covered by: Rote
Brubaker
Porter
Hanna
Kropp

Paper: Don Rotes Paper: Current uses and requirements for A.Q. models

Questions:

Warren Johnson:	I have a comment to your statement on the connection between the Environmental Impact Statement (EIS) and the Air Quality Management (AQM) or the implementation of the EIS. I know that in California there is a connection between the environmental impact statement, the adverse effects stated in these and the rejection of plans.
Answer: Rote	California is probably one of the most developed regions in the sense that they really apply the EIS. That is, however, not the case in all countries. As an example I could mention that in one country I visited the construction of a new industrial site started before the meteorological data from the site had been collected, and the EIS was thus presented after construction of the plant.
Question: L. Prahm	You stated in your paper that more complex models only are better than simple models for short averaging times. Are you then thinking about urban models only? It is not our experience in modeling long range transport of air pollutants.
Answer: Rote	I have only looked at available urban data, were models have been validated.

Paper: A method for the comparison of air quality simulation models, K. Brubaker

Question: J. Padro	Are the initial and boundary conditions taken into account in the parameters specified for the users. I am especially thinking about the user's choice of numerical grid models.

Answer: Brubaker	The user has to specify influx of pollutants or background pollution levels. The user is informed of difficulties in boundary conditions in the documentation of the different models, so the user is informed about what kind of input information he has to provide.

Paper: Comparative study of four mathematical air dispersion models for a new urban industrial complex of Sines, Portugal
R. Porter

Question: D. Jost	We have earlier to day heard that only 40 - 60 % of the variance of pollution data can be explained from meteorological data. How do you know that your calculated valued of groundlevel concentrations are on the safe side of the air quality standard? Were the models for calculating short term concentration validated for these averaging times?
Answer: Porter	I am not sure that these models were properly validated at all, and I am aware of the uncertainties in the calculated concentrations.
Question: T. Schneider	To be sure that your calculated concentrations really are below the stated air quality standards, I think you should try to after cheque the emission data.
Answer: Porter	Part of the future plan includes emission evaluation.
Question: Sivertsen	You are preparing an environmental impact statement for a large industrial area, including a petrochemical complex, based upon emissions of SO_2. Do you have plans for also considering the impact of hydrocarbon and nitrogenoxide emissions? I would think that photochemical oxidants and particulate sulphate might lead to as large problems in the future as SO_2, at the latitude of south of 40° N.
Answer: Porter	I don't know a proper photochemical model that can solve these problems, wo we will not go into the evaluation of photochemical smog potential
Question: Brubaker	I understood that the site was close to the coast. Have you considered the extent of the seabreeze effect on the ground level concentrations?

Answer: Porter We have not taken the seabreeze into consideration in the calculations, but I expect it to have a strong effect on the maximum short term concentrations.

Question: W. Johnson Do you have any significant terrain features that complicate the model calculations?

Answer: Porter No, the terrain in the area is faily flat.

Question: Runca Have anyone tried to categorize the atmospheric stability of the area. I think this will lead to difficulties, because you have to specify the parameters for the specific application.

Answer: Porter The stability data originated from data at Lisbon, as did the mixing depths. The mixing depth data is probably the least appropriate, and there is a programme to get better data on mixing depths.

Question: M. W. Williams How far would you go to justify the 95 % half-hour concentrations based on annual average emission data?

Answer: Porter I feel faily comfortable as most of the emissions are continous emissions.

Question: Knox What was the background for the decision that 20 % of the air quality standard is allocated to the power plant?

Answer: Porter That decision was taken before we started our modeling work, and was based upon the fact that 20 % of the fuel was to be used by the power plant.

paper: Application of the ATDL simple urban dispersion model to Frankfurt, West Germany, St. Hanna

Question: Slater The relative small contribution of the point sources in your complex model, is that due to your assumption of a faily high background concentration of 40 ug/m^3, which probably would obscure the results

Answer: Hanna The point sources did not contribute to more than 10 ug/m^3 in any point of the area.

Question: Prahm If you compare the slope of the regression line between calculated and observed data it seems like you over estimate the highest concentrations, while you are close at the lower concentrations.

Answer: Hanna — Yes I think you are right.

Question: Kretzschmar — How did you arrive at a background concentration for Frankfurt at 40 ug/m^3? It seems to high to me.

Answer: Hanna — I have got the background concentrations through all available literature, and I more or less had to work by guesswork. If you have good data I would appreciate seeing them.

Question: Berger — Your simple model use the wind only as a factor. Do you mean that other meteorological variables have nothing to do with air pollution problems?

Answer: Hanna — In calculating the total concentration with more complex models, all the small variations due to the different parameters are well hidden under the integrals carried out.

Question: Nieuwstadt — In comparing the model results with measurements you have used correlation coefficients. I think you should be careful of using these coefficients based on only 6 points. I don't think you can say that one model is better than another one.

Answer: Hanna — I did not say that.

Question: Knox — The slopes of Larsen's frequency distributions that you have used to establish frequency distributions in Frankfurt varies from one station to another in USA. At least that is the case for the frequency distributions of oxidants in the LA-region.

Answer: Hanna — The slopes for the different distributions in US-cities, that I have used varies from 1.8. - 2.5 with an average of 2.22.

Paper: Comparison of dispersion calculations and measurements in the Cologne area, L. Kropp

Question: Berger — In your east-west cross sections the computed values were lower than measured in the northern part of your area, while the opposite was the case in the south. Have you used information of background concentrations, or influx from outside in your calculations?

Answer: Kropp	No I do not think so. We over estimate, in general, the concentrations in the city center, where we have good emission data, while we under estimate in the outer parts where we have bad emission data.
Question: Schorling	Don't you think that you use the model to too large distances? The o-values are not good at long distances from the source. The values of o are usually only given at specified distances, where measurements are done.
Answer: Kropp	Yes, I think one should only use these models on distances between 100 m to 10 km. Further out it is only a guess.

8th NATO/CCMS INTERNATIONAL TECHNICAL MEETING ON AIR POLLUTION MODELING

TOPIC 3

GUIDELINES FOR THE APPLICATION OF AIR QUALITY SIMULATION MODELS IN THE NATO COMMUNITY

8th International Technical Meeting on Air Pollution Modeling and its Application

Influence of Meteorological Data on the Dispersion Calculation Results

L. Kropp, W. Bahmann
TÜV Rheinland, Köln, F.R.G.

September 20 - 23, 1977
Louvain-La-Neuve
Belgium

Influence of Meteorological Data on the Dispersion Calculation Results

Dr. L. Kropp and Dipl.-Met. W. Bahmann
TÜV Rheinland, Köln, FRG

Introduction

Air quality forecasting during licensing procedures of new plants in Germany is generally performed via statistical Gaussian plume models. Characteristical values to be calculated are annual mean values and 95 to 99 percentiles, corresponding to excess frequencies of 5 to 1 %, (see /1/, /2/). Such calculations therefore require joint frequency distributions of wind direction, wind speed and turbulence class.

Annual change of meteorological data

Observations of the meteorological data are to be performed through several years (minimum 5, better 10 years). Differences in the frequency distributions as shown in fig. 1, where wind direction data of Cologne for three time periods (1962-1966, 1972 and 1972-1975) are displayed, result in deviations of calculated air pollution load especially for low excess frequencies (5 or 1 %). There may exist locations for which only 1 year distributions are available. The more frequent occurence of westerly winds results in higher concentrations in a favorite residential district. This effect would be increased by the special topography of the Cologne area with gentle highlands of about 100 m towards the east in a distance of less than 10 km. Even the annual mean values will be significantly different when using e.g. the different wind direction distributions as shown in fig. 2 for the neutral turbulence condition.

Shifts of wind speed distributions to lower wind speeds as shown in fig. 3 will results in slightly higher concentration values. This effect is of course to be expected small against influences due to the choice of diffusion parameters or plume rise formula.

Day/night change of meteorological data

A much stronger effect on air quality forecasts follows from a day/night or a seasonal change of meteorological conditions. Up to now these facts have not been taken into consideration in regular dispersion calculations. Kolb /3/ published investigations for an Austrian area. (Turner turbulence classification; Singer/Smith diffusion parameters, same as used in /2/.) Fig. 4 represents the frequency of excess for a source of 70 m height during day and night. The probability of concentrations above 0,2 $mgSO_2/m^3$ during day time is 2 to 4 times higher than during night time for directions north as well as south of the source due to more stable turbulence conditions in the night. Taking into account that industrial emissions very often are much higher during day time, the discrepancy of air pollution load calculations between day and night time becomes much stronger. The real situation is much more complicated because the concentration peak occurs during the morning hours as starting period of power plants, residential emittents and traffic.

Looking to mean concentrations estimated for day and night time, respectively, the result is quite similar. Fig. 5 shows for different distances north or south of the source that during the night time average air pollution load is to be expected only 20 - 50 % of day time load at distances of less than about 3 km. At larger distances the ratio between night and day time mean load becomes 1 (south of the source) to 2 (north of the source). The shift of the point of maximum load to higher distances during night because of more stable conditions is more clear north than south of the source.

From these facts it can be deduced that the confidence in air quality calculations using annual joint frequency distributions of meteorological data depend on the time dependence of emissions:

Air quality forecast calculations for continuous emissions through day and night will be much more accurate than calculations for emissions depending on the hour of the day as e.g. emissions from households and traffic.

Seasonal including day/night changes of meteorological data

Further to the influence of annually averaged day and night meteorological data the influence of seasons including day and night variation was investigated. The 10 year average wind data were available for a station near Aachen for days and nights of the four seasons. The wind direction distributions during day and night time show no significant deviations. However, there was a seasonal dependency of the wind direction. There were less winds from NE in summer than in winter. The frequency of calms was much higher during the night than at day time (about two times higher in winter and nearly 5 times higher in summer regarding to the day frequencies respectively).

Calculations performed for receptor points at 1 and 3 km distance north from the source show significant deviations for the high percentile values as well as for the mean values. Fig. 6 represents excess frequency distributions for four different times:

(a) summer during day time
(b) summer during night time
(c) winter during day time
(d) winter during night time.

Fig. 6,1) corresponds to 1000 m distance and fig. 6,2) to 3000 m distance and a source height of 100 m. (Klug turbulence classification; Jülich diffusion parameters; no plume rise.) Deviations of the distributions at 1000 m distance due to seasonal dependencies are up to 40 % regarding the 1 % excess frequency values (99 percentiles) being reduced to about 25 % with respect to the 5 % excess frequency values (95 percentiles).

The corresponding deviations for the load calculations at 3000 m are 50 % (1 % excess frequency values) and 40 % (5 % excess frequency values).

The mean concentration values relative to the annual mean values at both places for the four cases are as follows:

Time	distance from the source	(on annual values) normalized concentrations 1000 m	3000 m
day in summer		1.14	1.21
night in summer		0.81	0.76
day in winter		1.15	1.12
night in winter		0.91	0.91

The annual mean concentration at 3000 m was about 40 % of that at 1000 m.

From these results it can also be deduced that in cases of continuously operating sources calculations of the air quality at the point of maximum load using annual frequency distribution differ by about 15 % only from calculations with seasonal and day/night joint frequency distributions. At larger distances the differences may however be greater while the absolute values have decreased.

Further aspects

There are a lot of problems which could be investigated in the near future to get more real dispersion calculations. But the results of these investigations must become applicable by the different administrative environmental protection authorities in the regular licensing procedures. The solutions of the problems mentioned would lead to:

- registers of representative areas concerning wind distribution of special stations and guidelines for taking into account topographical influences
- consideration of the height-dependent variation of wind-direction in combination with registers of roughness categories
- registers of mixing height and averaged wind speed combined with a climatology in regard to critical weather situations, i.e. with shallow mixed layers and little ventilation, their duration and the increase of pollutant concentrations by assimilation.

Listing of figure captions

Fig. 1	frequency distribution of wind direction at Cologne
Fig. 2	frequency distribution of wind direction at Cologne for neutral stability
Fig. 3	sum frequency of wind speed at Cologne
Fig. 4	excess frequency as function of distance during day and night time
Fig. 5	average concentration as function of distance during day and night time
Fig. 6	excess frequencies of air pollution load for a source of 100 m height at different distances

References

/1/ Technische Anleitung zur Reinhaltung der Luft
1. VwV zum Bundes-Immissionsschutzgesetz vom
28.8.1974 und Berichtigung
Gemeinsames Ministerialblatt vom 4. Sept. 1974
(Technical Guideline for Monitoring Air Quality)

/2/ Verwaltungsvorschrift zum Genehmigungsverfahren
für Mineralölraffinerien und petrochemische Anlagen zur Kohlenwasserstoffherstellung
RdErl. d. MAGS, Ministerialblatt für NRW, 31.5.197
(Administrative Regulation for Licensing Procedure
of Refineries and Petrochemical Plants)

/3/ H. Kolb
Immissionclimatology for Graz, Austria.
Publication No. 15 of "Lehrkanzel für Theoretische
Meteorologie der Universität Wien", 1975

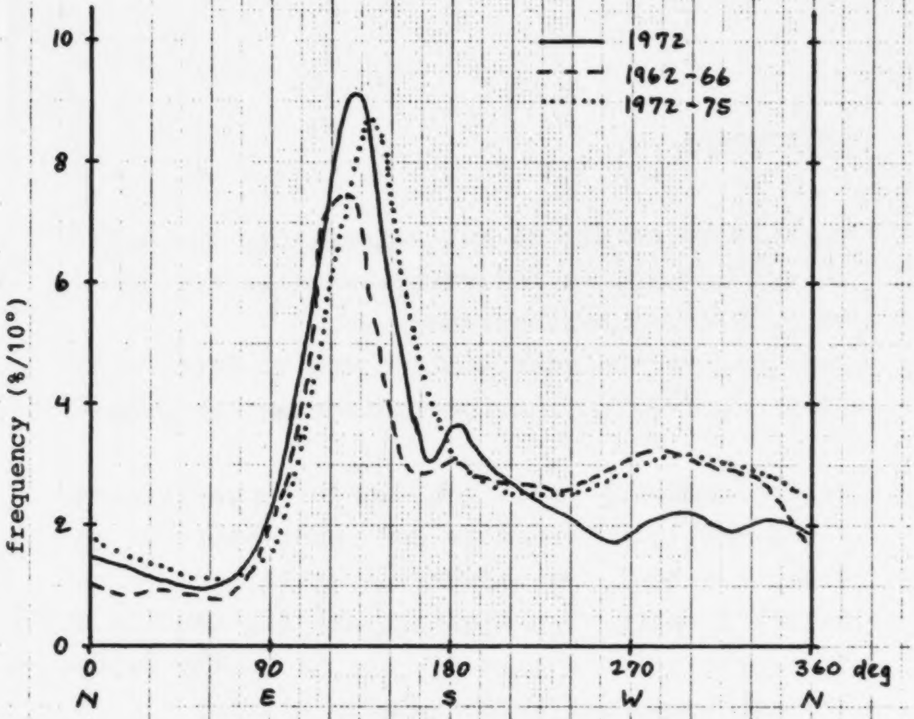

Fig. 1 frequency distribution of wind direction at Cologne

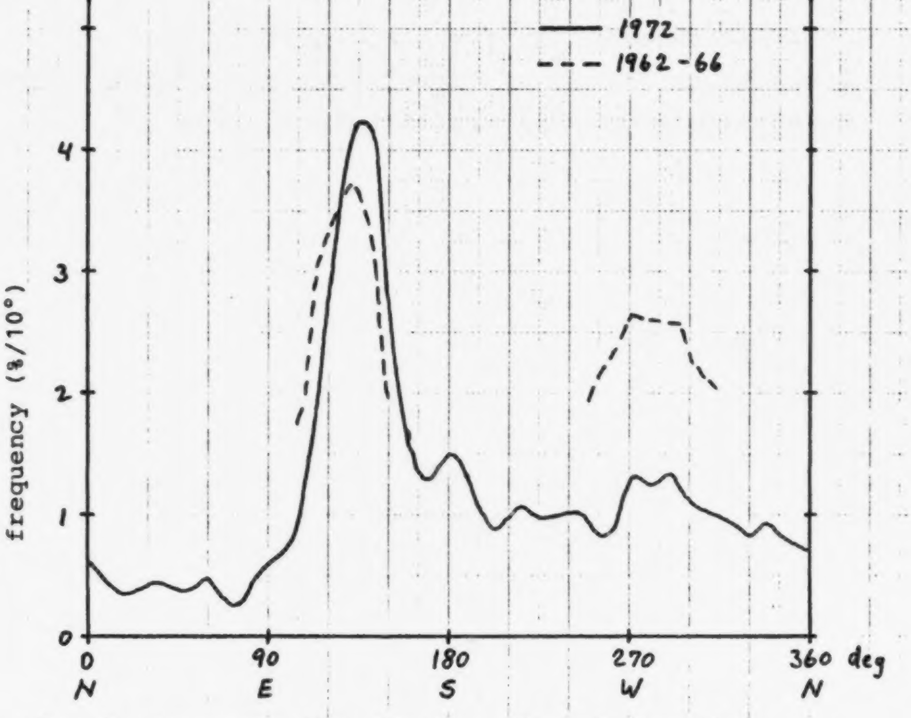

Fig. 2 frequency distribution of wind direction at Cologne for neutral stability

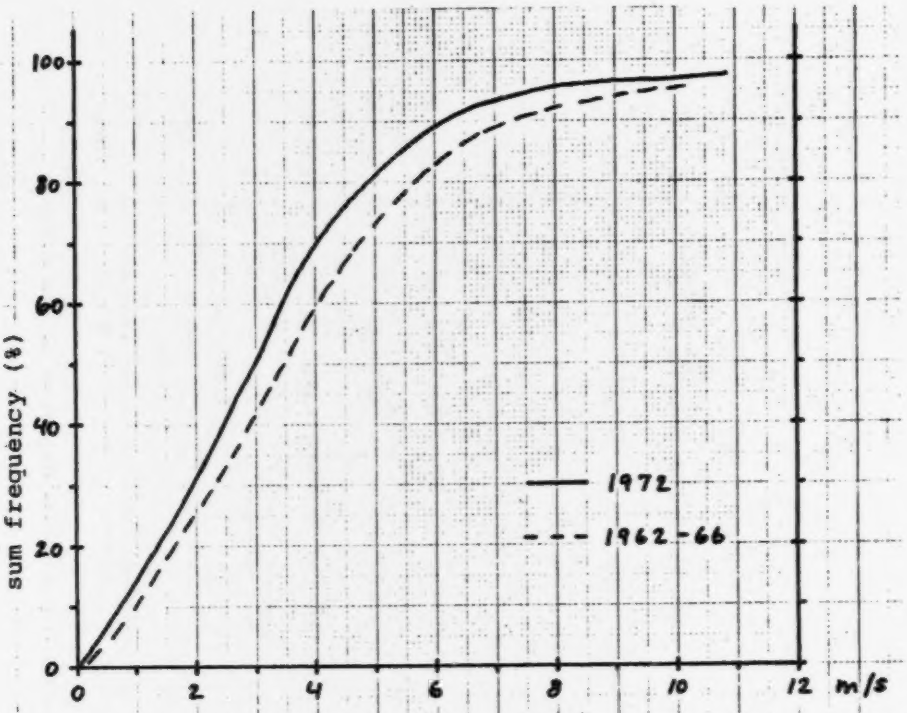

Fig. 3 sum frequency of wind speed at Cologne

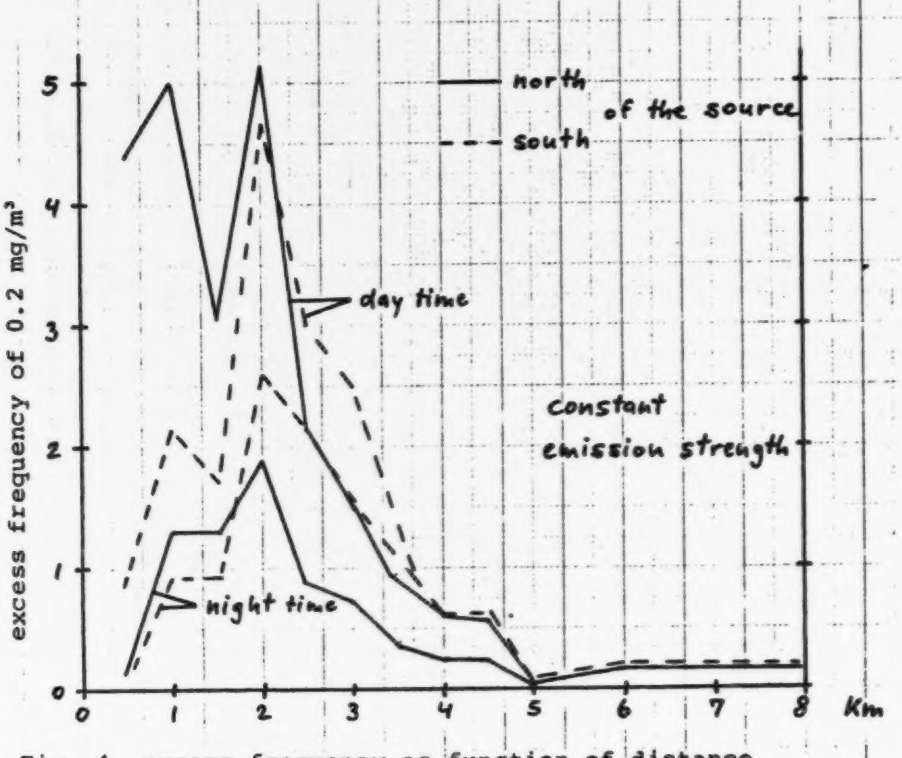

Fig. 4 excess frequency as function of distance during day and night time

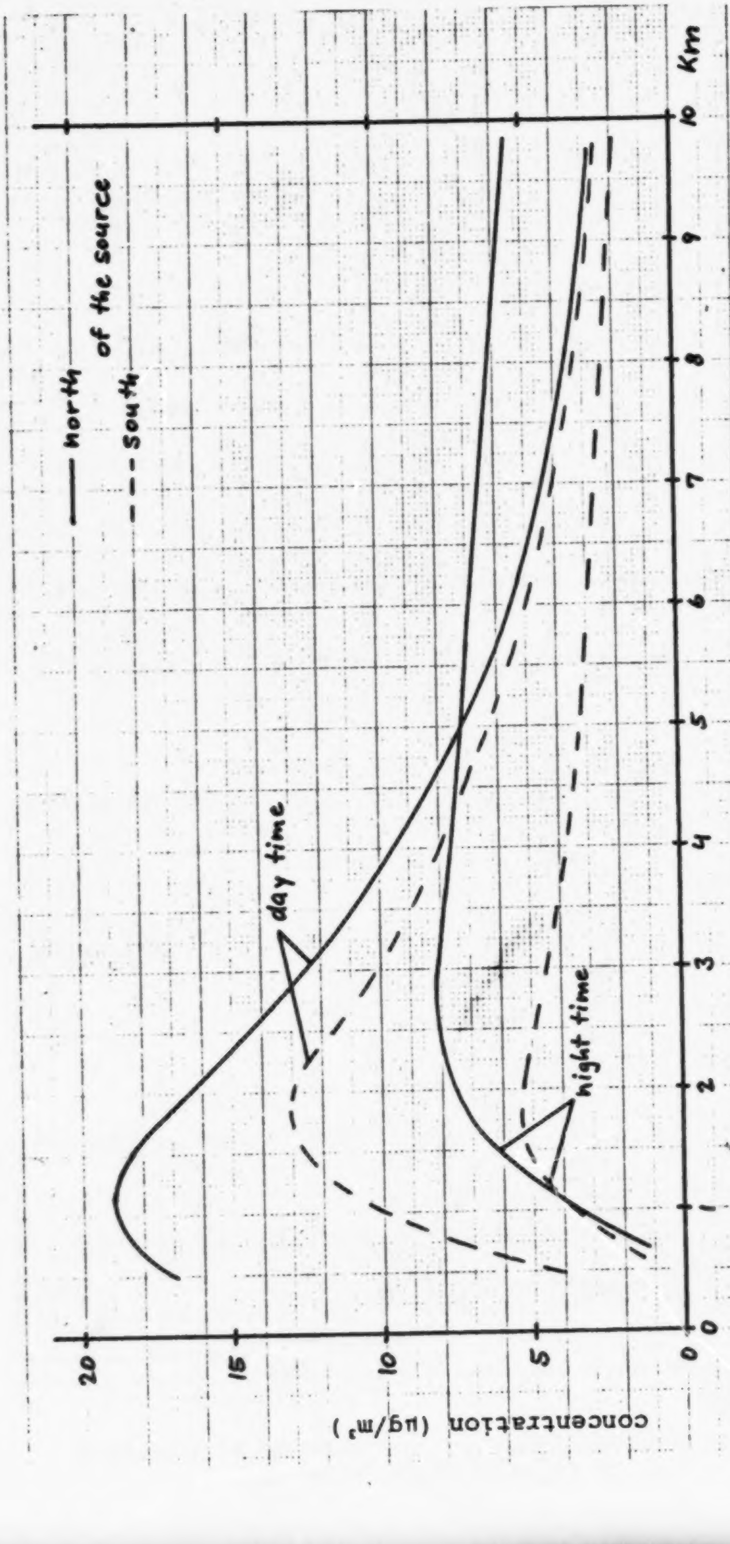

Fig. 5 average concentration as function of distance during day and night time

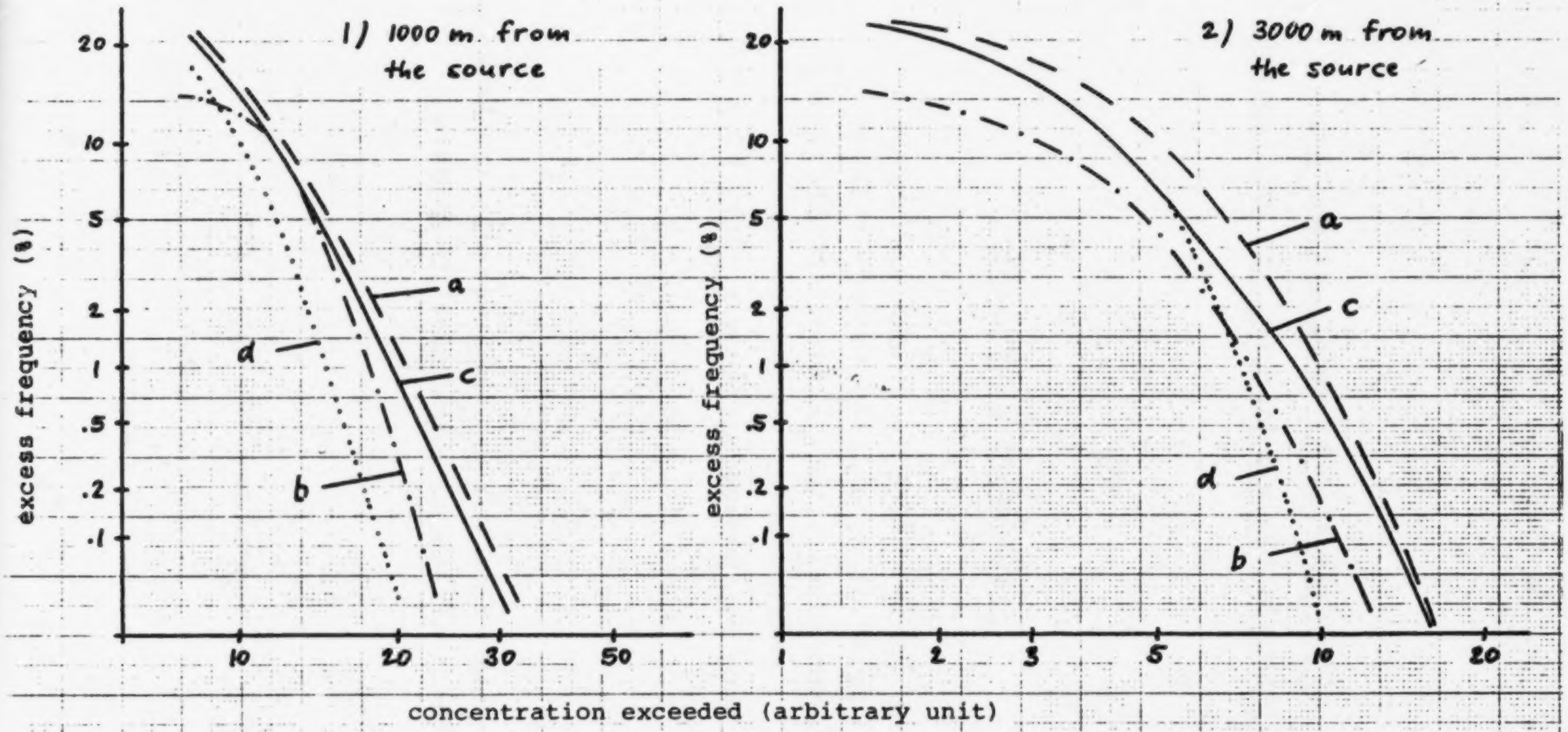

Fig. 6 excess frequencies of air pollution load for a source of 100 m height at different distances

8th International Technical Meeting
on Air Pollution Modeling and its Application

EXPERIENCE WITH UNAMAP

D. BRUCE TURNER* AND ADRIAN D. BUSSE*
Meteorology and Assessment Division
Environmental Sciences Research Laboratory
Environmental Protection Agency
Mail Drop 80, Research Triangle Park, NC 27711

* On Assignment from the National Oceanic and Atmospheric Administration, Department of Commerce

September 20 - 23, 1977

Louvain-La-Neuve

Belgium

EXPERIENCE WITH UNAMAP

by

D. Bruce Turner and Adrian D. Busse

Abstract -- The Meteorology and Assessment Division of the U.S. Environmental Protection Agency started UNAMAP (Users Network for Applied Modeling of Air Pollution) in October 1972 by making interactive (conversational) versions of various air quality simulation models available to EPA users. Successful use within the agency encouraged the establishment of a similar service for other users on an existing nationwide network in May 1973. Over 30 users have applied UNAMAP on the nationwide network. Alternative availability of these programs on magnetic tape utilizing the facilities of the National Technical Information Service began in April 1974. Over 120 user groups have purchased the tape since it has become available. Six categories of users and their geographical distribution are presented. Models currently contained in UNAMAP and their appropriate application are indicated. Problems encountered in utilizing the UNAMAP system and their solutions are discussed.

INTRODUCTION

Recognizing that it was desirable to make air quality simulation models available for use in application to air quality management problems and in a computer compatible form to shortcut both time and manpower expense, the Meteorology and Assessment Division of the Environmental Protection Agency (EPA) has formulated and supported UNAMAP (Users Network for Applied Modeling of Air Pollution, Hosler, 1975).

The following discussion considers the contents of UNAMAP, the history and problems, and the users of UNAMAP. The presence of a model in the UNAMAP system constitutes neither an endorsement by the Agency nor an indication as to the state of validation of the model. Models are placed in UNAMAP to make them readily available for air quality estimates by any user. Most of the models (APRAC, CDM) have been validated; one model (HIWAY) has however, been made available for use with only a few comparisons between model estimates and field measurements.

CONTENTS OF UNAMAP

UNAMAP contains six air quality simulation models. Two are urban models (APRAC and CDM), one is a line source model (HIWAY), and three are point source models (PTMAX, PTDIS, and PTMTP). Each model has a specific application. APRAC is available to estimate carbon monoxide or other relatively non-reactive pollutants from motor vehicles. CDM is useful for seasonal or annual estimates of non-reactive pollutants from point and area sources in urban areas. HIWAY may be used to make short-term (hourly) estimates of non-reactive pollutants from a single roadway segment. The point source models (PTMAX, PTDIS, and PTMTP) are useful for short-term estimates of non-reactive pollutants from point sources located in rural areas. Highlights of each model are outlined in Appendix B.

From conversations with users and potential users, UNAMAP models are estimated to be applicable to some 5 to 15 percent of the problems in which the user anticipates that some form of dispersion modeling should be an aid to an understanding of the problem that the user is facing.

Detailed vertical profiles of wind and temperature, and fluctuation statistics of wind azimuth angle and wind elevation angle are extremely useful to estimate concentrations, but are not always available. Therefore, UNAMAP models require simple meteorological input data. These data can generally be obtained or inferred from routine surface observations.

Several topics may be discussed that are common to more than one model in UNAMAP.

PLUME RISE

The equations of Briggs (1969, 1971, and 1972) for determining the effective height of a positive buoyancy dominated plume are used in the CDM, PTMAX, PTDIS, and PTMTP models. Only the form for neutral and unstable conditions is used in CDM because stable conditions seldom occur in the lower layers over an urban area. Equations for both stable and unstable-neutral are used for the three point-source models.

Domination by momentum, consideration of negative buoyancy, stack downwash, and effects due to buildings or terrain are considerations that can enter into plume rise computations for point sources, but are not considered in these programs.

WIND SPEED

Wind speed is an important input parameter for all the UNAMAP models except PTMAX (six stability classes and appropriate wind speeds for each stability are selected internally). The input wind speed for APRAC, HIWAY, PTDIS, and PTMTP should be representative of the source. In these models wind speed and direction are not varied either in the horizontal or in the vertical. A power law variation of wind speed with height (with the power dependent upon stability) is used in CDM.

WIND DIRECTION

The variation of wind direction with height is a difficult parameter to estimate when wind information from towers or radiosondes is not available. The input wind direction is assumed to indicate the direction of transport of the source(s). For multisource models such as CDM and PTMTP, the wind direction is the same at all sources regardless of height.

DISPERSION PARAMETERS

Although horizontal and vertical wind fluctuation statistics from measurements at a representative height are generally preferred, computations of the impact of a source or sources are frequently required without such measurements being available.

For the three point source programs in UNAMAP, the standard deviations of the plume concentration distribution (σ_y and σ_z), commonly referred to as Pasquill-Gifford dispersion parameters (Pasquill, 1961; Gifford, 1960) as shown in Figures 3-2 and 3-3 in Turner (1970), have been used. It has been recently pointed out by Pasquill (1976) that the Pasquill-Gifford σ_z's are appropriate for sampling times up to one hour, but that the σ_y's are most appropriate for 3 minutes. It was previously thought that the σ_y's were representative of sampling times from 10 to 15 minutes. In these three point source models, both parameters have been used to estimate concentrations which have been treated as hourly averages. The use of these 3-minute σ_y's for hourly estimates results in overestimates of centerline concentrations and underestimates of off-axis concentrations. For usual situations, actual centerline concentrations may be on the order of 55 to 70 percent of those calculated. For more unusual situations that produce maxima, with wind directions for the twenty 3-minute periods in an hour more persistent, the errors are much less.

These parameters are appropriate for use in essentially rural environments with flat or gently rolling terrain. Although most appropriate for low-level releases, the point source models have been applied to elevated sources such as large power stations with generally good results.

The Pasquill-Gifford dispersion parameters are also used in the HIWAY model. A virtual point source method is used to account for the initial dispersion taking place in the wakes of vehicles.

The Climatological Dispersion Model (CDM), since it is intended for urban application, modifies the input stability class (determined from parameters measured at airport locations) toward more unstable conditions to account for additional heat and roughness effects of a city. Also in this model, a virtual point source method is employed, giving an initial plume size in the vertical to account for general building downwash effects in urban areas upon low-level releases.

A need exists for more appropriate field measurements that can be used to improve dispersion estimates. The effects of height-of-release and surface roughness in dispersion estimates also need to be determined and included in an improved method. Also, for large buoyancy dominated sources, the initial spreading due to stack induced turbulence should be included (Pasquill, 1976).

HISTORY AND PROBLEMS

To facilitate the application of air quality simulation models, it became clear in the early 1970's that models should not be made available just through descriptions or by publishing the computer program source code. Also, the answer was not to have the originator of a model bogged down by reproducing punch card decks or copying magnetic tapes for each and every potential user. Executing models on a central computer or furnishing a computer compatible product would simultaneously relieve the developer of the responsibility of meeting requests for models while serving each user's needs.

Because air quality simulation modeling is a rapidly developing area, the ability to make changes in the models and to rapidly disseminate these changes was given prime consideration. If programs were compiled on a central computer and users were allowed to execute only the compiled codes on that computer, then changes and control of these changes could remain with the model developer. The developer would simply modify the source code and recompile, replacing the previous compiled version with the new version. Then, the next time a user executed the model, the new version would be used.

UNAMAP FOR EPA USERS

With this philosophy, the Users Network for Applied Modeling of Air Pollution (UNAMAP) was started in October of 1972 by making interactive (conversational) versions of several air quality simulation models available to EPA users on EPA's computer facility located in Research Triangle Park, North Carolina. This allows not only EPA users at Research Triangle Park to utilize UNAMAP, but, because the computer facility is accessible by telephone, users in the ten EPA regional offices and at EPA laboratories in Washington, D. C.; Cincinnati, Ohio; Las Vegas, Nevada; Corvallis, Oregon; and several other EPA facilities can also use UNAMAP. Credit is due to Dr. Warren Johnson and Dr. Donald Ruff for initially forming UNAMAP.

UNAMAP ON A NATIONAL COMPUTER NETWORK

Experience during the initial phase of operation on the EPA computer was very good. An investigation was made on how to make these air quality simulation models available to users outside EPA. It was learned that Computer Sciences Corporation (CSC), which was already under contract to provide certain teleprocessing services to the General Services Administration of the U. S. Government, operated a nationwide computer network called INFONET. Arrangements were made to use the services of the network and the UNAMAP series of programs were installed on INFONET in May 1973. The programs were stored on magnetic tape to be read into the computer system as required.

A number of problems arose as a result of placing UNAMAP into INFONET. They were partially due to relative independence of each of the four computers in the INFONET system. Access was initially difficult because of problems in transferring information from the tape on one computer to the other three computers. Difficulties were also encountered in the dissemination of how to access UNAMAP through INFONET.

Early in the use of UNAMAP with Computer Sciences Corporation, it was common practice to copy UNAMAP, or parts of UNAMAP, into storage files for each user. This presented three problems: 1) The user was charged for these storage files. 2) Because programs were not being obtained from the central source each time they were to be executed, users were executing outdated programs that had been replaced since the initial storage into their file. 3) Instead of users having access to only compiled executable programs, FORTRAN source code was also made available so it was possible for individual users to modify the models stored in their files. Further, many users would obtain copies of individually modified model versions from another user which were inconsistent with the EPA UNAMAP versions. Thus, there were no assurances that a given model would give a unique answer to a specified problem. These difficulties were decreased with the establishment of a single point of contact within CSC for inquiries about UNAMAP by the company's local offices.

A larger problem became apparent when it was learned that potential users having their own computer facilities found it difficult to justify use of additional computer facilities outside their own organization. Thus a large number of potential users were unable to execute the EPA models.

UNAMAP AVAILABILITY THROUGH NTIS

In seeking a solution to this significant problem, EPA learned that the National Technical Information Service (NTIS) of the Department of Commerce in Springfield, Virginia not only would duplicate technical reports for requesters, but also would duplicate computer compatible products. To make UNAMAP available to the large number of potential users with their own computer facilities, a magnetic tape containing a file of the FORTRAN source programs of the UNAMAP models and a file containing test data for APRAC and CDM was sent to NTIS. The tape was available for duplication and sale to the public in April 1974. NTIS was asked to send a copy of a form letter that EPA had prepared to all purchasers of the UNAMAP tape. Purchasers were asked to write their name and address on the bottom of the letter, tear off and return to the EPA's Environmental Applications Branch. In this way, EPA knew who to inform when UNAMAP tape changes were made.

Although this action solved the major problem of availability, it compromised the original objectives of UNAMAP. Three of the objectives were 1) to have the ability to change programs when required, 2) to make these changes available to users quickly, and 3) to make available compiled executable programs rather than source codes in order to prevent unauthorized modification.

It was decided to accomplish changes in two ways. If a change was minor, involving only FORTRAN coding changes for a few statements, it could be accomplished by mailing a list of the changes to tape purchasers. If a change was major, involving many statements, the following procedure could be used: 1) The current UNAMAP tape would be withdrawn from NTIS and a new tape with all the changes incorporated would take its place. 2) A change tape that would allow previous purchasers of the tape to update their UNAMAP program would also be placed with NTIS (The charge for this tape is typically much less than for the tape of the entire UNAMAP system.) 3) Previous purchasers would be notified by letter of this addition to UNAMAP.

Making source programs available, rather than compiled executable programs, has caused problems since users modify the programs to suit specific needs. The problems are reduced if the person modifying the program uses a different name for the modified program so that two (or more) different algorithms do not exist with the same name. Despite these problems, in retrospect the decision to make the programs available through the National Technical Information Service made the UNAMAP programs available to a large number of users who would not otherwise have had the opportunity to use EPA models.

In the meantime, during the first half of 1973, the EPA computer facility replaced an IBM 360, model 50 with a UNIVAC 1110. Many difficulties were encountered during the transition. Minor coding changes to the UNAMAP models were made and the models installed on the UNIVAC in September 1973.

Source codes made available from NTIS were the same conversational versions as placed on INFONET. However, most users who had their own computers, preferred versions that they could operate in a batch mode rather than in a conversational mode. Since most of the models had been developed in batch versions initially, this demand was easily met.

In the summer of 1975, it was found that one of the models, HIWAY, produced some erroneous results with certain combinations of input. The model was reprogrammed and the difficulty removed. Since this was a major change, a new tape and a change tape were placed with NTIS. Both tapes contained batch versions of all six UNAMAP models. Conversational versions were retained for HIWAY and the three point source programs. This revision, referred to as UNAMAP Version II, became available in November 1975.

USERS OF UNAMAP

As stated previously, UNAMAP may be accessed by EPA users on the UNIVAC 1110 at EPA's National Computing Center at Research Triangle Park, North Carolina. Information is relayed to the users through the UNAMAP files. No records are kept as to which users access the EPA system. However, the EPA UNAMAP system has been accessed more than 450 times between January 23, 1976 and July 14, 1977, an average of 25 times per month.

UNAMAP is available to users outside the Environmental Protection Agency either by accessing the nationwide network, INFONET, or by purchasing the magnetic tape from the NTIS for use with their own computer systems. Since it is important to inform users of updates, Computer Sciences Corporation periodically furnishes a list of users of the INFONET system, and purchasers of the tape are requested to inform EPA's Environmental Applications Branch of their address. By this means, EPA has a general, though not complete, knowledge of the users outside of the Agency.

A statistical compilation of known UNAMAP users, complete as of July 1, 1977, is shown in Table 1. Six categories of users are shown. The term 'consultants' is taken broadly and includes engineering firms and research organizations. 'State and local governments' include Air Pollution Control Districts, Highway Departments, Health Agencies, and Planning Authorities. 'Federal government' includes any agency of a national government. 'Industry' and 'University' are self-explanatory. 'Other' is the category selected if a home address is available without an affiliation.

The geographic distribution is shown by five areas in the United States and by country outside the U. S. The Northeast includes 10 states, from Maine to Pennsylvania and Delaware. The Southeast includes 10 states and the District of Columbia, from West Virginia and Tennessee to Florida plus Puerto Rico. The Midwest includes 13 states, from Ohio and Kentucky to Kansas and North Dakota. The Southwest includes 9 states, from Arkansas and Louisiana to Nevada and California plus Hawaii. The Northwest includes 8 states, from Colorado and Utah to Washington plus Alaska.

As of July 1, 1977, there were 156 known users of UNAMAP outside EPA with just over half in the consultant category.

SUMMARY

The availability of some air quality dispersion models comprising UNAMAP (Users Network for Applied Modeling of Air Pollution) has been discussed. This discussion has included the contents of the system, the history and problems encountered, and a statistical summary of the 156 known users outside the Environmental Protection Agency. UNAMAP is not expected to remain static, but will have additional air quality simulation models added to the system as they become available.

ACKNOWLEDGEMENTS

The authors are grateful to Warren B. Johnson and Ronald E. Ruff, the "fathers" of UNAMAP, and to Lea Prince, John S. Irwin, and Alan M. Cope for their assistance.

REFERENCES

Briggs, Gary A., 1969: Plume Rise, USAEC Critical Review Series, TID-25075, National Technical Information Service, Springfield, VA 22161. 81 p.

Briggs, Gary A., 1971: Some recent analyses of plume rise observation, in Proceedings of the Second International Clean Air Congress, edited by H. M. Englund and W. T. Beery, Academic Press, New York, pp 1029-1032.

Briggs, Gary A., 1972: Discussion on chimney plumes in neutral and stable surroundings. Atmos. Environ. 6, 507-510.

Gifford, Franklin A., Jr., 1960: Atmospheric dispersion calculations using the generalized Gaussian plume model, Nucl. Safety, 2 (2) 56-59.

Hosler, Charles R., 1975: The meteorology program of the Environmental Protection Agency. Bull. Amer. Meteorol. Soc. 56, 12, 1261-1270.

Pasquill, Frank, 1961: The estimation of the dispersion of windborne material, Meteorol. Mag., 90 (1063): 33-49.

Pasquill, Frank, 1976: Atmospheric Dispersion Parameters in Gaussian Plume Modeling, Part II. Environmental Monitoring Series. EPA-600/4-76-030b. US EPA, Research Triangle Park, NC. 44 p.

Turner, D. Bruce, 1970: Workbook of Atmospheric Dispersion Estimates, Office of Air Programs Publication No. AP-26. US EPA, Research Triangle Park, NC. 84 p.

TABLE 1. UNAMAP USERS (1 JULY 1977)

	TAPE PURCHASERS							NETWORK USERS							
	CONSULTANTS	INDUSTRY	UNIVERSITY	STATE & LOCAL GOVT.	FEDERAL GOVT.	OTHER	SUB TOTAL	CONSULTANTS	INDUSTRY	UNIVERSITY	STATE & LOCAL GOVT.	FEDERAL GOVT.	OTHER	SUB TOTAL	GRAND TOTAL
USERS, U.S.															
NORTHEAST	21	9	3			1	34	6	2		1		1	10	44
SOUTHEAST	9	3	3	1	1		17	1				2		3	20
MIDWEST	15	8	3	5		1	32	3	3	1	1			8	40
SOUTHWEST	14	12	1	2			29	3			1			4	33
NORTHWEST	2	1	1	3			7	3	1		2		1	7	14
SUBTOTAL	61	33	11	11	1	2	119	16	6	1	5	2	2	32	151
USERS, OUTSIDE U.S.															
CANADA	1						1								1
ENGLAND				1			1								1
JAPAN					1		1								1
NORWAY					1		1								1
SWITZERLAND	1						1								1
SUBTOTAL	2			1	2		5								5
	63	33	11	12	3	2	124	16	6	1	5	2	2	32	156

APPENDIX A

INFORMATION ON UNAMAP MODELS

PUBLICATIONS

APRAC - User's Manual for the APRAC-1A Urban Diffusion Model Computer Program (available from NTIS, accession number PB 213-091)

A Practical, Multipurpose Urban Diffusion Model for Carbon Monoxide (NTIS accession number PB 196-003)

Field Study for Initial Evaluation of an Urban Diffusion Model for Carbon Monoxide (NTIS accession number PB 203-469)

Evaluation of the APRAC-1A Urban Diffusion Model for Carbon Monoxide (NTIS accession number PB 210-813)

Dabberdt, Walter F.; Ludwig, F.L.; and Johnson, Warren B., Jr.,1973: Validation and Applications of an Urban Diffusion Model for Vehicular Pollutants, *Atmos. Environ.*, *7*, 603-618.

Johnson, W. B.; Ludwig, F. L.; Dabberdt, W. F.; and Allen, R. J.,1973: An Urban Diffusion Simulation Model for Carbon Monoxide. *J. Air Poll. Control Assoc.*, *23*, 6, 490-498.

CDM - Busse, A. D., and Zimmerman, J. R., 1973: User's Guide for the Climatological Dispersion Model. U. S. Environmental Protection Agency. Research Triangle Park, NC. Environmental Monitoring Series, EPA-R4-73-024, 131 p. (NTIS accession number PB 227-346/AS)

HIWAY - Zimmerman, J. R.; and Thompson, R. S., 1975: User's Guide for HIWAY: A Highway Air Pollution Model. U. S. Environmental Protection Agency, Research Triangle Park, NC. Environmental Monitoring Series, EPA-650/4-74-008, 59 p. (NTIS accession number PB 239-944/AS)

PTMAX,PTDIS, and PTMTP - Turner, D. B.; and Busse, A. D., 1973: Users' Guides to the Interactive Versions of Three Point Source Dispersion Programs: PTMAX,PTDIS, and PTMTP. unpublished manuscript, Meteorology Laboratory, U. S. Environmental Protection Agency. Research Triangle Park, NC 27711.

Guzewich, David C., and Pringle, William J. B., 1977: Validation of the EPA-PTMTP Short-Term Gaussian Dispersion Model. J. Air Poll. Control Assoc., 27, 6, 540-542.

MAGNETIC TAPES OF UNAMAP MODELS

Users Network for Applied Modeling of Air Pollution (UNAMAP) - NTIS accession number PB 229-771. This Version II tape containing batch FORTRAN source codes for APRAC, CDM, HIWAY, PTMAX, PTDIS, and PTMTP, and conversational (interactive) FORTRAN source codes for HIWAY, PTMAX, PTDIS and PTMTP replaced the original tape in January 1975. Tape normally furnished is 9 track, 800 bits per inch, EBCDIC code, odd parity. Physical records each contain 10 logical records in card image format (that is, 80 byte logical records; 800 byte block size). Other configurations can also be obtained: BCD code, ASCII code, or 7 track (556 or 800 bpi), etc.

Price: $175.00, foreign orders: $219.00

Change tape for UNAMAP, PB 240-273, allows purchasers of original UNAMAP tape to update their UNAMAP system.

Price: $97.50, foreign orders: $122.50

NTIS - National Technical Information Service
U. S. Department of Commerce
Springfield, VA 22161

APPENDIX B

BRIEF DESCRIPTIONS OF UNAMAP MODELS

ACRONYM: APRAC
NAME: SRI'S URBAN CO MODEL
TYPE: GAUSSIAN, URBAN
POLLUTANT: CARBON MONOXIDE
INPUT
    EMISSIONS: FROM ALL ROADWAY LINKS IN URBAN AREA
    METEOROLOGY: REPRESENTATIVE HOURLY
RECEPTOR: ANY LOCATION
CONCENTRATIONS: HOURLY AVERAGES

ACRONYM: CDM
NAME: CLIMATOLOGICAL DISPERSION MODEL
TYPE: GAUSSIAN, URBAN
POLLUTANT: SO_2 AND SUSPENDED PARTICULATE
INPUT
    EMISSIONS: ALL POINT AND AREA SOURCES
    METEOROLOGY: JOINT FREQUENCY OF STABILITY, WIND SPEED, AND WIND DIRECTION
RECEPTOR: ANY LOCATION
CONCENTRATIONS: AVERAGE FOR PERIOD OF JOINT FREQUENCY DATA (USUALLY ANNUAL)

ACRONYM: **HIWAY**
NAME: HIGHWAY
TYPE: GAUSSIAN, OPEN COUNTRY
POLLUTANT: GASES OR AEROSOLS FROM MOTOR VEHICLES
INPUT
    EMISSIONS: FROM SINGLE ROADWAY SEGMENT
    METEOROLOGY: REPRESENTATIVE HOURLY
RECEPTOR: ANY OFF ROADWAY
CONCENTRATIONS: HOURLY AVERAGES

ACRONYM: **PTMAX**
NAME: MAXIMUM FROM A POINT SOURCE
TYPE: GAUSSIAN, OPEN COUNTRY
POLLUTANT: ANY NON-REACTIVE GAS OR AEROSOL
INPUT
    EMISSIONS: FOR SINGLE STACK
    METEOROLOGY: NONE, INTERNALLY USES RANGE OF STABILITY AND WIND SPEED
CONCENTRATIONS: MAXIMUM HOURLY AT POINT OF MAXIMUM

ACRONYM: PTDIS
NAME: CONCENTRATIONS WITH DOWNWIND DISTANCE
TYPE: GAUSSIAN, OPEN COUNTRY
POLLUTANT: ANY NON-REACTIVE GAS OR AEROSOL
INPUT
    EMISSIONS: FOR SINGLE STACK
    METEOROLOGY: STABILITY, WIND SPEED, WIND DIRECTION, AND MIXING HEIGHT FOR AN HOUR
RECEPTOR: AT VARIOUS DOWNWIND DISTANCES
CONCENTRATIONS: AVERAGE FOR GIVEN HOUR

ACRONYM: PTMTP
NAME: MULTIPLE POINT SOURCES AND RECEPTORS
TYPE: GAUSSIAN, OPEN COUNTRY
POLLUTANT: ANY NON-REACTIVE GAS OR AEROSOL
INPUT
    EMISSIONS: FOR UP TO 25 STACKS
    METEOROLOGY: FOR ONE TO TWENTY-FOUR HOURS
RECEPTOR: UP TO 30 POINTS AT OR ABOVE GROUND LEVEL
CONCENTRATIONS: HOURLY AND AVERAGE OVER THE PERIOD, ALSO PARTIAL (DUE TO EACH SOURCE).

8th International Technical Meeting on Air Pollution Modeling and its Application

Air Pollution Studies In Canada

by

F.H. Fanaki and M. Kwizak

Atmospheric Environment Service
Toronto, Canada

September 20 - 23, 1977
Louvain-La-Neuve
Belgium

Air Pollution Studies In Canada

1. INTRODUCTION

The atmosphere plays an integral part in dispersing pollutants from sources to receptors. Its complex motions control both the transport and the dilution of the pollution. The mechanisms involved vary from place to place depending on the nature of the underlying surface and on the local climate.

Canada occupies most of the northern portion of North America, except for Alaska. It forms an irregular basin with its lowest part in the St. Lawrence River valley and its highest part in the Rocky Mountains. Canada is dotted with countless lakes, the most important and largest of which are known as the Great Lakes.

The Canadian climate is as complex as its terrain. In general it is temperate and is characterized by a variety of conditions. These conditions range from coastal to continental and from arctic to boreal.

There is a wealth of both theoretical and experimental information on the transport and diffusion of pollutants in the atmosphere. However, since the transport and diffusion is strongly dependent on the topography and meteorology of the area, it is extremely difficult to generalize and to assess the air quality of areas about which little is known. To illustrate this point, the paper reviews some of the studies in the air pollution field made in Canada. It describes briefly the different studies with a view towards solving air pollution problems and demonstrating the limited applicability of the diffusion formulas when applied to some practical situations.

2. Experimental Field Studies

a. Plume Dispersion from Stacks

The purpose of using a stack is to help elevate the exhaust fumes above the ground where man lives. It is believed that this, in turn, reduces the magnitude of the pollution problem. With an increase in production comes an increase in the amount of exhaust wastes, and thus stack heights have been increased. In 1960 stack height had reached 97.5 m and by 1970 the height had been doubled. At present the International Nickel Company (INCO) operates a 381-m stack in Sudbury, Ontario, area.

(i) Dispersion from Tall Stacks

Tall stacks as a preventive of air pollution are controversial; there are other factors as important as the height of the stack that influence the rise and the diffusion of the smoke plume. These factors are wind speed, wind direction, topography of the area and thermal stability of the atmosphere. These factors may combine to bring the exhaust smoke to the ground at a short distance from the stack. They also may produce an inversion layer which, in a limited region, may prevent the plume from rising and dispersing the pollutants.

Such a "lid" on the smoke rise increases the concentration of pollutants.

The problem of dispersion from tall stacks has been discussed in some detail at the last NATO meeting (see Fanaki and Turner 1976), and will not be repeated here. Recently, however, some interesting characteristics of tall stack plume dispersion have been found by Millan et al (1976). Using three correlation spectrometers (COSPECs) simultaneously at different downwind locations up to 38 km from the source, Millan et al examined the temporal and spatial behaviour of the INCO plume. Figure 1 displays a sample of their results. The profiles describe the vertically integrated SO_2 concentrations of the INCO plume during a 1 hour period.

The figure includes also average Eulerian and Langrangian profiles as well as the meteorological conditions during the time of observations. The Eulerian profile represents the space averaging of the different profiles. The Lagrangian profile was obtained by superimposing the individual profiles with respect to their center of gravity. This profile shows the relative diffusion of the plume as compared with the absolute diffusion shown by the Eulerian profile.

Upon examination of the SO_2 vertically integrated profile, one will note that the center of gravity of the plume was drifting to the one side during the time of observations. Over approximately a one hour period, the plume drifted by about 20°, a value which agrees well with the observed change in the wind direction at the plume height (900m). Further observations showed that the Eulerian profile was rarely Gaussian, for the averaging time period of 1 hour. It appears also that wind shear, both in speed and direction, affects the diffusion of the plume and yields a skewed Lagrangian profile.

Values of the horizontal standard deviations σy obtained from this study were compared with the equivalent ASME values in Figure 2. Two observations may be made. Firstly, these values are generally large for the observed neutral-stable category. Secondly, there is no apparent relationships between the measured coefficients and their corresponding stability class. The results in this case reflect increased horizontal plume growth due to vertical wind shear, a dominant effect under these stability conditions.

(ii) Plume Dispersion from Short Stacks

In contrast to tall stacks, there are some industrial complexes in Canada that use relatively short stacks to exhaust their waste. For example, the pulp and paper mill in Point Tupper, Nova Scotia uses a stack which is a few meters in height situated on the roof of their main building. The plume in this case is greatly affected by the wake of the building. Above a certain wind speed the plume may be downwashed (e.g. 7 m sec^{-1}). During a study in which downwash occurred, the ground concentration of SO_2 peaked at 0.6 ppm at a few tens of meters from the source.

Another short stack example is the dispersion from the Creat Canadian Oil Sands (CGOS) plant at the Oil Sands area, Alberta, Canada. This part of Canada is characterized by cold winter season, during which air temperatures may drop to -40°C. The dispersion and rise of the plume is largely determined by the intensity of the nocturnal inversions. These inversions result from radiative cooling of the ground during the night and may persist for relatively long periods.

The GCOS plant is located 40 km north of Fort McMurray, Alberta, on the west bank of the Athabasca River. The elevation of the area ranges from 200 m along the Athabasca River to over 1000 m MSL around the river valley. The land slopes gently upwards to the northeast. The topography around the river is slightly variable, ranging from undulating to rolling land.

The major emission sources in the GCOS plant are three stacks, the Power Plant Stack (A), the Refinery Flare Stack (B) and the Incinerator Stack (C). They discharge SO_2 and other gases into the atmosphere. The physical characteristics of the stacks are given in Table I.

TABLE I

Physical Characteristics of the GCOS Stacks

Parameter	Magnitude		
	Stack A	Stack B	Stack C
Height above ground (m)	106	99	107
Inside Diameter (m)	5.89	1.1	1.8

There are numerous formulas for modeling the rise of a buoyant plume (see Briggs, 1969). In order to model the rise of buoyant stack plumes, in the Tar Island area, these widely used formulas require re-evaluation. In this study the most commonly used formulas, namely Briggs (1969, 1971 and 1972), TVA 1971 and 1972 (see Montgomery et al, 1971 and 1972), Holland (1953), CONCAWE (see Brummage, 1968) and Moses and Carson (1967) were selected to examine their predictive capability in determining the rise of the GCOS from Stack A plume. This was done by comparing the observed plume rise with the predicted value. A sample of the results is shown in Figure 3. Mean wind speed between the stack top and the top of the plume was used in this comparison. Values of the wind speed were obtained from the minisonde observations that were made at the lower Syncrude site. It can be seen by the scatter of the points in the figures that none of the models are good predictors for the measured values. Briggs, TVA 1971 and Moses and Carson's formulas underpredict the rise of the plume which in turn will lead to overestimate the maximum ground-level pollutant concentration. The reverse is true with the remaining formulas.

The predictive capability of the formulas depends on the wind speed. Table II shows the mean values of the ratio of the observed plume rise to the predicted value of the plume rise for different ranges of wind speed. With all the formulas except Briggs', the fit becomes steadily worse with increase in the wind speed. By comparison, Holland's model appears to perform best but the correlation is still low when one considers the strong dependence of predicted concentrations upon assumed plume rise.

In addition to the determination of the plume rise, some interesting observations on the behaviour of the plume are recorded. On some occasions during the morning, the plumes from the GCOS plant were trapped under the inversion layer and fanned. This in turn limited their rise to the inversion base height and the plume outlines appeared as a thin ribbon. On other occasions, some of the plumes were able to penetrate the inversion layer and continue to rise till they lost their buoyancy and momentum.

An attempt was made to determine the vertical dispersion co-efficient (σ_z) of the plume from Stack A using the relation.

$$\sigma_z = \frac{D_z}{4.3}$$

TABLE 5.III

RATIOS OF OBSERVED TO PREDICTED PLUME RISE FOR DIFFERENT WIND SPEED RANGES

Wind Speed Range ($m\ sec^{-1}$)	Ratios of Observed to Predicted Plume Rise					
	Briggs	TVA(1971)	TVA(1972)	Holland	Concawe	Moses & Carson
U<2	1.46	0.59	1.8	0.66	0.77	1.28
2<U<3	1.19	0.43	1.42	0.73	0.76	0.83
3<U<4	1.33	0.74	1.09	1.09	0.98	1.74
4<U<6	1.15	1.01	1.14	1.15	0.97	2.03
6<U	1.3	0.82	2.36	0.95	0.71	0.78

Here D_z is the plume width averaged over 5 minutes. In this case the plume is assumed Gaussian. It is also assumed that the concentration at the edge of the plume is equal to one tenth that of the plume centerline.

The estimated values of σ_z were grouped according to stability categories determined by applying the algorithm of Turner (1964) to the hourly observation from Fort McMurray airport. A comparision between the estimated σ_z is made with calculations based on Pasquill-Gifford dispersion parameters as given by Turner (1967)(Figure 4). The values of the estimated σ_z are slightly large and mostly compare with Pasquill-Gifford values for unstable and neutral conditions. There is no apparent relationship between the observed and the predicted values of σ_z. One also will note that during stable conditions the measured σ_z tend to lie at the middle of the scattered points on the Figure. However, the neutral condition cases tend to spread across the whole stability range. This disagreement may be attributed to the plume buoyancy which tends to make the observed σ_z larger than that estimated.

Cramer (1957) derived a relationship between σ_z and the downwind distance from the source x in a power law form,

$$\sigma_z = ax^b$$

where a and b are constants.

The above relationship was examined. Assuming that a power law can fit the observations, the variables are plotted logarithmically (Figure 5). The data was grouped according to the three different wind speed ranges at the plume level, $U<2.4$, $2.5<U<5$ and $U<5$ m sec^{-1} obtained from the lower syncrude minisonde observations. The least square method was applied to fit a straight line to each group. The power law appears to hold for each velocity group, each with different values of a and b. Value a decreases with increasing wind speed and b increases with increasing wind speed.

b. Plume Dispersion in a Valley

One of the challenging problems in the field of air pollution is to determine the dispersion of pollutants in a valley. The complex terrain and the local meteorology greatly affect the air flow producing nonuniform and unsteady dispersion conditions in the valley.

In May, 1974, a plume dispersion study was made at a deep valley site in Trail, British Columbia. The main object of the study was to determine the behaviour and diffusion of pollutants in a valley under different meteorological conditions. The industrial source, in this case, was the Cominco smelter which is located on the west bank of the Columbia River overlooking the city of Trail. Trail is situated on a relatively flat plateau about 75 meters above the river. The terrain of the area is rugged (some mountains reaching a height of 1220 m) with a few side valleys sloping into the Columbia River valley. The valley is from 800 m to 5,000 m in width with sharply rising sides near the plant.

The smelter's main function is to produce base metals (lead and zinc) from concentrate. The major emission sources are three stacks: the zinc stack, the Dwight and Lloyd stack, and the lead Furnace Baghouse stack. The emission characteristics are tabulated in Table III.

Table III Emission Characteristics of Cominco Smelter

PARAMETER	STACK A	STACK B	STACK C
Chimney height (m)	122	122	87
Stack inside diameter (m)	3.6	7.6	3.9
Average Emission rate ($m^3\ min^{-1}$)	3161.6	5392.1	6779.8
Average SO_2 concentration (ppm)	1409	729	382
CO_2 concentration (%)	0	1.0	2.2
Average gas temperature (^oK)	306	319	331
Exit velocity ($m\ sec^{-1}$) calculated	5.8	2	9.5

Irregularities in both the topography of the valley and convective heating of the air over the sunny side of the valley cause local variations in wind direction, wind speed, and temperature. Figure 6 shows vertical profiles of wind and temperature to a height of about 2 km at two meteorological stations in the valley. Changes in wind direction are more pronounced than the changes in wind speed and temperature. These local changes affected the behaviour of the smoke plume from the Cominco smelter.

At first the plumes from the two stacks moved in the same direction. Local changes in the wind direction, however, caused the plume from one stack to behave differently from the other stack. During the study, the two plumes moved both away from each other and towards each other, some times combining.

Occasionally, the plume from one of the stacks travelled in a spiral path and one some occasions, parts of the plume reached the ground, with the point of impingement ranging from tens of meters, to hundreds of meters from the stack.

Cool air drainage flow and the cross-valley gradient winds generated by the valley's complicated topography displace and disperse the plume laterally as well as vertically (Whaley and Lee 1975). As a result the plume is characterized by large vertical and horizontal extent. Figure 7 and 8 show side and plan view respectively of SO_2 isopleths marking the plume outline, during stable atmospheric conditions. The nonuniform wind carries the plume first in one direction, and then back, causing the plume width to be about 7 km at a height of about 800 m as it passes over the source. Under neutral atmospheric conditions, the plume thichness is normal (Figure 9). Its width, however, is exceptionally large (Figure 10).

Whaley and Lee (1975) estimated the dispersion parameters of this plume (σ_y and σ_z) and compared the observed values with theory for both stable and neutral atmospheric conditions. (Figures 11 and 12) They indicated that the regression lines through σ_y and σ_z values have a shallower slope than the corresponding Pasquill's curves. The discrepancy is due to the severe nonuniform motion created by irregular topography and heating in the valley.

c. Diffusion in an Urban Environment

The transport and the dispersion of pollutants in an urban environment is more complex than that from a rural environment. They are strongly influenced by the magnitude of the urban mean wind, turbulent intensity generated by buildings, and street canyons, and thermal stability.

Types of pollutants in the urban area include anthropogenic heat, gases and particulates. The anthropogenic heat contributes to the formation of the heat island. Urban gases and large particles produced by the city vehicular traffic and industry help to produce the well known urban haze.

The heat island effect has been documented by many investigations and reviewed extensively (see eg. Chandler, 1976).

In order to determine the characteristics and variations of the urban haze, Summers (1966) analyzed measurements of Soiling Index from three smoke analyzers which were located in the centre of the city of Montreal, Quebec. He concluded that the haze concentration is directly proportional to the following:

a) Rate of production of gases and particulate

b) Square root of the city size

c) Square root of the potential temperature gradient ($\delta\theta/\delta z$)

d) Square root of the reciprocal of the average urban wind speed

He found that the city of Montreal has a marked seasonal cycle of haziness (Figure 13).

The weekly cycle of pollution was also discussed in this study (Figure 14). There is a pronounced reduction in the Soiling Index during the weekend by about 23% of the mean weekday value. This reduction is a consequence of the shutting down of many industries and commercial activities during the weekend.

It appears also that urban haziness is inversely proportional to the urban ventilation coefficient. The monthly variation of the ventilation coefficient for the city of Montreal was obtained by Summers (1966) (Figure 15). By examining Figs. 13 and 15, one will note that the ventilation coefficient is a maximum and a minimum during the winter and summer respectively. The reverse is true with respect to the Soiling Index (Fig. 13). The highest value of the Soiling Index occurred in mid-winter. At that time, the Soiling Index reached a value up to three times the summer values.

Another pollutant which appears to be widespread in urban environment is ozone (0_3). This photochemical air pollutant can cause eye and throat irritation and impairment of lung function. Mukammal (1965) found that 0_3 can cause some damage to certain vegetation (e.g. tobacco, bean and spinach). Recently ozone has been found in alarmingly high concentrations on a regional scale, outside or urban areas. Indeed an appreciable fraction of the ozone measured within urban areas may have already existed in the incoming air, rather than being produced from locally emitted pollutants. Since few non-urban measurements are available in Southern Ontario, Lusis et al (1976) have measured 0_3 in the vicinity of Metropolitan Toronto. A sample of their observations is shown in Figure 16. The figure shows the profiles of 0_3 concentrations along with some meteorological profiles. The measurements indicate the existence of an inversion layer at the 1600 m level. At that level 0_3 concentration decreased sharply from 100 ppb to about 50 ppb at the Toronto water front while days with a lake breeze, there was a build-up of ozone here.

Their findings indicate that ozone is of anthropogenic origin rather than stratospheric. Chung (1976) using 0_3 data for 1973-75 inclusive, found that 0_3 concentration increases when an anticyclonic ridge passes over the region. Chung also found two maxima in the diurnal cycle of 0_3 for the cities of Toronto and Montreal. These maxima usually occur between 1400 and 1500 and at 0400.

3. Air Pollution Models

Numerous mathematical models of urban and regional air pollution are being developed in Canada. The models are designed to predict the distribution of concentration of pollutants, as a function of the local meteorological conditions, on a day to day or on a climatological basis.

They are used to forecast episodes of air pollution or for land use planning. There are four types of models which are commonly used, namely box, puff, plume, and K-theory models. A detailed discussion on these four types can be found in many previous NATO publications, so therefore will not be repeated here.

For illustrative purposes, two examples of air pollution models will be discussed. This by no means covers all the modelling experiments being carried out in Canada.

Western Research & Development Limited (1976) applied a model which is based on the box model (air column trajectory model) to predict the concentration of CO and NO_x at a location in the city of Calgary, Alberta, Canada. The model also predicts the excess of moisture and heat emitted in the urban environment. The model assumes that both mechanical and thermal turbulence are strong enough to distribute the pollutants uniformally along the vertical within the urban mixing depth.

The following two figures (17) and (18) show a sample of the predicted values of the NO_x and CO concentrations respectively. It is assumed that the city is characterized by a 5% daily flow of traffic, stable atmospheric conditins, south wind of 2 m sec^{-1} and an ambient air temperature of $4^{o}C$.

It will be noted that the largest concentration of CO and NO_x occured at the downwind edge of the city. For that city NO_x appeared to be of more concern than the CO.

In this study concurrent meteorological and air quality data were available and were used to verify the model.

The correlation coefficients between the predicted and observed NO_x and CO concentrations were 0.6 and 0.84 respectively.

Another example of the application of an air pollution model was described by Walmsley and Bagg (1977). They applied a Climatological Dispersion Model (CDM) to determine the annual ground level concentrations of pollutants at the Oil Sands area, Alberta.

The CDM model was described in detail by Buss and Zimmerman (1973).

Walmsley and Bagg used a power law to parameterize the increase of wind speed along the vertical, with an exponent that depended on atmospheric stability. They used Briggs' formulae to describe the rise of the plumes from the existing sources and a Gaussian dispersion of pollutants. The meteorological input to this model was the long-term joint frequency distribution of winds in the vicinity of the sources. Other input information for this model consisted of emission rates and characteristics of the stacks.

Figure 19 illustrates a sample of the CDM predicted values of the annual ground level concentration of SO_2.

In order to simulate the removal of SO_2 processes in that area, Walmsley and Bagg assumed a 20 hour half life for SO_2.

There appear to be two maxima of 21 and 22 μg m^{-3} of SO_2 concentration. They are located respectively 2.3 km south southeast and 2.3 km north northwest of the source. The low values of SO_2 concentrations that exist to the east and west of the source reflect the low frequency of occurrence of wind along that direction.

Since the CDM assumes a flat terrain, Walmsley and Bagg attempted to examine the effect of topography on the CDM predictions. This was done by assuming that the polluted flow followed a path governed by the terrain. The results of this modification indicated that the terrain of that area had a negligible effect on the CDM predicted values.

The results obtained using the CDM were reasonably well correlated with the available observations.

4. Concluding Remarks

Many aspects of air pollution problems have been discussed in this paper to illustrate the important role that meteorology and topography play in their dispersal.

Meteorology determines what happens between the pollution source and the receptor. Changes in meteorological conditions may cause potentially harmful pollutants to travel to an unexpected remote location, adversely affecting humans, animals and agriculture crops.

Despite all measures taken to date to control the emission rates of pollutants and to increase the stack height, it is not unlikely that air pollution damage can occur in some instances, for example in valleys and in cold calm conditions when inversion layers occur. It is true that tall stacks may improve the air quality of the local area but at the same time they introduce air pollution problems on a larger scale. At the moment, it appears that there are several aspects of dispersion of tall stack plumes that require more study. There is a need to understand the impact of wind shear both in direction and speed to parameterize the growth of the plume.

The rise of the plume from relatively short stacks in a cold environment is complicated by the frequent occurrence of inversion layers in the morning.

Holland and Briggs formulas appear to predict the rise of the plume better than other reported in this paper. The correlation, however, between the observed and predicted values is low. The model proposed by Briggs for windy conditions does not predict well the final rise of the plume for wind speed less than 4 m sec^{-1}.

The lack of agreement between the observed and the predicted σ_z may be due to the fact that Turner's algorithm may not apply for snow covered surfaces.

Our present understanding of the diffusion of pollutants in Canadian urban environments is limited. This is due in part to the fact that the methods applied in diffusion calculations by many investigators are based on information obtained using idealized meteorological conditions and flat terrain. Interpretations of the removal processes of pollutants in urban areas are also open to question. It is apparent that more field studies similar to the ones reported in this Chapter are needed.

With regard to the air pollution modelling it must be stated that although model studies shed a favorable light on this type of investigation, they are based on a limited amount of field observations. Their representativenes must be treated with caution. One, however must admit that numerical models offer many possibilities in the study of air pollution.

Acknowledgements

The authors are greatly indebted to Drs. H. Martin and C. Matthias for their friendly advice and constructive criticism of the manuscript.

5. REFERENCES

Briggs, G.A. 1969, "Plume Rise". AEC Critical Review Series TID-25075, 81 pp, National Technical Information Service.

Briggs, G.A. 1971, "Some Recent Analyses of Plume Rise Observation" Proc. Second International Clean Air Congress, Academic Press, 1029-1032.

Briggs, G.A. 1972, "Discussion on Chimney Plumes in Neutral and Stable Surroundings". Atmos. Environment 6, 507-510.

Brummage, K.G. 1968, "The calculation of Atmospheric Dispersion from a Stack" Atmos. Envir. 2, 197.

Buss, A.D. and Zimmerman, J.R., 1973 "User's Guide for the Climatological Dispersion Model" U.S. Environmental Protection Agency Rep. EPA-R4-73-024, Research Triangle Park, N.C.

Chandler, T.J., 1976 "Urban Climatology and its Relevance to Urban Design", WMO Tech. Note No. 149.

Chung, Y.S., 1976 "Photochemical Ozone and Regions transport of Air Pollutants in the Boundary Layer". Paper presented at the Joint Int. Symp. on Atmospheric Ozone (I.U.G.G.), Dresden, Germany.

Cramer, H.E. 1957 "A practical Method for Estimating the Dispersal of Atmospheric Contaminants" Proc. of the Conf. on Applied Meteorol. AMS.

Fanaki, F.H. and Turner, H.E. 1976 "Plume Dispersion from the Sudbury Tall Stack". Proceedings of the Seventh International Technical Meeting on Air Pollution Modelling and its Application, NATO Committee on Challenges of Modern Society, Airlie House, Virginia, USA.

Holldand, J.Z. 1953 "A Meteorological Survey of the Oak Ridge Area. U.S. Atomic Energy Commission Report ORO 99, 554.

Lusis, M.A., Anlauf, K.G., Chung, Y.S. and Wiebe, H.A. 1976 "Aircraft O_3 Measurements in the Vicinity of Toronto, Canada" Paper presented at the 69th Annual Meeting of the Air Pollution Control Association, Portland, Oregon, USA.

Millan, M.M., Gallant, A.J. and Turner, H.E., 1976 "The Application of Correlation Spectroscopy to the Study of Dispersion from Tall Stacks", Atmospheric Environment, 10, 499.

Millan, M.M., Hoff, R.M. and Gallant, A.J., 1976 "Tall Stacks, Plume Dispersion and Emission Calculations by Correlation Spectroscopy" Paper presented at the 69th Annual Meeting of APCA Portland, Oregon, USA.

Montgomery, T.L., Carpenter, S.B., Colbaugh, W.C. and Thomas, F.W., 1971, "Full-Scale Study of Plume Rise at Large Electric Generating Stations - Bull Run Supplement. Air Quality Branch, TVA, Muscle Shoals, Alta. 58 pp.

Mongomery, T.L., Carpenter,S.B., Colbaugh, W.C. and Thomas, F.W. 1972, "Results of Recent TVA Investigations of Plume Rise. J. Air Pollution Control Assoc., 22, 779-784.

Moses, H. and Carson, J.E. 1967, "Stack Design Parameters Influencing Plume Rise". Paper presented at the 60th Annual Meeting of the Air Pollution Control Association, Cleveland, Ohio. Paper 67-84.

Mukammal, E.I., 1965 "Ozone As a Cause of Tobacco Injury" Agricultural Meteorology, 2, 145.

Summers, P.W., 1966 "The Seasonal, Weekly and Daily Cycles of Atmospheric Smoke Content in Central Montreal APCA Journal, 16, No. 8, 432.

Turner, D.B., 1964, "A Diffusion Model for an Urban Area". J. Appl. Met. 3, 83-91.

Turner, D.B., 1967, "Workbook of Atmospheric Dispersion Estimates", Public Health Service Publication 999-AP-26, U.S. Dept. of Health, Education and Welfare.

Walmsley, J.L. and Bagg, D.L., 1977 "Calculations of Annual Averaged Sulphur Dioxide Concentrations at Ground Level", Alberta Oil Sands Environmental Research Program Report, Sub-Project ME 4.1.

Whaley, H. and Lee, G.K., 1975 "Plume Dispersion in a Mountainous River Valley During Spring". Paper presented at the Pacific North Western International Section Annual Meeting of APCA, Vancouver, B.C., Canada.

Western Research and Development Ltd., 1976 "Application of an Urban Air Pollution Model to the City of Calgary" Alberta Dept. of the Environment Report, Alberta, Canada.

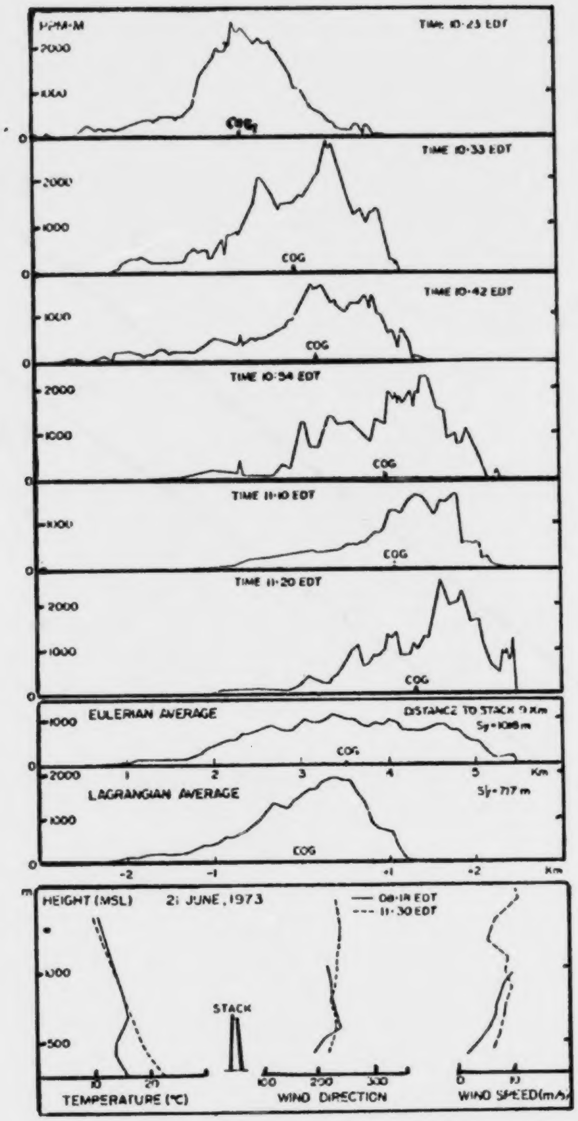

Figure 1 Six plume profiles at 9 km from the source. The Eulerian (space) average represents the lateral (absolute) diffusion, including relative diffusion, wind shear effects and plume meandering. The Langrangian (centre of gravity) average would include only the effects of the first two. The times shown indicate the beginning of each transect (from Millan et al 1976a).

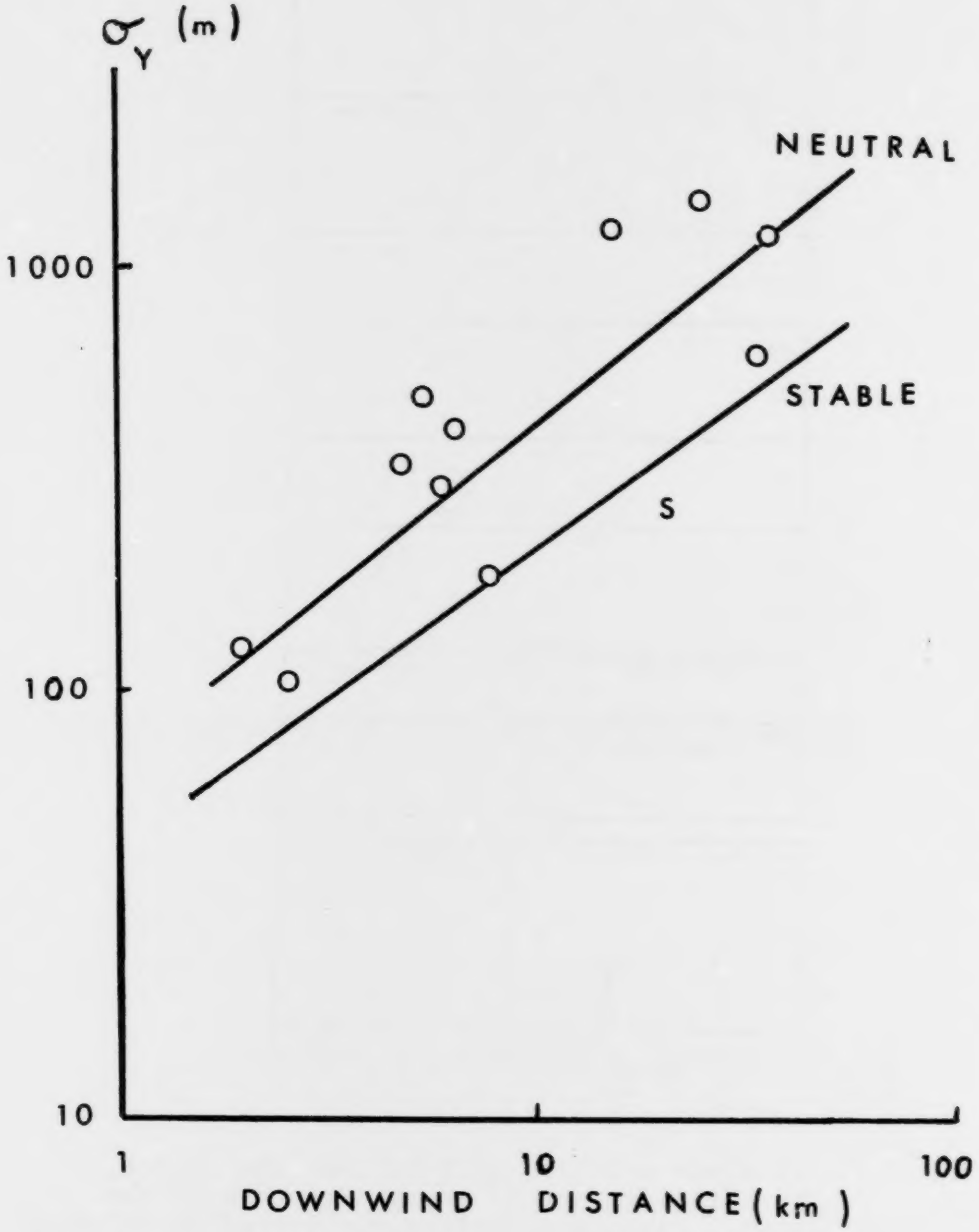

Figure 2 Comparison of Observed Vertical Dispersion with ASME predictions for the Sudbury Study (from Millan et al 1976a).

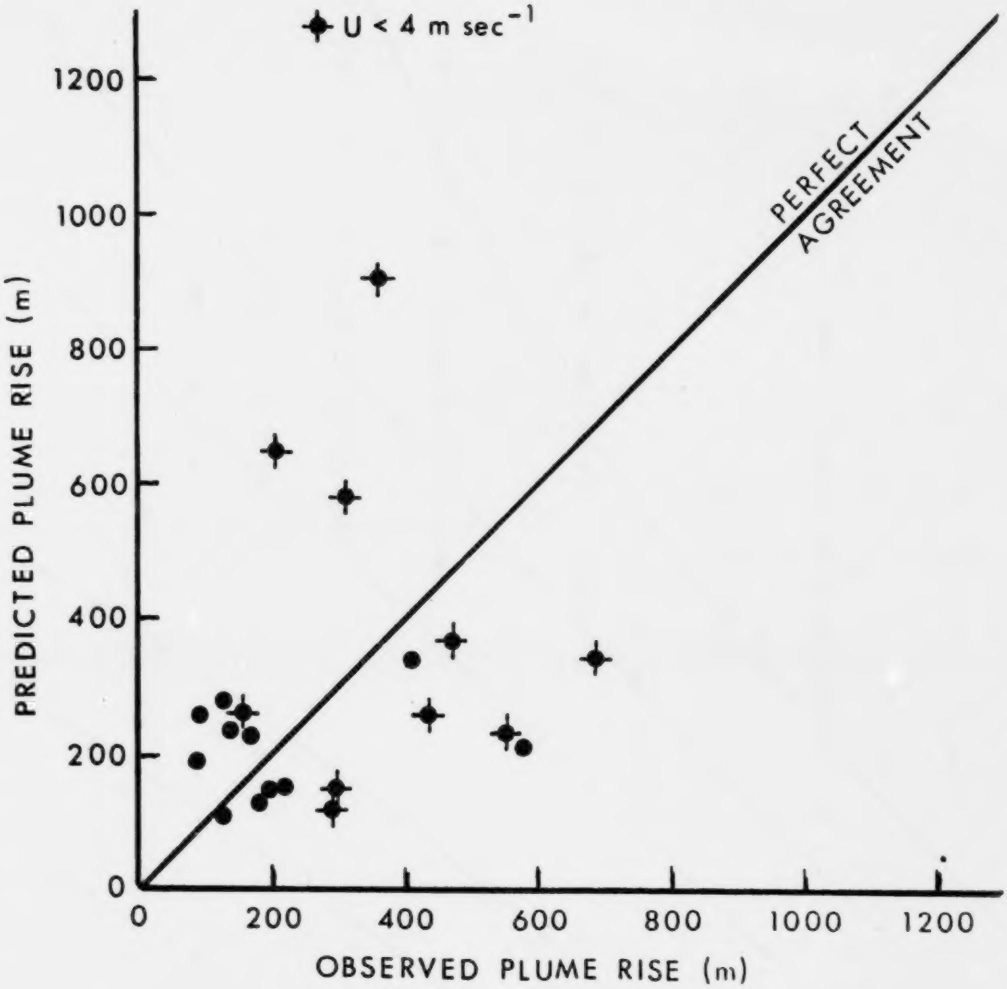

Figure 3 Comparison of predicted versus observed plume rise using Briggs' model. Solid line represents perfect agreement.

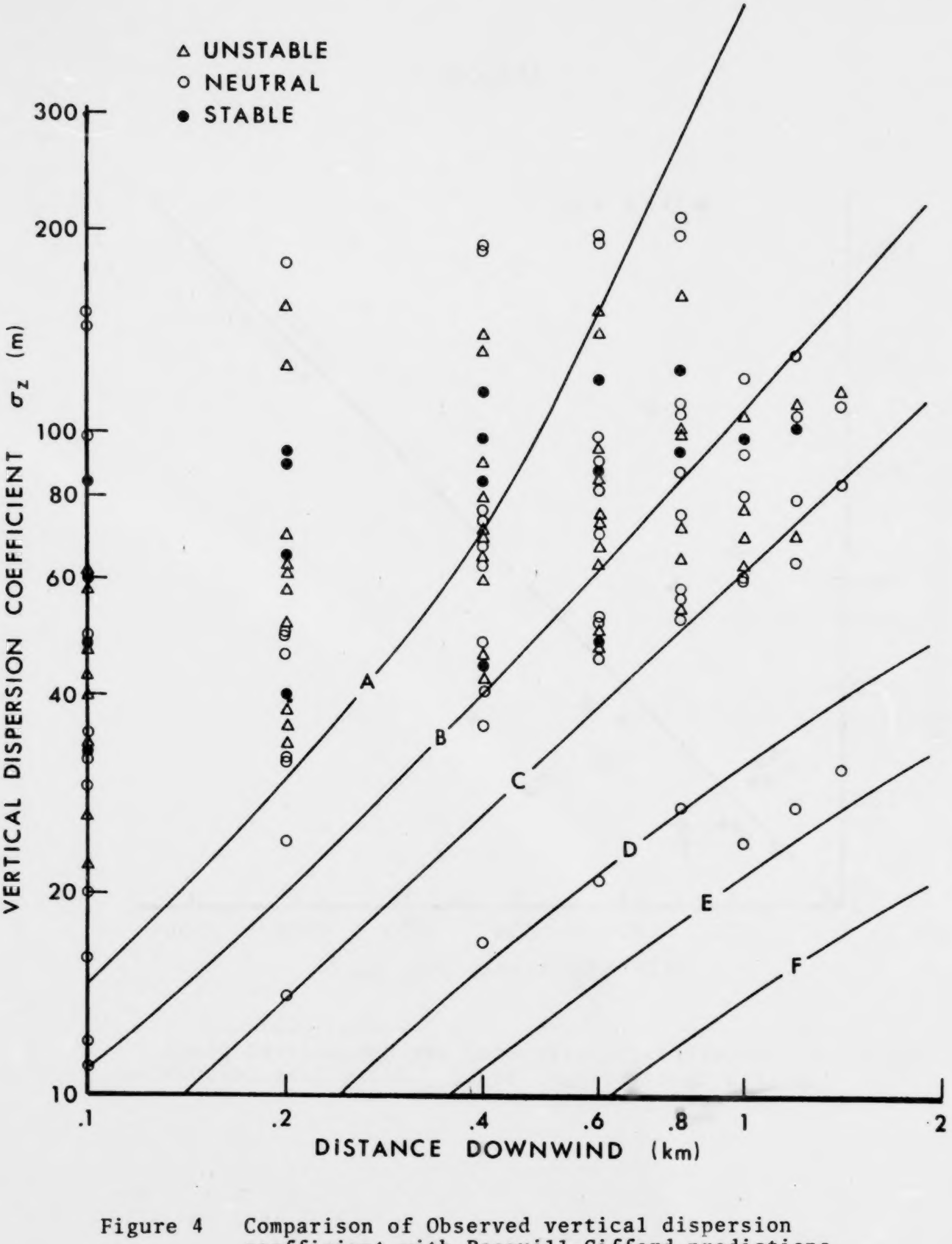

Figure 4 Comparison of Observed vertical dispersion coefficient with Pasquill-Gifford predictions.

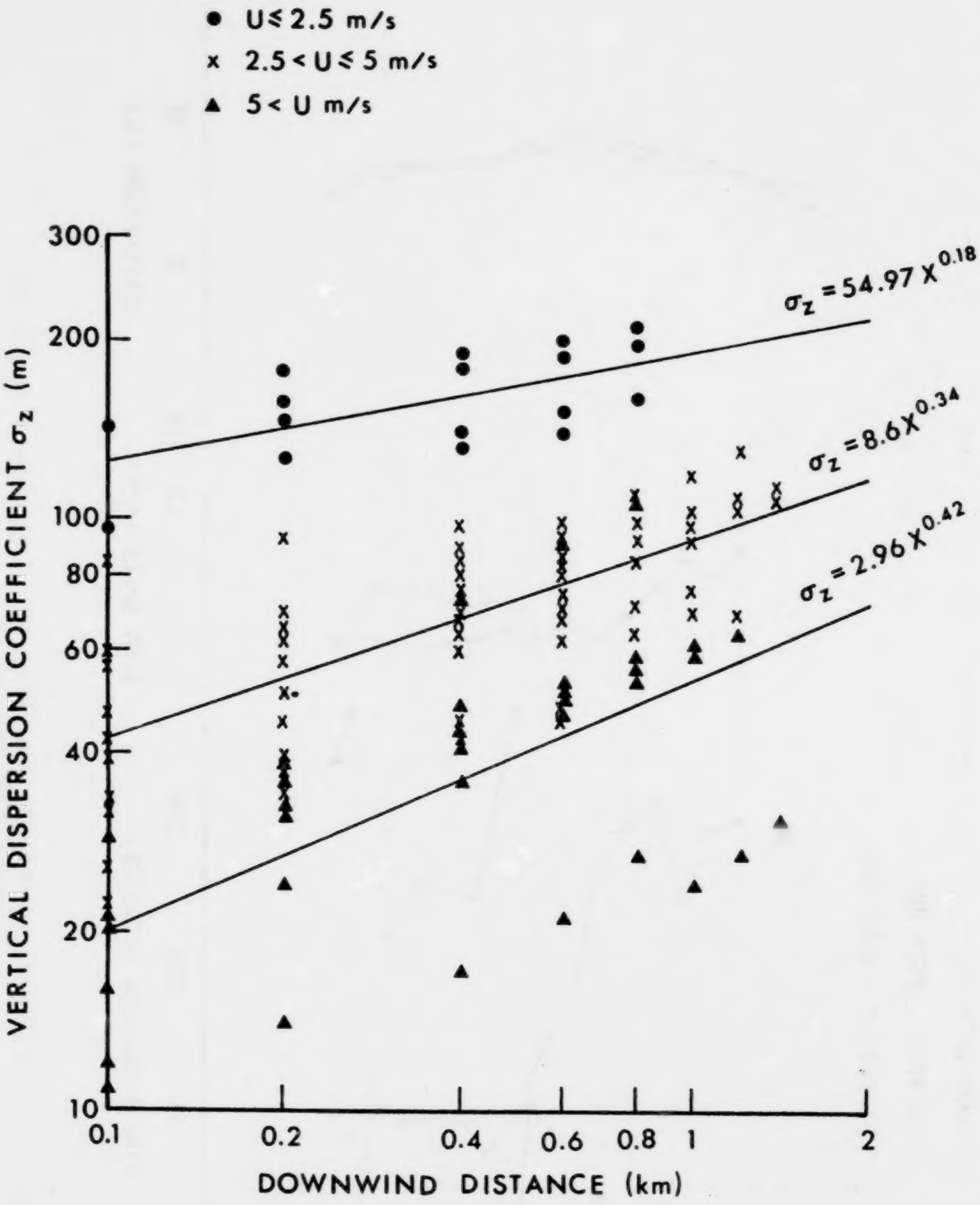

Figure 5 Vertical Dispersion Coefficient of the GCOS plume as a function of downwind distance from the source (Stack A). The solid line represents the best fit for each wind speed group.

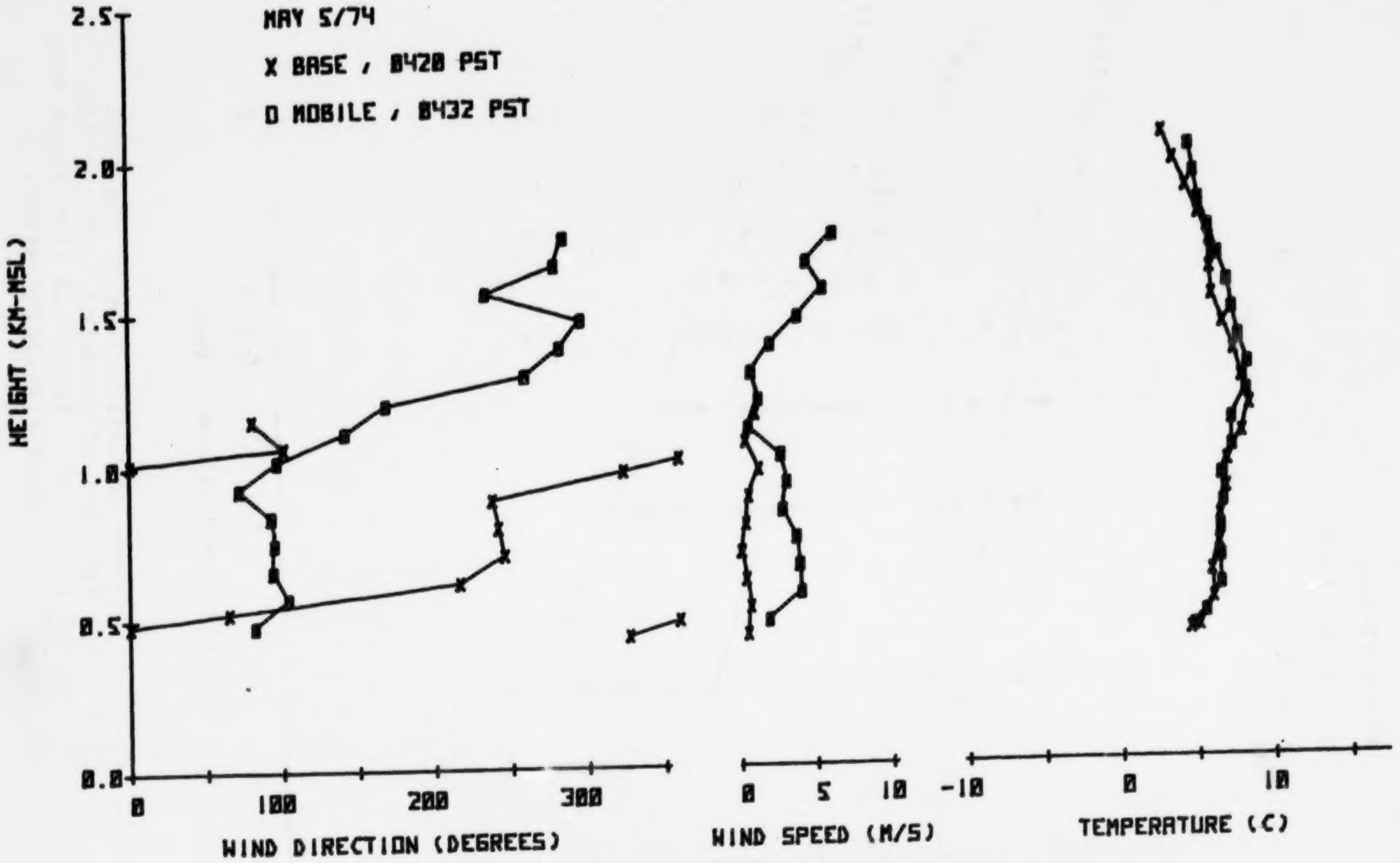

Figure 6 Vertical profiles of wind direction, wind speed and temperature.

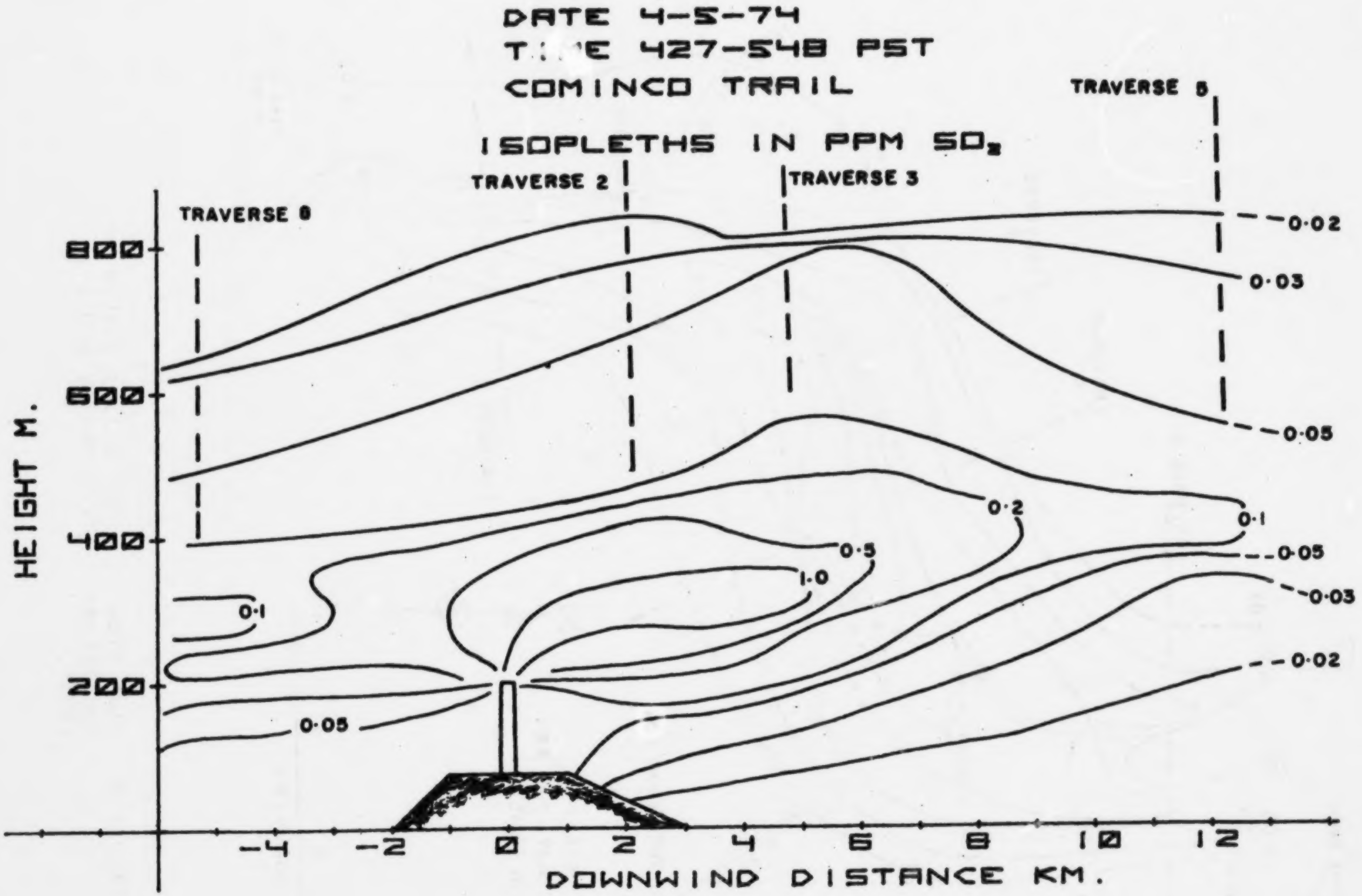

Figure 7 Side view of plume during stable conditions. (From Whaley and Lee 1975).

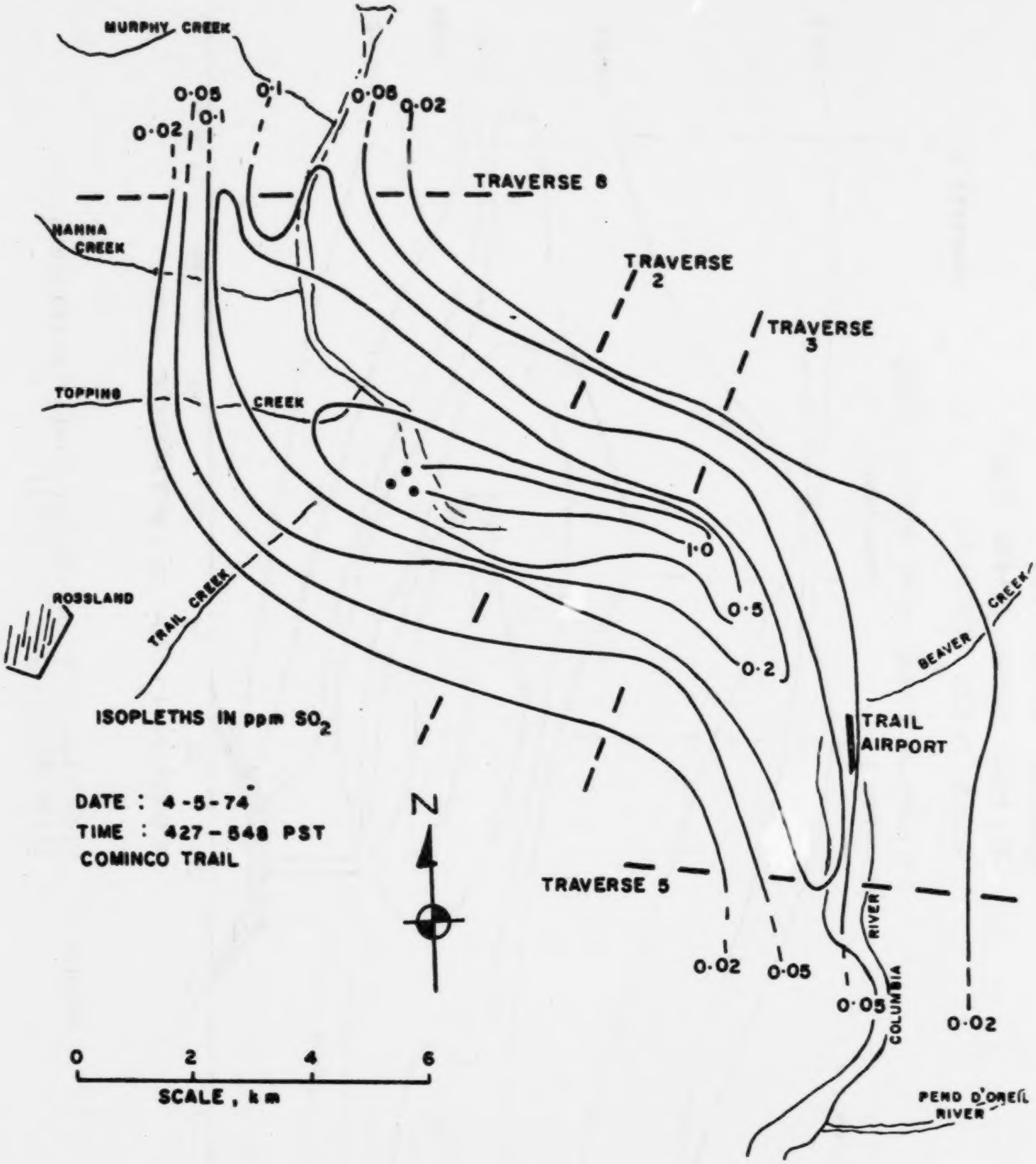
MURPHY CREEK
HANNA CREEK
TOPPING CREEK
TRAIL CREEK
ROSSLAND
TRAVERSE 8
TRAVERSE 2
TRAVERSE 3
TRAVERSE 5
0·02
0·05
0·1
0·1
0·05
0·02
1·0
0·5
0·2
0·02
0·05
0·05
0·02
BEAVER CREEK
TRAIL AIRPORT
COLUMBIA RIVER
PEND D'OREIL RIVER
ISOPLETHS IN ppm SO2
DATE : 4-5-74
TIME : 427-548 PST
COMINCO TRAIL
N
0
2
4
6
SCALE, km

Figure 8 Plan view of plume during stable conditions. (from Whaley and Lee 1975).

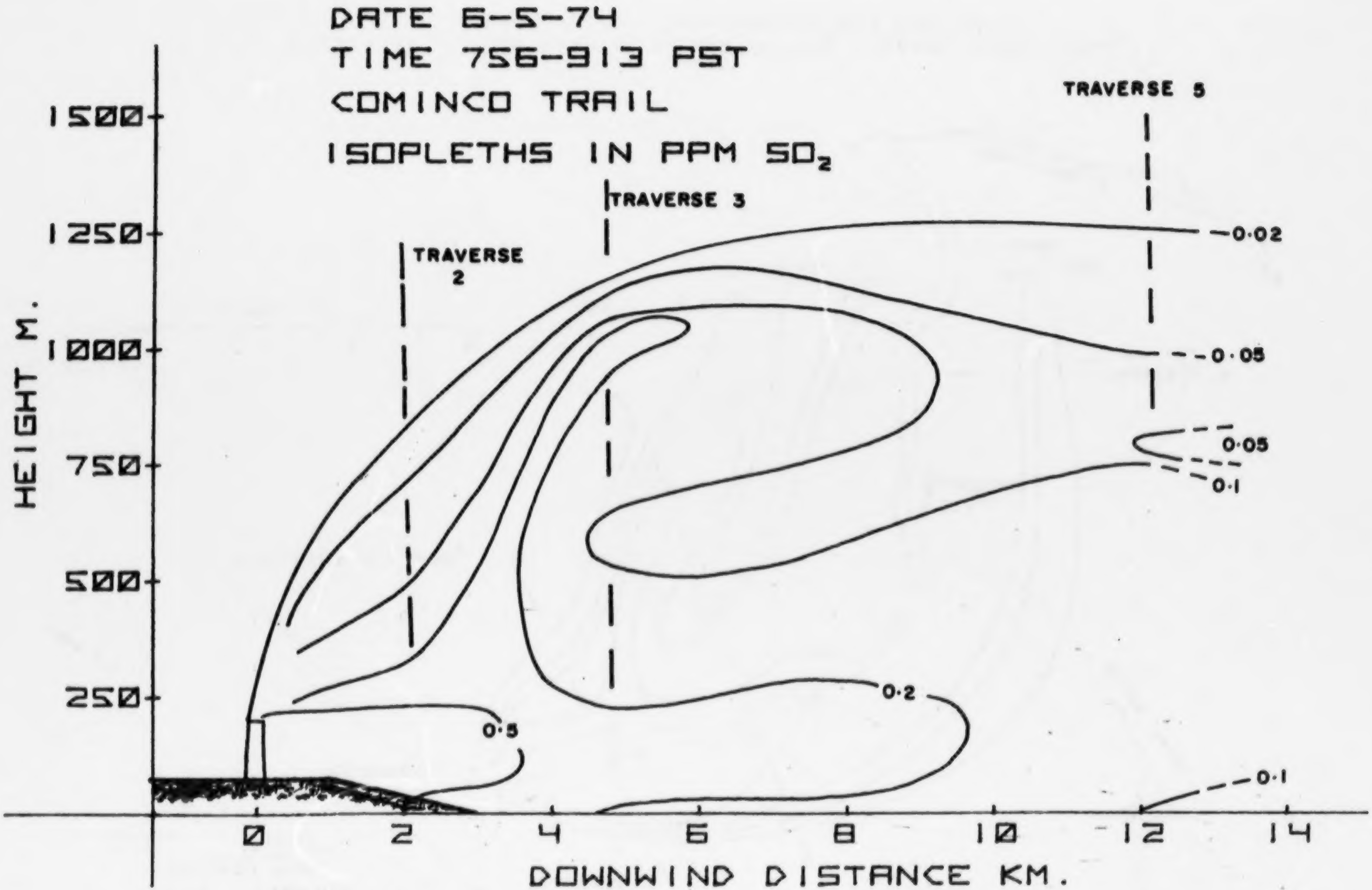

Figure 9 Side view of plume during neutral conditions, mid-morning (from Whaley and Lee 1975).

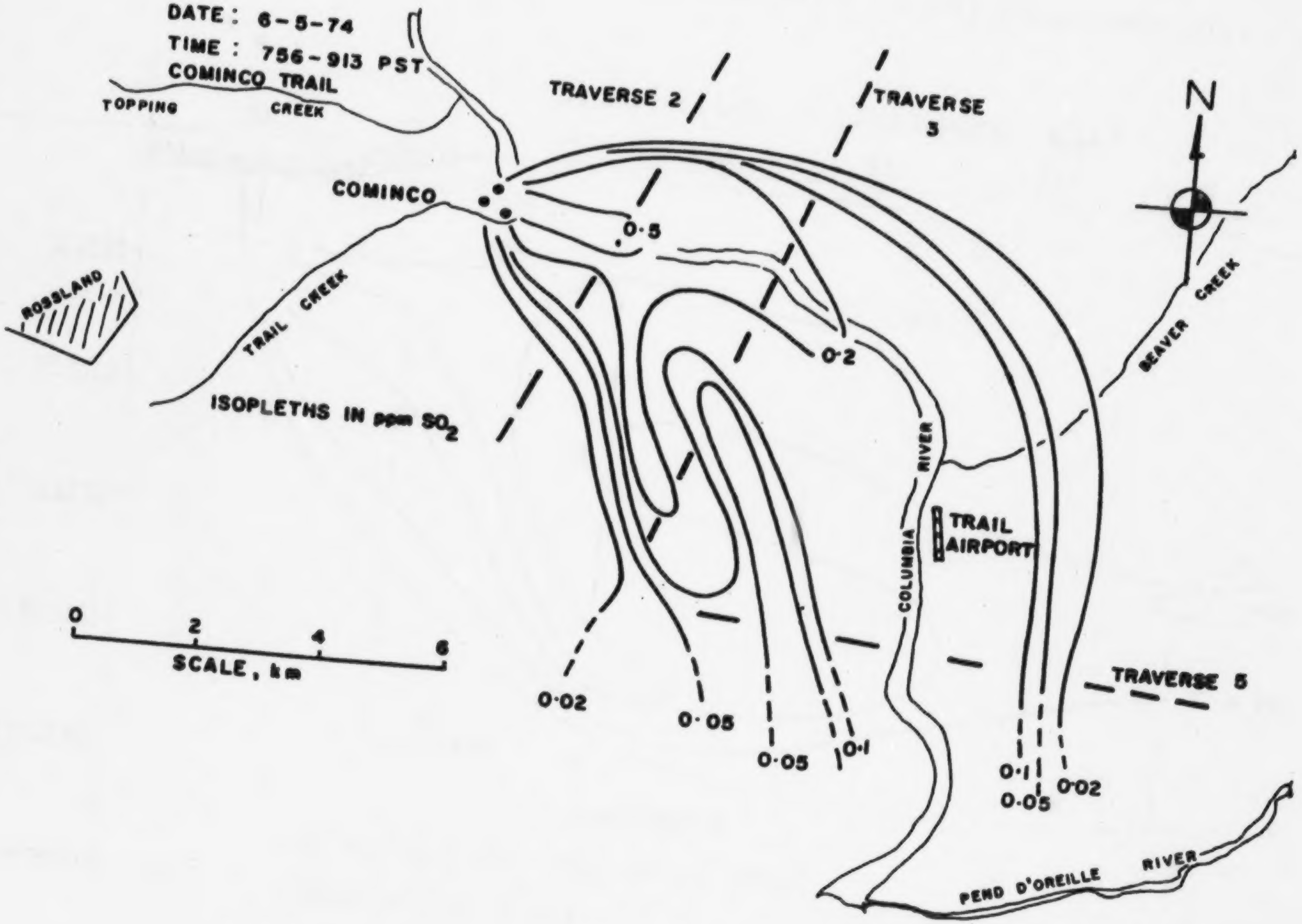
DATE : 6-5-74
TIME : 756-913 PST
COMINCO TRAIL
TOPPING
CREEK
COMINCO
ROSSLAND
TRAIL CREEK
ISOPLETHS IN ppm SO_2
TRAVERSE 2
TRAVERSE 3
TRAVERSE 5
N
BEAVER CREEK
0·5
0·2
COLUMBIA RIVER
TRAIL AIRPORT
0
2
4
6
SCALE, km
0·02
0·05
0·05
0·1
0·1
0·05
0·02
PEND D'OREILLE RIVER

Figure 10 Plan view of plume during neutral conditions, mid-morning (from Whaley and Lee 1975).

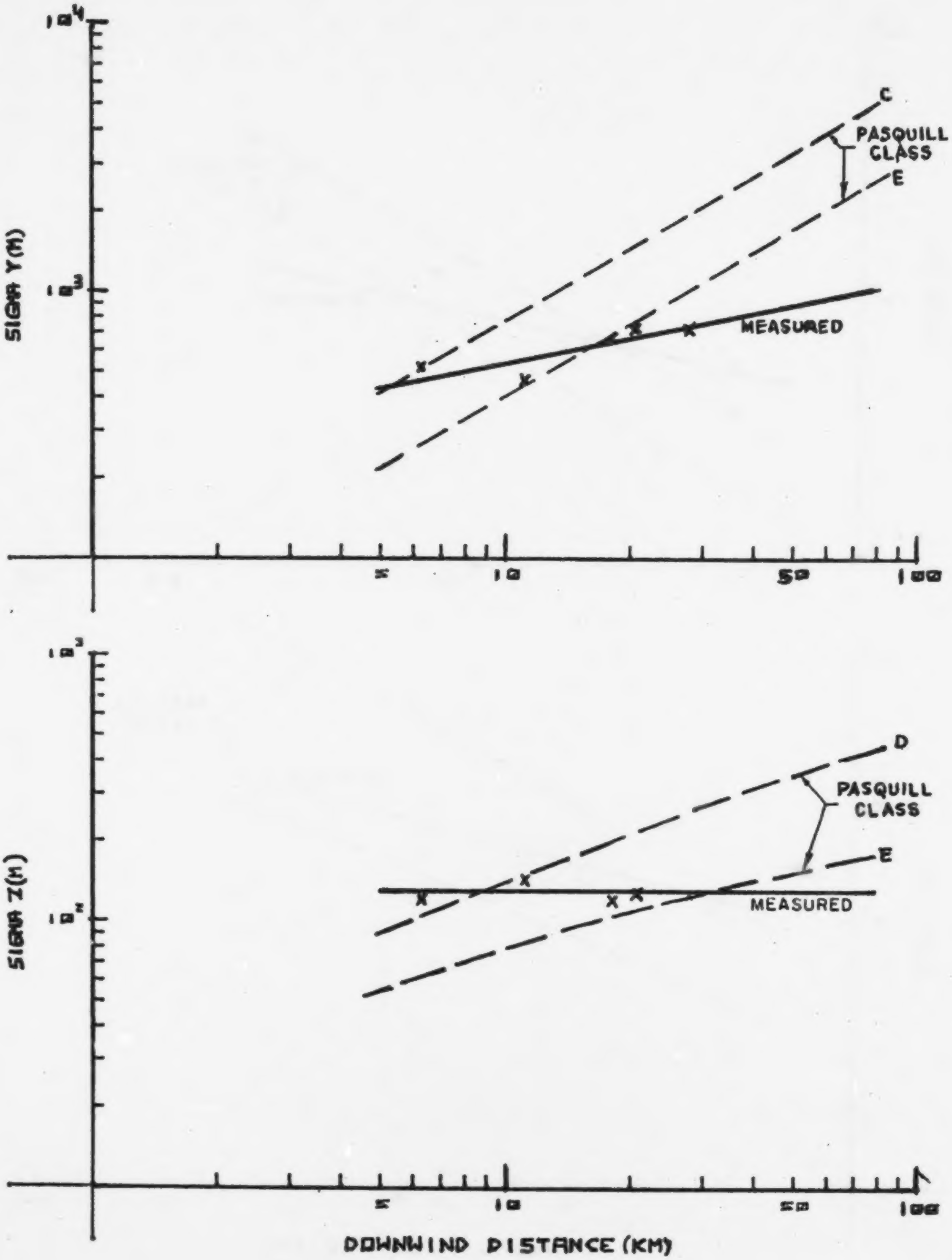

Figure 11 Standard deviations of plume spread during stable conditions. (From Whaley and Lee 1975).

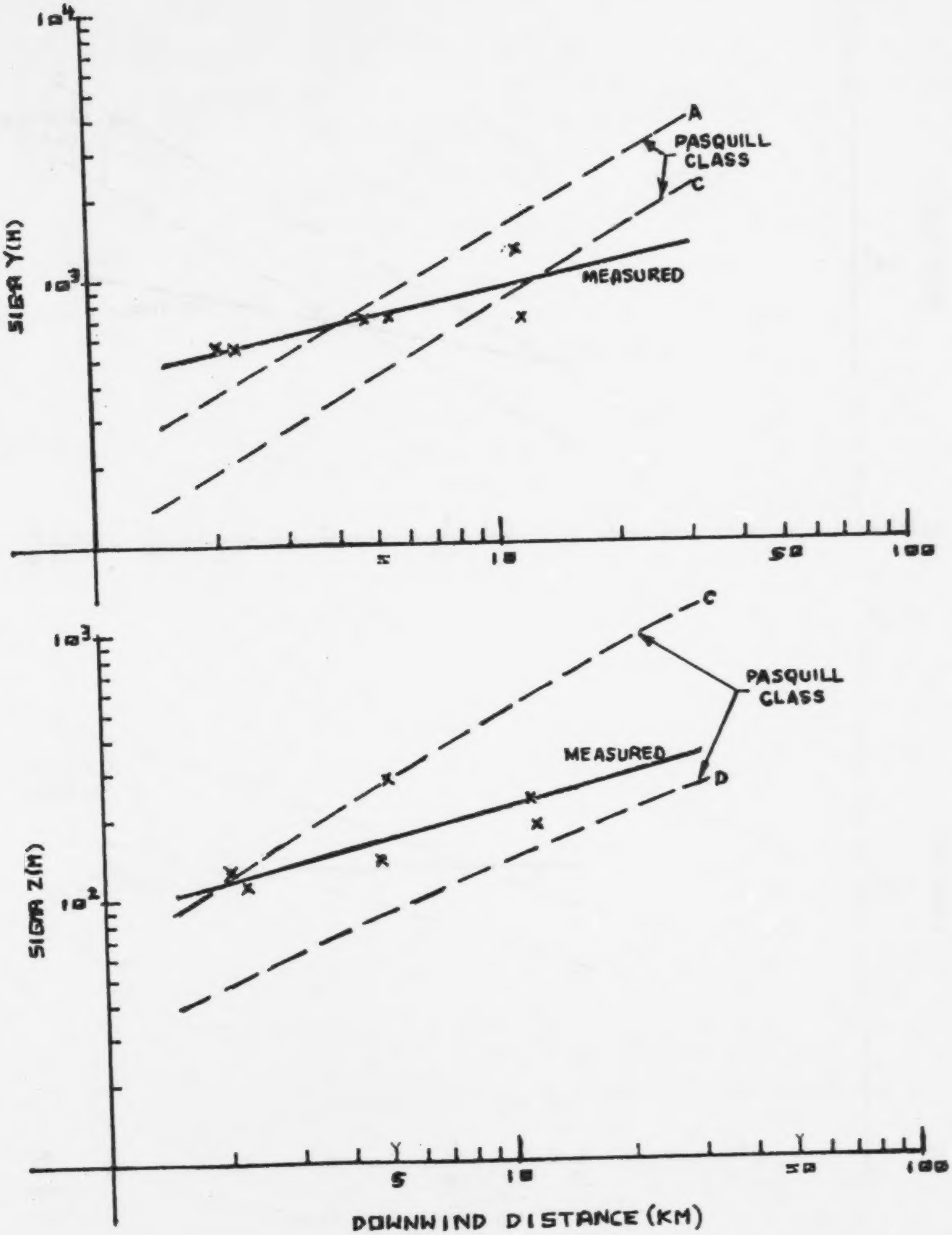

Figure 12 Standard deviations of plume spread during neutral conditions. (From Whaley and Lee 1975).

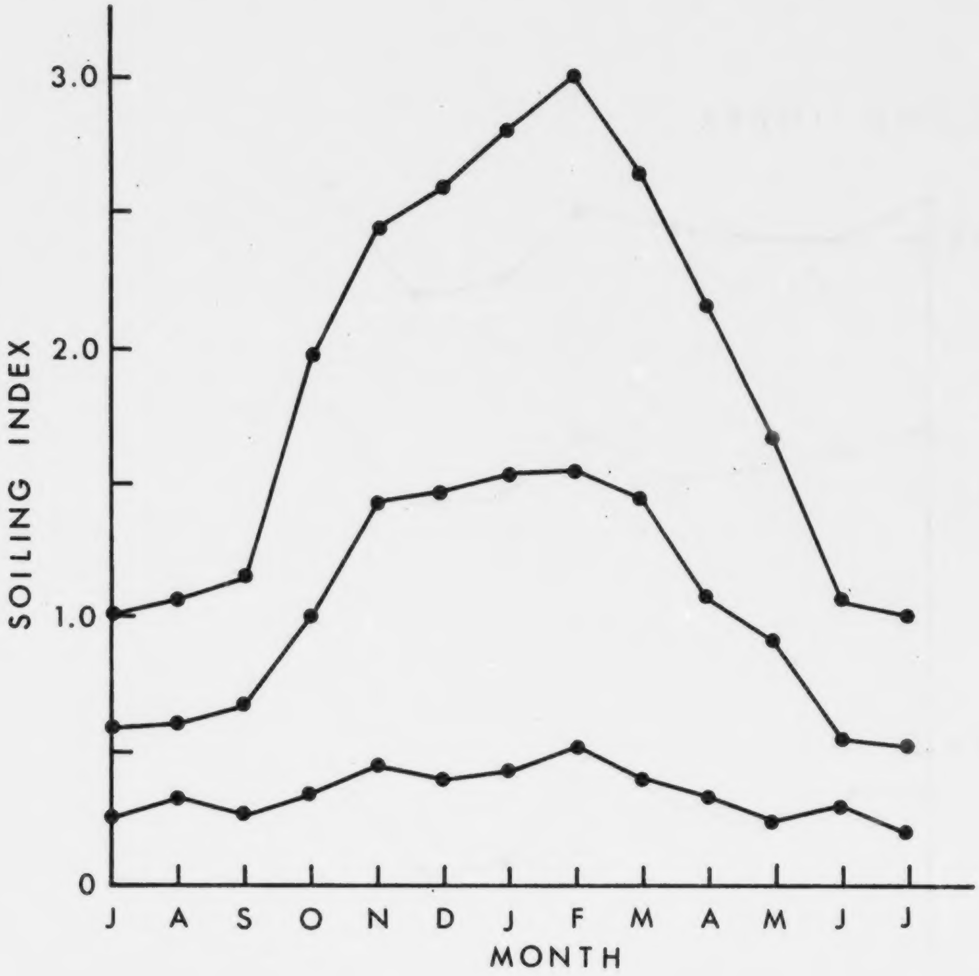

Figure 13 Seasonal cycle of Soiling Index at three different locations in Central Montreal. (From Summers 1966).

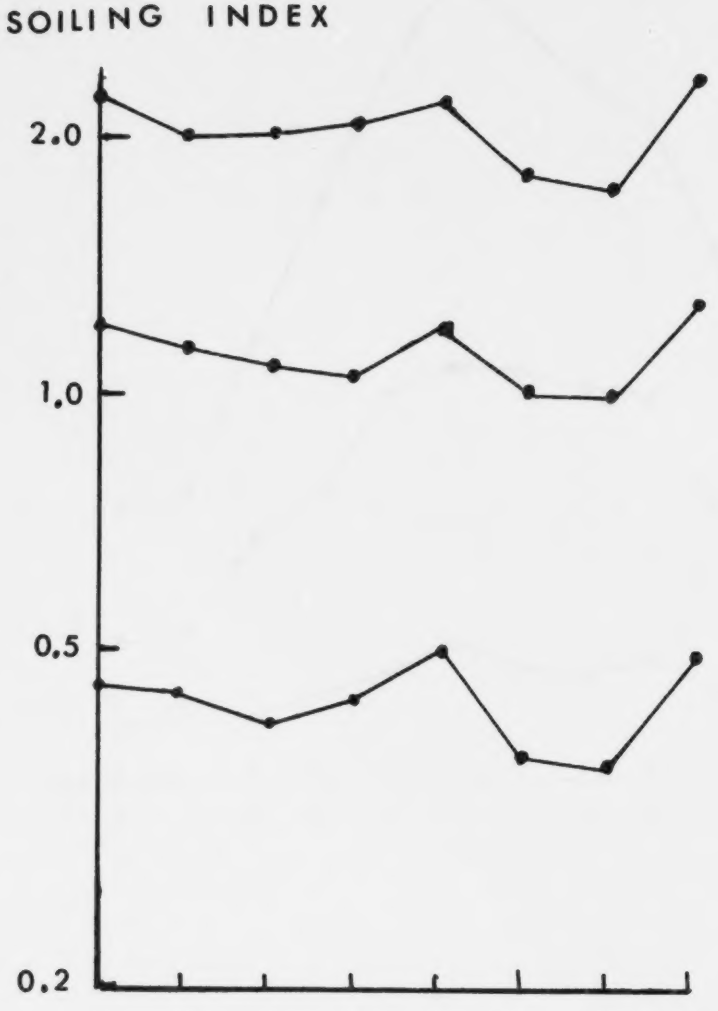

Figure 14 Weekly cycle of Soiling Index in Montreal. (From Summers 1966).

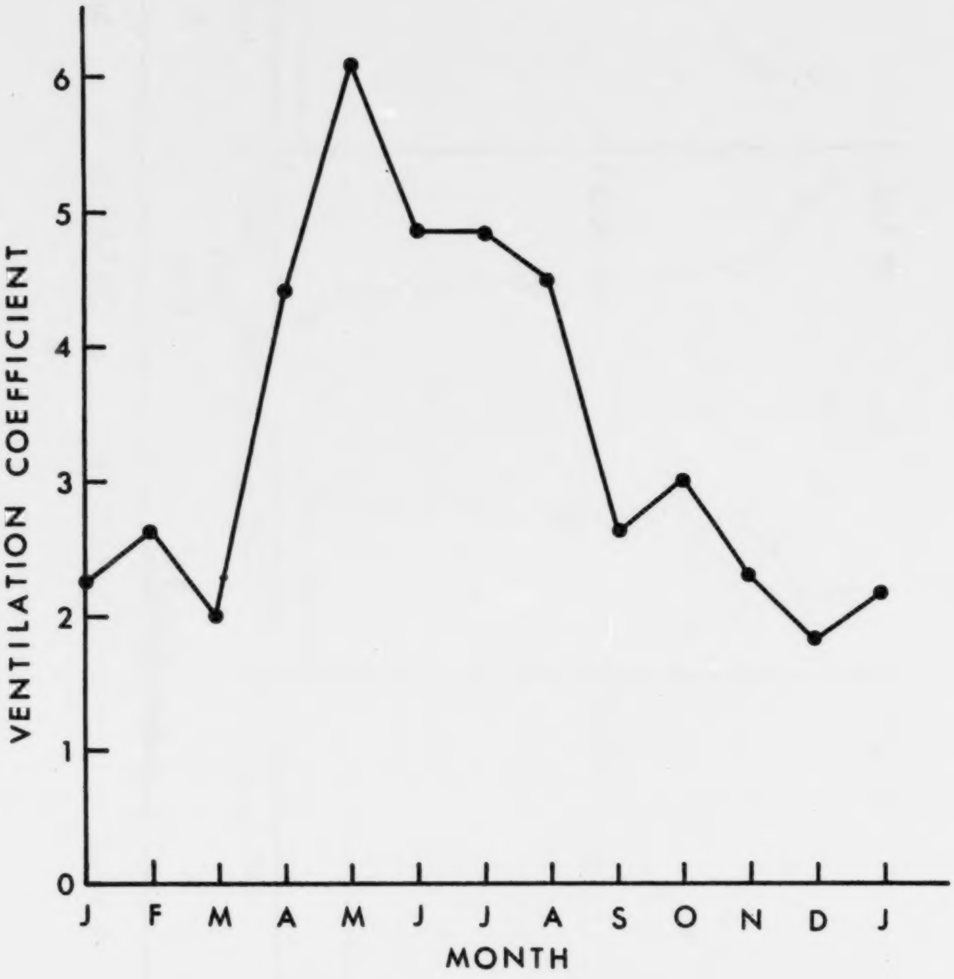

Figure 15 Monthly variation of the afternoon ventilation coefficient. (From Summers 1966).

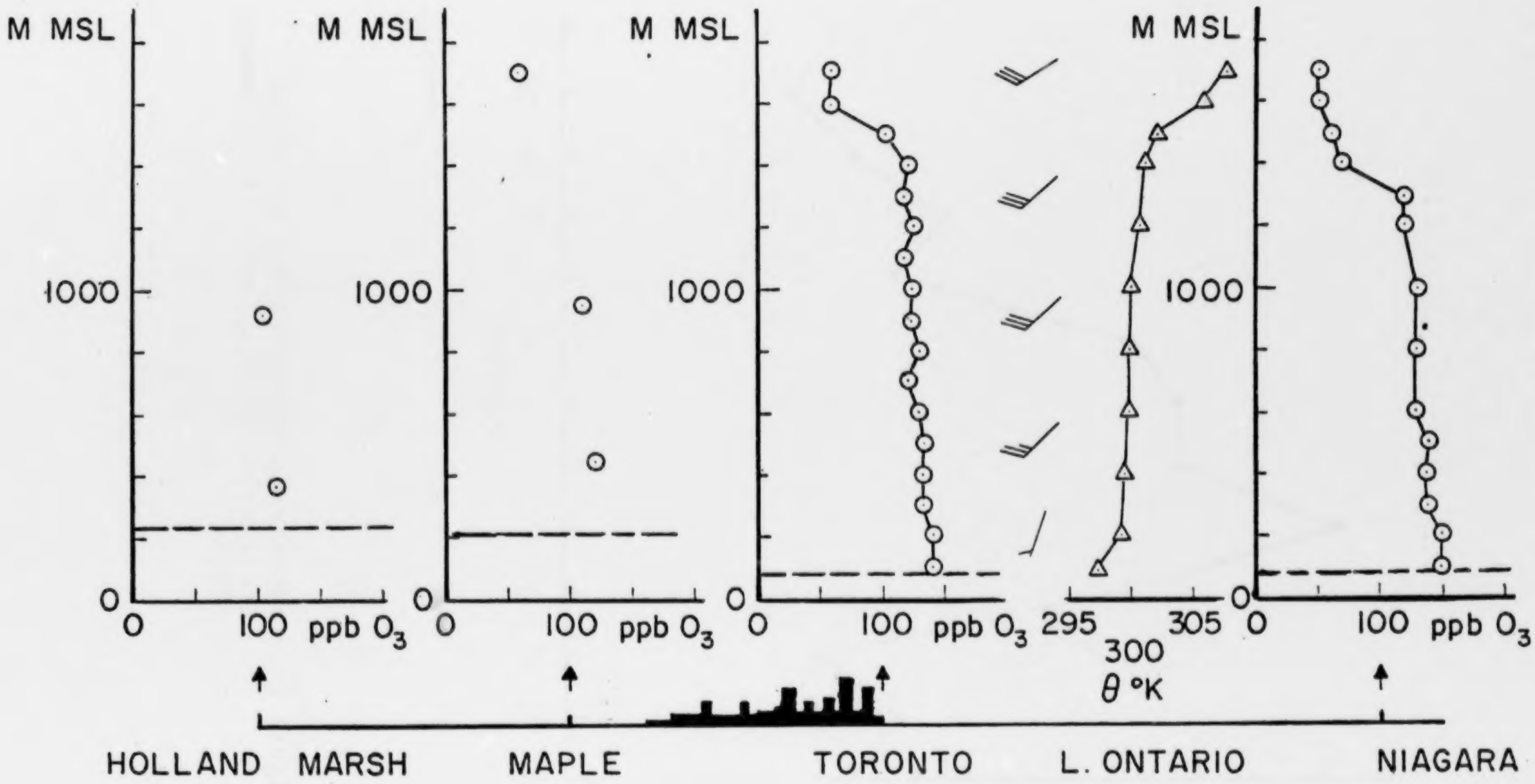

Figure 16 Ozone measurements on August 9, 14-16 EST (from Lusis et al. 1976).

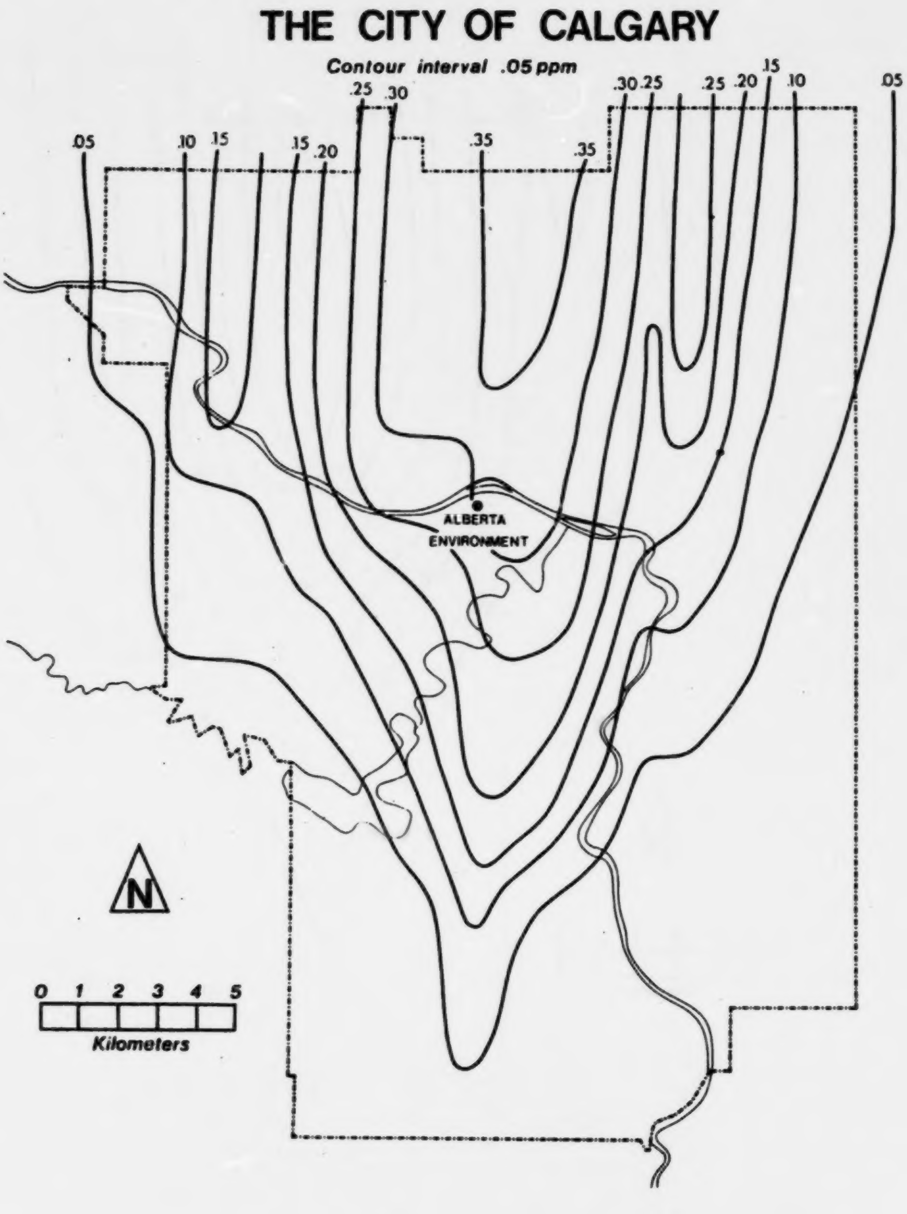
THE CITY OF CALGARY
Contour interval .05 ppm
.05
.10
.15
.15
.20
.25
.30
.35
.35
.30
.25
.25
.20
.15
.10
.05
ALBERTA ENVIRONMENT
N
0 1 2 3 4 5
Kilometers

Figure 17 Predicted values for the NO_x concentration (ppm) on a day with very stable air and an ambient temperature of 4°C. A south wind of 2 ms^{-1} and a traffic flow of 5 per cent were assumed in the calculations (from Western Research and Development Ltd. 1976).

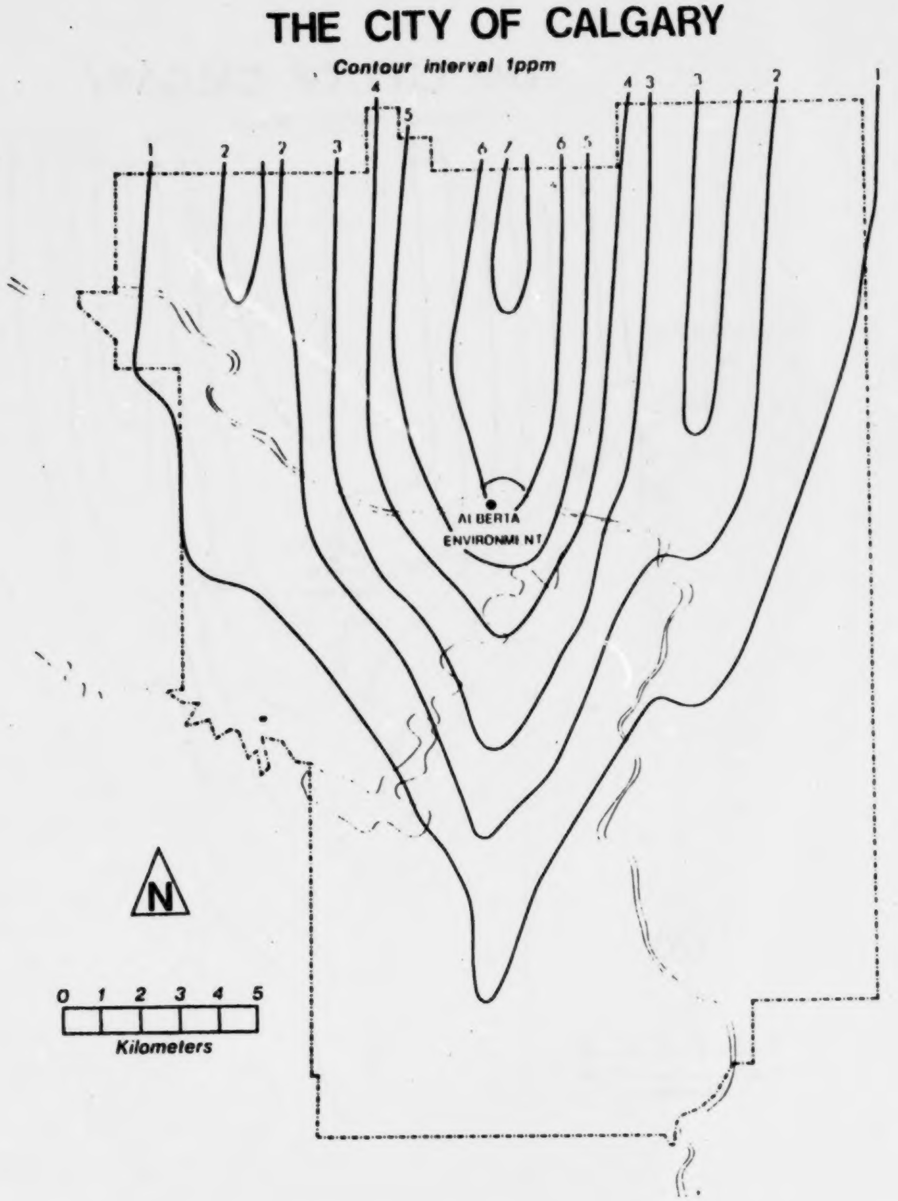
THE CITY OF CALGARY
Contour interval 1ppm
1
2
2
3
4
5
6
7
6
5
4
3
3
2
1
ALBERTA ENVIRONMENT
N
0 1 2 3 4 5
Kilometers

Figure 18 Predicted values for the CO concentration (ppm) on a day with very stable air and ambient temperature of 4°C. A south wind of 2 ms^{-1} and a traffic flow of 5 percent were assumed in the calculations. (From Western Research and Development Ltd. 1976).

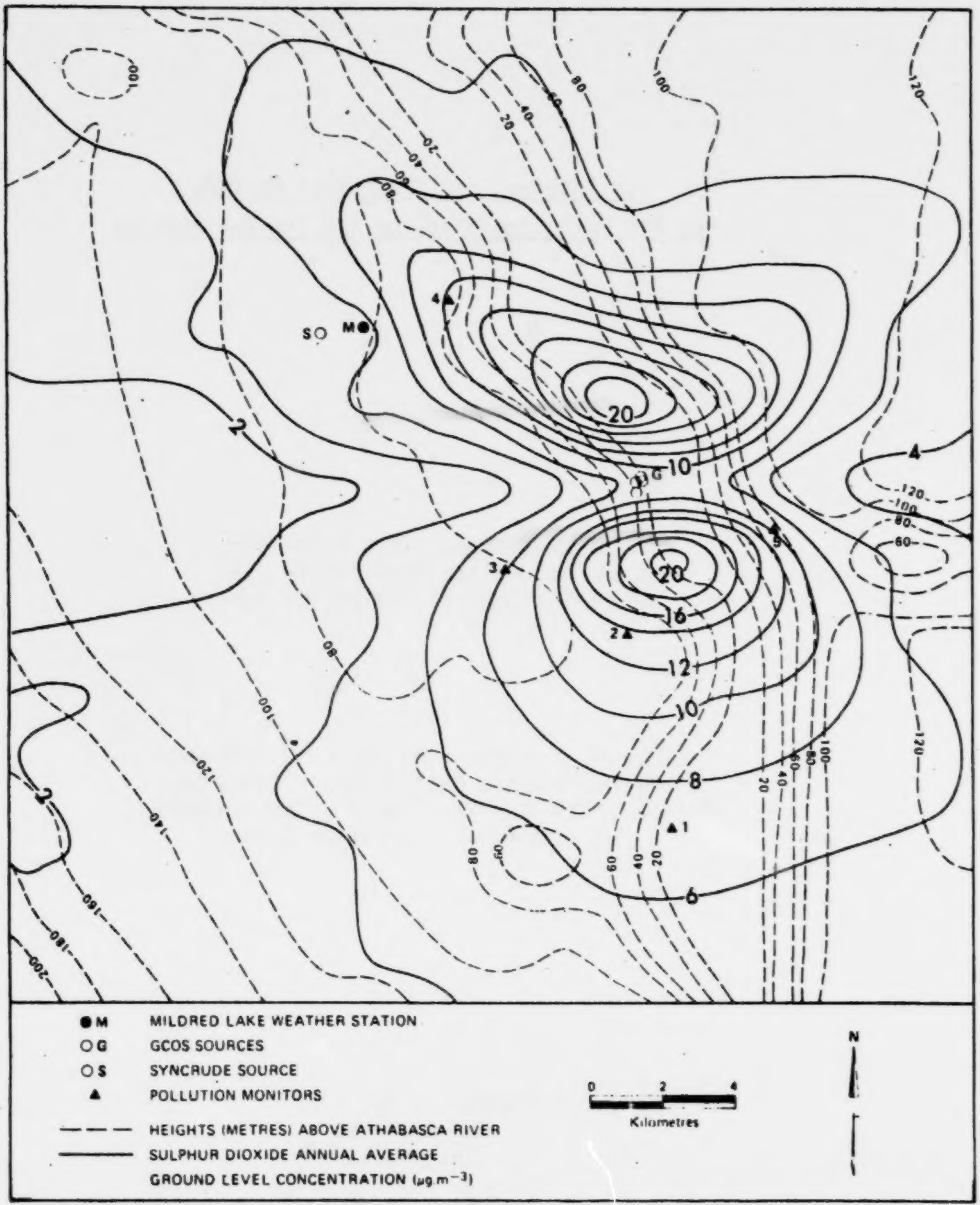
●M MILDRED LAKE WEATHER STATION
○G GCOS SOURCES
○S SYNCRUDE SOURCE
▲ POLLUTION MONITORS
HEIGHTS (METRES) ABOVE ATHABASCA RIVER
SULPHUR DIOXIDE ANNUAL AVERAGE GROUND LEVEL CONCENTRATION (µg.m⁻³)
0 2 4
Kilometres
N
S
M
G
1
2
3
4
5
20
20
16
12
10
10
8
6
4
2
2
20
40
60
80
100
120
140
160
180
200

Figure 19 Annual Averaged Sulphur Dioxide Concentrations at Ground Level: Four Sources, 20 Hour Half-Life (from Walmsley and Bagg 1977).

310

8th International Technical Meeting on Air Pollution Modeling and Its Application

The Development of A Guideline on Air Quality Modeling by the U.S. Environmental Protection Agency

by

Herschel H. Slater and Joseph A. Tikvart
Monitoring and Data Analysis Division
Office of Air Quality Planning and Standards
Environmental Protection Agency

September 20-23, 1977
Louvain-La-Neuve
Belgium

INTRODUCTION

The two general approaches followed in the United States "to protect and enhance the quality of the Nation's air resource" are the air quality standards and emission standards strategies (CAA, 1970). Each has its advantages. The emission standards strategy is simple to administer and easy to enforce. However, it may not be cost-effective. The same stringent controls may be required on a facility located in a remote area as in a congested area even though the facility is unlikely to threaten ambient air quality standards in the remote area.

The air quality standards strategy is the dominant strategy in United States air pollution law. It is more cost-effective than the emission standards approach, but it is less convenient to enforce and far from simple to administor (de Nevers, 1977). Emissions, meso-meteorology, measured air quality, and plausible control methods must be considered in a systematic way to determine what pollutants must be controlled, by whom, by what timing, by how much and by what methods in order to meet ambient air quality standards. A system or procedure which can relate all of these factors is called an air quality model. The infinite variety of climatological, meteorological and topographical circumstances, chemical reactions, source configurations and distributions challenges the ingenuity of atmospheric scientists to meet the need for general models. Since the Clean Air Act of 1970 became United States law, control officials and others have called for consistent, uniform, easily applied analytical procedures, or models, for relating emissions to air quality.

The Agency set out to respond to calls for it to specify acceptable models for developing the data required by environmental laws. The procedure used by The Netherlands in developing a general model for national use was studied with interest (TNO Comm., 1976). However, in the United States, the interests and concerns of those affected are extremely diverse. Great care was taken to provide an opportunity for the Nation's scientific community, its industrial associations, and public interest groups to become involved in the guideline development process.

A prominent judge, Chief Justice David L. Bazelon, U.S. Court of Appeals for the District of Columbia, who has ruled on several important environmental issues, stresses the importance of providing all parties an opportunity to participate. Addressing the Atomic Industrial Forum, he said that the courts are not the proper place

> ". . . To resolve the factual disputes or to make painful value choices" . . . regarding scientific or technical issues.

* * *

> ". . . What the courts and judges can do - and do well when conscious of their role and limitations - is scrutinize

> and monitor the decision-making process to make sure that it is thorough, complete, and rational: that all relevant information has been considered; and that insofar as possible, those who will be affected by a decision have had an opportunity to participate in it."

* * *

> "[Decision makers should openly disclose] where and why the experts disagree as well as where they concur, and where information is sketchy as well as complete. . . when the issues are controversial, any decision which is reached may be unsatisfactory to large portions of the community. But those who are dissatisfied with a particular decision will be more likely to acquiesce in it if they perceive that their views and interests were given a fair hearing."

* * *

EPA 's approach is consistent with the concepts expressed by Judge Bazelon.

PROCEDURE

As a first step toward developing a guidance document, a draft guideline on the use of air quality models was prepared. Secondly, a conference of specialists was immediately convened at Chicago in February 1977 to review the draft. The conferees, who were by training engineers, physical scientists and meteorologists, recognized the need for greater uniformity in the analytical procedures which should be followed in air quality management. Their prior experience included service with large corporations and as consultants to the entire spectrum of the Nation's industrial activity. Scientists from Canada and the United Kingdom brought experience and procedures followed in Europe and Canada. Those associated with the public sector were involved at the federal, State and local levels. Several were valued consultants to both the private and public sector as well as to public-interest and environmental associations. All were highly knowledgeable of the capabilities and limitations of air quality modeling. Their conference report constituted a critique of the draft guideline (Roberts, 1977).

As a third step, the guideline was rewritten to respond to the recommendations of the conferees.

The fourth step was to offer the revised draft guidance for public comment. Public participation meetings were held in five major cities: Atlanta, Chicago, Denver, San Francisco, and New York (EPA, 1977). EPA encouraged representatives of control agencies, industries, environmental groups, consultants and the scientific community to attend. Nearly 500 individuals participated. Comments were solicited, and a written transcript of the proceedings was made. Additional comments in writing were accepted for a few days after the conference.

The final step was to prepare the guideline in a form convenient for use by State agencies and the EPA's Regional Offices. Its value and the need for revision will be decided by time and experience.

ISSUES

The conference and public meetings showed widespread, but not unanimous, agreement that the Environmental Protection Agency should issue a guideline on air quality modeling. There was also a consensus that the Gaussian approach is the state-of-the-science technique for estimating the dispersion of the stable, or relatively non-reactive, pollutants such as suspended particulate matter, sulfur dioxide, and carbon monoxide.

However, there were many issues concerning a modeling guideline on which the participants could come to a general understanding, but not agreement, only after lengthy and intense discussions. The paramount issue concerned the degree of detail that the guidelines should use to prescribe procedures for analyzing air quality problems. Roberts (1977) summarized the problem, "The desirability of some guidance is generally recognized; the degree of specificity of that guidance is the issue."

There are two basic positions on this issue. The first contends that control agencies, industry and the public require a consistent, well-documented basis for determining the degree that a polluting source deteriorates air quality. Consistency in the procedures is deemed by some to be more important than the accuracy of the results. Therefore, an authoritative group should specify in detail the models to be used and how they should be applied for a great variety of source types and site characteristics. The specification should be sufficiently objective that technicians could perform the required calculations.

This position has the advantage of apparent fairness. All sources are subject to the same procedures. Trials, hearings and appeals to regulatory commissions are unnecessary. There are also disadvantages. There is little flexibility to address problems created by the diversity of plant configurations, meteorology and terrain that is encountered across the Nation. The specified models tend to acquire special legal status. They tend to be applied with little perception. The incentive for research to improve models is discouraged.

The opposing position is that the characteristics of the sources, topography and climatology are so diverse that each situation requires professional attention. Each situation needs case-by-case analysis. This position has the disadvantage of only limited uniformity of approach and analysis. Similar situations tend to be treated differently. Inevitably, delays in reaching agreements among contending parties aggravate the delays in issuing permits to construct new facilities or to modify existing ones. Assuming a degree of flexibility is allowed someone must decide whether the chosen analytical procedure fits the case. Eventually, the control agency involved must make the decision. Such a decision in turn may be challenged, creating further delays. An appropriate solution is early discussions and understandings among the principal parties as to the critical aspects of the problem, the data required and the most useful modeling methodologies.

Some uniformity is possible. Several models have been applied so often in similar situations that specifying their use arouses few objections. Examples are the Climatological Dispersion Model (Busse and Zimmerman, 1973) and the Briggs plume rise model (Briggs, 1969). The Netherlands has adopted a uniform approach. The documentation of their model very explicitly identifies the sources of meteorological data, the selection of dispersion coefficients and the characteristics of the sources and the source configurations to which the model applies (TNO Comm. 1976).

Most participants of the Chicago conference and the public meetings felt that the guideline should recommend the use of one model if there is no doubt as to its applicability. Adequate flexibility must be permitted to address those situations where the recommended model is inappropriate. In such circumstances, the guideline must permit, even encourage, the application of modified or new techniques. Nevertheless, the guideline must not be so general as to cause a proliferation of procedures, each a slight variation of the basic model.

The second issue concerns screening procedures. Most new and modified sources are relatively small. Many do not constitute serious threats to air quality standards. In such situations, it is not cost-effective to the source, the industry, the control agency or the governing body to require that a complex and sophisticated assessment procedure be undertaken. There was a concensus among those who reviewed the draft guideline that a preliminary, simple screening procedure, which requires only a hand calculator or small computer, should be inititally applied. The procedures should be conservative. "Worst case" emission and weather conditions should be assumed. If the results indicated that the impact would be less than an agreed upon fraction of the allowable concentration, then no further analysis would be required. If the results showed greater than the agreed concentration, more refined analyses would be undertaken.

A third issue deals with validation and performance standards for models. Many people involved in environmental matters have spent their professional careers concerned with producing materials with small tolerances and high reliability. They understandably call for high standards of performance and assurances of reliability from air quality models. It is logical to limit the models recommended in a guideline to those which have met predetermined standards of performance. Unfortunately, uniform validation procedures and standards of performance have not been developed and are not generally accepted by the scientific community. The conferences and meetings did provide the EPA a needed impetus to expand and intensify its research efforts in this area. Unfortunately, criteria for selecting, comparing and validating models will continue to require more subjectivity than is desirable.

A fourth issue involves the determination of representative meteorological data. There are two aspects to this matter. One aspect involves the period of record that is required to assess a source's impact on the air environment. Historically, one year of meteorological and emission data have been applied. This period has been used mostly for convenience and for economic reasons - to keep costs of data acquisition and computation within available funds. Unfortunately, there is no standard method of ascertaining whether the selected data is "typical." The problem is particularly perplexing when it is necessary to estimate the frequency of occurrence of concentrations of given magnitudes. For example, several U.S. air quality standards specify a concentration that may not be exceeded more than once per year (CFR 1975). The concensus was that five years of meteorological data were adequate to obtain a likely range of meteorological conditions. Some climatological studies have used data periods of similar length (Doty, et al, 1976).

However, a requirement of five years of data may create very substantial analysis costs. Further, more refined statistical procedures are likely to be more scientifically sound and less costly. An air quality model may be applied to a limited meteorological base. The results may be fitted to a suitable cumulative frequency distribution and extrapolated to concentrations that would be occur with lower frequency. The approach would be similar to the design of structures to withstand rarely occurring natural phenomena like floods, hurricanes, tornadoes, heavy snow falls and earthquakes. As yet, statistical procedures for estimating the occurrence of such events have not been generally accepted for application to air pollution matters.

Another aspect of the representative meteorological data issue concerns the determination of whether the data appropriately describes the dispersion and transport of the pollutants. Are the locations, exposures, types and number of sensors adequate to ascertain the character of the dispersion that is prevalent near the source? Does the sensing data provide information as to the frequency of adverse and beneficial circumstances? Assuming that the record is of sufficient length to apply statistical extrapolation techniques with a theoretically high degree of reliability, are the data still inherently flawed? The problem was recognized by the specialists and participants of the public meetings. However, objective methods for addressing this aspect of the representativeness of data issue were not forthcoming.

The fifth major issue is the frequency of guideline revision and how the revision should be conducted. A significant part of each meeting was spent discussing the need for improved methodologies. No models have been shown to simulate, in necessary detail, the plume characteristics and physical processes for many commonly experienced situations, such as plume interaction with elevated terrain, aerodynamic downwash, sea or lake breeze circulations, inversion-breakup fumigation, plume trapping and the influences of an elevated inversion and plume impacts beyond 50 - 100 kilometers. Other concerns centered on turbulence characterization methods and the applicability of familiar vertical dispersion rates to analyze sources having very tall stacks.

No consensus on these matters was reached. In fact, the proper forums to address such questions are meetings of scientific groups or the publications of scientific societies, not closed symposia or meetings of the public. The deficiencies in current modeling capability emphasize the need for periodic, if not continuous, review of the guideline, and for timely revisions as these and other uncertainties are resolved or clarified. Revisions should be frequent enough to initiate the use of improved procedures promptly. However, the revisions should not be made in such a manner that reanalysis of an pollution control plans or impact estimates would be required whenever a more refined technique is proposed or becomes available. A revised guideline at one or two year intervals is expected initially. Somewhat greater intervals will likely prevail after one or two revisions.

SUMMARY

This paper describes a procedure to develop a guideline which encourages more consistent use of air quality models. The process purposely involved as many interested parties as possible. All were encouraged to criticize in depth and to comment in detail. Highly qualified scientists and engineers formally reviewed initial drafts of the document. Following revisions were offered for comment to all interested parties.

The Gaussian model is considered the state-of-the-science for the relatively non-reactive pollutants. Uncertainties in many applications require that models often be used as screening procedures only. The guideline, as issued, cannot be specific for all applications, as there are many atypical situations. With experience, and with critical and periodic review, an acceptable level of specificity will become evident in the guideline.

ACKNOWLEDGEMENT

The specialists conference which reviewed and criticized early approaches to the guideline was organized and conducted by Argonne National Laboratories under EPA auspices. The deliberations and the final report of the conference were largely due to Dr. J. J. Roberts, Dr. D. M. Rote, Dr. A. E. Smith and Dr. K. L. Brubaker. J. L. Dicke, NOAA assignee to EPA, with the authors organized and lead the public participation meetings. The cooperation, innovations and recommendations of these associates are gratefully acknowledged.

REFERENCES

Bazelon, D. L., 1977: Speech before Atomic Industrial Forum, Jan. 27, 1977. Environmental Reporter, v. 7, No. 38, Bureau of National Affairs, Inc. Washington, D.C. 20037.

Busse, A. D. and J. R. Zimmerman, 1973: "User's Guide for the Climatological Dispersion Model", Publication No. EPA-RA-73-024, Environmental Protection Agency, Research Triangle Park, North Carolina 27711.

Code of Federal Regulations, Title 40, Part 50 (40 CFR 50) July, 1975, U.S.G.P.O., Washington, D.C. 20460.

de Nevers, N., 1977: "Air Pollution Control Philosophies," J. Air Pollution Control Assoc., v. 27, No. 3, pp. 197 - 205.

Doty, S. R., B. L. Wallace, and G. C. Holzworth, 1976: "A Climatological Analysis of Pasquill Stability Categories Based on "Star" Summaries." National Climatic Center, NOAA, Asheville, North Carolina 28802.

Environmental Protection Agency, 1977: Guideline on Air Quality Models: Meetings. Federal Register, volume 42, No. 76, P. 20492. Apr. 20, 1977.

Nieuwstadt, F.T.M., C. M. Verheul and J. Addicks, 1976: "The Validation of the Gaussian Dispersion Model for Long-term Average Ground Level Concentrations in the Rijnmond Region." NATO/CCMS Proceedings of the 7th International Technical Meeting on Air Pollution and Its Application NATO/CCMS. No. 51, 1976.

Roberts, J. J., Ed., 1977: "Report to the U.S. EPA of the Specialist's Conference on the EPA Modeling Guideline." Environmental Protection Agency, Research Triangle Park, North Carolina 27711.

"The Clean Air Act, 1970" 42 U.S.C. 1857 et seq, Washington, D.C. Sec. 101.

TNO Commission, 1976: Models for the Calculation of the Dispersion of Air Pollution (translation): Modellen voor de berenkening van de Verspreiding van Luchtveron treininging, Staatsuitgeverig/The Hague, Netherlands.

Rapporteur's Summary Report:

Prepared by: J. G. Kretzschmar

Papers covered by: Bahman / Kropp
Turner
Fanaki
Slater

Paper: Influence of meteorological data on the dispersion calculation Results, Dr. Bahman, TÜV L. Kropp

Questions:

J. G. Kretzschmar: Is it sound practice to compare statistics over many years with statistics for one year.

Answer: Licensing procedures must be based on 10 years observation. In many cases this information is not available. The paper points out that one has to be very careful with the results obtained on the basis of one year of meteorological data.

Fronza: Did you do any statistical tests to see how significant your results are.

Answer: Not yet.

Fischer: At what height above ground-level were the data obtained.

Answer: 20 m above ground-level (airport observation).

Paper: Experience with UNAMAP, D. B. Turner, EPA

Questions:

Fischer: What kind of models are PTMAX and PDIS.

Answer: GAUSSian with BRIGGS' plume rise formula.

Fischer: Is it possible to do emergency calculations.

Answer: Yes, in the conversational mode on obtains a fast answer.

Fischer: Which meteorological data are required to use UNAMAP.

Answer: Depends upon the specific model but primarily based on estimates of the hourly average wind direction, wind speed, stability class and mixing height.

Fischer: How do you obtain the mixing depth.

Answer: With radiosondes the maximum daily mixing depth is obtained for 60 stations in the U.S.

Fischer: Was there any validation of the models in UNAMAP.

Answer: Yes. Those validations are described in specific reports e.g. The users guide of CDM.

Padro: Do the models calculate daily averages.

Answer: The models calculate the maximum daily average occurring once a year.

Schneider: From your paper it looks like there are not too many users of UNAMAP in Europe. What is the price of the file.

Answer: As you know magnetic tapes are copied sometimes. The actual price is 219 U.S. dollar.

Paper: Air Pollution field studies in Canada.
F. H. Fanaki

Question:

Gillani: Could you comment on the $SO_2 \longrightarrow SO_4^{--}$ rate.

Answer: An average conversion rate of 1 % has been used but this rate varies of course with meteorological conditions such as rain, fog, ...

Paper: The Development of a Guideline on Air Quality Modeling by the U.S. Environmental Protection Agency, H. Slater, EPA.

Comments by Knox:

It must be pointed out that the U.S. Nuclear Regulatory Commission in its Regulatory Guide 1.111 accepts the following model types for nuclear impact studies

- variable trajectory models such as the particle-in-cell model and the plume element models
- constant mean wind direction models such as the GAUSSian straight-line trajectory model.

8th NATO/CCMS INTERNATIONAL TECHNICAL MEETING ON AIR POLLUTION MODELING

TOPIC 4

INFLUENCE AND CHOICE OF METEOROLOGICAL INPUTS

SIMULATION OF DAILY TEMPERATURES FOR ENVIRONMENTAL MODELLING

R.Cecchi,M.Marseguerra,S.Morelli,S.Pugnaghi and
R.Santangelo

Istituto di Fisica e Osservatorio Geofisico
Università di Modena,Italy

Work performed within the Program "Promozione della Qualità dell'Ambiente" of CNR,Italy

1. Introduction (why to simulate daily temperatures)

It is certainly important to have available input tapes of statistically equivalent meteorological data, in order to test the effects of the meteorological conditions in the environmental planning. With such input tapes it is not only possible to evaluate the average effect but also the uncertainty arising from the fluctuating nature of the data.

In particular simulated daily temperatures may result useful in problems connected with air pollution or saving of energy. For instance the energy consumption and the amount of pollutants due to the heating and the refrigeration of buildings strongly depends on air temperature and other meteorological quantities (e.g. wind;humidity,etc.). Fair estimations can be obtained by the knowledge of the diurnal variation of the temperature(1).Its pattern can be reasonably parametrized by the minimum,mean and the maximum temperature reached in each day. In conclusion the daily temperatures in both average and extreme conditions are important pieces of information for the estimation of a part of energy consumption and of air pollution.

Measurements of these temperatures over a long period of time (e.g. 50 years) are necessary in order to set up a statistical model of their behaviour. At the Geophysical Observatory in Modena,Italy a long record of such temperatures was available.This has allowed the construction of a stochastic model, whose general features should still hold in similar climatic regions. In section 2. we recall shortly the results which were obtained for the minimum,mean and maximum temperatures(2). However we have checked that the same statistical behaviour is followed also by the daily temperatures measured at fixed hours of each day.

In section 3. we present an autoregressive-moving average model (AR-MA), which has the same statistical properties of the model discussed in section 2.(3)(4). This AR-MA model allows a statistical prediction of the daily minimum, mean and maximum temperature, which could be very useful in the management of the environment(5). Moreover this model is particularly suited for the simulation of the temperatures.

Finally in section 4. we discuss how to use this model in other locations for which long records of meteorological data are not available.

2. Stochastic Behaviour of the Daily Minimum, Mean and Maximum Temperature (short summary of results already achieved)

Daily temperatures measured in the period 1892-1975 have been analyzed in order to obtain the stochastic behaviour. The temperature T(t) as a function of the sequential number t which orders the days, can be represented as a sum of a deterministic function D(t) and a stochastic function $\Delta T(t)$:

$$T(t) = D(t) + \Delta T(t)$$

The deterministic function results to be the sum of a constant and the first three harmonics having as a fundamental period one year :

$$D(t) = a_0 + a_1 \cdot \cos \frac{2\pi}{365}\left(t - t_1^{max}\right) + a_2 \cdot \cos \frac{2\pi}{365/2}\left(t - t_2^{max}\right) + a_3 \cdot \cos \frac{2\pi}{365/3}\left(t - t_3^{max}\right)$$

The 7 parameters: $a_0, a_1, a_2, a_3, t_1^{max}, t_2^{max}, t_3^{max}$ are fixed.

The stochastic function $\Delta T(t)$ fluctuates around zero and is fairly stationary. It has a gaussian distribution with standard deviation shown in Table I. It is perhaps worthwhile to remark that in this case the meaning of the standard deviation is not that of a standard error but of a standard fluctuation.

TABLE I

	maximum	mean	minimum
stand.dev.	3.19 °C	2.81 °C	2.81 °C

$\Delta T(t)$ is autocorrelated. Its autocovariance is fitted by the sum of two decreasing exponentials as a function of the time-lag Δt: $b_1 \cdot e^{-\lambda_1|\Delta t|} + b_2 \cdot e^{-\lambda_2|\Delta t|}$

up to values of 30 days.

In Table II the values of the amplitudes and the decay constants of the two exponentials are reported.

TABLE II

	maximum	mean	minimum
b_1	7.92 °C^2	6.81 °C^2	6.92 °C^2
λ_1	0.39 d^{-1}	0.27 d^{-1}	0.27 d^{-1}
b_2	2.21 °C^2	1.12 °C^2	0.90 °C^2
λ_2	0.05 d^{-1}	0.03 d^{-1}	0.02 d^{-1}

The second exponential however is rather small in amplitude and slow in the decay constant. Therefore for time-lags up to $\sim$7 days the process is approximately markovian since its autocovariance is mainly given by only one decreasing exponential.

3. Autoregressive-moving average model of daily temperatures (a model for simulation and forecasting)

It is known that a stationary markovian process is an autoregressive process of the first order AR(1)(3)(4). For the stochastic part of the temperatures, then :

$$\Delta T(t+1) = \phi \cdot \Delta T(t) + a(t+1)$$

ϕ is a constant,satisfying the condition $-1 < \phi < +1$ in order to have a stationary process. a(t) is a gaussian stochastic function with zero mean and standard deviation σ_a. Its autocovariance is typical of a white noise, i.e. $\sigma_a^2 \delta_{0,\Delta t}$.

The parameters of this AR(1) process are connected with the parameters of $\Delta T(t)$ (only one exponential !) :

$$\sigma_a^2 = b \cdot (1-\phi^2) \qquad , \qquad \phi = e^{-\lambda}$$

In Table III are presented the values of the parameters of the AR(1) model for the three temperatures considered. The first row of Table III contains the values already shown in Table I. The fourth row shows the standard deviation of the experimental values of a(t) as obtained from the recursive formula of AR(1).

TABLE III

	maximum	mean	minimum
$\sigma(\Delta T)$	3.193 °C	2.806 °C	2.805 °C
ϕ	0.676	0.761	0.766
σ_a	2.353 °C	1.827 °C	1.798 °C
σ_a^{exp}	2.249 °C	1.724 °C	1.830 °C
$\sigma_a^{exp}/\sigma(\Delta T)$	0.70	0.61	0.65

If the assumption of markovian behaviour for ΔT were correct,then the autocovariance of a(t) should vanish for $\Delta t > 0$ (white noise).In fig. 1 we show the autocovariance of a(t) only for the maximum daily temperature,

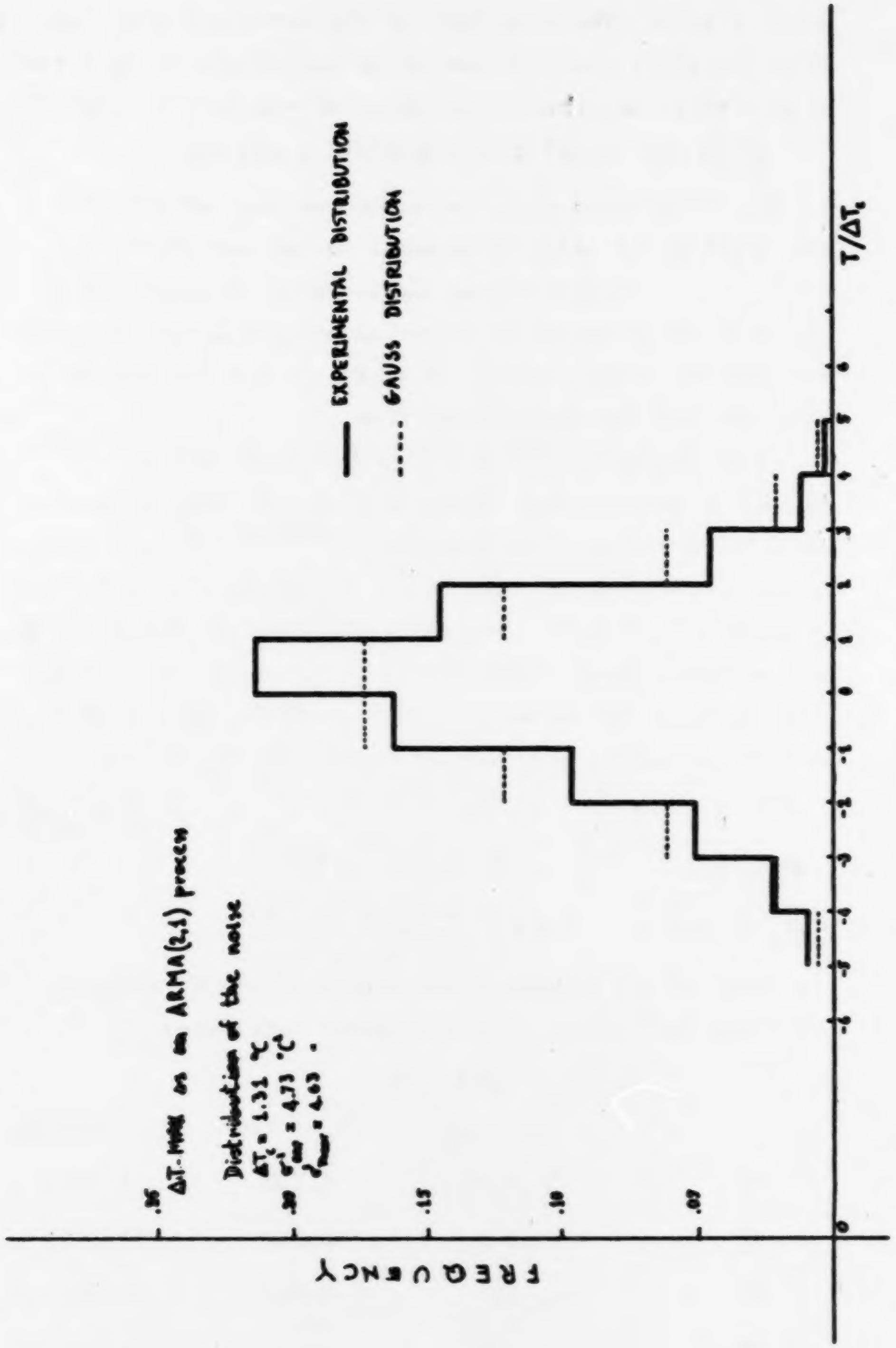

ΔT-MAX as an ARMA(2,1) process
Distribution of the noise
ΔT_c = 1.31 °C
σ²_exp = 4.73 °C²
σ_exp = 4.63 .
EXPERIMENTAL DISTRIBUTION
GAUSS DISTRIBUTION
FREQUENCY
T/ΔT_c
.25
.20
.15
.10
.05
0

Fig. 1

since the behaviour for the other two temperatures is quite similar. The long tail of the autocovariance implies that the AR(1) model is not quite satisfactory. We tried also with an autoregressive model of the second order AR(2):

$$\Delta T(t+2) = \phi_1 \cdot \Delta T(t+1) + \phi_2 \Delta T(t) + a(t+2)$$

In fig. 1 is shown also the autocovariance of a(t) for the AR(2) model. Also this model is not satisfactory.

A much better agreement is instead achieved with an autoregressive-moving average model of order two and one respectively: AR(2)-MA(1). For the stochastic part of the temperature then :

$$\Delta T(t+2) = \phi_1 \cdot \Delta T(t+1) + \phi_2 \cdot \Delta T(t) + \theta \cdot a(t+1) + a(t+2)$$

ϕ_1 and ϕ_2 are constant which must satisfy some inequalities which follow from stationarity$^{(3)(4)}$. θ is a constant satisfying: $-1 < \theta < +1$ for invertibility. a(t) is a gaussian stochastic process with standard deviation σ_a and autocovariance typical of a white noise.The connection between the parameters of this AR(2)-MA(1) model and the parameters of the autocovariance of ΔT is :

$$\phi_1 = e^{-\lambda_1} + e^{-\lambda_2} \quad , \quad \gamma_0 = b_1 + b_2 \quad ; \quad \sigma_a^2 = \frac{(1-\phi_2)\gamma_1 - \phi_1 \gamma_0}{\theta}$$

$$\phi_2 = - e^{-(\lambda_1 + \lambda_2)} \quad , \quad \gamma_1 = b_1 e^{-\lambda_1} + b_2 e^{-\lambda_2}$$

$$\theta = R + \sqrt{R^2 - 1} \qquad R = \frac{1}{2} \frac{(1 - \phi_2^2 + \phi_1^2)\gamma_0 - 2\phi_1 \gamma_1}{\theta \cdot \sigma_a^2}$$

In Table IV are reported the values of the parameters obtained for the three temperatures considered.

TABLE IV

	maximum	mean	minimum
ϕ_1	1.624	1.736	1.748
ϕ_2	-0.641	-0.742	-0.752
θ	-0.912	-0.958	-0.970
σ_a	2.152 °C	1.719 °C	1.711 °C
σ_a^{exp}	2.176 °C	1.626 °C	1.728 °C
$\sigma_a^{exp} / \sigma(\Delta T)$	0.68	0.58	0.61

In fig. 2,3,4 we show the autocovariance of a(t) for the daily maximum,mean and minimum temperature. The agreement with a white noise process is very good. In fig. 5,6,7 we show the distribution of a(t) for the three temperatures. For comparison a true gaussian distribution is also shown. The experimental standard deviation σ_a^{exp} is very close to the standard deviation computed with the formulas given above (see also Table IV).

4. Input tapes with simulated daily temperatures (some practical prescriptions for the construction of the tapes)

In locations where long records of daily minimum,mean and maximum temperatures are available,the long record itself can be used as input tape. However adding other simulated data the effects of meteorological conditions in the environmental planning could be better estimated. Instead the need of simulation strongly arises in locations where long records are not available. By several splittings of our data we have checked that daily temperatures measured over 10 years are a reasonable minimum in order to obtain stable parameters for the model discussed in sections 2. and 3.

The simulated temperatures are given by the sum of the deterministic part and the stochastic part. This last term is built with the recursive formula of AR(2)-MA(1) model. The values of a(t) are chosen randomly in a gaussian distribution of standard deviation σ_a. The first two values of $\Delta T(t)$ are put equal to zero or chosen randomly in a gaussian distribution of standard deviation $\sigma(\Delta T)$ (see Table I). Usually we started from t = -20 in order to wash out the effects of the arbitrary and uncorrelated choice of the first two $\Delta T(t)$.

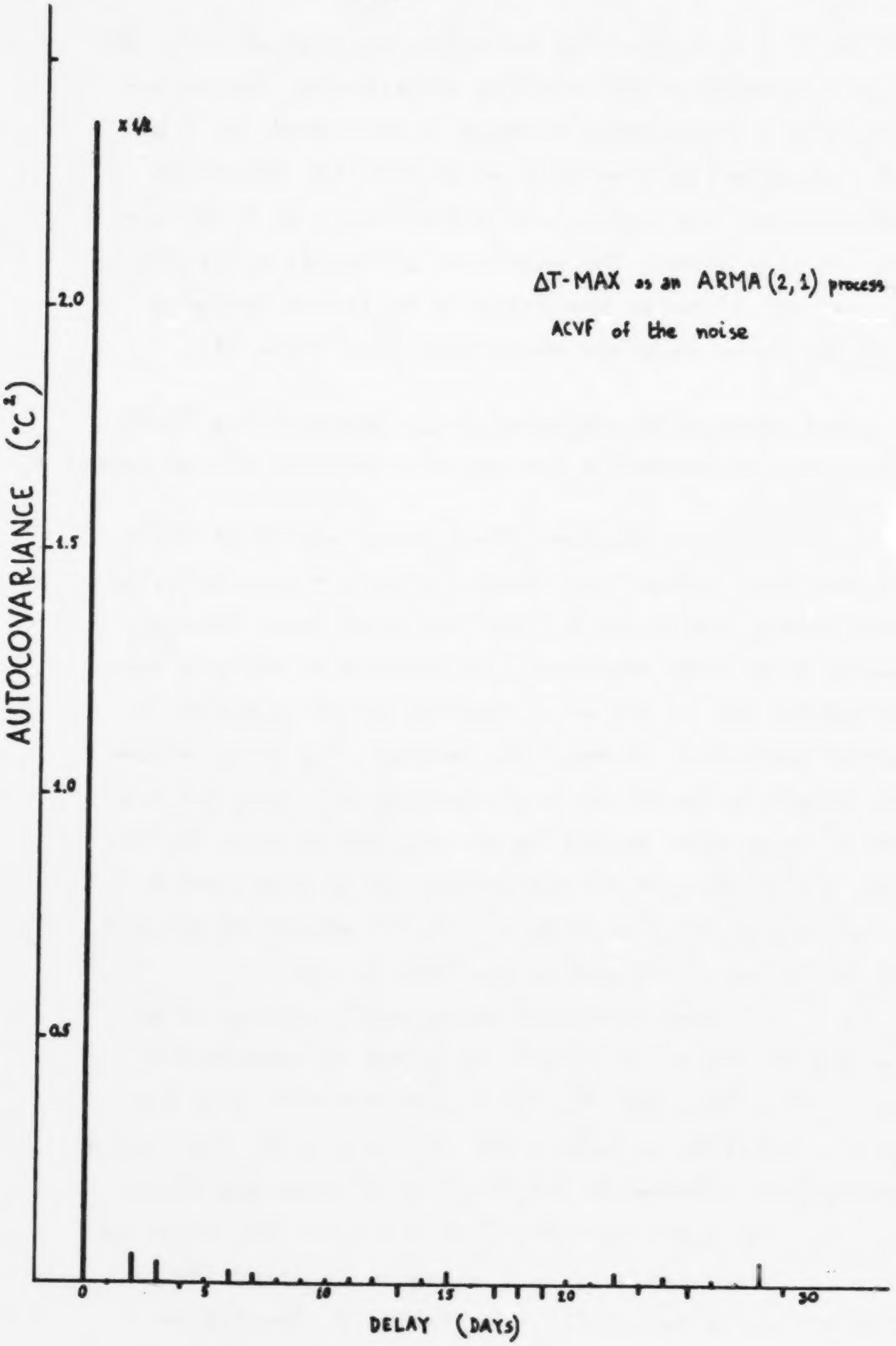
x 1/2
ΔT-MAX as an ARMA (2,1) process
ACVF of the noise
AUTOCOVARIANCE (°C²)
2.0
1.5
1.0
0.5
0
5
10
15
20
30
DELAY (DAYS)

Fig. 2

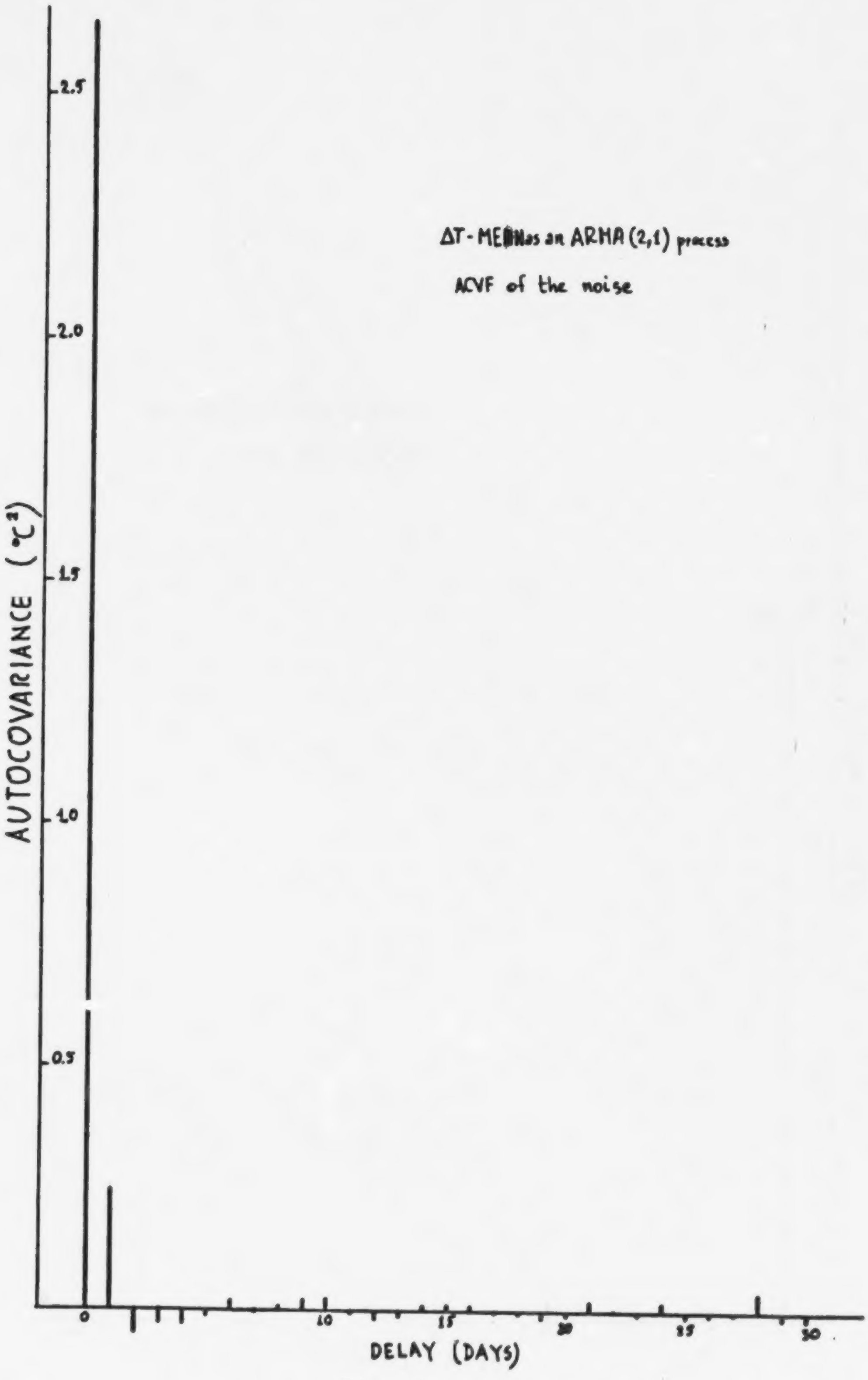
ΔT-ME[illegible]as an ARMA (2,1) process
ACVF of the noise
AUTOCOVARIANCE (°C²)
2.5
2.0
1.5
1.0
0.5
0
10
15
20
25
30
DELAY (DAYS)

Fig. 3

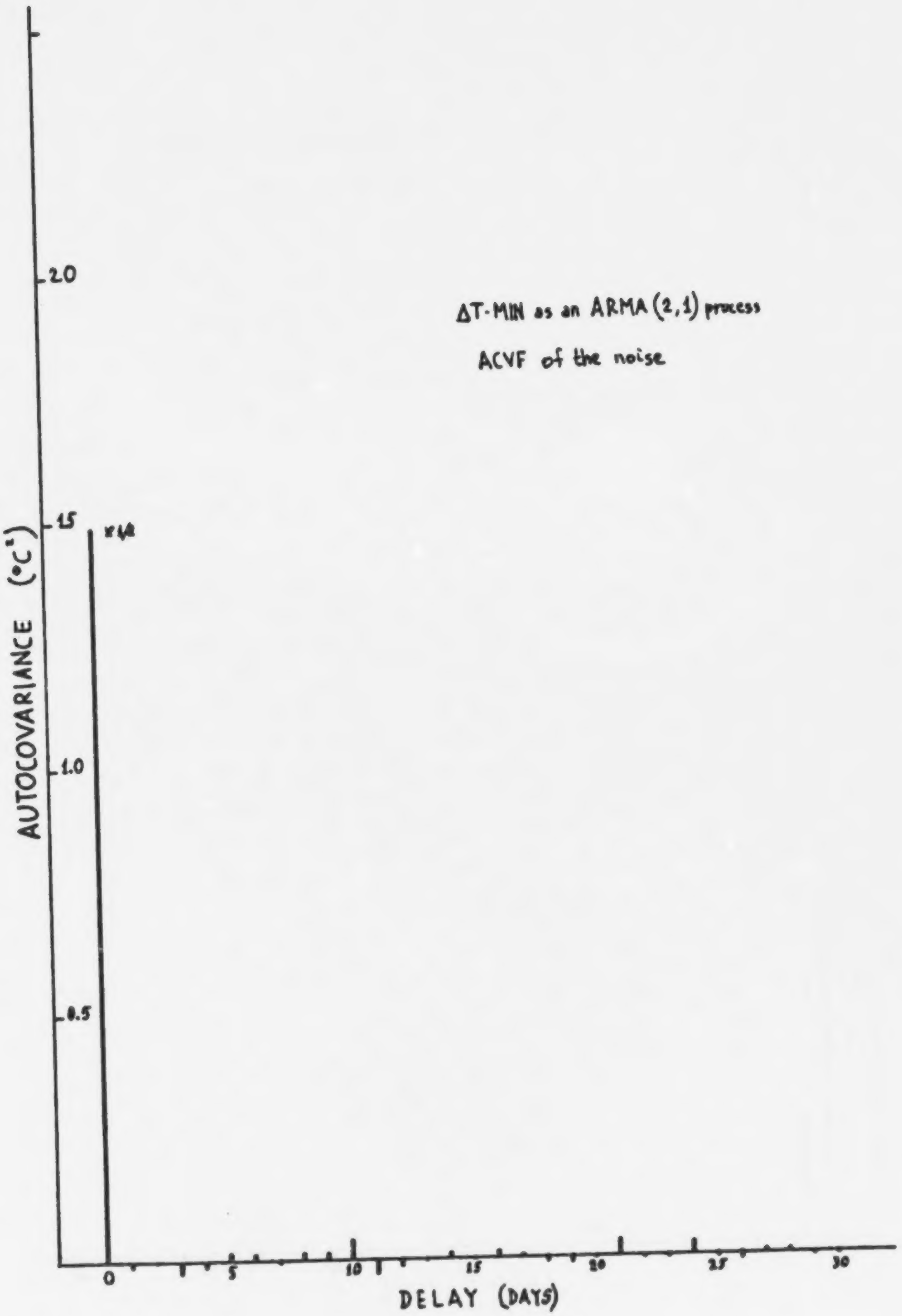
ΔT-MIN as an ARMA (2,1) process
ACVF of the noise
AUTOCOVARIANCE (°C²)
2.0
1.5
1.0
0.5
x 1/2
0
5
10
15
20
25
30
DELAY (DAYS)

Fig. 4

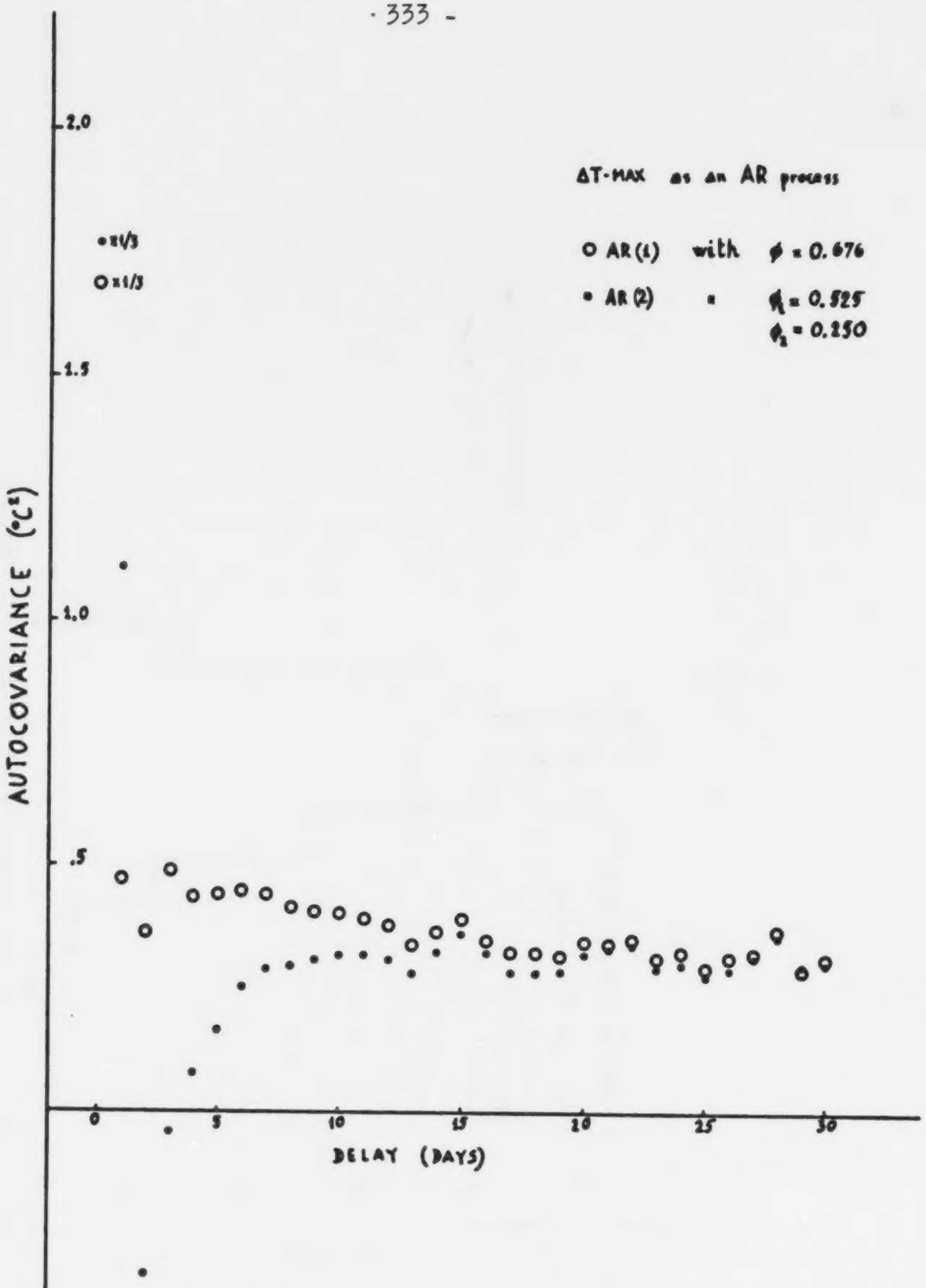
ΔT-MAX as an AR process
○ AR(1) with φ = 0.676
● AR(2) " φ₁ = 0.525
φ₂ = 0.250
● x1/3
○ x1/3
AUTOCOVARIANCE (°C²)
2.0
1.5
1.0
.5
0
5
10
15
20
25
30
DELAY (DAYS)

Fig. 5

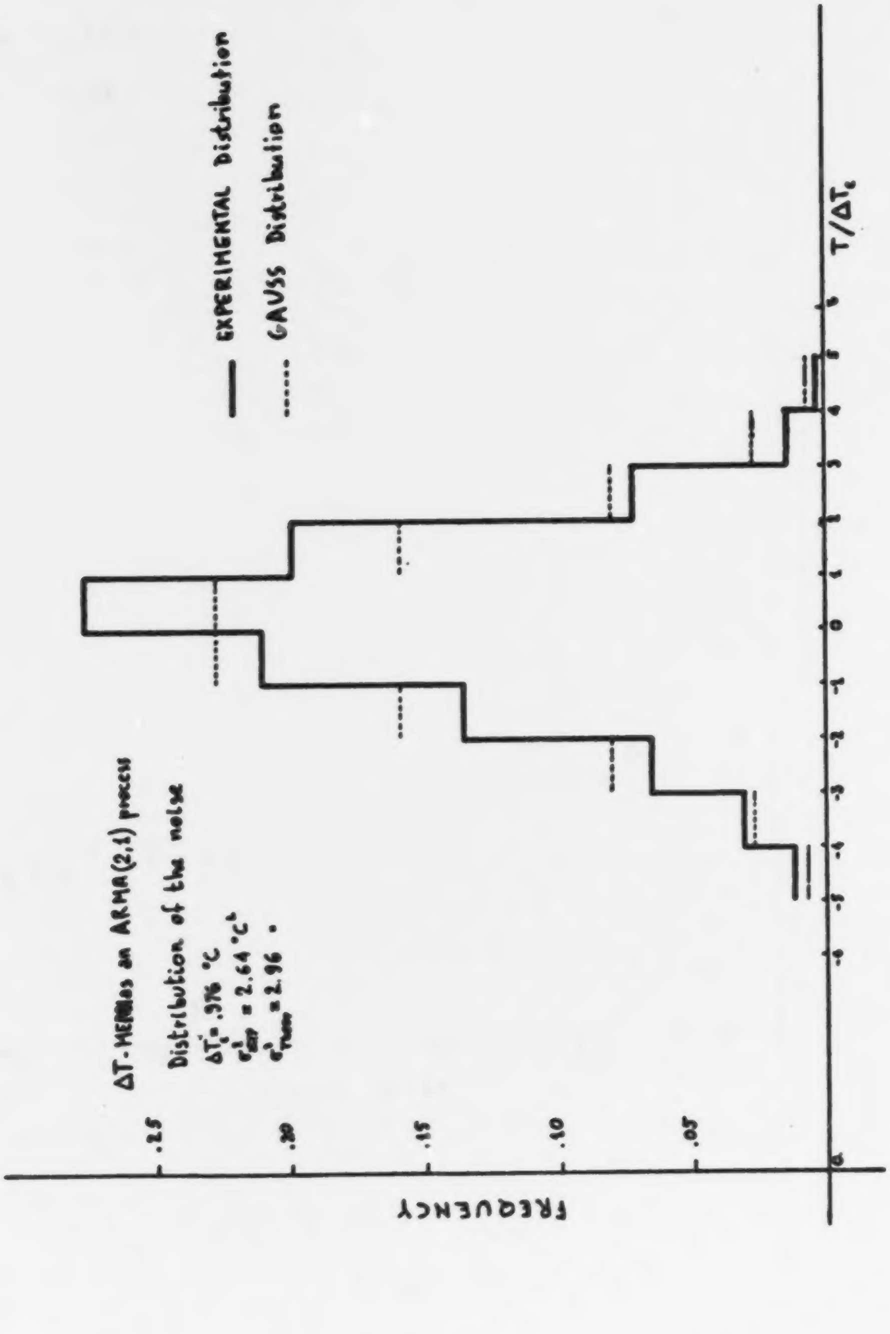
ΔT-HERMES an ARMA(2,1) process
Distribution of the noise
$\Delta T_c = .976\ ^\circ C$
$\sigma^2_{exp} = 2.64\ ^\circ C^2$
$\sigma^2_{theor} = 2.96$ "
EXPERIMENTAL Distribution
GAUSS Distribution
FREQUENCY
T/ΔT$_c$
.25
.20
.15
.10
.05
0
-6
-5
-4
-3
-2
-1
0
1
2
3
4
5
6

Fig. 6

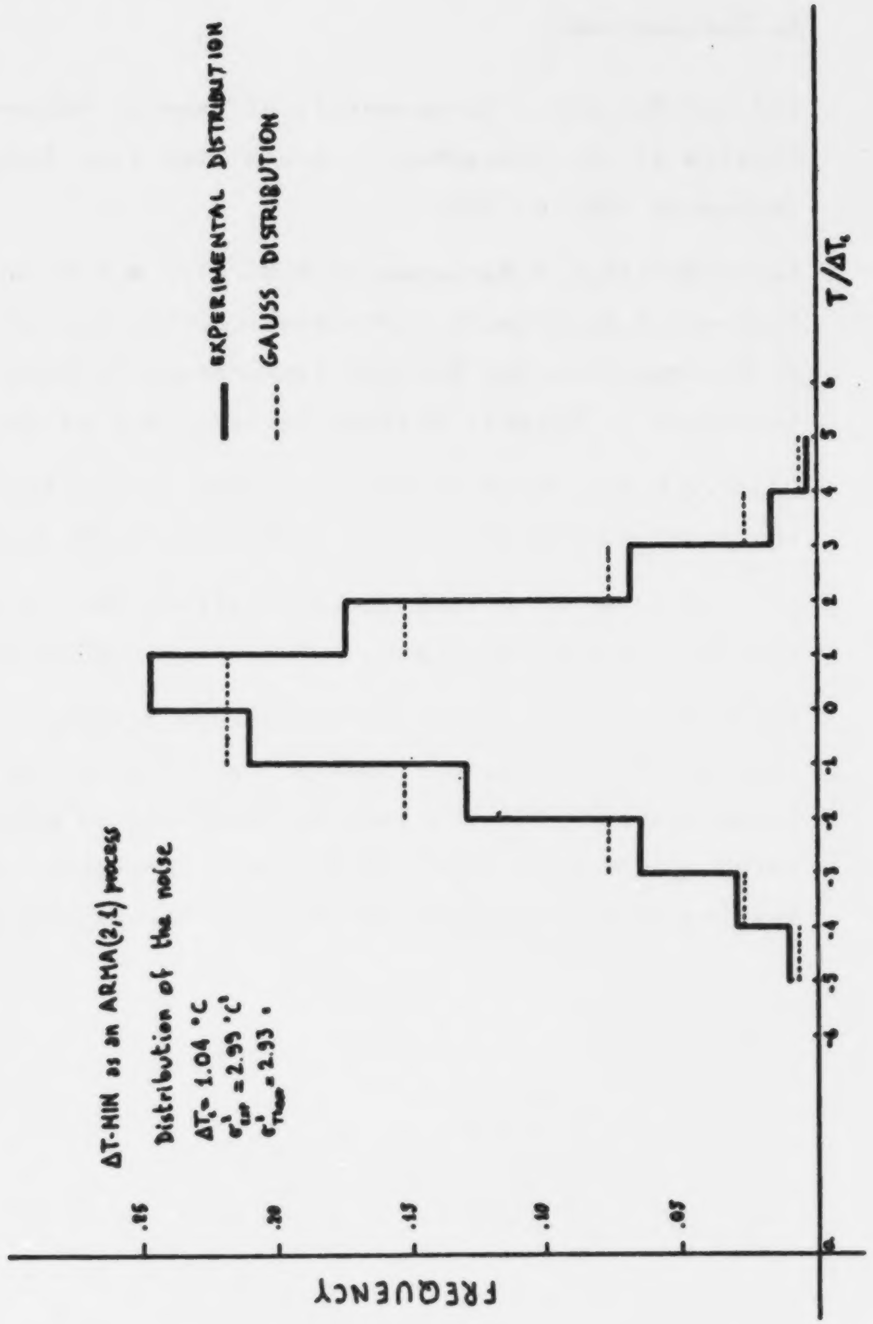
ΔT-MIN as an ARMA(2,1) process
Distribution of the noise
$\Delta T_c = 1.04$ °C
$\sigma^2_{exp} = 2.99$ °C²
$\sigma^2_{Theo} = 2.93$ "
EXPERIMENTAL DISTRIBUTION
GAUSS DISTRIBUTION
FREQUENCY
.25
.20
.15
.10
.05
0
-6
-5
-4
-3
-2
-1
0
1
2
3
4
5
6
$T/\Delta T_c$

Fig. 7

5. Bibliography

(1) L.T.Matveev - Fundamentals of General Meteorology: Physics of the Atmosphere - translated from Russian, Jerusalem 1967 p. 205.

(2) G.Aprilesi,M.Marseguerra,S.Morelli,M.R.Rivasi,G.Saltini and R.Santangelo - Stochastic Behaviour of the Daily Minimum,Mean and Maximum Temperature in Modena,Italy-to appear in Monthly Weather Review,issue of November 1977.

(3) G.E.P.Box and G.M.Jenkins - Time Series Analysis (Forecasting and Control) - Holden Day 1976, p.53-80.

(4) O.D.Anderson - Time Series Analysis and Forecasting (The Box-Jenkins Approach) - Butterworth 1976,p.15-53.

(5) L.Balestri,R.Cecchi,M.Marseguerra,S.Morelli,M.R.Rivasi and R.Santangelo - Statistical Forecasting of Daily Temperatures - EOS Transactions,American Geophysical Union vol 58,No 9 Sept. 1977 p. 907 (presented at the Meeting of the European Geophysical Society,Munich 1977).

8th International Technical Meeting
on Air Pollution Modeling and its Application

The dispersion
# of pollutants over a water surface

F.T.M. Nieuwstadt
Royal Netherlands Meteorological Institute

September 20-23, 1977
Louvain-La-Neuve
Belgium

1. Introduction

There is a growing demand for estimates of dispersion of pollutants over a water surface.

In the Netherlands the feasibility is studied of an artificial island in the North Sea. On this island industries will be installed, which will emit a considerable amount of pollutants. An important part in the development of this project will be the assessment of the pollutant concentrations due to these emissions, both on the island and in the coastal regions in the neighbourhood.

As an increasing number of ships will transport dangerous loads, e.g. liquefied natural gas, the consequences of a spill, e.g. whether danger for explosions exists, should be estimated. For this purpose it is necessary that the dispersion over a water surface should be understood.

Recently several ships have been built that incinerate toxic chemical wastes at sea. The effluents of these ships contain a large amount of toxic compounds, primarily hydrochloric acid. Dispersion calculations of the emissions are necessary in order to estimate the deposition of these substances on the sea surface and to estimate the concentration level in nearby coastal regions.

In the USA the problem of diffusion over a water surface has atracted attention because of proposals to install nuclear power plants on floating platforms on offshore locations along the Atlantic Coast (Raynor et al., 1975).

Dispersal of pollutants in the atmospheric boundary layer is caused by turbulent motions of the air. An increasing turbulence intensity results in increasing dispersion. As turbulence is a property of the airflow, its qualitative description will be the same over land as over water, except in the neighbourhood of the surface where the surface characteristics are important. This means that many results of research of turbulence over a land surface can be applied to turbulence over water after they have been rescaled with parameters that are representative of the situation over a water surface.

Turbulence in the atmospheric boundary layer is determined by buoyancy forces and shear forces.

The effect of buoyancy forces is determined by the stability. In unstable conditions turbulence is generated by buoyancy forces. This results in a high turbulence intensity, so that dispersion is good. In stable conditions turbulence is suppressed by buoyancy forces, so that dispersion is poor.

Turbulence by shear forces occurs when a gradient in the mean wind velocity is present, e.g. in the neighbourhood of a fixed surface. In this case the surface roughness is an important parameter. Increasing surface roughness results in increasing turbulence intensity, and therefore in better dispersion.

Because turbulence over a water and over a land surface is qualitatively the same, dispersion estimates that are based on experimental results over land may be transformed to be representative for dispersion over water. However, this hypothesis must be tested with experimental data on the dispersion over a water surface. These experimental data are very scarce,which is a major obstacle in the development of dispersion estimates over a water surface.

A review of the few experimental results that are available has been given by Portelli (1977). The extensive experiments on diffusion over a water surface performed by the Brookhaven National Laboratory (Raynor et al., 1975) deserve to be mentioned separately. They find that over a water surface dispersion is generally less than over a land surface. In a later paper by the same group (Raynor et al., 1977) additional results were published together with the results of dispersion experiments from a small island.

2. Stability of the atmosphere over a water surface

In the atmospheric boundary layer the stability can be described by the well-known Obukhov length (Businger, 1973). Over a land surface this parameter is defined as

$$L = -\frac{u_*^3 \, \overline{T}}{kg \, \overline{wT}} \qquad (2.1)$$

where u_* is the friction velocity, $\overline{T}$ the average boundary layer **temperature**, $\overline{wT}$ the heat flux, g the acceleration of gravity and k the von Karman constant. A negative value of L indicates an unstable situation, a positive value a stable situation. For neutral conditions L becomes infinite.

A typical daily cycle of the stability over a land surface under sunny conditions is shown in figure 1. In this figure are shown the insolation G in J/cm^2, the temperature at 2 m T_2 and the inverse of the Obukhov length L^{-1} as measured on August 4, 1975 at the meteorological tower in Cabauw, in the Netherlands. For a full description of this tower and its instrumentation one is referred to Van Ulden et al. (1976). The Obukhov length was determined from the wind speed and temperature profiles as described by Nieuwstadt (1977).

After sunrise, when the insolation is sufficiently strong, the surface starts to warm up. This results in a positive heat flux, which then causes the air above the surface to warm up as shown by the behaviour of T_2. The resulting unstable situation is therefore driven by the insolation. Before sunset, when the insolation has become sufficiently small, the surface will start to cool due to radiative losses. The heat flux becomes negative and the air temperature T_2 will gradually decrease. The situation is then stable.

The value of L can be evaluated directly, provided the turbulent fluxes of heat and momentum are known, However, this is seldom the case. Therefore, in diffusion estimates the stability is characterized by stability categories, which are based on routinely measured meteorological parameters. The definition of the stability classes is based on the daily cycle of stability over a land surface as discussed above. The most widely used system of stability classes was developed by Pasquill (1961). The main parameters in this scheme are the wind speed together with the insolation during the day-time and with the cloud cover during the night-time.

Over a water surface the stability can also be characterized by the Obukhov length. However, in this case the influence of humidity on the stability should be included (Busch, 1973). The definition of L then becomes

$$L = - \frac{u_*^3 \overline{T}}{kg(\overline{wT} + 0.61 \, \overline{T} \, \overline{wq})} \qquad (2.2)$$

where $\overline{wq}$ is the humidity flux. The term $0.61 \, \overline{T} \, \overline{wq}$ is often of the same order of magnitude as the term $\overline{wT}$, so that the influence of humidity on stability cannot be neglected. Also the term $\overline{wq}$ is mostly positive (evaporation), so that the sign of the stability condition is determined by the magnitude and direction of the heat flux.

A daily cycle of the stability over a water surface is shown in figure 2. In this figure are shown the air temperature T, the water temperature T_w and the inverse of the Obukhov length L^{-1} as measured on August 4, 1975 at the light-vessel Noordhinder, which is situated in the southern part of the North Sea, about 40 km off the coast of the Netherlands. As the day that was considered was cloudless over the Netherlands and the North Sea, it is assumed that the global radiation G, as measured at Cabauw (figure 1) is also representative for the insolation at the light-vessel. The Obukhov length can be calculated from the temperature and the humidity differences between the air and the sea surface, as will be discussed below.

It follows that the insolation during the day-time and the radiation during the night-time only slightly affect the difference between the air and water temperature. Therefore, the same stability (in this case a stable condition) persists during the whole day. A transition from stable to unstable conditions, as found over a land surface, is not present.

The small daily cycle in the air temperature, which seems to be present in figure 2, also follows from figure 3, where is shown the average diurnal variation of the air and water temperature for each month as measured at the light-vessel Noordhinder (Verploegh, 1959). The cycle in the air temperature is caused by absorption of short wave radiation by the humid air over the water surface during the day-time, which explains the dependence of the amplitude of this cycle on the time of year, and by radiation losses during the night-time (Roll, 1965; Kraus, 1972). The amplitude of the cycle in the water temperature is much smaller, due to the large heat capacity of water. The amplitude of the air-water temperature difference is shown in figure 3 to be 2-3° C in the summer months, in contrast with the values of about 0.5° C mentioned by Roll (1965) and Kraus (1972). This overestimate is probably caused by an error in the air temperature measurement at the light-vessel.

From this daily cycle of the air-water temperature difference may be concluded that conditions over a sea surface are more stable during day-time than during night-time, which is quite opposite to the cycle of stability over a land surface.

The annual cycle of the daily average air and water temperature is shown in figure 4. These climatic data were also obtained at the light-vessel Noordhinder (Verploegh, 1959).

Roughly, two periods can be distinguished. During fall and early winter the sea water is warm with respect to the air, which results in an unstable situation. During spring and early summer the situation can be characterized as stable, because the water temperature is lower than the air temperature.

This stable condition generally does not occur over the open ocean (Roll, 1965). Therefore, it must be assumed that over the North Sea these conditions are caused by coastal effects.

To estimate the stability over a water surface direct measurements of L are hardly ever available. It also will be clear that the stability class definitions based on the daily cycle of stability over a land surface cannot be applied to the situation over a water surface.

However, the stability over a water surface can be estimated from routinely measured meteorological parameters. These data generally include wind speed u, temperature T, humidity q, which are all measured at a certain height z, and the water temperature T_w. The L can be evaluated from these data by substituting the following relations into (2.1)

$$\begin{aligned} u_*^2 &= C_D\,(u-u_s)^2 \\ \overline{wT} &= C_H\,(u-u_s)\,(T-T_w) \\ \overline{wq} &= C_q\,(u-u_s)\,(q-q_w) \end{aligned} \tag{2.3}$$

where u_s is the velocity of the sea surface, which here is taken as 3-5 % of the wind velocity (Deardorff, 1968). The specific humidity q_w close to the water surface is taken as the saturation value at the temperature T_w. The influence on q_w by for instance salinity or the pollution of the water surface is neglected.

The coefficients C_D, C_H and C_E are the transfer coefficients for momentum, heat and humidity respectively. Theoretically, these transfer coefficients depend on the measuring height z, the roughness of the water surface z_o and also on the stability L (Hicks, 1975).

Several experimental results indicate that the transfer coefficients are only weakly dependent on stability (SethuRaman et al.; 1975; Emmanuel, 1975). With respect to the dependence of the transfer coefficients on the surface roughness several proposals have been made (SethuRaman, 1975; Smith et al., 1975; Kitaygorodskiy et al., 1973). However, considering the scatter in the values obtained for the transfer coefficients, we propose here to use a constant transfer coefficient for routine estimates of the stability over a water surface.

In a review of a large number of experimental results Pond et al. (1974) suggest for the transfer coefficients at a height of 10 m in moderately unstable conditions, which are generally present over open sea

$$C_D = C_H = C_q = 1.5\ 10^{-3} \qquad (2.4)$$

3. Roughness of a water surface

The roughness of a water surface is determined by the wind-driven waves on the surface (Kitaygorodskiy, 1973). By simple dimensional arguments Charnock (1955) has proposed the following relation for the roughness length z_o

$$z_o = a\, u_*^2/g \qquad (3.1)$$

Many values for the constant a have been proposed: 0.012 (Charnock, 1958), 0.014 (Smith and Banke, 1975), 0.035 (Kitaygorodskiy, 1970); SethuRaman and Raynor (1975) propose a range of 0.012 - 0.072 for a, depending on the state of roughness of the water surface.

A characteristic value for the roughness of a water surface can be estimated to be $z_o \cong 10^{-3}$ m. This value is much smaller than the characteristic roughness values of a land surface, which ranges between 10^{-2}- 1 m. In the introduction the effect of the surface roughness on the turbulence intensity has been discussed. Therefore it may be concluded that in comparable stability conditions the dispersion over a water surface will be considerably smaller than the dispersion over a land surface.

As an extension of (3.1) z_o should also depend on wave parameters. Hsu (1974) and Kitaygorodskiy (1973) propose z_o to be dependent on u_*, wave height and phase velocity of the waves.

Because of the fact that wave parameters are usually not available, it is proposed to use (3.1) to obtain the roughness of a water surface.

4. Dispersion over a water surface

a. Vertical dispersion

In routine dispersion calculations over a land surface the Gaussian plume model is widely used (e.g. Pasquill, 1974). The diffusion of a plume in this model is described by dispersion coefficients, which are categorized according to stability classes.

As has been discussed in section 2, the stability classes used over a land surface cannot be directly applied to the situation over a water surface. An equivalent stability class, however, can be obtained by relating the Obukhov length, which can be estimated over water, to a stability class. This method was also suggested by Gifford (1976).

However, no unique relation exists between the stability classes and the Obukhov length, so that one value of L may occur in several stability classes (Smith, 1973). Nevertheless, several relationsships were proposed, e.g. by Pasquill and Smith (1970), as shown in the table below.

Table I. Relation between Pasquill classes and Obukhov length L for a roughness length z_o = 1 cm.

Stability class	L in m
A	- 2 to - 3
B	- 4 to - 5
C	-12 to -15
D	∞
E	35 to 75
F	8 to 35

From experimental results Golder (1972) gives a relation as shown in figure 5.

The dispersion coefficient related to the equivalent stability class can then be applied over a water surface, after it has been corrected for the reduced roughness of the water surface. Based on a graph given by Pasquill (1974) the following correction factor is proposed

$$\sigma_z(z_{o_1}) / \sigma_z(z_{o_2}) = (z_{o_1}/z_{o_2})^{0.53\, x^{-0.22}} \qquad (4.1)$$

where x is the distance from the source in m.

By this method a rough estimate can be obtained of the vertical dispersion over a water surface. This approach can be applied in climatological dispersion models by which long-term average concentrations can be computed (e.g. Nieuwstadt et al., 1976).

Several alternative estimates of the vertical dispersion coefficient based on the standard deviation of the horizontal wind direction fluctuations are discussed by Hosker (1974). He also makes a comparison with experimental results. However, his results are rather inconclusive, due to the fact that the standard deviation of the horizontal wind direction fluctuations is not representative of the vertical wind direction fluctuations which determine the vertical dispersion.

Raynor (1975) compares his experimental results for σ_z with an expression based on the well-known diffusion theory of Taylor (1921). Although he claims to find good agreement, the theory of Taylor should not be applied to this case, because the basic assumption of homogeneity is not satisfied.

Because the stability over a water surface can be described by an Obukhov-length, an estimate of the vertical diffusion related directly to this length is preferable. For a stationary and continuous source at ground level such an estimate can be found from a solution of the diffusion equation, which reads (Pasquill, 1974)

$$u(z;u_*,z_o,L)\,\frac{\partial \chi}{\partial x} = \frac{\partial}{\partial z}\left(K_z\,(z;u_*,L)\,\frac{\partial \chi}{\partial z}\right), \qquad (4.2)$$

where χ is the concentration, u(z) the wind velocity profile and K_z the mass diffusivity coefficient.

In the atmospheric surface layer the u(z) and $K_z(z)$ can be expressed in similarity forms depending only on the parameters u_*, z_o and L (Businger, 1973). After substitution of these expressions in (4.2) estimates of the vertical diffusion can be found, which also depend only on the parameters u_*, z_o and L (Nieuwstadt and Van Ulden, 1977; Van Ulden, 1977).

For the concentration at ground level, χ_o, for instance the following similarity form can be found (Van Ulden, 1977)

$$\frac{\chi_o u_* z_o}{Q} = F\,(x/z_o,\ z_o/L)\ , \qquad (4,3)$$

where Q [g/sm] is the source strength. This function is plotted in figure 6. From this figure follows that in neutral conditions a reduction of the roughness length with a factor 100 results in an increase of the χ_o by a factor 2 - 2.5, assuming the wind speed at 10 m to remain constant.

These results can also be applied to an elevated source inside the atmospheric surface layer by applying a correction discussed by Van Ulden (1977).

b. Horizontal dispersion

Horizontal dispersion is caused not only by turbulence but also by wind direction fluctuations with larger time scales. An estimate of horizontal dispersion should therefore preferably be related directly to the standard deviation of the wind direction fluctuations σ_θ. Hosker (1974) mentions several models of the horizontal dispersion coefficient σ_y that are directly related to σ_θ. After a comparison with experiments he found that the model for σ_y based on the theory of Taylor (1921) and modified by Fuquay et al. (1964) gave the best results. The equation for this model for σ_y reads

$$\sigma_y = \sqrt{A\ \ x/u - \frac{A^2}{2(\sigma_\theta\, u)^2}\left\{1 - \exp\left(-\frac{2(\sigma_\theta\, u)^2\ x/u}{A}\right)\right\}} \qquad (4.4)$$

where $A = 13 + 232\ \sigma_\theta u$.

The ratio of the observed and calculated values for σ_y averaged 1.033 with a standard deviation of 0.477. The scatter between the observed and the calculated values therefore is appreciable. Reasonable results were found also with several other models, the σ_y values by Pasquill-Gifford (Slade, 1968) and the model of **Islitzer (1961).**

Gifford (1959) made an attempt to separate the dispersion by turbulence from the dispersion by large time scale wind direction fluctuations. He argued that the instantaneous plume diffuses due to turbulence, while the meandering of the plume causes the diffusion due to large time scale wind direction fluctuations. The total horizontal dispersion coefficient σ_y is then given by

$$\sigma_y = \sqrt{\sigma^2_{y_{turb}} + \sigma^2_{y_{meander}}} \qquad (4.5)$$

The $\sigma_{y_{turb}}$ should depend on the turbulent wind direction fluctuations $\sigma_{\theta_{turb}}$. In terms of surface layer parameters it follows that

$$\sigma_{\theta_{turb}} = \frac{\sigma_v}{\bar{U}} = \frac{\sigma_v}{u_*} C_D^{\frac{1}{2}} \qquad (4.6)$$

where σ_v is the standard deviation of the horizontal wind fluctuations perpendicular to the mean wind velocity. The drag coefficient C_D has been discussed in section 2. Leavitt (1975) puts $\sigma_v/u_* = 3$, independent of stability. Raynor (1975) finds $\sigma_v/\bar{u} = 0.07$, which results in $\sigma_v/u_* = 1.9$ approximately, if $C_D = 1.4.10^{-3}$. The results of measurements in the atmospheric surface layer over land indicate that $\sigma_v/u_* = 1.6 - 1.7$ (Busch, 1973). Panofsky et al. (1977) suggest that in unstable conditions the influence of the stability on σ_v/u_* should be related to the ratio z_i/L, where z_i is the mixing height.

The $\sigma_{y_{meander}}$ should be related to wind persistence data (Nieuwstadt, 1975).

Conclusions

The stability over a water surface can be characterized by the Obukhov length, which should include the effect of humidity. This length can be determined from routinely measured meteorological parameters.

In contrast with the situation over a land surface the same stability condition can persist over a water surface during the whole day.

A small daily cycle in the air temperature over a water surface is present, caused by radiative processes. The result of this daily cycle is that the condition is more stable during day-time than during night-time, in contrast with the daily cycle of stability over a land surface.

Due to the annual variation of the air and water temperature over the North Sea conditions are primarily stable during the spring and the summer, and conditions are primarily unstable during the fall and the winter.

The roughness of a water surface is much smaller than the characteristic roughness of a land surface. Therefore dispersion over water is smaller than dispersion over a land surface under comparable stability conditions.

The vertical dispersion estimates over a water surface should be related directly to the Obukhov-length. The horizontal dispersion estimates should be related directly to the horizontal wind direction fluctuations.

Acknowledgement

Mr. R. Agterberg assisted with the preparation of the diagrams.

References

Busch, N.E. 1973: On the mechanics of atmospheric turbulence.
Workshop on micrometeorology.
Publ. by American Meteorological Society.

Businger, J.A. 1973: Turbulent transfer in the atmospheric surface layer.
Workshop on micrometeorology.
Publ. by American Meteorological Society.

Charnock, H. 1955: Wind stress on a water surface.
Quart. J. R. Met. Soc. 81, p. 639-640.

Charnock, H. 1958: A note on emperical wind-wave formulae.
Quart. J. R. Met. Soc. 84, p. 443-447.

Deardorff, J.W. 1968: Dependence of air-sea transfer coefficients on bulk stability.
J. of Geoph. Res. 73, p. 2549-2557.

Emmanuel, C.B. 1975: Drag and bulk aerodynamic coefficients over shallow water.
B.L.M. 8, p. 465-474.

Fuquay, J.J., Simpson, C.L., Hinds, W.T. 1964: Estimates of ground-level air exposures resulting from protracted emissions from 70-m stacks at Hanford.
Pacific Northwest Laboratory, rep. HW-80204.

Gifford, F.A. 1959: Statistical properties of a fluctuating plume mode.
Advances in geophysics, Vol. 6, Acad. press, p. 117-118.

Gifford, F.A. 1976: Turbulent diffusion-typing schemes: a review.
Nuclear safety, Vol. 17 No. 1, p. 68-86.

Golder, D. 1972: Relations among stability parameters in the surface layer.
B.L.M. 3, p. 47-58.

Hicks, B.B. 1975: A procedure for the formulation of bulk transfer coefficients over water.
B.L.M. 8, p. 515-524.

Hosker, R.P. 1974: A comparison of estimation procedures for over water plume dispersion.
Proc. of the symp. on atm. diff. and air poll., Santa Barbara, p. 281-288.

Hsu, S.A, : A dynamic roughness equation and its application to wind stress determination at the air-sea interface.
J. of phys. ocean. 4, p. 116-120.

Islitzer, N.F. 1961: Short range atmospheric dispersion measurements from an elevated source.
J. Meteorol. 18 (4), p. 443-450.

Kitaygorodskiy, S.A. 1970: The physics of air-sea interaction (translated from Russian and published by Israel program for scientific translations, ltd., Jerusalem).

Kitaygorodskiy, S.A.
Kuznetsov, O.A.
Panin, G.N. 1973: Coefficients of drag, sensible heat and evaporation in the atmosphere over the surface of a sea.
Izv. Atm. and Ocean. physics 9, No. 11, p. 1135-1141.

Kraus, E.B. 1972: Atmosphere-ocean interaction.
Clarendon press-Oxford.

Leavitt, F.
Paulson, C.A. 1975: Statistics of surface layer turbulence over the tropical ocean.
J. of phys. ocean. 5, p. 143-156.

Nieuwstadt, F.T.M. 1975: The use of wind persistence data for the calculation of concentration statistics.
Royal Netherlands Meteorological Institute, Scientific Report 75-9.

Nieuwstadt, F.T.M.
Verheul, C.M.
Addicks, J. 1976: The validation of the Gaussian dispersion model for long-term average ground level concentrations in the Rijnmond area.
Proc. of the 7th international technical meeting of air pollution modeling of the NATO/CCMS, Airlie, Virginia, USA.

Nieuwstadt, F.T.M.
van Ulden, A.P. 1977: Vertical dispersion of passive material from a continuous point source in the atmospheric surface layer.
To be published.

Nieuwstadt, F.T.M. 1977: The computation of the friction velocity u_* and the temperature T_* from temperature and wind velocity profiles by least square methods.
To appear in B.L.M.

Panofsky, H.A.
Tennekes, H.
Lenschow, D.H.
Wyngaard, J.C. 1977: The characteristics of turbulent velocity components in the surface layer under convective conditions.
B.L.M. 11, p. 355-361.

Pasquill, F. 1961: The estimation of the dispersion of windborne material.
Meteor. Magazine 90, p. 30-49.

Pasquill, F.
Smith, F.B. 1970: The physical and meteorological basis for the estimation of the dispersion of windborne material.
Proc. of the 2nd Intern. Clean Air Congress, Washington, p. 1067-1072.

Pasquill, F.
1974: Atmospheric diffusion.
John Wiley & Sons, New York.

Pond, S.
Fissel, D.B.,
Paulson, C.A.
1974: A note on bulk aerodynamic coefficients for sensible heat and moisture fluxes.
B.L.M. 6, p. 333-339.

Raynor, G.S.
Michael, P.
Brown, R.M.
SethuRaman, S.
1975: Studies of atmospheric Diffusion from a near-shore oceanic site.
J.A.M. 14, p. 1080-1094.

Raynor, G.S.
Brown, R.M.
SethuRaman, S.
1977: A comparison of diffusion from a small island and an undisturbed ocean site.
To be published.

Roll, H.U.
1965: Physics of the marine atmosphere.
Academic Press.

SethuRaman, S.
Raynor, G.S.
1975: Surface drag coefficient dependence on the aerodynamic roughness of the sea.
J. of geoph. res. 36, p. 4983-4988.

Slade, D.H. (ed.)
1968: Meteorology and atomic energy.
T.I.D.-24190.

Smith, F.B.
1973: Estimation of dispersion of pollutants over distances up to 100 km.
Lecture in the course on Atmospheric turbulence and diffusion and their influence on air pollution.
Von Karman Institute, Rhode-Saint-Genese, Belgium.

Smith, S.D.
Banke, E.G.
1975: Variation of the sea surface drag coefficient with wind speed.
Quart. J. R. Met. Soc. 101, p. 665-673.

Taylor, G.I.
1921: Diffusion by continuous movements.
Proc. of Lond. Math. Soc., ser. 2 XX, p. 196-212.

van Ulden, A.P.
van der Vliet, J.G.
Wieringa, J.
1976: Temperature and wind observations at heights from 2-200 m at Cabauw 1973.
Roy. Neth. Met. Inst. Scientific Report 76-7.

van Ulden, A.P.
1977: Similarity predictions for vertical diffusion from a source at the ground.
To be published.

Verploegh, G.
1959: Climatological data of the Netherlands light-vessels over the period 1910-1940.
Roy. Neth. Met. Inst., MV 67.

-o-o-o-

Captions to the figures

1. Daily cycle of the Obukhov-length L, the insolation G and the temperature at a height of 2 m, T_2, over a land surface.

2. The daily cycle of the Obukhov-length L, the insolation G, the water temperature T_w and the air temperature T over a water surface.

3. The average daily cycle of the air and water temperature for each month as measured at the light-vessel Noordhinder.

4. Daily averages of the water and air temperature measured at the light-vessel Noordhinder.

5. Relation between Pasquill stability classes and the Obukhov-length according to Golder (1972).

6. The dimensionless ground **level** concentration as a function of the dimensionless distance x/z_o for several values of the dimensionless stability parameter z_o/L.

-o-o-o-

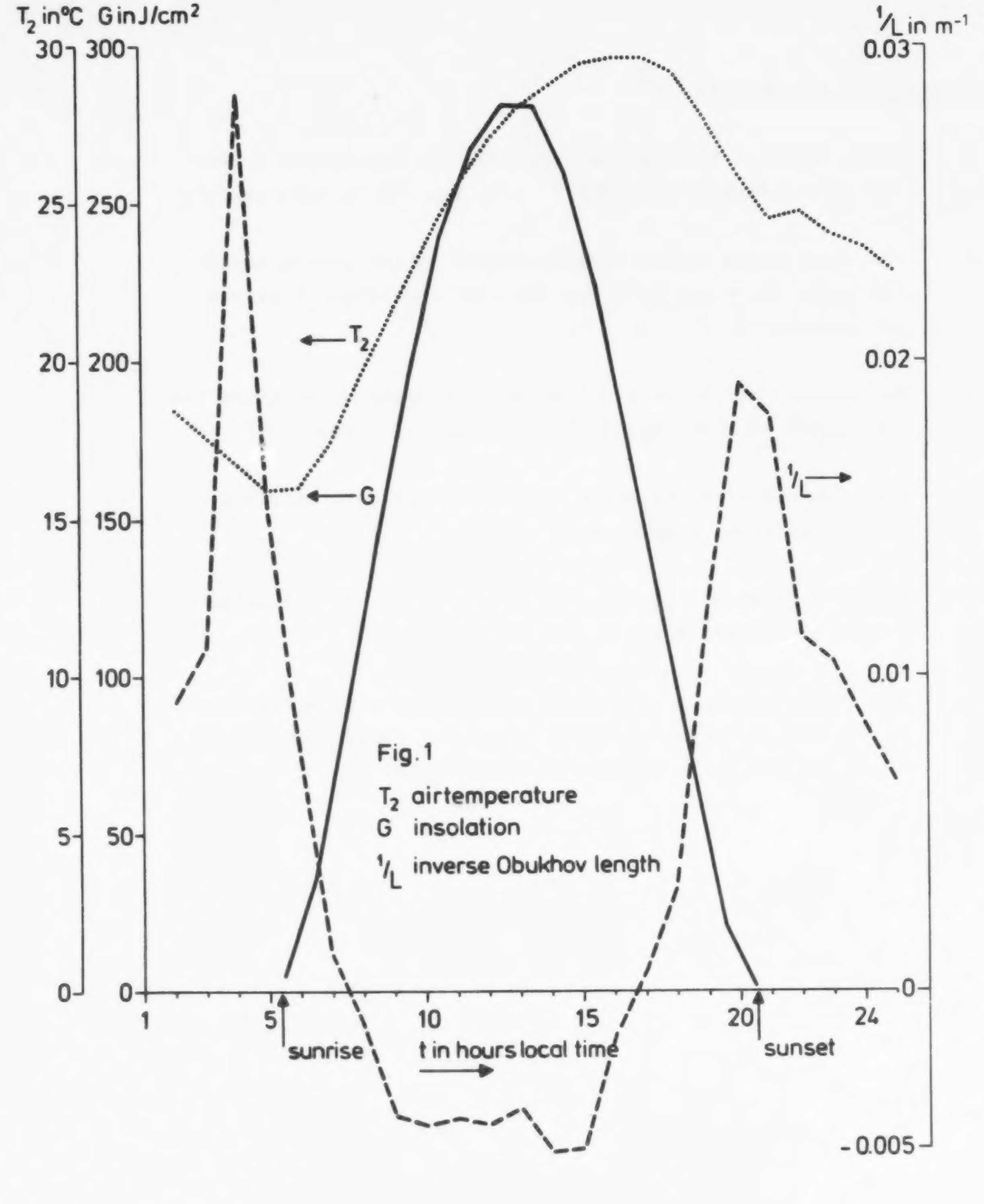

Fig. 1

T_2 airtemperature

G insolation

$1/L$ inverse Obukhov length

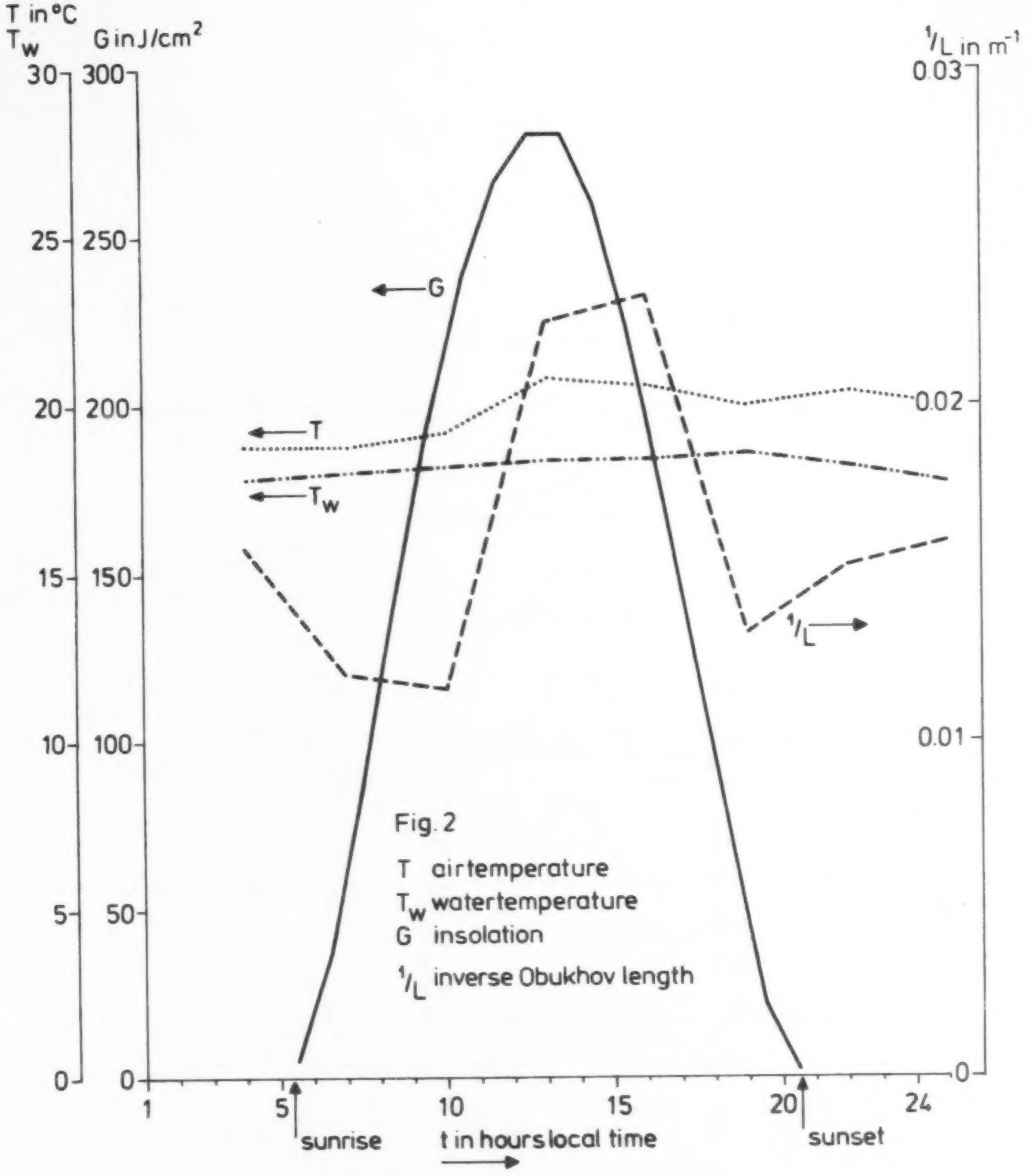

Fig. 2

T airtemperature

T_W watertemperature

G insolation

$^1/_L$ inverse Obukhov length

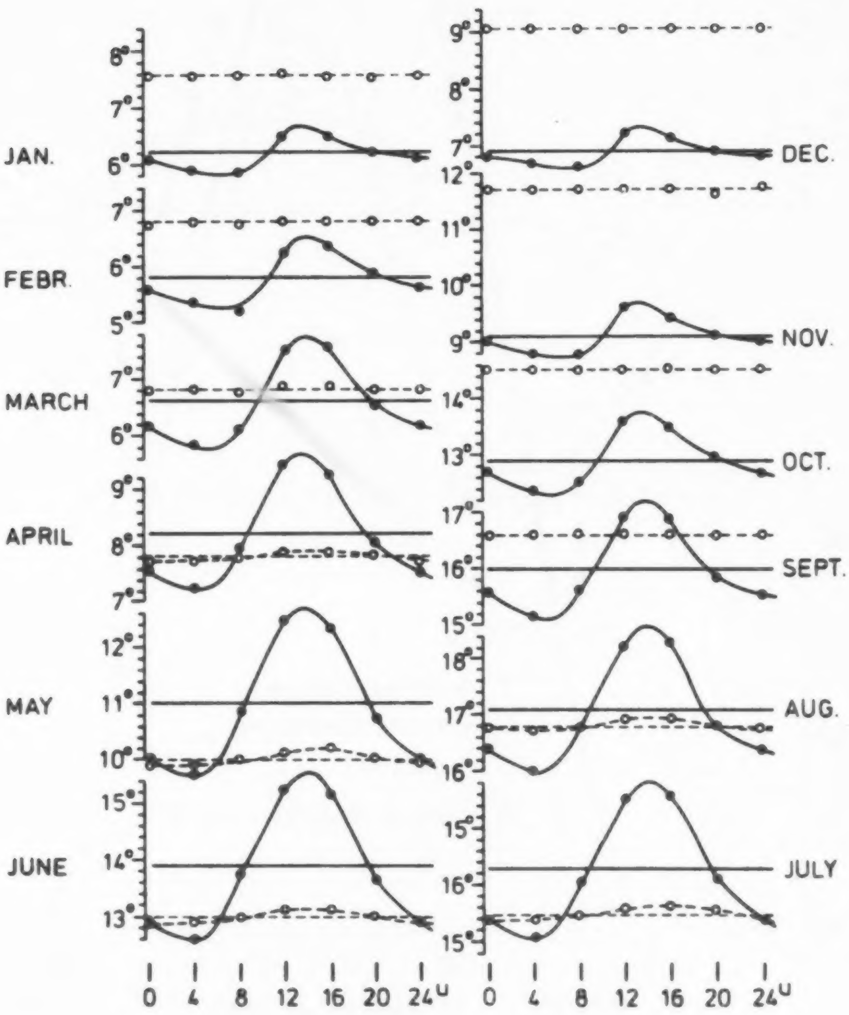

Fig. 3 ——— air temperature
----- sea surface temperature

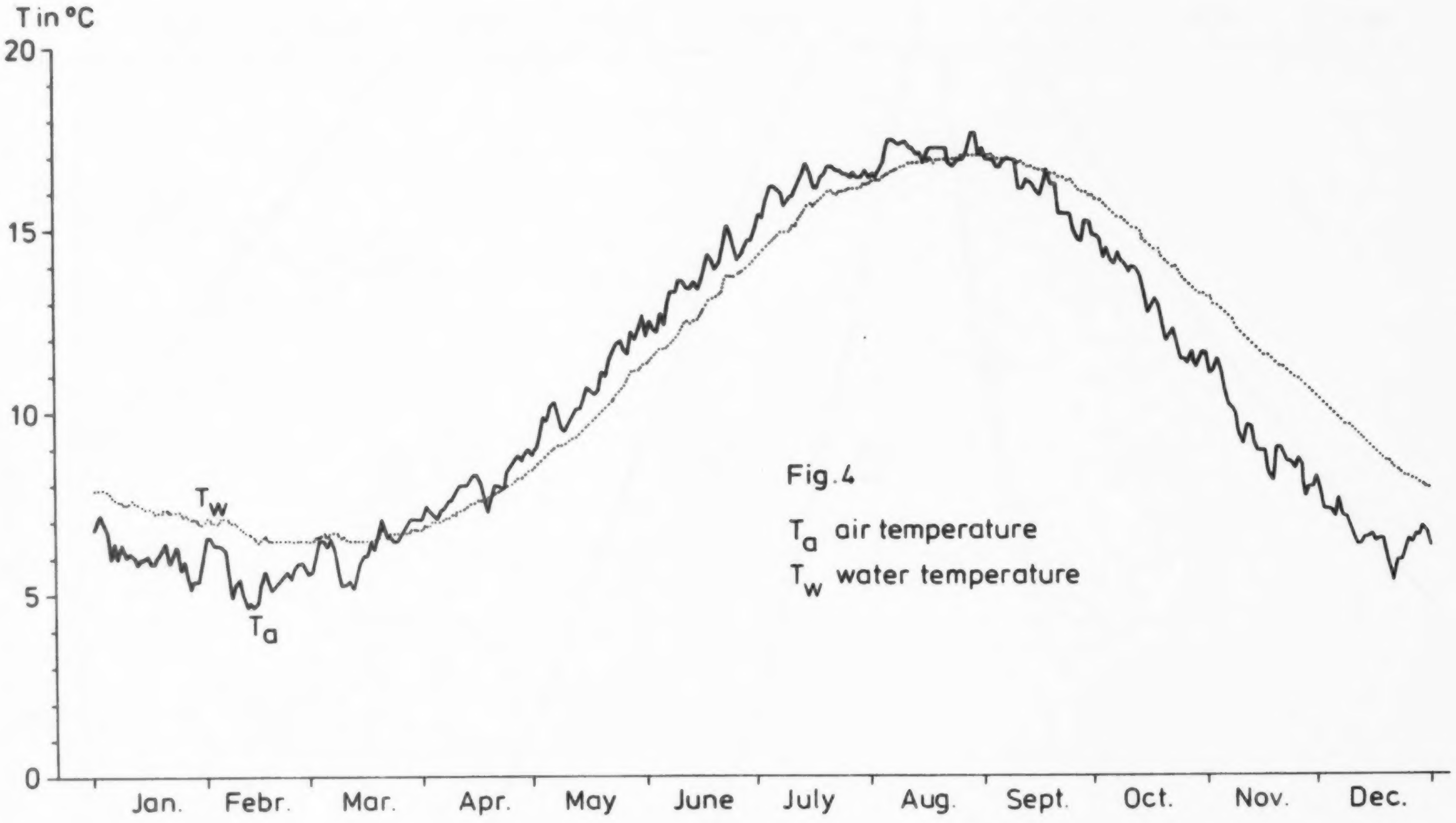

Fig.4

T in °C
20
15
10
5
0
Jan.
Febr.
Mar.
Apr.
May
June
July
Aug.
Sept.
Oct.
Nov.
Dec.
T_w
T_a
T_a air temperature
T_w water temperature

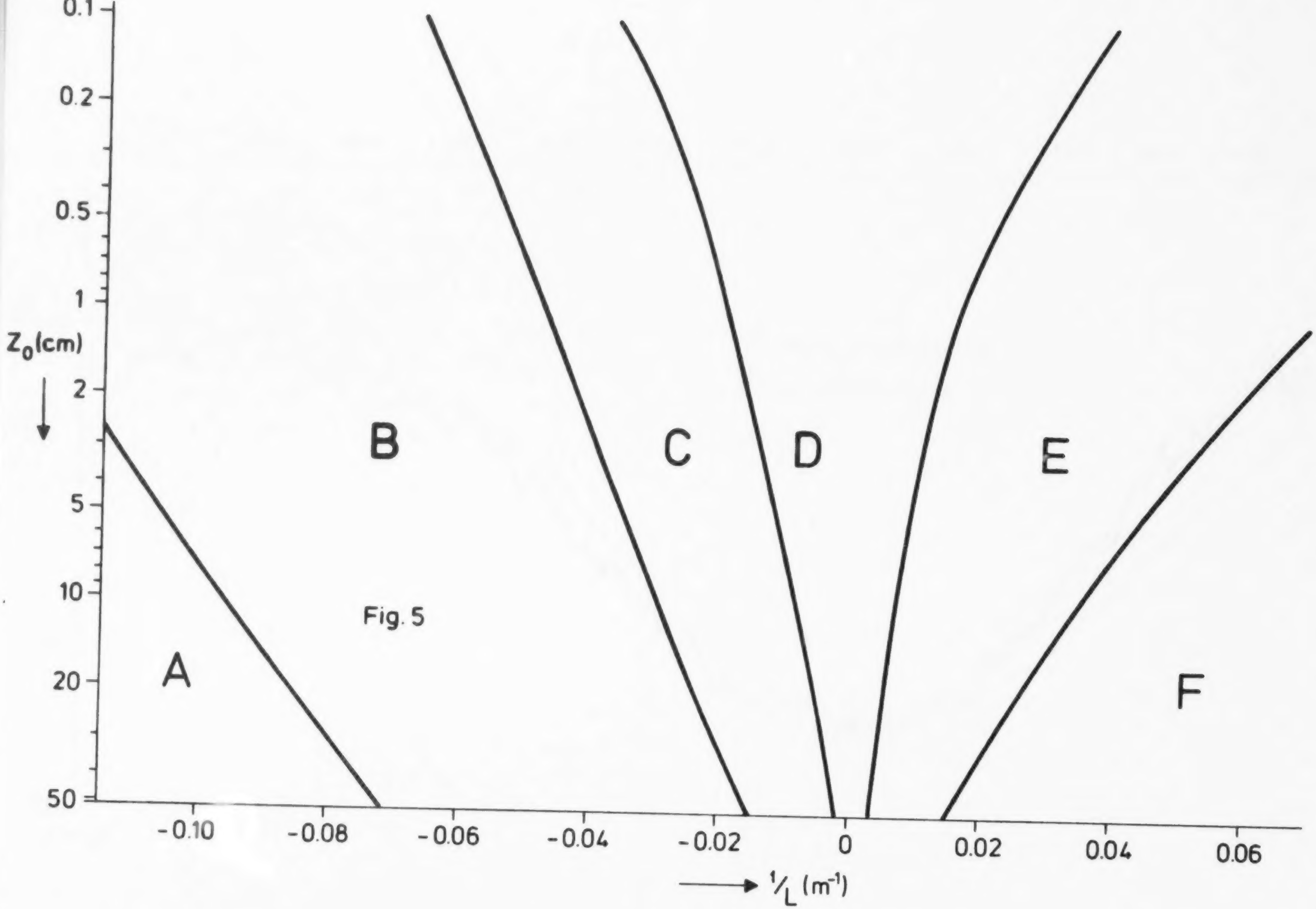

Fig. 5

Z_0(cm)
0.1
0.2
0.5
1
2
5
10
20
50
A
B
C
D
E
F
-0.10
-0.08
-0.06
-0.04
-0.02
0
0.02
0.04
0.06
$^1/_L$ (m^{-1})

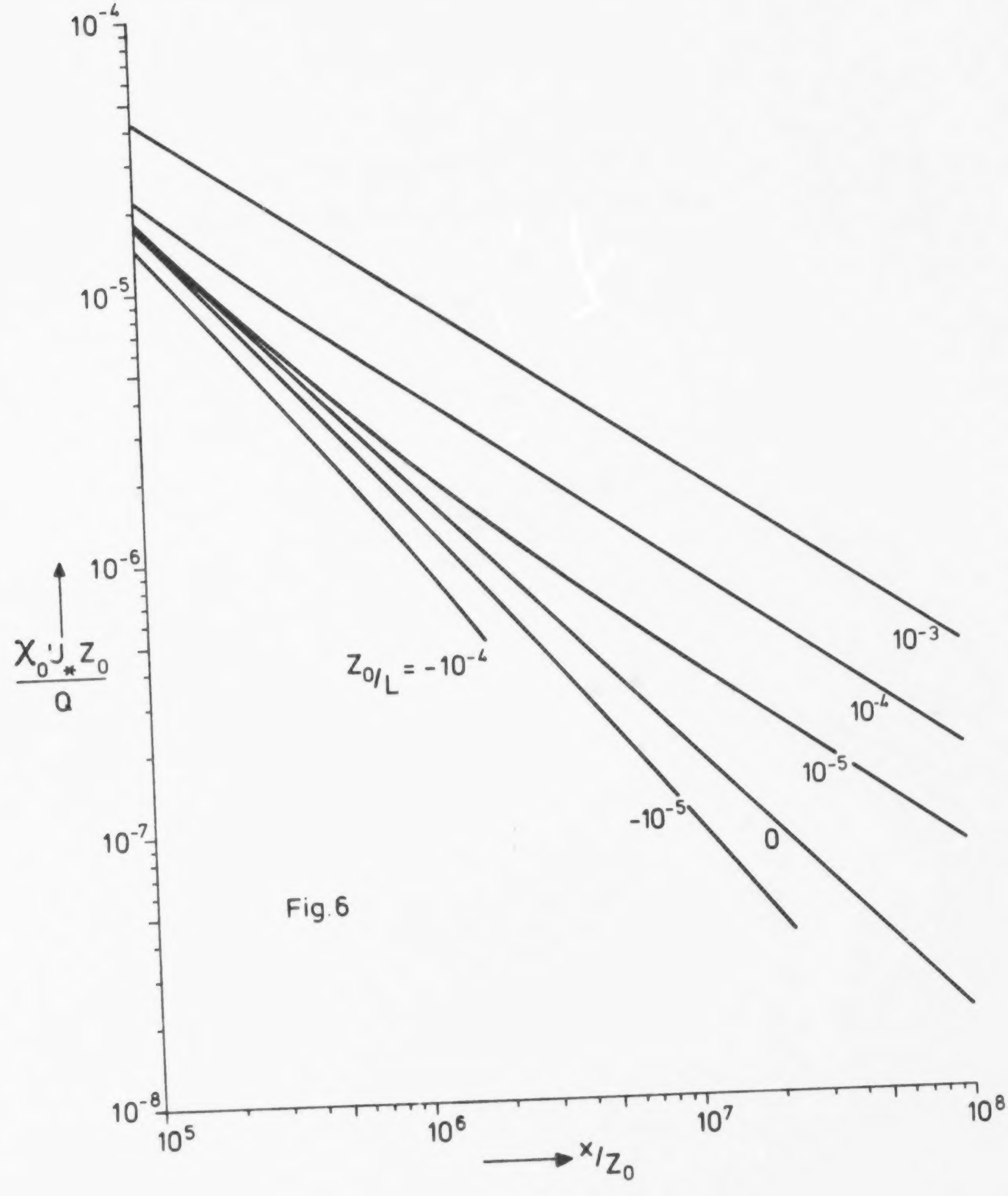

10^{-4}
10^{-5}
10^{-6}
10^{-7}
10^{-8}
$\frac{X_0 U_* Z_0}{Q}$
10^5
10^6
10^7
10^8
x/Z_0
$Z_0/L = -10^{-4}$
-10^{-5}
0
10^{-5}
10^{-4}
10^{-3}

Fig. 6

8th International Technical Meeting on
Air Pollution Modeling and its Application

A PROCEDURE FOR COMPUTING VERTICAL WIND PROFILES IN THE PLANETARY BOUNDARY LAYER

BY

JACOB PADRO

ATMOSPHERIC ENVIRONMENT SERVICE
4905 DUFFERIN STREET
DOWNSVIEW, ONTARIO M3H 5T4
CANADA

September 20 - 23, 1977
Louvaine-La-Neuve
Belgium

A PROCEDURE FOR COMPUTING VERTICAL WIND PROFILES IN THE PLANETARY BOUNDARY LAYER

JACOB PADRO
TORONTO, ONTARIO, CANADA

1. INTRODUCTION

Applied problems in numerical modelling of the planetry boundary layer (PBL) find it inconvenient to extend the integrations of time-dependent equations to the surface of the earth. Instead, the models replace the lowest layer of the PBL by an approximately constant flux layer and apply the Monin-Obukhov similarity theory. This approach is used by models which have stringent computer and data constraints. Gerrity (1967) and Padro (1974) have formulated such restrictive models. The constant flux equations provide lower boundary conditions for equations which govern the rest of the PBL.

Most air quality dispersion models use restricted vertical wind profiles in the boundary-layer. Attempts to remove these restrictions have been made by Egan and Mahoney (1972) and Parker and Baxter (1975) by resorting to similarity theory formulations. The present paper describes a procedure for predicting vertical profiles of wind in the absence of initial wind information. The input consists of stability, geostrophic wind and roughness length. Application is made of the theories of Monin-Obukhov and Monin-Kazanski and the universal functions of Businger (1971).

2. FORMULATION

(a) Constant Flux Layer

The constant flux equations in the manner of Monin-Obukhov similarity theory can be written in terms of universal functions as,

$$\phi_m(\zeta) = \frac{kz}{u_*}\frac{\partial S}{\partial z} \quad \text{, for momentum} \tag{1}$$

$$\phi_h(\zeta) = \frac{kz}{u_*}\frac{\partial \theta}{\partial z} \quad \text{, for heat} \tag{2}$$

where $\zeta \equiv z/L$ is a dimensionless stability parameter,

$L \equiv \dfrac{\bar{\theta}\, u_*^3}{k^2 \beta\, \theta_*}$ is Monin-Obukhov length,

$\beta \equiv g/\bar{\theta}$ is the buoyancy parameters

θ_* is a temperature scale,

and u_* is friction velocity,

The fluxes can be expressed in terms of diffusion coefficients.

$$K_m \frac{\partial S}{\partial z} = u_*^2 \tag{3}$$

and

$$K_h\left(\frac{\partial T}{\partial z} + \gamma_d\right) = k\, u_*\, \theta_* \tag{4}$$

From equations (1), (2), (3) and (4), we obtain

$$K_m = \frac{k u_* z}{\phi(\zeta)} \quad , \quad K_h = \frac{\phi_m(\zeta)}{\phi_h(\zeta)} K_m$$

$$\frac{z}{\theta_*}\left(\frac{\partial T}{\partial z} + \gamma_d\right) = \phi_h(\zeta) \tag{5}$$

Using Businger's forms for $\phi(\zeta)$ for various stability conditions it is possible to obtain θ_* from conventional meteorological data or predictions of temperature. Friction velocity u_* and the cross-isobaric angle can be independently obtained from Monin-Kazanski type of Resistance Laws.

(i) Stable case ($\zeta > 0$)

$$\frac{z}{\theta_*}\left(\frac{\partial T}{\partial z} + \gamma_d\right) = (0.74 + 4.7\, z/L) \equiv \phi_h(z/L)$$

integration yields,

$$\int_{z_0}^{z}\left(\frac{\partial T}{\partial z} + \gamma_d\right) dz = \int_{z_0}^{z} \frac{\theta_*}{z}(0.74 + 4.7\, z/L)\, dz$$

i.e. an equation for θ_* of the form

$$a\theta_*^2 + b\theta_* + c = 0$$

$$a \equiv 4.7\beta k^2 (z_2 - z_0)$$

$$b \equiv 0.74\, u_*^2 \ln z_2/z_0$$

$$c \equiv -u_*^2 \left[T(z_2) - T(z_0) + \gamma_d (z_2 - z_0)\right]$$

Only the positive root is accepted for the stable case. Wind speed can be obtained from

$$\frac{\partial S}{\partial z} = \frac{u_*}{k}(1 + 4.7\, z/L)$$

$$S(z_2) = \frac{u_*}{k}\left[\ln \frac{z_2}{z_0} + 4.7\, \frac{(z_2 - z_0)}{L}\right]$$

(ii) Unstable case ($\zeta < 0$)

$$\frac{z}{\theta_*}\left(\frac{\partial T}{\partial z} + \gamma_d\right) = 0.74(1 + 9\zeta)^{-1/2} \equiv \phi_h(z/L)$$

integration leads to

$$\int_{z_0}^{z_2}\left(\frac{\partial T}{\partial z} + \gamma_d\right) dz = \theta_* \int_{z_0}^{z_2} \frac{0.74}{z(1 - 9\, z/L)^{1/2}}\, dz$$

$$\theta_* = \frac{\left[T(z_2) - T(z_0) + \gamma_d (z_2 - z_0)\right]}{0.74 \ln\left[\frac{(a-1)(b+1)}{(a+1)(b-1)}\right]}$$

where $a \equiv (1 - 9\, z_2/L)^{1/2}$

$b \equiv (1 - 9\, z_0/L)^{1/2}$

A solution is obtained by iteration. Wind speed is obtained by integrating

$$\frac{\partial S}{\partial z} = \frac{u_*}{k}\left(1 - 15\, z/L\right)^{-1/4}$$

This yields,

$$S(z_2) = \frac{u_*}{k}\left[2(\tan^{-1} a - \tan^{-1} b) + \ln \frac{(a-1)(b+1)}{(a+1)(b-1)}\right]$$

where $a \equiv \left(1 - 15\,\frac{z_2}{L}\right)^{1/4}$, $b \equiv \left(1 - 15\,\frac{z_0}{L}\right)^{1/4}$

(iii) Neutral case (ζ=0)

$$S(z_2) = \frac{u_*}{k} \ln z_2/z_0$$

Wind components (u, v) can be expressed in terms of geostrophic wind (u_g, v_g) wind speed S and the cross-isobaric angle α as follows,

$$u(z_2) = \frac{S}{V_g}(u_g \cos\alpha - v_g \sin\alpha)$$

$$v(z_2) = \frac{S}{V_g}(u_g \sin\alpha + v_g \cos\alpha)$$

where $V_g = (u_g^2 + v_g^2)^{1/2}$

(b) Resistance Laws

From the theory of Monin-Kazanski (1960) and similar to Fiedler and Panofsky (1972), the following form for the Resistance Laws has been derived,

$$\ln R_0 = \left(\frac{k^2}{C_d} - k^2 B_2^2(s)\right)^{1/2} - \ln C_d^{1/2} - k B_1(s) \qquad (6)$$

$$\frac{\theta_*}{\Delta\theta} = \frac{1}{0.74 k^{-1}(\ln C_d^{1/2} R_0) + B_3(s)} \qquad (7)$$

$$s = \frac{\theta_*}{\Delta\theta}\,\frac{1}{C_d^{1/2}}\,S \qquad (8)$$

and $$\tan\alpha = \frac{B_2(s)}{k\ln\left[C_d^{1/2} R_o\right] + B_1(s)} \tag{9}$$

where $C_d \equiv \left(\frac{u_*}{V_g}\right)^2, \quad s = k^{-2}\mu$

$\frac{\theta_*}{\Delta\theta}$ can be eliminated from these equations to yield s, C_d and α as functions of the external parameters Ro and S. By an iterative procedure, nomograms for α and $C_d^{1/2}$ have been constructed in Figs. 1 and 2.

The universal functions $B_1(s)$, $B_2(s)$ and $B_3(s)$ are illustrated in Fig. 3. These are approximated by polynomials in terms of the internal stability.

3. RESULTS AND CONCLUSIONS

The wind field of a surface map for 0000 GMT, August 30, 1972 is shown in Fig. 4 for part of the North American Continent. Model results superimposed upon the same map indicate, in general, a very good agreement in Fig. 5. The winds cross the isobars into areas of low pressures and troughs and out of areas of high pressure.

Time height sections of wind are shown in Figs. 6, 7, 8 for Sault St. Marie (SSM), Moosonee (MO) and Montreal (UL) respectively. In response to thermal stability the section for SSM shows light winds at night and stronger winds during the day. The winds at the highest level are observed geostrophic winds, the lowest level wind is computed from the present formulation and the rest of the profile is obtained from a solution of the Ekman equations. A feature to be noted is the clockwise turning of the wind with height.

We conclude that vertical profiles of horizontal winds can be computed from external parameters of geostrophic wind, and two levels of temperature. For non-homogeneous terrain, it is recommended that an effective roughness length be used in each grid area.

REFERENCES

Barker, E.H. and T.L. Baxter, 1975: A note on the computation of atmospheric surface layer fluxes for use in numerical modelling. J. Appl. Meteor., 4, 620-622.

Businger, J.A., A. Wyngaard, J.C. Izumi, and E.F. Bradley, 1971: Flux-profile relationships in the atmospheric surface layer. J. Atmos. Sci., 28, 181-189.

Clarke, R.M., 1970: Observational studies in the atmospheric boundary layer. Quart. J. Roy. Meteor. Soc., 96, 91-114.

Egan, B.A. and J.R. Mahoney, 1972: Applications of a numerical air pollution transport model.to dispersion in the atmospheric boundary layer. J. Appl. Meteor., 11, 1023-1039.

Fiedler, F. and H.A. Panofsky, 1972: The geostrophic drag coefficient and the 'effective' roughness length. Quart. J. Roy, Meteor. Soc., 94, 213-220.

Gerrity, J.P., 1967: A physical-numerical model for the prediction of synoptic-scale low cloudiness. Mon. Wea. Rev., 55, 281-267.

Kazanski, A.B. and A.S. Monin, 1961: On dynamical interaction between the atmosphere and the earth's surface, Izvestia Ann. SSSR. Ser. Geophys., 5, 786-788.

Padro, J., 1974: Forecasting in the planetary boundary layer. Proceedings, Forecast Res. Symposium, May 27, A.E.S., Toronto.

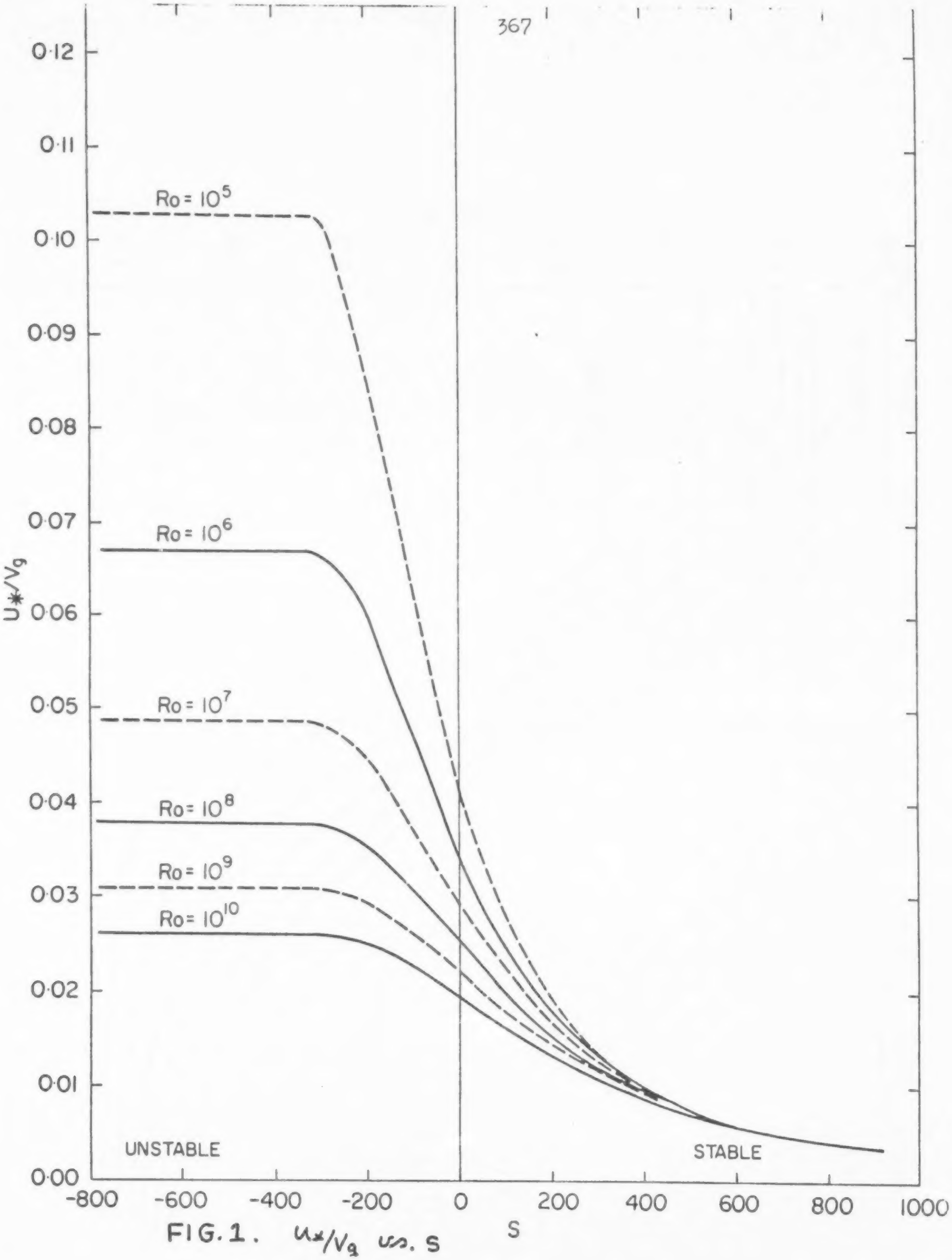
0·12
0·11
0·10
0·09
0·08
0·07
0·06
0·05
0·04
0·03
0·02
0·01
0·00
U*/Vg
Ro = 10^5
Ro = 10^6
Ro = 10^7
Ro = 10^8
Ro = 10^9
Ro = 10^10
UNSTABLE
STABLE
-800
-600
-400
-200
0
200
400
600
800
1000
S

FIG. 1. u_*/V_g vs. S

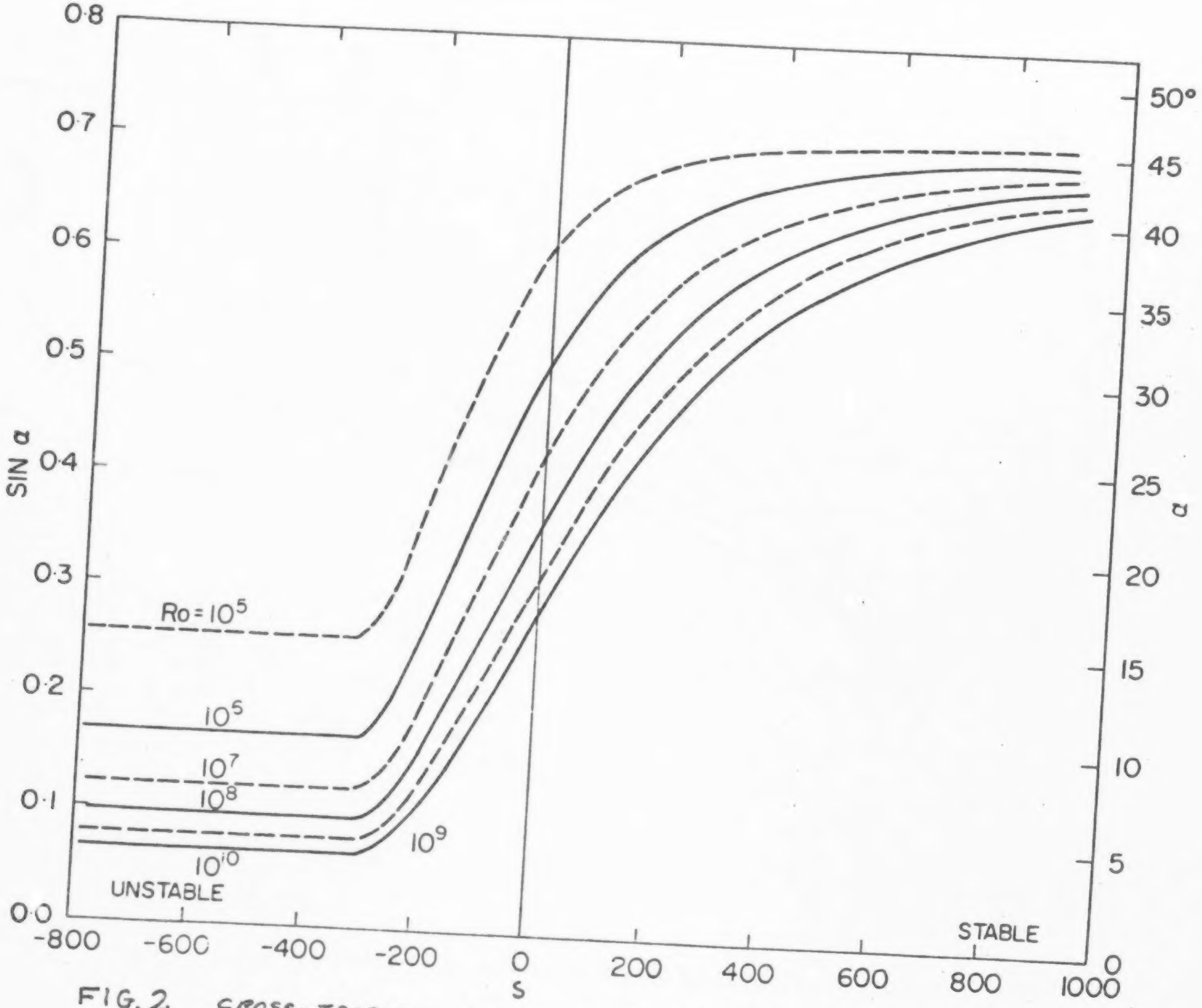

FIG. 2 CROSS-ISOBARIC ANGLE α VS. S.

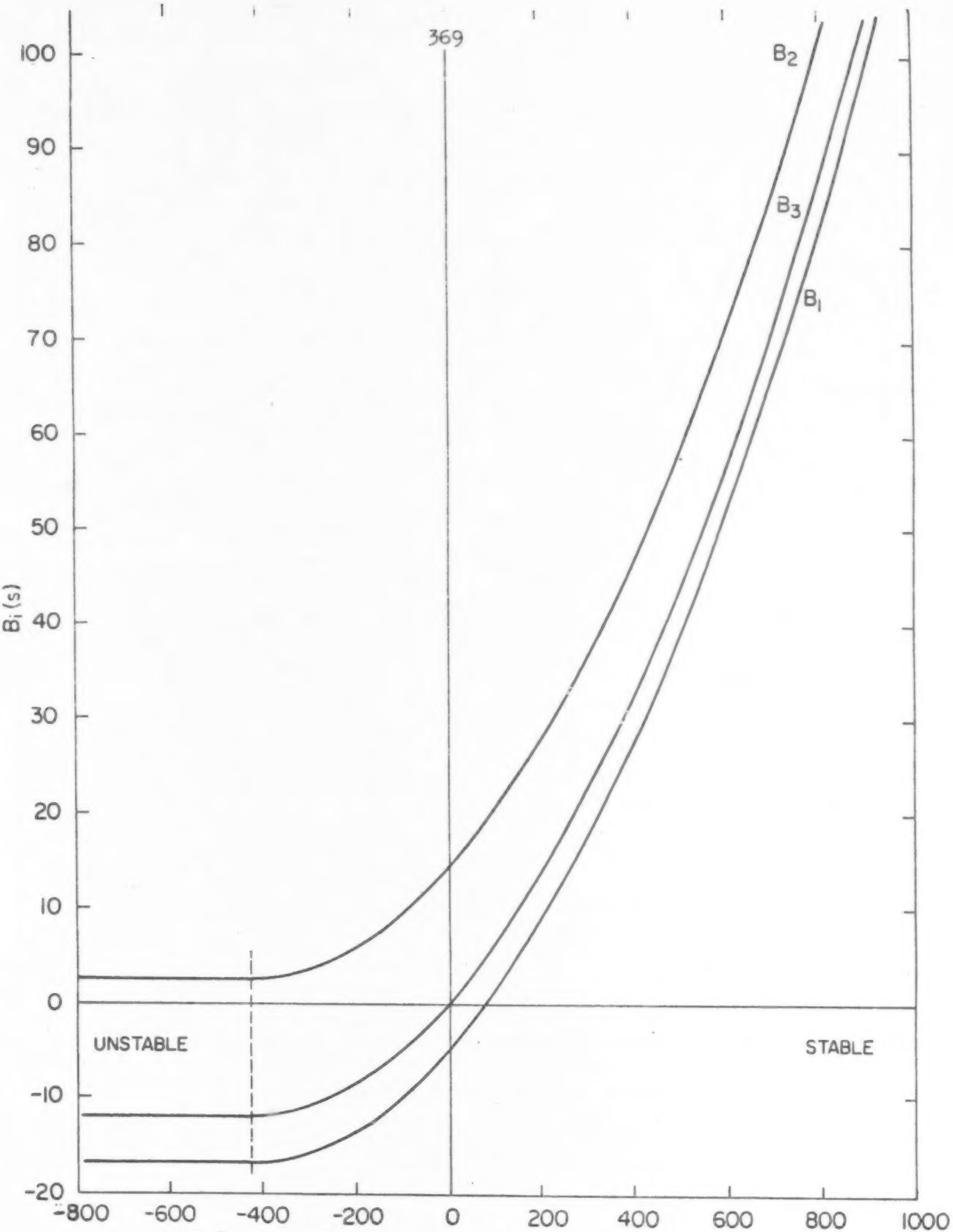

FIG. 3. UNIVERSAL FUNCTIONS

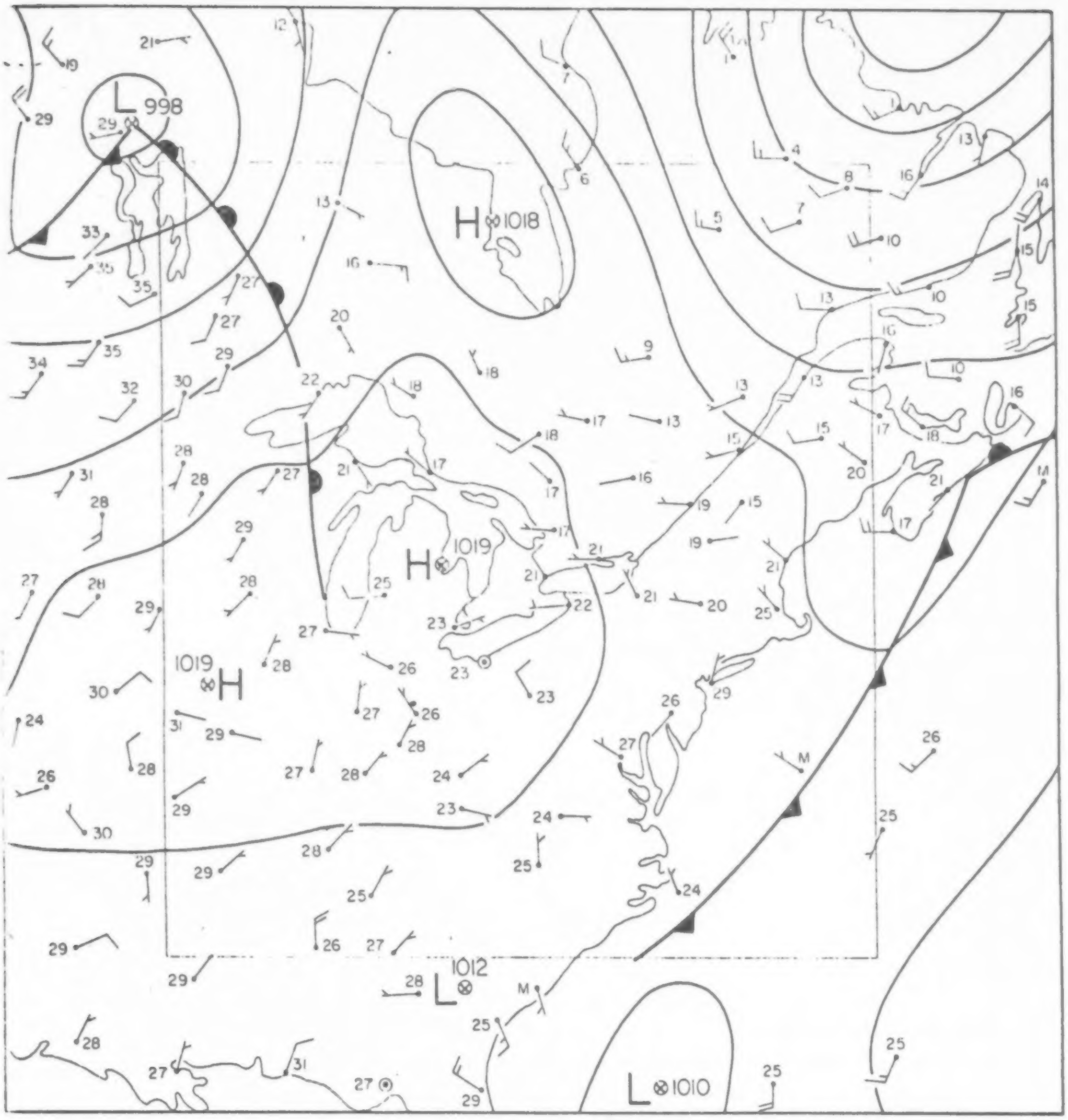
L 998
H 1018
H 1019
1019 H
L 1012
L 1010

Figure 4. Surface chart for 0000 GMT 30 August

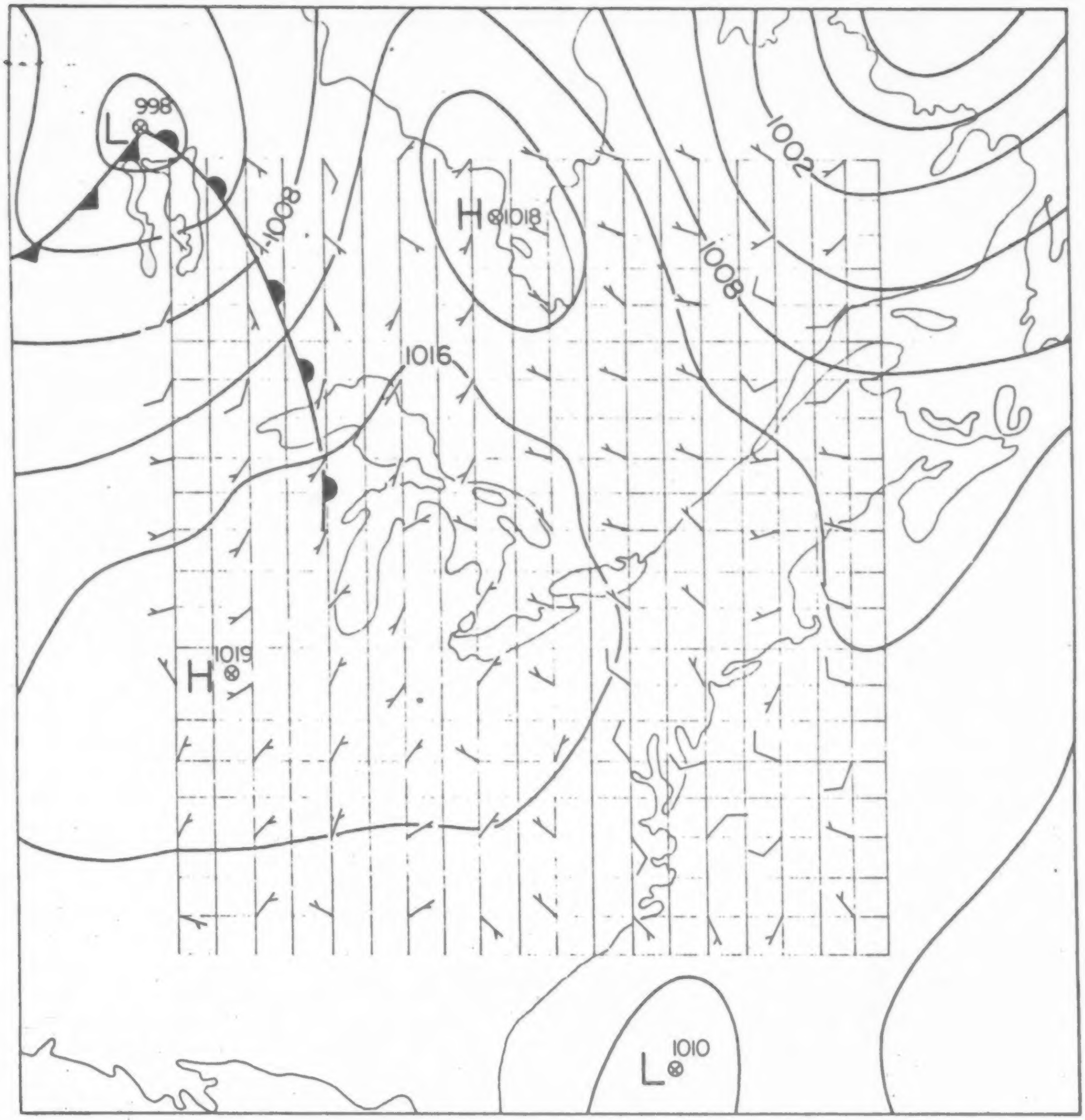
L 998
-1008
1002
1008
H 1018
1016
H 1019
L 1010

Figure 5. Diagnosis of 50-m winds, superimposed upon the surface chart of Figure 4.

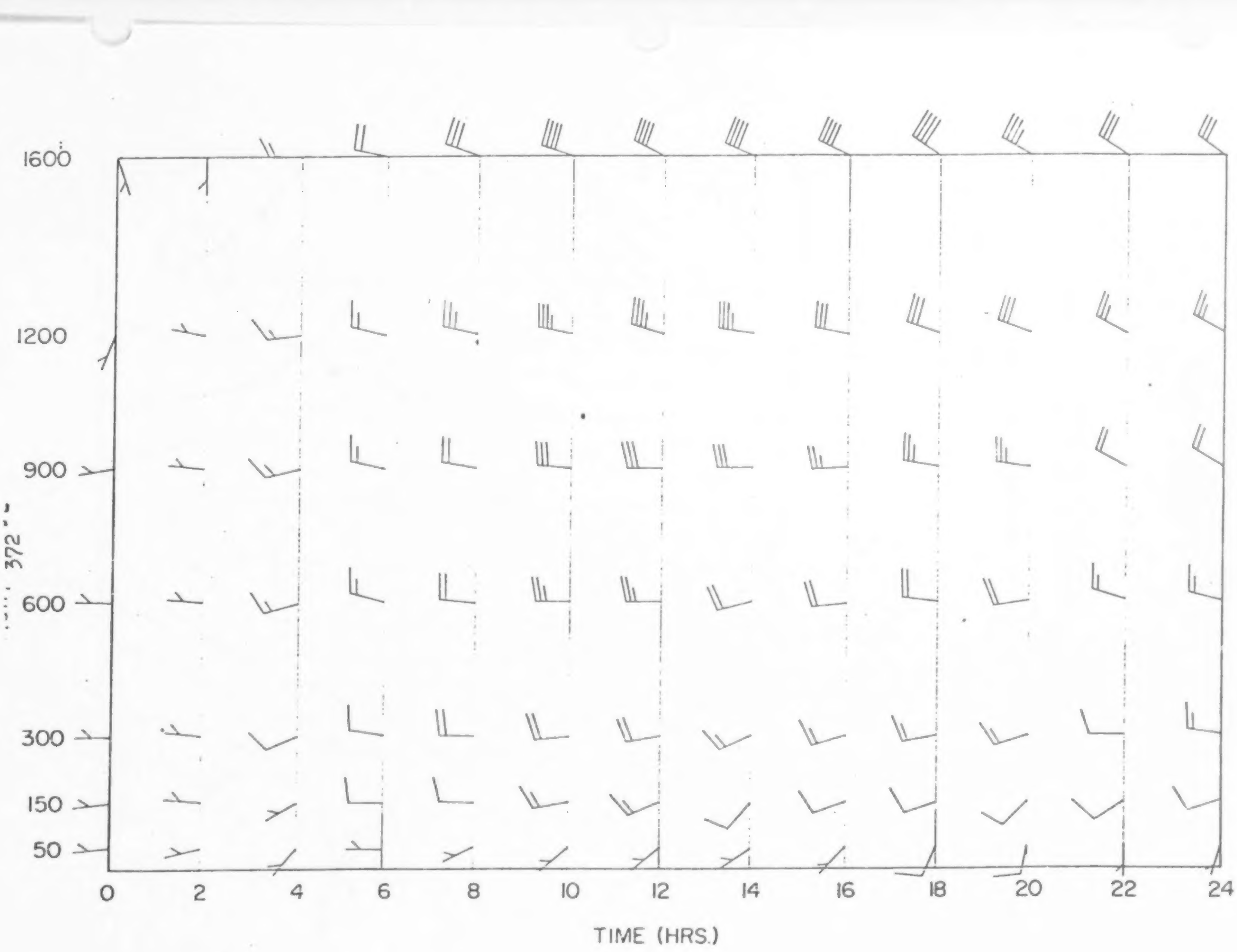

Figure 6. Time-height section of forecasts of winds for Sault St. Marie.

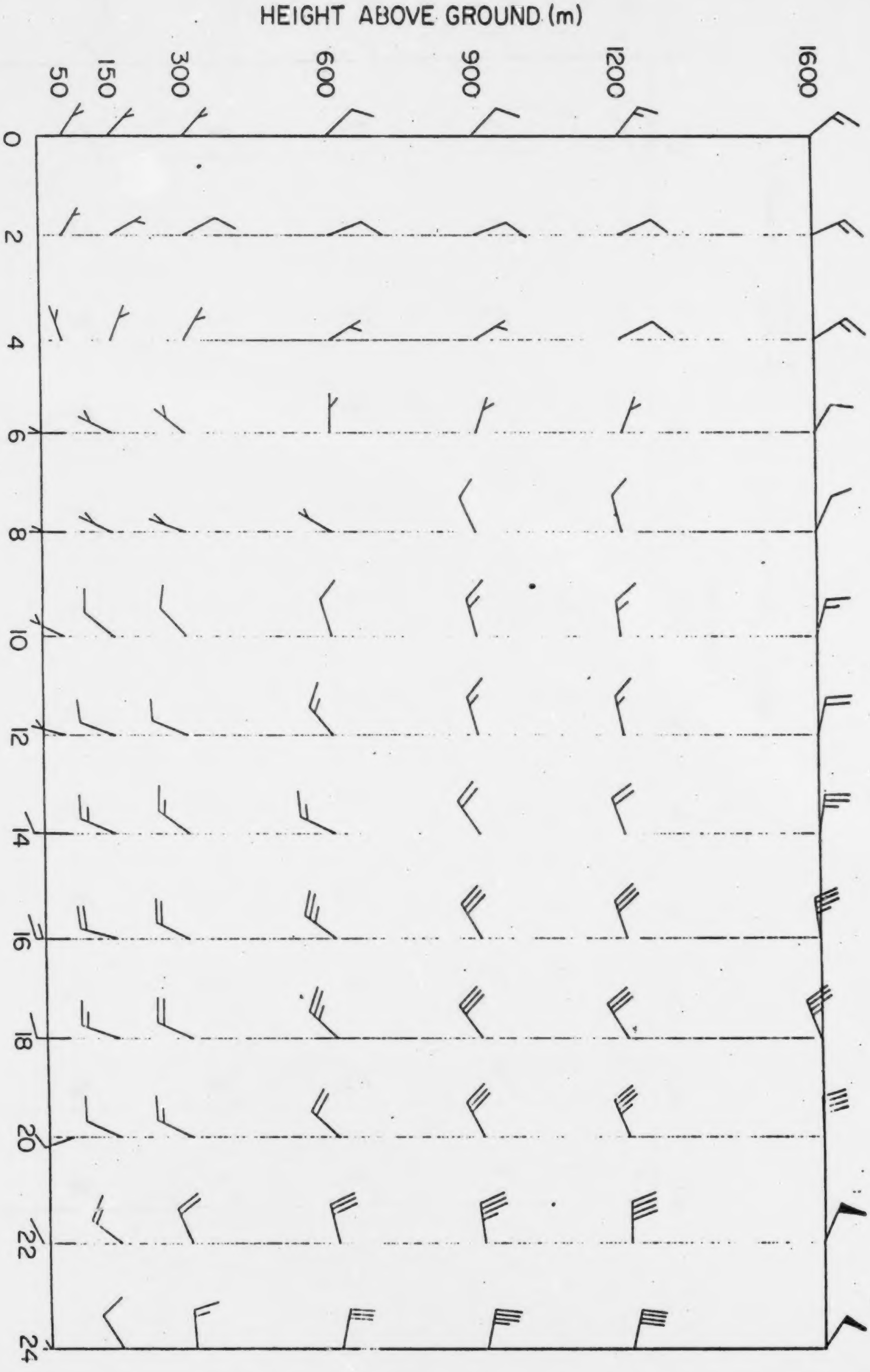

Figure 7. Time-height sections of forecasts of winds for Moosonee.

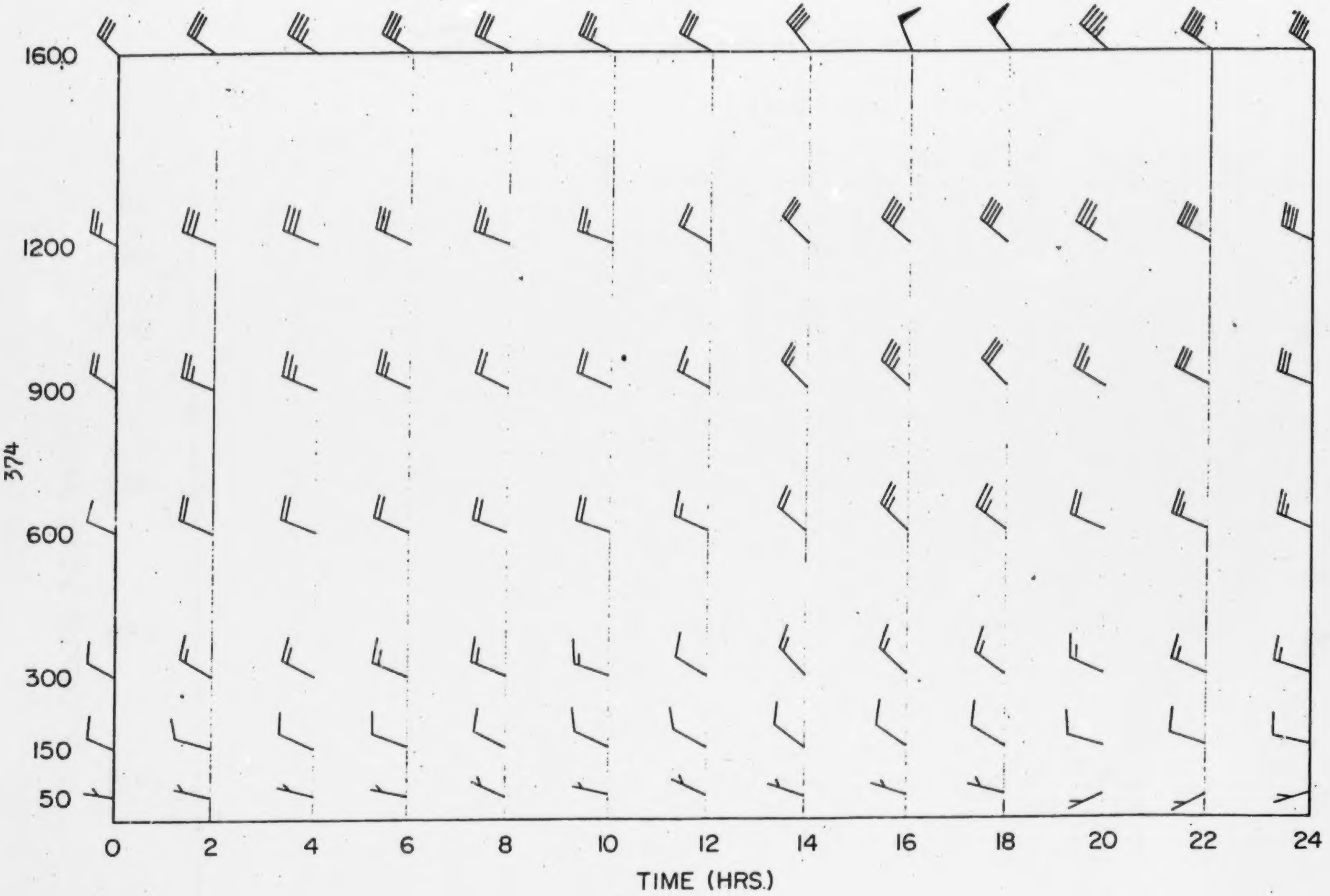

Figure 9. Time-height section of forecasts of winds for Montreal.

Rapporteur's Summary Report:

Prepared by: C. A. Velds

Papers covered by: Santangelo
Nieuwstadt
Padro

The papers presented in this session pertain to the meteorological aspects of modeling; they were

R. Santangelo:	"Simulation of daily temperature for environmental modeling";
F. Nieuwstadt:	"The dispersion of pollutants over a water surface";
J. Padro:	"A procedure for computing vertical wind profiles in the planetray boundary layer".

Simulation of daily temperatures for environmental modeling.

The presentation started from the principle that some emission rates are dependent on meteorological factors, as for instance the fuel consumption for space heating depends on temperature.It is therefore useful to simulate the meteorological data by a model. The author discussed a model for the yearly variation of the daily mean, minimum and maximum temperature, assuming that the times series can be divided into a deterministic part and stochastic (Markovian) part.

In the discussion it was remarked that the simulation of daily temperatures can be considered a starting point, temperaturebeing the most important parameter. In the future it will be tried to simulate other relevant meteorological parameters.

The dispersion of pollutants over a water surface

The dispersion of pollutants over a water surface has become an increasingly important problem. The stability classes, with the dispersion parameters belonging to them, used over a land surface, cannot be used for dispersion calculations over water. The presentation described a method to define stability classes over water based on the Obukhov-length L, which can be determined from measured meteorological parameters. Due to the small roughness of a water surface the dispersion over water is generally smaller than the dispersion over land. Data from a light-vessel in the North Sea showed that conditons are primarily stable during the spring and summer and primarily unstable during the autumn and winter.

In the discussion Dr. Turner remarked that the EPA is engaged in the estimation of the dispersion from incinerators at sea.

He considered the paper very interesting, as it can contribute to estimate the dispersion of waste gases from these incinerators.

When asked, the author replied that there are at the moment no meteorological restrictions to burning at sea. The emission consists largely of hydrochloric acid. Good incineration of chemical wastes requires a well-defined very high temperature of the combustion furnaces.

To define a value for the Obukhov-length from routinely measured data the following substitutions are made in the formula for L:

$$u_*^2 = C_D\,(u-u_s)^2$$

$$\overline{wT} = C_H\,(u-u_s)(T-T_w)$$

$$\overline{wq} = C_q\,(u-u_s)(q-q_w)$$

The coefficients C_D, C_H and C_q are transfer coefficients for momentum, heat and humidity; they all have been taken 1.5 10^{-3},
u is the wind speed at about 10 m above sea level,
u_s is the velocity of the sea surface, which is taken 3-5 per cent of u,
T is the temperature measured on board the light-vessel, 2-3 m above sea level,
T_w is the water temperature measured with a bucket,
q is the specific humidity measured on board the ship,
q_w is the specific humidity close to the water surface, which is taken equal to the saturation value at temperature T_w.

The accuracy of the transfer coefficients has not been determined. A best guess has been made from data taken from literature. Speaker believes the accuracy to be about 50 per cent.

By the above mentioned substitutions in the formula for the Obukhov-length it is possible to get only a rough value of L. According to the author this inaccuracy is not serious, as L is only used to define the 6 stability classes in a stability class climatology, which will have the same accuracy as a comparable climatology over land.

The Obukhov-length is a measure for the stability in the surface layer, which is about 10 meter high over a water surface. A difficult question is, if the stability determined closely above the sea may be extrapolated to the levels of the effective plume height, which may reach several hundreds of meters. Until now the given data on stability are the best that can be determined, but in the near future measurements will be made at greater heights above the sea level on a platform.

It was remarked in the discussion that the roughness length z_0 over sea is dependent on wind speed through the eight of the winddriven waves. This dependence has not been taken into account.

Air masses and subsidence do determine the eight of the mixing layer over the sea. In the future measurements will be performed closer to the coast where the influence of land- and sea-breezes is dominant.

The frequency of the stability classes above the sea depends on the place of measurement, it will differ from the ocean to the North Sea. The frequency is also dependent on the season. During the autumn and early winter the frequency of unstable classes is higher than the frequency for a station on the coast. During the spring the frequency of stable classes is higher.

There was some discussion on the method using L and z_0 to define stability chlasses and from these the dispersion coefficients. Dr. Hanna asked if it was not possible to measure the dispersion parameters σ_θ and σ_φ directly above the sea by using tridimensional vanes. The author remarked that the project had been started to answer the questions posed to his Institute; a quick determination of diffusion over the sea had to be made. Therefore use could be made only of parameters which were routinely measured on board the light-vessels. At this time, σ_θ is measured on an existing platform in the North Sea.

Finally, some examples on diffusion over water surfaces were given from the floor. Dr. Sivertsen drew the attention to the measurements of the plume's cross section of the Ecofisk accident. These have given rather good values of σ, from which it could be concluded that due to low roughness the dispersion was small. Dr. Brubaker remarked that satellite photographs of the plume across Lake Michigan have shown narrow plumes over 100 km distance, so that it can be deduced that the increased stability extends to greater altitude. It must be doubted, however, if these results can be transferred to the open sea.

A procedure for computing vertical wind profiles in the planetary boundary layer

This paper describes a procedure for predicting vertical profiles of the wind in the planetary boundary layer from thermal stability, geostrophic wind and roughness length as input variables. Application is made of the theories of Monin-Obukhov and Monin-Kazanski and Businger's universal functions. Computations of the vertical wind profiles agree, in general, very well with measurements from 3 radiosonde stations.

When asked, the author replied in the discussion that the diffusion coefficients K are height-dependent, but are independent of the height of the mixing layer. The mixing layer is so high that its height is well above the friction layer.

Advection of air masses on a large scale does not influence the procedure; according to Yaglom one uses mean values for large-scale effects. It was remarked that the barotropic assumption underlying the theory is seldom true in situations with advection. Is the model applicable in baroclinic situations? According to the author baroclinic regions, as for example with frontal disturbances, are small-scale phenomena, which are time-dependent. Therefore the barotropic assumption has been taken, which is also used by several authors (Tennekes and others) in matching the surface layer and the boundary layer.

In the abstract it is stated that the procedure is suitable to long-range transport of pollutants. Trajectories, however, have not yet been calculated, until now only the wind speed as a function of height has been computed. For trajectories it is common practice to use the geostrophic wind or a balanced wind, also taking into account the stability.

The lowest length- and time scale to which the procedure is applicable are the synoptic scale, grid areas of 100 x 100 km and a daily time scale.

8th International Technical Meeting on
Air Pollution Modeling and its Application

ASSESSMENT OF STABILITY CATEGORIES AS METEOROLOGICAL INPUT OF AIR POLLUTION MODELING

A. Longhetto[◆], P. Bacci[◆], L. Briatore[●■], G. Elisei[◆], L. Santomauro[▲]

◆ Laboratorio Ricerche Ambientali ENEL:CRTN, Milano, Italy

● Istituto di Fisica Generale dell'Università, Torino, Italy

▲ Osservatorio Meteorologico di Brera - Director - Milano, Italy

■ Laboratorio di Cosmo-geofisica, CNR, Torino, Italy

September 20 - 23, 1977
Louvain-La-Neuve
Belgium

1. Introduction.

The primary object of people working on air pollution modeling is to improve the accuracy and reliability of estimates of ground level concentrations. To do that, one needs to better understand turbulent processes responsible of the spreading of airborne pollutants, both from a theoretical and from an experimental point of view. In fact, if it is true that we have now a satisfactory understanding, for many respects, of the main characteristics of atmospheric boundary layer, it is also true that there is a less good knowledge of the relations between these atmospheric structures and the diffusing properties of atmospheric turbulence (Gifford, 1976).

The need for an improvement of our knowledge of these phenomena is therefore felt, but, of course, this is a very impracticable road and so, generally, air pollution modelers attempt to improve the accuracy of their estimates constructing more and more sophisticated models (from a computational and analytical point of view).

But this last procedure generally fails to give valuable improvements in respect of simplest models (which have, on the contrary, the advantage of low cost and high speed answers), if one cannot utilize meteorological input of comparable degree of sophistication (i.e, detailed both in space and in time, affected by low measuring errors and typical of every site of interest).

As a consequence, it is necessary to increase the confidence level of the empirically established diffusional schemes and stability criteria in order to choose, for a given site, the most suitable one, that is, that better describing the various atmospheric situations more frequently occurring in that place, on the basis of the available instrumentation.

Therefore, if we refer to thermodynamic stability of air in the first hundred metres, which represents the most important parameter governing the spreading of airborne pollutants, we must recall that it has been evaluated, from Porton experiments up to now, in numerous different ways, all more of less qualitative and reliable (Slade, 1968; Pasquill, 1974, Stern, 1976).

For this reason we thought it useful to study in particular this problem, from an experimental point of view, making a climatological classification of the stability conditions recorded by the meteorological tower (120 m high) and by the conventional aerological instrumentations of Trino Vercellese ENEL Environmental Research Laboratory.

The meteorological tower is located at the western extremity of the Po Valley, in a prevailingly agricultural zone (rice fields), and was built near the PWR ENEL nuclear power station "Enrico Fermi", for studies in boundary layer dynamics and climatology chiefly connected to air pollution problems.

It stands near an hilly chain extending mainly in direction W-E, whose altitude is typically of about 100 metres above the plain, while at a distance of about 90-100 km is surrounded by the Alpes for a sector of about 150 degrees. Therefore the climatology of our site is of continental type (Santomauro) and is mainly determined by the Alpes whose blocking of general circulations brings about weak circulations and a certain stationarity of air masses.

In the present study two of the most widely used criteria, lapse rate's and Richardson's stability classifications have been evaluated and critically compared.

2. Dispersion data requirements.

The choice of the above two stability criteria follows from a classification of model input data according to minimal, typical and additional requirements, established by R.C. Sklarew and J.C. Wilson (1976) on the ground of a thorough inquiry among modeling community.

As to dispersion data, the simplest-prescription for stability class is that relating stability class to easy to measure meteorological parameters, i.e. wind speed, cloud cover and whether it is day or night. In this sense, Pasquill's classification of air stability can be taken as a "minimal" dispersion data requirement.

Greater reliability in the classification of atmospheric stability can be gained through the observation of vertical temperature variation, even if the relation of turbulence type to lapse rate has proved to be very variable from site to site (Gifford 1976).

The measured temperature gradients are generally translated into stability classes, amenable both to Pasquill's turbulence types and to BNL turbulence types. This second classification represents a "typical" dispersion data requirement.

At last, "additional" input variables, required by some models, include, among other descriptions of atmospheric turbulence (σ_ϑ and σ_φ, or vertical heat flux, or spatial and temporal variation of surface temperatures), the Richardson number R_i, it also related to stability classes.

3. Evaluation of diffusion categories.

As above said, our analysis refers to a "typical requirement" (Pasquill's turbulence type defined on the ground of temperature gradients) and an "additional" input variable (Richardson number).

Temperature and wind speed readings along the tower have been used to evaluate the Richardson number in the layers 120 - 100, 120 - 80, 120 - 40, 100 - 80, 100 - 40 and 80 - 40 m. A first general feature of air stability, as given by the Richardson criterium shown in fig. 1, is represented at any level by the large occurrence of neutral and near-neutral conditions, and the fairly low frequency of occurrence of unstable conditions, irrespectively of the layer considered. Going deep into the diagrams of fig. 1, shows that the largest frequencies of neutral conditions occur in the thinnest layers (120-100 and 100 - 80 m) and in the lowest one (80 - 40 m), while stable and unstable conditions are quite independent on both height and depth of layers. This last fact sounds a little strange, as stability should increase, as well as instability decrease, with increasing height in the surface layer; we have, however, to keep in mind the very weak circulation of air (average values of wind speed, are less than 3 m/s) in the Po valley, particularly in the first 150 m of the atmosphere, which could make not completely meaningful the definition of stability conditions through the Richardson number.

The diagrams of fig. 1 have been compared with the results of a climatological study of stability conditions distribution, carried out for the period jan. - oct. on a time basis of 8 years (from jan. 1966 to oct. 1973). This latter analysis gave us the bulk distribution, in the 120 - 40 m layer, of Pasquill's turbulence types obtained by reading the 10 min average lapse rate, along the meteorological tower, at synoptic hours (03, 06, 09, 12, 18, 24 h local time). Fig. 2 shows the distribution we obtained, from which it appears that the most probable condition for air at Trino is one of fairly stability, followed by neutral stability and, to a less extent, by strong stability. As in fig. 1, here also unstable conditions are extremely rare, and this could lead to think of a consequence of the fact that thermal gradients were not evaluated from ground level to 120 m, but from 40 to 120 m, for which a considerable fraction of lowest superadiabatic conditions have not been observed. However, if we refer to a previous analysis (Briatore et al, in press) we carried out on temperature differences measured from between 1, 5 and 120 m at the same location (fig. 3), we can conclude that there is no appreciable difference when stability conditions are evaluated higher up in the Po Valley.

As to the diurnal trend of atmospheric stability conditions, the hourly frequency distribution of Richardson number values is shown in fig. 4. From the trend of the distribution we can recognize well separated stationary and evolutive periods during the day, connected to the thermal cycle of heating and cooling of ground surface. After a strong transition from the highest negative values of Ri number in the afternoon (at 02 h p.m., local time), to the highest positive ones at midnight due to surface cooling, air stability keeps constant still 08 h a.m. (even local time). It is interesting to observe that the first period of ground surface heating from down to 10 h a.m. does not seem to have sensible influence on stability conditions, while from 10 h a.m. to 0.2 h p.m. convective motions start their actions and atmosphere gets its maximum unstable conditions. The above situation refers, we must remember it, to a ten - monthsperiod, during which the climatology of the site undergoes very large modifications.

As we did for the stability distribution frequencies, also the diurnal trend of Ri number has been compared with the trend of the above defined Pasquill's categories, evaluated at each synoptic hour, during an 8 years observation period, for the same months. Fig. 5(a) shows the time distribution of Pasquill's categories during 24 hours, while fig. 5 (b) shows a continuous line, obtained rather arbitrarily from the curves of (a), which should represent a qualitative trend of stability conditions to compare to the curve of Ri number previously shown. From such a qualitative point of view, there is a fairly good agreement between the two representations of the air stability diurnal course, even if the ratios between stable and unstable conditions are quite different.

Conclusions.

A critical review carried out on two atmospheric stability criteria, widely used as dispersion input data in most air pollution models, gave us the following results:

- the Pasquill's type of turbulence, evaluated from vertical temperature profiles between 20 and 120 m and relating to a ten months period (on a time basis of 8 years) yields prevailing stable conditions and a minimum of unstable situations
- the Richardson's type of turbulence, relating to the same ten months period (on a time basis of 1 year) yields prevailing neutral conditions, with a minimum of stable situations.
- the above results are confirmed by the diurnal trend of the two criteria. In fact, while similar on a qualitative point of view, thermal gradient classifications shows a stable-unstable conditions ratio which is opposite to that given by the Richardson's number classification.

We have not got, at this time, any reason to consider one of the two criteria most reliable than the other, also on account of the different sampling time (1 year's statistics against an 8 years' one); so, we are planning to carry out, in the future, diffusion experiments with lagrangian tracers in order to assess which of the two stability classifications is more correlated with actual dispersion conditions of the atmosphere.

Figure captions.

Fig. 1 - Richardson number distributions at different heights along the tower.

Fig. 2 - Distribution of Pasquill's stability categories in an 8 years climatology, evaluated on the basis of the lapse-rate.

Fig. 3 - Frequency distribution of the vertical temperature gradient along the tower. Dotted line refers to data belonging to the same class of wind speed and angular sector the wind is blowing from.

Fig. 4 - The hourly frequency distribution of the Richardson number in a six-months period (jan.-jun.)

Fig. 5 - (a) diurnal distribution of Pasquill's categories in the quoted ten months period and (b) the resultant mean diurnal trend of the stability conditions.

References.

- F.A. Gifford (1976) - Turbulent Diffusion-Typing Schemes: a Review - Nuclear Safety - vol. 17 - n. 1.
- R.C. Sklarew - J.C. Wilson (1976) - Air Quality Models - Required data characterization - /EC - 137 (Research Project 677 - 1) Final Report - Elctric Power Research Institute, Palo Alto, California.
- L. Santomauro (1972) - 3 th CCMS/NATO - Paris.

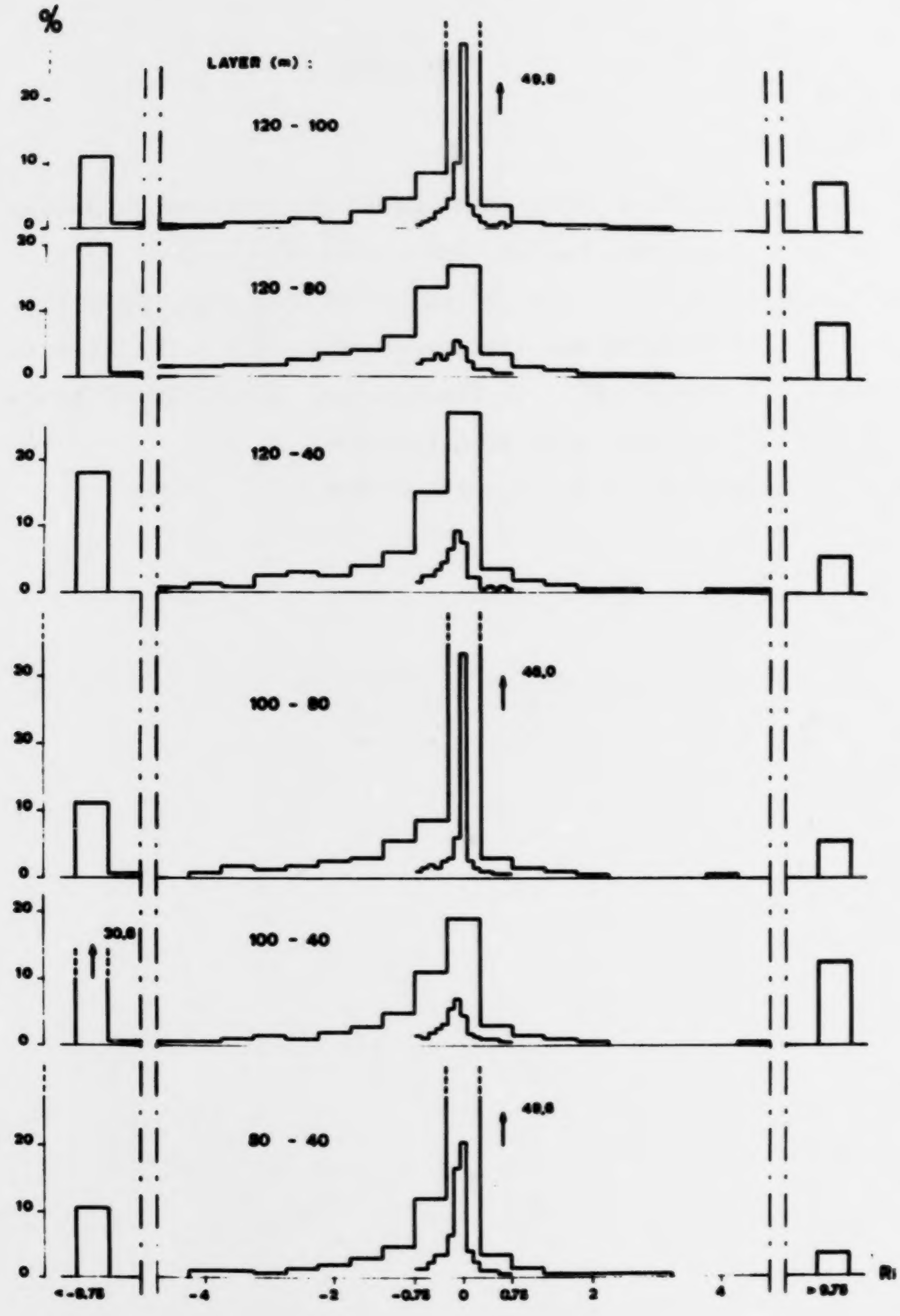
%
LAYER (m) :
120 - 100
49,8
120 - 80
120 -40
100 - 80
48,0
100 - 40
30,8
80 - 40
48,6
0
10
20
30
< -0,75
-4
-2
-0,75
0
0,75
2
4
> 0,75
Ri

Fig.1

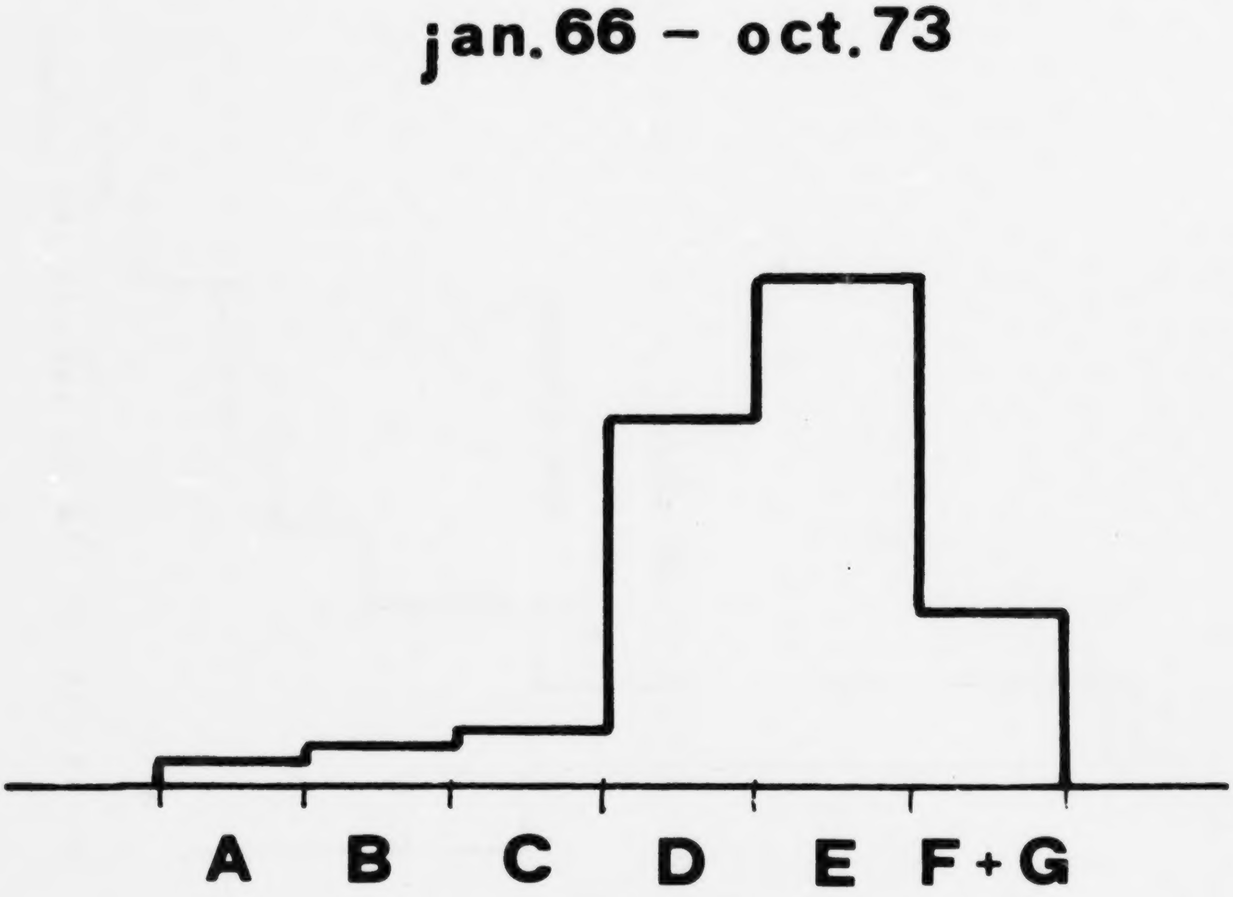

Fig.2

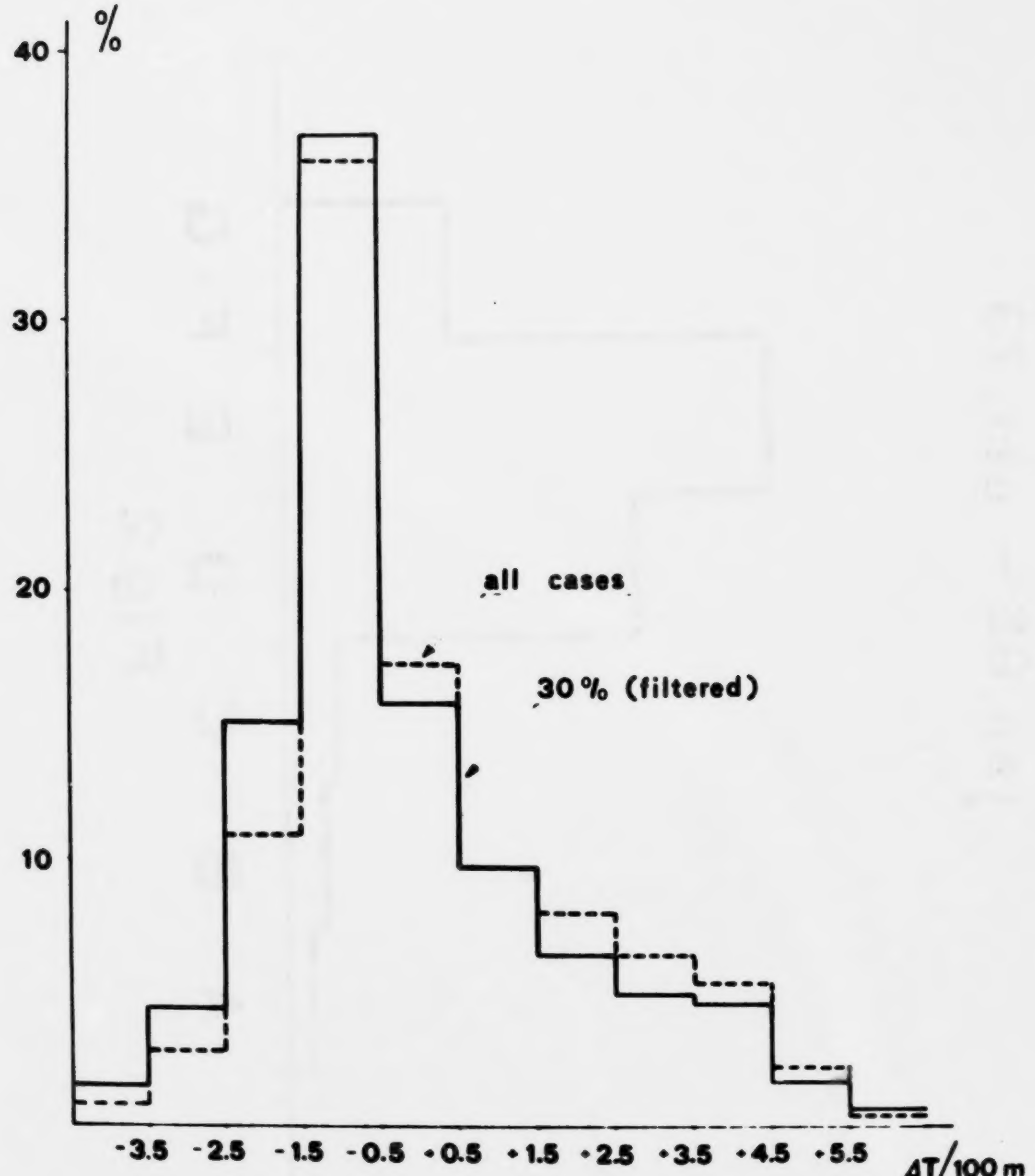
%
40
30
20
10
all cases
30 % (filtered)
-3.5
-2.5
-1.5
-0.5
+0.5
+1.5
+2.5
+3.5
+4.5
+5.5
ΔT/100 m

Fig.3

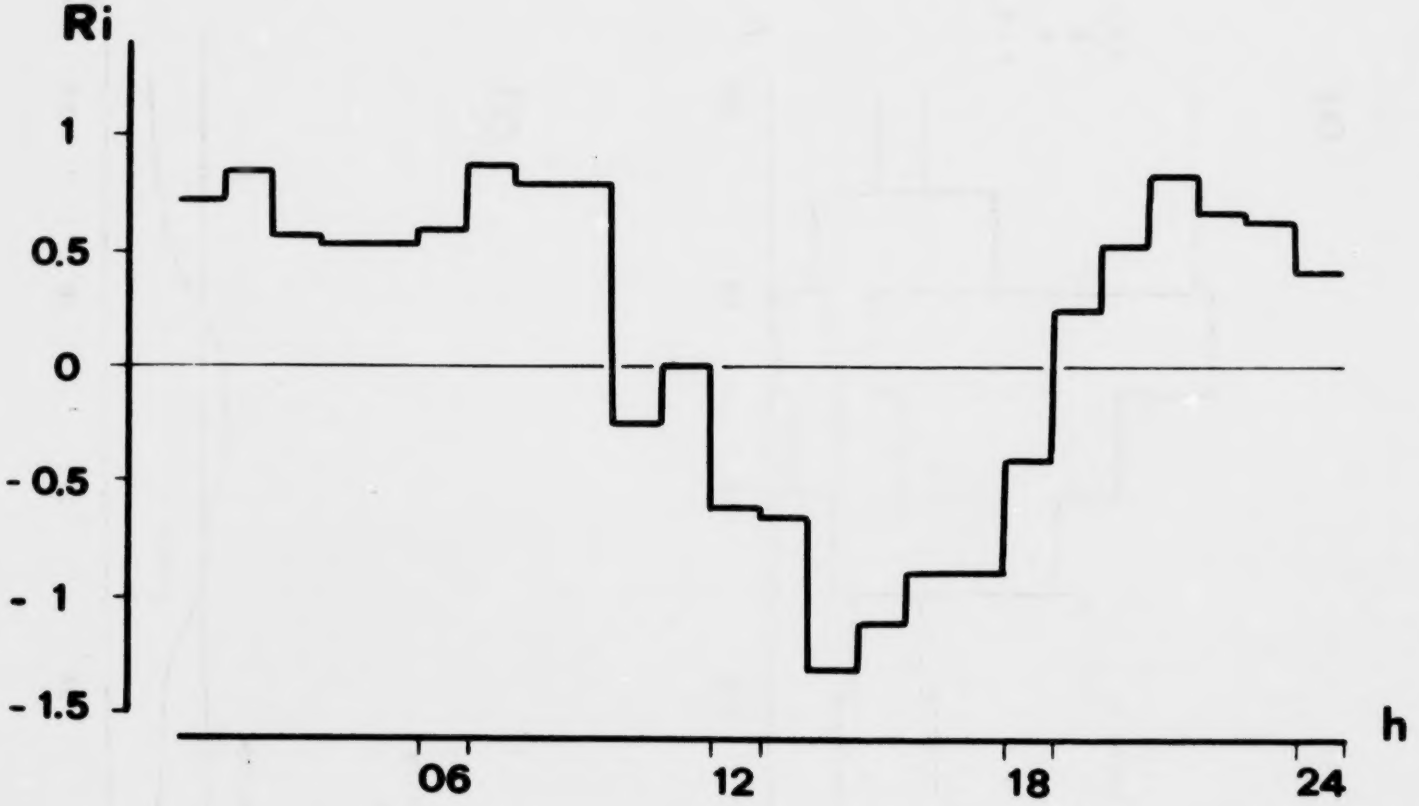

Fig. 4

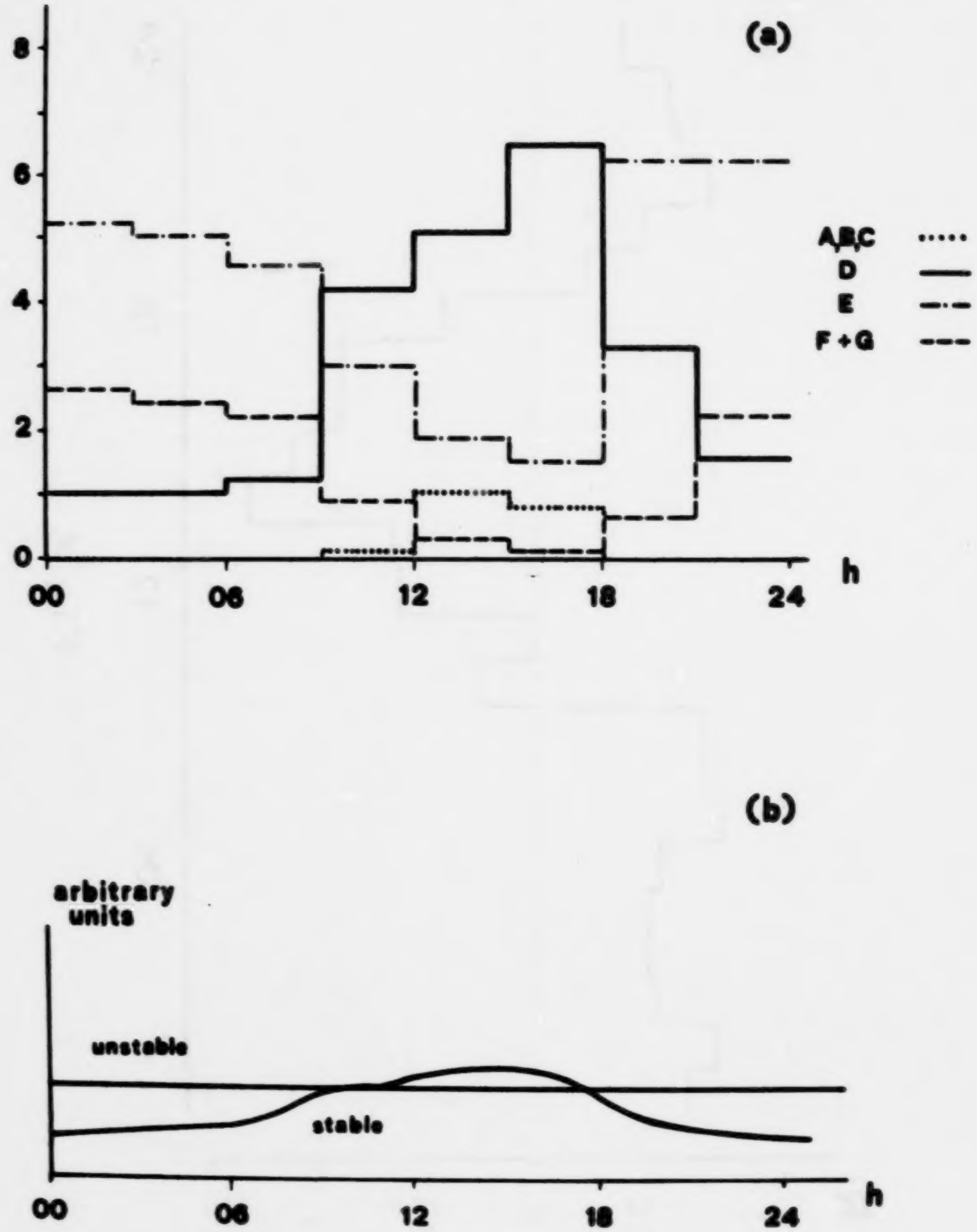
(a)
8
6
4
2
0
00
06
12
18
24
h
A,B,C
D
E
F + G
(b)
arbitrary units
unstable
stable
00
06
12
18
24
h

Fig. 5

8th International Technical Meeting on
Air Pollution Modeling and its Applications
NATO/CCMS

NEW TECHNICS OF ESTIMATION
OF DISPERSION COEFFICIENTS
- GENERALIZATION OF THE DIFFUSIVITY CONCEPT -

SAAB A. - GRANIER J.P.
Direction des Etudes et Recherches
ELECTRICITE DE FRANCE

Septembre 20-23 . 1977
LOUVAIN-LA-NEUVE
BELGIUM

NEW TECHNICS OF ESTIMATION OF DISPERSION COEFFICIENTS: GENERALIZATION OF THE DIFFUSIVITY CONCEPT

INTRODUCTION

In the light of recent works using the "second order closure modeling" to calculate atmospheric turbulent flows, we have followed PASQUILL's recommandations in order to give a better quantitative estimation of crosswind and vertical spread from an elevated source especially in extreme stabilities where the effects of vertical wind shear, turning of the horizontal wind components and buoyancy are predominant (which leads to different intensity and length or time scales).

Keeping in mind the conceptual validity of gradient transport model -even for the 2nd order closure modeling as discussed by CORRSIN and LUMLEY- an attempt for specifying the eddy diffusivity dependence on measurable properties of the turbulent flow is developped using a tensorial form of diffusion coefficient which can be derived from turbulence theory.

Thus a three-dimensional numerical model is developped using this tensorial form for diffusivity which is more reliable than a scalar form. The results of the model are presented for 4 typical conditions in the atmospheric boundary layer : unstable, neutral, strong wind and stable. Comparisons made with TESKE and LEWELLEN's calculations of atmospheric dispersion (using second order closure modeling) show good agreement for the following applications : variation of the ground level concentration for different stack heights ; lateral and vertical concentration contours for different stack heights.

SECOND ORDER CLOSURE MODELING

As you know, the starting point is the definition of a closure for the flux of species $\overline{u_i'c'}$ to solve the mass continuity equation which is described in a turbulent field by means of :

$$\frac{\partial \overline{C}}{\partial t} + \overline{U_i}\,\frac{\partial \overline{C}}{\partial x_i} = -\frac{\partial}{\partial x_i}\,(\overline{u'_i c'}) + D\,\frac{\partial^2 \overline{C}}{\partial x_i^2} + S$$

where $\overline{C}$, $\overline{U_i}$ are the mean values of concentration and velocity ; c', u'_i are the turbulent fluctuations ; D, the molecular diffusivity ; S, a source term.

Rather then closing the system with a gradient approach (mixing length hypothesis), we generate an exact equation for the species flux $\overline{u'_i c'}$:

$$\begin{aligned}\frac{\partial \overline{u'_i c'}}{\partial t} + \overline{U_j}\,\frac{\partial \overline{u'_i c'}}{\partial x_j} = &- \overline{u'_i u'_j}\,\frac{\partial \overline{C}}{\partial x_j} - \overline{u'_j c'}\,\frac{\partial \overline{U_i}}{\partial x_j} \\ &+ \frac{g_i}{\theta_o}\,\overline{c'\theta'} - \frac{\partial}{\partial x_j}\,\overline{u'_i u'_j c'} \\ &- \overline{\frac{c'}{\rho_o}\,\frac{\partial p'}{\partial x_i}} - D\,\overline{\frac{\partial u_i}{\partial x_j}\,\frac{\partial c'}{\partial x_j}}\end{aligned}$$

This equation which is similar to the transport equation of heat is undetermined because of the introduction of unknown quantities : third order correlations, pressure and temperature correlations, dissipation terms.

The problem is reduced then to specify these unknown quantities by means of additional equations or closure modeling which must be limited to the explicit variables of the system (mean values and second order moment) and the characteristic length scales. The modeling must respect the properties of dimensional homogeneity, tensor invariance and symetry.

The full description has been set out in general notation by DONALDSON and LUMLEY, and a simplified formulation may be written as :

- Pressure correlations

$$\overline{\frac{c'}{\rho_o}\,\frac{\partial p'}{\partial x_i}} = \frac{1}{\rho_o}\,\frac{\partial}{\partial x_i}\,\overline{c'p'} - \overline{\frac{p'}{\rho_o}\,\frac{\partial c'}{\partial x_i}}$$

where $$\overline{\frac{p'}{\rho_o}\,\frac{\partial c'}{\partial x_i}} = \gamma_1\,\overline{u'_i c'} + \gamma_2\,\frac{g_i}{\theta_o}\,\overline{c'\theta'}$$

$\frac{1}{\rho_o}\,\frac{\partial \overline{c'p'}}{\partial x_i}$: diffusion term

- Third order correlation

$$\frac{\partial}{\partial x_j}\overline{u'_i u'_j c'} + \frac{1}{\rho_o}\frac{\partial}{\partial x_j}\overline{c'p'} = \alpha \frac{\partial}{\partial x_j} \beta \frac{\partial \overline{u'_j c'}}{\partial x_j}$$

- Dissipation terms : the isotropic hypothesis for the small scale dissipative eddies allows to link this term to the dissipation rate ε.

The species flux equation is written then :

$$\frac{\partial}{\partial t}\overline{u'_i c'} + \overline{U_j}\frac{\partial \overline{u'_i c'}}{\partial x_j} = - \overline{u'_i u'_j}\frac{\partial \overline{C}}{\partial x_j} - \overline{u'_j c'}\frac{\partial \overline{U_i}}{\partial x_j}$$

$$+ (1-\gamma_2)\frac{g_i}{\theta_o}\overline{c'\theta'} + \alpha \frac{\partial}{\partial x_j} \beta \frac{\partial \overline{u'_i c'}}{\partial x_j} - \gamma_1 \overline{u'_i c'}$$

To close the system, we generate a similar equation for $\overline{c'\theta'}$

$$\frac{\partial}{\partial t}\overline{c'\theta'} + \overline{U_j}\frac{\partial \overline{c'\theta'}}{\partial x_j} = - \overline{u'_j\theta'}\frac{\partial \overline{C}}{\partial x_j} - \overline{u'_j c'}\frac{\partial \theta_i}{\partial x_j}$$

$$+ \alpha \frac{\partial}{\partial x_j} \beta \frac{\partial \overline{c'\theta'}}{\partial x_j} - \gamma_3 \overline{c'\theta'}$$

The parameters α, β, γ_1, γ_2 and γ_3 introduced in the closure modeling provide the correct dimensionality by means of characteristic length, time and kinetic energy of scales.

In our applications, it is realistic to specify analytically the length scales (referring to the plume dimension and to the height of mixing) and to generate an equation for the turbulent kinetic energy to take into account the spatial and temporal variations of dynamic and thermal structure of atmospheric turbulence (Fig. 1) :

$$\frac{1}{2}\left[\frac{\partial q^2}{\partial t} - \frac{\partial}{\partial x_j}\left(\frac{5}{3}\Lambda q \frac{\partial q^2}{\partial x_j}\right)\right] = - \overline{u'_i u'_j}\frac{\partial \overline{U_i}}{\partial x_j} + \beta g \overline{u'_j\theta'} - \frac{q^3}{\Lambda}$$

where Λ is a length scale.

GENERALIZATION OF THE DIFFUSIVITY CONCEPT

The above system may be reduced to a set of algebraic equations if we assume the following hypothesis :

- quasi-equilibrium approximations where the advective and diffusive terms can be neglected in the second order equations ;
- horizontal homogeneity

$$\overline{u_i'c'} = -\frac{1}{\gamma_1}\left(\overline{u_i'u_j'}\,\frac{\partial\overline{C}}{\partial x_j} + \overline{u_3'c'}\,\frac{\partial\overline{U_i}}{\partial x_3}\right)$$

$$\overline{u_3'c'} = -\frac{1}{\gamma_1}\,(\overline{u_3'u_j'}\,\frac{\partial\overline{C}}{\partial x_j} - \frac{g}{\theta_o}\,(1-\gamma_2)\,\overline{c'\theta'})$$

$$\overline{c'\theta'} = -\frac{1}{\gamma_3}\left(\overline{u_j'\theta'}\,\frac{\partial\overline{C}}{\partial x_j} + \overline{u_3'c'}\,\frac{\partial\theta_3}{\partial x_j}\right)$$

Using the tensorial form for diffusivity which is more reliable than a scalar form $\overline{u_i'c'} = -K_{ij}\,\frac{\partial\overline{C}}{\partial x_j}$, we can express the components of the tensor diffusivity

$$K_{ij} = A_1\left(\overline{u_i'u_j'} - K_{3j}\,\frac{\partial\overline{U_i}}{\partial x_3}\right) \qquad i = 1,2$$

$$K_{3j} = A_2\,(\overline{u_3'u_j'} + B_2\,\overline{u_j'\theta'})$$

The tensor components are then expressed in terms of quantities determined by the properties of the atmospheric boundary layer : the gradients of the mean wind components and temperature, the turbulent covariances of velocity components and temperature, and the characteristic scales of the atmospheric turbulence.

All of the turbulent covariance terms are obtained from a similar reduction to an algebraic system of the 10 differential equations for $\overline{u_i'u_j'}$, $\overline{u_i'\theta'}$ and $\overline{\theta'^2}$. These may be described in terms of the turbulent kinetic energy, the gradients of mean flow quantities, the gradient RICHARDSON number and the time or length scales. The spatial and temporal evolution of the kinetic energy allows to extend the validity of this approximation, referring to the correlations between the turbulent covariance terms and the kinetic energy.

It is clear that this approximation will be unsuitable under special conditions such as strong spatial variations in the turbulence field or fast thermal evolution when a quasi-equilibrium state is not respected.

APPLICATIONS

Our purpose is to test the sensitivity of the three dimensional numerical model to the variation of a few meteorological parameters describing different dynamic and thermal structure of the atmospheric boundary layer : MONIN length scale L, friction velocity U_*, convective velocity scale W_*, surface heat flux H, effective surface roughness z_0, RICHARDSON number R_i, ROSSBY number R_0, height of mixing layer z_i.

Assuming a kinetic energy profile and an analytical formulation of length scales, the procedure consists of describing in terms of altitude z, successively :

- profiles of mean wind components and temperature,
- the turbulent covariances using the quasi-equilibrium approximation,
- the diffusivity tensor components,
- and then the solving of a three dimensional numerical equation of mass continuity for a steady turbulent flow using finite difference techniques :

$$\overline{U_i} \frac{\partial \overline{C}}{\partial x_i} = - \frac{\partial}{\partial x_i} \left(K_{ij} \frac{\partial \overline{C}}{\partial x_j} \right) + S$$

  where we neglect the molecular diffusion, and the along-axis diffusion term.

A CRANK-NICHOLSON discretization in x directions (time-like) and a divergence form discretization in y, z directions are used.

The numerical procedure consists -rather than operating directly on this parabolic partial differential equation- of a set of blocks formed by a three-dimensional grid network. The program allows to compute the properties of a volume of fluid located at one point i+1,j,k from the previous point i,j,k using the mass continuity equation.

The discretized systems are solvable by the method of successive over-relaxation by blocks.

We summarize in the following table the main parameters selected for four typical stability conditions that we use to apply the model : "q_{max}" is the maximum of the kinetic energy profile, "H" is the surface heat flux, "$\partial\theta/\partial z$" is the gradient of mean potential temperature, "U_G" the geostrophic wind.

	UNSTABLE	NEUTRAL	STRONG WIND	STABLE
$1/L (m^{-1})$	< -0.17	~ 0	~ 0	> 0.016
$\partial\theta/\partial z$ (°C/m)	-1×10^{-3}	0	0.50×10^{-3}	1×10^{-3}
$H (mW/m^2)$	~ 200	~ 10	~ 0	-20
q_{max}/u_*	6.2	3.4	2.2	< 2
U_∞ (m/s)	5	8	12	10

$z_o = 15$ cm, $z_i = 1\ 000$ m, $\theta_o = 290°$

Figures 2, 3, 4 show the profiles of horizontal mean wind and K_{yy}, K_{zz} diffusivities obtained for the 4 stabilities : the vertical diffusivity is denoted by a maximum and then a slow decrease in the upper layer for neutral and stable cases, whereas K_{zz} is still increasing in unstable case. The horizontal diffusivities increase and reach a limit value in the upper part, which is in accordance with the influence of horizontal dispersion in terms of distance from an elevated source.

Figures 5, 6, 7, 8 show the profiles of K_{yy}, K_{yz}, K_{zy} and K_{zz} for the four stability classes. The off-diagonal terms of tensor diffusivity may be negative for certain values of wind shear and having comparable values to the diagonal terms.

Figure 9 represente the kinetic energy profiles calculated by the model which are in accordance with the input values referring to the solution of kinetic energy evolution equation.

To illustrate the applications of the numerical model, figures 10 and 11 give the distributions of normalized ground concentrations as a function of distance downwind for the three heights (50, 100, 200 m) of an elevated point source and for neutral and unstable cases. The empirical form expressing the decrease of maximum ground concentration as a function of height using a power law $H^{-\alpha}$ gives for α a value varying from 2.15 to 2.3 in neutrale case, and from 1.7 to 1.9 in unstable case. This result is in accordance with TESKE and LEWELLEN's calculations using the 2nd order closure modeling.

Figures 12, 13, 14, 15 give the concentration contours in the planes x.y and x.z for neutral and unstable cases.

The effect of convecting the plume in the direction of wind shear is increased with the height of emission. The model is not yet improved for the free convection situation where the maximum concentrations could increase above the height of emission (DEARDORFF's laboratory measurement), and we don't think that it will be appropriate in counter-gradient situations.

CONCLUSIONS

The solving of a general three-dimensional diffusion equation using a tensorial form of diffusion coefficient which can be derived from turbulence theory seems to give useful results. Through this technique we are able to derive estimations of atmospheric dispersion, with a good degree of accuracy, for a variety of situations and diffusion problems.

REFERENCES

BRIGGS (1975) - Plume Rise Predictions. Workshop on Meteorology and Environmental Assessment. Boston.

CORRSIN (1974) - Limitation of Gradient Transport Models in Turbulence. Adv. in Geophysics vol. 18 A.

DEARDORFF, WILLIS (1975) - A Parametrization of Diffusion into the Mixed Layer. Journal of App. Meteo. vol. 14, p. 1451-1458.

DONALDSON (1972) - Construction of a Dynamic Model of the Production of Atmospheric Turbulence and the Dispersion of Pollutants. Workshop in Micrometeorology. Boston.

FAVRE et al. (1976) - La Turbulence en Mécanique des Fluides. Gauthier-Villars.

FORTIER (1975) - Transfert de Chaleur et de Masse. Masson.

LUMLEY, TENNEKES (1973) - A First Course in Turbulence. M.I.T. Press.

MATHIEU (1972) - Remarks on Turbulent Flows. V.R.I. for Fluid Dynamics, LS 36 Rhode Saint-Genèse, Belgique.

MERY, DENIAU (1972) : Les Moyens d'Estimation de la Dispersion des Pollutants à l'aval des Cheminées Industrielles. E.D.F. Bull. D.E.R. série A.3.

NGUYEN VAN CHI, SAAB (1976) - A Three-Dimension Numerical Model of Atmospheric Diffusion. 3rd Symposium of Atmospheric Turbulence. Raleigh, N.C.

PASQUILL (1974) - Atmospheric Diffusion. 2nd edition, John Wiley & Sons.

SAAB, ROLIN (1977) - Développement d'un Modèle Turbulent de Diffusion. Généralisation du concept de diffusivité. Rapport E.D.F. (à paraître).

SAAB et al. (1975) - Some Features of Turbulent Diffusion Process resulting from Experimental Field Tests NATO/CCMS Int. Meeting, Frankfurt.

SPALDING, LAUNDER (1972) - Mathematical Models of Turbulence. Academic Press New-York et Londres.

TESKE, LEWELLEN (1976) ; Example Calculations of Atmospheric Dispersion using 2nd Order Closure Modelling. 3rd Symposium of Atmospheric Turbulence. Raleigh, N.C.

YAMADA, MELLOR (1975) - A Simulation of the Wangara Atmospheric Boundary Layer Data, J. Atm. Sci. 32, 2309-2329.

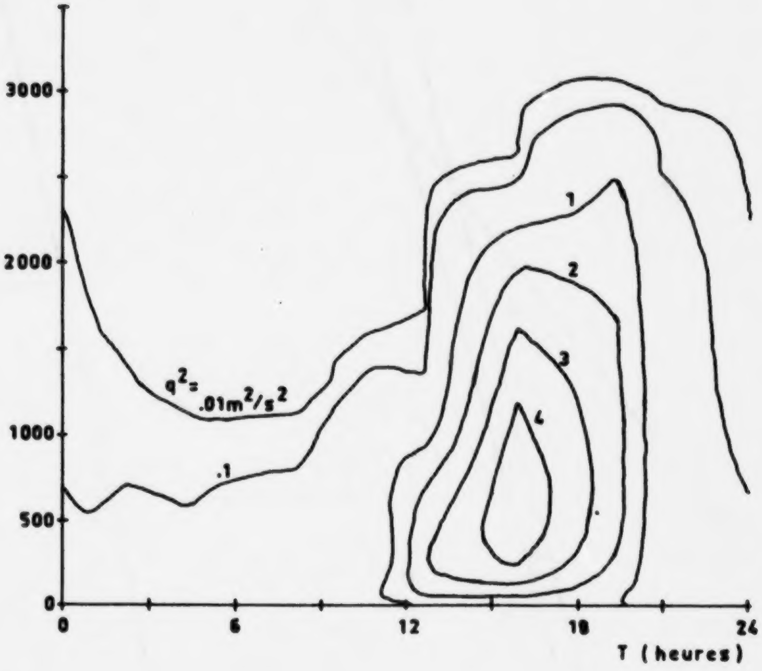

Fig.1: Diurnal variations of the turbulent kinetic energy q^2. (After LEWELLEN and TESKE)

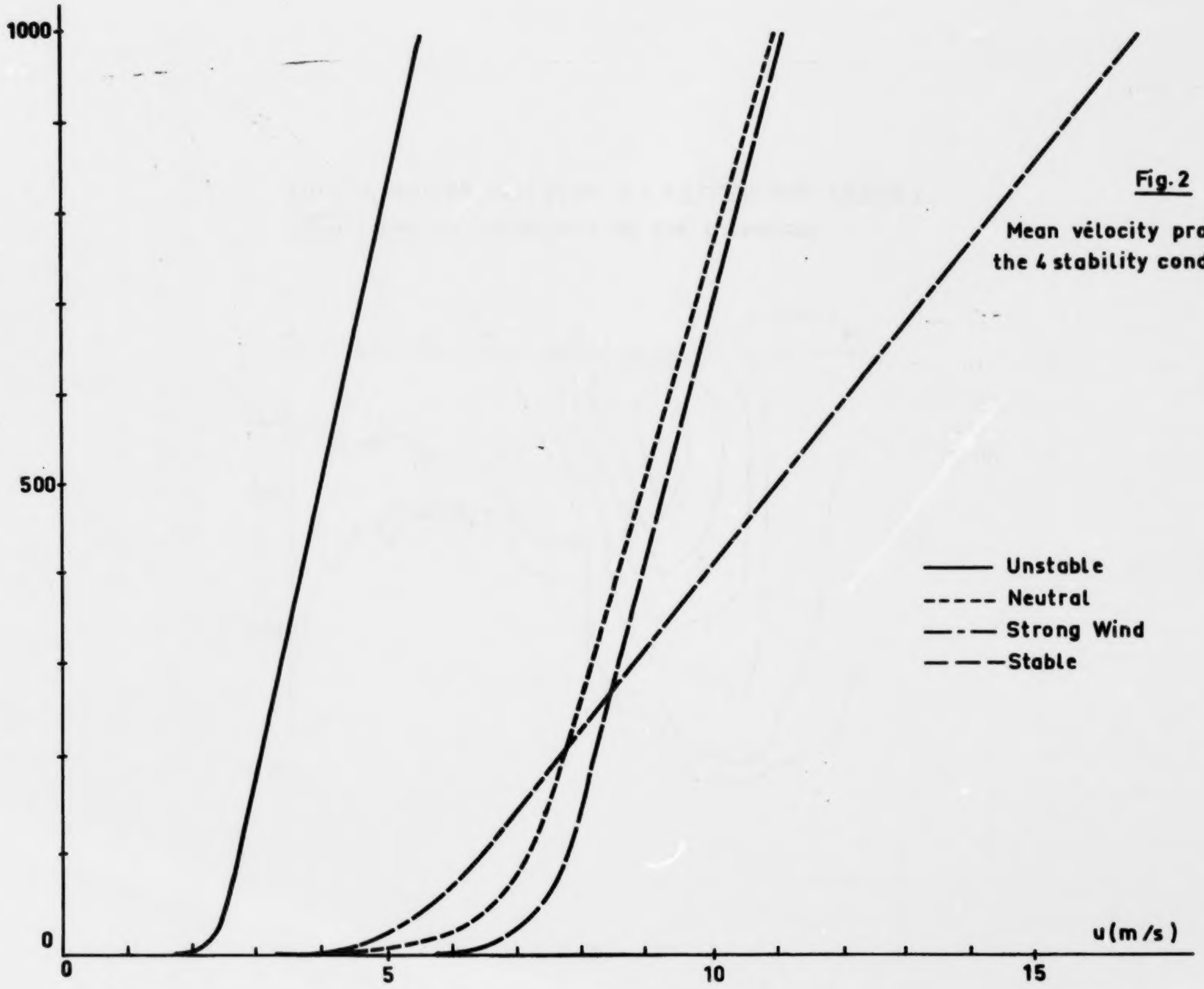

Fig. 2

Mean vélocity profiles for the 4 stability conditions

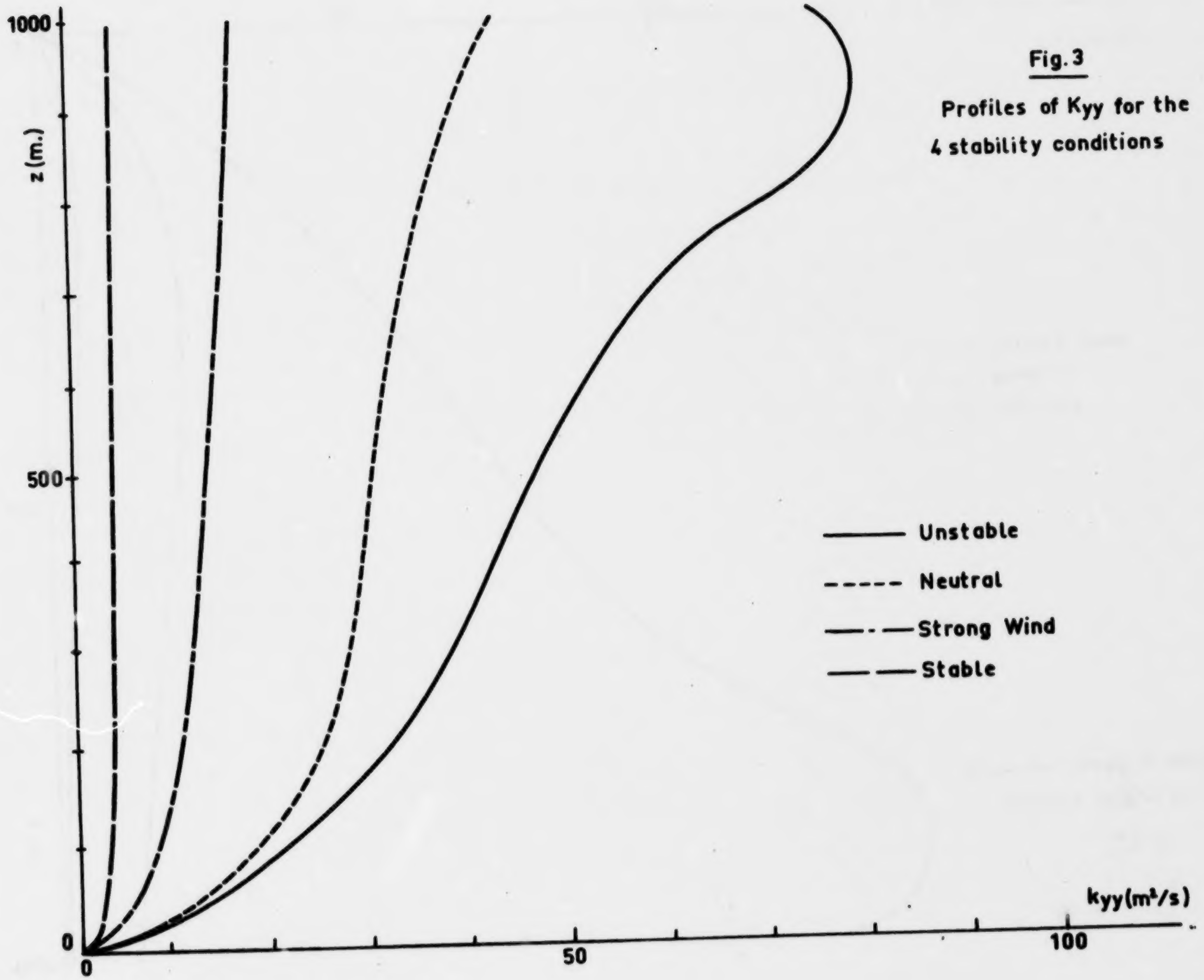

Fig. 3

Profiles of Kyy for the 4 stability conditions

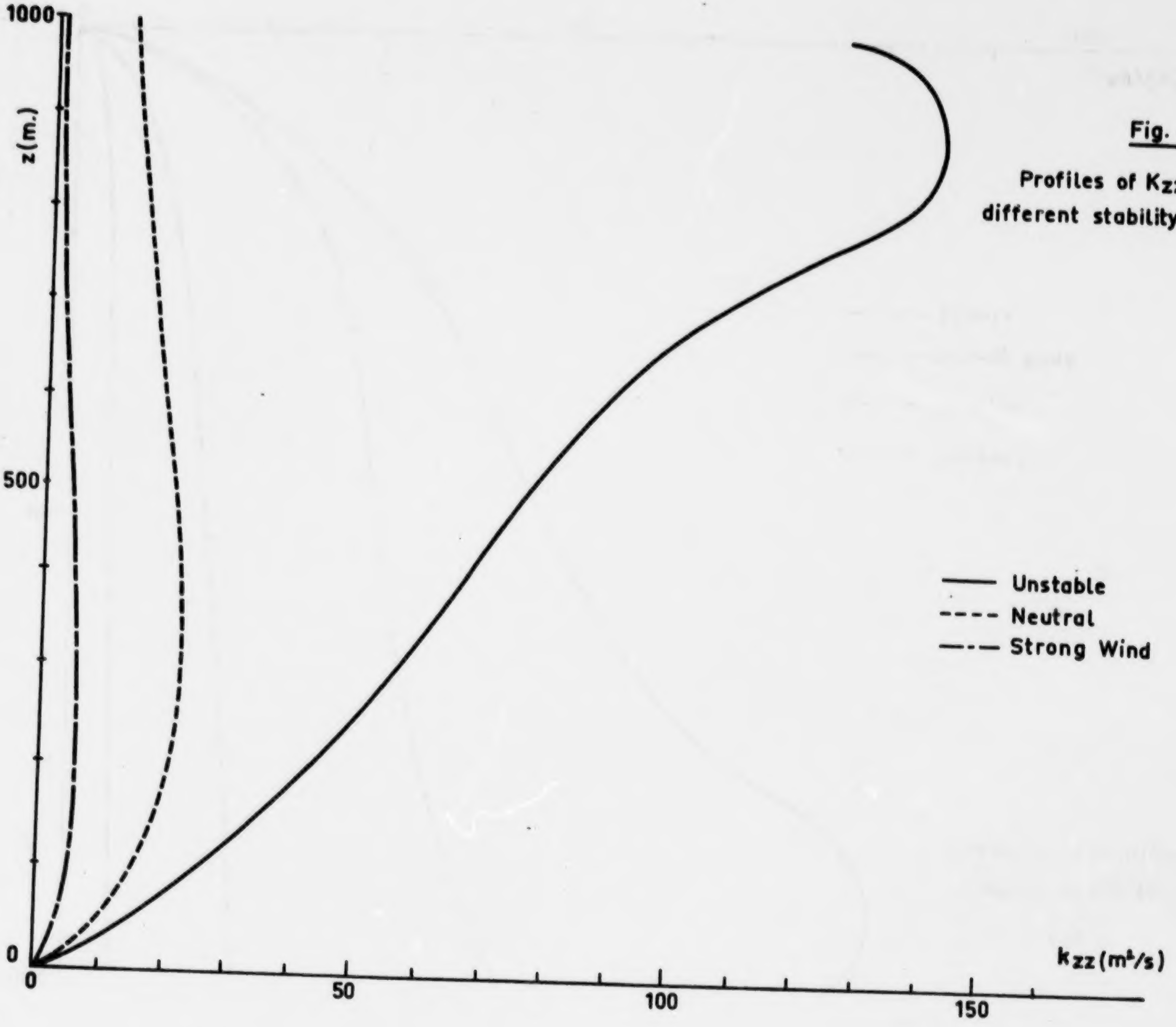

Fig. 4

Profiles of Kzz for the different stability conditions

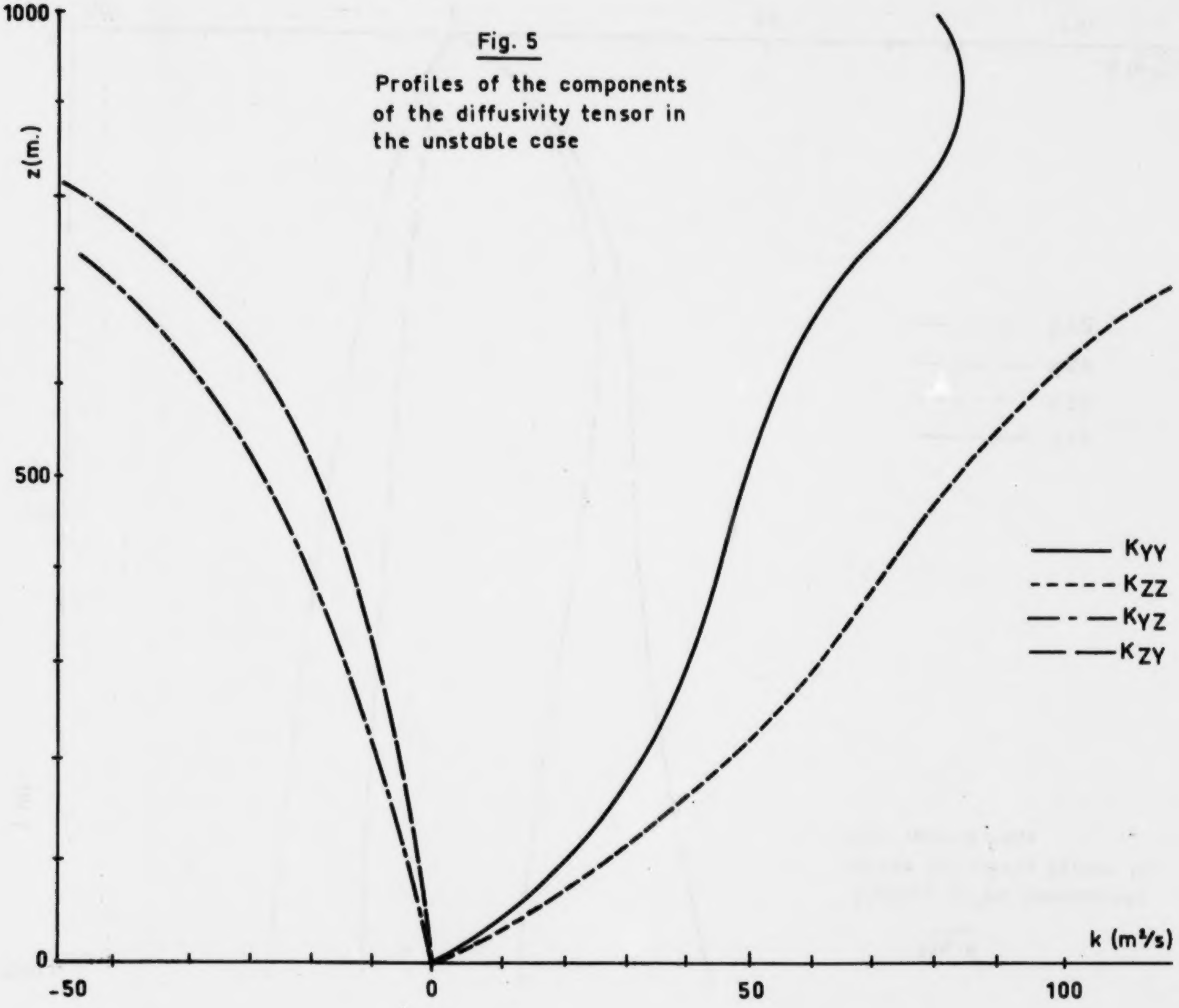

Fig. 5

Profiles of the components of the diffusivity tensor in the unstable case

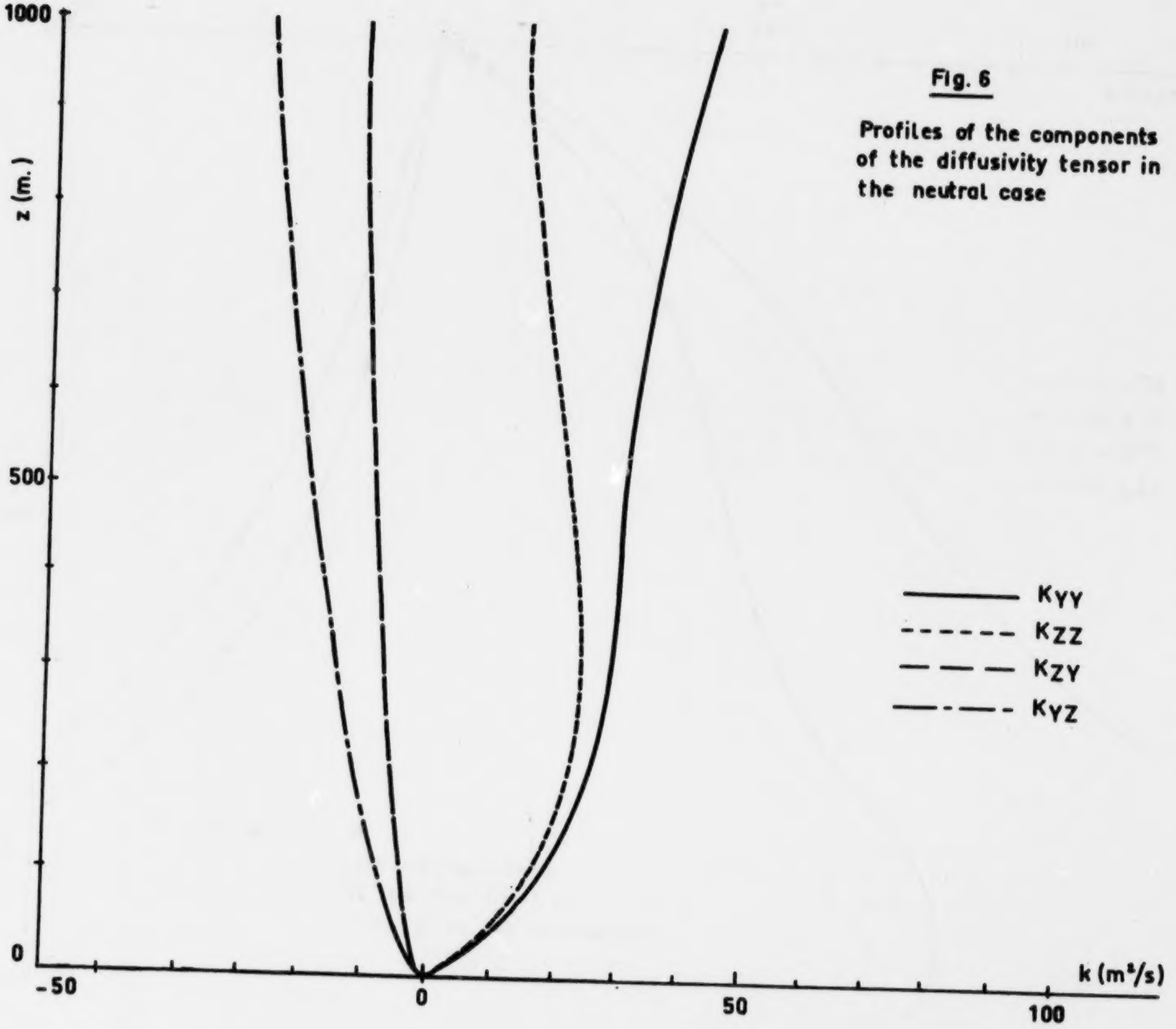

Fig. 6

Profiles of the components of the diffusivity tensor in the neutral case

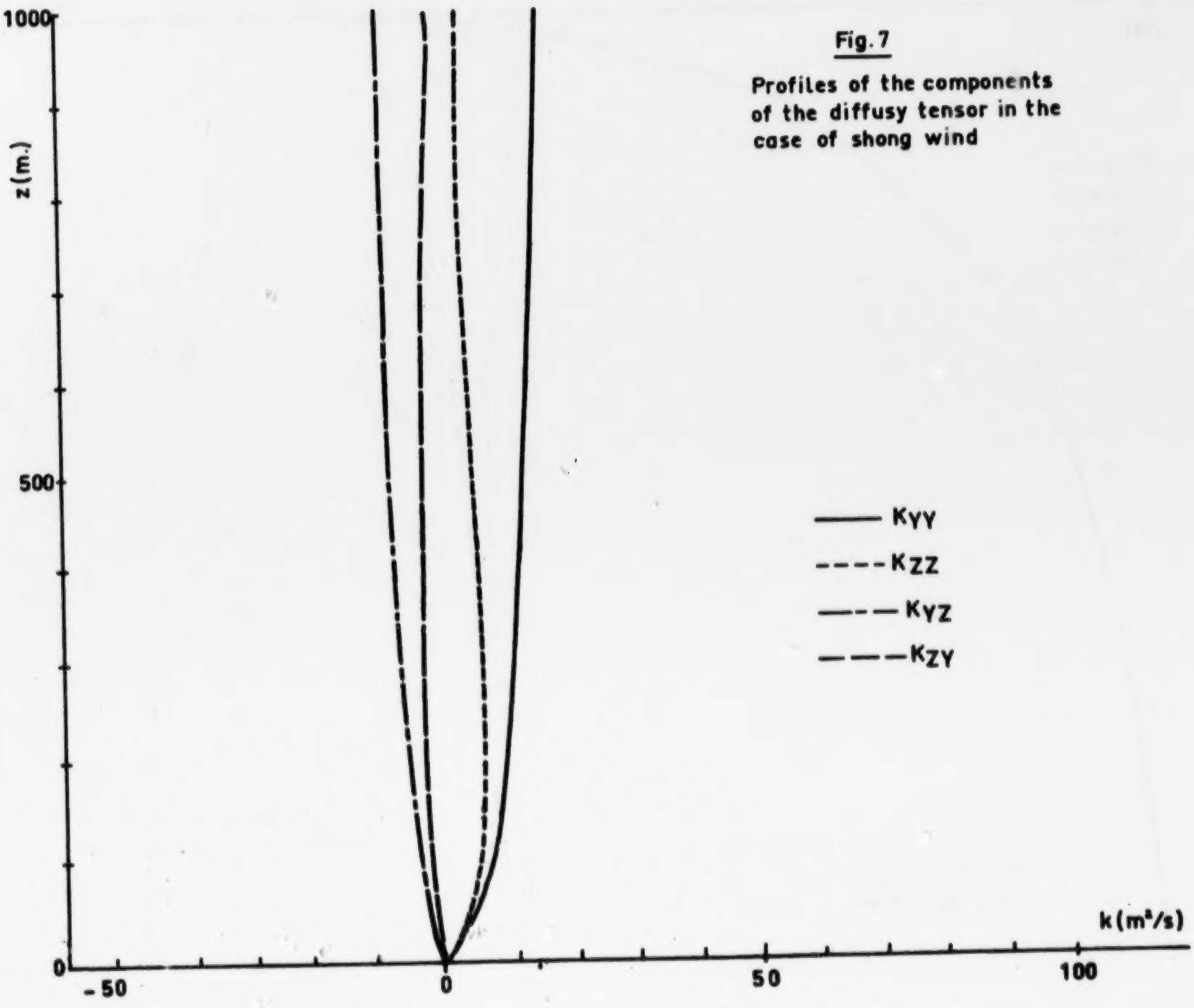

Fig. 7

Profiles of the components of the diffusy tensor in the case of shong wind

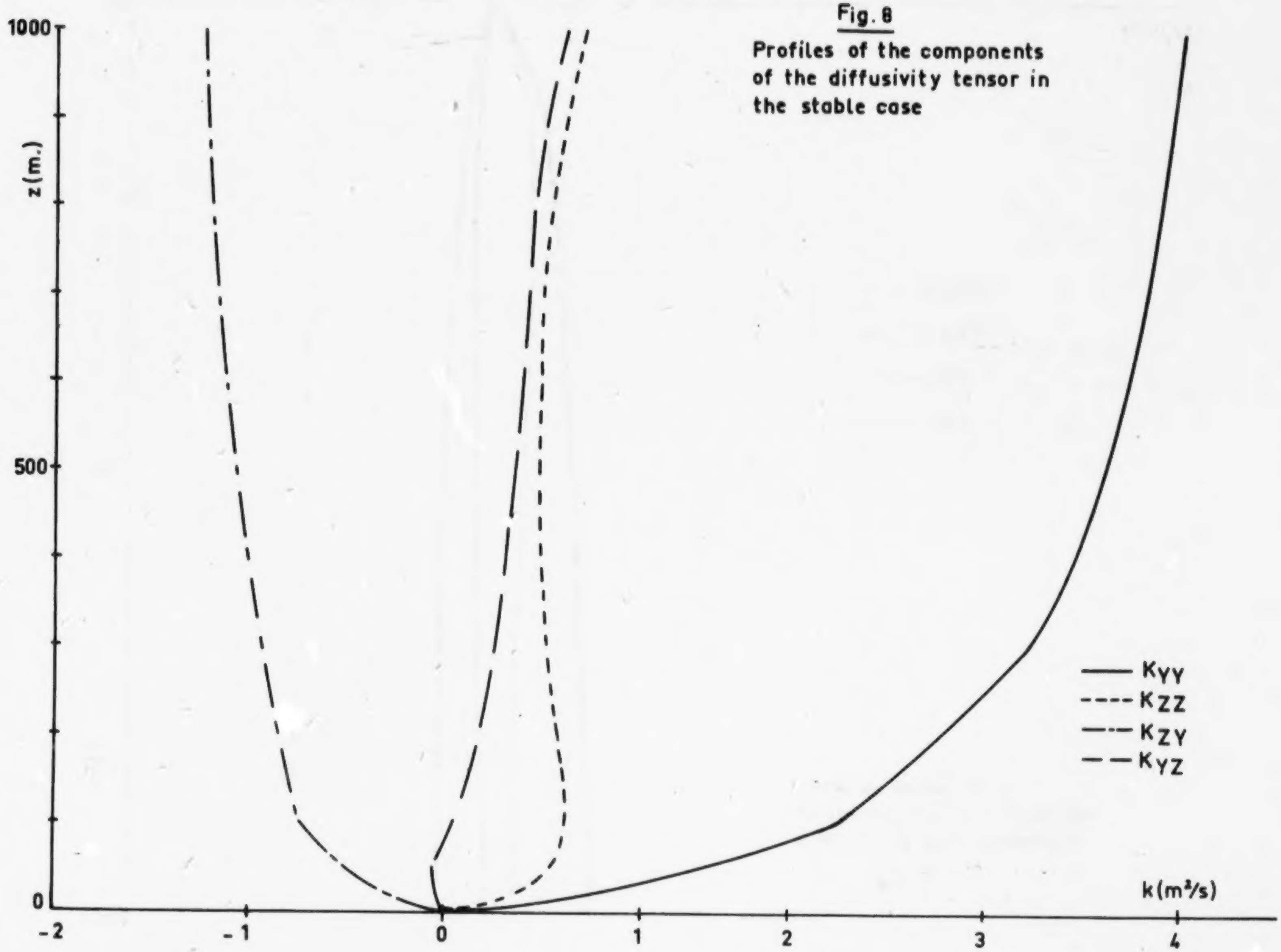

Fig. 8

Profiles of the components of the diffusivity tensor in the stable case

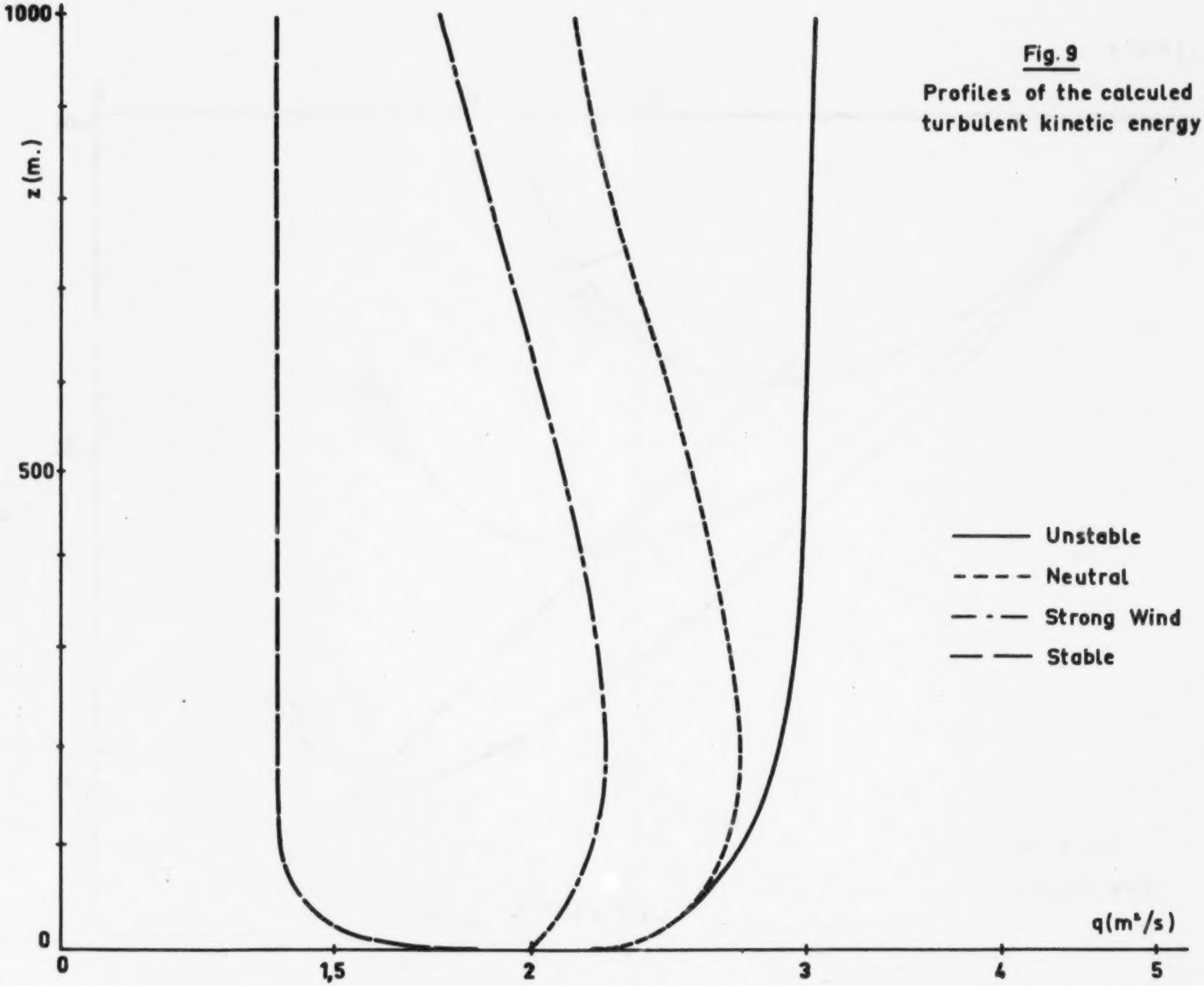

Fig. 9

Profiles of the calculed turbulent kinetic energy

Fig.10

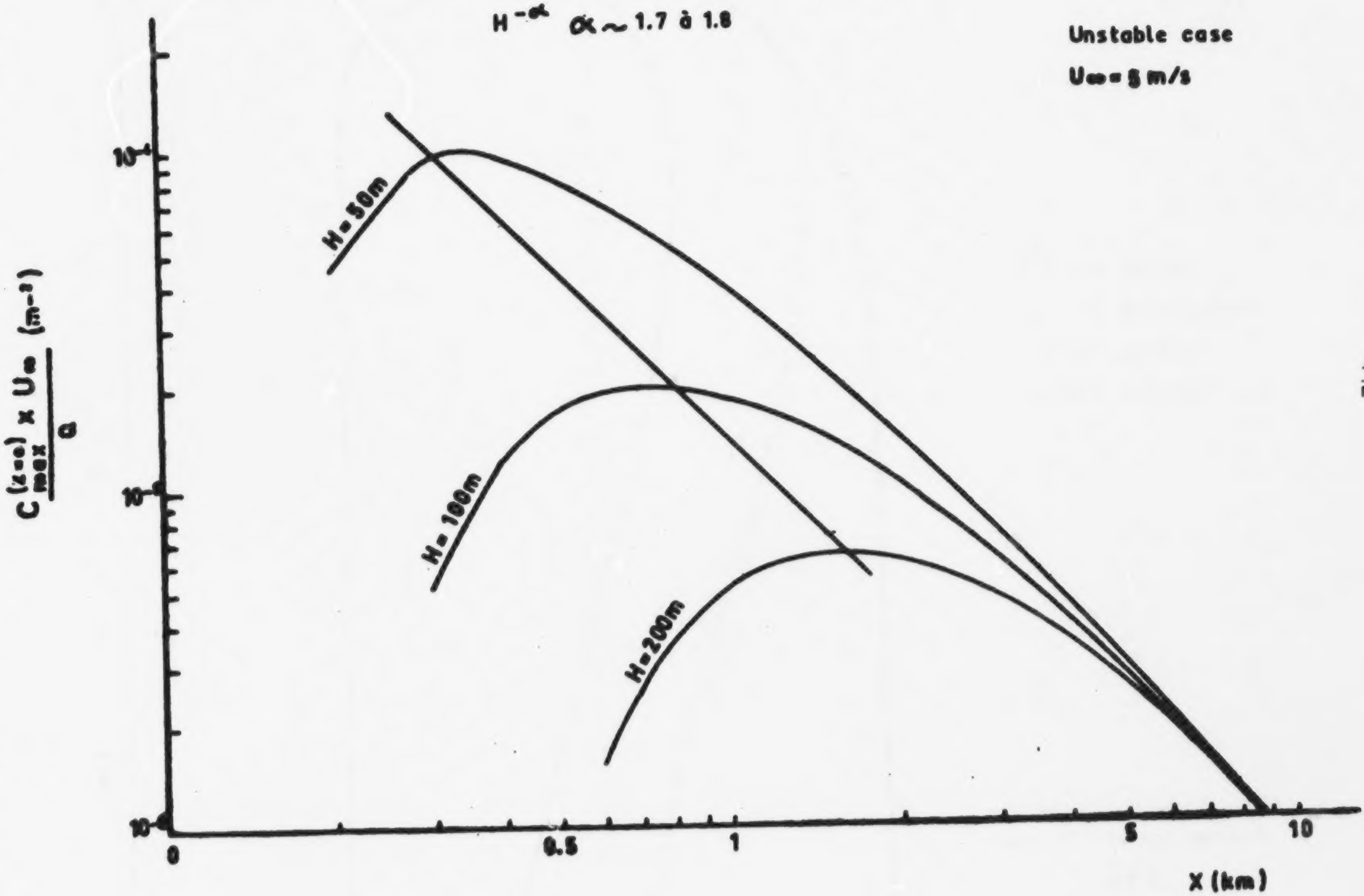
$H^{-\alpha}$ $\alpha \sim 1.7$ à 1.8
Unstable case
$U_\infty = 5$ m/s
$\frac{C_{max}^{(z=0)} \times U_\infty}{Q}$ (m^{-2})
10^{-4}
10^{-5}
10^{-6}
0
0.5
1
5
10
X (km)
H=50m
H=100m
H=200m

Fig. 11

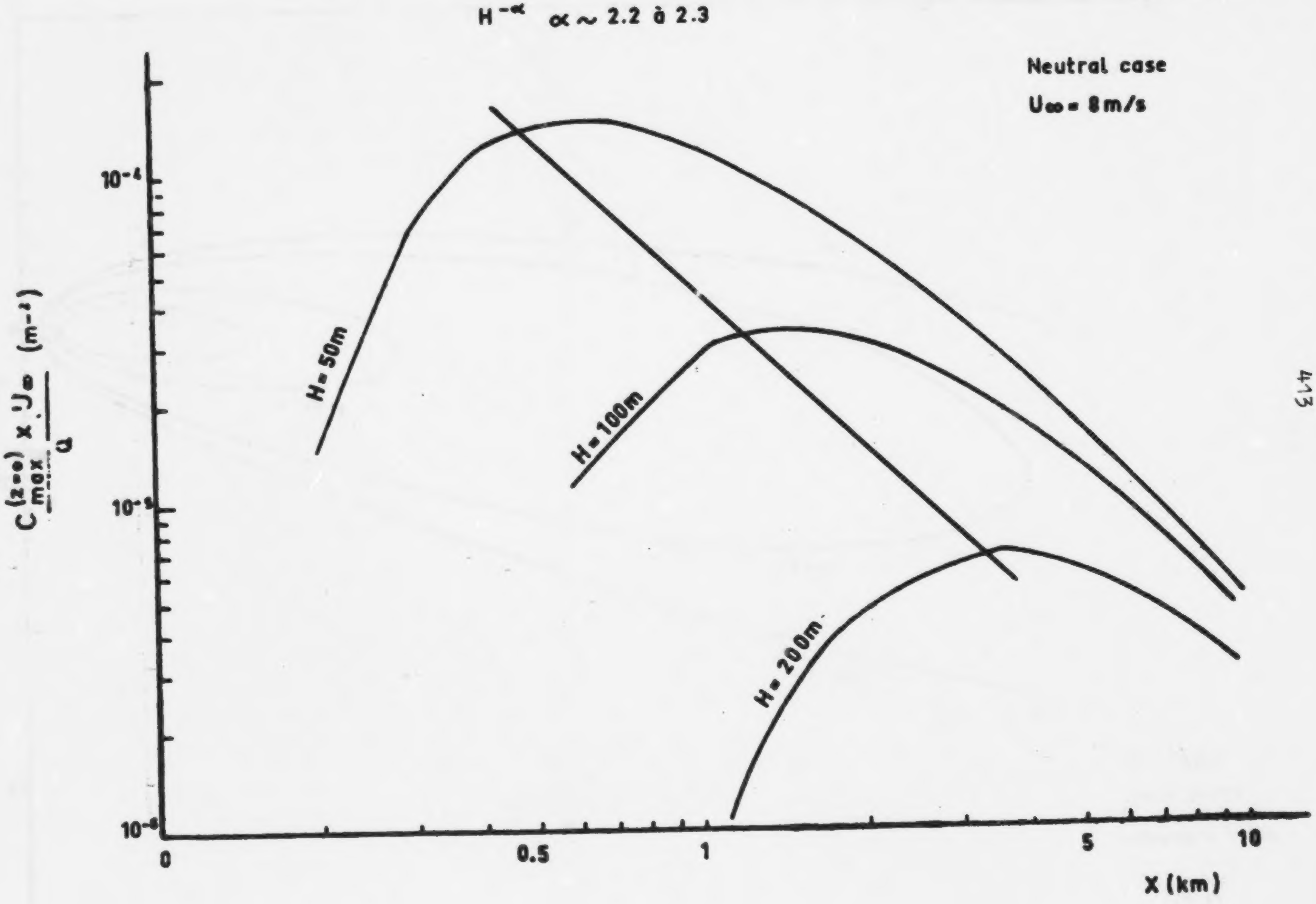
$H^{-\alpha}$ $\alpha \sim 2.2$ à 2.3
Neutral case
$U_\infty = 8 m/s$
$\frac{C_{max}^{(z=0)} \, x \, U_\infty}{Q}$ (m^{-2})
10^{-4}
10^{-5}
10^{-6}
0
0.5
1
5
10
X (km)
H = 50m
H = 100m
H = 200m

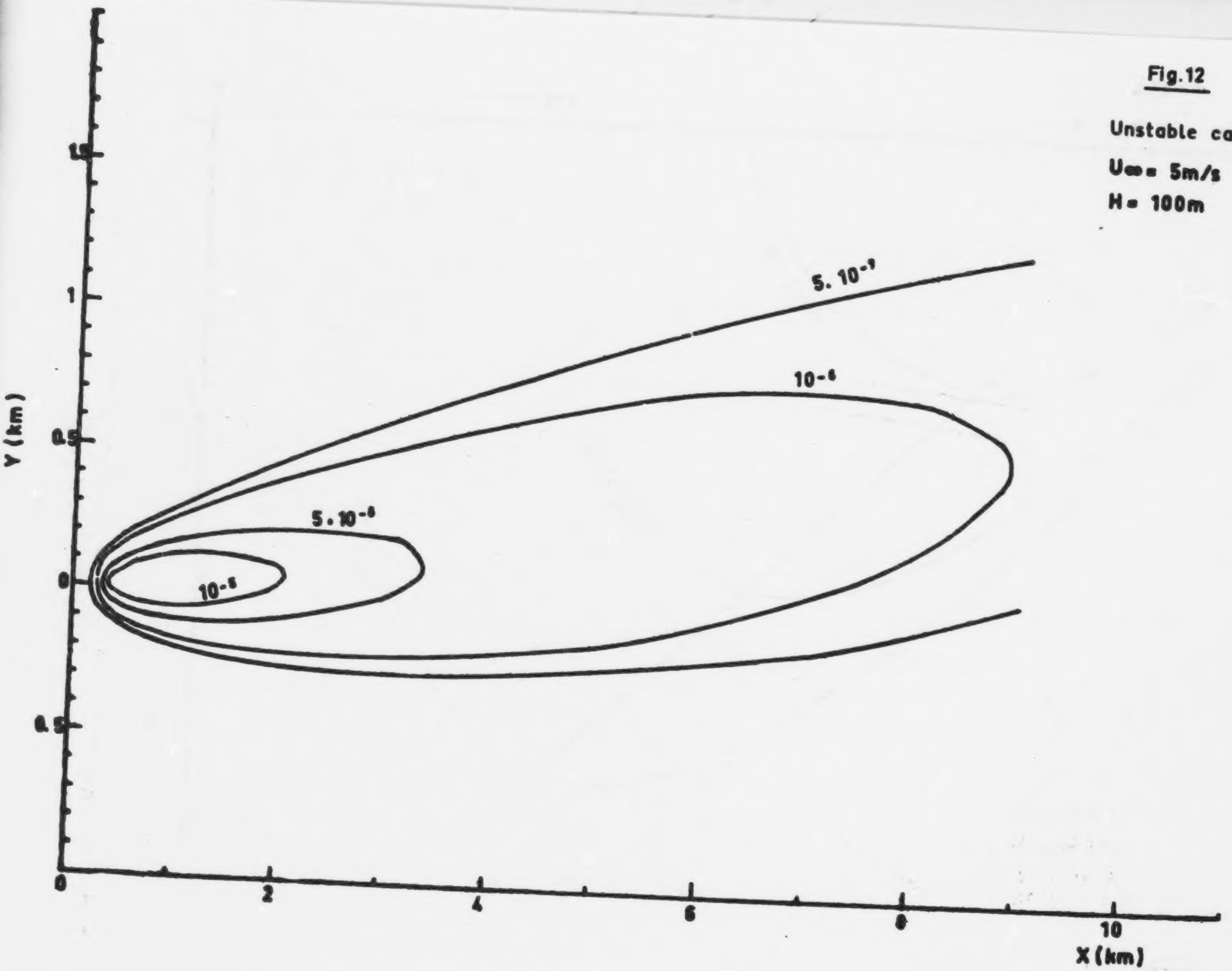

Fig.12

Unstable case

U_∞ = 5m/s

H = 100m

Fig.13

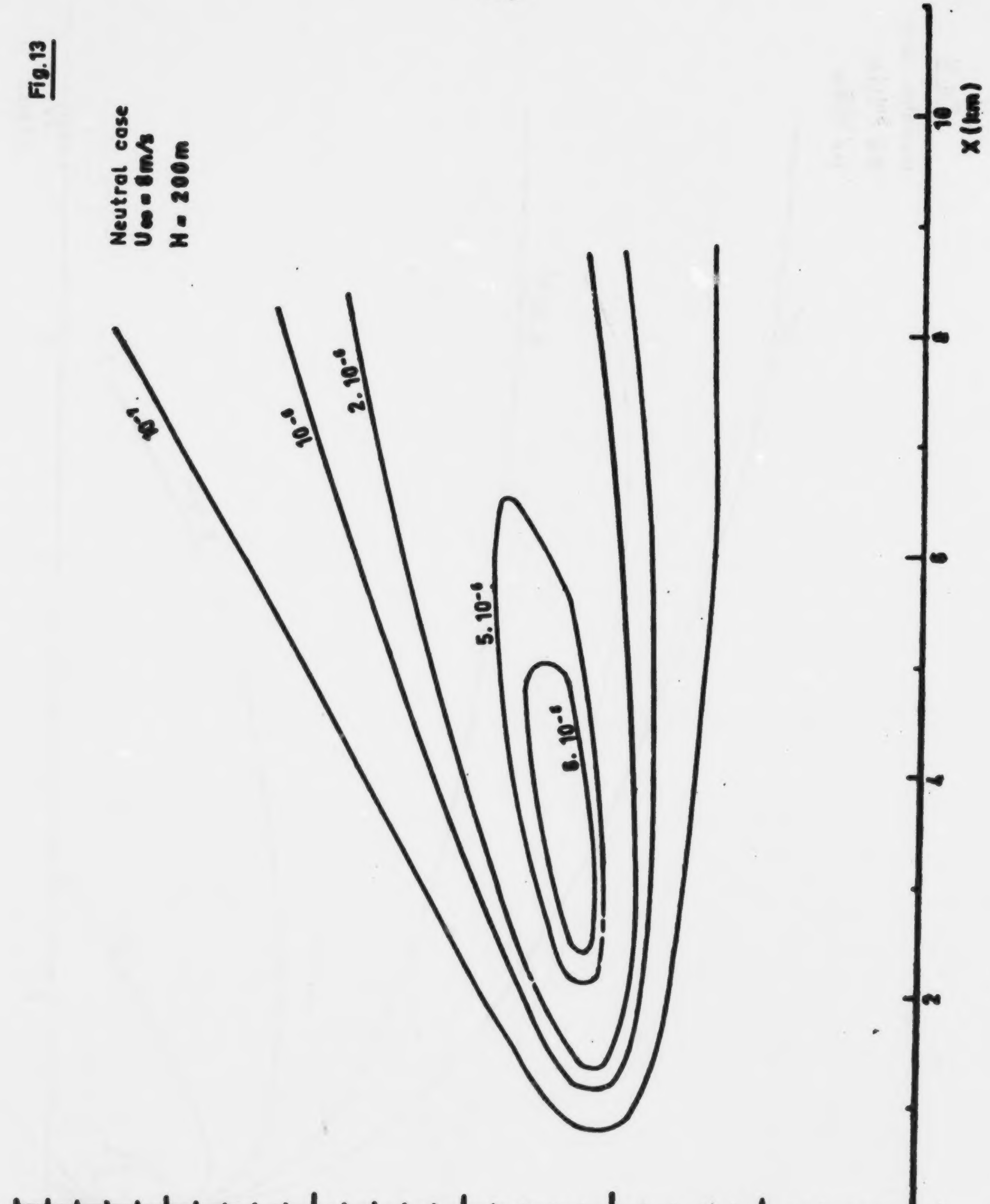
Neutral case
$U_\infty = 8$m/s
H = 200m
10^{-7}
10^{-6}
2.10^{-6}
5.10^{-6}
8.10^{-6}
X (km)
0
2
4
6
8
10
Y (km)
1.5
1
0.5
0
0.5

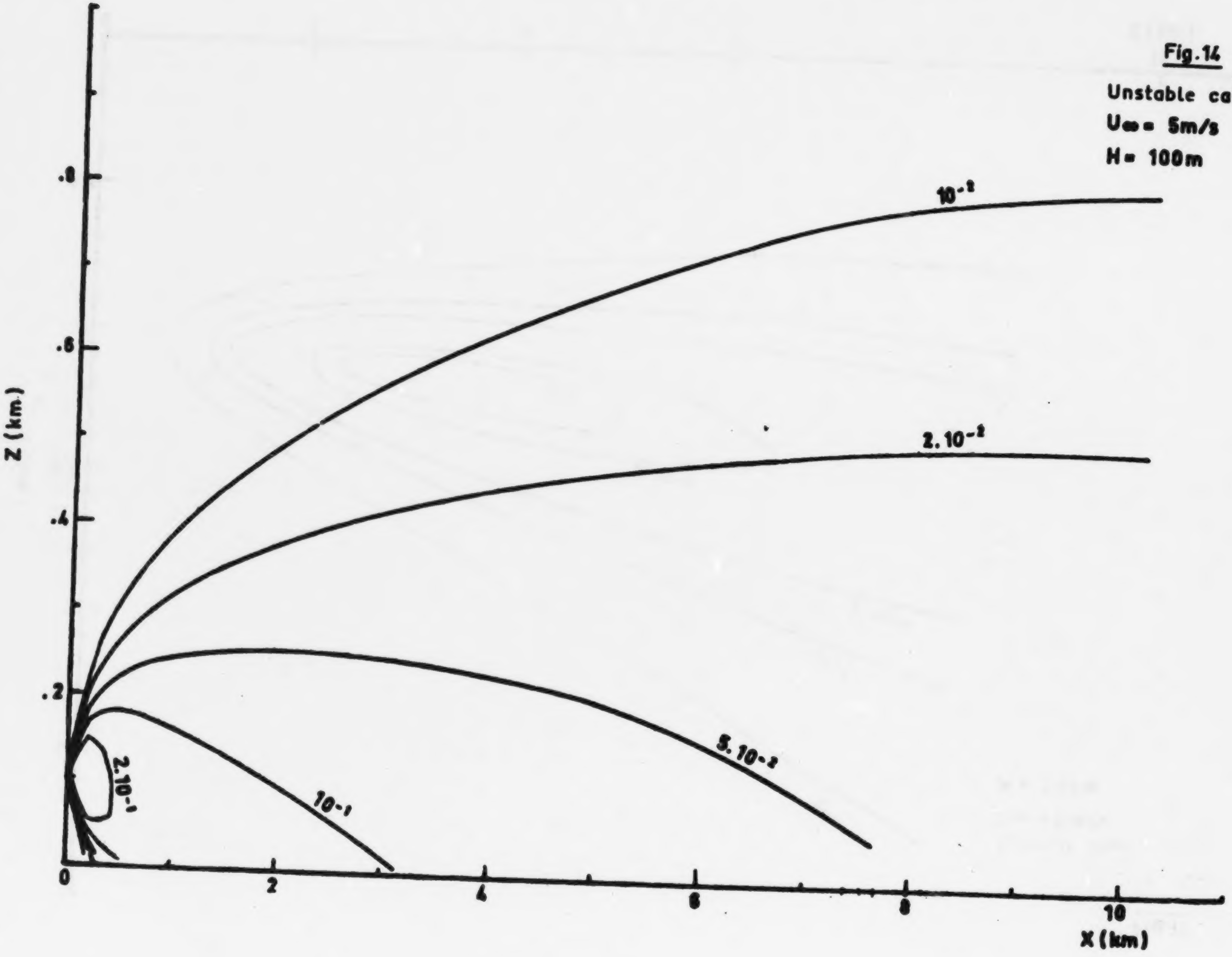

Fig.14

Unstable case
$U_\infty = 5m/s$
$H = 100m$

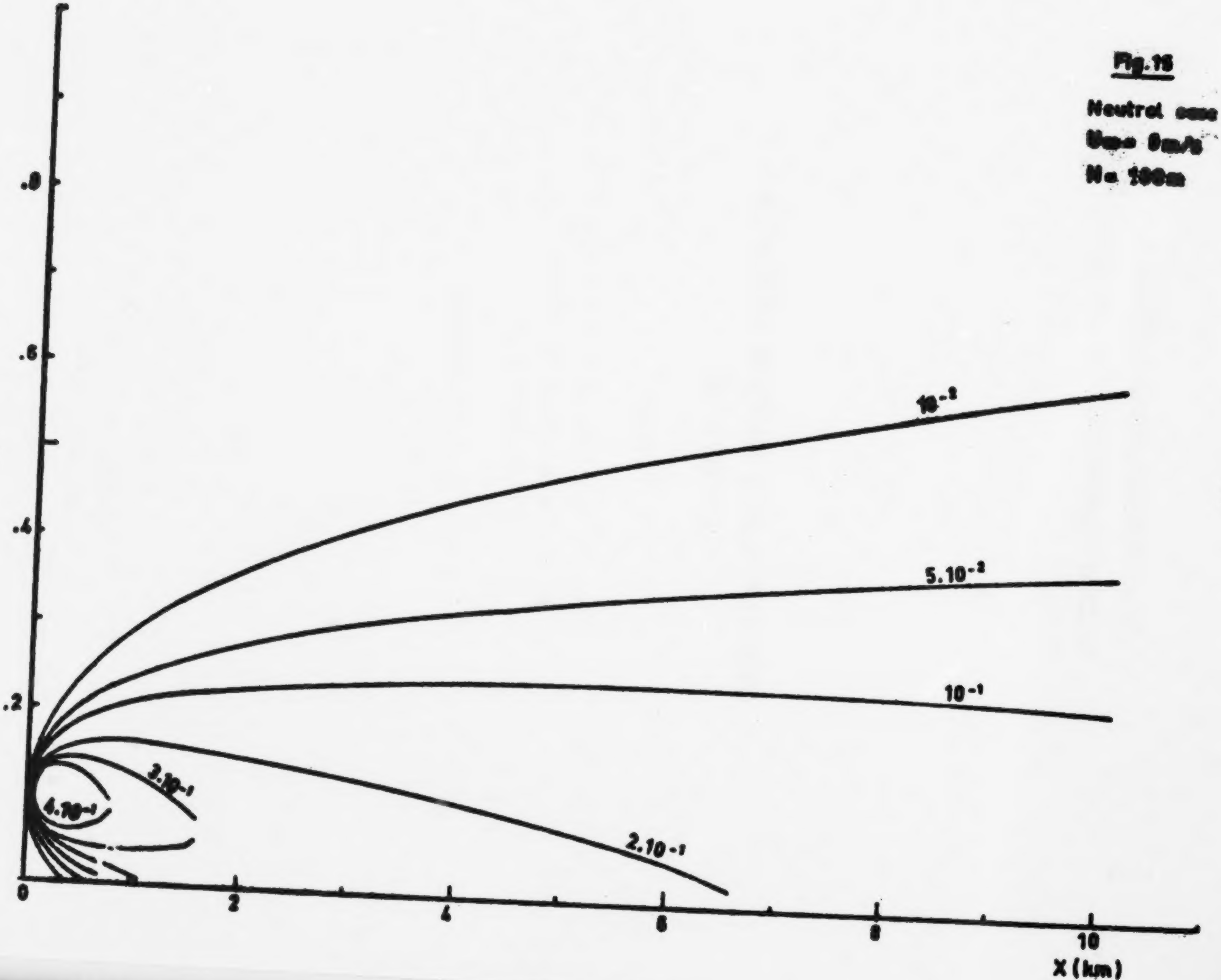

Fig.16

Neutral case
Ug= 0m/s
H= 100m

8th International Technical Meeting on

Air Pollution Modelling and its Application.

COMPARISON BETWEEN INVERSION OBSERVATION AND MODELLING

G. SCHAYES.

Institut d'Astronomie et de Géophysique
Université Catholique de Louvain
Chemin du cyclotron, 2

B-1348 LOUVAIN-LA-NEUVE
BELGIUM

September 20-23, 1977
Louvain-la-Neuve

Belgium.

COMPARISON BETWEEN INVERSION OBSERVATION AND MODELLING.

G. Schayes.

An important parameter of all dispersion models is the height of the mixing layer. This is why we have focused our attention on the behaviour of nocturnal inversions, as their top is related with the height of the mixing layer.

Recently, Anfossi and his colleages (1) have designed an inversion model that seems to be a significant improvement on the classical model of Brunt, because it follows more closely the physical processes involved in the developpement of a temperature inversion close to the ground.

In this preliminary work, we have fitted to the model temperature profile observations during inversion periods made by tethered balloon during the last two winter periods in Louvain-la-Neuve.(2,3,4).

The main features of the used model may be summarised as follows :

- heat exchange coefficient K_H constant with height and time;
- radiative effects are stronger than turbulent effects, this implies low wind conditions;
- no water vapour condensation;
- radiative flux f at ground level is constant
  $$f\ (o,t) = f_o;$$
- radiative flux at the top of the inversion z_i is 0
  $$f\ (z_i,t) = 0;$$
- inversion top height increases as a square root law of time
  $$z_i = (4K_H t)^{1/2}.$$

With these conditions the model has an analytical solution of the form :

(1) $$T(z,t) = T(o,o) - [T(o,o)-T(o,t)]$$

$$[\exp(-(\frac{z}{z_i})^2 - \frac{z}{z_i}(\pi)^{1/2}\operatorname{erfc}(\frac{z}{z_i}) + 0.278\frac{z}{z_i}]$$

(2) $$z_i = (4K_H t)^{1/2}$$

(3) $$T(o,o) - T(o,t) = \frac{2f_o}{k(1-\operatorname{erfc}(1))}(\frac{K_H t}{\pi})^{1/2}$$

An example of theoretical temperature profile evolution is shown in figure 1.

Two parameters f_o and K_H, respectively the ground radiative flux and the mean heat diffusivity of the layer determine the shape of the inversion profile. K_H is controlling the top height while K_H and f_o both control the temperature drop.

Nine inversion situations have been observed that fullfilled the initial conditions required by the model. The first results indicate that the radiative flux f_o needed to fit the observed profile is much less than what would have been expected, and in a few cases it has been measured. The descripancy ranges by a factor from 4 to 10.
The discripancy may be due to the fact that this model does not yet fit sufficiently the real physical world, mainly that turbulent processes are not negligeable and the radiative heat flux at the top of the layer is non zero $(f(z_i,t) \neq 0)$.

More significant are the results obtained for the K_H. The figure 2 shows a plot of the obtained K_H in function of the mean temperature gradient of the inverted layer. It comes out that high values of K are associated with low values of the gradient and reciprocally.

This simple application of the model enables us to find at least an order of magnitude of the mean K in the layer. As we know this value is also approximately equal to the eddy diffusivity of passive polutants in the same layer.

However, this method cannot give the K profile in the mixing layer, which is needed to run K dispersion models. We are now planning to estimate the vertical distribution of K by running turbulence measurements in the mixing layer. As we know, the general shape of these profiles can be represented as shown in fig. 3 and corresponds rather well to an expression of the form : (5)

$$K = a(\exp(-bz/z_T) - \exp(bcz/z_T)),$$

ruled by 4 parameters a, b, c and z_T. There is a unique relation between these parameters and the magnitude K_M and height Z_M of the maximu of the K profile. They have to be defined in situ in function of the main meteorological situations.

REFERENCES

(1) P. Anfossi, P. Bacci et A. Longhetto, "Forecasting of vertical temperature profiles in the atmosphere during nocturnal radiation inversions from air temperature trend at screen height? Quat. Journ. Roy. Met. Soc. 102, 173-180 (1976).

(2) F. Robert, "Mesure des profils dans les 300 premiers mètres de l'atmosphère", (unpublished), U.C.L. (1975).

(3) L. Nachtergaele, "Profils de la couche limite planétaire par Sodar et Radiosonde", (unpublished), U.C.L. (1977).

(4) J.P. Peters et G. Schayes, "Observation de la couche limite planétaire par radiosonde et sodar, premiers résultats", Contrib. n° 16 de I.A.G., U.C.L. (1977).

(5) Agee E., Brown D., Dowell, Chen, "A height dependent model of eddy viscosity in the planetary boundary layer", J. Appl. Met. 12, pp. 409-412, (1973).

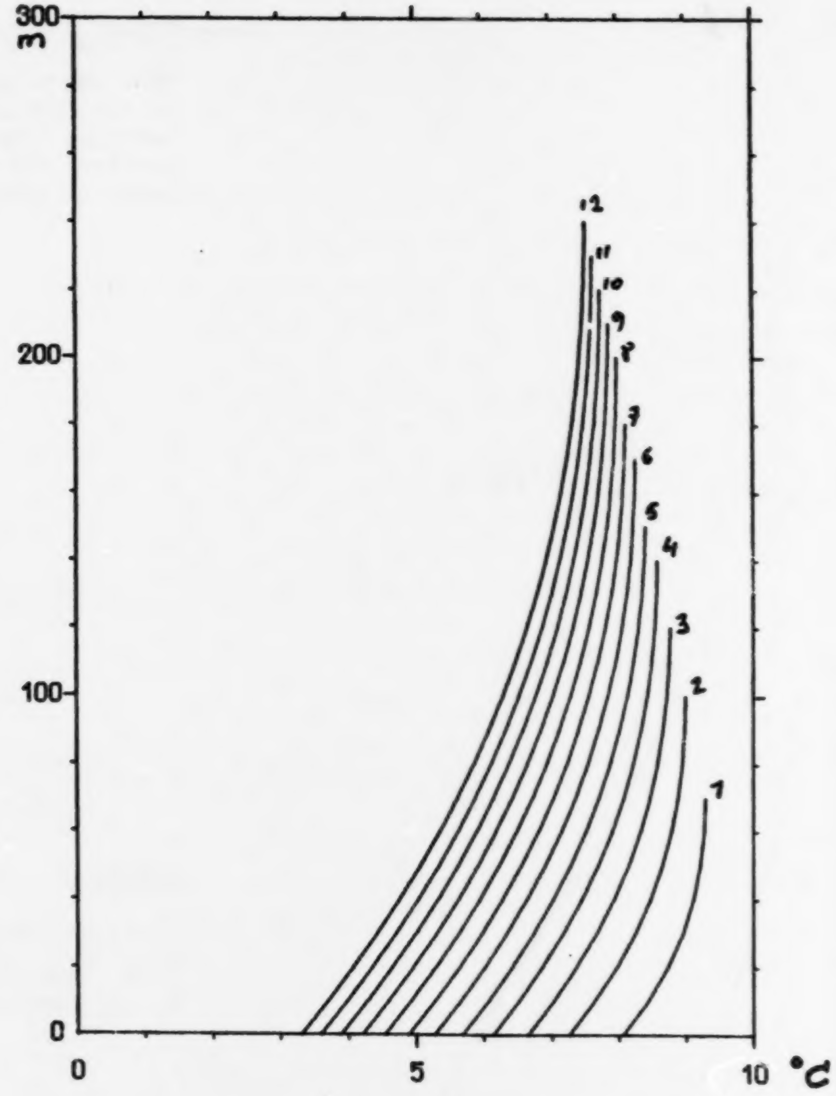

FIGURE 1 : Example of temperature profile evolution given by the model. Figures are hours after sunset (f_o = 18Wm^{-2}; K_M=0.3 m^2.s^{-1}).

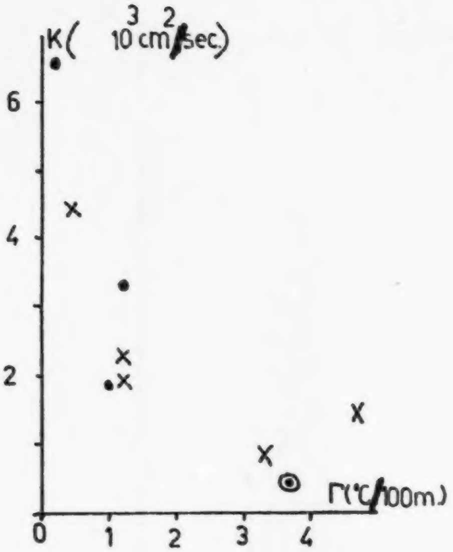

FIGURE 2

Heat conductivity in function of mean vertical temperature gradient for the observed inversions.

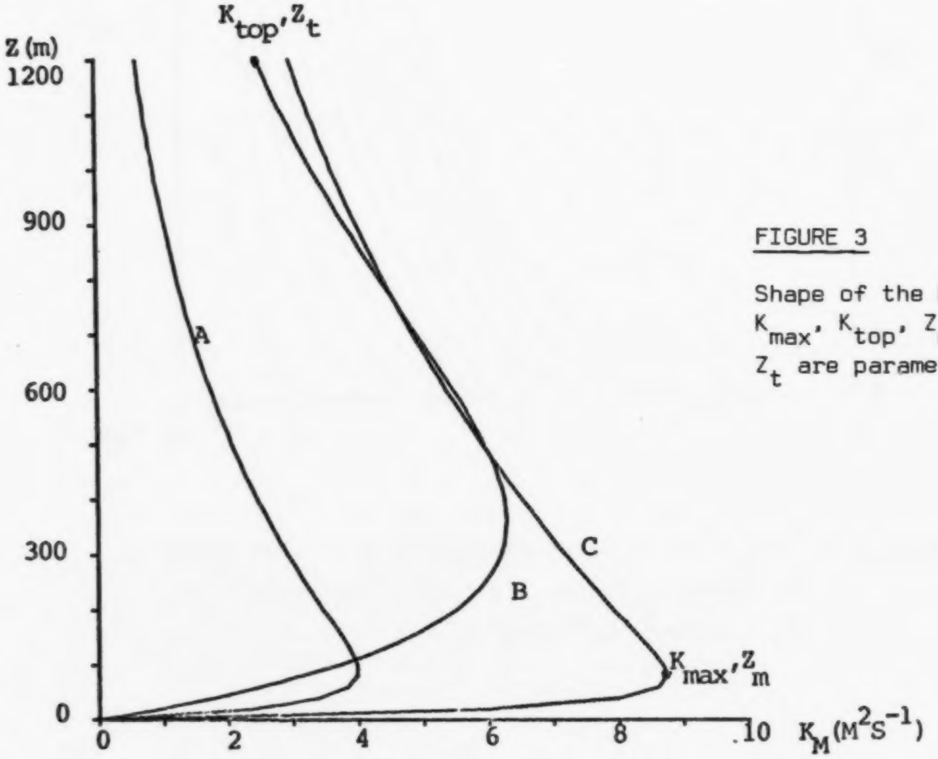

FIGURE 3

Shape of the K-profiles K_{max}, K_{top}, Z_m and Z_t are parameters.

Rapporteur's Summary Report:

Prepared by: D.B. Turner

Papers covered by: Longhetto
Saab
Schayes

Paper: Assessment of stability categories as meteorological input of air pollution modeling
A. Longhetto

Question: NIEUWSTADT asked if laminar flow occured beyond a critical Richardson number of about 0.2 ? There seemed to be values shown as 0.5 or higher.

Answer: LONGHETTO indicated that the data were shown in the first figure.

Paper: New technics of estimation of dispersion coefficients
A. Saab

Question: HANNÀ asked if he was suggesting that second order closure be used instead of GAUSSian modeling ?

Answer: SAAB indicated, no, they were trying to validate dispersion coefficients. There will be many cases where three dimensional modeling will be necessary such as wind shear and complex topography.

Question: PADRO asked SAAB if he was familiar with a paper on 4th order closure and if he would care to comment on it.

Answer: SAAB said he had seen it. He said to validate second order closure takes extreme situations such as extreme convection. It may be useful when determining evolving conditions such as early morning.

Paper: Comparison between inversion observation and modeling
G. Schayes

JOHNSON commented that with the building of the community, Louvain-la-Neuve, the opportunity existed to study increased urbanization.

General Comments after Morning Session:

KNOX commented on the patterns of the papers indicating that there must be suitable input data for these new types of models such as profiles of K_z The model inputs can either be from measurements or model outputs from boundary layer models.

JOHNSON said we must obtain more information on vertical structure. The emphasis must shift to better and more economical vertical measurements.

JOST stated that this would require special measurement networks.

RUNCA said that models should be compared with real data. Also sophisticated models may be used to test the applicability of simple models.

PADRO commented that instruments are required for studies and that measurements should be made to collect data relevant to both GAUSSian and K type models.

JOST said there are definite limitations to the regularly obtainable data.

8th NATO/CCMS INTERNATIONAL TECHNICAL MEETING ON AIR POLLUTION MODELING

TOPIC 5

CONSIDERATIONS OF TRANSFORMATION PROCESSES OF AIR POLLUTANTS IN MODELS

8th International Technical Meeting
on Air Pollution Modeling and its Application

PROJECT MISTT: PLUME MODELING OF THE DISPERSION, TRANSFORMATION AND GROUND REMOVAL OF SO_2 OVER THE β-MESOSCALE RANGE (25-250 km)

N. V. Gillani and R. B. Husar
Air Pollution Research Laboratory
Mechanical Engineering Department
Washington University
St. Louis, MO 63130

September 20 - 23, 1977
Louvain-La-Neuve
Belgium

1. INTRODUCTION

The prevalence of high and increasing levels of atmospheric sulfates over wide regions of the eastern U.S. has now received official recognition (EPA, 1975), and its causes, nature and effects are the subject of several large and well-known research programs in the U.S. Of particular concern is the gas-to-particle conversion of sulfur compounds released to the atmosphere (primarily as SO_2) from large sources such as tall-stack power plants and large industrial complexes. Gas-to-particle conversions of atmospheric sulfur compounds are important because the secondary products have a longer lifetime in the air, and because they are believed to be more harmful than the precursor gases. The amount of secondary sulfate formation depends on two primary factors - the rate of the conversion process and the atmospheric residence time of SO_2. Under average atmospheric conditions, the conversion rates are believed to be of the order of only 1% ph. Consequently, observations of substantial amounts of sulfates over large regions are explained as the result of long range transport of SO_2 lasting a day or longer. Such a possibility immediately raises two questions of paramount practical significance. First of all, is the proliferation of modern tall-stack power plants which burn fossil fuels largely responsible for the observed distribution of sulfates in the U.S.? Secondly, what is the role of diurnal variations in emissions and ambient atmospheric and ground conditions in the overall formation of secondary sulfates?

Numerous efforts are under way in the U.S. and in Europe to develop mathematical models to simulate aspects of long range (synoptic scale) transport, transformation and removal of SO_2. Thus, the existing steady-state models developed for application over a range of a few tens of kilometers are now being joined by a new class of "regional" models whose range of applicability is of the order of 1000 km. Conspicuously rare in the existing family of models are those designed specifically for application in the intermediate β-mesoscale range, roughly between 25 and 250 km.(1) This dearth is particularly surprising in the case of models for isolated large plumes, because much of the current activity

---

*In meteorological literature, the mesoscale is often subdivided into γ-mesoscale (0-25 km), β-mesoscale (25-250 km) and α-mesoscale (250-500 km).

of airborne sampling of large plumes is within that range. It is also in the mesoscale range that the plume becomes dispersed throughout the mixing layer and first comes into contact with the ground. The effect of source height is also most pronounced in this range. The amount and distribution of the pollutant which become available to synoptic scale transport are determined by the mesoscale effects on emissions.

For the transport of large plumes over a short range (<50 km), the variability of the PBL and of SO_2 conversion and removal parameters is usually small, and steady-state models can provide an adequate simulation. During long range transport, source effects are no longer important and simple box-model simulations are valid. In the intermediate β-mesoscale range (25-250 km), source effects, spatial inhomogeneities of the PBL structure, and the diurnal variability of the PBL as well as of SO_2 conversion and ground removal parameters all exert important influence on the sulfur budget of the plume. This complexity, coupled with a general lack of suitable air quality and meteorological data, has discouraged past efforts at plume modeling in the β-mesoscale.

In this paper, the formulation and application of a diagnostic β-mesoscale plume model are described. This Lagrangian model incorporates the diurnal variability of the planetary boundary layer (PBL) structure and of the parameters governing the chemical conversion and ground removal of SO_2. It is a quasi-steady model which uses an existing steady-state model to perform the solution over one hour at a time, with inputs which are variable from one hour to the next. The vertical inhomogeneity of atmospheric dispersion is simulated by the use of an assumed height-dependent profile of the eddy diffusion coefficient. Application of the model using the field data of the transport and kinetics of SO_2 in the plume of a large coal-fired power plant yields quantitative information about the dispersion, transformation and ground removal of SO_2. This information is then used in the model to investigate the parts played by source height, eddy diffusion and time of emission in determining the overall mesoscale sulfur budget of the plume.

The model is designed specifically for implementation on a minicomputer with 56K bytes of core storage. The cost of running this model is thus insignificant in comparison with many existing grid models which require the use of a large computer.

The work reported here was performed as part of Project MISTT (Midwest Interstate Sulfur Transformation and Transport), an integrated, interdisciplinary research program of field, laboratory and theoretical studies sponsored by the U.S. Environmental Protection Agency, and carried out under the technical direction of William E. Wilson, Jr. The primary objective of the program is to obtain a physical understanding and quantitative assessment of the nature and fate of atmospheric sulfur released in large power plant and urban-industrial plumes. An intensive field program of increasing scope and duration, centered around aircraft sampling of the urban plume of St. Louis and of the plume of the Labadie power plant near St. Louis, has been conducted each summer since 1973. Details concerning the overall Project are given elsewhere (Wilson, 1978). Detailed descriptions of the field program and a study of the sulfur budget in a power plant plume are given by Husar et al. (1978). The spatial range covered in these plume mapping experiments increased steadily from 50 km in 1973 to more than 300 km in 1976. On July 9 and 18, 1976, the Labadie plume was sampled out to 300 km, representing plume transport times of 10-12 hours ranging over day and night. The data for these two days are used in the model application. They are presented in this paper only briefly; a much more detailed description and analysis of the sulfur kinetics on these two days is given by Gillani et al. (1978). The emphasis in this paper is on sulfur kinetics beyond the first two hours of plume transport.

1.1 Objectives of diagnostic plume models

The primary function of contemporary air pollution models is to identify and quantitatively characterize pollutant emission at its source, and its subsequent transmission through the atmosphere subject to meteorological transport, physical and chemical transformations, and a variety of wet and dry removal processes. All present air pollution models are diagnostic in that they all take certain observed fields of meteorological variables as inputs and attempt to diagnose a consistent distribution of the pollution variables. The emphasis in this paper is on the use of plume models as a diagnostic tool in an integrated program of field and laboratory work. The specific objectives of such a model are:

(i) to provide a quantitative framework for the physical interpretation of the findings of field experiments;
(ii) to identify the most important system parameters influencing the atmospheric fate of pollutants, and to estimate the sensitivity of primary pollutant variables to changes in these parameters;
(iii) to aid in the design of future field experiments by identifying types of data needed for more realistic model inputs, and finally,
(iv) to validate and upgrade the simulation capabilities of the model by incorporating new physical insights and better data acquired from the field program.

2. MODEL FORMULATION

2.1 Basic Equation

The mathematical formulation of a model requires the choice of a frame of reference (Eulerian or Lagrangian), the degree of resolution (integral or differential approach), and finally, the specific mathematical simulation of the physics, chemistry and initial and boundary conditions. The Lagrangian frame moves with the system of interest along the trajectory described by the mean flow field. It is necessary to compute the mean trajectory of the air volume of interest. Spatial resolution is partly lost in Lagrangian models because it is necessary to consider a homogeneous volume of definition. At least in the unstable, capped mixing layer of the daytime, the necessary assumption of uniform wind speed with height represents a reasonably good approximation (Townsend, 1967; Deardorff, 1970; Husar et al., 1978). In the U.S. Midwest and Great Plains, the approximation may be poor during the night hours when a low-level jet blows at a height of about 500 m (Blackadar, 1957; Husar et al., 1978; Smith et al., 1978).

The differential formulation of the principle of conservation of mass employed most commonly in mesoscale models pertaining to the transport over flat terrain of a plume from a single, isolated source is (for a single component such as SO_2)

$$\frac{\partial \bar{c}}{\partial t} + \bar{u}\,\frac{\partial \bar{c}}{\partial x} = K_H\,\frac{\partial^2 \bar{c}}{\partial y^2} + \frac{\partial}{\partial z}\left(K_z\,\frac{\partial \bar{c}}{\partial z}\right) + r \qquad (1)$$

where x,y,z denote the downwind, crosswind and the vertical co-ordinates, respectively. This formulation is based on the following assumptions:

a) molecular diffusion is negligible compared to eddy diffusion;

b) the vertical component of the velocity is negligible;

c) the x-coordinate is always aligned with the direction of the horizontal component ($\bar{u}$) of the wind;

d) the horizontal and vertical turbulent mass fluxes are assumed to be describable in terms of eddy diffusion, with K_H and K_z representing the corresponding eddy exchange coefficients;

e) eddy diffusion in the longitudinal direction is negligible compared to downwind advection.

In the above formulation, r represents the rate of internal generation or loss of the pollutant. In our model, it describes the conversion loss of SO_2.

The validity of assumption (b) diminishes with increasing transport time, and becomes questionable during long range transport (Pasquill, 1974). Also, in regions of local vertical transport such as a heat island, this assumption will fail. Assumption (c) neglects directional wind shear with height and can result in significant errors in the estimation of crosswind plume spread, particularly during long range transport. In a recent detailed analysis of the validity of the eddy diffusion approximation (d), Corrsin (1974) concluded that "the partial success of gradient transport models in turbulence is largely fortuitous, and certainly surprising." The principal limitations of the gradient transfer approach are that the length and time scales of the effective turbulent eddies must be sufficiently small in comparison with the corresponding scales of the plume. The eddy diffusion concept is thus least valid near elevated point sources where the scale of atmospheric turbulence is generally large and the plume dimensions are small. In practice, therefore, the exchange coefficients are sometimes expressed in power law functions of the distance x from the source, in order to account for progressively larger eddies as they take part in the diffusion process, until the action of the entire spectrum of eddies has been felt (Peters & Klinzing, 1971). During the initial stage of plume spread, the gradient transfer theory cannot simulate the translation of the whole plume in the vertical or crosswind directions due to eddy motion larger than the plume cross-section. The assumption of negligible longitudinal eddy diffusion is generally valid for $\bar{u} > 1$ m/s (Herrmann, 1976). In spite of their obvious shortcomings, eddy diffusion models have been relatively successful in simulating mesoscale plume transport whenever appropriate time and height-dependent models of K_z have been employed.

The validity of the above formulation is perhaps most restricted by the combined implication of assumptions (c) and (d) that crosswind plume spread may be adequately described by a lateral diffusivity. This approximation is frequently made in plume dispersion models because it greatly simplifies model solution. Its validity is least questionable during the daytime convective conditions when the directional shear of the wind with height is smallest (Husar et al., 1978). The application of the β-mesoscale model is considered here only for the daytime hours. Furthermore, as is shown later (section 3.3), model calculations and comparisons with the field data are considered only for crosswind integrals of the concentration of SO_2 rather than for crosswind distributions. Thus, the model is not actually applied to simulate the details of crosswind plume spread.

2.2 Non-dimensionalization

An important step in the mathematical formulation of the model is the proper non-dimensionalization of all variables, and it permits the identification of the system parameters which govern the physical processes. If τ, ℓ, u_c, K_c and C_c are chosen to denote characteristic values of time, length, speed, eddy diffusivity and pollutant concentration with respect to which the real variables are normalized, then equation 1 may be rewritten in the following non-dimensional form:

$$\frac{\partial\chi}{\partial T} + U\left(\frac{u_c\ell}{K_c}\right)\frac{\partial\chi}{\partial\xi} = g_H\,\frac{\partial^2\chi}{\partial Y^2} + \frac{\partial}{\partial Z}\left(g_z\,\frac{\partial\chi}{\partial Z}\right) + R, \qquad (2)$$

where

$T = t/\tau, \quad \xi = x/\ell, \quad Y = y/\ell, \quad Z = z/\ell,$

$U = \bar{u}/u_c, \quad g_H = K_H/K_c, \quad g_z = K_z/K_c,$

$R = r(\tau/C_c)$ and $\chi = \bar{c}/C_c$

The above formulation yields one important system parameter, $(u_c \ell / K_c)$, which has been identified as the Peclet number (Pe) of turbulent mass transfer (Gillani & Husar, 1975). Pe is an important meteorological parameter related to plume dilution. It may be used in the further reduction of the downwind distance parameter as

$$X = \xi / \mathrm{Pe}.$$

As will be demonstrated in a later section (3.1), the use of X permits the direct comparison of the St. Louis urban-industrial plume data gathered on different days under quite different meteorological conditions. The application of similar non-dimensionalization procedures to the surface boundary condition applicable to equation 2 yields another important system parameter, as will be shown later.

The proper choice of the characteristic quantities τ, ℓ, u_c, K_c and C_c is also important. For the problem of mesoscale dispersion within a confined mixing layer,

$\ell = h$ (the mixing height), and
$\tau = h^2/K_c$ (characteristic time of vertical turbulent dispersion of a particle through the mixing height)

are the natural length and time scales relevant to the physical situation. The particular choice of the characteristic transport velocity u_c is less obvious; the geostrophic wind speed, the average transport speed over the mixing height, or the wind speed at effective stack height at the time of emission (u_0) are all appropriate choices. $u_c = u_0$ is chosen in the present model application. K_c may be chosen as the maximum value of K_z in the mixing layer. $C_c = (Q_0/u_c h^2)$, where Q_0 is the pollutant emission rate, is a meaningful choice.

In the Lagrangian formulation of the model, application of Taylor's hypothesis, $t = x/\bar{u}$, leads to the equality $X = T$, and the left hand side of equation 2 reduces to just the first term.

2.3 The source and near-source effects

Anthropogenic sources of air pollution are generally classified as point sources (e.g. tall stack), line sources (roadway), or area sources (urban area). Area sources are usually made up of multiple stationary and moving point sources whose emissions rapidly become mixed. A short distance downwind of the horizontal area source, the emissions are distributed over a vertical plane. Consequently, it is sometimes convenient to consider an urban plume source to be a vertical area source of finite lateral width and a given vertical profile of emission distribution (see illustration in Fig. 5). If Q_0 is the overall rate of pollutant emission, $\bar{C}_0(z)$ is the corresponding vertical distribution of the pollutant source (assumed uniform in the lateral direction), and the source area is assumed to be bounded by $|y| \leq b$ and $z_1 \leq z \leq z_2$, then the pollutant mass balance may be expressed by the following "boundary" condition

$$Q_0 = \int_{z_1}^{z_2} \int_{-b}^{b} \bar{C}_0(z) \quad \bar{u}_0(z) \, dydz, \tag{3}$$

where $\bar{u}_0$ denotes the mean wind speed at the source. For sufficiently small values of b and z_2-z_1, such an area source model may be applied to point sources.

The emission of the pollutant is accompanied by an efflux of heat and momentum at the stack exit. Consequently, the plume is a buoyant jet. The interactions between plume buoyancy, the wind, and atmospheric turbulence result in plume rise, plume bending and plume spread by the entrainment of ambient air. Final plume rise is often much greater than the physical stack height. Thus, the knowledge of the effective stack height is of considerable importance in the plume model. There are basically three methods of determining plume rise: using empirical formulas, solving numerical models which simulate the buoyant plume behavior, and by direct observation of the plume, as from an aircraft. Of these, the last method is perhaps the most reliable, but generally the least available. Fortunately, appropriate aircraft data indicating the approximate location of the plume centerline at a distance of several kilometers from the source are quite often available in Project MISTT, and are used in this model study. The method of calculating plume rise from empirical formulas is often frustrating because there are many such formulas, and the results of using different formulas are quite different - often by a factor of 10 or more (Briggs, 1975).

2.4 Eddy exchange coefficients

The realistic simulation of the vertical dispersion of the plume is a principal requirement of a mesoscale dispersion model. It governs the rate of delivery of the pollutants to or away from the ground sink, depending on whether the source is elevated or near the ground. Thus, it influences the residence time of SO_2 in the air, and thereby indirectly the amount of sulfate formation. More directly, however, atmospheric mixing is responsible for the entrainment of background air into the plume. For the power plant plumes, such entrainment could make available air mass constituents such as ozone, hydrocarbons and free radicals which may promote sulfate formation.

Turbulent flux terms appear in the equations of conservation of mass, momentum and energy as cross-correlations of stochastic quantities. Thus $\overline{w'c'}$ represents the vertical turbulent mass transfer of the pollutant. In the plume model, such quantities must be expressed in analytical closed-form approximations which provide an adequate parametrization of turbulent mixing in the planetary boundary layer. Perhaps the most promising of the existing approaches is that using second and higher order closure schemes (Donaldson, 1973) in which dynamic equations modeling the subgrid fluxes are solved. Deardorff (1973) and Orlanski et al. (1974) have developed eddy coefficients which depend respectively on local turbulent energy and on local vertical gradients of potential temperature. For the exchange coefficients to be "local", this method of sub-grid scale parametrization requires the use of a fine grid. Both of the above methods of parametrization of turbulence require extensive computations on large computers.

The use of semi-empirical assumed vertical profiles of eddy diffusivities represents only a first-order closure approximation of turbulent transfer, but it gives reasonable simulations with substantially less effort and cost. The succcess of this approach depends on the choice of proper functional forms for K_H and K_z. The functional forms of K_H and K_z may be chosen as:

$$K_H = K_H(t) \, . \, (x)^{\gamma_0} \qquad (4a)$$

$$K_z = K_{zm} \, . \, (x/x_r)^{\gamma} \, . \, g(t,z) \qquad (4b)$$

According to Islitzer & Slade (1968), = 0.42 for the neutral case. In our model, we choose the following stability-dependent representation

$$\gamma = \begin{cases} \gamma_0 & x \le x_r \\ 0 & x > x_r \end{cases} , \qquad (5)$$

where $\gamma_0 = 0.4\ (1-3/L)$, $|L| > 3$. x_r is a reference distance within which the action of the entire spectrum of turbulence has been felt by the spreading plume; $x_r = 3h$ is used in our model. L is the Monin-Obukhov similarity length.

K_{zm} is the highest value attained by K_z in the mixing height during the entire duration of application of the model. Based on the application of the Lagrangian similarity theory in the constant-flux surface layer,

$$K_z = \frac{\kappa u_* z}{\phi(z/L)} , \quad z_0 \le z \le z_{SL} \qquad (6)$$

where ϕ is a stability correction factor and z_0 and z_{SL} are the roughness length and surface layer height respectively. For the case of heat and mass transfer, Businger et al. (1971) have suggested the following empirical expressions for ϕ:

$$\phi_n = 0.74, \quad \text{neutral case, } L = \infty \qquad (7a)$$

$$\phi_s = 0.74 + 4.7\ z/L, \quad \text{stable case, } L > 0 \qquad (7b)$$

$$\phi_u = 0.74(1-9\ z/L)^{-1/2} \quad \text{unstable case, } L < 0 \qquad (7c)$$

Above the surface layer, the similarity theory is not well developed and there is much greater uncertainty about the magnitude and height dependence of K_z. Several models for K_z have been used for this region. The models of O'Brien (1970) and Shir (1973) are well-known. They are derived to satisfy specified realistic boundary conditions. O'Brien's model is a cubic polynomial above the surface layer, and matches the surface layer value and slope of K_z at the interface. Shir's profile is based on a single continuous function which fits the specified boundary conditions at the ground and at the inversion base, and is also forced to attain a maximum value (K_m) at $z/h = 0.25$. The expressions for these two models are as follows:

$$\text{O'Brien:} \quad K_z = K_h + \left(\frac{h-z}{h-z_{SL}}\right)^2 \left\{ K_{SL} - K_h + (z-z_{SL}) \left[K'_{SL} + 2\,\frac{K_{SL}-K_h}{h-z_{SL}} \right] \right\}, \quad z \geq z_{SL} \qquad (8)$$

$$\text{Shir:} \quad \frac{K_z}{K_m} = 0.73\,(4Z) \left[e^{1-4Z} + \frac{1}{1+16Z^{1.6}} \right], \quad 0 \leq Z = z/h \leq 1 \qquad (9)$$

In the O'Brien model, K_h and K_{SL} are values of K_z at $z = h$ and z_{SL} (height of surface layer), and K'_{SL} is the derivative of K_z at z_{SL}. K_{SL}, K'_{SL} are determined from surface layer theory. The application of this model requires *a priori* knowledge of the thickness of the constant flux layer and is very sensitive to this choice. O'Brien's model is tested in our β-mesoscale model, and is henceforth referred to as K-Model 2. Time-height contours and vertical profiles of K_z, based on the O'Brien model, were constructed with $z_{SL} = |L|$ for each hour of the day for July 18, 1976 in St. Louis, and are shown in Fig. 1. Shir's model was used in our steady-state, short range plume model.

For application in the present β-mesoscale plume model, the author has developed the following simple model for K_z which varies with time and height and is responsive to changes in atmospheric stability. The model also permits adequate flexibility in varying the maximum value of K_z at each time in such a way as to provide a reasonable fit for the aircraft data. In the surface layer, the model employs the basic expressions of equations 6 and 7, with the choice $z_{SL} = |L|$. The evaluation of the Monin-Obukhov stability length L is based on hourly ground data, and is performed as described in Appendix A. The changing stability from hour to hour is thus incorporated into the model explicitly. For unstable stratification, the model uses the following expression for "free convection" immediately above the surface layer:

$$K_z = A\kappa\, u_* \, z \left|\frac{z}{L}\right|^{1/3}, \qquad -L \leq z \leq z_{m\ell} \qquad (10)$$

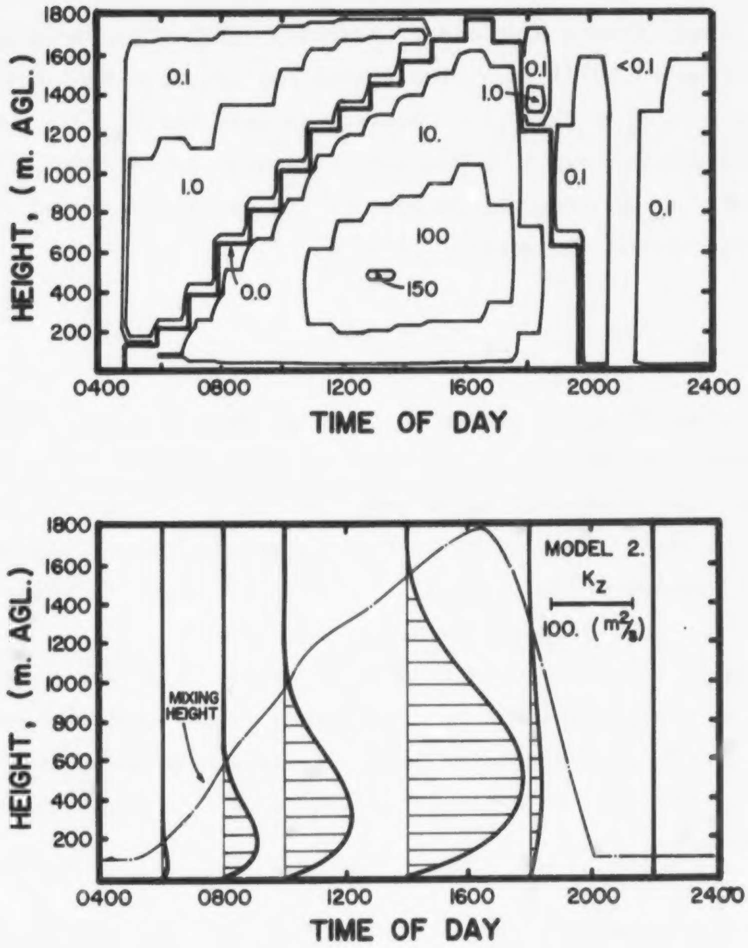

Fig. **1**: *Time-height contours (a) and selected vertical profiles (b) of K_z for July 18, 1976 according to the O'Brien model (K-Model 2). The contour for K_z=0 in (a) represents the simulated mixing height variation during unstable conditions.*

where A is chosen such that equations 6 and 10 give matching values of K_z at $z = -L$. This value is obtained as 4.2733. The above expression is based on the scheme proposed by Priestly (1954), and subsequently used by Yordanov (1972) in a plume model for emission from a high source. Above $z_{m\ell}$, $K_z = K_m = K_z(z_{m\ell})$ = constant is used for $z_{m\ell} \leq z \leq 0.9h$. Such a constant K above 50 m has been suggested by Deardorff (1967). The value of K_m is directly related to the stability parameter $-h/L$ of unstable conditions (Deardorff, 1970) by

$$K_z = -f_m \quad h/L, \qquad z_{m\ell} \leq z \leq 0.9h \tag{11}$$

where the constant f_m is chosen to fit the observed data. The choice of f_m determines the height $z_{m\ell}$ (by equating equations 10 and 11 at $z = z_{m\ell}$) above which the constant K value ($=K_m$) is used. Values of f_m are estimated to vary from 0.15 on a strongly unstable day (July 18) to 0.25 on a weakly unstable day (July 9). Above z = 0.9 h, the value of K is allowed to decrease linearly to $0.2\ K_m$ at $z = h$.

In stable conditions, surface layer values of K_z are obtained according to equations 6 and 7. The height of the surface layer is chosen as L. Above the surface layer, K_z is approximated by a slight variation of the O'Brien model for the case of $K_h = K_{SL}$. The resulting expression is

$$K_z = K_{SL}\ 1 + \beta\left(\frac{h-z}{h-L}\right)^2 \left(\frac{z}{L} - 1\right), \qquad z \geq L > 0 \tag{12}$$

where β 0.136 ensures that the slope of K at $z = L$ matches its value based on surface layer formula. Profiles of K_z based on the above model (henceforth referred to as K-Model 1) have been computed for each hour of July 9 and 18. Selected vertical profiles and the time-height contours of K_z for July 18 are shown in Fig. 2 .

2.5 Dynamics of the mixing layer

The fate of any given pollutant release within the lowest kilometer or so of the atmosphere is influenced by the evolution of the daily mixing layer. The existence of a well-defined daytime mixing layer in the continental U.S. is well documented (Holzworth, 1972). Such a

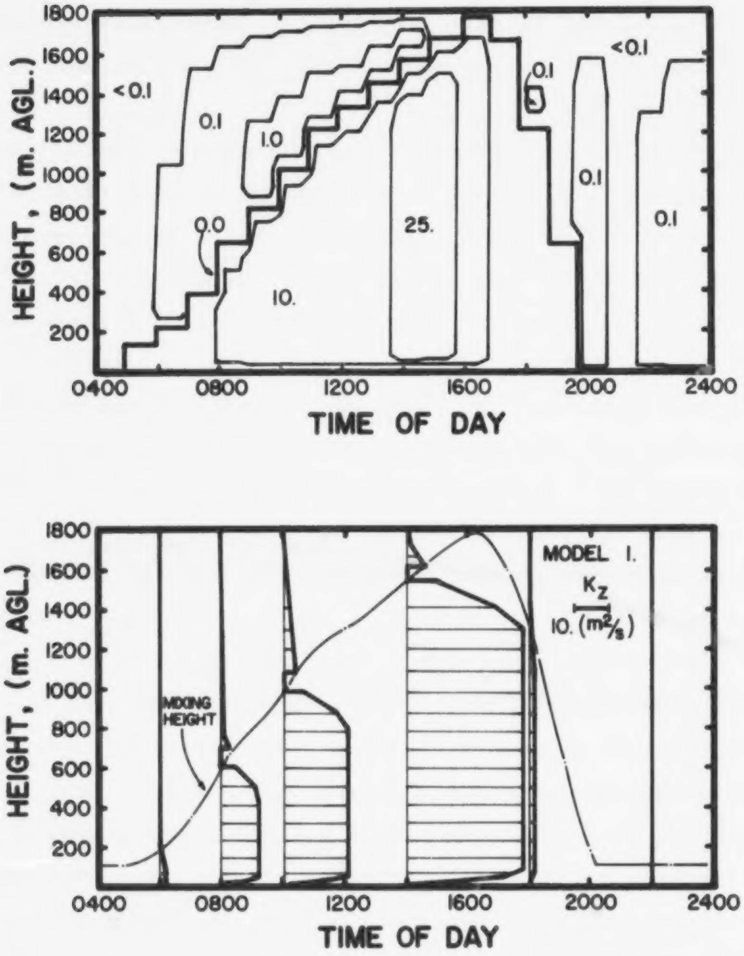

Fig. **2**: *Time-height contours (a) and selected vertical profiles (b) of K_z for July 18, 1976 according to the author's model (K-Model 1). Notice that the scales for K_z profiles in (b) are different in Figs. 1 and 2 by a factor of about 4.*

mixing layer is commonly characterized by an adiabatic or superadiabatic thermal gradient capped by a stable inversion layer, and good turbulent mixing within the layer which drops off sharply at the top of the layer. Aircraft vertical soundings reveal a rather uniform vertical profile of pollutant variables in the daytime mixing layer with a drop near the mixing height (see Fig. 3).

During the night, the air close to the ground is cooled by conduction and radiation, forming a shallow nocturnal inversion. Some degree of turbulent transfer will continue to prevail in the lowest layer near ground. Above the inversion, the PBL is stably stratified. After the sun rises, convection develops due to surface heating, and gradually the night inversion is eroded. As insolation increases, so does the magnitude of the ground-to-air sensible heat flux, and an unstable well-mixed convective layer grows rapidly upwards, typically reaching heights of 1 to 2 km in the afternoon. Our understanding of the structure and behavior of the PBL is perhaps the weakest for the evening transition period when the ground-to-air heat flux rapidly ceases and radiational cooling of the ground once again causes the formation of the nocturnal inversion above it, thus effectively "insulating" the elevated pollution layers from the ground below (Smith & Hunt, 1978). Based on the results of a large number of aircraft soundings, Sholtes (1972) has concluded that during the late afternoon, atmospheric turbulence and the mixing height undergo a very rapid decrease. The boundary layer measurements of the Sangamon Experiments (Argonne, 1975) revealed the existence of a transient multilayered, stably-stratified structure of the PBL during morning and evening transition periods. Presumably, the dispersive ability of the atmosphere diminishes drastically and the corresponding transient mixing layer structure is complex.

The simulation of the daytime PBL structure in the present β-mesoscale model is as a three-layer model: the surface layer of height $|L|$ (or 25 m, whichever is smaller), the bulk mixing layer capped by a rising elevated inversion of finite thickness (one grid spacing), and a stable layer above. The variable mixing height is denoted by $h(t)$ and the fixed height of the three-layer PBL (including the top stable layer) is H, chosen to be equal to the maximum value attained by h during

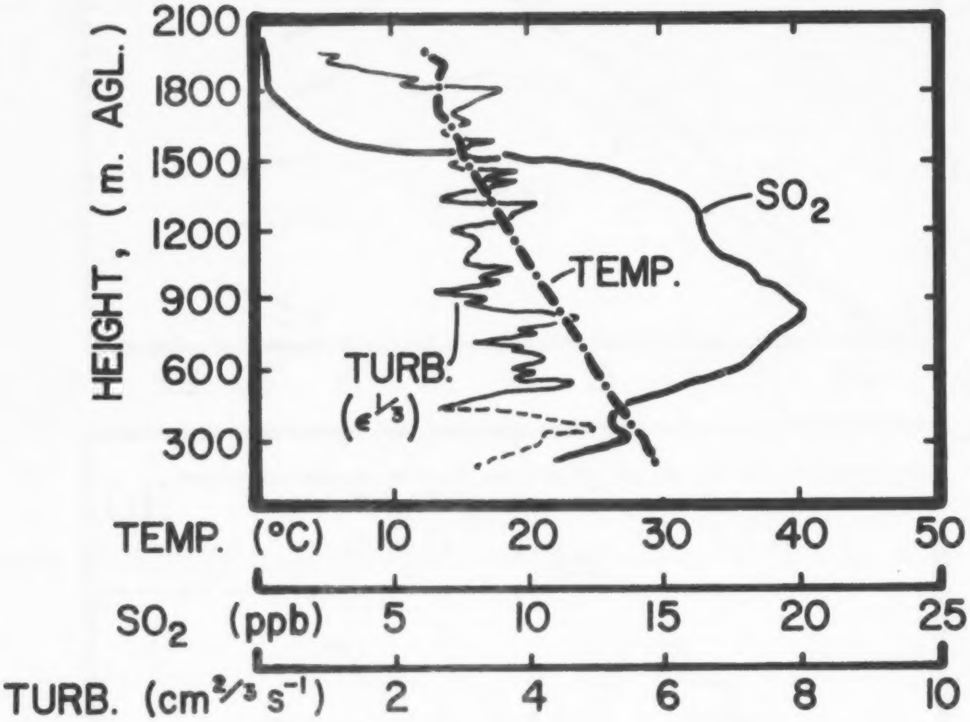

Fig. 3: *Aircraft data of vertical sounding at about 1630 CDT on July 18, 1976. Notice the temperature inversion layer between 1700 and 1900 m, and the corresponding sharp drop in turbulence at the mixing height.*

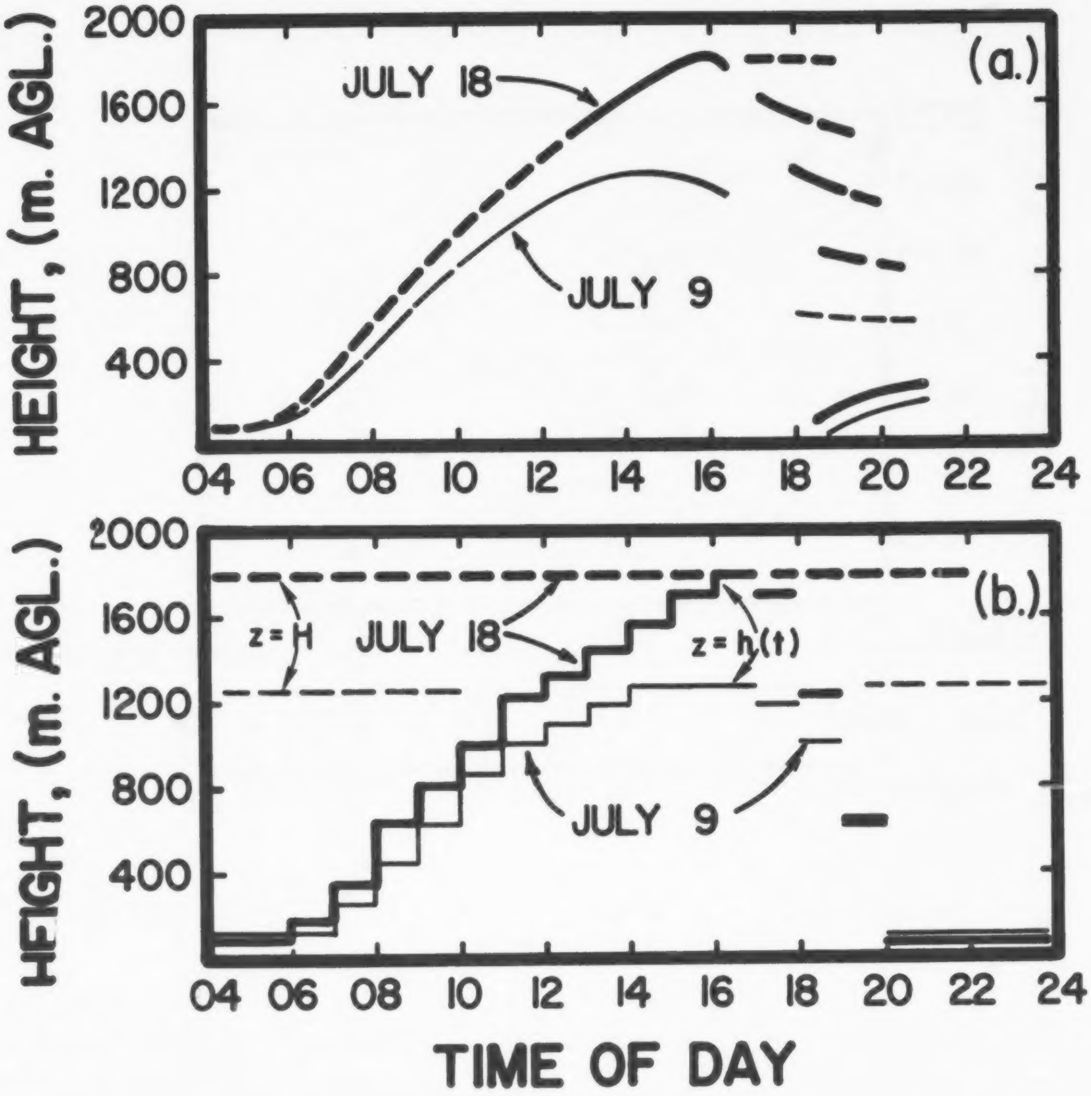

Fig. 4: Temporal variation of the observed (a) and simulated (b) mixing height, h, on July 9 and 18, 1976. Observe the multi-layered PBL structure (a) during the evening transition hours (1800-2000 CDT).

mid-afternoon. The mixing layer and the stable layer above it are effectively decoupled, without the introduction of an explicit boundary condition at the interface, by the insertion of an inversion layer of finite thickness Δ within which $K_z = 0$. In the stable layer, K_z decreases linearly from $K_h/2$ ($K_h = K_z$ at $z = h$) at $z = h + \Delta$ to zero at $z = H$.

For the sampling missions of July 9 and July 18, 1976, direct estimates of h (Fig. 4a) were made from the vertical aircraft sounding data, such as shown in Fig. 3 , collected in the afternoon and evening hours. These data were augmented by the temperature radiosonde data of the Regional Air Monitoring Systems (RAMS) of the St. Louis Regional Air Pollution Study (RAPS) of the U.S. E.P.A. (Myers & Reagan, 1975). Fig. 4b shows the corresponding discrete simulation of the PBL. The mixing height shows a stepwise increase after each hour. The evening transition is modelled by discrete elevated inversion layers, which no longer exist after 1900. Subsequently, the entire PBL is very stable. Values of K_z drop by at least two orders of magnitude between 1600 and 2000 (see Fig. 2).

The present model application is considered only for plume releases within the daytime mixing layer. Calculations of plume concentrations of SO_2 are made during the hours of mixing layer development as well as during the evening transition. Only during the latter case does the plume vertical spread extend into the stable region between h(t) and H. The structure of K_z in this layer thus enters into the model only during the evening transition hours.

2.6 Modeling of reactive plumes

Past field and laboratory research on SO_2 oxidation rates have implicated temperature, humidity, turbulent mixing, intensity of solar radiation, in-cloud residence time of the plume, catalytic heavy metals, soot, ozone, free radicals, hydrocarbons, ammonia, background haziness, air mass history, and various other factors as rate-controlling in the conversion kinetics. Reliable *in situ* measurements of these factors and of the concentrations of some of the reacting species are sparse or even non-existent. A wide range of uncertainty exists concerning the values of many of the reaction rate constants (Davis & Klauber, 1975). The complexity of the situation raises serious questions regarding the relevance of detailed numerical modeling of plume chemistry with the quality and quantity of available input data. One class of models is devoted to a detailed simulation of the formation of photochemical smog, with a focus on multi-component systems of hydrocarbons (HC) and oxides of nitrogen (NO_x). Recently some of these models have been extended to include reactions involving SO_2 (Liu et al., 1976; Isaksen et al., 1978). Another class uses the concept of "overall" conversion rate, α, in a formulation of the following form for a single component

$$r = -\alpha c^a \tag{14}$$

In general, α is a function of time and space, and through its time dependence, in particular, includes the bulk effect of all possible factors influencing the rate of conversion under given conditions. A proper application of this simple approach in a diagnostic model can probably provide results of competitive validity compared to the more complex reactive plume models. Many long range model applications use a constant average value of α (Sheih, 1976; Wendell et al., 1976; Rao et al., 1976; Eliassen and Saltbones, 1975) and a linear conversion process ($a=1$) as a representation of conditions during long range transport. Our β-mesoscale model is based on the concept of "overall" conversion rate.

The eddy diffusion equation is an attractive vehicle for modeling simple as well as complex chemical situations while retaining significant rigor in dispersion simulation. If r can be modeled as a linear term, i.e.

$$r = -\alpha(t)\,\bar{c}, \tag{15}$$

then the solution may be simplified by the following separation of variables:

$$\bar{c}(t,x,y,z) = e^{-\int \alpha(t)dt}\,\chi\,(t,x,y,z) \tag{16}$$

where χ represents the solution of the pure-diffusion problem. This decoupling of the dispersion and conversion problems means that the pure-dispersion concentration profiles remain self-similar even in the presence of conversion. It was shown by Friedlander and Seinfeld (1969) that such an assumption is valid as long as the rate of change of the concentration due to chemical reactions is much smaller than that due to turbulent diffusion. This condition is satisfied in the early hours of plume transport for SO_2 for which the rate of conversion is slow. Our β-mesoscale model uses the formulation of equation 15 and makes the assumption of equation 16.

2.7 Modeling ground removal

Surface dry deposition is most easily treated in the eddy diffusion model as the lower boundary condition, thus

$$K_z \frac{\partial \bar{c}}{\partial z} = v_d \bar{c} , \qquad z = z_r \tag{17}$$

where each side represents the vertical downward flux of the pollutant crossing a reference plane at z_r, commonly about 1 m from the ground. v_d is the so-called deposition velocity introduced by Chamberlain and later discussed by him in terms of a resistance analogy (Chamberlain, 1966). It is a turbulent mass transfer coefficient for the vertical transfer of the pollutant from z_r to its final absorption within the leaf, if the ground cover is vegetation. The mass transfer below z_r is subject to three resistances: the aerodynamic resistance to turbulent transfer above the surface, r_a; a laminar sublayer resistance, r_b; and the resistance at the surface itself, r_s. Then, $v_d = (r_a+r_b+r_s)^{-1}$. During the well-mixed daytime conditions, the surface resistance predominates as r_a is negligible. At night, the atmosphere is stable, and r_a may be expected to be high. The surface resistance is believed to be higher at night, except possibly in the presence of dew (Fowler & Unsworth, 1974). Consequently, v_d is probably smaller at night.

The above formulation of the surface boundary condition was introduced by Monin (1959) and discussed by Calder (1961). The left side of the equation represents the turbulent delivery of the material from above. Consequently, it is really the ratio (v_d/K_0), where $K_0 = K_z$ at z_r, which is the effective ground removal parameter. The non-dimensional formulation may be represented as

$$\frac{\partial \chi}{\partial Z} = Sh. \chi \qquad \text{at } Z = 0, \tag{18}$$

where

$$Sh = \frac{v_d \ell}{K_0} = \text{turbulent Sherwood number of vertical surface layer mass transfer.}$$

ℓ denotes any convenient length scale which may be chosen as h, the mixing height. This dimensionless system parameter governs the ground removal process. Since v_d, h and K_0 are all time-dependent quantities, so is Sh, in general. Typically, $v_d = .01$ m/s, h = 1000 m, $K_0 = 0.1$ m^2/s, and Sh = 100.

3. PROJECT MISTT PLUME MODELS

The principal objective of Project MISTT field studies and related activities is to determine the fate of sulfur emissions in the plumes of the large power plants and the urban-industrial complex of St. Louis. Specifically, the rates of SO_2-to-sulfate conversion and of the ground removal of SO_2 must be extracted from field data. Project MISTT plume modeling efforts started with an analytical, steady-state model with constant K_z (Gillani and Husar, 1975). The model was made numerical with the introduction of a height-dependent K_z (Gillani and Husar, 1976 a, b). The β-mesoscale model is still in the developmental stage. It is a quasi-steady numerical model. The two numerical models are described here.

3.1 Steady-state model

Fig. 5 shows a schematic drawing of an urban plume of near-ground origin, dispersing within a finite mixing layer of constant height, h. A constant steady wind speed is assumed over the mixing layer. Gas-to-particle conversion is modeled as a first order process with the conversion rate being a function of plume age. Vertical eddy diffusion is height-dependent. The applicability of such a model is believed to be

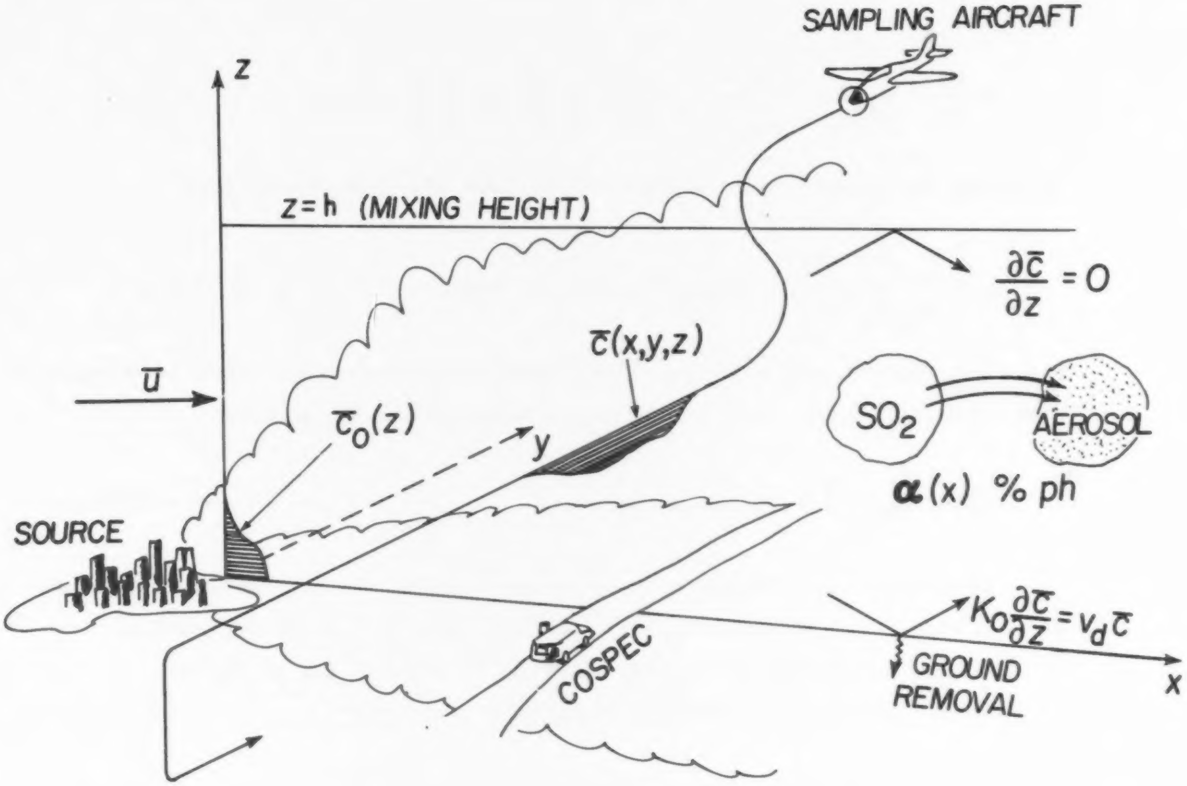
SAMPLING AIRCRAFT
z
z = h (MIXING HEIGHT)
$\frac{\partial\bar{c}}{\partial z} = 0$
$\bar{c}(x,y,z)$
$\bar{u}$
$\bar{c}_o(z)$
y
SO₂
AEROSOL
$\alpha(x)$ % ph
SOURCE
$K_o\frac{\partial\bar{c}}{\partial z} = v_d\bar{c}$
COSPEC
GROUND REMOVAL
x

Fig. **5** : *Illustration of aircraft sampling and modeling of the transport, diffusion, transformation and ground removal of an urban emission within a finite mixing layer.*

valid for periods of upto four or five hours of plume transport under relatively steady, near-neutral conditions. The model formulation is as follows:

$$\bar{u}\,\frac{\partial \bar{c}}{\partial x} = K_H\left(\frac{x}{x_r}\right)^{\gamma} \frac{\partial^2 \bar{c}}{\partial y^2} + K_m\left(\frac{x}{x_r}\right)^{\gamma} \frac{\partial}{\partial z}\left(g(z)\,\frac{\partial \bar{c}}{\partial z}\right) - \alpha(x)\bar{c} \qquad (19)$$

Applying the Taylor hypothesis $t = x/\bar{u}$, and the transformations

$$\chi = \frac{\bar{c}\; e^{\int \alpha(t)dt}}{(Q_0/\bar{u}h^2)} \quad \text{(equation 16)}, \qquad \text{and} \qquad T' = \int \left(\frac{T}{T_r}\right)^{\gamma} dT,$$

and carrying out the non-dimensionalization procedure outlined previously (Section 2), we get the following non-dimensional formulation

$$\frac{\partial \chi}{\partial T'} = g_H\,\frac{\partial^2 \chi}{\partial Y^2} + \frac{\partial}{\partial Z}\left(g(Z)\,\frac{\partial \chi}{\partial Z}\right) \qquad (20)$$

The source is treated as a vertical area source, symmetric laterally about the plane $Y = 0$ and of half width B and vertical distribution $\chi_0(Z)$. The distribution of the emission is assumed to be uniform laterally. Hence, the boundary conditions are

$$\int_0^1 \chi_0(Z)dZ = \frac{1}{2B}, \qquad |Y| \leq B$$

$$\chi \to 0 \text{ as } Y \to \pm\infty \quad ,$$

$$\frac{\partial \chi}{\partial Z} = 0 \quad \text{at} \quad Z = 1 \text{ , and}$$

$$\frac{\partial \chi}{\partial Z} = Sh \cdot \chi \quad \text{at} \quad Z = 0 \text{ .}$$

The following separation of variables solution is assumed

$$\chi(T',Y,Z) = \eta(T',Y) \cdot \zeta(T',Z) \qquad (21)$$

for which η may be determined analytically as

$$\eta(T',Y) = \frac{1}{4B}\left[\mathrm{erf}\left(\frac{Y+B}{2\sigma}\right) - \mathrm{erf}\left(\frac{Y-B}{2\sigma}\right)\right], \qquad (22)$$

where $\sigma = \sqrt{g_H T'}$.

The factor $\zeta(T,Z)$ is a solution of the following two-dimensional problem:

$$\frac{\partial \zeta}{\partial T'} = \frac{\partial}{\partial Z}\left(g(Z)\,\frac{\partial \zeta}{\partial Z}\right) \qquad (23)$$

$$\zeta(0,Z) = \zeta_0(Z)$$

$$\frac{\partial \zeta}{\partial Z} = 0 \text{ at } Z = 1 \text{ and } \frac{\partial \zeta}{\partial Z} = Sh \cdot \zeta \text{ at } Z = 0.$$

Shir's model (equation 9) for $K_z(Z)$ is used for $g(Z)$ in the present model application. The above plume model is solved by the so-called method of lines (Madsen & Sincovec, 1974), a semi-discrete numerical procedure in which the spatial term on the right hand side is discretized by a centered finite difference approximation over a fixed, non-uniform grid in the vertical direction. The semi-discretization yields the following system of simultaneous first order ordinary differential equations:

$$\frac{\partial \zeta_1}{\partial T} = \frac{2}{Z_2-Z_1}\quad g_{1+\frac{1}{2}}\,\frac{\zeta_2-\zeta_1}{Z_2-Z_1} - g_1 \cdot Sh \cdot \zeta_1 \qquad \text{at } Z = Z_1 = 0,$$

$$\frac{\partial \zeta_i}{\partial T} = \frac{2}{Z_{i+1}-Z_{i-1}}\quad g_{i+\frac{1}{2}}\,\frac{\zeta_{i+1}-\zeta_i}{Z_{i+1}-Z_i} - g_{i-\frac{1}{2}}\,\frac{\zeta_i-\zeta_{i-1}}{Z_i-Z_{i-1}} \quad , \quad i = 2,3,\ldots(N-1)$$

$$\frac{\partial \zeta_N}{\partial T} = \frac{2}{Z_N-Z_{N-1}}\quad -g_{N-\frac{1}{2}}\,\frac{\zeta_N-\zeta_{N-1}}{Z_N-Z_{N1}} \qquad \text{at } Z = Z_N = 1$$

In the above equations, the subscript i refers to the value of the variable at the node of the ith grid line above the ground. i = 1 corresponds to $Z = 0$, and $i = N$ to the top of the mixing layer at $Z = 1$. The subscript $i + 1/2$ refers to the value of the variable at the mid point between nodes i and $i + 1$. The equations for $i = 1$ and $i = N$ include the boundary conditions at the ground and the mixing layer top, respectively. The above set of N simultaneous first-order differential equations at each T are integrated numerically by means of Hammings modified predictor-corrector method (Ralston & Wilf, 1969).

Fig. 6 illustrates the role of the ground removal parameter, Sh, for the case of a broad source near the ground, such as an urban-industrial complex. For such an emission, the conversion process is slow in the initial stages of plume transport (White et al., 1976), and dry deposition may be expected to predominate. Consequently, SO_2 conversions are neglected. The plot shows the fractional mass of the gaseous sulfur emission which continues to remain airborne (M_g/M_0) as a function of dimensionless time of transport. For such a ground source, ground removal is seen to be quite rapid initially, and increases with increasing Sh. The data points shown are for the transport of the urban-industrial plume of St. Louis on three summer days in 1973 and 1974. The use of the dimensionless time coordinate includes the effect of meteorology and permits the direct comparison of data of different days for such a ground source. The Sherwood number values are seen to range between 40 and 260, and correspond to a midday range of values of v_d between 0.6 and 2.6 cm/s. Application of this model with height-dependent K_z to the urban plume data of 9/6/73 gave deposition velocities between 2.1 and 2.6 cm/s. The application of the analytical model with constant K to the same data gave corresponding values of 3.9 and 6.9 cm/s. The more realistic simulation of the surface layer resistance to vertical mass transfer in the height-dependent model thus has the effect of lowering the value of v_d significantly.

Fig. 7 illustrates the role of source height in the ground removal of SO_2. $Z_1 = z_1/h$ denotes the dimensionless source height. Four cases are considered, viz. $Z_1 = 0.1, 0.25, 0.50, 0.75$. The results plotted are for plume transport with $Pe = \bar{u}h/K_m = 200$ and $Sh = v_dh/K_0 = 100$. The ground loss of sulfur is seen to be about 18% at $x/h = 48$ for the

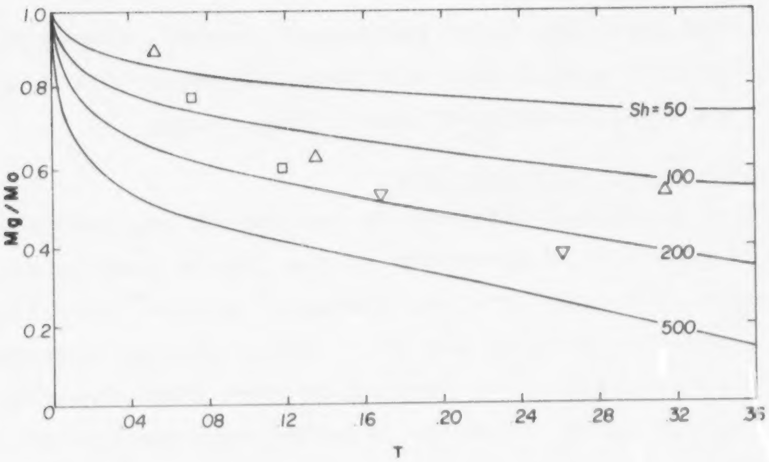

Fig. **6** : *The role of the parameter, Sh, in the ground removal of a surface level emission. The data points are for three different summer days.* M_g/M_o *denotes the airborne fraction of the sulfur emission from the urban-industrial complex of St. Louis.*

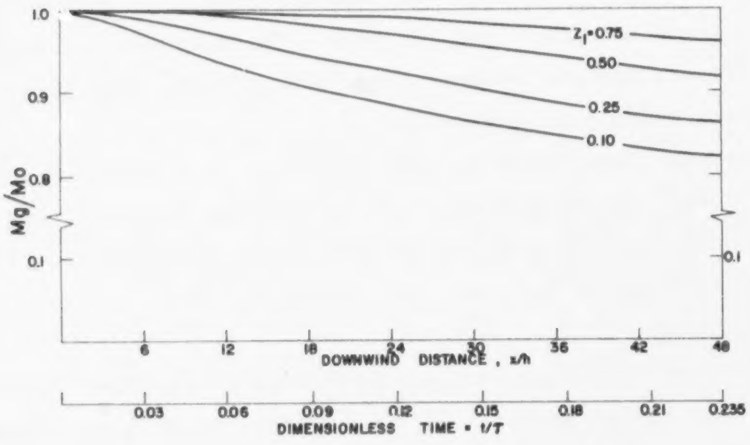

Fig. **7** : *The role of source height* ($Z_1 = z_1/h$) *in the depletion of* SO_2 *by ground removal during short range plume transport (<50 km).*

lowest source and less than 4% for the highest source. These results clearly point out the need to make this mesoscale correction in applications of the box model in transport over a longer range.

3.2 β-mesoscale model: The data base

The data of particular relevance in the present application of the β-mesoscale model are those pertaining to the Labadie power plant plume of July 9 and 18, 1976, and have been discussed in detail by Gillani et al. (1978). There are two main sources of data: aircraft sampling and the St. Louis RAPS network. Data related to power plant characteristics and operations, fuel usage and sulfur emissions were supplied by Union Electric Company. Details related to the aircraft sampling procedures are included in our companion paper (Husar et al., 1978).

Ground level measurements of ambient and dew point temperature, relative humidity, wind speed (10 m), total (direct + diffuse) incoming solar radiation intensity, R_T, in the spectral range 3950-7000A, and ozone monitored at the 25-station Remote Air Monitoring System (RAMS) of the St. Louis Regional Air Pollution Study (RAPS) of the U.S. Environmental Protection Agency (Myers & Reagan, 1975) were obtained in hourly-average form. In particular, the data of Station 118, a rural site to the south of the urban area, have been utilized (see Appendix A). This site was upwind of St. Louis on July 9 and 18, 1976. In addition, vertical profiles of temperature and wind at four RAPS stations were also available from hourly radiosonde measurements.

The above data constitute the level 1 data set. Using this data set, a level 2 data set is generated which consists of quantities directly required in the main plume model or in one of the sub-modules. The components of the level 2 data set are described below.

a) Meteorology:

Transport, $\bar{u}$ -- backward plume trajectories were constructed from the point of sampling to the source. In this manner, plume identification is verified and plume age is determined. These trajectories were computed by Dr. T. B. Smith of MRI utilizing the MISTT mobile pibal data and the RAPS upper air wind data. The upper air wind data of RAPS Station 142 located near Labadie were used to estimate u_0, the wind speed at emission time and height.

Mixing height, h -- mixing heights were determined from inspection of MISTT aircraft data of vertical spirals, and the RAPS vertical temperature profiles. Aircraft data parameters used for this purpose were turbulence, temperature, light scattering coefficient, aerosol charge, SO_2 and ozone.

Eddy diffusivity, K_z -- the quantities needed to determine $K_z(z)$ at each hour are u_*, L and h. The determination of u_* and L is described in Appendix A.

b) Kinetics:

Conversion and removal parameters, α, SH -- these parameters use the above level 2 meteorological data as well as the solar radiation data from level 1.

c) Air Quality:

For each constant-altitude aircraft traverse through the plume in the crosswind direction, the crosswind integrals of the concentrations of gaseous and particulate sulfur in excess of the background concentrations are computed. These are denoted as S_g and S_p ($\mu g/m^2$). For each set of aircraft traverses at different altitudes at a given plume cross-section, the vertical integrals of S_g and S_p are performed to yield the instantaneous mass contents M_g and M_p in vertical plume slabs of unit downwind depth. These line and area integrals of the concentrations are compared with the corresponding model results.

d) Source:

The Labadie power plant of the Union Electric Company is located about 60 km west of the St. Louis Arch. It is a coal-fired plant with four tangentially fired units feeding into one double and two single stacks of 214 m height. This base-load plant has a rated capacity of 2400 MW. The actual power outputs during the hours of interest were about 2250 MW on July 9 and about 1700 MW on July 18. Based on the monthly average of 3.17% sulfur content of the fuel for July 1976, the corresponding total sulfur emissions averaged about 13.6 and 10.2 kg/s (as SO_2) respectively on July 9 and 18.

3.3 β-mesoscale model: Description

For a proper simulation of plume transport beyond 50-100 km and 4-5 hours, the effect of unsteady winds and the dynamics of the mixing layer cannot be ignored. Project MISTT data analyses for the Labadie plume indicate that the overall rate of conversion of SO_2 varies diurnally in close relationship with the intensity of solar radiation (Gillani et al., 1978). The ground removal rate is also believed to be higher during the daytime (see section 2.7). The model presented here is a quasi-steady model in which all time-dependent variables are allowed to change in a stepwise manner after each hour. The steady state model described in section 3.1 is used as a building block. Hourly-averaged values of the input variables are used at any given hour to obtain a steady-state solution for plume dispersion, transformation and ground removal during that hour. At the end of the hour, the output solution (SO_2 concentration distribution) is treated as the initial condition for the next hour, the values of all input variables are updated, and the steady state solution is now computed for the new hour. In this manner, the solution is advanced as the mixing layer evolves, atmospheric stability changes, the transport wind changes, and the pollutant kinetic parameters (α and Sh) change.

The solution is performed in a Lagrangian manner by following a given pollutant release from the source in the quasi-steady manner described above. At any given time, all vertical variations are considered on a fixed Eulerian grid of 21 points extending from the ground ($z=0$) to the top of the PBL ($z=H=h_{max}$). The use of a fixed coarse grid in the vertical plane is not suitable in the early stages of plume spread. Therefore, the analytical solution of Gillani and Husar (1975) is used in the first hour of transport following plume release. This solution uses K_z which is a constant with respect to height, and is a power law function of time in this early stage of plume spread. In the numerical solution of subsequent hours, the chosen grid is coarse and approximately uniform above $Z=0.05$, and relatively fine in the surface layer below $Z=0.05$.

The evolution of the mixing layer is considered within the context of the three layer structure of the PBL described in section .5. Because the mixing height is variable, the constant PBL height, H, is used in the non-dimensionalization of the spatial co-ordinates, instead of h. The 21-point fixed grid extends to H, and the upper reflecting boundary condition is applied there. During the rise of the mixing layer in the daytime, the pollutant released within the mixing layer is effectively decoupled from the stable layer above because $K_z = 0$ in the inversion layer. Thus, the dispersion is confined within the mixing layer. In the evening, following the break-down of the well-defined capped mixing layer, the pollutant in the upper part of the former mixed layer continues to be transported in the stable boundary layer. The model for K_z developed by the author and described in section 2.4 (K Model 1) is used in the model solutions.

Based on observations, the conversion rate of SO_2 is chosen of the form

$$\alpha(t) = A_1 + A_2 \quad R_T(t), \tag{24}$$

where A_1 and A_2 are empirical constants and R_T is the intensity of solar radiation expressed in KW/m^2. Based on the analysis of Project MISTT data for the Labadie plume, nighttime conversion of SO_2 during the summertime is slow compared to the daytime rate (Gillani et al., 1978; Husar et al., 1978). $A_1 = 0$ is used in the present model computations. Solar radiation data are presented in Appendix A.

The ground removal parameter, Sh, is defined as

$$Sh = \frac{v_d H}{K_0} = \frac{v_d H}{K_{zm}} \; \frac{K_{zm}}{K_0} = Sh_m \cdot \frac{1}{g_1}$$

In the model formulation, the removal rate is chosen of the following form

$$Sh_m = S_1 + S_2 \cdot R_T(t) \tag{25}$$

on the assumption that ground removal is more efficient during the daytime than at night. Here, S_1 denotes the nighttime conversion rate. S_1 and S_2 are empirical constants whose values are extracted from the comparison of the model results and field data.

The general solution of the model has the form

$$\frac{\bar{c}(t,y,z)}{Q_0/u_0H^2} = e^{-\int\alpha(t)dt} \cdot \eta(T,Y) \cdot \zeta(T,Z) \tag{26}$$

The crosswind factor $\eta(T,Y)$ is such that

$$\int_{-\infty}^{\infty} \eta(T,Y)\, dY = 1$$

Consequently, as long as the desired outputs are the crosswind integral (S_g), and the cross-sectional area integral (mass M_g) of the excess plume concentration of gaseous sulfur, the factor η (T,Y) need not be computed at all. For this reason, the model solution is carried out only for the two-dimensional time-height plane.

The numerical solution remains stable and well-behaved for all hours under neutral and unstable conditions for which the solutions are carried out. The largest truncation error results from the finite differencing of derivatives with respect to height, and is limited to about 6%. The round-off error is limited by the double-precision accuracy of the computations.

3.4 β-mesoscale model: Comparison with field data

The model application is specifically considered for the field data of July 9 and 18, 1976. Sampling of the Labadie plume was performed beyond 300 km on each day. However, only single traverses were made at each of the sampling distances beyond 200 km. In this study, only those sampled plume cross-sections are considered for which the plume age was greater than 2 hours, and at which multiple crosswind traverses at different altitudes were made. There were three such sampled cross-sections on each of the two days. The corresponding sampling summary is as follows:

		July 9	July 18
Downwind distance	(km):	70, 135, 190	30, 110, 160
Approximate plume release time	(CDT):	0800, 0900, 1200	1400, 1000, 1000
Plume age at sampling	(hr):	3, 6.5, 8.5	2, 6, 9

On July 18, the 30 and 110 km measurements were made at about the same time by two sampling aircraft. It is pointed out that, in general, the sampling of a given day was not Lagrangian, i.e. different air parcels were sampled at different downwind distances. The trajectory and time history of each plume sample is thus independent and model simulation requires an independent run corresponding to each sampled distance. The last two samplings of July 18, at 110 and 160 km, however, approximated a Lagrangian air parcel.

The model is used as a diagnostic tool, in conjunction with the field data, to extract information about three sets of empirical model inputs, viz. $K_z(t,z)$, $\alpha(t)$ and $Sh(t)$. An attempt is made to choose these inputs such that a good match of the model results with the appropriate measured sulfur data is obtained. The corresponding sulfur data to be matched are S_g (the crosswind integral of gaseous sulfur for each traverse), M_p/M_0 (the fraction of the emission which has undergone conversion to particulate sulfur at each sampled plume section), and M_R/M_0 (the fraction of the emission which has been removed at the ground). Fig. 8 shows the comparison of S_g for both days corresponding to the following choice of model inputs:

	July 9	July 18
K-model	Model 1	Model 1
$K_{zm} (m^2/s)$	33.6	13.4
(A_1,A_2)	(0,.020)	(0,.032)
(S_1,S_2)	(0.5,1.5)	(.25,.75)

The above choices of A_1,A_2 and S_1,S_2, when combined with the solar radiation data in accordance with equations 24 and 25, give the following values for the kinetic parameter values:

	July 9	July 18
α, nighttime (%ph)	0	0
α, noon (%ph)	1.82	3.02
Sh, nighttime (-)	88	110
Sh, noon (-)	112	146
v_d, nighttime (cm/s)	0.53	0.47
v_d, noon (cm/s)	1.99	1.79

The comparison between the observed and computed values of S_g (Fig. 8) at each plume section is considered to be good. The comparisons between the observed and computed values of the conversion fraction, (M_p/M_0), and the ground removal fraction, (M_R/M_0), corresponding to the

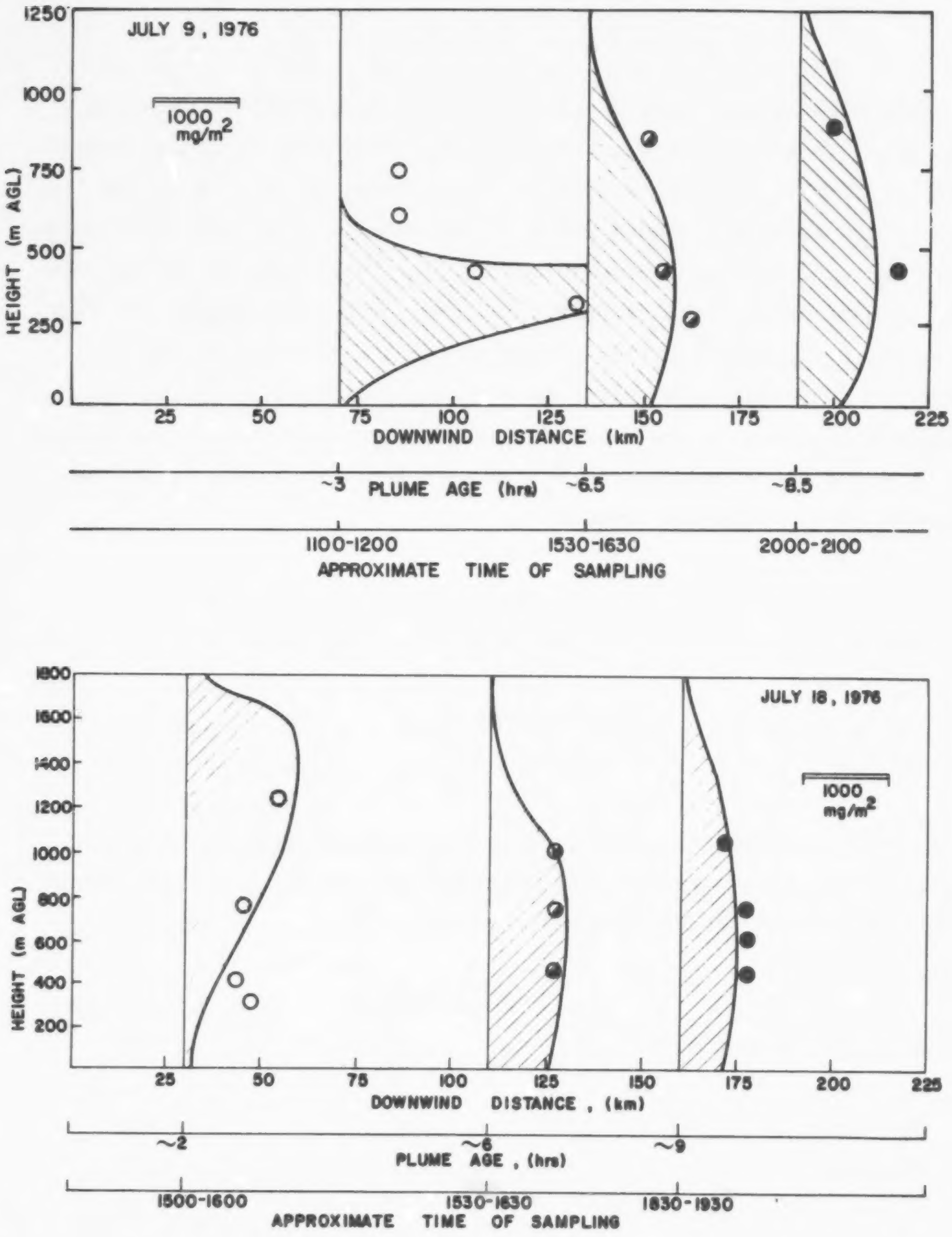

Fig. 8: Comparison of the observed (data points) and calculated values of the crosswind-integrated concentration of gaseous sulfur (S_g) for July 9 and 18, 1976 for the Labadie power plant plume.

above choice of the dispersion, conversion and removal parameters are given in Table V. The comparisons, particularly for the conversion fraction, are good. However, the reader is cautioned that the error margin on the observed data of mass ratios, particularly in the case of ground removal, is quite large.

The rationale for the particular choices of the kinetic rates used in the above comparisons is illustrated in Figs. 9 and 10. Fig. 9 shows the simulated sulfur mass balance for 9 hours of plume transport corresponding to the 1000 CDT plume release on July 18. This release was sampled in a quasi-Lagrangian mode at ages 6 and 9 hours. The sampled data points are also shown in the figure. Three model runs for this plume transport situation were carried out, each with $(A_1,A_2) = (0,.032)$, and each with a different set of values of (S_1,S_2), as shown in the figure. The particular choice of $(S_1,S_2) = (0.25,0.75)$ is made as an approximate representation of the prevailing removal conditions for the day. Near the top of Fig. 9 , the time variation of the chosen α is also shown. In Fig. 10, the effect of different values of A_2, and hence of α, is illustrated. The range of $A_2 = 0$ to 10 corresponds to peak daytime values of α in the range 0 to 9.4% ph. For the choice of $(S_1,S_2) = (0.25,0.75)$, the temporal behavior of v_d and the crosswind-integrated ground level concentration of gaseous sulfur are shown in the lower portion of Fig. 10. Comparison of the model results and the data show that the conversion rates on July 9 and 18 attained peak midday values of about 1.8% ph and 3.0% ph, respectively. The corresponding peak inferred values of v_d are between 1.5 to 2.0 cm/s.

3.5 The effect of diurnal variability on sulfur budget

The pronounced diurnal variability of the PBL has important consequences with respect to the ground removal and the gas-to-particle conversion of atmospheric sulfur. In particular, the existence of a nocturnal inversion near the ground is believed to cause an effective decoupling of the surface sink from the stable layers aloft within which the pollutant contents of the previous evening remain trapped and become available for overnight long range transport. The relatively longer atmospheric residence of nighttime emissions of SO_2, however, is accompanied by a substantially reduced nighttime sulfur conversion rate. It

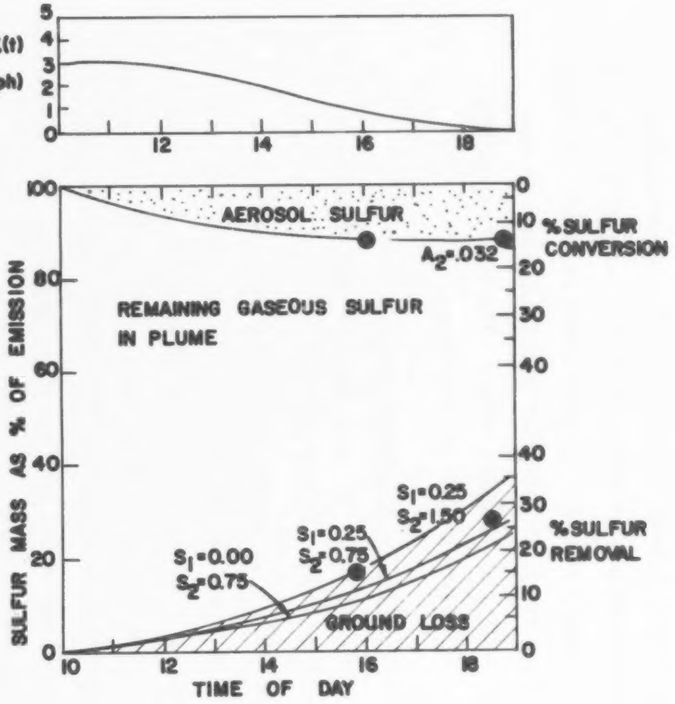

Fig. **9**: *Sulfur budget of the Labadie plume released at 1000 CDT on July 18, 1976 for different ground removal parameters. For the chosen values of the conversion coefficient* A_1 *and* A_2*, the temporal variation of conversion rate* α *is shown in the upper box.*

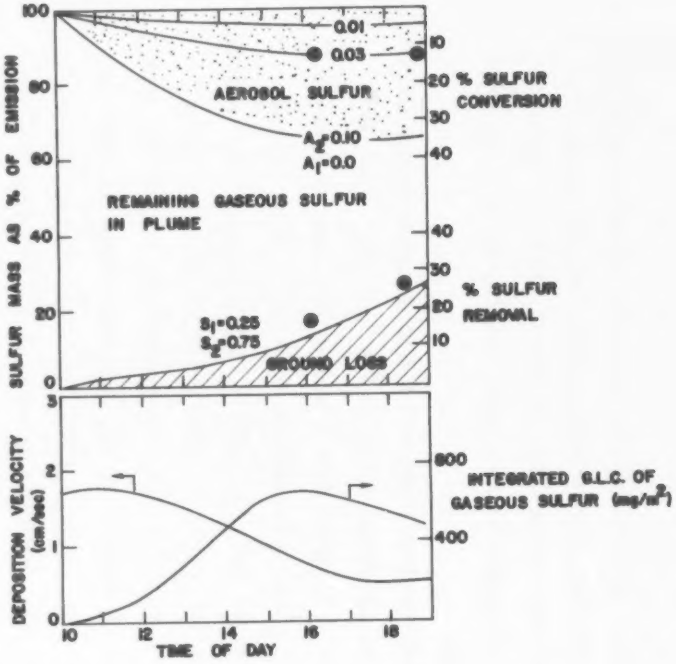

Fig. **10**: *Sulfur budget of the Labadie plume released at 1000 CDT on July 18, 1976 for different values of the conversion coefficient* A_2*. For the chosen values of the ground removal coefficients* S_1 *and* S_2*, the temporal variations of deposition velocity and crosswind-integrated ground level concentration of gaseous sulfur are shown in the lower box.*

is thus difficult to determine intuitively the time in the diurnal cycle corresponding to which the SO_2 emission from a large source will normally experience the maximum amount of conversion.

To investigate the role of time of emission on the overall fate of sulfur in the mesoscale, three plume releases of the Labadie plume on July 18 are considered at 0600, 1000 and 1400 CDT. For the latter two cases, plume measurements were made and the necessary inputs are available. The 0600 release is simulated on the assumption that the plume became trapped under the overlying rising inversion (h=280 m at 0600, stack height = 214 m). The same kinetic parameters (A_1,A_2,S_1,S_2) are used for all three releases. The effective source heights are observed to increase during the day as the vertical mixing domain grows. The results of model computations for the 0600, 1000 and 1400 releases are shown in Fig. 11 a,b,c, respectively. Fig. 12 shows the corresponding temporal plots of crosswind-integrated ground level concentration (a), and the fraction of the sulfur emission remaining airborne as gas (b). The early morning release is rapidly delivered to the ground (fumigation), the corresponding ground level concentration remains high for several hours of the morning, and the ground sink effectively removes about 50% of the sulfur mass by 1300. The 1000 release is subjected to the intense midday mixing, becomes effectively diluted over the entire deep midday mixing layer, with a smaller delivery of the pollutant to the ground compared to the 0600 case, and correspondingly smaller ground removal. Finally, the 1400 release rises to an effective stack height of over 1100 m, experiences a short period of intense mixing, which contributes more towards SO_2 accumulation near the top of the mixing layer than towards downward delivery to the ground. The result is that at 1900 when the residual atmospheric distributions of SO_2 for each of the three releases are compared, the early morning release is mostly depleted (to about 1/e), the 1000 release has also undergone much depletion (to 60%) and is well-mixed. In contrast, the 1400 release shows a preferential accumulation aloft, having experienced little depletion (about 10%). As these remaining pollutant burdens are made available for nighttime long range transport, the implications for sulfate formation within each of these air masses become a little more clear. The bulk of the 1400

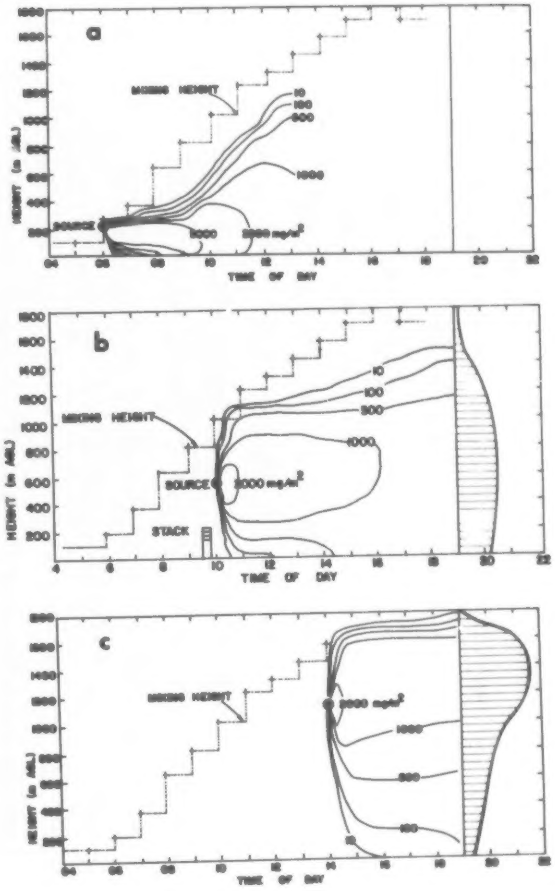

Fig. **11**: Time-height contours of the crosswind-integrated concentration of gaseous sulfur, S_g, for a) 0600 CDT release, b) 1000 CDT release, and c) 1400 CDT release of the Labadie plume of July 18, 1976.

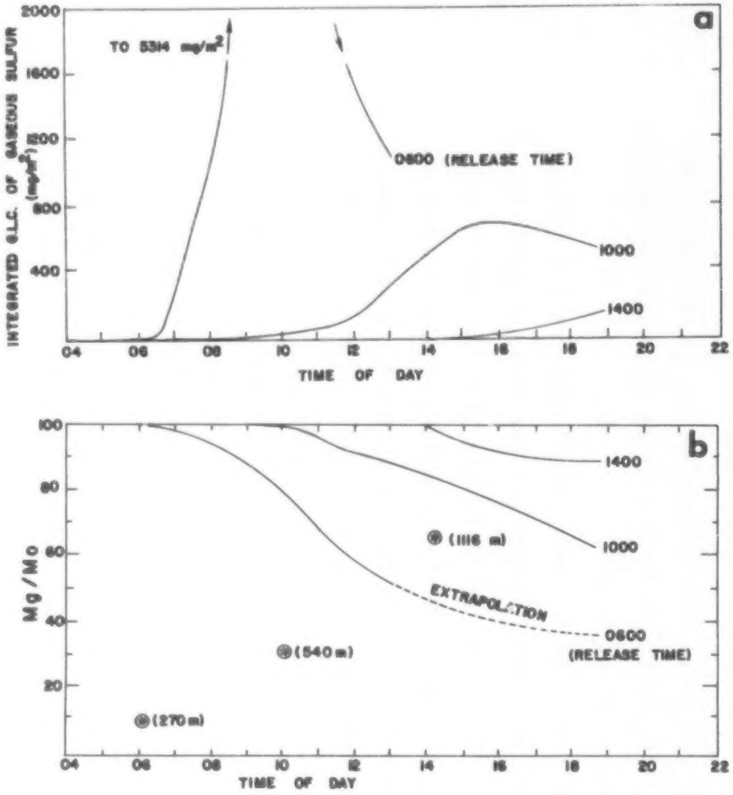

Fig. **12**: Temporal variations of a) the crosswind-integrated ground level concentration, and b) the airborne fraction of the gaseous sulfur emission for the 0600, 1000 and 1400 CDT releases of the Labadie plume of July 18, 1976.

release may be expected to remain aloft and not become entrained into the mixing layer of the next day until perhaps noon or later. Consequently, a significant portion of the sulfur in this air parcel may still remain airborne on the second evening, a substantial part of it already in the secondary particulate form. The remaining SO_2 may undergo yet more conversion during a third day of residence in the atmosphere. The 1000 release would start becoming entrained into the next day's mixing layer from the time the nocturnal inversion becomes eroded, and would presumably be subject to efficient ground removal throughout the day. The 0600 release would undergo a similar fate. It may be inferred from this analysis, that the 1400 release has the greatest potential of the three for maximum particulate sulfur formation. A qualitatively similar conclusion regarding the role of time of emission in overall plume sulfate formation was reached by Husar et al. (1978) based on a simpler box model analysis which was carried out for a period of several diurnal cycles. Such model exercises suggest that a reduction in the emission of SO_2 from large power plants during the late afternoon hours may be a more effective control measure aimed at reduction of large scale sulfate distribution than controlling SO_2 emission at other times of the diurnal cycle.

3.6 The effect of vertical eddy diffusion on the sulfur budget

Dry deposition on the ground is a major scavenging mechanism in the case of SO_2, and vertical eddy diffusion is the only link between elevated emissions of SO_2 and their dry removal. The effective decoupling of elevated plumes from the ground at night is the most obvious illustration of the importance of vertical eddy diffusion to ground removal. The box model assumes instantaneous delivery of matter to the ground from above. Scriven and Fisher (1975) showed that the effect of introduction of finite eddy diffusion (as compared to box model) was to reduce the effective value of v_d by the factor $(1 + \frac{4}{2} \frac{v_d h}{K_z})$, for constant K_z. Gillani and Husar (1975) present a comparison of dry removal of surface emissions for finite and infinite K_z, which points out a dual role of eddy diffusion: near the ground source, a finite K_z gives increased ground removal; far from the source, when the pollutant concentration is higher aloft than near the ground, eddy diffusion has the opposite effect, in conformance with the finding of Scriven and Fisher. Scriven and Fisher also showed that the introduction of a more realistic K-profile in the surface layer resulted in a further reduction in the effective value of v_d. Gillani and Husar (1976a,b) later confirmed this finding in their numerical solution using Shir's vertical profile of K_z. They pointed out that the effect of the surface layer resistance to vertical mass transfer was to slow down the delivery of elevated emissions to the ground as well as to slow down the diffusion away from the ground of surface-level emissions. In the present study, we investigate the effect on ground removal and conversion of SO_2 of different magnitudes and profile-shapes of K_z in the region above the surface layer.

The transport of the 1000 release of July 18 is considered in two runs of the plume model with different models of $K_z(t,z)$. Model 1 (Fig. 2) is that presented in section 2.4 as the author's formulation. The maximum value of eddy diffusion in the afternoon is $K_{zm} = 33.6\ m^2/s$. Model 2 (Fig. 1) is O'Brien's model also presented in section 2.4. This cubic polynomial profile reaches a maximum value of K_z of 150 m^2/s in the mid-afternoon. The two models are thus vastly different in the bulk mixing layer, but are identical in the surface layer of height $|L|$. Fig. 13 shows the vertical profiles of S_g at two-hour intervals using Model 1 for K_z. The corresponding profiles for Model 2 (not shown) are only slightly different. Delivery to the ground as well as to the upper portion of the mixing layer is a little more rapid for Model 2 during early transport. The effective difference in the sulfur budget results obtained using Models 1 and 2 is shown in Fig. 14. The upper figure shows a higher net removal of SO_2 for Model 2, mostly occuring in the first two or three hours of transport. At the end of 9 hours of transport, Model 2 gives 31% loss of gaseous sulfur to the ground compared to 27% for Model 1. A fraction of this difference is a result of a small difference in values of v_d for which the models were run (see lower figure). There is about 1% difference in the amounts of net sulfate formation for the two cases after 9 hours of daytime transport. This surprisingly small difference in dispersion, removal and conversion of SO_2 for the two different K-Models indicates that large differences in K-profiles in the bulk mixing layer are of small consequence in the long

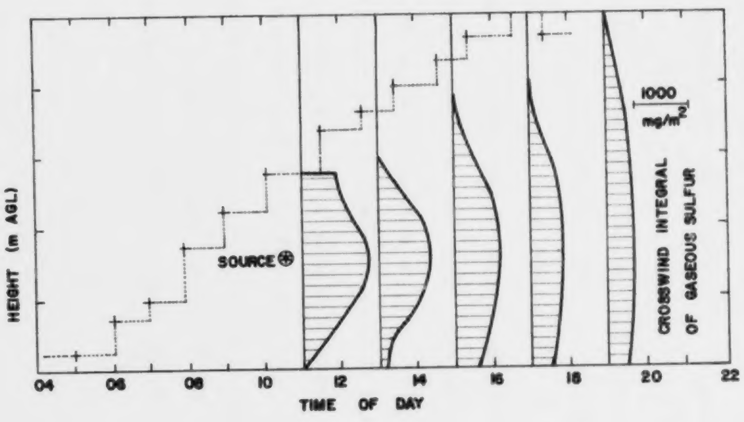

Fig. **13**: 2-hourly vertical profiles of the crosswind-integrated concentrations of gaseous sulfur (S_g) calculated using K-Model 1.

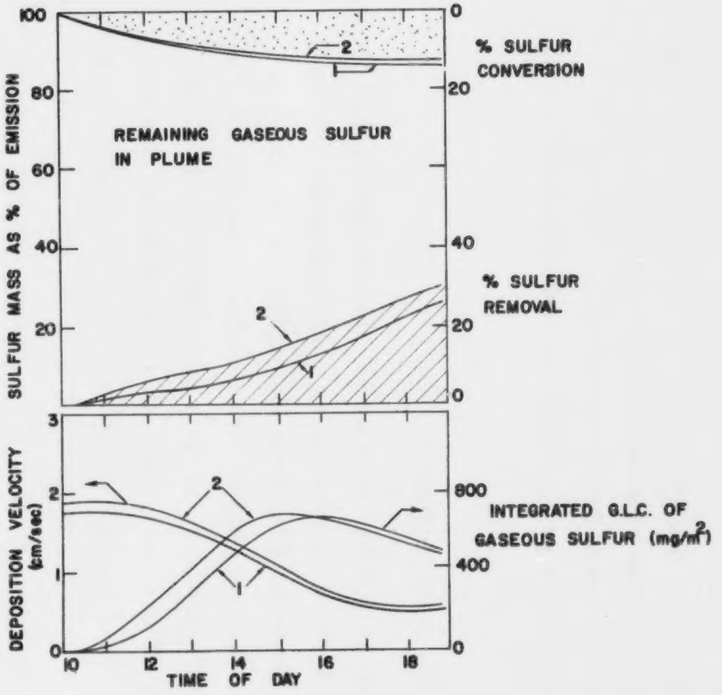

Fig. **14**: Comparison of the calculated sulfur budget of the power plant plume using K-Model 1 (author) and K-Model 2 (O'Brien).

range dispersion of pollutants. The profile of K_z in the surface layer is of dominant significance in the role of vertical eddy diffusion on ground removal. This finding lends further support for the use of a constant K_z in the bulk mixing layer, at least in unstable conditions.

4. CONCLUSIONS

As part of the summer 1976 field program of Project MISTT, the plume of the 2400 MW, coal-fired Labadie power plant was sampled from instrumented aircraft to downwind distances exceeding 300 KM on July 9 and 18. Both SO_2 and particulate sulfur were sampled. Detailed meteorological data were also available. These data provided the motivation for the development of the diagnostic β-mesoscale plume model described in this work. This quasi-steady, Lagrangian model was developed using an existing steady-state model as a building block. Its present application covers a transport range of 200 km over 9 hours. The model incorporates the diurnal variability of the PBL structure, and of the parameters governing the chemical conversion and ground removal of SO_2. A semi-empirical, dynamic, height-dependent submodel is developed for the vertical eddy diffusion coefficient. Two important dimensionless system parameters are identified: the Peclet number, $Pe = \bar{u} H/K_z$, governs plume dilution by transport and eddy diffusion; the Sherwood number, $Sh = v_d H/K_z$, governs ground removal.

The plume model is applied to the field data of July 9 and 18, 1976, and quantitative information about the dispersion, transformation and ground removal of SO_2 is extracted. The variable SO_2 conversion rates are shown to reach peak values of 1.8 and 3.0% ph at noon on July 9 and 18, respectively. Peak values of deposition velocity over open country are estimated at between 1.5 and 2.0 cm/s, also at noon.

The model is used to investigate the roles of Sh, source height, time of emission and eddy diffusion on the overall sulfur budget of the plume. Of the daytime emissions of SO_2, the early morning release becomes depleted to 1/e by 1900, while the mid-afternoon release tends to accumulate aloft and undergoes little depletion by 1900. The mid- and late-afternoon plume releases appear to have the highest potential for long range transport and sulfate formation. This suggestion based on model calculations has important implications regarding the formulation of sulfate control strategy. However, no direct evidence based on Labadie plume measurements has been presented here in support of this suggestion. The need for further measurements of the plume over the entire diurnal cycle is clearly indicated in order to assess the significance of time of plume release on overall sulfate formation.

The effect of finite eddy diffusion, in general, is to reduce the effective deposition velocity. A surface layer (∿50m) of high resistance to vertical mass transfer is of dominant importance in governing the ground delivery of SO_2 from elevated plumes. The profile of K_z above the surface layer appears to have relatively little effect on the overall sulfur budget, particularly after the first two or three hours of plume transport under unstable conditions.

Acknowledgements - The technical support of Dr. William E. Wilson, Jr. is gratefully acknowledged, and the patient review of this paper and useful suggestions of David Patterson are appreciated. To Morris Kahn, Stanley Nowak and Chandrashekhar Pradhan, the author is deeply indebted for their assistance, over and beyond the call of duty, in preparing and running the computer programs. This research was supported (in part) by the Federal Interagency Energy/Environment Research and Development Program through U. S. Environmental Protection Agency Grant No. R803896.

5. REFERENCES

Alkezweeny A. J. and Powell D. C. (1977) Estimation of transformation rate of SO_2 to SO_4 from atmospheric concentration data. Atmospheric Environment 11, 179-182.

Argonne National Lab. (1975) Radiological and Environmental Res. Div. Annual Report ANL-75-60, Part IV

Blackadar A. K. (1957) Boundary layer wind maxima and their significance for the growth of nocturnal inversions. Bull. Amer. Meteor. Soc. 38, 283-290.

Blumenthal D. L., Ogren J. A. and Anderson J. A. (1978) Airborne sampling system for Project MISTT. Atmospheric Environment 12 (1).

Breeding R. J., Klonis H. B., Lodge J. P. Jr., Pate J. B., Sheesley D. C., Englert T. R. and Sears D. R. (1976) Measurements of atmospheric pollutants in the St. Louis area. Atmospheric Environment 10, 181-194.

Businger J. A., Wyngaard J. C., Izumi Y. and Bradley E. F. (1971) Flux-profile relationships in the atmospheric surface layer. J. Atmos. Sci. 28, 181-189.

Calder K. L. (1961) Atmospheric diffusion of particulate material considered as a boundary value problem. J. Meteor. 18, 413-415.

Chamberlain A. C. (1966) Transport of gases to and from grass and grass-like surfaces. Proc. Roy. Soc., Series A, 290, 236-265.

Corrsin S. (1974) Limitations of gradient transport models in random walks and in turbulence. Advan. Geophys. 18A, 25-60.

Davis D. D. and Klauber G. (1975) Atmospheric gas phase oxidation mechanisms for the molecule SO_2. Int. J. Chem. Kinetics, Symp. No. 1, 543-556.

Deardorff J. W. (1967) Empirical dependence of the eddy coefficient for heat upon stability above the lowest 50m. J. Appl. Meteor. 6, 631-643.

Deardorff J. W. (1970) Preliminary results from numerical integrations of the unstable planetary boundary layer. J. Atmos. Sci. 27, 1209-1211.

Deardorff J. W. (1973) Three-dimensional numerical modeling of the planetary boundary layer. In Workshop on Micrometeorology, Amer. Met. Soc., 271-311.

Donaldson C. duP. (1973) Construction of a dynamic model of the production of atmospheric turbulence and the dispersal of atmospheric pollutants. In Workshop on Micrometeorology, Amer. Met. Soc., 313-392.

Eliassen A. and Saltbones J. (1975) Decay and transformation rates of SO_2 as estimated from emission data, trajectories and measured air concentrations. Atmos. Environment 9, 425-429.

EPA (1975) Position Paper on Regulation of Atmospheric Sulfates, U. S. Environmental Protection Agency, EPA 450/2-75-007, Research Triangle Park, N.C.

Fowler D. and Unsworth M. H. (1974) Dry deposition of sulfur dioxide on wheat. Nature 249, 389-390.

Friedlander S. K. and Seinfeld J. H. (1969) A dynamic model of photochemical smog. Environ. Sci. Technol. 3, 1175-1181.

Garland J. A. (1978) Dry and wet removal of sulfur from the atmosphere. Atmospheric Environment 12(1).

Gillani N. V. and Husar R. B. (1975) Mathematical modeling of air pollution - A parametric study. Proc. 2nd. Federal Conf. on the Great Lakes, Argonne, Ill.

Gillani N. V. and Husar R. B. (1976a) Mesoscale model for pollutant transport, transformation and ground removal. Preprints, 3rd Symposium on Atmospheric Turbulence, Diffusion and Air Quality, Raleigh, N.C.

Gillani N. V. and Husar R. B. (1976b) Analytical - numerical model for mesoscale transport, transformation and removal of air pollution. Paper presented at the 7th International Technical Meeting on Air Pollution Modeling and Its Application, NATO/CCMS, Airlie, Virginia.

Gillani N. V., Husar R. B., Husar J. D. and Patterson D. E. (1978) Project MISTT: Kinetics of particulate sulfur formation in a power plant plume out to 300 km. Atmospheric Environment 12(1).

Herrmann K. (1976) The role of turbulent diffusion in the direction of the mean wind in a numerical AQSM. Paper presented at the 7th International Technical Meeting on Air Pollution Modeling and Its Applications, NATO/CCMS, Airlie, Virginia.

Hill A. C. (1971) Vegetation: A sink for atmospheric pollutants. J.A.P.C.A. 21(6), 341.

Holzworth G. C. (1972) Mixing heights, wind speeds, and potential for urban air pollution throughout the contiguous United States. U. S. Environmental Protection Agency, AP-101.

Husar, R. B., Patterson D. E., Husar J. D. and Gillani N.V. (1978) Project MISTT: Sulfur budget of a power plant plume. Atmospheric Environment 12(1).

Isaksen I. S. A., Hov O. and Hesstvedt E. (1978) A chemical model for urban plumes: Test for ozone and particulate sulfur formation in St. Louis urban plume. Atmospheric Environment 12(1).

Islitzer N. F. and Slade D. H. (1968) in Meteorology and Atomic Energy. Ch. 4, D. H. Slade (ed).

Liu M. K., Yocke M. A. and Mundkur, P. (1976) Numerical simulation of reactive plumes. 1976 Air Series, Am. Inst. Chem. Engrg.

Madsen N. K. and Sincovec R. F. (1974) The numerical method of lines for the solution of non-linear partial differential equations. In Computation Methods in Nonlinear Mechanics, J. T. Oden et al., Eds., Texas Inst. for Computational Mechanics, Austin, Texas.

Monin A. S. (1959) On the boundary condition on the earth surface for diffusing pollution. Advan. Geophys. 6, 435-436.

Myers R. L. and Reagan J. A. (1975) The Regional Air Monitoring Systems, St. Louis, Missouri, U.S.A. Paper presented at the International Conference on Environmental Sensing and Assessment, Las Vegas, September 15-19.

O'Brien J. J. (1970) A note on the vertical structure of the eddy exchange coefficient in the planetary boundary layer. J. Atmos. Sci. 27, 1213-1215.

Orlanski I., Ross B. B. and Polinsky L. J. (1974) Diurnal variation of the planetary boundary layer in a mesoscale model. J. Atmos. Sci. 31, 965-989.

Pasquill F. (1974) Limitations and prospects in the estimation of dispersion of pollution on a regional scale. Advan. Geophys. 18B, 1-13.

Peters L. K. and Klinzing G. E. (1971) The effect of variable diffusion coefficients and velocity on the dispersion of pollutants. Atmos. Environment 5, 497-504.

Priestly C. H. B. (1954) Convection from a large horizontal surface. Austral. J. Phys. 6, 279-290.

Ralston A. and Wilf H. S. (1960) Mathematical Methods for Digital Computers, Wiley, N.Y., 95-109.

Rao K. S., Lague J. S. and Egan B. A. (1976) An air trajectory model for regional transport of atmospheric sulfates. Preprints, 3rd. Symp. on Atmos. Turbulence, Diffusion, and Air Quality. Amer. Met. Soc., Raleigh, N.C., 325-331.

Scriven R. A. and Fisher B. E. A. (1975) The long range transport of airborne material and its removal by depostion and washout - II. The effect of turbulent diffusion. Atmos. Environment 9 59-68.

Sheih C. M. (1976) Application of a Lagrangian statistical trajectory model to the simulation of sulfur pollution over northeastern United States. Preprints, 3rd. Symp. Atmos. Turbulence, Diffusion, and Air Quality. Am. Meteor. Soc., Raleigh, N.C., 311-317.

Shir C. C. (1973) A preliminary numerical study of atmospheric turbulent flows in the idealized planetary boundary layer. J. Atmos. Sci. 30, 1327-1339.

Sholtes R. S. (1972) The growth and decay of turbulent mixing in the planetary boundary layer. Environmental Monitoring Series EPA-R4-72-001.

Smith F. B. and Jeffrey G. H. (1975) Airborne transport of sulfur dioxide from the U.K. Atmospheric Environment 9, 643-659.

Smith T. B., Blumenthal D. L., Anderson J. A. and Vanderpol A. H. (1978) Transport of SO_2 in power plant plumes; day and night. Atmospheric Environment 12(1).

Smith F. B. and Hunt R. D. (1978) Meteorological aspects of the transport of pollution over long distances. Atmospheric Environment 12(1).

Townsend A. A. (1967) Wind and the formation of inversions. Atmos. Environment 1, 173-175.

Wendell L. L., Powell D. C. and Drake R. L. (1976) A regional scale model for computing deposition and ground level air concentration of SO_2 and sulfates from elevated and ground sources. Preprints, 3rd Symp. Atmos. Turbulence, Diffusion, and Air Quality, Amer. Met. Soc., Raleigh, N.C., 318-324.

Whitby K. T. (1977) Physical properties of sulfur aerosols. Atmospheric Environment 12(1).

White W. H., Anderson J. A., Blumenthal D. L., Husar R. B., Gillani N. V., Husar J. D. and Wilson W. E., Jr. (1976) Formation and transport of secondary air pollutants: Ozone and aerosols in the St. Louis urban plume. Science 194, 187-189.

Wilson, W. E. (1978) Sulfates in the atmosphere: A progress report for Project MISTT. Atmospheric Environment 12(1).

Yordanov D. (1972) Simple approximation formulae for determining the concentration distribution of high sources. Atmos. Environment 6, 389-398.

APPENDIX A

Determination of Monin-Obukhov stability length, L

By definition, $$L = \frac{\rho c_p T_o u_*^3}{\kappa g H_o} \qquad (1)$$

where ρ = density of air = 1.20 kg/m^3,

c_p = specific heat of air at constant pressure = 1.00 $\frac{\text{KW-sec}}{\text{kg}^o\text{K}}$,

T_o = ground level temperature, ^{o}K,

u_* = friction velocity, m/s,

κ = von Karman's constant = 0.4,

g = acceleration due to gravity = 9.81 m/s^2

H_o = sensible heat flux from the ground, KW/m^2.

In the surface layer, the shape of the wind profile is given by

$$(\bar{u}/u_*) = (1/\kappa)\cdot\left[\ln(z/z_o) - \psi_m(z/L)\right], \qquad (2)$$

where z_o is the ground roughness length, and the stability correction function for momentum, ψ_m is given by (Argonne, 1975).

$\psi_m(z/L) = 1$, Neutral

$\psi_m(z/L) = -5(z/L)$, Stable

$\psi_m(z/L) = 2\ln\left[(1+\chi)/2\right] + \ln\left[(1+\chi^2)/2\right] - 2\tan^{-1}\chi + \pi/2$, Unstable

where $\chi = 1-16(z/L)^{0.25}$.

Substitution of ψ_m into equation (2) gives an implicit relationship between u_* and L which is solved iteratively.

Equations 1 and 2 require five empirical inputs, viz. z_o, z, $\bar{u}(z)$, T_o and H_o. For the open country terrain over which the Labadie plume was transported on July 9 and 18, 1976, z_o = 5 cm is taken as a representative value. z = 10 m is chosen since the hourly data for $\bar{u}$ at 10 m are available for RAPS station 118, a rural ground monitoring station of the Regional Air Polluton Study in St. Louis (Myer & Reagan, 1975). The measured value of ambient temperature at 5 m height at the RAPS station is utilized for T_o. No direct measurements are available for H_o. Its hourly value is derived from values of R_T, the intensity of total (direct + diffuse) solar radiation in the spectral range 3950-7000 Å, as measured by a hemispherical pyranometer apparatus at RAPS station 118. Thus, $H_o = (H_o/R_T) \quad R_T$. The ratio H_o/R_T is determined based on hourly measured values of H_o and R_T on August 10, 1975 at the Sangamon Experiment site (a rural location approximately 100 km NE of St. Louis) of Argonne National Laboratory (Argonne 1975). The values of the ratio are adapted to the conditions of July 9 and 18, 1976 by assuming that H_o/R_T is directly proportional to the mixing height under peak midday convective conditions. These values of h_{max} are available from direct measurements, using the WHAT (wind, height and temperature) system at Sangamon on August 10, and from MISTT aircraft soundings on July 9 and 18.

The hourly values of T_o, $\bar{u}_{10}$, R_T, H_o, h, u_* and L for the hours 0500 to 2400 for July 9 and 18 are listed in Tables A-I and A-II, respectively.

TABLE A-1

METEOROLOGICAL DATA FOR JULY 9, 1976

TIME (CDT)	T_o (C)	$\bar{u}_{10}$ (m/s)	R_T (KW/m^2)	H_o (KW/m^2)	h (m)	u_* (m/s)	L (m)
0500	21.6	1.9	.022	-.030	100	.127	6.2
0600	22.5	2.0	.225	.001	150	.155	-258.2
0700	24.6	2.2	.533	.041	275	.198	-17.3
0800	26.3	2.2	.501	.048	450	.200	-15.5
0900	28.2	2.4	.652	.090	650	.226	-11.7
1000	29.6	3.4	.802	.123	850	.301	-20.6
1100	30.4	4.1	.888	.175	1000	.358	-24.3
1200	31.0	4.8	.909	.215	1100	.411	-30.1
1300	31.6	5.2	.869	.211	1200	.438	-37.2
1400	32.1	4.8	.760	.177	1250	.406	-35.3
1500	32.0	4.7	.600	.131	1250	.392	-42.9
1600	31.8	4.9	.426	.088	1220	.398	-67.2
1700	31.1	4.5	.233	.032	1120	.355	-130.7
1800	29.8	3.0	.070	.000	920	.226	∞
1900	27.9	2.6	0	-.018	600	.191	35.8
2000	26.1	2.6	0	-.036	100	.186	16.4
2100	25.1	3.1	0	-.050	100	.224	20.5
2200	24.3	3.0	0	-.050	100	.216	18.3
2300	23.9	3.0	0	-.050	100	.216	18.2
2400	23.9	3.0	0	-.050	100	.216	18.2

TABLE A-2

METEOROLOGICAL DATA FOR JULY 18, 1976

TIME (CDT)	T_o (C)	$\bar{u}_{10}$ (m/s)	R_T (KW/m^2)	H_o (KW/m^2)	h (m)	u_* (m/s)	L (m)
0500	14.1	1.6	.046	.003	100	.130	-64.8
0600	15.8	1.5	.210	.019	150	.140	-12.7
0700	19.7	1.7	.406	.047	350	.165	-8.6
0800	22.9	2.1	.591	.089	600	.204	-8.7
0900	25.3	2.2	.744	.152	800	.222	-6.6
1000	26.8	2.6	.842	.190	1000	.255	-8.0
1100	27.7	3.1	.931	.272	1200	.300	-9.1
1200	28.2	3.6	.944	.347	1350	.342	-10.7
1300	28.7	3.3	.886	.330	1500	.319	-9.1
1400	29.2	2.8	.776	.287	1600	.280	-7.0
1500	29.3	2.6	.623	.192	1700	.255	-8.0
1600	29.1	2.7	.443	.123	1800	.253	-12.1
1700	28.5	2.7	.247	.046	1700	.234	-25.8
1800	27.2	2.8	.075	.000	1200	.211	∞
1900	24.9	2.2	0	-.018	650	.159	20.3
2000	23.3	2.8	0	-.036	100	.202	20.9
2100	22.5	2.3	0	-.050	100	.155	6.8
2200	21.6	2.5	0	-.050	100	.173	9.4
2300	21.0	3.0	0	-.050	100	.216	18.0
2400	20.0	3.0	0	-.050	100	.216	18.0

An improved source depletion model for deposition from a Gaussian plume

J. Giebel

1. Introduction

Dry deposition on the surface is an important sink for a number of pollutants. It reduces the ambient concentration of an emitted pollutant in dependance on the effective height of the emission source. The depletion increases with decreasing effective stack height.

In the case of a Gaussian plume there are mainly two ways to calculate the depletion of a pollutant by deposition: the source depletion model originally proposed by Chamberlain /‾1, 2_7 and the surface depletion model developed by Horst /‾3_7.

In this study the source depletion model is expanded by accepting

the dependance of the deposition velocity on wind speed and

the altering of the transport velocity of the pollutant with increasing source distance because of the diffusion of the pollutant in the vertical.

Additionally, dispersion coefficients dependant on stack height are applied.

To consider dry deposition, Chamberlain modified the Gaussian plume formula by replacing the source term Q_o by an effective depleted source term, Q_x. The correction factor for deposition $\frac{Q_x}{Q_0}$ has the form

$$1.\quad \frac{Q_x}{Q_0} = \exp\left[-\left(\frac{2}{\pi}\right)^{\frac{1}{2}} \frac{\bar{v}_g}{\bar{u}} \int_0^x \frac{1}{\sigma_z(x)} \exp\left(\frac{-h_{eff}^2}{2\sigma_z(x)^2}\right) dx\right]$$

$\chi(x,y)$	air concentration of pollutant [mg/m^3]
Q_0	emission rate of pollutant [mg/s]
$\frac{Q_x}{Q_0}$	correction factor for dry deposition
$\bar{v}_g$	mean deposition velocity [m/s]
$\bar{u}$	mean transport velocity [m/s]
h_{eff}	effective height of emission [m]
$\sigma_z(x)$	vertical dispersion coefficient [m]
$\sigma_y(x)$	crosswind dispersion coefficient [m]

The method is based on the assumptions that the deposition rate ω equals the immediate ground-level air concentration $\chi(x,y,0)$ multiplied by the mean deposition velocity v_g

and that the shape of the concentration profile is unaltered by deposition:

Thomas W. Horst developed a model which selectively depletes the Gaussian plume in the vicinity of the deposition surface rather than throughout the vertical extent of the plume. Therefore he called his model surface depletion model.
In general it predicts smaller surface concentrations than does the source depletion model. With stable atmospheric conditions and high deposition velocities the differences are greatest.

A deposition velocity of 1 cm/s is representative for pollutants readily absorbed on the ground /‾4_7. Average atmospheric conditions are represented by stability class *D* , a wind speed of 3 m/s in anemometer level and a transport velocity of 5 m/s in greater source distances. With these parameters and an effective emission height of 1o m, for source distances between 2 and 5o km, the surface depletion model predicts a concentration 1 m above the ground which is about 88 % of the concentration predicted by the source depletion model.

With an effective stack height of 1oo m at a source distance of 1o km the difference is 1/4 of the concentration predicted by the source depletion model.
With decreasing distance the difference increases and in distances between 1o and 5o km the difference

decreases. For the very high value of

$$v_g / \bar{u} \quad = 0{,}01$$

the differences are greater.
But this value will not be reached with a mean deposition velocity of 1 cm/s. This is shown in the next section, where the source depletion model is expanded.

2. Expanded model

2.1 Dependance of the deposition velocity on wind speed

Experimental investigations, among other those of Hill [5], show that the deposition velocity increases with increasing windspeed. Therefore Stratmann [6] developed an equation which considers the dependance of the deposition velocity on wind speed:

$$2. \quad v_g\,(u) \qquad 1/4\;\bar{v}_g + 1/4\,\bar{v}_g\;\frac{u}{u_o}$$

v_g (u)	momentary deposition velocity m/s
$\bar{v}_g$	average deposition velocity m/s
u	wind speed in anemometer level m/s
u_o	reference velocity of 1 m/s

Which values can the quotient $v_g\,(u)/\bar{u}$ reach according to this equation? The Gaussian model, for which the discussed deposition models are developed, can be used, when the wind speed in anemometer level is greater than 1 m/s. When the transport velocity equals this windspeed, the quotient $v_g\,(u)/\bar{u}$ reaches its highest value. It then equals half of the mean deposition velocity. But this value is only to be expected in the neighbourhood of low sources.

With increasing source distance, respectively effective source height, the transport velocity u quickly reaches a value which is twice as big as the windspeed in anemometer level. Therefore the maximum value of the quotient $v_g\ (u)/\bar{u}$ ist usually only 1/4 of the mean deposition velocity in m/s. (With the mean deposition velocity of 1 cm/s only about o.oo25.)
Up to this value, however, the differences between the surface concentrations predicted by the two models remain low.

2.2 Consideration of the changing transport velocity with increasing source distance.

In addition to the dependance of the deposition velocity on windspeed the changing of the transport velocity with increasing source distance will be considered. In the depletion models known to the author the transport velocity is a constant value. There is no objection to this method as long as the transport velocity is calculated for the vicinity of the source. However, when concentrations are simulated for source distances of more than about 5 km, or in the case of low sources already for source distances of more than 2 km, the application of a constant transport velocity may cause greater deviations from the true concentrations.

While travelling downwind the pollutants disperse in the vertical until the top of the mixing layer is reached. With the pollutants spreading in the vertical, the transport velocity changes however, because the wind speed increases with height.

The dispersion of the plume in the vertical is described by the standard deviations of plume concentration distribution $\sigma_z(x)$, which increase with increasing source distance. Therefore, the changing of the transport velocity with increasing source distance is connected with the increase of $\sigma_z(x)$.

In the Gaussian plume model, mainly used in North Rhine Westfalia, the transport velocity is the mean wind speed between the earth and the effective height of emission. In this study the following method is proposed: To the effective height of emission h_{eff}, $\sigma_z(x)$ is added, and transport velocity is the mean wind speed between the ground and the height obtained in this way. When the sum of h_{eff} and $\sigma_z(x)$ becomes bigger than the height of the top of the mixing layer, then the transport velocity is the mean wind speed between the ground and the top of the mixing layer.

$$3. \quad \bar{u}(x,u) = \left(\frac{h(x)}{z_0}\right)^m * \frac{u}{1+m}$$

$$\text{with } h(x) = \sigma_z(x) + h_{eff} \quad \text{when } \sigma_z(x) + h_{eff} \leq H$$

$$\text{and } h(x) = H \quad \text{when } \sigma_z(x) + h_{eff} > H$$

$\bar{u}$ (x, u)	transport velocity
u	wind speed in anemometer level
h (x)	sum of h_{eff} and $\sigma_z(x)$
σ_z (x)	standard deviations of plume concentration distribution in the vertical

m	exponent for calculating the vertical wind profile
h_{eff}	effective height of emission
H	height of the top of the mixing layer
z_a	anemometer level (usually 1o m)

2.3 Expansion of the source depletion model for dry deposition

When the dependance of the deposition velocity on wind speed and the proposed method to calculate the transport velocity are taken into account the equation for dry deposition, originally proposed by Chamberlain, has the following form

$$4. \quad \frac{Q_x}{Q_0} = \exp\left[-\left(\frac{2}{\pi}\right)^{\frac{1}{2}} * \left(\frac{1}{4}\bar{v}_g + \frac{1}{4}\bar{v}_g * \frac{u}{u_0}\right) \int_0^x \frac{1}{\bar{u}(x,u)\,\vec{\sigma}_z(x)} * \exp\left(\frac{-h_{eff}^2}{2\vec{\sigma}_z(x)^2}\right) dx\right]$$

3. Comparison of the two models

The expanded source depletion model predicts smaller deposition rates and therefore higher surface concentrations than the original model. (In the calculation with the original model transport velocity is the windspeed in anemometer level when the effective height of emission is 1o m. With an

effective stack height of 1oo and 2oo m, transport velocity is the mean wind speed between the ground and the effective height of emission.)
Table 1 and figures 1 to 8 show the differences for a deposition velocity of 1 cm/s. The stability class is mainly D, windspeed in anemometer level 1 and 3 m/s.

With a windspeed of 1 m/s in anemometer level, stability class D and an effective emission height of h_{eff} = 1o m, the original model predicts that up to a source distance of 5 km more than half of the amount of the emitted pollutant is deposited on the ground, wereas the expanded model predicts only a removal of about 1/4. Surface concentration is reduced to about 5o % respectively to about 75% of the concentration values without deposition.

The dependance of the deposition velocity on windspeed has here a somewhat greater influence on the concentration than the dependance of the transport velocity on source distance.

With an effective stack height of 1oo m the surface concentration decreases about 1o% up to a source distance of 1o km, according the expanded model; whereas the original model predicts a decrease of about 1/4. (stability class D, windspeed in anemometer level 1 m/s)

At a windspeed of 3 m/s in anemometer level the differences are not so great. At this windspeed, the momentary deposition velocity equals the mean deposition velocity and therefore the consideration of the dependance of the deposition velocity on windspeed does not change the depletion of the pollutant in comparison to the original model.

With increasing windspeed the differences between original and expanded model decrease further. Because of the high transport velocity, however, the depletion of the pollutant is relatively low.
For a windspeed of 3 m/s in anemometer level and stability class D the two models give the following results:
With an effective stack height of 1o m, according to the expanded model up to a source distance of 1o km dry deposition reduces the surface concentration to 76 % of the value obtained when dry deposition is not considered.
The original model on the other hand predicts a surface concentration of 64 % of the concentration values without deposition (Table 1, figure 3).
With an effective stack height of 1oo m up to a source distance of 5o km the corresponding values are 78 and 71 % (Table 1, figure 4)

Figures 5 and 6 show the depletion for class A (unstable equilibrium)and class F (stable equilibrium).
In comparison to class D, depletion is decreased for unstable conditions and increased for stable conditions

The figures 7 and 8 and table 1 show the quotient of the surface concentration with deposition and the surface. concentration without deposition in dependence on source distance for the average annual concentration, according to the original and the expanded source depletion model.
The effective heights of emissions are 1o and 1oo m.
The values were calculated on the basis of the Meteorological Parameters of Düsseldorf-Flughafen. (Table 2)
The mean windspeed at anemomter level is 3.8 m/s.
For this windspeed, according to equation 2. the mean deposition velocity is 1.2cm/s, when the mean deposition velocity for a mean windspeed of 3 m/s is 1 cm/s.
To be able to compare the values calculated with the different deposition models, the simulation with the original model was done with the deposition velocity of 1.2 cm/s.

With an effective stack height of 1o m the original model predicts a decrease of the surface concentration of 6o % up to a source distance of 1o km, whereas the expanded model predicts a decrease of 32 %.
With an effective stack height of 1oo m the corresponding values are 17 and 7 %.

Figure 9 shows the ratio between the surface concentration with deposition and the surface concentration without deposition for the effective stack heights of 1o, 1oo and 2oo m for stability class D and a windspeed of 1 m/s in anemometer level, according to the expanded model. With an effective stack height of 1o m and a source distance of 2o km about 3o % of the emitted pollutant is deposited on the ground. With an effective stack height of 1oo m the corresponding value is about 14 % and with an effective stack height of 2oo m about 6 %.

The figure 7 shows that the depletion decreases with increasing effective height of emission.

The differences however, are low in comparison to the fact that, according to the Gaussian model the maximum concentration at the surface is nearly proportional to the inverse value of the square of the effective height of emission.

$$\chi_{max} \sim \frac{1}{h_{eff}^2}$$

Table 1

Comparison between original and expanded model
Decrease of the surface concentration by an average deposition velocity of 1 cm/s.

A) Stability Class D (Turner), Windspeed in Anemometer level 1 m/s

Source Depletion Model	5oo m	1 km	5 km	1o km	5o km
	effective height of emission h_{eff} = 1o m				
a) unchanged (equation 1)	21 %	33 %	62 %	73 %	92 %
b) transport velocity $\overline{u}$(u) replaced by $\overline{u}$ (x,u)	12 %	2o %	47 %	57 %	75 %
c) expanded by u(x,u) and the equation proposed by Stratmann (equation 5)	6 %	11 %	27 %	35 %	5o %
	effective height of emission h_{eff} = 1oo m				
a)	-	-	12 %	27 %	66 %
b)	-	-	1o %	22 %	54 %
c)	-	-	5 %	12 %	31 %

B) Stability Class D(Turner), Windspeed in Anemometer level 3 m/s (average atmospheric conditions)

	5oo m	1 km	5 km	1o km	5o km
	effective height of emission h_{eff} = 1o m				
a)	7 %	12 %	27 %	36 %	57 %
b)	4 %	7 %	2o %	24 %	37 %
c)	4 %	7 %	2o %	24 %	37 %
	effective height of emission h_{eff} = 1oo m				
a)	-	-	4 %	1o %	29 %
b)	-	-	4 %	9 %	22 %
c)	-	-	4 %	9 %	22 %

C) Average annual concentration (Meteorological Parameters of Düsseldorf-Flughafen

	5oo m	1 km	5 km	1o km	5o km
	effective height of emission h_{eff} = 1o m				
a)	12 %	25 %	49 %	6o %	77 %
b)	8 %	14 %	28 %	39 %	58 %
c)	6 %	1o %	22 %	32 %	53 %
	effective height of emission h_{eff} = 1oo m				
a)	-	-	7 %	17 %	6o %
b)	-	-	3 %	9 %	33 %
c)	-	-	2 %	7 %	23 %

Table 2: Windspeed distributions of the stability categories of Düsseldorf-Flughafen for the period from 1962-1966) [8]

Windspeed m/s / Stability Categories	1	1.5	2	3	4.5	6	7.5	9	12
1+2	o.8	o.9	o.7	1.8	o.2				
3	1.o	1.1	o.9	2.7	3.1	o.5	o.o3	o.o1	o.oo2
4	1.4	2.2	3.8	15.7	17.8	13.3	6.8	2.6	1.6
5+6	2.8	3.7	3.3	8.6	2.7				

Table 3

Meteorological Parameters

Met. Parameters / Stability Class	Dispersion Parameters	Dispersion Parameters	Exponent for the windprofile in the vertical (m-value)
	h = 1o m (Parameters of Mc Elroy/ Pooler)		(Klugsche Parameter)
A and B	$(1.22x)^{o.76}$	$(o.1ox)^{1.28}$	o.11
C	$(1.15x)^{o.74}$	$(o.11x)^{1.11}$	o.22
D	$(1.78x)^{o.67}$	$(o.67x)^{o.74}$	o.28
E and F	$(o.54x)^{o.72}$	$(o.77x)^{o.59}$	o.4o
	$h \geq$ 1oo m (Parameters of Singer/ Smith)		
A and B	$(o.38x)^{o.9o}$	$(o.24x)^{o.92}$	o.11
C	$(o.31x)^{o.85}$	$(o.19x)^{o.8o}$	o.22
D	$(o.24x)^{o.77}$	$(o.18x)^{o.69}$	o.28
E and F	$(o.21x)^{o.77}$	$(o.o7x)^{o.68}$	o.4o
	The top of the mixing layer is assumed to be 1ooo m		

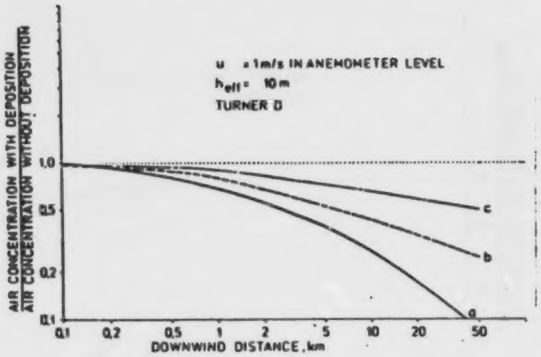

Fig. 1

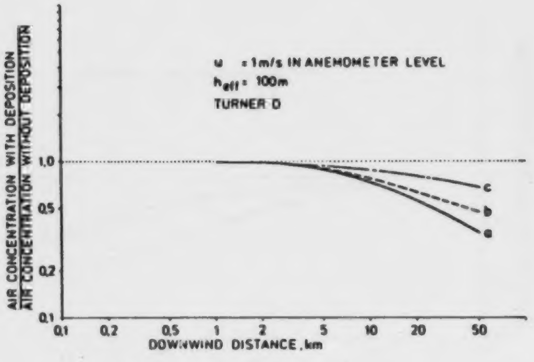

Fig. 2

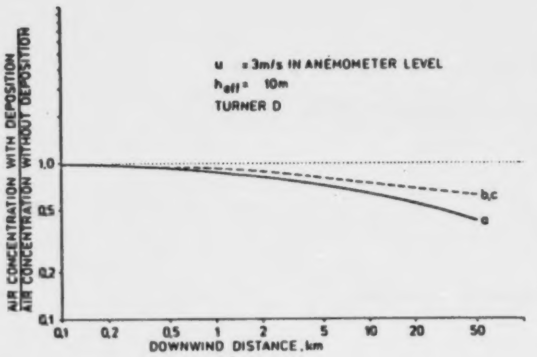

Fig. 3

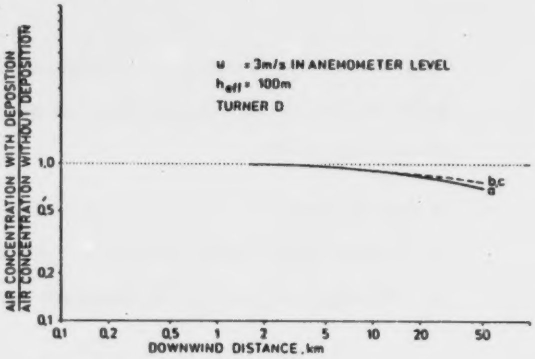

Fig. 4

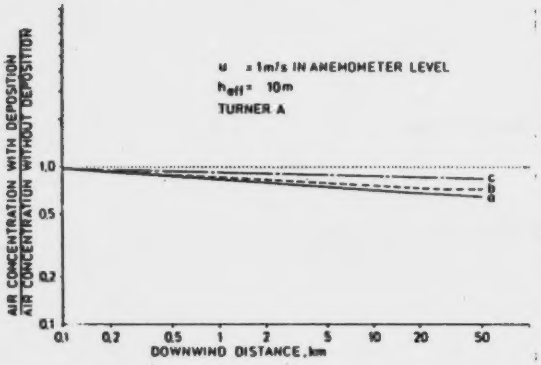

Fig. 5

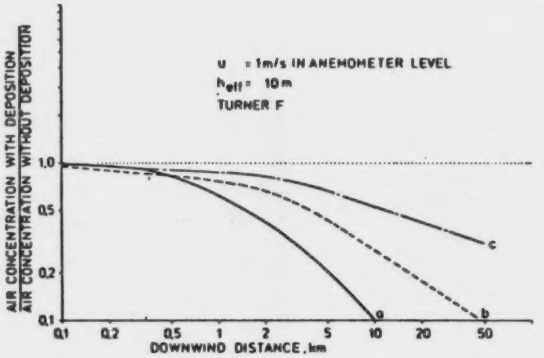

Fig. 6

Comparison between original and expanded source depletion model for a mean deposition velocity of 1 cm/s (related to a mean windspeed of 3 m/s in anemometer level)

a) original model

b) transport velocity $\overline{u}$ (u) replaced by $\overline{u}$ (u, x)

c) expanded by $\overline{u}$ (u, x) and the equation developed by Stratmann

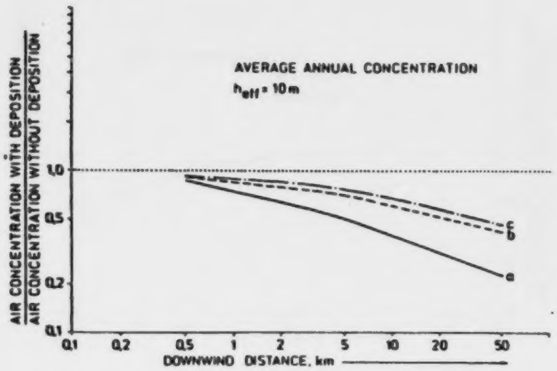

Fig. 7

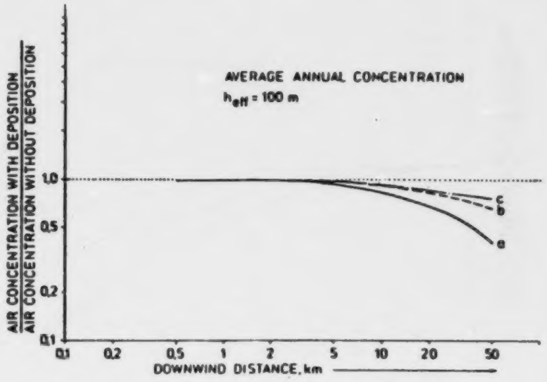

Fig. 8

Comparison between original and expanded source depletion model for a mean deposition velocity of 1 cm/s (related to a mean windspeed of 3 m/s in anemometer level)

a) original model

b) transport velocity $\overline{u}$ (u) replaced by $\overline{u}$ (u, x)

c) expanded by $\overline{u}$ (u, x) and thh equantion developed by Stratmann

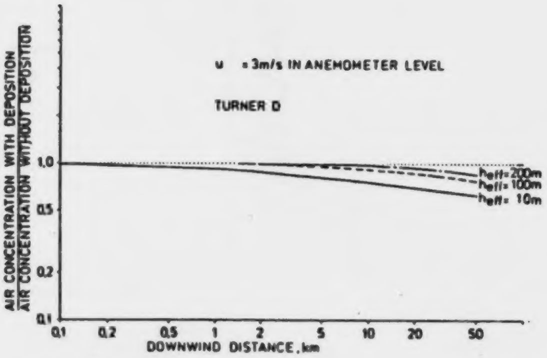

Fig. 9

Decrease of the surface concentration according to the expanded source depletion model for a mean deposition velocity of 1 cm/s.

Literatur

(1) Chamberlain, A.C.:
Aspects of the deposition of radioactive and other gases and particles
Int. J. Air and Water Poll. 3 (196o), S. 63-88

(2) Tadmor, J.:
Consideration of deposition of pollutants in the design of a stack height
Atmos. Environ., 5, (1971), pp. 473-482

(3) Horst, T. W.:
A surface depletion model for deposition from a Gaussian plume
Atmos. Environ., 11 (1977), pp. 41-46

(4) Beilke, S.:
Die Abscheidungsprozesse der Spurenstoffe aus der Atmosphäre
Promet, 5. Jg. 1975, Heft 2 und 3
Herausgeber: Dtsch. Wetterdienst, Offenbach/M.

(5) Hill, A. C.:
Vegetation: A sink for atmospheric pollutants
J. Air Poll. Contr. Assoc., 21 (1972), S. 341-346

(6) Stratmann, H.:
Private Mitteilung

(7) Külske, S.:
Der Stand der Anwendungstechnik von mathematisch-meteorologischen Ausbreitungsmodellen in der Praxis der Luftreinhaltung.
Schriftenreihe der Landesanstalt für Immissions- und Bodennutzungsschutz des Landes NW, Heft 35, S. 69-112, Verlag W. Girardet, Essen 1975.

8th International Technical Meeting
on
Air Pollution Modeling and its Application

ON THE DISPERSION OF CHEMICALLY REACTING POLLUTANTS

K.H. Müller
E.C. - JRC, Ispra Establishment
Italy

September 20-23, 1977

Louvain-La-Neuve
Belgium

1. PROBLEM DESCRIPTION

Thousands of organic and inorganic substances are continuously emitted into the atmosphere by natural and man-made sources. They stay there for some time. Unstable molecules decay, and some of their fragments join other components. The photochemical transformations are of particular importance. Most of the gaseous species released become "digested" and therefore play only a minor role in atmospheric polution. Main sinks are wash-out, biological interactions and decomposition after absorption of radiation. Unfortunately, there are also chemical reactions with pollutants, surface materials and "natural" gases leading to extremely noxious reaction products.

A detailed knowledge of the fundamentals of air chemistry proves to be important in the definition and identification of air polutants and is a valued contribution to air quality management systems (AQMS). Here, however, the aim is to apply such knowledge to AQMS, rather than to augment basic knowledge of air chemistry.

Reliable predictions in air hygienics can only be given by a simulation of the physical and chemical processes governing pollutant dispersion and transformation. Their full complexity, however, cannot be simulated experimentally on a laboratory scale. Here, a numerical simulation, i. e. a modelling, using an electronic computer, is inevitable. The formulation of an all-round satisfactory mathematical description of the complex physical, chemical and meteorological interplay is extremely difficult. The subsequent numerical evaluation of the model makes high demands on computer-time and -storage.

The aim and purpose of an atmospheric modelling consists both of obtaining insight into the interactions between radiation, chemistry and dynamics and of predicting possible environmental modifications caused by intentional or unintentional human interventions in nature. The importance and utility of pollution models for analysis, episode-control, long-term planning and legislation can hardly be overemphasized.

Since a detailed simultaneous modelling of pollutant-chemistry and -dispersion proves rather troublesome, one tends to purchase a detailed description of one phenomenon with a rough approximation of another one. To what extent this is justified has to be checked carefully from case to case.

The availability of big computers enables us to use very sophisticated models. The bottleneck here is the scarcity of the experimental data necessary both to characterize uniquely a given situation and to verify the adequate model, rather than computer-time and -storage.

One first needs to formulate a description as realistic as possible, without any regards to computer-time and -storage, somewhat like a "start-investment" or a "basic study", which can give a survey of both the relevance of the single phenomena occurring in the atmosphere, and of their interrelations. Only after that, i. e. during a second phase of modelling, can one start an economization of the model chosen. Unfortunately in practice, little notice is taken of this recommendation. One usually contents oneself with a so-called "simple" model, without knowing whether the inherent simplification ignores vital phenomena; in short, a criterion for relevance is lacking. One has to stress once more that the task of modelers is to construct a realistic model, rather than a simple one. Only a simulation containing very detailed mechanisms can decide whether one phenomenon is more important than another. Via a sensitivity analysis varying the characteristic parameters and relating these variations to their consequences, a reaction of minor significance can be traced and subsequently eliminated from the model.

First of all, one will check usefulness and completeness of the experimental data available by applying simply-structured models (sub-models) and, after that, if necessary, ask for additional measurements. A more complete data set will then represent a more reliable base, suitable for updating and generalizing the previous model version, etc. Such a procedure is somewhat like that of successive approximations. Finally, one will be able both to distinguish between relevant and unimportant events and to extrapolate to situations experimentally accessible with difficulty or even not at all.

An important task of a model consists in unifying numerous disparate atmospheric and air-hygienic data to give a coherent picture of the atmospheric processes underway. The final aim is, however, to construct a compact mechanism capable of simulating reaction-chamber experiments quite well and containing a sufficient number of free parameters necessary to adapt it to in-field measurements. The most effective approach is one which incorporates both the model and the experiment, somewhat like a semi-empirical model.

The vitality of a model lies in the availability of an extensive parametrization which allows a study of a wide span of response characteristics of the physical system in question. Basically, it is not difficult to construct a model and to fix its parameters by a fitting to measured data, if only a few species are to be treated; it becomes difficult, however, if several species and all possible atmospheric conditions occurring in a region, have to be taken into account.

Input-parameters are: dimensions of reaction -space and boundary conditions, transport coefficients, reaction rates, photodissociation coefficients, etc. It is clear that a specific parametrization of the model input determines the overall structure of the model itself. One could, for instance, say that the reality of a model manifests itself via the accuracy of the characteristic response time of the individual processes; and one could take this as a guide-line for a "realistic" description of the interplay of the different processes underway. Certainly, with rather simple models one can already get a good survey of the whole situation and the trend of an evolution. The crux here is, however, to find a suitable parametrization of the characteristic processes and of their causes and consequences. Also, one has to ensure that the fitting approach, hinging mainly on variations of parameters, gives reasonable orders of magnitude for each process under study.

Air quality models will usually be judged by a comparison of their output with measured concentrations of atmospheric trace species. The corresponding validation experiments rely mostly on a small number of reactants. It may not be disregarded that a model for only a few reactants may not be unique, e.g. in respect of smog formation, since several different mechanisms can be constructed and adapted to given reaction-chamber experiments just by a suitable choice of parameters. The simulation of the same experiment by the models of different authors shows that the corresponding results sometimes diverge to extreme degrees. This fact is obviously bad for the reputation of model simulations.

Also the available reaction-chamber data show, - even for "equal" experiments -, substantial divergencies both quantitative and qualitative. Causes include different chamber-constructions, initial concentrations etc. A real comparison between experimental data is only possible when the experiments are standardized. Without that, a validation of a model, i.e. a comparison of model output and experiment, remains questionable.

The main purpose of air quality models is to predict air pollution levels for hypothetical future conditions. A corresponding proof of efficiency can be given only by verifying predictions. One, therefore, has to take registered pollution concentrations and meteorological information as model input, to calculate a pollution level forecast for today and to compare its results with actually measurable data. If coincidence is obtained, there will be some confidence in the prediction mechanism.

Pollutant transport and chemistry in the atmosphere is a domain where one assumes that the basic principles are known. But theoretical treatment is possible only in the simplest cases. It is obvious that a decision maker and one who is engaged in solving practical problems cannot wait until someone publishes a theoretical solution of his problems. Only models can interpret incoming measured data and interpolate or extrapolate into regions where no measurements have been performed. It is our business to provide suitable and reliable models.

2. MATHEMATICAL FORMULATION

The most general principles in physics, such as the conservation of mass, momentum and energy, form its basis. The mathematical expression for a conservation principle is a continuity equation. Such equations must be established for each chemical species with a space-time varying particle density. The resulting equations, coupled to each other, due to all the interactions occurring in the atmosphere, have to be solved simultaneously to obtain the real space-time behaviour of the concentrations. It is clear that this set of equations, a model of the chemical kinetics transport, can only be solved numerically, and that only such a numerical simulation of the true interplay of the different atmospheric phenomena enables us to study it and to infer trends and consequences from the actual situation.

We are interested in properties of matter which can be described without referring to their micro-structure, but we are also interested in the interpretation, rationalization and codification of the bulk properties in terms of the micro-structure itself.

The kinetic theory of gases represents a uniform basis for models formulating the full interaction between radiative, photochemical and aerodynamic processes, and is, therefore, a suitable starting point for the mathematization (HUANG, 1963). The first task is to formalize the classical transport of mass, momentum and energy for a continuum. Because of this, continuous functions of space and time have to be assigned to the bulk matter properties, such as mass density, energy density, velocity field etc. One can speak of "sufficient smoothness" only when it is possible to define a volume element of macroscopic dimensions which still contains a sufficient number of molecules; only then can one speak of local density, local velocity etc. in the sense of average values.

Simultaneously, a time interval has to be defined, macroscopically small but large enough so that a sufficient number of molecular events, like collisions, fluctuations etc., can be processed to reasonable average values. The main task of the molecular theory is to show that such mean values can reasonably be defined and that they satisfy continuum equations.

One is interested in the particle distribution function $f_i(\vec{r}, t, \vec{v})$ counting the number of molecules of species S_i within the phase-space volume element, rather than in the motion of single molecules. This volume element is not infinitesimally small, in the literal sense, but finite. The functions f_i are considered to be continuous in all their variables. In this sense, the normalization holds

$$\int f_i(\vec{r}, t, \vec{v})\, d^3v = N_i(\vec{r}, t) = \text{number of particles in } (d^3r.\, dt).$$

The aim of the kinetic theory is to find the distribution functions f_i corresponding to given molecular interactions. The limit $\lim\limits_{t \to \infty} f_i \to f_i^*$ will then contain all the equilibrium properties of the system.

Our task is now to establish a continuity equation for each f_i. The density f_i changes in time, since molecules enter and leave the volume element $dV = d^3r. d^3v$ all the time. This transfer can be split up into a "streaming" and a "scattering" interpreting the particle motion as consequences of collisions between molecules. In case of a collision-free motion, the density function f_i satisfies the "streaming" equation

$$Df_i \equiv \left(\frac{\partial}{\partial t} + \vec{v}\cdot\frac{\partial}{\partial \vec{r}} + \vec{a}\cdot\frac{\partial}{\partial \vec{v}}\right) f_i = 0 \qquad (1)$$

$\vec{a}$ denotes the acceleration field acting on the molecules. In case of simultaneously occurring collisions, however

$$Df_i = \left(\frac{\partial f_i}{\partial t}\right)_{\text{collision}} \neq 0 \qquad (2)$$

holds. Obviously, one has to know the formal structure of the right-hand "collision" term which is a measure for the rate of change of f_i due to collisions.

The basic assumption of the kinetic theory is: the gas is dilute: i.e. the mean distance between the gas molecules is much larger than the range of their inter-molecular forces. Occasionally, a molecule hits another one; and, much more rarely, three molecules collide simultaneously. Within a mathematical analysis, this fact can be expressed by the statement that there are only two-body or binary collisions. Having constructed a corresponding binary theory, one will try to generalize it to three-body collisions, etc.

A gas is called non-equilibrium, when its distribution function f_i deviates from the Maxwell-Boltzmann distribution. Causes are heterogeneous temperature-, density-, or velocity-fields. The system of molecules tries to equalize these irregularities by transport of energy, momentum and mass. The corresponding transport mechanism is molecular collision. One usually assumes, as a working hypothesis, that the molecules fly freely between two subsequent collisions, i.e. $\vec{a} \equiv 0$, and that velocity $\vec{v}$ and position $\vec{r}$ of a molecule are uncorrelated ("molecular chaos").

The number of pairs of molecules in d^3r of two different substances, S_j and S_k, whose velocities are $\vec{v}_j$ and $\vec{v}_k$, is given by

$$\left[f_j(\vec{r}, t, \vec{v}_j). d^3r. d^3v_j\right] . \left[f_k(\vec{r}, t, \vec{v}_k). d^3r. d^3v_k\right] .$$

The molecules of substance S_j will be "attacked" by the current

$$f_k(\vec{r}, t, \vec{v}_k).\, d^3v_k \, |\vec{v}_j - \vec{v}_k|$$

of S_k molecules.
The number of collisions occurring during the time interval dt is

$$f_j(\vec{r}, t, \vec{v}_j).\, dt.\, \sigma_{jk}(\vec{v}_j, \vec{v}_k) f_k(\vec{r}, t, \vec{v}_k).\, d^3v_k . |\vec{v}_j - \vec{v}_k|$$

where σ_{jk} denotes the "cross section" characterizing the collision mechanism. During such collisions, chemical transformations may occur. The corresponding changes in particle densities are assumed to be proportional to the number of collisions. The proportionality factors, p and q, are called (positive or negative) production rates. The velocity of f_i-changes, due to collisions, is therefore given by

$$\left(\frac{\partial f_i}{\partial t}\right)_{\text{collision}} = -f_i(\vec{r}, t, \vec{v}) \int d^3v_k \sum_k p_{ik}(\vec{v}, \vec{v}_k)\, \sigma_{ik}(\vec{v}, \vec{v}_k) f_k(\vec{r}, t, \vec{v}_k) \, |\vec{v} - \vec{v}_k| +$$
$$+ \int d^3v_j \int d^3v_k \sum_{j,k} q_{ijk}(\vec{v}, \vec{v}_j, \vec{v}_k)\, \sigma_{jk}(\vec{v}_j, \vec{v}_k) f_j(\vec{r}, t, \vec{v}_j) f_k(\vec{r}, t, \vec{v}_k) \, |\vec{v}_j - \vec{v}_k| \tag{3}$$

The balance equation resulting from eq. (2) and (3) and including reactive scattering is a correct dynamical description of a combined transport-transformation process in a dilute gas; it is equivalent to the uncorrelated binary collision theory of chemical kinetics.

The continuity equations of the mass-, momentum- and energy-transport can be derived from this "Boltzmann equation" by applying a weighted averaging of the molecular velocity $\vec{v}$ onto it.

Our interest lies in deriving a compact model for the pollutant-mass transport including the simultaneously occurring chemical transformations in an atmosphere characterized by a given velocity- and temperature-field. Using the already defined density N_i and the particle current

$$\vec{g}_i = \int \vec{v}.\, f_i.\, d^3v$$

and the following mean values

$$\int p_{ik} \sigma_{jk} |\vec{v} - \vec{v}_k| \, f_k.\, d^3v_k = \alpha_{ik}(\vec{v}) \int f_k.\, d^3v_k = \alpha_{ik}(\vec{v}).\, N_k$$
$$\iint q_{ijk} \sigma_{jk} |\vec{v}_j - \vec{v}_k| \, f_j.\, f_k.\, d^3v_j.\, d^3v_k = \beta_{ijk}(\vec{v}) \int f_j.\, d^3v_j. \int f_k.\, d^3v_k = \beta_{ijk}(\vec{v}) N_j N_k \tag{4}$$

the Boltzmann equation can be rewritten as follows

$$\left(\frac{\partial}{\partial t} + \vec{v}.\frac{\partial}{\partial \vec{r}} + \vec{a}.\frac{\partial}{\partial \vec{v}} + \sum_k \alpha_{ik} N_k\right) f_i = \sum_{j,k} \beta_{ijk} N_j N_k \qquad (5)$$

An integration of this equation over the whole velocity space and the introduction of

$$\int \alpha_{ik}.f_i.d^3v = a_{ik}.\int f_i.d^3v = a_{ik}.N_i \quad ; \quad \int \beta_{ijk}.d^3v = b_{ijk}$$

leads to the parameterized form (with $\vec{a} = 0$):

$$\frac{\partial N_i}{\partial t} + \operatorname{div} \vec{g}_i = -L_i N_i + P_i \qquad (6)$$

of the macroscopic mass balance of combined processes.

The abbreviations

$$\begin{array}{lccc} L_i = \sum_k a_{ik}.N_k & \text{"loss"} & & \\ & \text{symbolize} & & \text{of } S_i. \qquad (7) \\ P_i = \sum_{j,k} b_{ijk}.N_j.N_k & \text{"production"} & & \end{array}$$

Before trying to parametrize the current $\vec{g}_i$ one introduces the mean velocity $\vec{u}$ of all molecules actually present in the volume element ($d^3r.dt$); i. e.

$$\vec{g}_i = \int \vec{v}.f_i.d^3v = \vec{u}.N_i - \int (\vec{u}-\vec{v}) f_i.d^3v = \vec{u}.N_i - \vec{\Gamma}_i$$

The space-time dependent function $\vec{\Gamma}_i$ expresses a sort of mean-dispersion-behaviour of substance S_i. According to the classical macroscopic diffusion theory one could perform a parameterization by a linear ansatz of the type

$$\vec{\Gamma}_i = \mathbb{K}.(\vec{c}.N_i + \operatorname{grad} N_i) \ . \qquad (8)$$

The tensor $\mathbb{K}$ serves to quantify the dispersion behaviour. COLGROVE et al. (1965) tried to include the influence of a given temperature field T on the chemical kinetics transport by the ansatz

$$\vec{c} = \nabla(\ln T) + \text{constant} \ .$$

Inserting the above $\vec{\Gamma}_i$ into eq. (6), and putting $\nabla.\vec{u} = 0$, a non-linear "diffusion equation" results:

$$\frac{\partial N_i}{\partial t} + \vec{u}.\nabla N_i - \nabla(\mathbb{K}.\nabla N_i) + (L_i - \nabla.\mathbb{K}.\vec{c}).N_i = P_i \qquad (9)$$

Such diffusion equations may be completely wrong, since they are based on an ad-hoc assumption, the linear gradient hypothesis (8). There is, indeed, a series of cases where this hypothesis cannot be justified. Here, there is no other alternative but to integrate eq. (6) or even (5).

Sometimes, velocity field $\vec{u}(\vec{r},t)$ and temperature field $T(\vec{r},t)$ are derived from so-called circulation models. In the most practical cases, however, the velocity- and temperature-fields are experimentally determined, i.e. by measurements. The advection of pollutants might be described afterwards by correlating meteorological data.

Since the topography of an urban region is far too complex to be described analytically, one renounces exact solutions of the basic aerodynamical equations and contents oneself with stochastic numerical solutions.

Molecular and turbulent diffusion can be quantified by the above mentioned $\mathbb{K}$-tensor which is usually calculated from measured temperature-, velocity- and trace-gas distributions, via a more or less complex formalism. It seems best, however, to take $\mathbb{K}$ as a free parameter to be fixed indirectly by fitting N_i to measured pollutant concentrations.

The evaluation of L_i and P_i requires the consideration of both the solar radiation and the molecular scattering- and absorption cross sections; i.e. one needs a detailed knowledge of the reaction mechanisms governing the chemical processes in the atmosphere. Because of the multiplicity of those phenomena, the theory is here confronted with unsurmountable difficulties. With regard to the determination of the characteristic parameters, a_{ik} and b_{ijk}, there is no alternative to calculating them from reaction-chamber concentration measurements by an inversion of the kinetic equations

$$\frac{dN_i}{dt} = - L_i . N_i + P_i \qquad (10)$$

valid for homogeneous mixtures (LEIGHTON, 1961).

There were comments in a previous chapter concerning the accuracy and reliability of such experiments and data. Experiments of this kind show a strong temperature dependence of the reaction rates, a_{ik} and b_{ijk}. One, therefore, tries to find out their, at least approximate, T-structure. The literature shows some possible ways; we illustrate here only the basic idea underlying them.

Suppose there is a reaction: A + B → C. The kinetics is quantified by

$$- \frac{d[A]}{dt} = - \frac{d[B]}{dt} = \frac{d[C]}{dt} = k.[A][B] \qquad (11)$$

where the brackets denote the corresponding concentrations, and k measures the reaction velocity.

The theory says that the fundamental relation between macroscopic and microscopic pictures of the kinetics of binary reactions can be formulated via

$$k \sim T^{-3/2} \int Q(E,T) . \exp(-E/RT) . E . dE$$

where E denotes the required activation energy. Having selected a suitable functional form for Q, able to describe the microscopic collision mechanism sufficiently well, the integral can be evaluated. The temperature behaviour of most of the reactions relevant to air pollution follow the formula of ARRHENIUS:

$$k = A . T^{B} . \exp(-C/T) . \tag{12}$$

The parameter A is related to the collision frequency and to the probability that a reaction occurs during a collision, B depends on the temperature of this collision frequency and C is proportional to the activation energy.
In practice, the numerical values of A, B, and C are to be determined by fitting the Arrhenius equation (12) to experimental data.

Photolytical reactions, e.g. $S_i + h\nu \rightarrow S_j$, are usually parameterized by so-called photodissociation coefficients, like

$$I = \int d\lambda . \sigma^{i}(t) . R(i \rightarrow j) . I_{o} . \exp(-s(\vec{r}, t))$$

which depend in a rather complex way on wave length λ, attenuation factor s, absorption cross section σ^{i}, temperature T and "quantum yield" R of the corresponding process. The attenuation factor (optical depth) is again an integral over all absorptions and scatterings of the quanta of a given wave length caused by all the chemical species present in the irradiated atmosphare.
It is clear that here too, simplifying assumptions have to be made to obtain, - at least approximately -, useful relations from the integral. The radiation also causes secondary effects, like diffusion, heating etc., which in their turn create further consequences. Part of the incoming radiation becomes absorbed and excluded from further radiochemical reactions. When including the radiation effects proportional to the intensity J of the radiation, the loss- and production-operators defined by eq. (7) have to be modified as follows

$$\begin{aligned} L_i &= \sum_k a_{ik} . N_i + \nu_i . J \\ P_i &= \sum_{j,k} b_{ijk} . N_j . N_k + \sum_k \mu_{ik} . N_k . J \end{aligned} \tag{13}$$

The parameters ν_i and μ_{ik} also have to be determined by a fitting to corresponding experimental data. The hypothesis that the part of space impermeable is proportional to the absorbed radiation, gives a complementary equation

$$\frac{\partial J}{\partial r} = - J.(\alpha + \sum_{i} \chi_j . N_i) \tag{14}$$

which can formally be integrated. Using the resulting expression, the intensity J can be eliminated from the diffusion equation governing the mass balance. An integro-differential equation results (MÜLLER, 1961). Most authors, however, assume J to be constant.

The generalization of the presented theory of chemical kinetics transport to interactions including three-particle collisions does not require excessive effort.

3. NUMERICAL TREATMENT

A simulation of combined transport-transformation processes occurring in the atmosphere deals with systems of partial differential equations, symbolically written as:

$$\frac{\partial N_i}{\partial t} = \phi_i(\vec{r}, t, N_k/k=1, 1, \ldots\ I) \tag{15}$$

where ϕ_i is the combined transport-transformation operator.
The corresponding physical problem is an initial-boundary value problem with widely differing time constants. One knows from experiments that the chemical reaction rates span a range of time constants from about 10^{-6} sec to 10^{+5} sec; the atmospheric transport processes, sometimes, have characteristic times up to 10^{8}-10^{9} sec. Because of these huge differences in time scale, the application of procedures based on the usual techniques of operator-splitting and fractional steps seem to be adequate. But soon, however, it becomes clear that each time the transport operator is used, the chemical system is rudely perturbed out of equilibrium, and that subsequent smoothing requires an excessive effort. In connection with this, the question arises of how the system reacts to such perturbations. We shall see later that those perturbations are more natural than spurious.

3.1 Eulerian Models

A frequently used approach to solving system (15) is to replace the spatial derivatives by the corresponding finite differences. The pollution distribution $\vec{N}(\vec{r}, t) = \{ N_i(\vec{r}, t)/i=1, 2, \ldots I \}$ will be replaced by the I.E-dimensional vector $\vec{n}(t) = \{ n_k(\vec{r}_\varepsilon, t)/k=1, 2, \ldots\ I/\varepsilon=1, 2, \ldots\ E \}$ whose components $n_i(t)$ satisfy non-linear differential equations

$$\frac{dn_i}{dt} = F_i(t, n_k/k=1, 2, \ldots \varepsilon \cdot I) \tag{16}$$

which possess the unpleasant property of "stiffness". One calls a system stiff, if - roughly speaking - its representative time constants differ in orders of magnitude. Time constants are quantities $\tau_m > 0$ such that the solution $n_i(t)$ of eq. (16) can locally be approximated by a linear combination of terms with damping factors $\exp(-t/\tau_m)$. These quantities are analytically given by $\tau_m = -1/\mathrm{Re}(\lambda_m)$, where $\{\lambda_m\}$ are the eigenvalues of the Jacobian matrix

$$\left\{\frac{\partial F_i}{\partial n_k}\right\}.$$

Stiffness occurs if there are λ-values horizontally widely spread over the left λ-half plane. The space between the largest and smallest eigenvalue measures the degree of stiffness of the system of differential equations under study.

The initial value problem of eq. (16) is usually solved by a stepwise method of some sort. In the beginning, when the state variables n_i are still changing very rapidly due to the fast reactions, one has to use a time step Δt of the order of $\tau_{min} = \min \tau_m$, so that all quantities behaving like $\exp(-t/\tau_m)$ can be represented, as functions of time, in a sufficiently accurate manner. Sometimes, one or two λs may be found in the right λ-half plane; i. e. indicating temporarily increasing concentrations. But a short while later, the fast reactions are complete and the rapid "transient" solutions vanished.

Now one should use a time step Δt comparable to $\tau_{max} = \mathrm{Max}\ \tau_m$. Unfortunately, such a large time step causes - for most of the classical integration techniques - badly diverging numerical errors, i. e. these methods are in the presence of stiffness, no longer numerically stable.

To integrate the set of ordinary differential equations (16) resulting from a spatial discretization of eq. (15), one replaces the first-order derivatives by a finite difference form, e. g.

$$\frac{dn_i}{dt} \approx \frac{n_i^{j+1} - n_i^j}{\Delta t} \tag{17}$$

The index j counts the time steps. The resulting set of algebraic equations can be solved in three different ways. The simplest one follows the so-called explicit technique:

$$n_i^{j+1} = n_i^j + F_i^j \cdot \Delta t \tag{18}$$

working sufficiently well for small time steps.
Numerical stability also requires small time steps here.

LOMAX and BAILEY (1967) developed an explicit multistep-predictor-corrector algorithm with a large induced stability boundary. Since there are no matrix inversions, a relatively short calculation time is necessary. This approach allows much larger time steps than, for instance, the classical approaches of Euler and Runge-Kutta.

The much stabler implicit technique evaluates F_i at time step $(j+1)$ or at some weghted average of j and $(j+1)$.

GEAR (1969) proposed a multistep-predictor corrector method which works much faster than the usual Runge-Kutta methods. Today, there are numerous modifications of this approach (e.g. CHANG et al., 1973; CRUTZEN, 1974; GRAEDEL et al., 1976). Their basic form is

$$n_i^{j+1} = n_i^j + F_i^{j+1} \cdot \Delta t \tag{19}$$

It uses a time step comparable with τ_{max} and controls only by the criterion of representing the truly active reaction accurately, rather than being limited by the inactive rapid reactions. The solution of eq. (19) can be obtained by a modified Newton-method based on the inversion of a matrix of the type

$$S = I - \gamma \left\{ \frac{\partial F_i}{\partial n_k} \right\}.$$

Using the structure $\vec{F}(\vec{n}) = A(\vec{n}).\vec{n}$ in conjunction with successive over-relaxation, one can solve equation (19) quite efficiently. During the calculation, S is kept unchanged until it becomes negative, i.e. it is re-evaluated only after a failure of the corrector convergence.

The semi-implicit technique takes only part of F_i at time point $(j+1)$, e.g. L_i. Such a procedure has the advantage of separating the equations in view of the species-index i.

AMES (1969) discussed this method in considerable detail. It has, however, the disadvantage of introducing spurious sources and sinks for the reacting substances, because of the sequential instead of a simultaneous calculation of the densities. Using iterations at fixed time steps, these perturbations can be eliminated afterwards. Unfortunately, such an iteration is very computer-time consuming.

The so-called Eulerian multibox models represent nothing but a slightly different interpretation of the finite difference technique and, therefore, do not need further explanation.

A completely different structured integration formalism discretizes eq. (15) only with respect to time; it ignores, for the moment, the production term P_i. This procedure follows the so-called "first collision concept" successfully used elsewhere (SOODAK, 1962). A subsequent second step calculates the corresponding production rates according to the stoichiometry of the species involved in the chemical reactions underway.

Using the abbreviations

$$D_i = -\vec{u}.\nabla + \nabla.(\mathbb{K}\nabla), \qquad \lambda^2 = 1/\Delta t \tag{20}$$

and opting for the explicit technique, eq. (15) can be written as follows:

$$(D_i - \lambda^2).N_i^{j+1} = (L_i^j - \lambda^2)\,N_i^j \tag{21}$$

The introduction of the corresponding Green's function satisfying

$$(D_i - \lambda^2).G_i = 4\pi\delta(r)$$

for the same geometry, allows a formal integration of eq. (21) resulting in the recursion formula

$$N_i^{j+1} = \int G_i(\vec{r}-\vec{\rho})\,\left[L_i^j - \lambda^2\right]N_i^j\,d^3\rho \tag{22}$$

easily to evaluate starting from the initial concentration $N_i^0(\vec{r})$.

One can show that the approximative solution $N_i^j(\vec{r})$ constructed in such a way converges uniformly in $\vec{r}$ and j with $\Delta t \rightarrow 0$ to the desired density distribution $N_i(\vec{r},t)$. (MÜLLER, 1961).

The corresponding implicit form

$$(D_i - \lambda^2 - L_i^{j+1}).N_i^{j+1} = -\lambda^2.N_i^j \tag{23}$$

can formally be integrated to the Fredholm integral equation

$$N_i^{j+1} = \int G_i(\vec{r}-\vec{\rho}).\left[L_i^{j+1}.\,N_i^{j+1} - \lambda^2.N_i^j\right].d^3\rho \tag{24}$$

or to a slightly different form

$$N_i^{j+1} = \int H_i(\vec{r}-\vec{\rho})\left[(L_i^{j+1} + \lambda^2).N_i^{j+1} - \lambda^2.N_i^j\right].\,d^3\rho \tag{25}$$

where H_i satisfies the equation: $D_iH_i = 4\pi.\delta(r)$.

Inserting one of the extrapolation formulae of the type

$$N_i^{j+1} \approx \sum_{k=0}^{j} \alpha_{ik} N_i^{j-k} \quad \text{in } L_i^{j+1} \tag{26}$$

published in literature, the integral equations (24) and (25) can be linearized. There are a series of methods for solving such linear equations.

Example: For the operator $D_i = -u_o z^\beta.\frac{\partial}{\partial x} + K_2(x)z^\beta.\frac{\partial^2}{\partial y^2} + K_3(x)\frac{\partial}{\partial z}\left(z^\gamma\frac{\partial}{\partial z}\right)$

and the infinite $\vec{r}$-space we get the following Green's function (MÜLLER, 1976)

$$H_i(r) = \varkappa_2^{-1/2} \varkappa_3^{-b} \exp\left(-\frac{u_o y^2}{4\varkappa_2} - \frac{u_o z^c}{c^2 \varkappa_3}\right)$$

$$\varkappa_i = \int_o^x K_i(\xi)\, d\,\xi \;;\; b = \frac{\beta+1}{c} \;;\; c = \beta - \gamma + 2 \qquad (27)$$

The corresponding Green's function for the half space $z \geq 0$ results from a superposition according to the classical mirror method.

Finally, one should mention that numerical Green's functions, i. e. K-models, can also be inserted into eq. (22), (24) and (25).

3.2 Lagrangean Models

The so-called moving-cell methods consider homogeneous air parcels or vertical air columns travelling along their trajectories with the velocity $\vec{u}$ of the wind field and taking up pollution during their crossing of source regions. The horizontal dimensions of such columns remain unchanged, while their heights vary with the local inversion- or mixing height. Such models generally ignore the horizontal diffusion. ESCHENROEDER and MARTINEZ (1973) treated the vertical diffusion inside a column assuming it to be composed of vertically stacked cells. The diffusion equation connects the cell motion and the history of pollutant concentrations inside the cell. SKLAREW et al. (1972) applied the so-called particle-in-cell method frequently used in the mechanics of continua. Here the continuous mass flow is separated and the centroids of these discrete masses are tracked. A system of Eulerian boxes serves to determine the pollutant concentrations from the calculated space-time dependent particle densities.

Cell models are based on the assumption that each cell represents a closed system. This hypothesis holds, of course, only for a limited time-interval. One observes in nature quasi-stable air parcels, eddies, representing temporarily closed systems. They have a certain life-time, at the end of which they decay or coagulate with other eddies. This fact suggests a generalization of the above mentioned cell models which takes into account the phenomenon of "life-time" (MÜLLER, 1977). The "free" flights of the eddies between subsequent collisions are nothing but another interpretation of this life-time.

The pollutant transport can be interpreted as a superposition of a continuous "streaming" (convection) and a statistical motion of air parcels (eddy diffusion). One can, in addition, imagine the streaming to be the average of stochastic particle motions. By such a reasoning one returns to the basic idea of the kinetic gas theory. The most obvious difference between a molecular and an eddy-gas consists in the dimensions of the space time volume elements they refer to; i. e. an eddy-gas requires an eddy-scale volume element. Relating eddy-mass to eddy-velocity one can get, finally, a full con-

formity in modelling of both molecular and eddy-gas. The mechanisms of neither the molecular nor the eddy collisions are uniquely determinable; they must be suitably parameterized and indirectly quantified by a fitting to pollutant density measurements.
Such an eddy-gas model has, because of the temporarily closed-system-structure of the eddies, the advantage that the chemical transformations occurring during the free flight can be treated completely uncoupled from the transport mechanism itself, as each eddy possesses its "own" chemistry. At the collision points, however, the different chemistries interact with each other (MÜLLER, 1977). The modeller has the choice between some alternative interacting mechanisms. One possible approach is based on the assumption that the chemical transformations occur inside the closed eddies during their free flight and that the collisions represent nothing but an instantaneous mixing. An alternative assumes that there are no transformations at all during the flight, but only during the mixing process, this time of finite duration. In nature, of course, these two mechanisms take place simultaneously. The number of collisions per Eulerian box and time element is a measure of the eddy number density, and so for the pollutant densities.

The local substance composition, $N_i(\vec{r}, t)$, in a given box changes in the subsequent time interval Δt, as a result of both the chemical transformations and the continuously occurring eddy transport. Since most of the chemical reactions possess a time constant $\Delta\tau$, far smaller than that of the transport processes, one will quantify the incoming and outgoing flow according to the $\Delta\tau$-steps; i. e. assume that, during a $\Delta\tau$-step, only chemical transformations occur, and that the modifications of the chemical composition caused by the transport need to be taken into account only at the end of the different time steps, $(t+k.\Delta\tau)$ where $k=1, 2, \ldots$

A possibly acceptable approximation accumulates the incoming and outgoing pollutant masses over the whole transport time step Δt, before combining them with the chemical transformations. The changing density rates are measured, then, via the difference of the corresponding collision densities C_i, at subsequent time points, i. e.

$$\Delta C_i = C_i(\vec{r}, t + \Delta t) - C_i(\vec{r}, t)$$

ΔC_i will be related to the rate ΔN_i. Starting from the actual density, $N_i(\vec{r}, t)$, one integrates, in time steps $\Delta\tau$, the kinetics equation (10) over the time interval $(t, t + \Delta t)$. An "intermediate" density $N_i^*(\vec{r}, t + \Delta t)$ results. The "final" density including transport is given by

$$N_i\,(\vec{r}, t + \Delta t) = N_i^* + \Delta N_i.$$

Intermittent interventions use fragments of ΔN_i calculated by an interpolation based on the previous time behaviour of N_i.

3.3 Stochastic Models

To construct a model as realistic as possible, one also has to pay regard to the results of the theory of chemical reactions in non-homogeneous mixtures, usually subsumed under the key words: stochastic formulation of reaction kinetics (McQUARRIE, 1967). One considers it as an improvement of the classical deterministic formulation, in so far as the former is able to simulate the fluctuations of reactant densities and reaction products within small subvolumes.

The stochastic formulation assumes that the molecules follow Markovian paths and are activated during the collision undergone with other molecules or radiation quanta. After a series of such energy exchanges, a molecule accumulates enough energy to overcome the potential barrier of a collision partner which previously prevented chemical interaction. For a gas the rate of barrier-crossing equals the rate of the reaction.

The solution of the stochastic formulation of chemical kinetics becomes asymptotically identical with the solution of the deterministic formulation - in the thermodynamic limit (OPPENHEIM et al., 1969).

One could try to simulate the random walks of the single molecules, in analogy to the real events. The corresponding calculation time would directly be proportional to the number of individual molecular reactions taken into account. The excessive calculation effort forces us to a simplification which has, at any rate, to cover all the relevant phenomena. Since the collisions without chemical consequences are much more frequent than the so-called active reactions, one decides to ignore the inactive ones. Between two subsequent active collisions, as in this picture, a free flight represents the vector sum of the intermediate paths interrupted by the inactive collisions. This simplification is in harmony with the deterministic formulation of the kinetic equations which obtain their reaction coefficients from chemical reaction rates only. The stochasticity is not lost during this Monte Carlo procedure.

In the reaction volume V are, - in addition to a series of inert substances -, homogeneously distributed molecules of I chemically active species, S_i, reacting with each other in M different ways. z_m distinct molecular reactant combinations for reaction m are possible. Each reaction is characterized by a numerical parameter, c_m. Reversible reactions are considered to be different. The c_m are defined as follows:

$c_m dt$ = mean probability that a m-reaction occurs in the subsequent time interval dt.

They are related to the corresponding reaction constants, k_m, of the deterministic formulation by

reaction	k_m
$S_1 + h\nu$	c_m
$S_1 + S_1$	$c_m . V/2$
$S_1 + S_2$	$c_m . V$
$S_1 + S_2 + S_3$	$c_m . V^2$ etc.

The stochastic approach starts from the reaction probability density function, $p(\tau, m)$, defined by

$p(\tau, m). d\tau$ = probability that the next reaction occurring in the time interval $(t+\tau,\ t+\tau+d\tau)$ is an m-reaction.

With this, one can construct a sort of Monte Carlo procedure simulating the stochastic reaction process. The corresponding formula

$$p(\tau, m) = a_m . \exp(-a.\tau) \quad \text{with} \quad a_m = z_m . c_m \text{ and } a = \sum_{m=1}^{M} a_m$$

can easily be factorized:

$$p(\tau, m) = \left(\frac{a_m}{a}\right) . a. \exp(-a.\tau) = p_1(m). p_2(\tau)$$

Using a random number generator, one calculates, from p_1 and p_2, a pair (τ, m) of random numbers. With their aid one can proceed from t to $(t+\tau)$ and find out the index m of the presently most probable reaction. Now one identifies all species, S_i, involved in reaction m, and calculates the corresponding reaction rates according to the appropriate stoichiometric ratios, and then updates the density distributions. One repeats this step sequence just mentioned until a given time limit is reached or no more reactions occur due to the lack of substance (GILLESPIE, 1976). In this way, one constructs a single possible realization of the stochastic transformation process taking place in V. To get a statistically complete picture of the whole evolution, one has to construct, for the same initial conditions, numerous realizations independent from each other, and to calculate averages from these different "runs". Such mean values converge for an increasing number of runs to the real time-behaviour of the reactions in V. BUNKER et al. (1974) proposed the use of the mean value $\hat{\tau} = 1/a$ instead of statistically distributed τ-values.

In air chemistry, the probability $p_1 = a_m/a$ corresponding to the so-called "slow" reactions, is usually extremely small. One, therefore, separates all reactions into different classes, e.g. fast reactions and slow reactions.

Sometimes such a binary classification is not sufficient, and one is well advised to introduce three or more classes. For an illustration of the procedure to the applied, one contents oneself with a binary classification; a generalization to more classes does not create any difficulty. One divides into

$$m \underset{>}{\leq} s \qquad \begin{matrix}\text{fast}\\ \text{slow}\end{matrix} \qquad \text{reactions}$$

$$a = \sum_{m=1}^{S} a_m + a' \quad \text{and} \quad a' = \sum_{s+1}^{M} a_m$$

and uses the following scheme

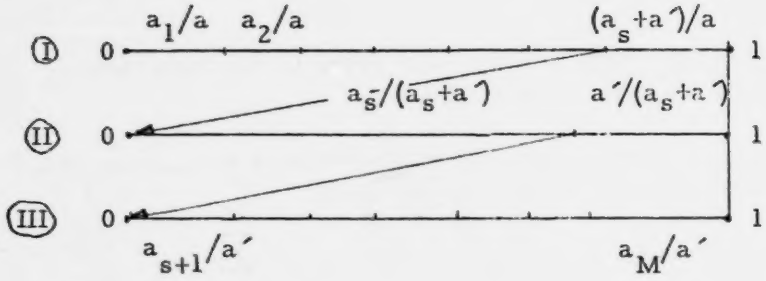

A random number generator produces numbers ξ_i equally distributed on the interval (0;1). ξ_i thrown on scale Ⓘ picks out a reaction $m \leq s$. If, however $m = s$ one calculates a new random number, ξ_2, and throws it on scale (II), which now decides whether a slow reaction is meant or not. If yes, a third random number, ξ_3, thrown on scale (III), determines the index of a slow reaction.

In the case of reaction velocities differing in several orders of magnitude, as is usual in practice, one can dispense with scale (II). For $m = s$, however, one has to take into account both the reaction $m = s$ and a slow one to be identified via scale (III). Additionally, an "importance weight", $w = a'/a_s$ has to be attached to the slow reaction, while $w = 1$ holds for the fast one. In this way, one is able, with only a limited quantity of random numbers, to pay sufficient regard to slow reactions as well. The corresponding life times are to be calculated from the adequately modified $p_2(\tau)$-distributions.

An extension of the presented stochastic approach to spatial inhomogeneities can easily be performed; one has to subdivide the reaction volume V into a system of boxes, each of them homogeneously structured, and to couple the life times with the distances covered by the particles and calculated from the given particle density distributions (MÜLLER, 1977).

Most of the calculation time to be spent by the stochastic approach requires the determination of the reaction index m. A "bundling" of runs is, therefore, recommended; i.e. one assumes that after each time step several elementary reactions occur simultaneously. The use of (artificial) particles disposing of a complete a_m/a-spectral composition much reduces calculation time.

Finally, it should be said that the algorithm just presented offers a convenient way of by-passing the stiffness-difficulties which generally dominate the integration of the coupled kinetics equations.

4. CONCLUSION

The photochemistry of the natural atmosphere is rather complex, but when the effluents of civilization are added, it becomes extremely complex. As, unfortunately, certain aspects of this photochemistry manifest themselves in increasingly unpleasant ways, the scientific effort engaged in understanding and solving related practical problems becomes substantial. Regrettably, our actually corresponding level of understanding is still very low. The reason is partly that the critical substances exist only in extremely low concentrations and, thus, render their measurement difficult, and partly that many reactions happen via unstable intermediate products and therefore have not been directly measured, and partly that no really satisfactory simulation models are available for the study of supposed reactions in connection with measured reactions. Adequate models would also allow the inference of future situations from the present one, and, because of this, become an indispensable tool for effective air hygiene management.

A concluding remark concerns ozone depletion in the stratosphere (HARD and BRODERICK, 1975; McCRACKEN, 1975). It has been known for a long time that the ozone layer covering our planet protects us from the sun's harmful ultraviolet rays; but less than ten years ago we did not appreciate the significance of oxides of nitrogen in maintaining the ozone balance; and it was only a few years ago that it was shown that fluor-carbons may pose a serious threat to the integrity of the ozone layers. In this case, damage which some consider significant may be inevitable, because of past releases of the chemicals. The time between the use of CFMs at ground level and the maximum depletion they subsequently produce in the stratospheric ozone layer is of the order of a decade, and it requires decades for the stratosphere to recover fully.

This long time-lag, together with the fact that there are appreciable long-term natural fluctuations in the ozone layer, means that if no action were taken until the CFMs produced a directly measured reduction in the ozone layer, it would then be too late to avoid further, more drastic long-term effects. As a consequence, mathematical models must be used to analyze the sequence of events and to predict its outcome decades in the future. The accuracy of such predictions depends not only on many directly measurable molecular properties, such as photochemical decomposition and chemical reaction rates, but also on the manner in which the models approximate the motions of the atmosphere and its interactions with the solar radiation. Since it would not be prudent to wait until ozone depletion can be directly measured to see if it agrees with predictions, it is extremely important to identify promptly and to measure those quantities needed to test and refine the accuracy of the predictions of the current models.

Given the vital significance of this activity in our increasing urbanized, populated, and mechanized planet, it behooves us to make progress in this field.

5. REFERENCES

AMES, W.F.: "Numerical Methods for Partial Differential Equations", N.Y. 1969

BUNKER, D.L., GARRET, B., KLEINDIENST, T., LONG, G.S.: Combust. Flame, 23 (1974) 37

CHANG, J.S., HINDMARSH, A.C., MADSEN, N.K.: UCRL - 74823 (1973)

COLGROVE, F.D., HANSEN, W.B., JOHNSON, F.S.: J. Geophys. Res. 70 (1965) 4931

CRUTZEN, P.J.: Can. J. Chem., 52 (1974) 1569

ESCHENROEDER, A.Q., MARTINEZ, J.R.: Adv. Chem. Ser., 113 (1973) 101

GEAR, C.N.: Commun. ACM, 14 (1971) 176

GILLESPIE, D.T.: J. Comp. Phys., 22 (1976) 403

GRAEDEL, T.E., FARROW, L.A., WEBER, T.A.: Atm. Env., 16 (1976) 1095

HUANG, K.: "Statistical Mechanics", N.Y. 1963

LEIGHTON, P.A.: "Photochemistry of Air Pollution", N.Y. 1961

LOMAX, H., BAILEY, H.E.: NASA-Techn. Note D - 4109 (1967)

McQUARRIE, D.A.; J. Appl. Prob., 4 (1967) 413

MILLER, K.H.: Zeitschr. Angew. Math. Phys., 12 (1961) 242
EUR-5564 e (1976) and EUR-6533 e (1977)

OPPENHEIM, I., SHULER, K.E., WEISS, G.H.: J. Chem. Phys., 50 (1969) 460

SKLAREW, R.C., FABRICK, A.J., PRAGER, J.E.; J.A.P.C.A., 22 (1972) 865

SOODAK, H.: "Reactor Handbook", 3 A, N.Y. 1962.

HARD, T.M., BRADWICK, A.J.: DOT-TSC-OST-75-38 (1975)

McCRACKEN, M.C.; UCRL-51336 (1975).

Rapporteur's Summary Report

Prepared by: S. Hanna

Papers covered by: Gillani
Giebel
Müller

Paper: Project MISTT.: Plume Modeling of the dispersion, transformation and ground removal of SO$_2$ over the B-Mesoscale Range, N. V. Gillani
Paper interrupted by projector failure. The chairman asked whose talk did not need a slide projector. Consequently the paper on CO diffusion by Schorling was given.

Question: When you say CO concentration is prop. to immission, is this estimated or measured emission?

Answer Schorling: Measured emission. This conclusion is not valid for very small concentrations and emissions, where there is much noise in the data.

Question Johnson: Your conversion rate for SO$_2$ was variable. What is your feeling about using a single number?

Answer Gillani: The conversion rate is a function of time of day. If I had ro use single number, I would use 2 % per hour.

Question Prahm: You fit or tune the model with the data. How general are the results?

Answer Gillani: The rate constants are fairly good. You are right that by varying K the results will change. The current model is the result of much trial and error.

Paper: An improved source depletion model for deposition from a GAUSSian plume, J. Giebel.

Question Steenkist: I found the same results. The stability class is important, though. Also, what mixing height is used?

Answer Giebel: I agree that stability is important. The mixing height is 1000 m.

Question Fischer: These calculations are not close to reality unless they are compared with observations. For example, the effects of stability are not well known.

Answer Giebel: I used a single stability class: D

Paper: On the dispersion of chemical reacting pollutants,
K. H. Müller

Question Rote: How do you decide the cluster or box size?

Anser: This is just a mean of providing a box for the chemical reactions.

Question Prahm: Do you compare your solutions with those of simpler models?

Answer: We have compared this technique only with another complicated computer model.
The results are nearly the same. Our model reduces the computer time, however.

Summary

1. GILLANI:

A three dimensional plume model employing K coefficients, is applied to the diffusion of SO_2 from the 2400 MW Labodie power plant near St. Louis. Observations of SO_2 concentrations were made by airplane in the plume at distances out to 300 km from the plant on two days in July 1976. By adjusting the parameters in the model, it is found that the model can sucessfully simulate the variation of SO_2 with downwind distance. Conversion of SO_2 to sulfate and stability effects on K are accounted for.

2. SCHORLING:

The APRAC model for CO diffusion is applied to the problem of whether or not to construct a new expressway in Frankfurt. The expected CO concentrations for a variety of different road designs are shown, and it is seen that the CO standard is exceeded in some cases. Using this model, the road design which has the least environmental effect can be chosen.

3. GIEBEL:

Source and surface depletion models for dry deposition are compared. Chamberlain's source depletion model is improved by making the deposition velocity a function of wind speed, and accounting for the increase of the effective wind speed with distance. It is shown that the models often give significantly different estimates of dry deposition, but there are no data available to tell which model is best in reality.

4. MÜLLER:

Use his abstract. It is only two sentences.

8th NATO/CCMS INTERNATIONAL TECHNICAL MEETING ON AIR POLLUTION MODELING

TOPIC 6

MODELING IN COMPLEX TERRAIN

8th International Technical Meeting
on Air Pollution Modeling and its Application

The Austrian Alps Air Pollution Study

Walter W. Kofler
Institut für Hygiene der Universität
Innsbruck

September 20 - 23, 1977
Louvain-La-Neuve
Belgium

THE AUSTRIAN ALPS AIR POLLUTION STUDY (AAAS)

Walter W.Kofler

In the years 1971 - 1977 air pollution studies covering an area of 30 000km2 carried out in the entire provinces of the Tyrol, Salzburg and Carinthia according to orders given by the respective provincial governements. The objective was to estimate the large scale concentration levels of sulfur dioxide and dustfall as a basis for land use planning with regard to health.

For that purpose we had to find out and to line out the areas with too high concentration levels and very clean areas for resort.

Two thirds of the study area cover the mountainous areas of the Alps, while one third covers the hilly parts of the Alpine foothills. Therefore our study area is complex terrain. In such areas inversions, calms and low-speed wind appears frequently. According to the geographical structures various direct and indirect effects on the transport of air pollutants may occur. There is only little information available concerning the absorption of pollutants on surfaces and other effects according to the residence time of air pollutants. Besides these reasons in the study area there are only few meteorological stations established. So fundamentally the use of dispersion models did not seem to be adiceable for the solution of these questions.

Methods of investigations

A new system was therefore developed in order to solve our problems with help of a combination of data gathered from the emission, the concentration levels of air pollutants and the geographical situation.
Our studies contain therefor three, sometimes four or five steps:

1) geographical characteristics of the study area
2) determination of emissions
3) determination of concentrations
4) meteorological measurements (if possible)
5) biological measurements (if possible)

Geographical characteristics and determination of emissions

The first two steps are the basis to establish the network for the measuring points for total sulfation and dustfall. Depending on the emission situation the distance between the measuring points are one, two, four or more kilometers based on the GAUSS-KRÜGER-network. The determination of emission e.g. using emission maps is very helpful for the interpretation of the results of the concentration studies. As I will show later this is a prerequisite for the separation of the areas of influence of various emitters.

Determination of concentrations

For the determination of dustfall we used the BERGERHOFF-method. Sulfur dioxide measurements werde done by combining two different measuring systems: Continous monitoring instruments were situated on selected measuring points with high pollution levels. Such measurements are very costly and require intensive work. Therefore we used only on 28 points monitors. Over the whole study area we used a lot of measuring stations for total sulfation (lead dioxide candles) These network were based on the emission situation, the geographical situation and the GAUSS-KRÜGER - network. All in all more than 1 600 measuring stations for total sulfation were used.
The time span of the air pollution measurements in one study area is usually one year with 13 measuring periods of 28 days for the measurements of total sulfation and dustfall.

Meteorological measurements

In some studies we had the possibility for additional meteorological measurements besides the routine meteorological stations e.g. in the Salzburg-study and in the Carinthia-study. I am very sorry that it was impossible to arrange investigations by ballons, acustic radar or similar systems. Meteorological results are very helpful for the interpretation of concentration results especially with regard to transport of pollutants. For our primary problem - the finding and outlining of high polluted and low polluted areas - the use of meteorological data is not absolutely necessary.

Air quality measurements using bio-indicators

In different studies extra measurements were done to test the effects of air pollution on biological systems. E.g. in the Innsbruck-study and in the Bad Gastein-study was tested the influence of air pollution on lichens, needles and barks (5,6)

Results in regard to hygienic aspects

By this used method it was possible to answer the required questions. Beyond that, general statements could be given concerning the transport of pollutants in the study areas. It was also possible to show some relations between geographical parameters and concentration levels. I will report about these later.
The estimation from the medical point of view was done in this way: For the estimation of dustfall there are different international standards. Fortunately the measuring results of our resort areas were very low. Therefore we suggested new limits for these areas (7)

Using the results of total sulfation areas of different pollution levels could be discovered and outlined. It was also possible to determine the changes of the pollution levels during the year. But these statements are only relative. Using only results of total sulfation measurements it is impossible to give answers about health effects. Therefore we need results of continuous monitoring instruments. Such monitors were used at representative points. In this way the characteristic pattern of the sulfur dioxide levels, their courses their changes with varied meteorological conditions and the necessary absolute figures of the concentration could be determinated. So we could correlate the results of total sulfation with the simultanous results of the monitors for each measuring period.

Stress categories

According to the results of international epidemiological and physiological studies about health effects of SO_2 we organized the data of total sulfation in relation to the concentration results into four stress categories. Table 1 shows the four categories and their limits for the total sulfaltion, used in the Salzburg-study. It is important to know, that these limits are not transferable to an other study area or to other years. We developed the limits for the stress categories for each study. Stress categories were developed only for results of winter-measuring periods. Apart from few relative small areas near industrial plants in the study areas significant SO_2-levels were found only in wintertime. Using these limits it is possible to organize different areas according to their total sulfation level into these stress categories. In this way we evaluted all municipalities of the three countries separately according to settled areas, rural areas in valleys and rural areas on terasses and other higher ground.

Because of the short time I have no possibility to give more details or same examples to the questions I mentioned before. I can not report also about the different concentration levels which we found out in different famous towns and resort areas.

Table 1: Stress categories, Total Sulfation
Salzburg, Wintertimt 1973/74

Category	SO_2-level by area sources mg SO_3/28d/1dm2	SO_2-level by point sources mg SO_3/28d/1cm2	Characterisation
1	5,0	5,0	not any SO_2-level to speak of (Resort area)
2	5,0 - 14,9	5,0 -11,9	slight SO_2-level (resort area)
3	15,0 - 35,0	12,0 -25,0	the possibility of danger to health cannot be excluded
4	35,0	25,0	danger to health must be counted in winter when anfavorable wether conditions prevail

In the second part of my paper I want to speak about different experiences with geographical parameters and their effects on the concentration of air pollutants in the ambient air.

Influence of the altitude above ground level

In situations with stable conditions you can expect sudden changes of the concentration levels depending on the altitude above the ground. In wintertime in Alpine areas inversions are frequent. Therefore the concentration level of different measuring points depends strongly on their height above ground level. You can demonstrate the changes of concentrations very easily using lead dioxide candles in different altitudes above ground. In this way you can also establish changes in the height within the measuring periods. In our studies, which were accomplished in different kinds of complex terrain, we found some conformities about the height, where the total sulfation level usually sudden decreased. During the winter periods (October - March) this height was never higher than 300m. In mountainous areas we could establish a decrease of this height to 150 to 100m and lower with decreasing average temperature. Except for regions influenced by big lakes (see later) we found this effect also in hilly areas.

Influences of different heights of the mixing layers and the geographical situation on the concentration levels

The height of the mixing layer is one of the limiting parameters of the volume of the air for the dilution of pollutants. In complex terrain, the form of the valley, and the height of the surrounding mountains or hills are other limiting factors. In special geographical situations therefore relative small variations of the effective mixing height can be the reason for fundamental changes in the immission situation. For this an example:

In Klagenfurt we found essentially higher SO_2-concentrations and total sulfation levels during a milder winter (1974/75) than in a much more severe winter (1975/76) The reason for this surprising situation we see in different heights of the effective mixing height in the average of the two winters.

Map 1 shows the concentration pattern for measuring period 5 (18.1.-15.2.1975) produced by computer mapping.

Klagenfurt is a small town in Carinthia with about 90.000 inhabitants. The town is situated in a basin, cloused in the NW by relative low hills with 100 -120m height, in the N and NE by 220 - 300m high hills. In the S a range of hills with perhaps 300m height limits the basin. From S two valleys run into the basin: one is only 40m higher than the ground level of the basinm the other is coming from the hills. In the West of Klagenfurt a big lake, the Wörthersee is located. In the East the basin is open. The winter 1974/75 was much warmer and dryer than in the longtime average. Because of this the lakes did not freeze as usual. Only on a few days the soil was covered by snow. However there were daily inversions during the winter. Windspeed and -direction (Airport Klagenfurt) were very similar on the average. On the average the windspeed is between 0,8m/sec (December) and 1,4m/sec (March) during the wintermonths. The frequency of wind with more than 5m/sec is only 1,3%. In the average of the wintermonths in 50,1% are calms with a maximum of 52% in December. The wind shows a typical West-East-system.

The SO_2-level - measured by continuous monitoring instruments, lead dioxide candles and by West-Gaeeke method, reached the limiting values specified by the WHO. The concentration pattern of measuring period 5 is typical for the concentration situation of this winter. Map 1 and map 2 show computer maps of this measuring period. The maximum of the concentration is situated in the center of the town. Relative high levels were observed only on the bottom of the basin. The measuring points on the hills and behind the hills showed very low levels. Because of the atypical warm winter the measurements had to be continued in the winter 1975/76.

This winter was much more severe than the winter 1974/75. E.g. the average temperature in January was -2,2°C, that is 1,9° lower than the same month 1975. The whole lake was frozen for some weeks. The precipitation was less than the longtime average, but the number of days with snow cover was greater than the winter before. There were no characteristic deviations in windspeed and windfield from the longtime average. This winter showed a totally different concentration situation as you can see on the computer maps 3 and 4. They show the total sulfation pattern of measuring period 18, the comperable measuring period of measuring period 5. During MP 18 high total sulfation levels and high concentration levels were measured in the center of the town, but they were lower than the year before. This result is especially surprising if you concider the increasing emission rate according to the decrease of the temperature. In contrast to the situation of measuring period 5 the measuring points situated on hills and behind hills showed new also high concentrations. This you can see very easily at the measuring point in the northwest. During the winter 1975/76 the height if the effective miximg layer was a little higher on the average than the year before. This you can see an the higher pollution level of the measuring points on hills and slopes. So the pollutants were spreaded over a much larger area than in 1974/75. The range of hills separating the basin to the NE is at the lowest part only about 70m above the ground level of the basin. The lower valley in the S is only about 40 m higher than the basin. Therefore, the increase of the concentration level is very clear in these areas.

Effects of a lake

As a reason for this increase of the effective mixing layer we developed following hypothesis: During the stronge winter the lake was frozen for many weeks. The surface of the frozen lake produced much more cold air than open water. Because of this multiplied cold air production also the thickness of the stable layer of the daily inversion was increased. As soon as the height of this layer was higher than the surrounding hills, the cold and polluted air could flow into the areas beyond the hills. Especially the hills in the NW are not very high. Therefore only a small increase of the effective mixing layer is necessary for this mechanism. Snow cover magnifies this effect. This hypothesis is in accordance with the concentration pattern of the different measuring periods and the numbers of days with frozen lake and snow cover. Our hypothesis is corresponding also with statements of BRANDL et al. They pointed out the disproportion between the temperature and the SO_2- concentration measured by continuous monitoring instruments in Klagenfurt in December 1967 and in February 1968.

In December 1967 they observed higher SO_2-concentrations accompanied by warmer temperature than in February 1968. (8)

Surfaces of lakes do not only influence the concentration levels when they are frozen, but also when they are open. According to different results of our studies it seems to be probable that the surface of an open lake is an efficient sink for SO_2. Our frozen lake surface did not show this effect. This two different situations of the surface of the lake could be the reason of the different total sulfation levels measured at the points on the other side of the Wörthersee in the West of Klagenfurt in measuring period 5 and 18. The SO_2-levels in this part of the study area are caused in first line by emissions shifted from Klagenfurt and damed up by the slopes which raise from the lakeside.
A considerable absorption effect of snow cover - especially of old snow - was not observed then.

The importance of windward slopes in the air quality

Windward slopes are often the reason for local high concentration of air pollutants in our study areas. Therefore these geographical factors must be considered estimating the air quality situation of such terrains. In Klagenfurt, for example, you can see easily the importance of windward slopes. In measuring period 18 the absolut maximum of total sulfation was observed at a slope in the NE of Klagenfurt about 100m above ground level. The SO_2 responsible for this effect was shifted from Klagenfurt to the windward slope. It seems reasonable that the effect of the windward slope coincides with the effect of crossing lines of the height of the temperaure inversion and the slopes. At such crossing lines we observed higher concentrations than at the ground in several cases.
In the map of MP 18 the maxima outside of the town in the SE, S and W are coused also by the effect of windward slopes.
We did not find significant effects of obstacles only on slopes but also in the areas situated in front of the barriers. In

some cases we observed some higher pollution levels in these areas e.g. south of the small mountains in downtown Salzburg. Such substantial increases were only found in areas not farther than two kilometers from the barriers.

The separation of the areas of influence of various emitters

It is possible in favorable situations to separate the areas of individual emitters one another with our method. This I will demonstrate by an example of the Lower Inn Valley of the Tyrol (Diagram. 1) We use the results of the determination of emissions and the results of the measurements of total sulfation during the measuring periods. The results of total sulfation of the study area were sumed for each measuring period and the percentage was calculated for each measuring point. By this the comparability of the results during the various measuring periods is greatly increased. In a graph the results in percent of a measuring point for the different measuring periods result in a curve. This shows the changing importance of the measuring points in the study area.
The Lower Inn Valley is approximately two kilometers wide and 12 kilometers long in the study area. The topography raises rather steadily to a height of over 2 000 meters above sea level. Approximately five kilometers up-valley from the illustred segment lie point source sulfur dioxide emitters in an industrial region with a population of approximately 4 000 people (Wattens). The valley regions up this point are primarily used agriculturally, so that no SO_2 emissions are expected. Point sources exit in Schwaz und Jenbach. The curves of the different measuring points are shown at the bottom of the diagramm. The level of the total sulfation for measuring point F4 (in the middle of the diagram) sank continuously from one periode to the next (Measurements were started in December) i.e. it decreased more and more with the increase in the wind blowing up the valley. As the frequence of up-valley winds increases, the influence of the sources kilometers down-valley (Schwaz) increases also, but this influence

could not compensate for the loss of the contribution of the up-valley sources. The situation was different at measuring points H 5 (three kilometers NW of Schwaz) in MP 6 and J 6 (two kilometers NW from Schwaz) during measuring period 5 and 6. Down-valley from Schwaz the emissions from Schwaz dominate for about three kilometers against the up-valley emissions of Jenbach.(see measuring point M 10) The increases in measuring point L8 in MP 4 and MP 5 are due to increased levels in domestic combustions from the village down-valley and not due to emissions from Jenbach. The small amounts of total sulfations in N 11 were more compensated for by larger levels of total sulfation from emissions from Jenbach, which is down the valley from N 11 approximately 1,5 kilometers. The relative total sulfation of the measuring stations O 13 and P 14, which are located down-valley from Jenbach, became smaller from measuring period to measuring period. Two factors are contributing to this: First the next sulfur dioxide emitter of importance is located approximately six kilometers up-valley and secondly the mouth of a broad side-valley is found one kilometer down-valley, thus creating better meteorological conditions for dilution the air pollution.

References

1) W.Kofler: Large Scale Estimation of the Sulfur Dioxide Concentration Levels and Concentration Changes in Mountainous Regions as a Basis for Land Use Planning with Regards th Health, Air Pollution Control Assoc. Publ. 76-17.02 Portland 1976

2) Amt der Tiroler Landesregierung: Untersuchung der Grundbelastung der Luft mit SO_2 , Tiroler Raumordnung, Bestandsaufnahmen 1, 1973

3) Amt der Salzburger Landesregierung: Die Belastung der Luft durch SO_2 und Staub im Land Salzburg, 1975

4)Amt der Kärntner Landesregierung: Lufthygienische Modellstudie für das Land Kärnten (im Druck)

5)M.Hutter: Die Pflanze als Indikator für Luftverunreinigungen, Inst. für Botanik, Hausarbeit 1973

6)W. Kofler, J. Benger: Luftreinhalteplan Bad Gastein, unveröffentlichtes Gutachten im Auftrag der Salzburger Landesregierung, Innsbruck 1977

7)W.Kofler, J.Benger: Basic Concept for the Judgement of the Results of Dustfall Measuring in the Alps, Zbl.Bakt. Hyg.,I.Abt. Orig.B 161, 351-361,1976

8)J.Brandl, H.Janach,F.Panger and F.Wiedermann: Messungen der Luftverunreinigung der bodennahen Atmosphäre im Raum Klagenfurt, Stadtmagistrat Klagenfurt 1968

9) W.Kofler:The Determination of Resort and Stress-Areas by Air Pollution 1. and 2. Communication, Zbl Bakt Hyg., I.Abt.,Orig.B 164 159-178, 1977

Figure 1:

KLAGENFURT MG SO_3/DM^2 MEASURING PERIOD 5 (18.1. - 15.2.1975)

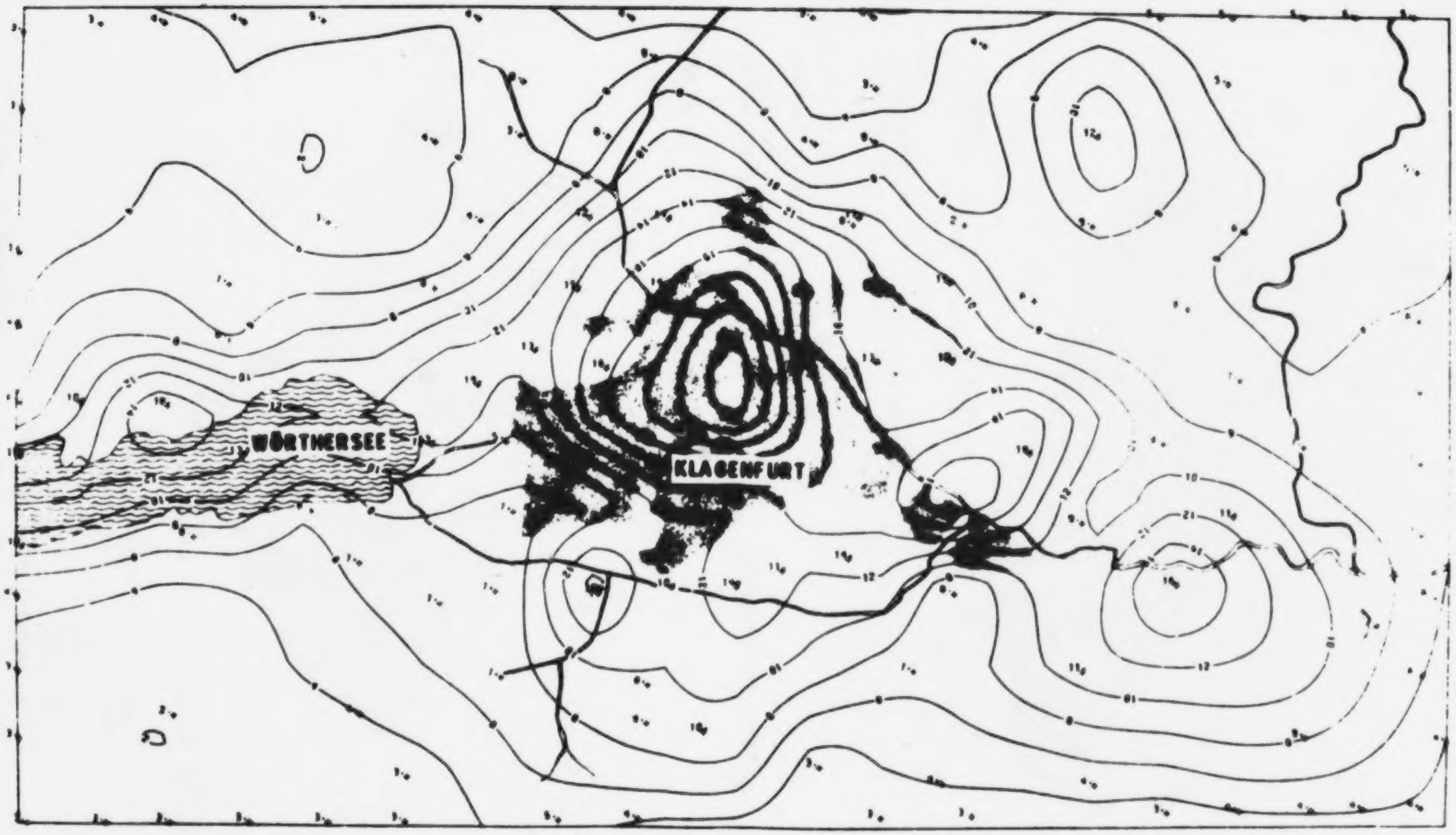
WÖRTHERSEE
KLAGENFURT

Figure 2:

Klagenfurt mg SO_3/dm^2

MEASURING PERIOD 5
18.1.-15.2.1975

Average temperature: +2,0°C
7h : -1,3
14h : +5,1
21h : +1,7

Snow cover : 2 days
Wörthersee : open

SO_3:

Klagenfurt centre : 24,2mg SO_3/dm^2
Walddorf : 4,1mg SO_3/dm^2

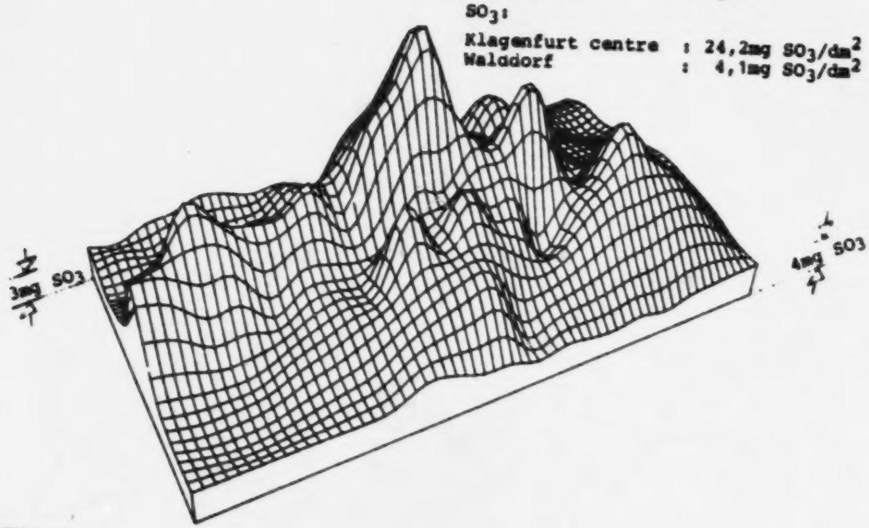

Figure 3:

MEASURING PERIOD 18
17.1.-14.2.1976

Average temperature: -1,4°C
7h : -4,9
14h : +1,8
21h : -1,5

Snow cover : 5 days
Wörthersee : 28 days under ice

SO_3:

Klagenfurt centre : 15,4mg SO_3/dm^2
Walddorf : 11,2mg SO_3/dm^2

Klagenfurt mg SO_3/dm^2

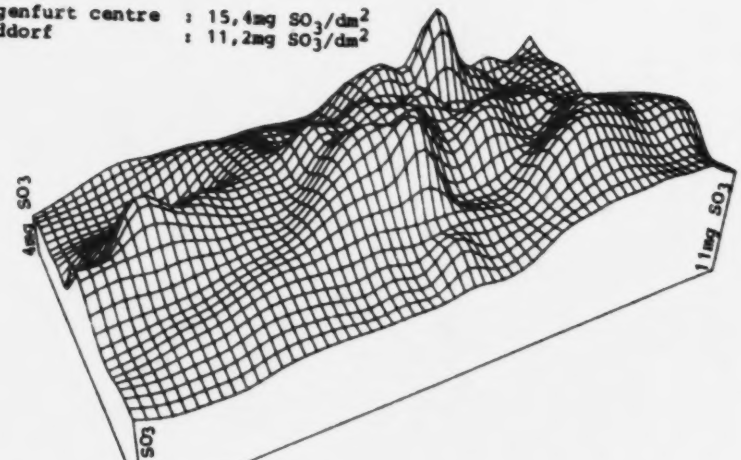

Figure 4:

KLAGENFURT MG SO_3/DM^2 MEASURING PERIOD 18 (17.1. - 14.2.1976)

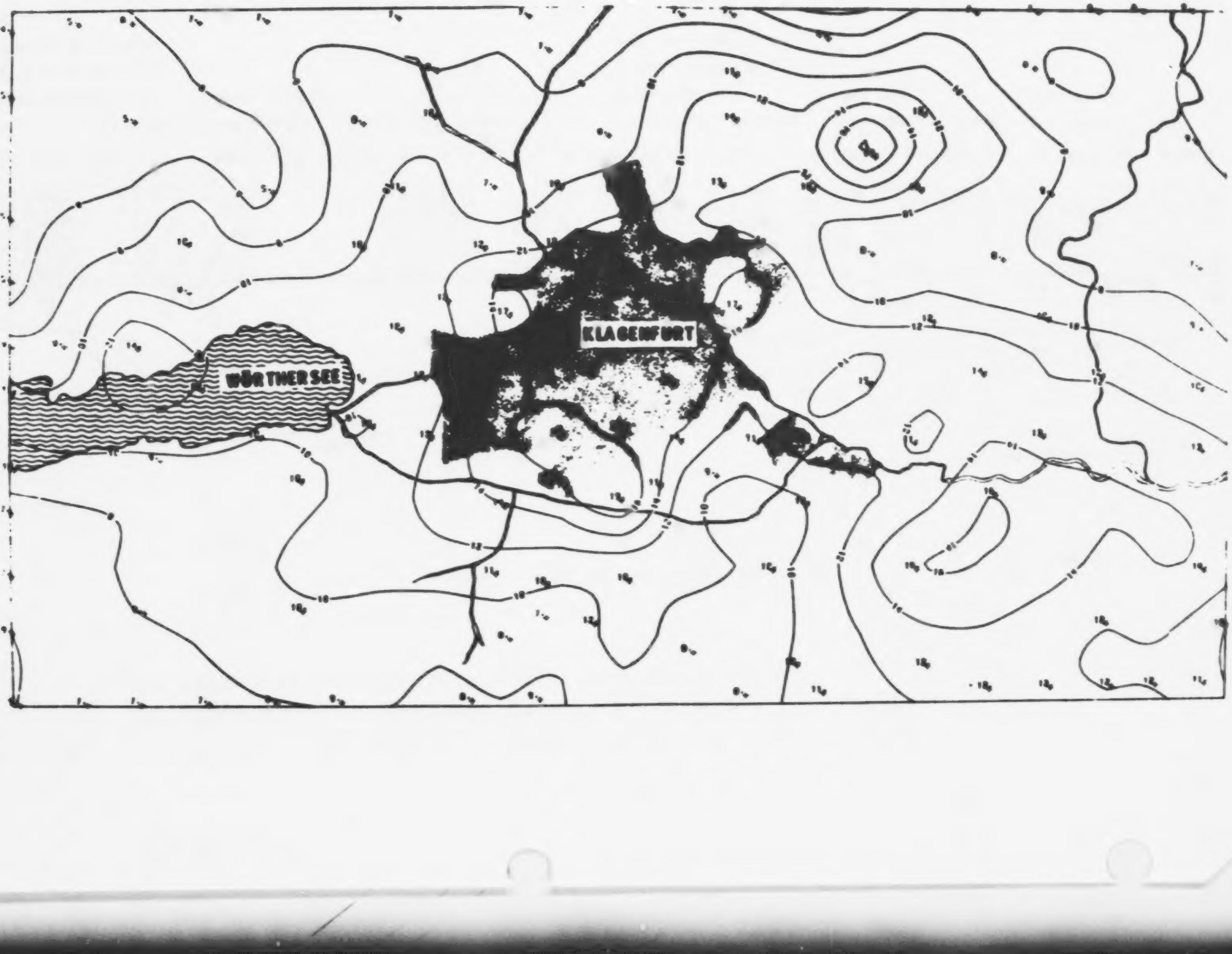
WÖRTHERSEE
KLAGENFURT

Diagram 1: The changing importance of measuring points (total sulfation) according to the different measuring periods 1 - 6 (1971-11-22 to 1972-5-9) and the location of various emitters

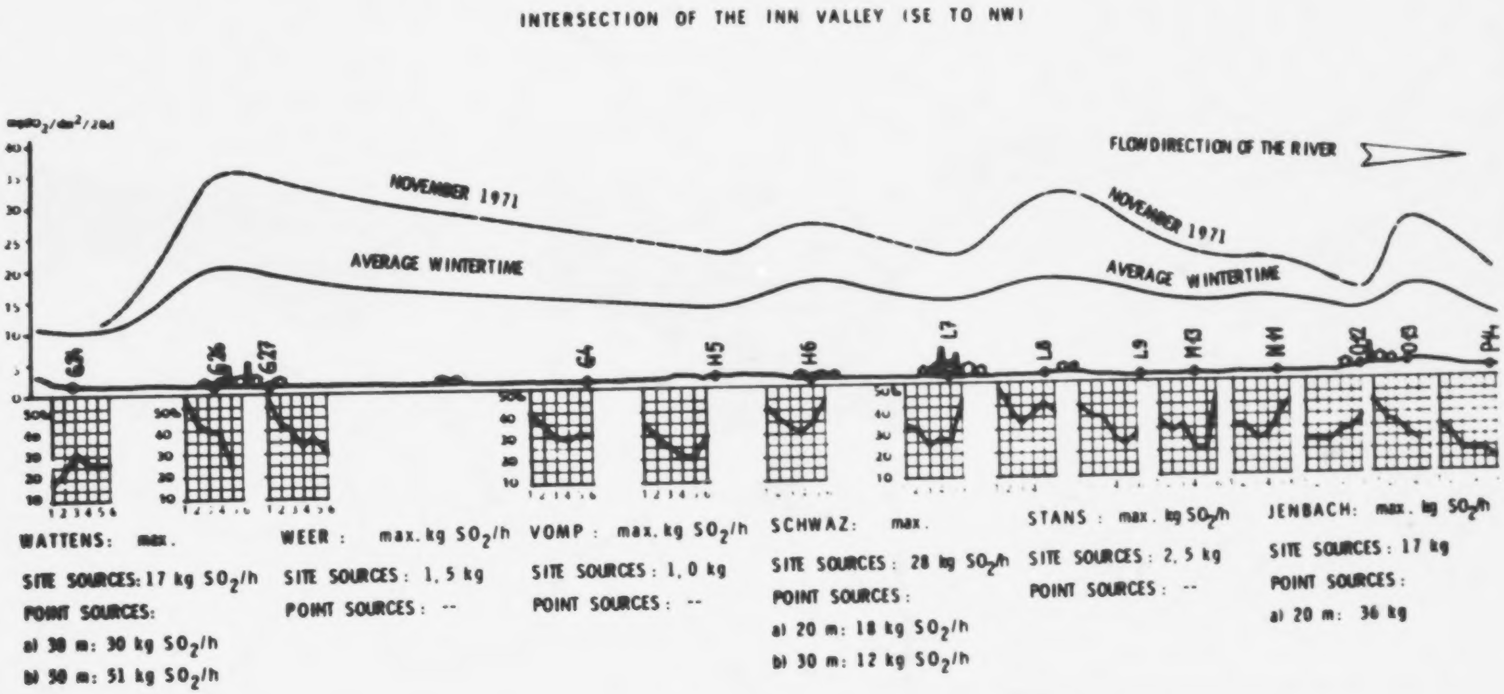

8th International Technical Meeting
on Air Pollution Modeling and its Application

MICROSCALE ATMOSPHERIC MODEL

by
J. VANDERBORGHT
ROYAL METEOROLOGICAL INSTITUTE
OF BELGIUM

September 20 - 23, 1977
Louvain-La-Neuve
Belgium

MICROSCALE ATMOSPHERIC
MODEL

INTRODUCTION

Before testing diffusion models of pollutants, it is essential to elaborate models that characterize air displacements over a well-known geographical region.

Our purpose is to build an atmospheric circulation model at town scale for a region with important orography. That model is especially designed to study the influence of orography on the circulation in the lower atmospheric layers.

For this study, we choose the city of Liege which has an orography varying between 55 to 280 meters above see-level.

We consider a domain extending vertically from the ground surface to the pressure surface of 900 mb. The area covers a square of 400 km2 (20 km x 20 km).

This domain is described by a 4-layers model, each layer having a constant thickness of 25 mb, except for the lowest one. This layer is supposed to include the entire orography. Therefore, its thickness ρ is variable (fig.1).

THE MODEL

The adopted model has the following physical properties :
The atmosphere is a perfect, non viscous gas whose motion is non turbulent and adiabatic.
Vertically, there is hydrostatic equilibrium.
Mass and energy conservation are imposed.

Because we consider only the small scale phenomena, we can neglect the non divergent part of the horizontal wind. Hence we keep the divergent part only.

List of symbols :

x^i, $i = 1, 2$	two coordinates defining a position on the terrestrial sphere
p	pressure (vertical coordinate)
t	time
θ'	velocity potential
T	temperature
ρ	thickness of the surface layer
δ	thickness of the three higher layers (25 mb)
g_{ij}	metric tensor
γ	metric tensor determinant
e_{ij}	LEVI-CIVITA anti-symmetric tensor
ε_{ij}	$e_{ij} / \sqrt{\gamma}$
A'	$\partial A / \partial p$
$\dot{A}$	$\partial A / \partial t$
ϕ	geopotential
Δ	LAPLACE operator
$J(A,B)$	$(1/\sqrt{\gamma})\, \varepsilon^{ij} (\partial A/\partial x^i) (\partial B/\partial x^j)$
$Q(A,B)$	$g^{ij} (\partial A/\partial x^i) (\partial B/\partial x^j)$
$R(A,B)$	$(1/\sqrt{\gamma})\, \frac{\partial}{\partial x^i} \left(\sqrt{\gamma}\, g^{ij} A \frac{\partial B}{\partial x^j} \right)$
c_p	specific heat at constant pressure

SCALAR FORM OF THE EQUATIONS :

We shall write the equations of the model in scalar form.

For the three higher layers, the system of differential equations can be expressed as [1]:

$$\Delta\dot{\theta}'_i = \frac{1}{2}\Delta\left(Q(\theta'_i,\theta'_i)\right) + \frac{1}{2} R(\Delta\theta'_i,\theta'_i) + \frac{1}{2}\Delta(\phi_{i+.5} + \phi_{i-.5}) - \frac{1}{2\delta} R(\Delta\theta_{i+.5}, \theta'_{i+1}) + \frac{1}{2\delta} R(\Delta\theta_{i-.5}, \theta'_{i-1}) + D_{\theta'_i}$$

$$\dot{T}_i = R(T_i,\theta'_i) + \frac{1}{2c_p}(\phi_{i+.5} + \phi_{i-.5})\Delta\theta'_i + \frac{1}{\delta}\Delta\theta_{i-.5}\left(\frac{T_i + T_{i-1}}{2} + \frac{\phi_{i-.5}}{c_p}\right) - \frac{1}{\delta}\Delta\theta_{i+.5}\left(\frac{T_i + T_{i+1}}{2} + \frac{\phi_{i+.5}}{c_p}\right)$$

where

$$D_{\theta'_i} = \mu_{i+.5}\left(\Delta\theta'^{*}_{i+1} - \Delta\theta'^{*}_{i}\right) + \mu_{i-.5}\left(\Delta\theta'^{*}_{i-1} - \Delta\theta'^{*}_{i}\right)$$

In this expression, θ'^{*} is the deviation of θ' with respect to its large scale value and the parameters μ are defined by the atmospheric basic structure.

For the ground layer, the equations take the following form :

$$\dot{\rho} = R(\rho,\theta') + \Delta\theta_{n-.5}$$

$$R(\rho, \dot{\theta}') = \frac{1}{2} R(\rho, Q(\theta', \theta')) + R\left(\frac{\phi_{n-.5} - \phi_s}{2}, \rho\right)$$

$$+ R\left(\rho, \frac{\phi_{n-.5} + \phi_s}{2}\right) + R\left(\Delta\theta_{n-.5}, \frac{\theta'_{n-1} - \theta'_n}{2}\right) + D_s\theta',$$

$$\rho\dot{T} = \rho\, Q(T, \theta') + \Delta\theta_{n-.5}\left(\frac{T_{n-1} - T_n}{2} + \frac{\phi_{n-.5} - \phi_s}{c_p}\right)$$

$$+ (\rho/2c_p)(\phi_{n-.5} - \phi_s)\,\Delta\theta'_n,$$

where

$$D_s\theta' = R\left(k \cdot \sqrt{Q(\theta'_n, \theta'_n)} \cdot \text{density}, \theta'_n\right)$$

in which k is the surface roughness coefficient.

INTEGRATION OF THE SYSTEM

Our purpose is to study the influence of the perturbation constituted by the orography on the basic meteorological parameters.

The equations of the model must be integrated till the situation describing the small scale phenomena becomes stable : in the atmosphere, there is generally a link between spatial and temporal scale. For the small scale phenomena, we obtain a stable atmospheric situation after an integration of one hour.

A 41x41 grid (mesh of 500 meters) has been defined. The 1681 gridpoints give a good representation of the topography of Liege.

Since every term appearing in the equations has to be calculated for each gridpoint, the numerical integration of this system of differential equations is very time consuming.

Because of the presence of high speed gravity waves in the model, we have to take a very small integration time step : a propogation speed ranging about 300 m s^{-1} implies an integration time step smaller then 0.25 second.

We are thus faced with the same problems as in large scale numerical weather prediction. That means that we have to control the gravity waves in such a way that we can take a longer time step.

If we integrate the equations of the model containing the high speed gravity waves, we need 9600 computation hours, on I.B.M. 360/44, to reach a stable atmospheric situation. It is evident that this solution is unacceptable. Therefore, we have developed a semi-filtered model which is integrated by a semi-implicit scheme.

SEMI-FILTERED MODEL

The equations of the model are linearized and the propagation velocities of the linear waves are calculated. One of these velocities corresponds to the gravity wave and is eliminated (semi-filtering).

For the slower waves, the equations are prognostic so that we can perform a time integration. For the gravity wave, the equations are diagnostic.

To reduce even more the total integration time, a progressive grid system has been considered. The model is first run with a 11x11 grid (mesh of 2 km) to a steady state solution.

Starting with this result, the system is integrated for a 21x21 grid (mesh of 1 km) to a steady state solution. Details are finally obtained by defining a 41x41 grid (mesh of 500 meters).

Heat sources and roughness are uniformely introduced in the model : it means that they have the same value at the same distance of the town centre (circular repartition). This hypothesis is not restrictive, because the roughness coefficients and heat sources can easily be modified numerically. In fact, the difficulty is to estimate a priori the roughness due to the terrain and the buildings, and to measure correctly the heat sources.

APPLICATIONS

Results are presented, for two different situations, in graphical form. The graphs show the horizontal wind field (surface wind) (figures 2 and 7), the velocity potential at the surface (figures 6 and 11), the velocity potential (figures 5 and 10) and the temperature field (figures 4 and 9) in the middle of the surface layer and the thickness of the surface layer (figures 3 and 8).

The (7 to 11) five graphs correspond to the situation obtained from UCCLE's sounding of 29/2/1972 at 0h, which gives the starting situation at large scale.

Pressure	Temperature Centigrades	Wind direction	Wind speed
100 cb	2°	80°	1.5 m s^{-1}
96.5 cb	4°	70°	2 m s^{-1}
85 cb	- 1°	40°	3 m s^{-1}

In this case, the wind is weak. The lower atmospheric layers are stable and the upper layers are unstable. The heat sources decrease uniformely from the town centre (value of 2 degrees centigrades in one hour) to the grid edges.

The five following graphs correspond to the situation obtained from UCCLE's sounding of 24/6/1972 at 12h.

Pressure	Temperature	Wind direction	Wind speed
100 cb	13°	240°	4 m s-1
93.8 cb	8°	-	-
90 cb	6°	230°	7.5 m/sec.

In that case, the atmosphere is unstable and there are no heat sources (summer situation).

In figures 2 and 7, the length of the arrows is proportional to the wind speed :
1 grid interval corresponds to 2.37 m s^{-1} for surface wind on 29/2/1972 at 0h and to 6.32 m s^{-1} on 24/6/1972 at 12h.

The mean executation time of the model, on I.B.M. 360/44 takes about two hours.

This microscale atmospheric model is part of the meteorological dynamical software (SMD), which has been developed in the I.R.M. by Professor J. VAN ISACKER [2]. Let us note that the program used to integrate the equations of this model cannot be used outside this context.

The program is written in LMD (Dynamical Meteorological language).
It has access to the large scale meteorological data and uses the methods of objective analysis [3], decoding [4] and plotting employed by the daily weather numerical prediction.

REFERENCES

[1.] : J. VAN ISACKER : private communication

[2.] : J. VAN ISACKER : Le système de météorologie dynamique (SMD), Note interne de l'I.R.M.

[3.] : J.P. STESSEL : Méthode d'analyse objective des cartes météorologiques. Publications de l'Institut Royal Météorologique de Belgique, série A n° 94.

[4.] : J.P. STESSEL : Sur une méthode pratique de décodage des messages météorologiques. Publications de l'Institut Royal Météorologique de Belgique, série B, n°74.

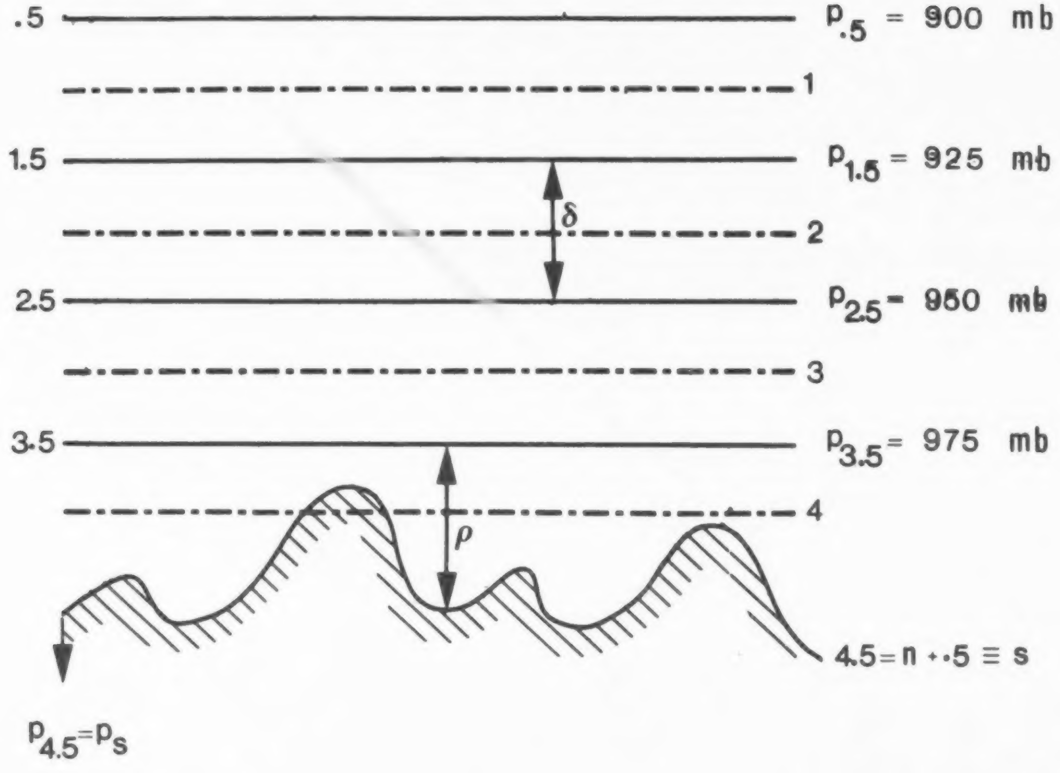
.5
$p_{.5}$ = 900 mb
1
1.5
$p_{1.5}$ = 925 mb
δ
2
2.5
$p_{2.5}$ = 950 mb
3
3.5
$p_{3.5}$ = 975 mb
4
ρ
4.5 = n + .5 ≡ s
$p_{4.5} = p_s$

FIGURE 1 : the four-layers model

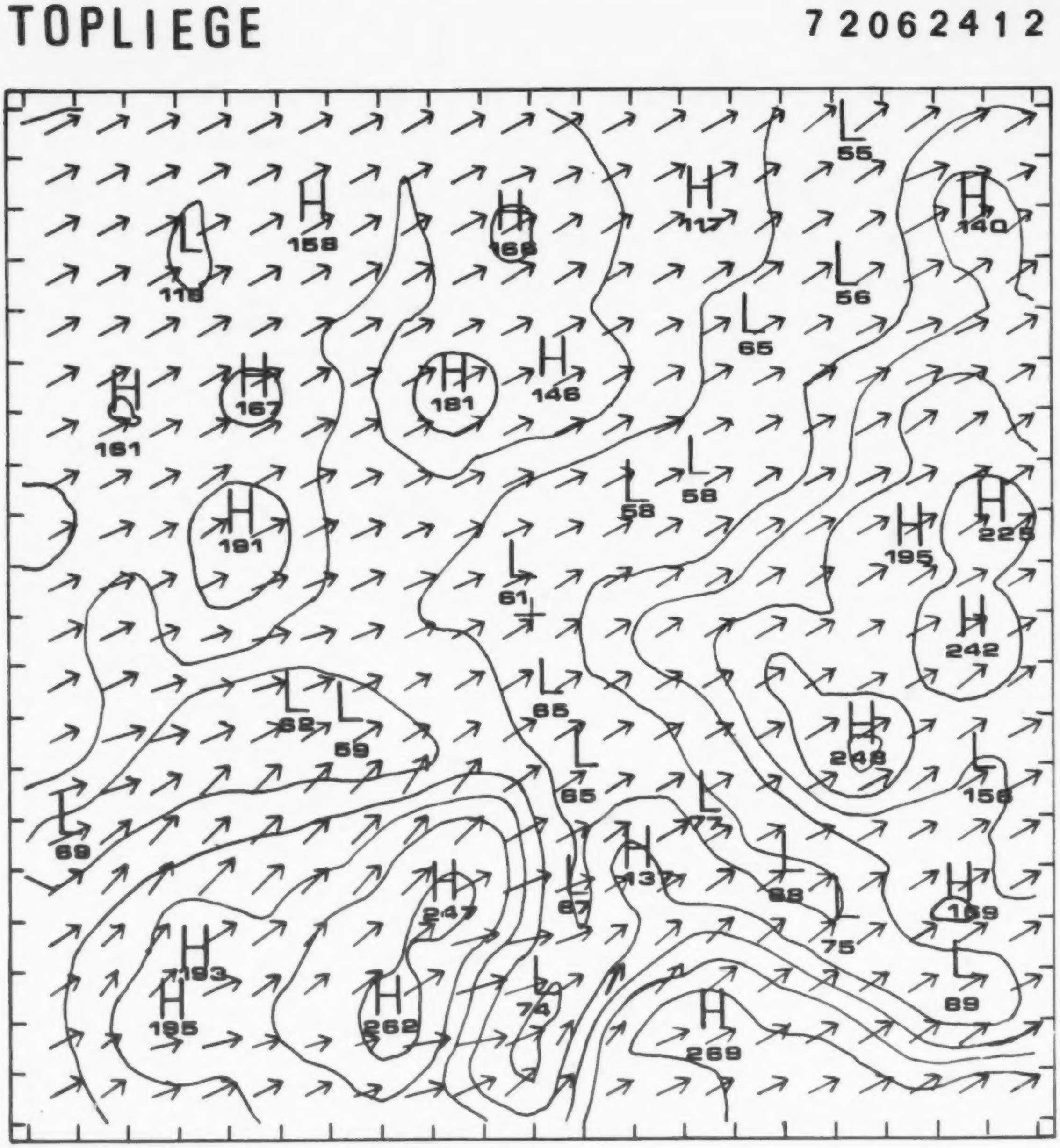
TOPLIEGE
72062412

FIGURE 2 : horizontal surface wind field

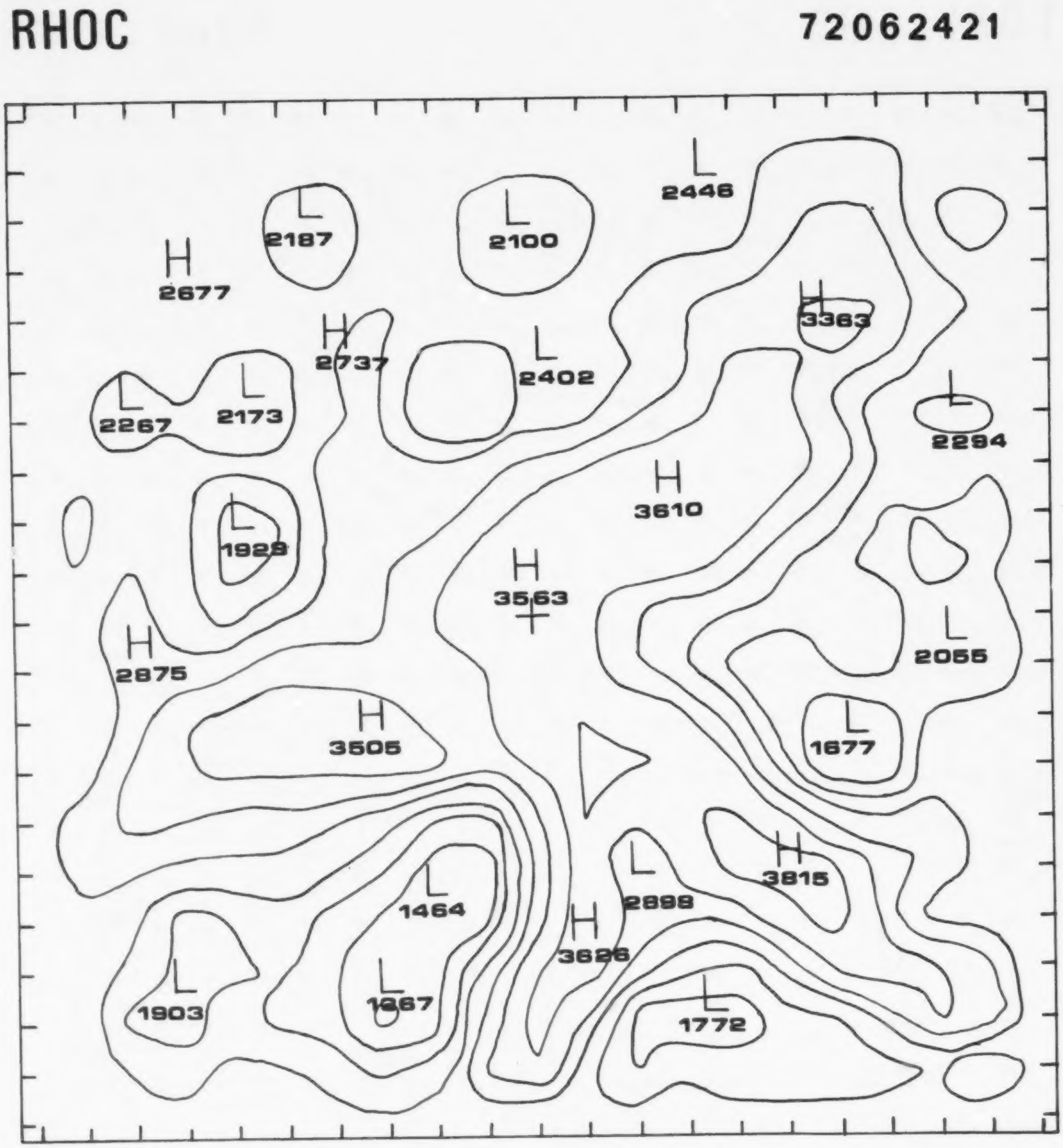
RHOC
72062421
L
2446
L
2187
L
2100
H
2677
H
2737
L
2402
H
3363
L
2267
L
2173
L
2294
H
3610
L
1929
H
3563
L
2055
H
2875
H
3505
L
1677
H
3815
L
1464
L
2898
H
3626
L
1903
L
1867
L
1772

FIGURE 3 : thickness of the ground layer (mb/100)

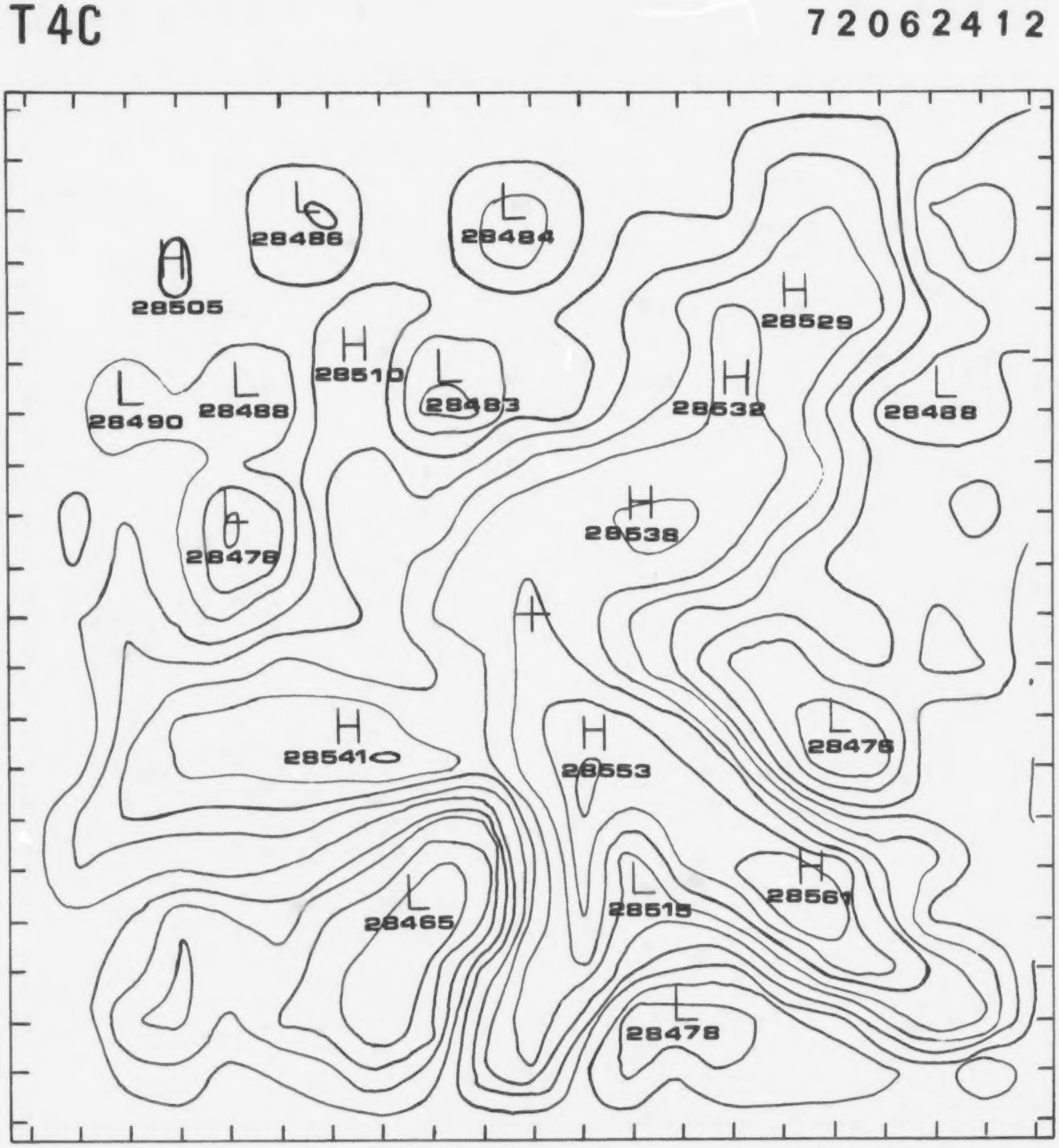
T4C
72062412
28486
28484
28505
28529
28510
28490
28488
28483
28532
28488
28538
28478
28541
28553
28476
28465
28515
28561
28478

FIGURE 4 : temperature field (°K/100)

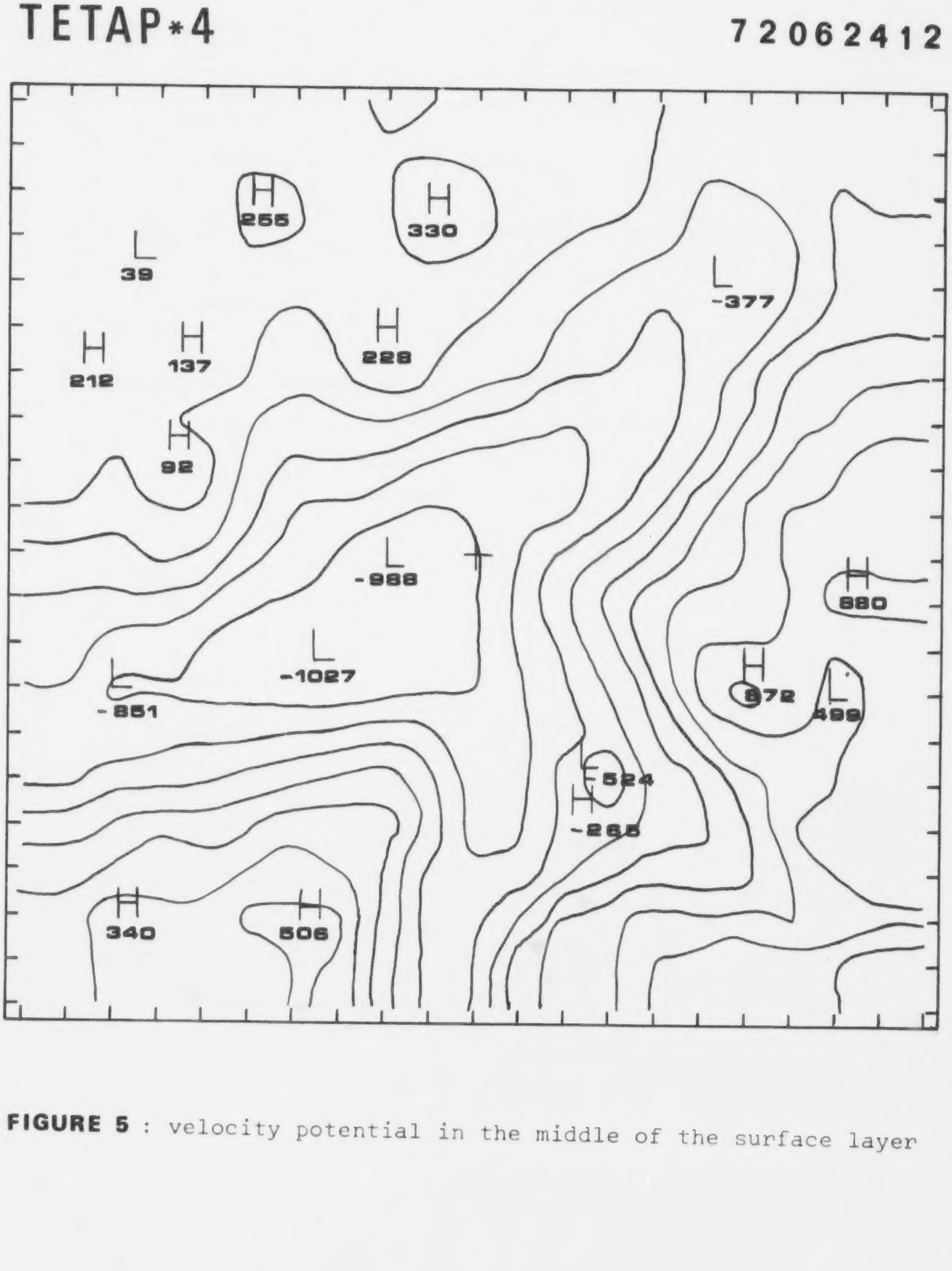
TETAP*4
72062412
H 255
H 330
L 39
H 212
H 137
H 228
H 92
L -377
L -966
L -1027
L -851
H 680
H 572
L 499
L 524
H -265
H 340
H 506

FIGURE 5 : velocity potential in the middle of the surface layer

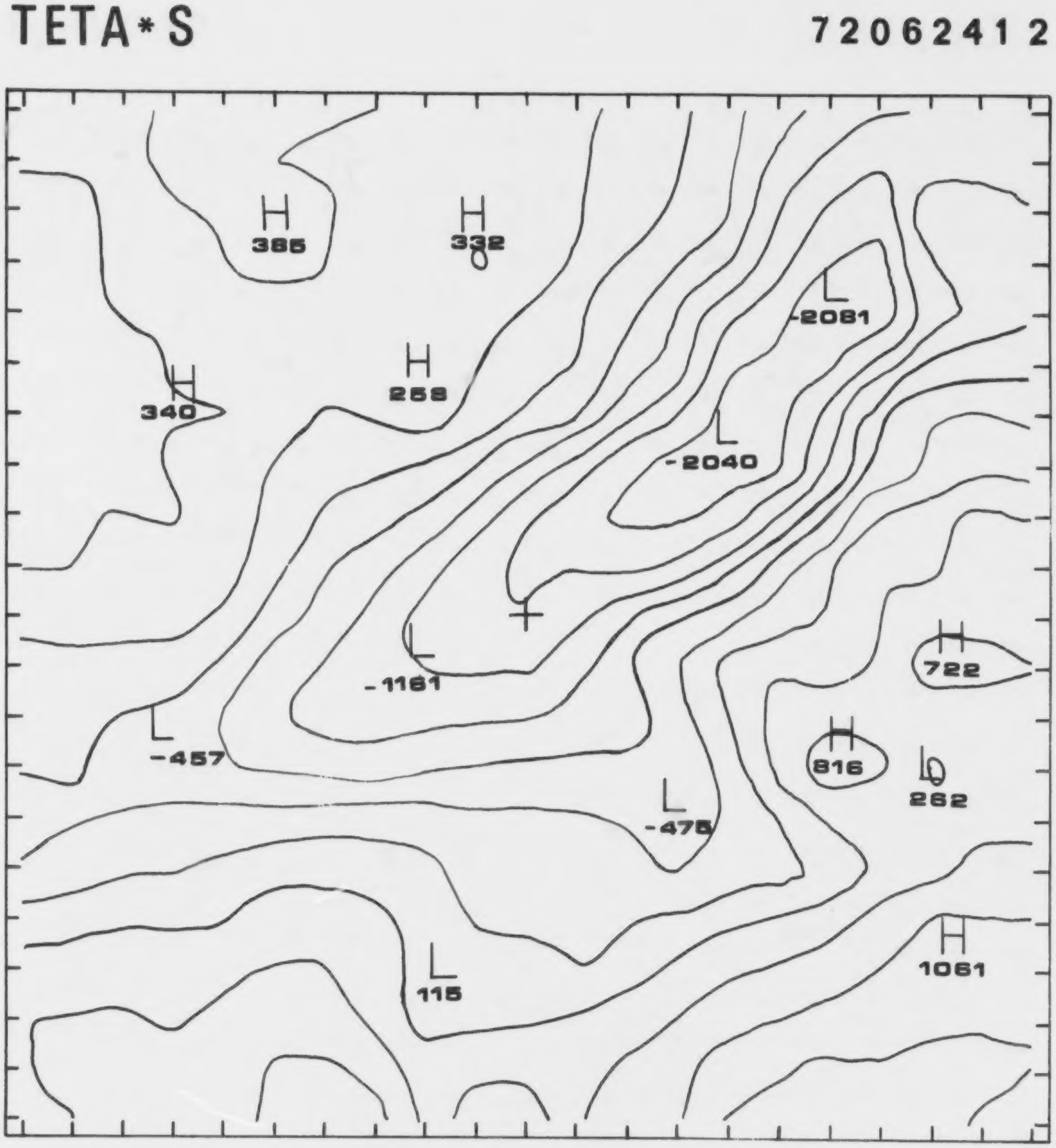
TETA*S
72062412
H
385
H
332
L
-2081
H
340
H
258
L
-2040
+
L
-1161
H
722
L
-457
H
816
L
262
L
-475
H
1061
L
115

FIGURE 6 : velocity potential at the surface

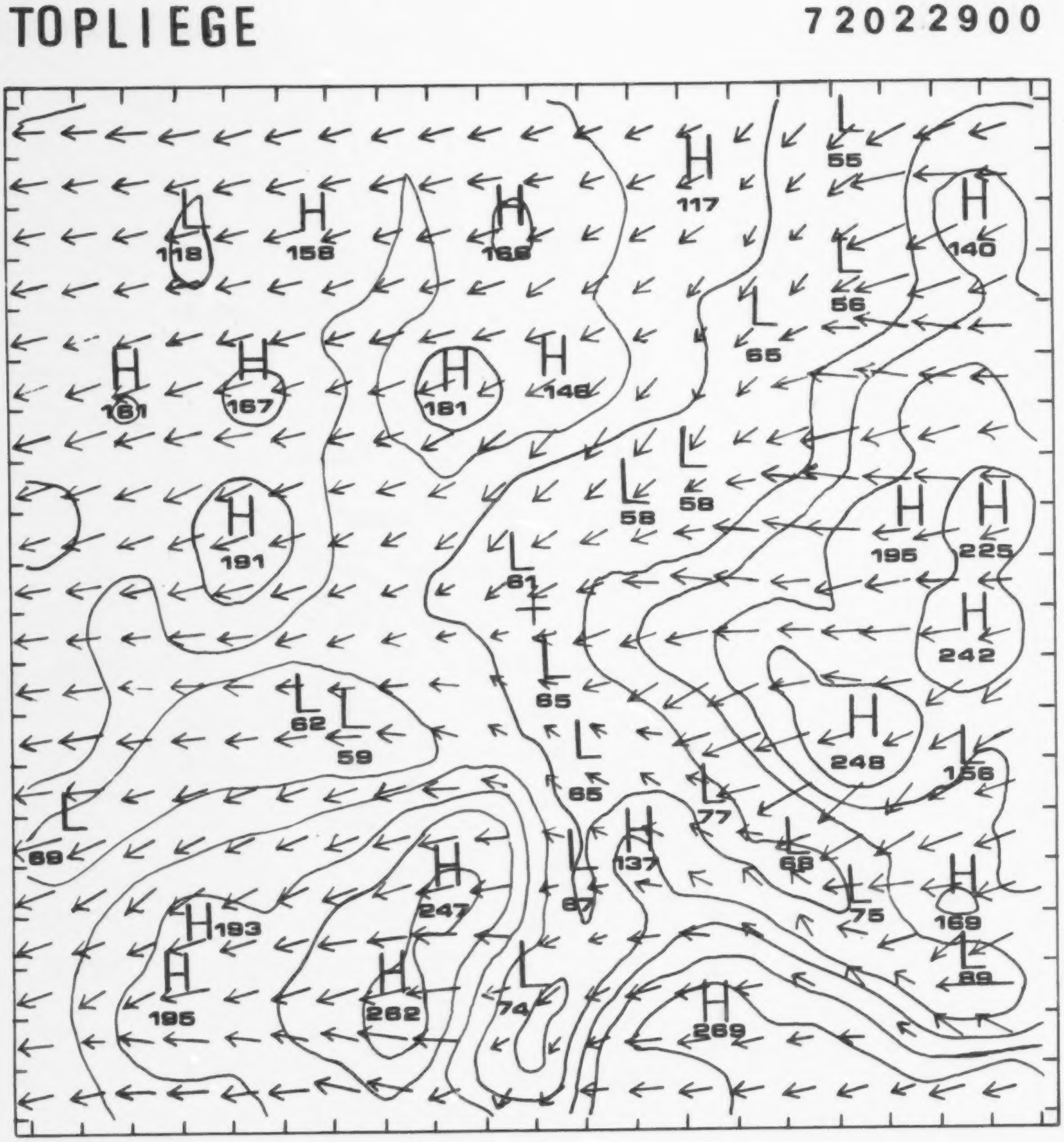
TOPLIEGE
72022900
H 117
L 55
H 140
L 118
H 158
H 169
L 56
L 65
H 161
H 167
H 181
H 146
L 58
L 58
H 191
H 195
H 225
L 61
H 242
L 65
L 62
L 59
H 248
L 65
L 156
L 69
L 77
H 137
L 68
L 67
L 75
H 169
H 193
H 247
H 195
H 262
L 74
H 269
L 89

FIGURE 7 : horizontal surface wind field

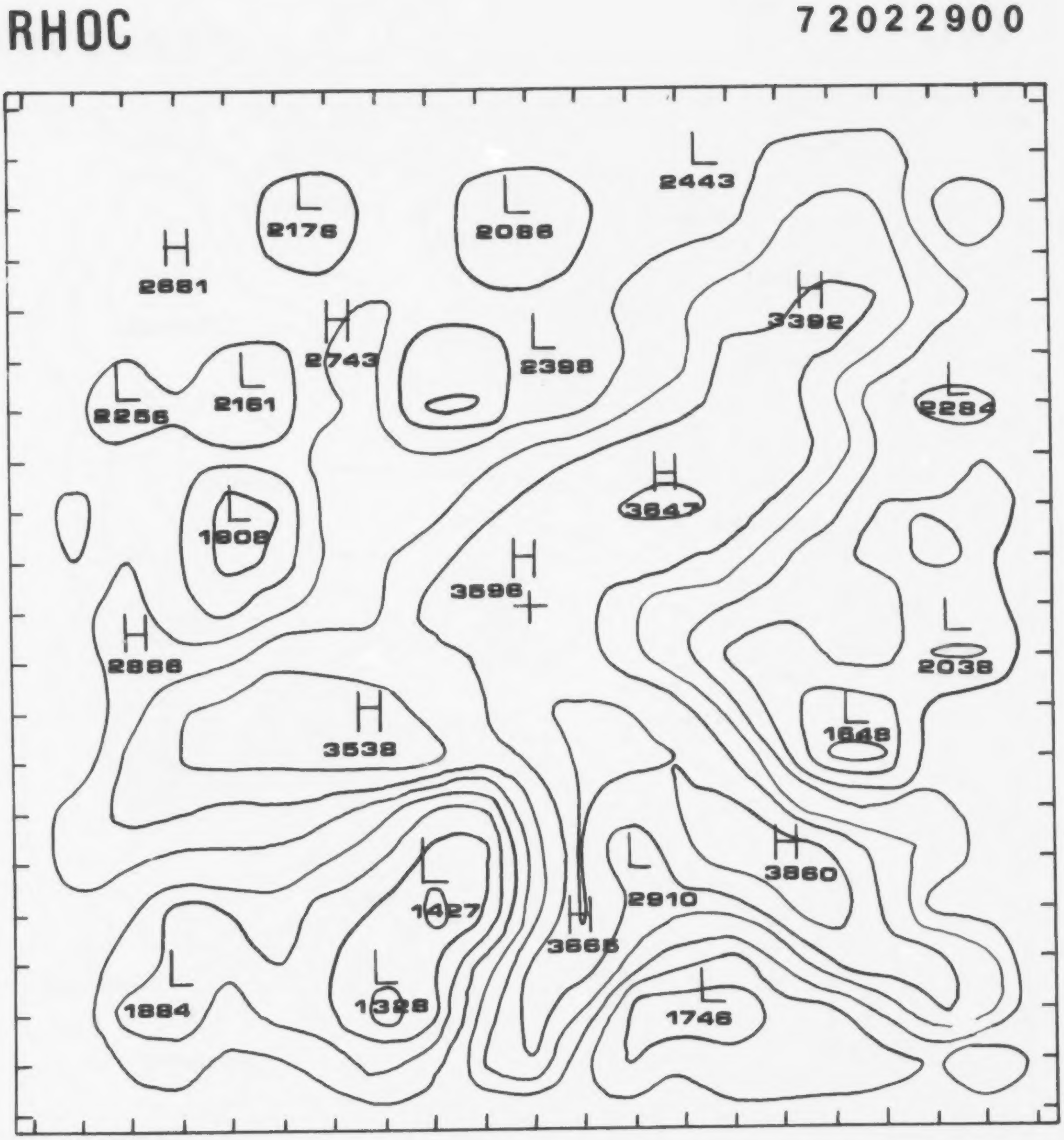
RHOC
72022900
L
2443
L
2176
L
2086
H
2681
H
2743
L
2398
H
3392
L
2256
L
2161
L
2284
H
3647
L
1808
H
3596
H
2886
L
2038
H
3538
L
1648
H
3860
L
1427
L
2910
H
3666
L
1884
L
1328
L
1746

FIGURE 8 : thickness of the ground layer (mb/100)

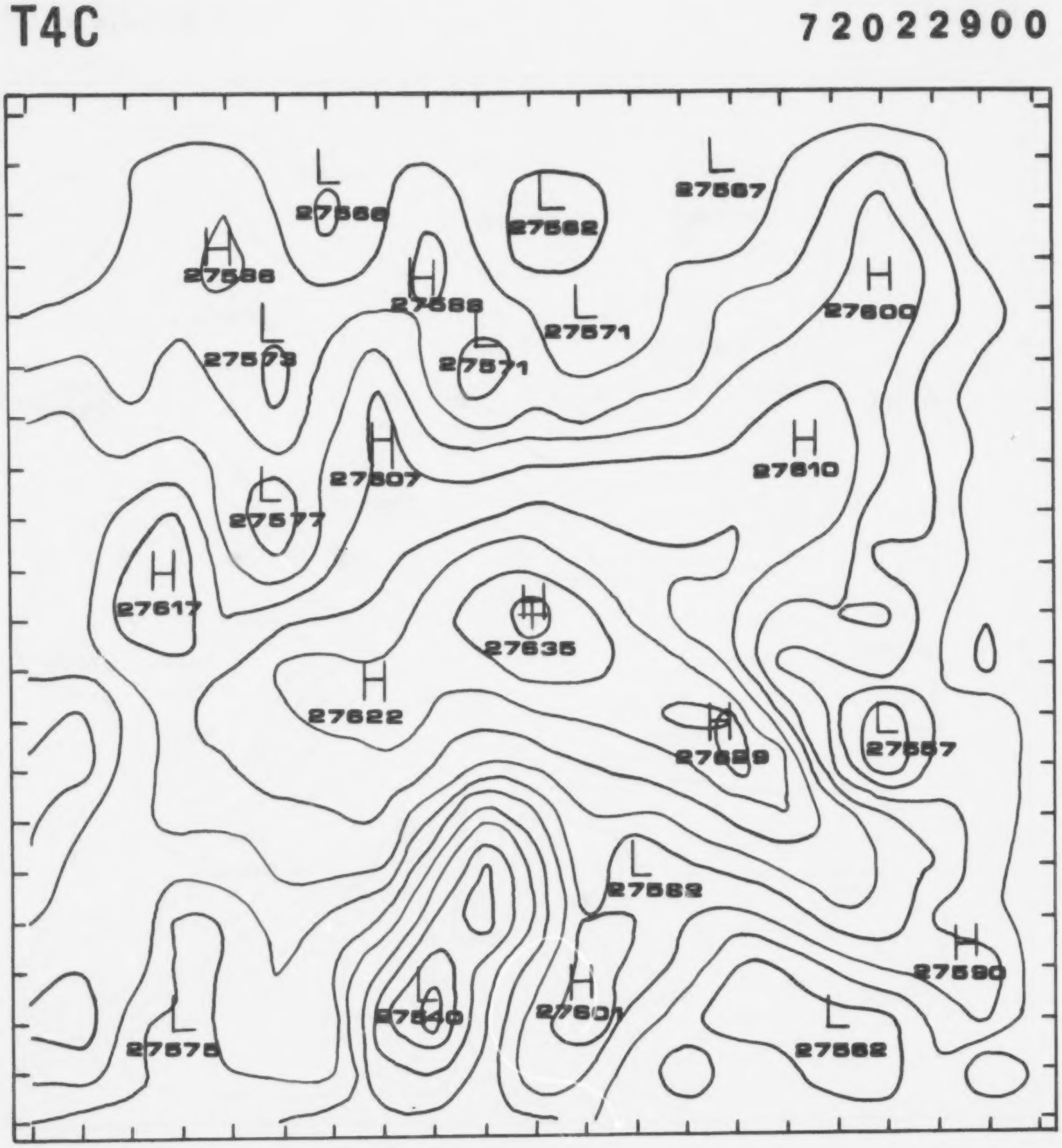
T4C
72022900
L
27566
L
27562
L
27567
H
27586
H
27588
L
27571
L
27573
L
27571
H
27600
H
27607
H
27610
L
27577
H
27617
H
27635
H
27622
H
27629
L
27557
L
27582
H
27590
L
27540
H
27601
L
27575
L
27582

FIGURE 9 : temperature field (°K/100)

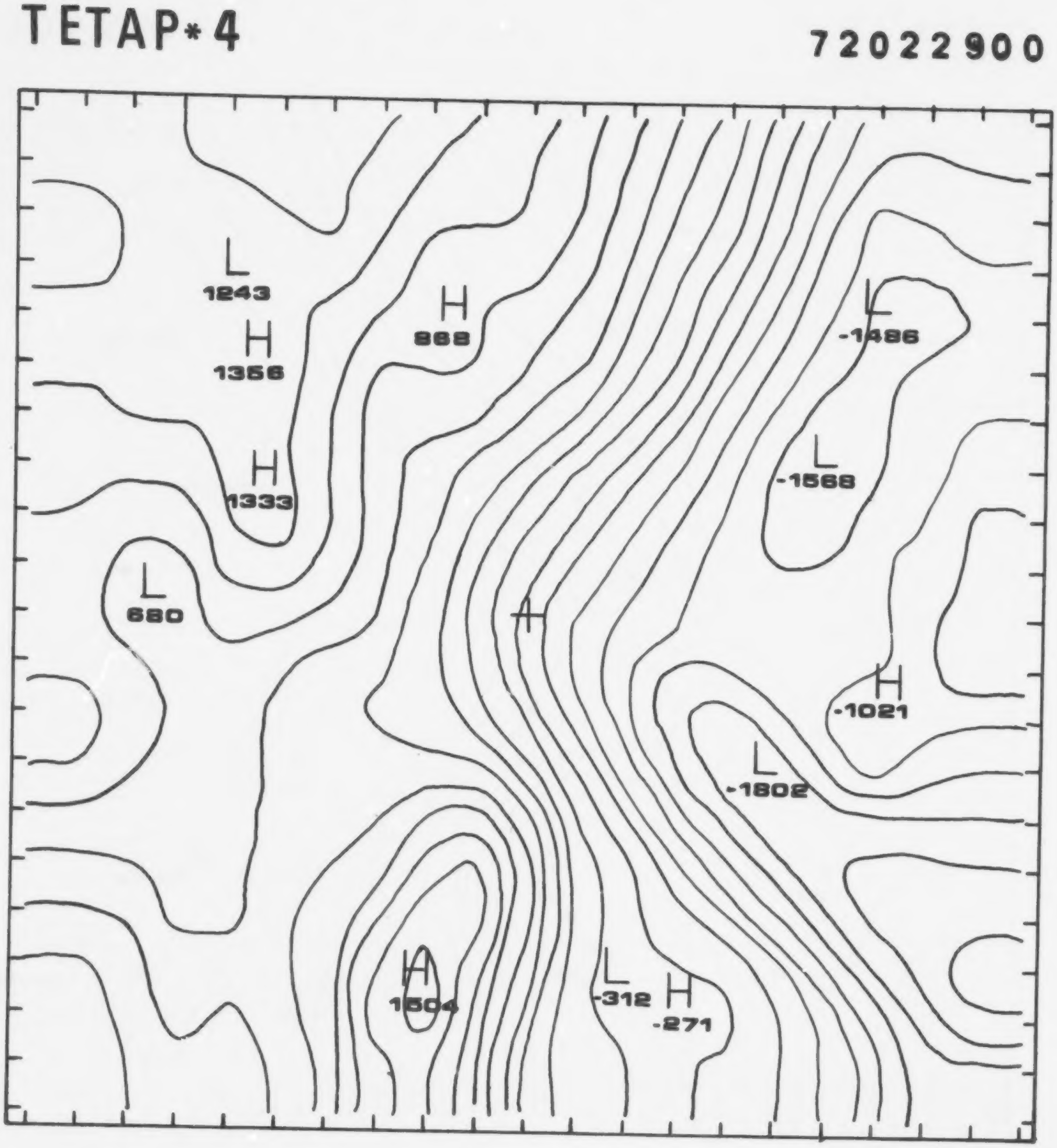
TETAP*4
72022900
L
1243
H
1356
H
968
H
1333
L
680
L
-1486
L
-1568
H
-1021
L
-1802
H
1504
L
-312
H
-271

FIGURE 10 = velocity potential in the middle of the surface layer

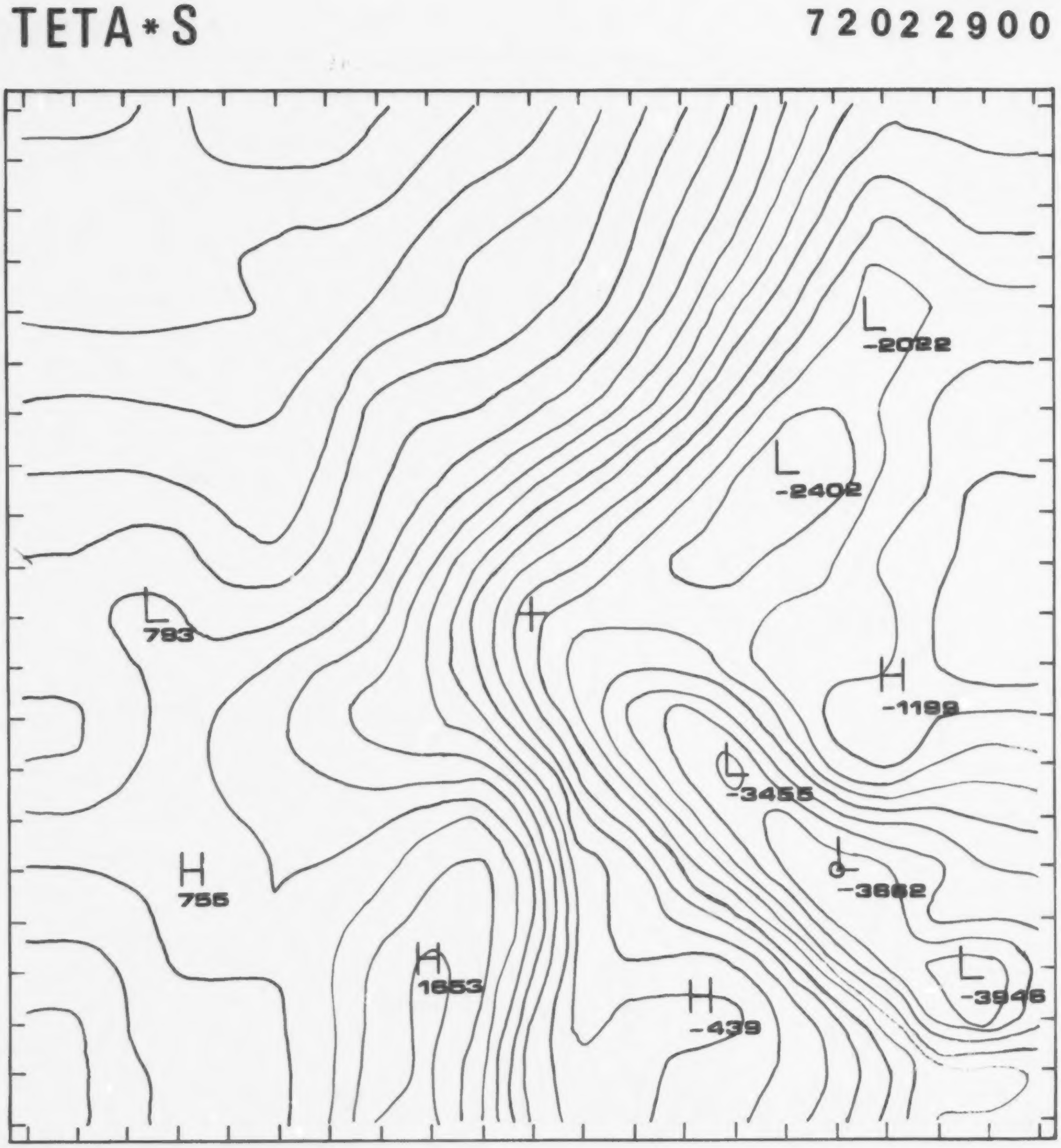
TETA*S
72022900
L
-2022
L
-2402
L
783
H
-1199
L
-3455
L
-3662
H
755
H
1653
H
-439
L
-3946

FIGURE 11 : velocity potential at the surface

8th International Technical Meeting on
Air Pollution Modeling and its Application

CALCULATION OF CARBON MONOXIDE CAUSED BY TRAFFIC

by

Michael Schorling
Industrieanlagen-Betriebsgesellschaft
Abteilung Planungsforschung für
öffentliche Aufgaben
8012 Ottobrunn bei München

Louvain-la-Neuve, Belgium
September 20-23, 1977

Calculation of Carbon Monoxide Caused by Traffic

1. Preliminary notes

Carbon monoxide is a poisonous gas. It can neither be seen, smelled, or tasted by its prospective victims. When carbon monoxide is inhaled it enters the capillary blood vessels through the alveoli. Because of its high affinity for the hemoglobin of the blood, which is more than 200 times greater than that of oxygen, it displaces the oxygen and forms with the hemoglobin carboxyl-hemoglobin. So it comes to a deficient supply of oxygen in - above all - the brain and the heart. This might lead to an asphyxiation.

Although there are a great number of reports about chronic phases of intoxication due to carbon monoxide, there are no known absolute safe threshold limits values for CO. In Germany the maximum concentration (MIK) for carbon monoxide is considered to be*):

MIK	1/2 hour mean	24 hour mean	1 year mean
CO	50 mg/m^3	10 mg/m^3	10 mg/m^3

CO-Concentration Threshold MIK (Chart 1)

---

*) VDI-Richtlinien zur Reinhaltung der Luft 2310

Besides that there are definitions given in the TA-Luft[*] for short and long period threshold values:

short period threshold (IW2)	30 mg/m^3
long period threshold (IW1)	10 mg/m^3

CO-Concentration Threshold TA Luft (chart 2)

The procedure to calculate the corresponding concentration value which must be compared with the IW1 and IW2 value is explained in the TA Luft. Unfortunately both guidelines don't apply to the traffic situation and there is no legal guiding rule for the maximum tolerable threshold for CO concentrations in urban road traffic. In the atmosphere, carbon monoxide is considered to be quite stable; it reacts only slightly under varied environmental conditions. A minimal amount of it is slowly converted to carbon dioxide.

CO is a product of incomplete combustion. Motor vehicle traffic contributes about 50 % of the overall carbon monoxide concentration in the Federal Republic of Germany (and 25 % of the nitricoxide loads and 19 % of the hydrocarbon loads). In cities, up to 99 % of the carbon monoxide concentration is attributed to exhaust gases from vehicles.

---

*) TA Luft = Technische Anleitung zur Reinhaltung der Luft, 1974

To underline the importance of this atmospheric pollutant, some figures on the emission of carbon monoxide by the motor vehicle traffic will be given.

	Consumption 1974 in FRG	rough emission factor	CO-emission
Gasoline	18 Mio tons	250 g CO/liter	5,1 Mio tons
Diesel Fuel	10 Mio tons	30 g CO/liter	0,3 Mio tons
		Total	5,4 Mio tons

Carbon Monoxide Emission in the FRG 1974 (chart 3)

About only half of that number - 2,7 Mio tons - was calculated to be the sulfer dioxide emission by power plants and industry in the same period in Germany.

2.0 Results from a Study: CO-Calculation in the City of Frankfurt

The results and findings reported here stem from a study undertaken for the German Ministry of Transportation in 1976.

By means of a cost benefit analysis, the environmental impacts of a planned city expressway in Frankfurt were investigated. Three alternative traffic concepts were analysed: a bridged expressway, a tunnel, and an expressway at ground level.

The analysis includes the calculation of the carbon monoxide loads along the highway in question and in the neighborhood as well.

To satisfy the requirements of the cost benefit analysis, the CO concentrations had to be expressed in monetary terms by applying the principle of cost avoidance. (However, this will not be covered here.)

2.1 Description of the Road Construction Project

The highway considered in this calculation will be situated in the north of the City of Frankfurt and is to connect two autobahn intersections, the Miquelknoten in the west and the Seckbachjunction in the east. Its length will be about 2,5 kilometers. Presently about 50,000 cars commute daily along the road, however, in the rush hours from 7 - 9 a.m. and 4 - 7 p.m. traffic jams prevail. (Figure 1)

The conceptual design of the future expressway is planned to handle about 110,000 cars a day. This should be accomplished by:

- a bridged expressway in connection with a highway on ground level, or
- a tunnel in connection with a highway on ground level, or
- a superhighway on ground level; here, the cross traffic will be led underneath.

The height of the buildings along the highway is quite heterogeneous: in parts, the area is built on both sides of the street with 3 - 4-storied houses, partly the area is open and only built on one side. To calculate the carbon monoxide concentrations due to the road traffic, the Stanford APRAC 1-A /1/ model has been used.

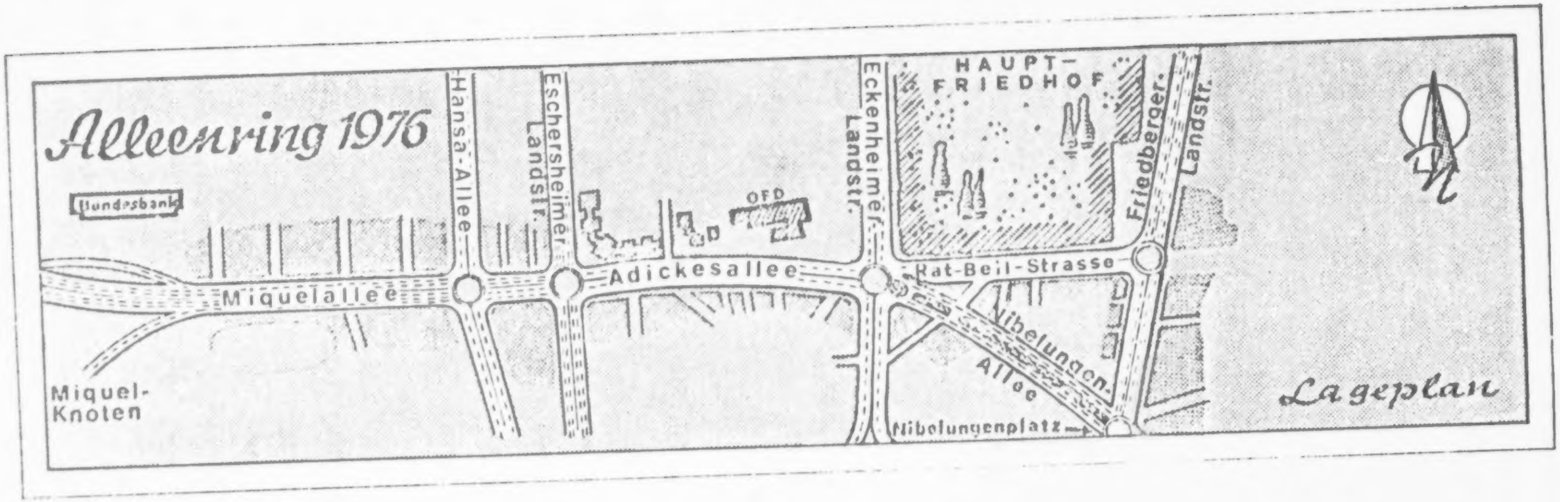
Alleenring 1976
Bundesbank
Hansa-Allee
Eschersheimer Landstr.
OFD
Eckenheimer Landstr.
HAUPT-FRIEDHOF
Friedberger-Landstr.
Miquelallee
Adickesallee
Rat-Beil-Strasse
Nibelungen-Allee
Nibelungenplatz
Miquel-Knoten
Lageplan

Fig. 1: Plan of Site of Alternative Expressway Project in Frankfurt

3. Application of a Diffusion model

3.1 Input Data

Here, some explanations for the input data used will be given.

3.1.1 Topography

To model the line sources the main traffic roads have been listed with its coordinates and street width. Figure 2 shows the street map of Frankfurt containing the linear road segments.

3.1.2 Traffic volume data

By means of a capacity restraint function a traffic assignment model has been used to forecast the daily traffic volume for the alternate highways. The hourly distribution of the daily traffic was assumed to accord with the data given in chart 4.

	Time	Frequences	Percentage of DTV
Mean night value	22-6	8 hrs.	4 %
mean day value off-peak-time	6-7, 9-16, 19-22	11 hrs.	54 %
mean day value peak time	7-9, 16-19	5 hrs.	42 %

Hourly Distribution of Daily Traffic Volume (DTV) (chart 4)

A more detailed hourly distribution of the traffic data could have been used within the APRAC Model. However, because of the uncertainty of the daily traffic volume and the meteorological data no more resolution in time was wanted.

Fig. 2 COMPUTER DRAWN STREET MAP OF FRANKFURT

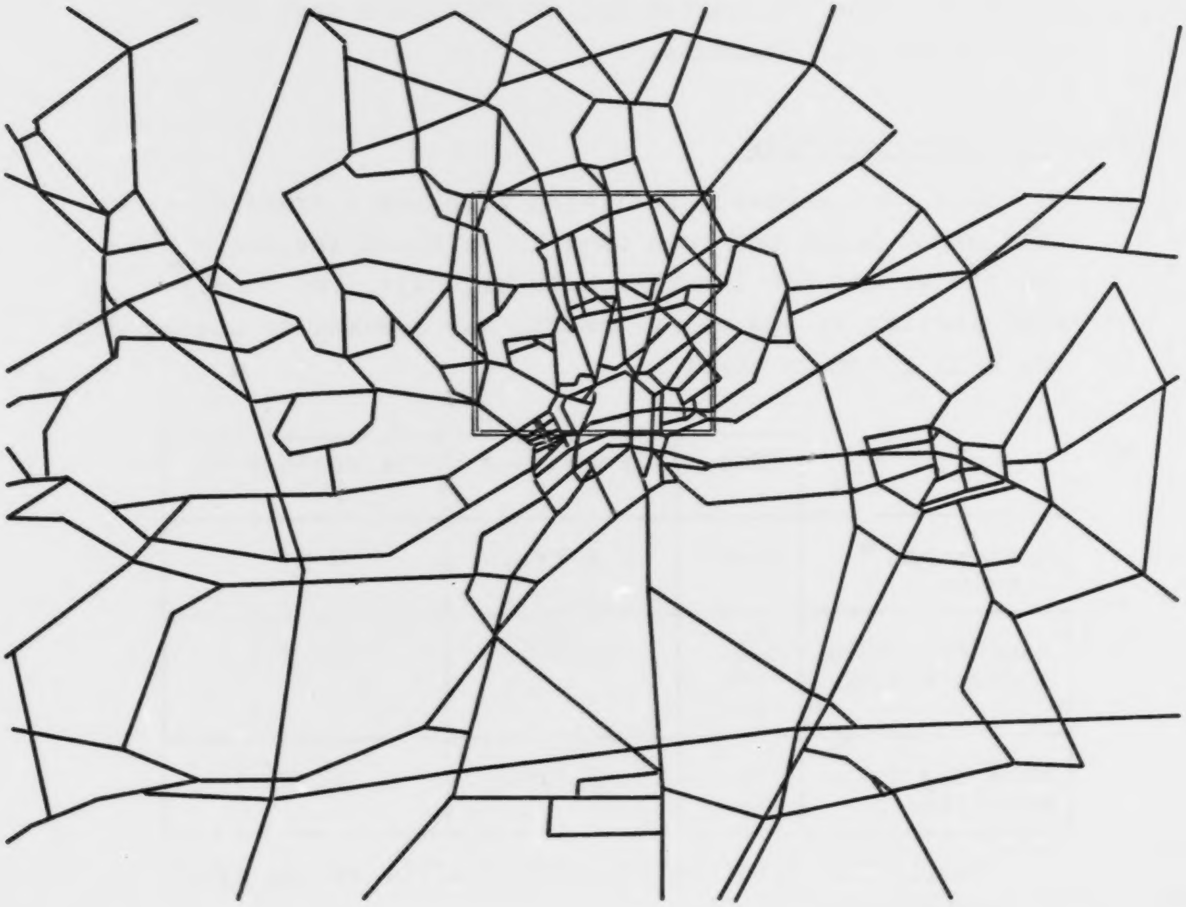

3.1.3 Emission Inventory

In the FRG there exists a very detailed investigation of the emission volume of the City of Cologne /2/. In that study the emission data for the average passenger car and truck for specifically defined driving modes have been derived. The corresponding emission factors with the car speed as parameter are listed in chart (5).

Driving mode	1	2	3	4	0	5	6
mean speed km/h	100	60	42.5	26	19.5	13.5	6.0
CO-emission g/car-hour	1571	1036	822	752	794	725	586

CO-Emission Factors for passenger Cars
(chart 5) /2/

A similar table of data exists for the carbon monoxide emission of trucks.

Assuming that 6 % of urban traffic is truck traffic a broken rational function of the fifth degree for the specific carbon monoxide emission can be derived:

$$e = \frac{1}{p(v)} + 4$$

with

$$p(v) = 1{,}08 \cdot 10^{-2} - 3{,}96 \cdot 10^{-4} \cdot v + 1{,}12 \cdot 10^{-4} \cdot v^2$$

$$- 2{,}27 \cdot 10^{-6} \cdot v^3 + 1{,}73 \cdot 10^{-8} \cdot v^4 - 4{,}59 \cdot 10^{-11} \cdot$$

The mean speed v should be expressed in km/h to obtain the specific Co-emission in g/car-km. The given formula is valid for any speed within the intervall 6 - 100 km/h.

Considering the hourly traffic volume $m_{j,k}$ passing a point j at the hour k the local emission $E_{j,k}$ is given by:

$$E_{j,k} = \frac{m_{j,k}}{3600} \cdot e_{j,k} \quad \frac{mg}{m \cdot sec}$$

This context is presented in figure 3 .

In the calculation the avarage speed in the city of Frankfurt had been as follows:

Time	Average Speed
mean night value	26,6 km/h
off-peak day time value	25,5 km/h
peak day time value	17,5 km/h

Average Car Speed (chart 6)

Here, stops at traffic lights have been included into the calculation. This explains the relatively low speed at night. The average speed along the highway in question, however, was 7 km/h at peak day time.

Fig. 3 CO-EMISSION DATA WITH MOTOR VEHICLE SPEED AND TRAFFIC VOLUME AS PARAMETERS

(m = 1 000 - 10 000 cars/h)

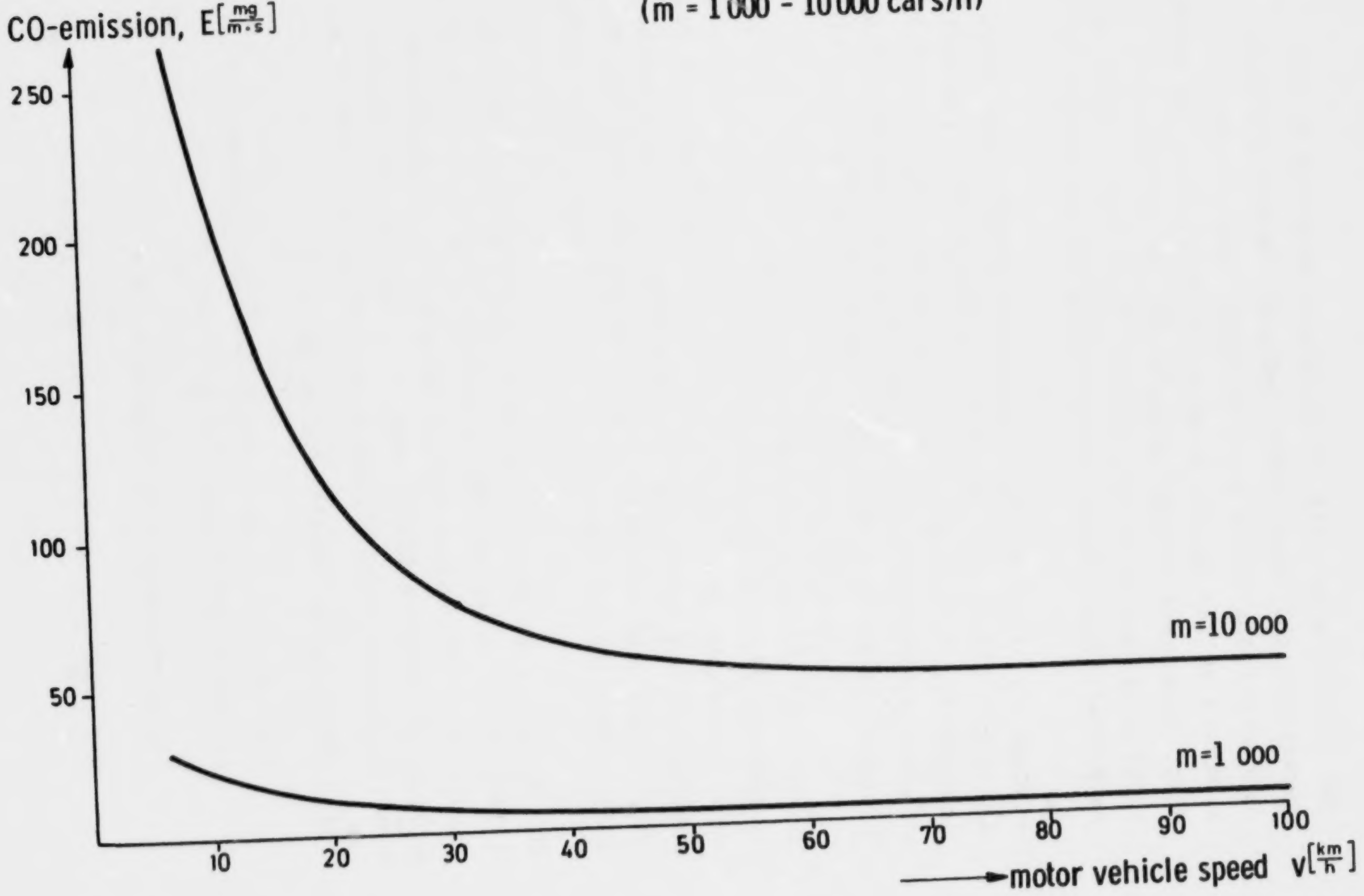

3.1.4 Meteorology

The diffusion process is extremely sensible to the meteorological conditions. Leeward carbon monoxide concentrations might be five times larger than windward values in the same cross section of the street. Here, increased concentrations are due to the wind blowing obliquely to the street. Roof level values might vary from street level measurements by the factor of 50.

Because of the specific differences between the rural and urban climate it would be desirable to use meteorological data which represent the climatology of a city or even a district of the city. Usually, however, only the meteorological data from the nearest airport are available.

To satisfy the requirements of the APRAC Model, hourly measurements of the ground temperature, cloud cover, windspeed and direction have been collected at the Frankfurt airport. Because of the dense air traffic, radiosonde data could not be provided for Frankfurt but only for the station of Essen which is in crow-fly distance of about 200 kilometers.

One drawback to the use of diffusion models is the computing time, which naturally increases with the number of simulations of weather conditions. Hence, to represent adequately the Frankfurt area, 3 typical atmospheric conditions have been chosen from each of the four seasons.

These atmospheric conditions were:

- the south-west wind condition. The probability of the event during the year is .4
- the north-east wind condition. p = .4
- the calm weather condition. p = .15

Consequently twelve days have been examined at 10 appropriately distributed receptor points. The resulting data for each receptor point have been condensed to daily, seasonal, and annual means. The calm weather condition, however, as the worst condition was agreed upon to give the criteria by what amount the concentration should be reduced to tolerable levels.

3.2 Results

Detailed information on the APRAC Model is given in /1/, hence no further descriptions of the Model need to be made.

For ten receptor points along the highway in question as well as in the adjacent streets, the mean values of the windward and leeward carbon monoxide concentration have been calculated. The concentration data of three weather conditions with known statistical probability in each of the four seasons had been condensed to daily, seasonal and annual means.

Figure 4 gives an overview of the mean annual concentration I1 for the receptor points as indicated. Here, the first five receptor points are situated along the highway under investigation, the rest in adjacent streets. The value I2 which comprises 95 % of all individually calculated data is shown in the same figure. 5 % of the individual data might exceed the threshold IW2 = 24 ppm if under these conditions the threshold IW1 = 8 ppm is observed.

Figure 5 shows the hourly distribution of the CO-concentration for receptor point 3 (Adickesallee) during

Fig. 4: CO - CONCENTRATION

Overview of short and long period concentrations for 10 receptor points within the area of the alternative highway concepts

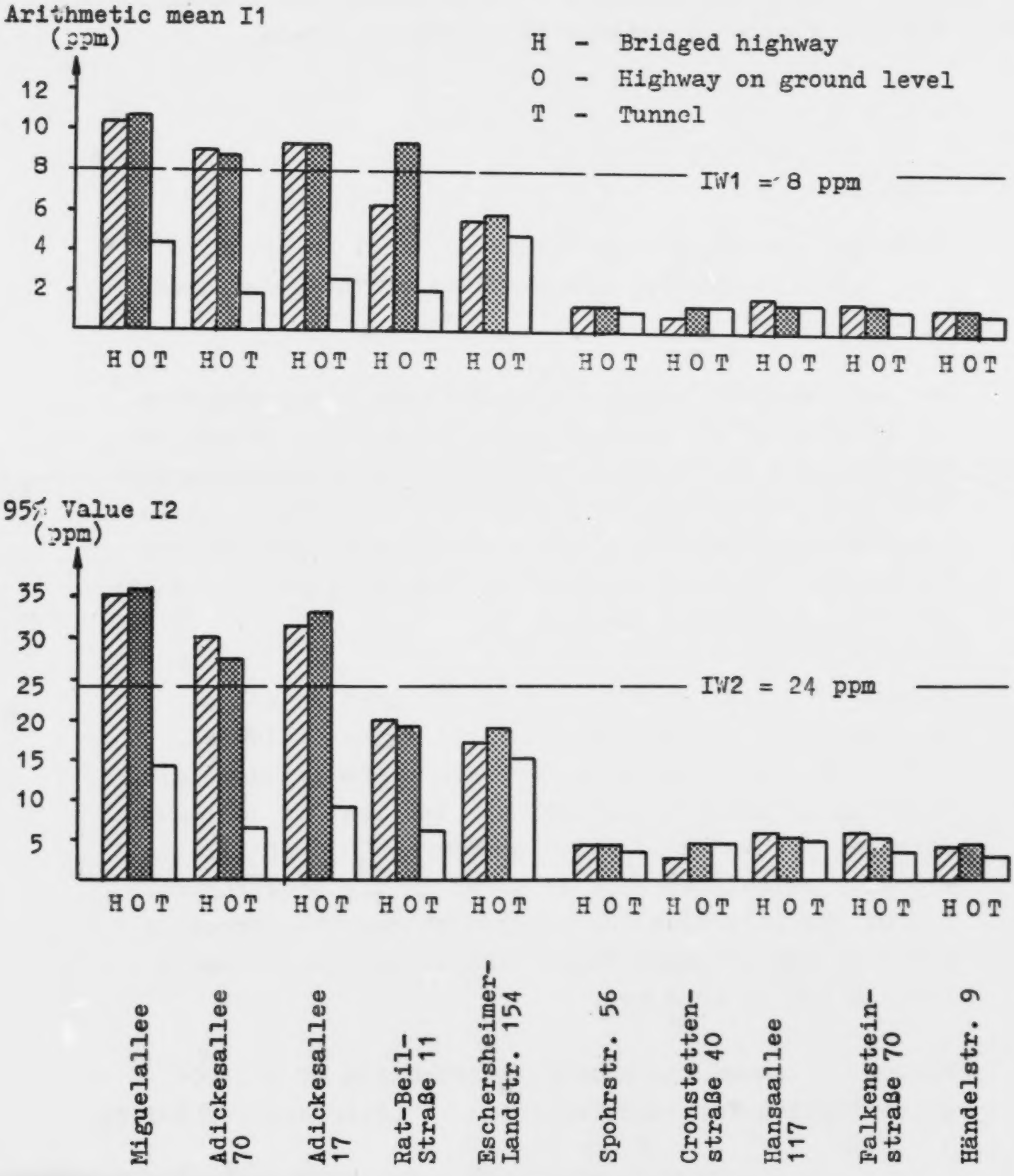

Fig. 5: HOURLY DISTRIBUTION OF CO-CONCENTRATION
Calm weather condition in fall
Receptor point 70, Adickesallee
Highway on ground level

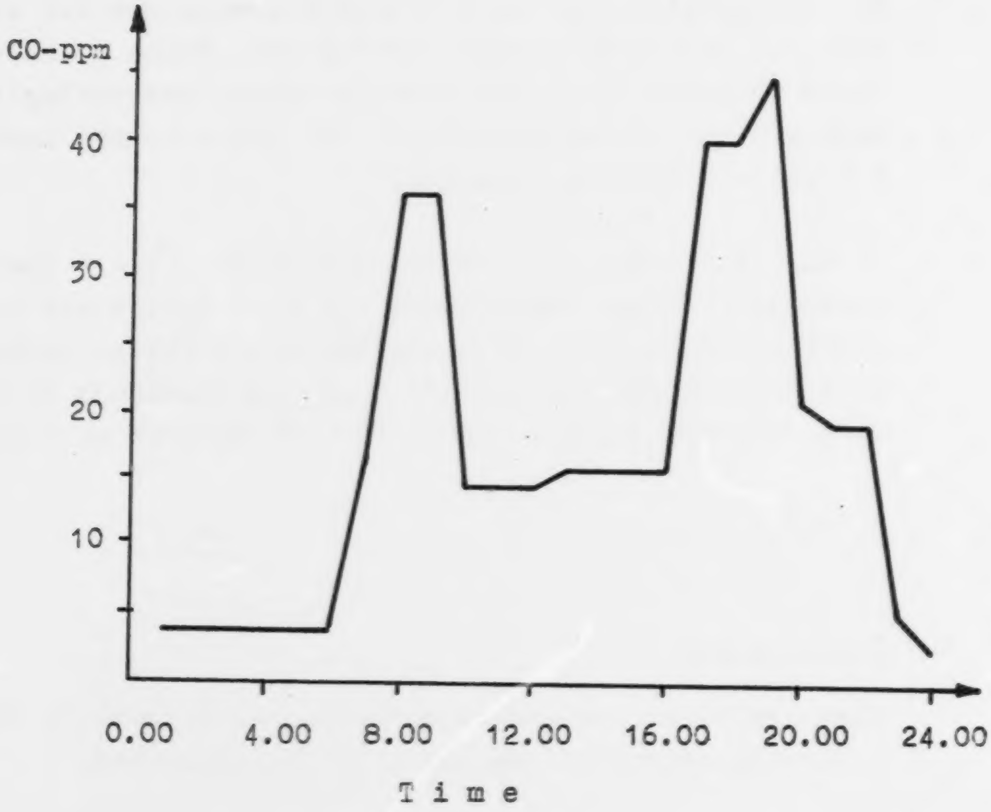

the "fall calm weather" condition for the ground level expressway alternative. Here, the hourly traffic volume distribution can be quite clearly recognized. According to these figures, the advantage of the tunnel concept is apparent.

To substantiate the calculations, measurements for some receptor points have been carried out. These measurements included the traffic volume data, meteorological data and the CO concentration. For the measured conditions the calculation was repeated.

It was found that for low concentrations (1 - 5 ppm) the agreement between measurement and calculation was insufficient. However, with concentration values higher than about 6 ppm the agreement got increasingly better. Here, the deviation was only 10 - 20 percent as a rule.

4. Consequences

When analysing the carbon monoxide concentrations the following contributions could be distinguished:

1. The primary loads at a given receptor point is evoked only by the traffic in that street.
2. The secondary loads of that receptor point is caused by the traffic in adjacent streets.
3. The background level brought on by the wind stems from far away sources.
   The present calculations proved the background level to be less than .5 ppm. For practical purposes it can therefore be neglected.

In general, the primary loads satisfy relations such as $X_{j,k} \approx \frac{E_{j,k}}{U_{j,k}}$, where $U_{j,k}$ is the hourly local wind speed. The calculation of the primary loads apparently does not require a great amount of input data. Here, an adequate factor of proportionality may reduce the procedure of calculation.

However, the calculation of the secondary loads requires the record of the propagation of the gas from the source to the receptor point and, with this, the compilation of the voluminous input data.

Our preliminary investigation showed that under specific conditions the primary loads approximately equal the secondary loads *).

These conditions are

- high traffic loads passing the receptor point under investigation
- both street sides bordered with buildings about 25 m high
- leeward and windward concentration data are comprised to an arithmetic mean.

The assumption of high traffic loads excludes in general the application of these findings for night-time calculations and the evaluation of the concentration in secondary streets.

---

*) Dabberdt et al reported about similar findings in the 1974 Seattle carbon monoxide investigation /3/

Under the mentioned conditions an approximate solution for the overall CO concentration can be derived. Using here an approach from Johnson and Ludwig /1/ in a slightly modified form, one gets - if the primary loads approximately equal the secondary loads - for the arithmetic mean of wind and leeward values:

$$X_{j,k} = \frac{7 \cdot E_{j,k}}{U_{j,k}} \left[\frac{1}{l + lo} + \frac{H - z}{b \cdot H} \right]$$

Here l = distance between receptor point and line source

$= \sqrt{x^2 + z^2}$

lo = a representative vehicle size

H = average building height

z = height of receptor point over ground level

b = street width

given $H = 24$ m, $z = 2{,}5$ m, $lo = 1{,}5$ m and $x = 7{,}5$ m a band of curves can be drawn for the quotient $X_{j,k}/E_{j,k}$ with the quantities wind speed and street width as parameters.

This is shown in figure 6

Remarkable here is the slight influence of the street width for high wind speeds. For wind speeds less than about 1 m/sec fundamental assumptions of the mathematical approach get violated, hence no valid results can be expected in this area.

In this simple empirical rule the wind direction is eliminated. It is assumed that the wind is blowing obliquely to the street. When, however, the wind is parallel to the street to be investigated, another approach must be used.

Fig. 6 RATIO BETWEEN CO-CONCENTRATION AND EMISSION LOADS DEPENDENT ON STREET WIDTH AND WIND SPEED

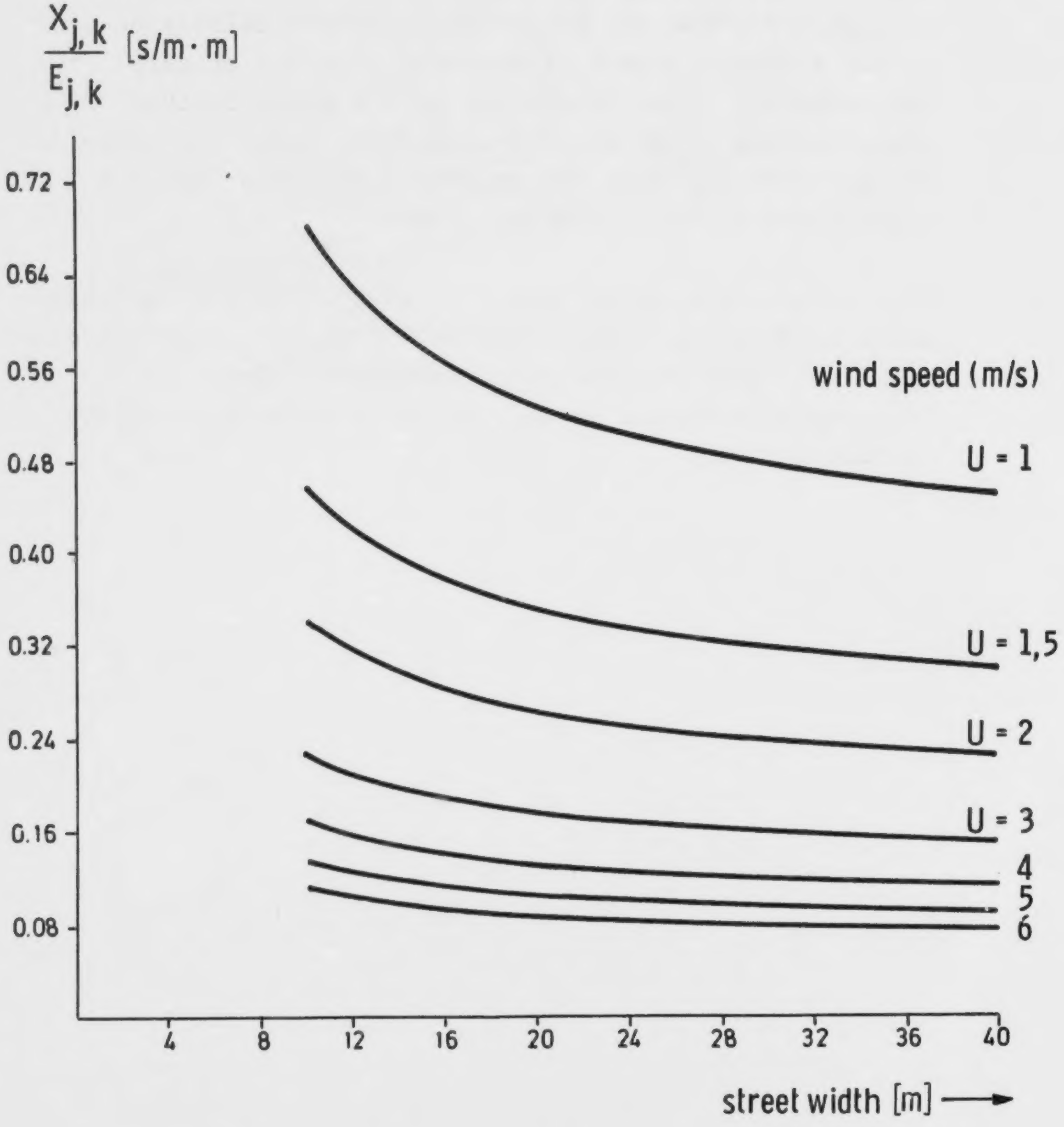

The quantity mixing depth does not occur in this empirical rule, which therefore might not be applied for serious inversion conditions.

To substantiate this approximation an hourly concentration distribution for one receptor point is given in figure 7. Here the total concentration calculated by the diffusion model is compared with the primary concentration loads determined by the above-derived approximating solution. The comparison shows for peak- and off peak day time the primary loads to be in fact approximately half the total loads.

This simple rule is not meant to substitute the diffusion model calculations. It is merely a tool for quick approximation of loads for the first assessment. Detailed investigation should be carried out with an appropriate diffusion model.

Fig. 7 COMPARISON OF RESULTS ACCORDING TO THE DIFFUSION MODEL AND APPROXIMATE SOLUTION

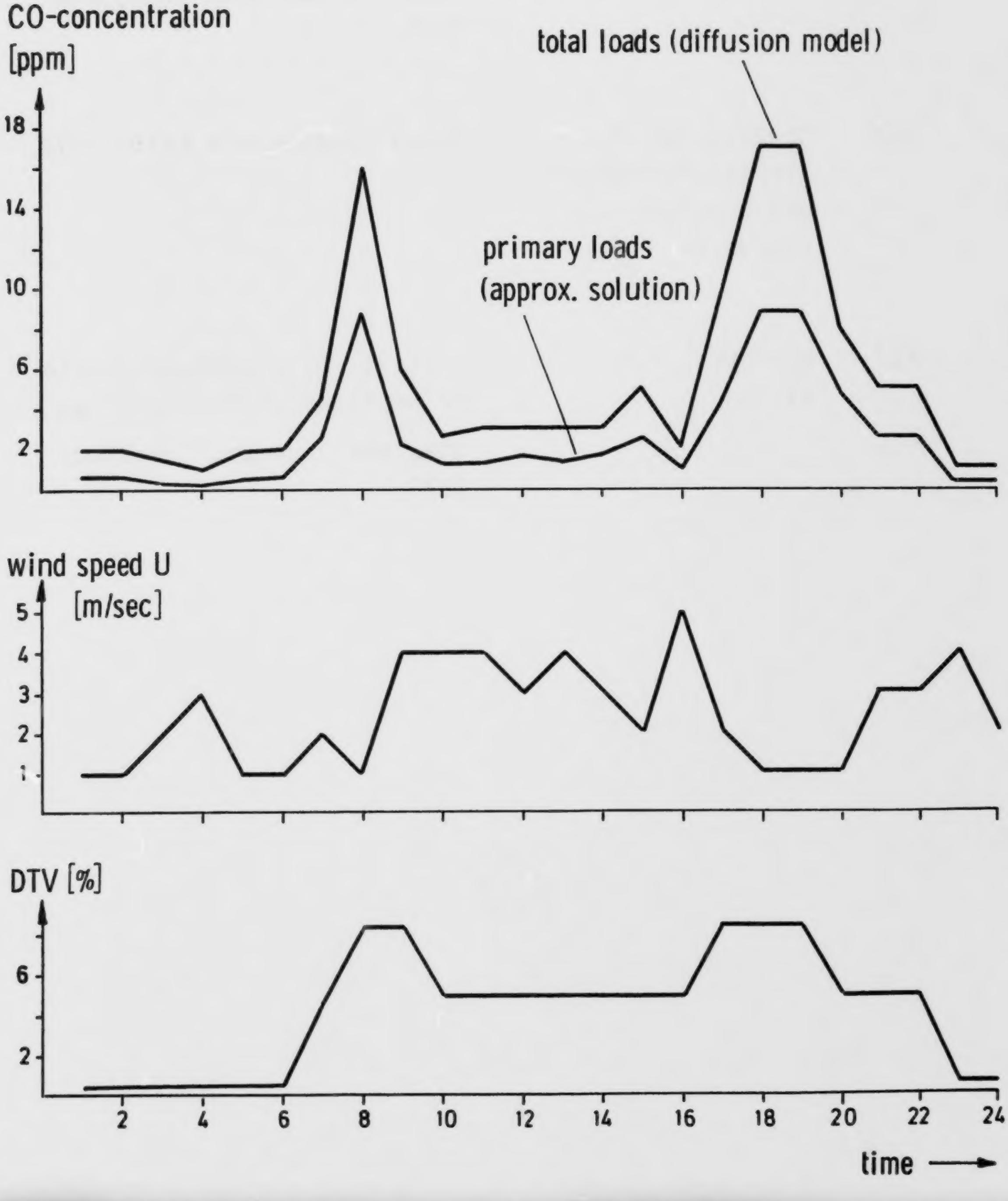

References

/1/ Mancuso, R.L.
Ludwig, F.L.
Users Manual for the APRAC-1A Urban Diffuion Model Computer Program
Stanford Research Institute
1972

/2/ Ministerium für Arbeit, Gesundheit und Soziales des Landes NW
Emissionskataster Köln, 1972

/3/ Dabberdt, W.F.
et ali
Analysis of Washington State Transportation Control Plan
Stanford Research Institute
1975

8th NATO/CCMS INTERNATIONAL TECHNICAL MEETING ON AIR POLLUTION MODELING

TOPIC 7

NOVEL APPROACHES IN AIR QUALITY MODELING

8th International Technical Meeting

on Air Pollution Modelling and its Application

Air Pollution Studies Using Planetary Boundary Layer and K-Models

Eli Runca
IBM Italia Scientific Center
Venice, Italy

and

Robert D. Bornstein
San Josè State University
San Josè , California

September 20-23, 1977
Louvain-La-Neuve
Belgium

AIR POLLUTION STUDIES USING LINKED PLANETARY BOUNDARY LAYER AND K-MODEL

Eli Runca
IBM Italy Scientific Center
Venice, Italy
and
Robert D. Bornstein
San Josè State University
San Josè, California

The two dimensional URBMET planetary boundary layer model has been used to simulate the flow dynamics induced from horizontal gradients due to discontinuities in the surface temperature and roughness.

Output from this model is used to provide input values for a three dimensional air pollution model based on the numerical integration of the advection diffusion equation written according to K--theory. This model has been solved including linear parameterization of removal processes for the case of a single point source of SO_2 whose concentration in the region very near the stack is analytically modelled in order to avoid problems associated with the approximation of the delta function.

INTRODUCTION

The computation of pollutant concentration downwind of a continuous point source is needed in order to assess the impact of emission on the air quality level. Solution to this problem can be derived from the continuity equation written for the pollutant under investigation. By assuming that the flux of matter due to the atmosphere turbulent eddies can be expressed as the product of a coefficient of diffusivity and the gradient of the mean concentration, that the air flow is non divergent, and that molecular diffusion is negligible if compared with turbulent diffusion, the continuity equation can be reduced formally to the Fickian equation in which the coefficients of diffusivity are variable in such a way that experimental data are satisfied (see, for example, Seinfeld (15)). Because of the empirical evaluation of the diffusion coefficients this equation is termed the "semiempirical equation of atmospheric diffusion" or simply "atmospheric diffusion equation".

From an analytic solution of this equation obtained under certain assumptions recalled below, a formula has been derived by Sutton (17) for the computation of steady state concentrations at the ground downwind of a continuous point source. This formula, which is at present commonly known as "Gaussian plume formula", does not describe the true plume behaviour, since its derivation assumes steady emission rate, no spatial or temporal variations in the wind or atmospheric stability, no upper level inversion, no deposition of the contaminant or chemical reactions between it and other substances. Because of these limitations the Gaussian plume formula can be applied to a restricted class of problems, and is not adequate for a rigorous analysis of the spatial and temporal distribution of concentrations downwind of a point source.

An improved analysis of air pollutant dispersion is achieved by integrating the atmospheric diffusion equation in the general case of spatial and temporal variability of the parameters entering the equation, including deposition, chemical and photochemical transformation of the pollutant in question. This integration can be only achieved numerically, and due to the nature of the problem must be generally performed in three dimensions. A dispersion model based on the "atmospheric diffusion equation" is termed K-model. This model allows an improved description of the plume behaviour even in complex situations, such as those of sea breeze circulations provided that the flow dynamics is described either through experimental measurements or through simulations by a planetary boundary layer model.

We have applied the latter approach in a recent work (Bornstein and Runca (3)), in which the URBMET urban planetary boundary layer model by Bornstein (1) was used to simulate the flow dynamics of a well developed sea breeze circulation.The atmospheric parameters computed by Bornstein's model were then used as an input to the K- model developed by Runca (13), to simulate dispersion from a stack located on the edge between the land and the water. This approach is similar to that used by Dieterle and Tingle (4).

Since the linkage of Bornstein's and Runca's model was done to obtain additional insight into the air pollution problem of Venice, the geometry, to which the models were applied, was derived from the geography of the Venetian area. Our previous study concentrated on the effects of sea breeze circulations on SO_2 concentrations in the area of Venice. In addition, since the decay of the artistic patrimony in Venice is associated with the presence of sulphuric acid, linear chemical transformation and surface deposition were also included in the K-model. These processes are generally considered to have only insignificant effects on concentration levels over short travel distances, but the combined effects of high atmospheric moisture content and metallic ions possibly associated with industrial processes may produce a significant sink of SO_2 by catalytic oxidation, see Kalthoff (5). Results from our work showed that they can significantly affect SO_2 concentration in the Venetian area.

This paper, after introducing the models developed by Bornstein and Runca, and recalling the results presented in their study, discusses the effects of the vertical air flow on the air pollutant distribution.

PLANETARY BOUNDARY LAYER MODEL

The URBMET planetary boundary layer model by Bornstein produces solutions to the hydrodynamic, thermodynamic and moisture equations in a vertical plane.

Vertical fluxes of heat and momentum are assumed constant with height, but variable with atmospheric stability, in a lower analytical surface boundary layer. Fluxes generally decrease with height in an upper finite-difference transition layer, assumed to be hydrostatic and Boussinesq.

With the above assumptions the transition layer equations can be written as:

$$\frac{\partial \zeta}{\partial t}+\frac{\partial}{\partial x}(u\zeta)+\frac{\partial}{\partial z}(w\zeta)=-\frac{g}{T_m}\frac{\partial \theta'}{\partial x}+f\frac{\partial v}{\partial z}+\frac{\partial^2}{\partial z^2}(K_M\zeta)+K_{HOR}\frac{\partial^2 \zeta}{\partial x^2} \tag{1}$$

$$\frac{\partial v}{\partial t}+\frac{\partial}{\partial x}(uv)+\frac{\partial}{\partial z}(wv)=f(u_g-u)+\frac{\partial}{\partial z}\left(K_M\frac{\partial v}{\partial z}\right)+K_{HOR}\frac{\partial^2 v}{\partial x^2} \tag{2}$$

$$\frac{\partial \theta'}{\partial t}+\frac{\partial}{\partial x}(u\theta')+\frac{\partial}{\partial z}(w\theta')=\frac{\partial}{\partial z}\left(K_H\frac{\partial \theta'}{\partial z}\right)+K_{HOR}\frac{\partial^2 \theta'}{\partial x^2} \tag{3}$$

$$\zeta=\frac{\partial u}{\partial z}=\frac{\partial^2 \psi}{\partial z^2} \tag{4}$$

$$u=\frac{\partial \psi}{\partial z} \tag{5}$$

$$w=-\frac{\partial \psi}{\partial x} \tag{6}$$

where x, y, and z are the Cartesian coordinates in the cross shore, along shore, and vertical directions, respectively, and ζ is the hydrostatic vorticity . All other symbols have their normal meaning and are defined in Bornstein (1). The equations are identical with those in Bornstein (1), with the exception that the horizontal diffusion term was not included in the previous study. The vertical eddy exchange coefficients in the transition layer in the present study are computed following the method of O'Brien (9), while the horizontal coefficients are arbitrarily set to 10^4 m^2/sec . Further details concerning the formulation of both the transition layer and constant flux layer equations can be found in Bornstein (1).

Integration of Equations (1)-(6) is carried out using forward differencing procedure, using variable and unequal time steps for the diffusive and advective processes (Bornstein and Robock (2)). The advection terms are approximated using the donor-cell finite difference scheme of MacCracken and Bornstein (8).

The current version of URBMET assumes lateral invariability. It has been applied to simulate temporal and spatial distributions in a vertical plane, whose boundary at ground level is defined on the basis of the Venetian area which includes a mainland, a lagoon and the Adriatic sea.

The boundary conditions used in the present application are those given in Bornstein (1), except for that of the surface temperature which is specified as follows:

$$\vartheta_o(t) = \vartheta_m + \bar{\vartheta}_o + \Delta\vartheta_o\left[0.454\sin(15t+159.75) + 0.161\sin(30t+257.50)\right] \quad (7)$$

which is derived from an expression given by Kuo (6), and in which ϑ_m is 304.33^{o} K. Values for $\bar{\vartheta}_o$ and $\Delta\vartheta_o$ in each of the three regions of the area under consideration are given in table 1 as are values of their surface roughness parameter, z_o.

Table 1

Surface Parameters

Region	$\bar{\vartheta}_o$ (°K)	$\Delta\vartheta_o$ (°K)	z_o (cm)
Mainland	1. 17	11	20
Lagoon	-0. 33	4	4×10^{-3}
Adriatic	-0. 83	1	8×10^{-3}

K-MODEL

Under the assumptions recalled in the introduction, the process of turbulent dispersion of air pollutant, from a point source of emission rate Q, is governed by the atmospheric diffusion equation which takes the following form:

$$\frac{\partial c}{\partial t} + u\frac{\partial c}{\partial x} + v\frac{\partial c}{\partial y} + w\frac{\partial c}{\partial z} = \frac{\partial}{\partial x}\left(K_x\frac{\partial c}{\partial x}\right) + \frac{\partial}{\partial y}\left(K_y\frac{\partial c}{\partial y}\right) + \frac{\partial}{\partial z}\left(K_z\frac{\partial c}{\partial z}\right) + Q\,\delta(x_s-x)\,\delta(y_s-y)\,\delta(z_s-z) + R \quad (8)$$

where (x_s, y_s, z_s) is the source location. The vertical diffusivity has been taken equal to the heat exchange coefficient K_H in equation (3), and the horizontal eddy diffusion coefficients Kx and Ky have been set, arbitrarily equal to 500 m^2/sec. R is the removal term, which in this study has been taken to be a linear function of the average concentration, i.e.: $R = -K_T C$. For SO_2, the pollutant to which it is assumed to apply equation (8), a recent review of oxidation rates by Levy et al. (7) sets the maximum transformation rate at 0.2 hr^{-1}, and this is the value used in this study.

In the current application transmissive boundaries are assumed at the top of the model and at the lateral extents. At the air-earth interface, surface deposition has been modelled by

$$K_z\frac{\partial c}{\partial z}\bigg]_{z=0} = -K_D\, C_{z=0} \quad (9)$$

where K_D is the velocity deposition which has been taken equal to 0 .8 cm/sec. overland (Shepherd, (16)) and 2.0 cm/sec. over water (Prahm, et al., (10)).

The numerical technique used to obtain the solution to equation (8) at $(t+\Delta t)$ involves, as described by Runca and Sardei in a paper to be published (12), summing the concentration C_b contributed by the puff emitted by the point source in the time interval Δt to the concentration field resulting from the effects of diffusion, transport and removal on the concentration field C_a existing at t. The mathematical formulation of this procedure is as follows:

$$\frac{\partial C_a}{\partial t}+u\frac{\partial C_a}{\partial x}+v\frac{\partial C_a}{\partial y}+\omega\frac{\partial C_a}{\partial z}=\frac{\partial}{\partial x}\left(K_x\frac{\partial C_a}{\partial x}\right)+\frac{\partial}{\partial y}\left(K_y\frac{\partial C_a}{\partial y}\right)+\frac{\partial}{\partial z}\left(K_z\frac{\partial C_a}{\partial z}\right)-K_T C_a \quad (10)$$

$$\frac{\partial C_b}{\partial t}+u\frac{\partial C_b}{\partial x}+v\frac{\partial C_b}{\partial y}+\omega\frac{\partial C_b}{\partial z}=\frac{\partial}{\partial x}\left(K_x\frac{\partial C_b}{\partial x}\right)+\frac{\partial}{\partial y}\left(K_y\frac{\partial C_b}{\partial y}\right)+\frac{\partial}{\partial z}\left(K_z\frac{\partial C_b}{\partial z}\right) \quad (11)$$

$$C_*^{t+\Delta t}=C_a^{t+\Delta t}+C_b^{t+\Delta t} \quad (12)$$

The initial conditions for equations (10) and (11) are

$$C_a=C_*^{t}$$

$$C_b=Q\Delta t\,\delta(x_s-x)\,\delta(y_s-y)\,\delta(z_s-z)$$

respectively. It is shown in the paper by Runca and Sardei (12) that C_* is a first order (in time) approximation of the solution to equation (8).

The replacement of equation (8) with equations (10)-(11) leads to the solution of two partial differential equations of which the first one has no singularities, while the second one has as initial condition a δ-function representig the instantaneous release of a puff having intensity $Q\,\Delta t$. Thus, equation (10) can be solved numerically by applying a finite or equivalent difference scheme without having to face the treatment of singularities. The numerical difficulties inherent to the approximation of the δ-function have been moved to equation (11).However, a pseudo analytic solution to equation (11) can be obtained by defining a time step τ submultiple of the original time step and by introducing around the source a subgrid whose dimensions are submultiple of the original grid dimensions. If τ is taken sufficiently small, the dispersion of the puff can be considered as affected, for the time interval τ, only by the value of $\vec{V}$ and $\vec{K}$ at source location. For uniform wind and diffusivity equation (11) has the solution;

$$C(x,y,z,\tau)=\frac{Q\Delta t}{8(\pi\tau)^{3/2}\left(K_{x_s}K_{y_s}K_{z_s}\right)^{1/2}}\exp\left\{-\frac{(x-u_s\tau-x_s)^2}{4K_{x_s}\tau}-\frac{(y-v_s\tau-y_s)^2}{4K_{y_s}\tau}-\frac{(z-w_s\tau-z_s)^2}{4K_{z_s}\tau}\right\} \quad (13)$$

Taking equation (13) as initial condition at time $t = \tau$, numerical integrations (using the same numerical scheme applied to equation (10)) are carried out on equation (11) with time steps of τ until a time interval of Δt is reached. The obtained pseudo analytic solution C_b is then transfered from the subregion to the original grid and it is added to C_a to compute C_*. The above described sub-grid sub-time step approach avoids the problems associated with the numerical approximation of the δ-function. An additional benefit of this approach is that point sources need not to be located at grid points.

The numerical integration of both equations (10) and (11) is carried out applying Carlson's and Crank Nicolson's schemes (see, e.g., Richtmyer and Morton (11)), with a fractional steps procedure, to the convection and diffusion processes, respectively. The resulting finite difference scheme is unconditionally stable, and, by virtue of the sequential treatment of convection and diffusion, makes the diffusion operator conforming closely to the path of air pollutant trajectories (Sardei and Runca (14)). In addition to that, it also allows for variable grid spacing and time step, selected such that the travel distance of pollutants particles in a time step is approximately equal to the grid size in the region near the source. This leads to a reduction of the truncation error in the region of maximum concentration gradients. This reduction of the truncation error and the above recalled approximation of the diffusion processes increase the accuracy of the numerical solution (Sardei and Runca (14)).

RESULTS

A stack, 175 m height, and whose SO_2 emission rate was set equal to 1 Kg/sec. was located on the edge between the mainland and the lagoon. It was switched on at 900 LST, time at which the simulation was begun. The initial SO_2 concentrations were taken to be uniformly zero and adiabatic lapse rates were assumed to exist (Kwo (6)). An initial geostrophic wind of 3 mps was specified to blow from land to the sea, and initial wind profiles consisted of equilibrium distributions (valid over homogeneous terrain) for each of the surface roughness given in table 1.

Horizontal temperature gradients produced by the surface warming rates given by equation (7) and table 1 produced a sea breeze front which first developed over the lagoon and then with time penetrated inland, as shown in figs. 1 and 2, which report the distribution of u and w components of the flow at 1500 and 2000 LST, respectively. The origin of the x-coordinate is located at the stack. At 1500 LST the center of the sea breeze circulation is at $x = 9$ Km and $z = 400$ m, approximately. At 2000 LST the sea breeze front has started to retreat from its inland penetration, and the center of the sea breeze circulation at this time is at $x = 3$ Km and $z = 1000$ m. Note that the scale for w is ten times larger than for u, and that the Coriolis force has turned the flow so that at 2000 LST, it has a major component in the "up coast" direction (i.e., into the figure).

The effect of the sea breeze front on the plume behaviour can be seen in the concentration fields in vertical planes perpendicular to the coast.

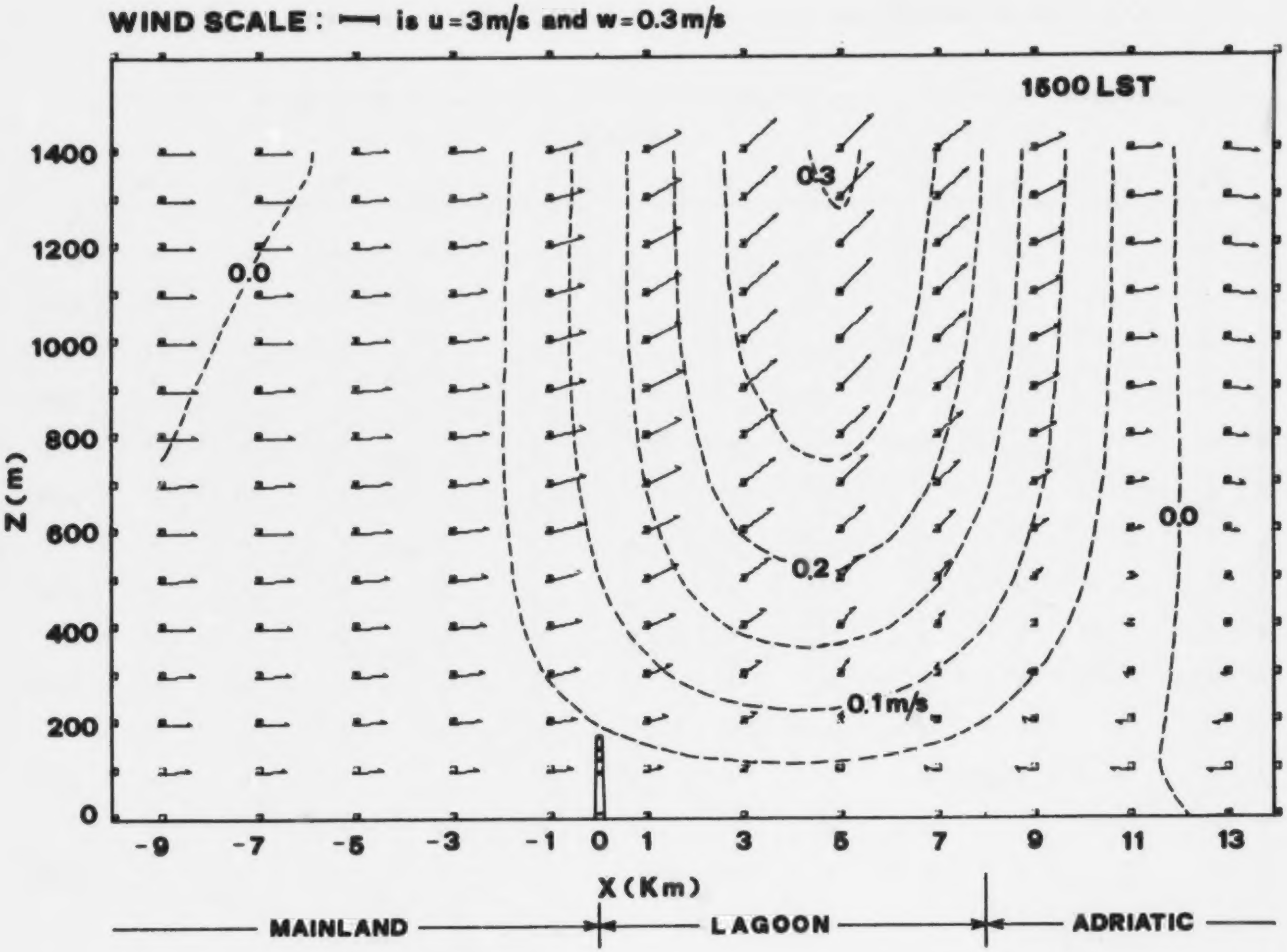

Fig. 1 - Vertical distribution of u and w wind components at 1500 LST.

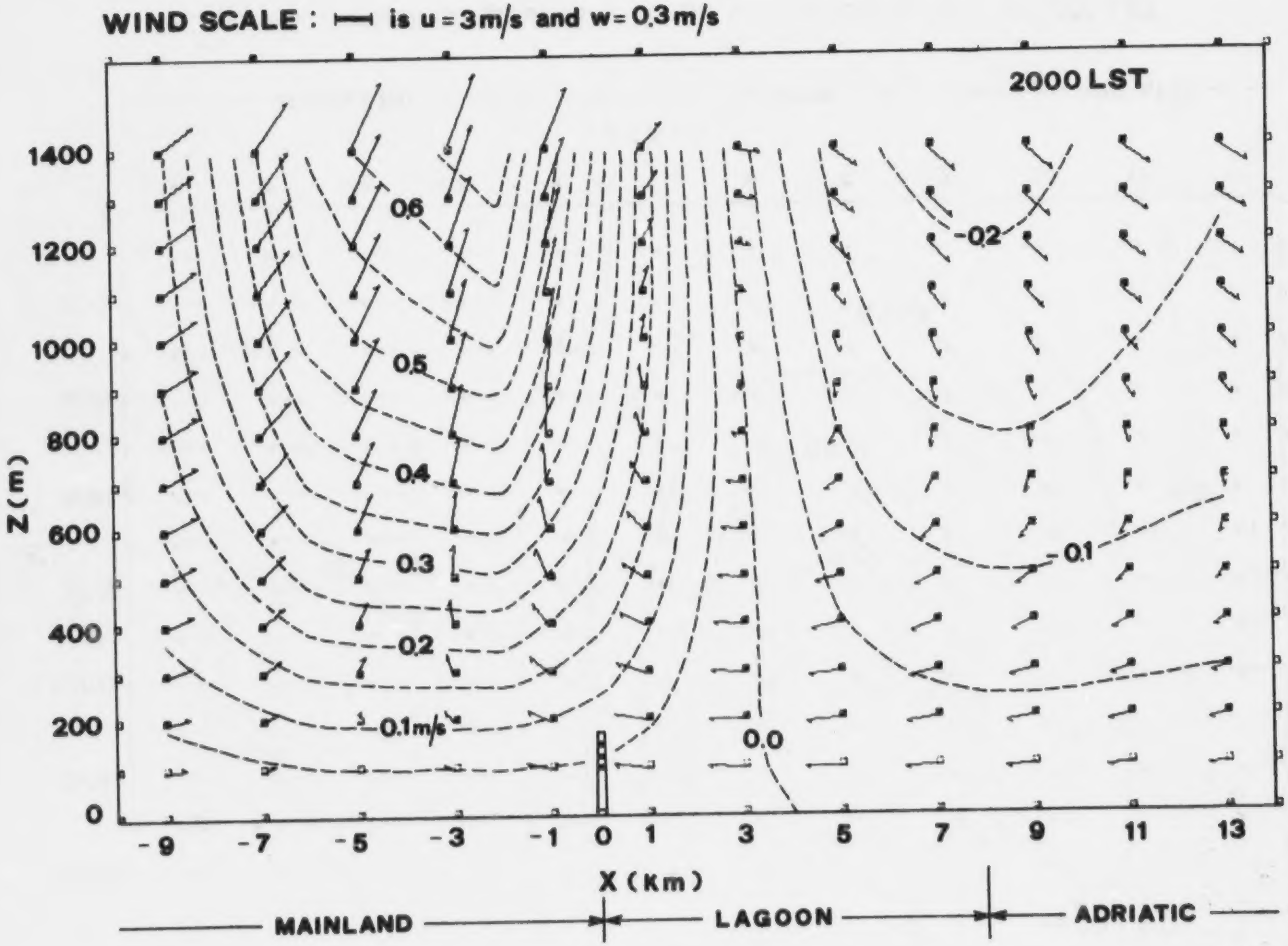

Fig. 2 - Vertical distribution of u and w wind components at 2000 LST.

The distributions in figs 3 and 4 are in a plane perpendicular to the coast and 3 Km "up the coast" from the source (looking with the water on the right). The distribution of fig. 3 is at 1000 LST, before the sea breeze has developed, and shows the advection produced by the synoptic flow, while the distribution of fig. 4 (at 1500 LST) shows clean maritime air pushing under and lifting the plume.

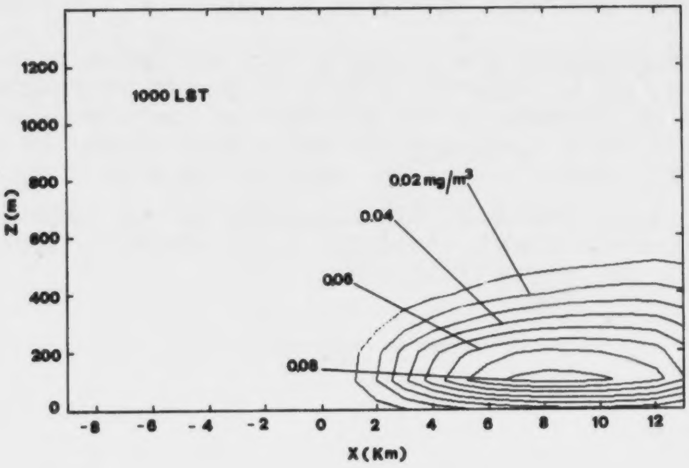

Fig. 3 - Distribution of SO_2 at 1000 LST in a vertical plane perpendicular to the coast and 3 Km "up the coast" from the stack.

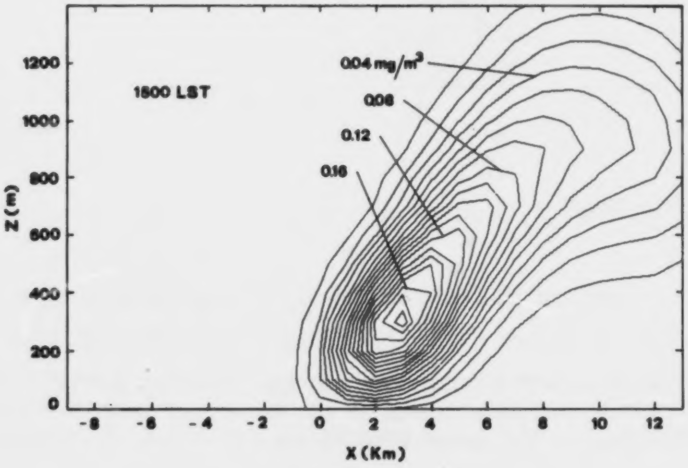

Fig. 4 - Distribution of SO_2 at 1500 LST in a vertical plane perpendicular to the coast and 3 Km "up the coast" from the stack.

The lifting of the plume shown in fig. 4 is due to the vertical flow. The intensity of the vertical flow increases during the development of the sea breeze circulattion up to the value of 0.85 m/sec., which is reached, during the simulation, at 1700 LST. Isopleths of the vertical velocity are given by dashed lines both in fig. 1 and 2. At 1500 LST the flow is ascending over the lagoon with maximum velocity equal to 0,3 m/sec at x = 5 Km, and is slowly descending over the mainland and the Adriatic sea, while at 2000 LST the air is lifted over the land with maximum velocity equal to 0.65 m/sec. at x = -3 Km, and it is descending over the water with a maximum downward velocity of 0.2 m/sec. at x = 8 Km.

Since meteorological measurements give generally only information on the horizontal flow, the vertical flow is neglected in many studies of air pollutant dispersion. In order to show its relevance on the behaviour of the plume a simulation was carried out in which the w component was set to zero. Except for the latter condition, fig. 5 gives SO_2 distribution in the same conditions as in fig. 4. The pollutant spreads in a region limited by "the downwind and the upwind flow", as the pollutant particles are not lifted to the upper layers where the synoptic flow is still prevailing on the sea breeze circulation.

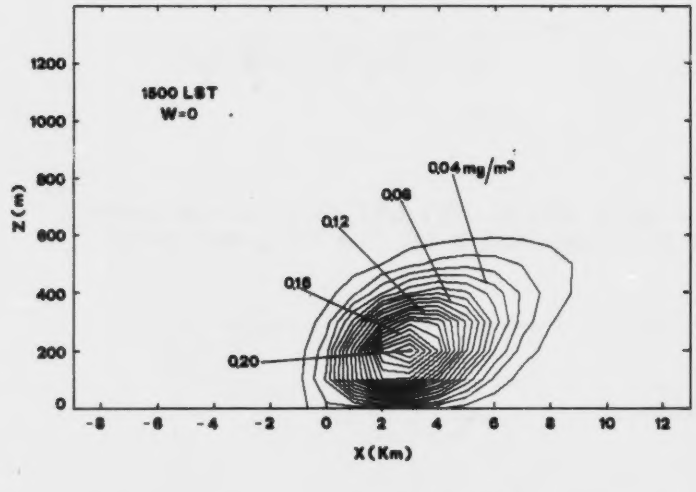

Fig. 5 - Same as in Fig. 4, but for w = 0

The effect of the vertical flow on the SO_2 distribution can be also seen on planes parallel to the coast. Fig. 6 shows SO_2 distribution at 1500 LST in a plane parallel to the coast and 6 Km downward from the source (looking towards the sea). The air flow has lifted the plume and has moved it up the coast from the source. Fig. 7 shows the SO_2 distribution in the same conditions as in fig. 6, except for the vertical flow which was set to zero. The center of the plume is 400 m lower than in fig. 6, less pollutants particles were able to reach this section. The distribution of SO_2 in fig. 7 is mainly due to diffusion processes, as the pollutant, forced to be confined to the lower layers, was not advected by the synoptic flow existing at the upper layers.

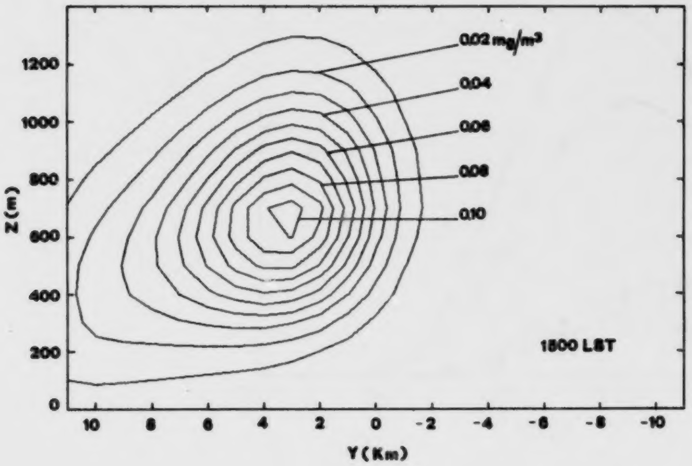

Fig. 6 - Distribution of SO_2 at 1500 LST in a vertical plane parallel to the coast and 6 Km downwind from the stack.

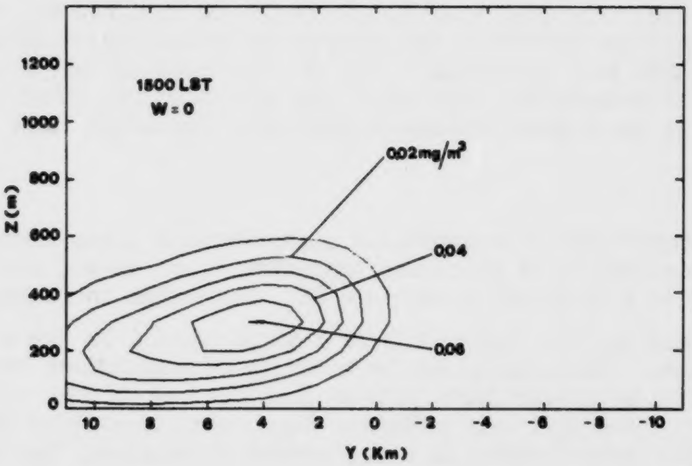

Fig. 7 - Same as in Fig. 6 but for w = 0

For the simulation described in figs. (3)-(7), both chemical transformation and deposition were taken into account. In our previous work (Bornstein and Runca (3)) a series of simulations was also carried out to determine the change in concentration produced by sequentially including the effects of chemical transformation and surface deposition. Results from those simulations are shown in fig.8 for a surface site 6 Km downwind and 3 Km "up the coast" from the stack.

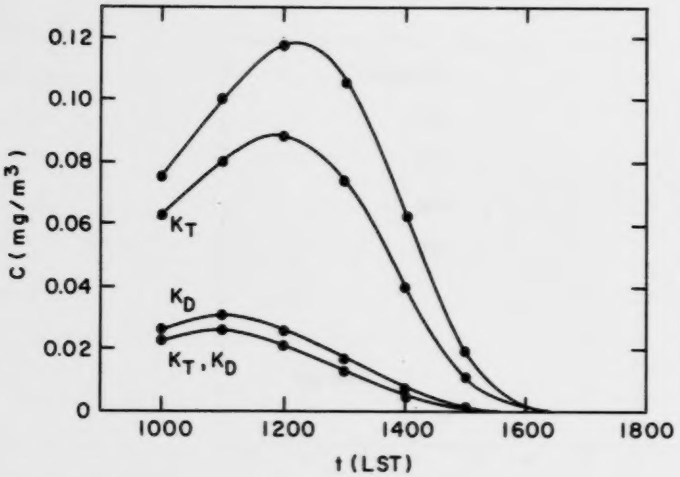

Fig. 8 - Time variations of surface SO_2 concentrations at a site 6 Km downwind and 3 Km "up the coast" from the stack. See text for explanation of four simulations.

The upper curve of fig. 8 is for zero transformation and deposition coefficients, the next curve includes only chemical transformation, the third curve is from a simulation having only surface deposition, and finally, the bottom curve includes both chemical transformation and deposition. Fig. 8 demonstrates that surface deposition and chemical transformation processes can significantrly affect SO_2 even on short distances if the highest transformation and deposition rates occur.

CONCLUSION

Spatial and temporal distributions of atmospheric parameters of a sea breeze circulation have been simulated by a planetary boundary layer model, and then have been used as input to a K-model to compute SO_2 dispersion, including linear chemical transformation and surface removal, from a stack located on the edge between the land and the sea. Results, given by a series of simulations carried out to determine the plume behaviour, have proved that the link of PBL and K-models is a suitable technique to investigate air pollutant dispersion in complex air flow dynamics. This study has proved that, in a sea breeze circulation, the vertical flow cannot be neglected, and that removal processes can affect SO_2 significantly even on short distances.

Future work should analyze to which extent a K-model describes correctly the pollutant distribution in the "pseudo real" situation simulated by a planetary boundary layer model. Tests concerning numerical errors, and treatment of boundary conditions, as well as comparison of different numerical techniques should be performed. Effects of relevant atmospheric parameters on concentration distribution should be investigated in detail. Plume rise and inversion layer height, neglected in this study, should also be included.

References

1. R. Bornstein: The two dimensional URBMET urban boundary layer model, J. Appl. Meteor. 14 (1975), 1459-1477.
2. R. Bornstein and A.D. Robock: Effects of variable and unequal time steps in the simulation of the urban boundary layer using the two-dimensional URBMET model, Mon. Weather Rev. 104 (1976) 260-7.
3. R.D. Bornstein and E Runca: Preliminary investigations of SO_2 patterns in Venice, Italy, using linked PBL and K-models, including removal processes, Proc. Joint Conference on Applications on Air Pollution Meteorology, Salt Lake City, Utah (American Meteorological Society, Boston, 1977, in press).
4. D.A. Dieterle and A.G. Tingle: A numerical study of mesoscale transport of air pollutants in sea-breeze circulations, Proc. Third Symposium on Atmospheric Turbulence, Diffusion, and Air Quality, Raleigh, N.C. (American Meteorological Society, Boston, 1976) 436-441.
5. D.R. Kalthoff: On SO_2 removal and sulfate formation processes in the atmosphere, Proc. Seventh Int. Technical Meeting on Air Pollution Modelling and its Application, Airlie, Virginia (NATO/CCMS, Bruxelles, 1976) 856 - 870.
6. H.L. Kuo: The thermal interaction between the atmosphere and the earth and propagation of diurnal temperature waves, J. Atmos. Sci. 25 (1968) 682 -706.
7. A.H. Levy, D.R. Drewes and J.M. Hales: SO_2 oxidation in plumes: a review and assessment of relevant mechanistic and rate studies (EPA Report, 1976, in preparation).
8. M.C. MacCracken and R.D. Bornstein, On the treatment of advection in flux formulations for variable grid models, with application to two models, of the atmosphere, J. Computational Physics, 23 (1977) 135-149
9. J.O'Brien: On the vertical structure of the eddy exchange coefficients in the planetary boundary layer, J. Atmos. Sci. 27 (1970) 1213 - 5
10. L.Prahm, U.Torp and R.M. Stern: Deposition and transformation rates of sulphur oxides during atmospheric transport over the Atlantic, Tellus 28 (1976) 355 - 372.
11. R.D.Richtmyer and K.W.Morton: Difference methods for initial value problems (Interscience, New York, 1967).
12. E.Runca and F.Sardei: An improved numerical representation of a point source, Technical Report (IBM Italy, Venezia, in preparation).
13. E.Runca: An efficent air quality K-model, Proc. Seventh Int. Technical Meeting on Air Pollution Modelling and its Application, Airlie, Virginia (NATO/CCMS, Bruxelles, 1976) 628-650.
14. F.Sardei and E.Runca: An efficient numerical scheme for solving time dependent problems of air pollution advection and diffusion, Proc. Seminar on Air Pollution Modelling (IBM Italy, Venezia 1975) 5.1 - 5.13.
15. J.H.Seinfeld: Air pollution: physical and chemical fundamentals (McGraw-Hill, New York, 1975) 261 - 346.
16. J.G.Sheperd: Measurements of the direct deposition of sulphur dioxide onto grass and water by the profile method, Atmos. Env. 9 (1974) 69 - 74.
17. O.G.Sutton: Micrometeorology (McGraw-Hill, New York, 1953) 273-295.

8th International Technical Meeting
on Air Pollution Modeling and its Application

Calculation of atmospheric pollutant dispersion by the computer program XPIC for instationary and inhomogeneous conditions

H. Schultz, E. Voelz, C.D. Wüneke

Arbeitsgruppe für Technischen Strahlenschutz
Technische Universität Hannover

September, 20 - 23, 1977
Louvain-La-Neuve
Belgium

Calculations of atmospheric pollutant dispersion by the computer program XPIC for instationary and inhomogeneous conditions

For calculations of atmospheric pollutant dispersion under instationary and inhomogeneous conditions, numerical computer codes using the particle-in-cell method are developed by several groups. This method simulates the dispersion by the transport of Lagrangian particles in an Eulerian grid mesh in a given wind field.

The main advantage of these programs in comparison to the other solutions of the transport equation is to avoid the so-called fictitious diffusion inherent in the conventional finite-difference techniques. In the program XPIC Lagrangian particles - called marker particles - are moved in the fixed Eulerian grid according to a given time step and to a velocity which is linearly interpolated from the velocities at the eight cell corners with respect to the position of the particle. The velocities $\vec{v}$ at the cell corners are composed of the advection velocities $\vec{u}$ given from the wind field and of net-diffusion velocities $\vec{w}$ calculated from the pollutant concentrations C by a difference-scheme.

The net-diffusion velocity is defined $\vec{w} = -\frac{\vec{j}}{C} = -\frac{K}{C}\,\mathrm{grad}\,C = -\frac{K}{C}\nabla C$ with $\vec{j}$ the net-current density and K the turbulent diffusion coefficient.

This model solves the non-linear transport diffusion equation

$$\frac{\partial C}{\partial t} + u\nabla C = \nabla(K\cdot\nabla C)$$

Under the assumption of incompressible air, where div $\vec{u} = \nabla\vec{u} = 0$, the transport diffusion equation can be rewritten as follows

$$\frac{\partial C}{\partial z} + \nabla(\vec{u}C) = \nabla(K\cdot\nabla C)$$

Introducing the net-diffusion velocity $\vec{w} = -\frac{K}{C}\nabla C$

$$\frac{\partial C}{\partial t} + \nabla(\vec{u}\cdot C) + \nabla(\vec{w}\cdot C) = 0$$

and a pseudo-velocity $\vec{u} + \vec{w} = \vec{v}$ we get

$$\frac{\partial C}{\partial t} + \nabla(\vec{v} \cdot C) = 0$$

Since therein $\nabla\vec{v}$ must not be zero, this equation corresponds to a compressible pollutant gas, which can be simulated by an adequate distribution of pollutant particles.

The flow chart of our program is shown in fig. 1.

On hand of this figure our program shall be explained as follows.

At the beginning the positions of the particles are created by a random number generator in correspondance to a given particle distribution. From this particle distribution a mean concentration at the cell centres is made for smoothing reasons by a special volume weighting (VOWIK), that means linear interpolation.

With a difference scheme (ENDF) the diffusion velocities at the cell corners are calculated from these concentrations using diffusion coefficients given by a subroutine.

In a subroutine (ADDI) the addition of these diffusion velocities to the advection velocities from the windfield gives the pseudo-velocities at the cell corners.

By a similar weighting process (VOWIV) we get the linearily interpolated pseudo-velocities at the positions of the particles.

With these velocities the transfer of each particle during the time step is calculated. Starting with the new particle positions the calculation is repeated for the next time step.

For practical use the code has been developed in two versions: A) for handling single clouds over wide ranges with an expanding cell system and B) for multiple sources in a limited area with a large number of fixed cells.

In version A) the grid system follows the cloud path with cells stepwise expanding in accordance to the cloud dimensions. At the moment in our computer CDC CYBER 73/76 the version A) can handle about 26 000 particles in a grid system of about 10 000 cells, whereby about 2 seconds per time step are needed.

To overcome these restrictions, in version B) the calculations are performed by tracking the particles groupwise and by handling the grid system in sections. Until now total grid systems of up to 100 000 cells can be handled this way with 6 seconds per time step.

For evaluating the correct concentration on the earth surface in spite of the strong initial theoretical decrease of the velocities and the diffusion coefficients we have arranged the following two procedures: In case (a) a linear interpolation according to the vertical position of the particle is performed between the diffusion velocity value zero on the surface and the value on the upper border of the lowest cell layer as calculated with the normal difference scheme.

In case (b) the velocity of the particles in the lowest layer is statistically sampled between both limiting values of case (a).

Case (a) seems to simulate the more theoretical assumption of linear decrease of eddies, whereas case (b) seems to correspond to a nearly constant eddy spectrum in the lowest layer what looks more realistic.

The time integral of the concentration at a reference point in version B is got by adding up all concentration values weighted by the time steps during the time of interest. Assuming that a single cloud is nearly unchanged during the passage across the reference point, in the version A) the concentration time integral can be calculated by adding up all concentrations along the trajectory across this point and multiplying with the time interval, which is needed for the passage of a cell along the reference point.

It could be shown that the mathematical model is now working correctly, if calculations for single clouds using the K-values in correspondance to the standard deviations of the Gaussian model are compared with the results of pure Gaussian model calculations.

Therefore now the main problem remains how to choose the right values of K_x, K_y, K_z and u for each cell corner in correspondance to the special weather situations and how much this choice influences the results.

Here the crucial question arises how turbulences with longer wave lengths and periods than the cell dimensions and time intervals shall be regarded in the numerical calculations. Especially for instable situations very large eddies have to be considered, which hardly can be simulated by independent eddy distributions within the cells as it is done with local K-values for each cell. If we use for this purpose local K-values that are long-time mean values for the impact of all eddies occuring within the total boundary layer we will overestimate the turbulence within each cell and underestimate the advection transport effect by large eddies through several cells and time steps. In principle for longer dispersion times these difficulties may be overcome by separating the eddies into such contributing to the K-values in the individual cells and into such possible simulated by a spectrum of wind waves swinging through the whole cell system.

But as long as there is a lack of information about the eddy distribution and their contribution to the K-values and to the wind waves, one can only try to estimate the effect of these uncertainties by test calculations under extreme assumptions.

There are some well-known methods to get K-values:

- Mean values for K_x, K_y and K_z averaged over a single cloud can be derived from the standard deviations of the Gaussian plume model.
  On the other hand, these K-values can be assumed as respresentative for a single cell, if a cloud dimension is comparable to the cell dimension.
- By means of the mixing length hypothesis, for neutral atmospheric stability Blackadar deduces height-dependent turbulent diffusion coefficients $K_z(z)$ that include the distribution of all eddies in the whole mixing layer.
- Another method to get such height-dependent $K_z(z)$-values is developed by Wippermann by solving Navier-Stokes Equations for the turbulent atmosphere with a complete set of all important parameters.

Corresponding vertical profiles of $K_z(z)$ are presented in fig. 2.

Since for the horizontal diffusion coefficients no values are given by the last two methods we choose for a first investigation comparable correlations of K_x and K_y to K_z as in the Gaussian model. Further parameter variations during the investigation concerned the vertical distribution of the wind speed and/or the wind direction. Some typical results are given on the following figures.

In fig. 3 concentration isopleths in the x-z-plane through the cloud center path for three different source distances are presented, which were calculated with version B for an emission height 100 m in a neutral atmosphere (class D) with a vertical wind speed profile in the power law form (exponent 0,28) and distant dependent K(x)-values according to the $\sigma(x)$ of the Gaussian plume model. From these and other diagrams for other K-values it can be seen, that the lagging between the cloud at the emission height and at the ground level increases roughly with a rate of 200 m per 1 km path length. This corresponds to an effective surface velocity in the lowest cell layer that is roughly 80 % of the velocity in the emission height. Since the corresponding value of the vertical wind speed profile is only 40 % of the speed in the emission height the important influence of vertical diffusion effects in the lowest layers on the effective cloud velocity at ground level is obviously.

The next fig. 4 shows the influence of different K-choices on the concentration time integral isopleths at ground level for calculations with the same emission conditions as in fig. 3. On behalf of the limited cell numbers and dimensions in the XPIC-programs, these calculations were made in two steps, - first with XPIC-A using an expanding cell system for distances from 0,7 to 4 km, beginning with a pure Gaussian cloud according to the Gaussian plume model - and then with XPIC-B up to 12 km, beginning with a source distribution transfered from the XPIC-A calculation at 3 km. Here XPIC-B gives correct values of the concentration time integral only between 3,5 km and 9 km, - that is the region, where the cloud as a whole passes the reference points.

Obviously the K(x)-values by the Gaussian plume model lead to broader distributions than the both other K-choices. With the K(z) by Blackadar the decrease of the local diffusion coefficients from the emission height to the ground level is apparently more important than the effect of the relative larger K-values compared to the Gaussian model at the beginning of the calculation.

With constant K-values, corresponding to the turbulence within each cell alone, the diffusion effect is obviously still more underestimated. Therefore realistic calculations for vertically inhomogeneous windfields seem to be possible only, when statistically varying wind waves through the whole windfield are added to the local K-values for each cell.

The next fig. 5 shows how the cloud transport is influenced by a vertical wind shear profile additionally to a homogeneous windfield and to a vertical wind speed profile. Within the middle region, where correct calculations of the concentration time integral are possible, the additional decrease of values and the distortion of isopleths under the influence of wind shear can be seen.

In the last fig. 6 a preliminary demonstration is given of automatically plotted isopleths calculated with XPIC-A for a case comparable to the last diagram of fig. 5. Additionally the wind direction turns with a constant angle velocity of -10° per 1 minute as soon as the cloud has reached a distance of 3 km from the source.

Summarising we conclude from our calculations so far made with XPIC-A and -B that the use of these programs may be restricted to more qualitative than quantitative investigations as long as there is a lack of information about realistic local diffusion coefficients for all three directions and for an adequate simulation of the long wave turbulences. Another handicap is the very lage computer memory and calculation time needed for sufficiently accurate results over larger regions and travel distances, if the vertical inhomogeneities in the lower boundary layer are to be considered. Therefore quantitative results seem to be aquirable at the moment only if the diffusion effects are nearly negligible compared to the transport effects within an inhomogeneous and/or instationary windfield.

Literatur:

Blackadar, A.K., The Vertical Distribution of Wind and Turbulent Exchange in a Neutral Atmosphere, J. Geophys. Research, Vol 67, No.8, July 1962

Lange, R., ADPIC - A Three-Dimensional Computer Code for the Study of Pollutant Dispersal and Deposition under Complex Conditions
Lawrence Livermore Laboratory
UCRL-51462 1973

Pasquill, F., Atmospheric Diffusion, van Nostrand, London 1962

Sklarew, R.C., Fabrick, A.J., Prager, J.E., A Particle-in-Cell-Method for numerical Solution of the Atmospheric Diffusion Equation, and Applications to Air Pollution Problems
3 SR-844 1971
Systems, Science and Software, La Jolla, California

Vogt, K.J., H. Geiß, Kurzzeit- und Langzeitausbreitungsfaktoren zur Berechnung der Umweltbelastung durch Abluftfahnen, Jul-1131-ST, Okt. 1974

Wippermann, F., The Planetary Boundary Layer of the Atmosphere, Annalen der Meteorologie, Deutscher Wetterdienst, Offenbach 1973

Fig. 1

Flow Chart of the XPIC-Code

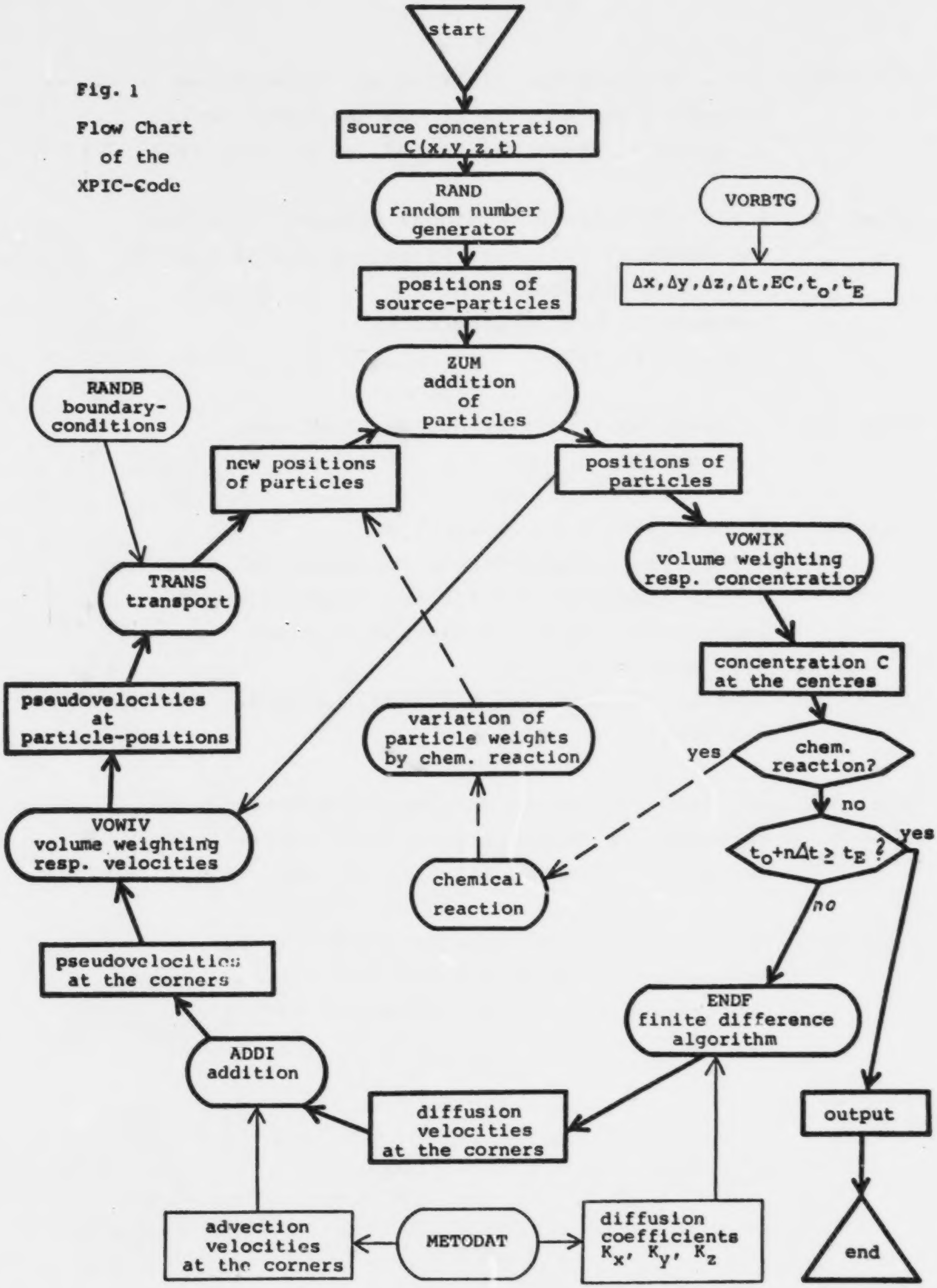
start
source concentration C(x,y,z,t)
RAND random number generator
positions of source-particles
VORBTG
Δx, Δy, Δz, Δt, EC, t_o, t_E
ZUM addition of particles
RANDB boundary-conditions
new positions of particles
positions of particles
VOWIK volume weighting resp. concentration
TRANS transport
concentration C at the centres
pseudovelocities at particle-positions
variation of particle weights by chem. reaction
chem. reaction?
yes
no
VOWIV volume weighting resp. velocities
$t_o+n\Delta t \geq t_E$?
yes
chemical reaction
no
pseudovelocities at the corners
ENDF finite difference algorithm
ADDI addition
diffusion velocities at the corners
output
advection velocities at the corners
METODAT
diffusion coefficients K_x, K_y, K_z
end

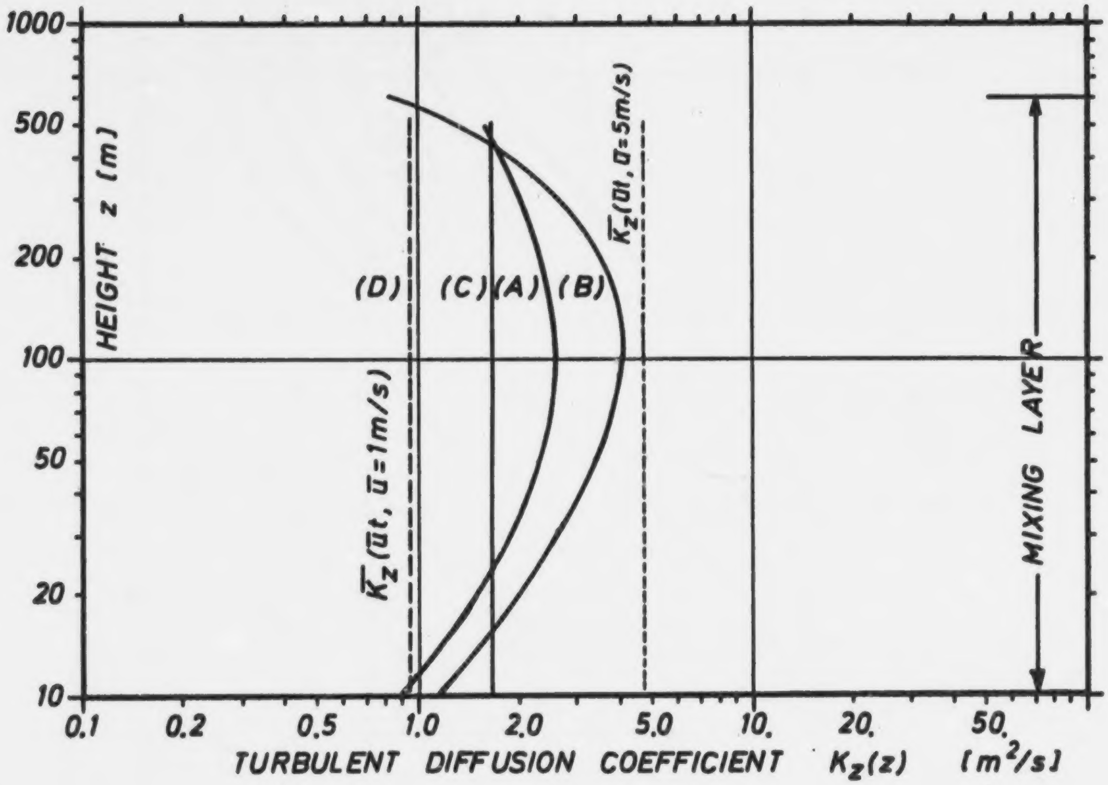

Fig. 2 Coefficients $K_z(z)$ for neutral atmospheric stability (D) from Blackadar (A), Wippermann (B) and for the mean turbulence within a cell dimension 15 m (C) and the mean value for the Gaussian plume model between ut = 600 and 3000 m (D).

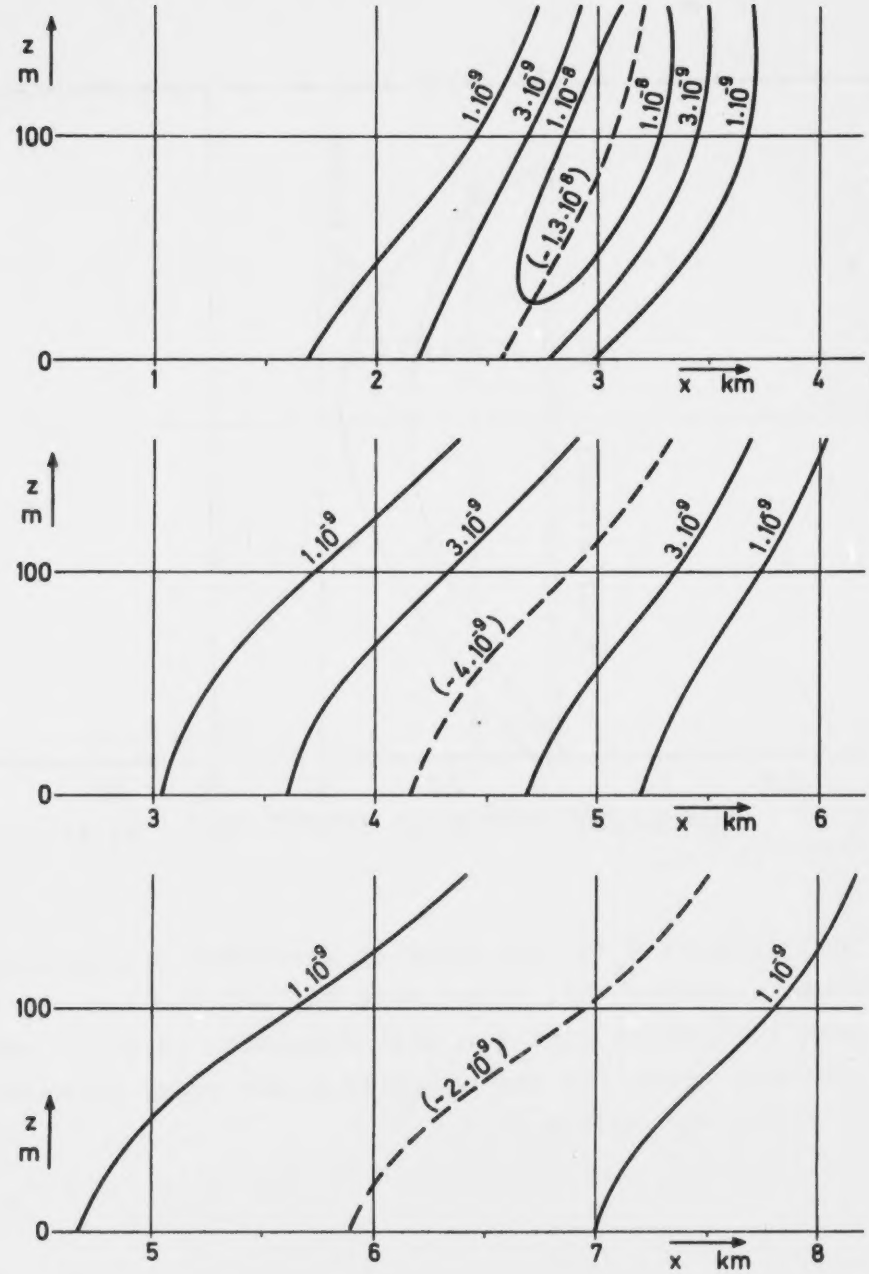

Fig. 3 Isopleths of the concentration (m^{-3})
in the x-z-plane at three positions of the cloud.
(——— isopleths; ------ positions of the maximum)
neutral atmospheric stability (D),
point source emission height 100 m,
vertical wind speed profile $u(z)/u(z_0) = (z/z_0)^{0,28}$,
$K(x)$ according to the $\sigma(x)$ of the Gaussian plume model

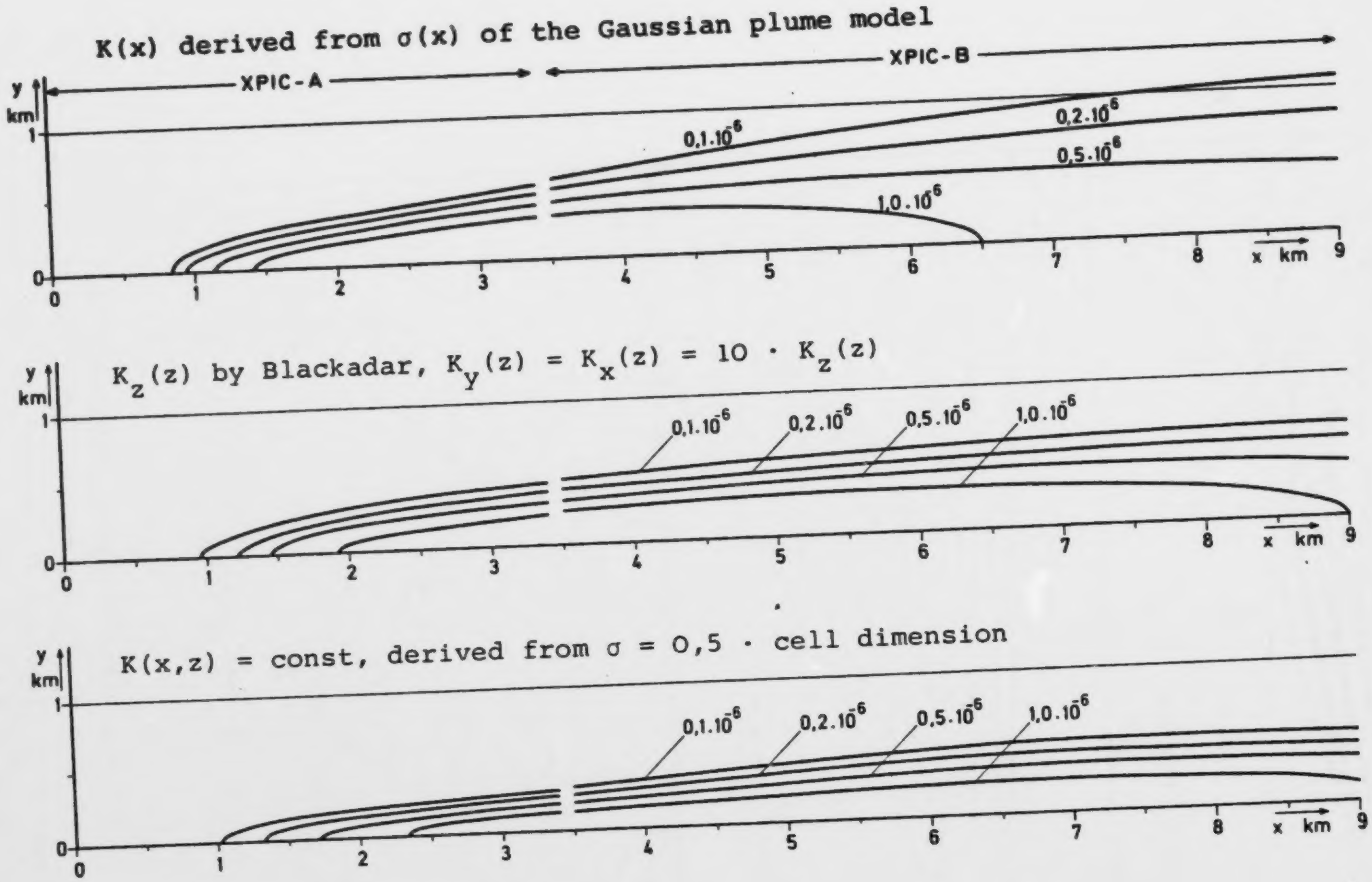

K(x) derived from σ(x) of the Gaussian plume model

$K_z(z)$ by Blackadar, $K_y(z) = K_x(z) = 10 \cdot K_z(z)$

$K(x,z)$ = const, derived from σ = 0,5 · cell dimension

Fig. 4 Isopleths of the concentration time integral (s/m^3) at ground level calculated by a combination of the program versions XPIC-A and -B for different K-values, neutral atmospheric stability (D),
point source emission at height 100 m,
vertical wind speed profile $u(z)/u(z_o) = (z/z_o)^{0,28}$

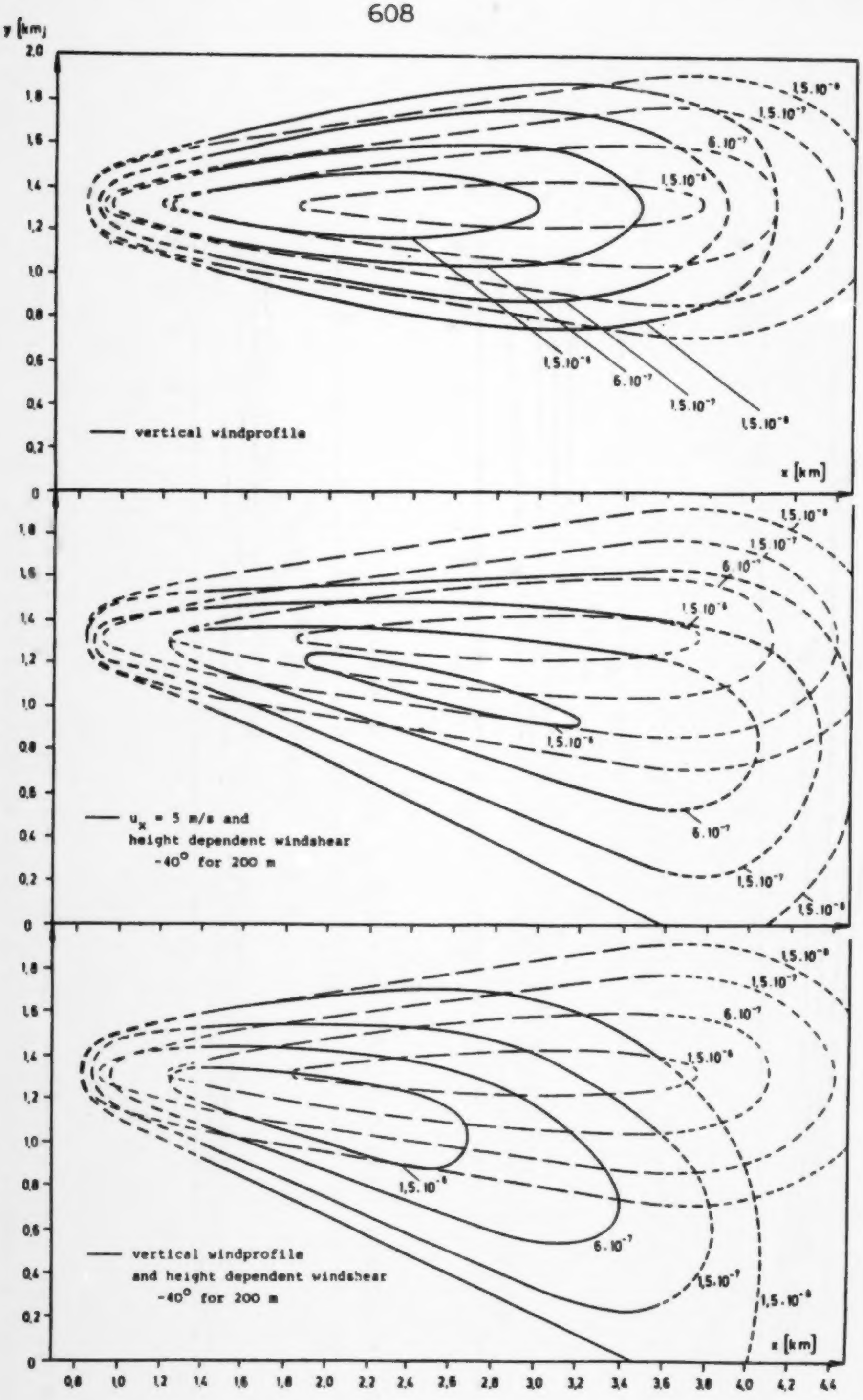

Isopleths of the concentration time integral (s/m^3) at ground level with height-dependent wind direction shear, neutral atmospheric stability (class D), Gaussian source at 1 km according to a point source emission height 100 m, wind speed u(100 m) = 5 m/s, ----- homogeneous wind field

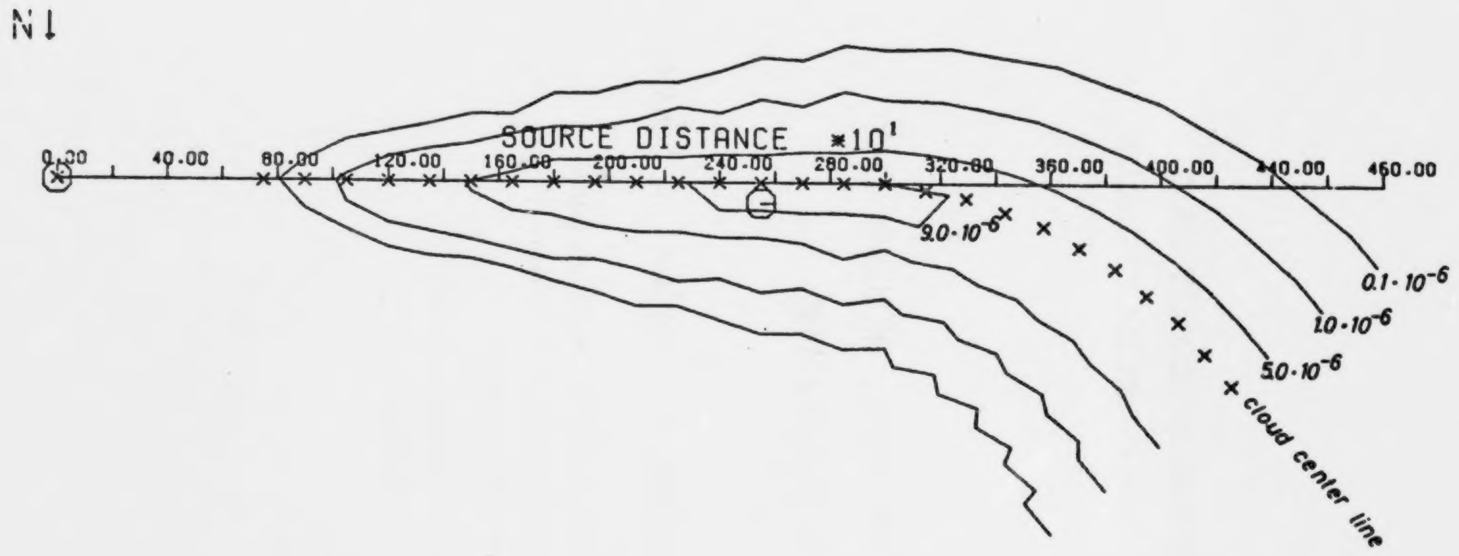

Fig. 6 Isopleths of concentration time integral (m^{-2}) normalized to 1 m/s, at ground level, under neutral atmospheric conditions (class D) for a point source at emission height 100 m, with a height-dependent wind speed profile $u(z)/u(z_o) = (z/z_o)^{0,28}$ and wind direction shear profile (-5^o/100 m). The wind with a speed 5 m/s at emission height begins to turn with an angle velocity (-5^o/30 s) at a distance 300,00 · 10^1 m.

8th International Technical Meeting on
Air Pollution Modeling and its Application.

A K ANALYTICAL MODEL, INCLUDING CALM WIND SITUATIONS.

CL. DEMUTH, A. BERGER, Y. JACQUART, G. SCHAYES

Institut d'Astronomie et de Géophysique
Université Catholique de Louvain
Chemin du cyclotron, 2
B-1348 LOUVAIN-LA-NEUVE
BELGIUM

September 20-23, 1977
Louvain-la-Neuve
Belgium.

A K ANALYTICAL MODEL,
INCLUDING CALM WIND SITUATIONS

1. INTRODUCTION.

The first stage in modelling atmospheric pollution due to a point source needs the knowledge of important physical mechanisms which are responsable for the dispersion of the pollutant when the turbulence produced by the plume in the initial phase is weak. Their introduction in only the continuity equation for the pollutant allows to define the mathematical model.

Three fundamental mechanisms occur in the dispersion of the pollutant : the advection, a turbulent diffusion and a "pseudo-turbulent" diffusion of advectif character.

The first mechanism refers to velocity field. The second is responsible for the dispersion of the pollutant in the atmosphere with a dissymmetry in its effects. The turbulence action along the vertical is more important than in the horizontal plane because the difference of the scale : the air is mixed vertically in layer of approximately one kilometer while horizontally the related dimensions are twenty times greater. The last mechanism, which takes into account horizontal fluctuations of the wind, expresses the mixing of the air through horizontal eddies with caracteristic scales much more important than the scales of the usual turbulence.

At each of those mechanisms is associated a caracteristic function such as the vertical wind profile for the advection, the profiles of the pseudo-turbulent diffusivity coefficient κ_y and the turbulent diffusivity coefficient K_z for the other phenomena. This decomposition of the diffusion in these principal elements in the case of the oriented wind admits a simple representation in a system of orthogonal axes (fig. 1).

The models presented here are stationary models of analytical type for oriented and calm wind. In order to understand their structure, it is necessary to look over fig. 1. If the function connected to the principal axes of the diffusion in plane (x,z) are only dependant upon the altitude (if we assume horizontal homogeneity) and if κ_y is related to the vertical wind profile, the solution of our diffusion equation can be expressed as the product of two distinct functions Y and Z. The function Y represents the diffusion in the horizontal plane and Z the diffusion in the vertical plane.

As far as a power law is assumed for the vertical profile of U and K_z,the problem of diffusion in both vertical and horizontal planes and for oriented winds has an analytical solution. If the calm wind situations have to be included, this analytical model can be generalized as far as power laws for vertical profiles are assumed. This is an extension of the Berlyand-Kurenbin study (1969) where the mixing height was not taken into consideration.

2. ANALYTICAL MODEL FOR ORIENTED WIND

a) Point source.

The model is based upon the analytical solution of the problem of the stationary diffusion :

$$(1)\quad \left|\begin{array}{l} U(z)\,\frac{\partial\chi}{\partial x} = \kappa_y\,\frac{\partial^2\chi}{\partial y^2} + \frac{\partial}{\partial z}\,K_z\,\frac{\partial\chi}{\partial z} \\[2ex] \chi(o,y,z) = \frac{Q}{U(H)}\,\delta(y)\delta(z-H) \text{ or } \int_o^{+\infty}\int_{-\infty}^{+\infty} U(z)\chi(x,y,z)\,dydz = Q \\ \hfill \text{for } x > o \\[2ex] K_z\,\frac{\partial\chi}{\partial z} = o \quad \text{for } z = o = L \\[2ex] \lim\limits_{x^2+y^2+z^2 \uparrow \infty} \chi = o \end{array}\right.$$

where the downstream diffusion term is considered to be negligible when compared to the advection.
The source, localized at the origin with the x-axis oriented in the direction of the mean wind, emits an amount Q of a pollutant at an effective height H in a mixing layer of depth L, where the limits made by two horizontal planes are supposed to be perfectly reflecting.

If the ratio between κ_y and the wind profile is constant in z and if the vertical profiles U and K_z follow some power laws, the concentration χ in the mixing layer is the product of the two functions :

$$(2)\quad Y = \frac{1}{x}\,\omega\,\left(\frac{y}{x}\right)$$

$$(3)\quad Z = \frac{2qQ}{LU(L)}\left\{\mu + \left(\frac{zH}{L^2}\right)^p \sum_{l=1}^{\infty} \frac{J_{\mu-1}(j_{\mu,l}H^q/L^q)\,J_{\mu-1}(j_{\mu,l}z^q/L^q)}{[J_{\mu-1}(j_{\mu,l})]^2}\right.$$

$$\left.\exp\left[-j_{\mu,l}^2\,\frac{q^2K_z(L)}{L^2U(L)}\,x\right]\right\}$$

where the function ω is the probability density of a wind-direction deviation over a given time period. The parameters occuring in (3) are defined in terms of an exposant m for the wind velocity $U=U_1 z^m$, and n for the profile of the turbulent diffusivity, $K_z = K_1 z^n$. The relations between p,q,m and μ can be expressed as follows :

$$(4) \quad \left| \begin{array}{l} 2p = 1 - n \\ 2q = m - n + 2 > 0 \\ \mu = (m+1) / (m-n+2) \end{array} \right.$$

and $j_{\mu,1}$ is the 1^{th} strictly positive root of the Bessel function of the first kind and of order μ.

The solution (3) is the exact solution of the problem of the diffusion in the plane (x,z) as opposed to Rounds (1955) and Tseytin (1965) formula (Demuth, 1977a).

The period of investigation is of importance to determine χ. If a long period is taken into account,as it will be considered in the example, function (2) has to be modified : the probability density ω has to be replaced by a density which introduces the joint frequency-function F. This function gives the joint frequency of occurence of a wind direction sector id, a wind speed class iw, and a stability category index is. For a wind rose divided into N sectors, the function (2) becomes

$$(5) \quad Y = \frac{1}{x} \frac{N}{2\pi} F(is, id, iw).$$

Consequently, the concentration on the ground is calculated (for P point sources ip and for 16 wind sectors) by

$$(6) \quad \chi = \sum_{ip=1}^{P} \sum_{is,id,iw} Y(ip,is,id,iw) Z(ip,is,id,iw)$$

where

$$(7)\quad Y = \frac{16}{2\pi} F\,(is,id,iw)\,\frac{1}{x_{ip}}$$

$$(8)\quad Z = \frac{Q_{ip}}{LU(L)} \{\,(1+m) + \frac{2q}{\Gamma(\mu)} (\frac{H}{L})^{p} \sum_{l=1}^{\infty} (\frac{1}{2}\, j_{\mu,l})^{\mu-1} \frac{J_{\mu-1}(j_{\mu,l} H^{q}/L^{q})}{[J_{\mu-1}(j_{\mu,l})]}$$

$$\exp\,[-\,j_{\mu,l}^{2}\,\frac{qK_z(L)}{L^{2}U(L)}\,x_{ip}]\}$$

b) Area source

The simulation of each area source, considered as a square source is realised applying the method by Gifford-Hanna (1970) and Lebedeff-Hameed (1975). Thus, assuming each point source plume as being a long and narrow plume, the concentration at each receptor is influenced only by sources strictly under the wind and is considered as being a ligne-source with a finite width. So, the concentration χ at the center of a square area source can be evaluated from the area sources contiguous to the receptor considered, according to the relation :

$$(9)\quad \chi = \frac{1}{U_1} (\frac{U_1}{4q^{2}K_1})^{\mu} \frac{2q}{(1-\mu)\Gamma(\mu)} (\frac{\Delta x}{2})^{1-\mu}$$

$$\{\,Q(0,0) + \sum_{i=\pm 1}^{4} \sum_{j=\pm 1}^{4} Q(i,j) f(i,j) [(2r+1)^{1-\mu} - (2r-1)^{1-\mu}]\}$$

where U_1 and K_1 : the coefficients in the power laws for U and K_z.
$Q(i,j)$: the matrix of area sources.
$f(i,j)$: the matrix of frequency distribution defined from F(is,id,iw).
Δx : the width of the grid mesh.
r : the number of the four circles centred at the receptor.

The other parameters are defined as for a point source. We have to note that (9) does not consider the height H and L.

c) Application.

The region under study is Antwerpen for which we have some informations about sources and meteorological parameters required for the elaboration of the joint frequency function F. The immission grid, fig. 2, is defined by a rectangle of 10 kilometers over 11 in a region which contains 142 point sources localized by their Lambert coordinates. Our study has been limited to summer to allow us to consider only the point sources as a first approximation.

The meteorological parameters are given in tables 1 and 2. The parameter U_i is defined by $U_0 z_0^{-m}$ where U_0 is the wind speed at the anemometer level z_0 (10m). Let us note that these parameters have not been measured in Antwerpen but are only representative parameters taken from the litterature (Vorontsov, 1968) for the considered meteorological situations. This is important for the analysis of the results. Table 3 gives the joint frequency function F for Deurne (6km north-west of Antwerpen) determined from the three-hourly meteorological data recorded from 1 April to 30 September 1974. The wind rose for each stability class is and for each wind speed class iw is presented at figure 3. It can be seen that the more frequent wind direction is South-West for "moderate" wind (iw=3,4) and North for "light" wind (iw=1,2).

d) Results

Table 4 shows for ten receptors the SO_2 concentration measured for the period April-September 1974 and the calculated concentration from the Gaussian model LPADM (Berger et al., 1976) and from the K-model described above. It has to be pointed out that the calculated concentrations do not take the calm wind into account in opposition to the measured concentration where all meteorological situations are considered. The Gaussian model is the same that has been used for the City Test of Frankfurt. The only modifications introduced here concern some parameters, as the temperature of the ambiant air, the mixing height and the absence of half-life.

The K-model has been run for three values of the K_z power law index. When the condition n=0 is choosen, the function K_z becomes constant in the whole mixing layer. Both other choices of n are introduced to simulate a profile of K_z which rapidly varies in the surface layer and which becomes constant in the remaining mixing layer. The results obtained by our model show a weak or even not decrease of the concentration at the nine first receptors when n increases from its minimum value. At receptor ZR826, there is, on the contrary, significant increase in the concentration. Moreover, if the results obtained from the K-model are compared against those obtained from the Gaussian plume model, a good agreement is shown for all receptors, except ZR826. These differences at that receptor ZR826 come from the proximity of many sources in the angular sector where the wind is more frequent. In such a case, the structure of the model becomes determinant in the computation of the concentration at one specific location close to the sources.

The comparison between theoretical and measured values has to be made with great care because no calibration has been made here. Nevertheless, from a theoretical point of view, we can already deduce some advantages of K-model upon Gaussian plume model. The two most important ones seem to be :

i) in the particular cases where dry deposition or any modification of functions U and K_z are taken into account, the analytical solution Z is then easily replaced by a numerical solution of a bidimensional diffusion problem. In that case, it is possible to take into account K_z profiles which show a well shaped maximum (Demuth, 1977 b).

ii) The calm wind situations can be analysed with the same model and this is probably the most advantage as far as calibration and validation are concerned.

3. ANALYTICAL MODEL FOR CALM WIND

The model we proposed is a stationary model which, by the symmetry around the vertical, is the solution of the following problem of diffusion :

$$(10)\quad \begin{cases} \dfrac{1}{r}\dfrac{\partial}{\partial r} rK_r \dfrac{\partial \chi}{\partial r} + \dfrac{\partial \chi}{\partial z} K_z \dfrac{\partial \chi}{\partial z} + \dfrac{Q}{2\pi r}\,\delta(r)\delta(z-H) = 0 \\ K_z \dfrac{\partial \chi}{\partial z} = 0 \quad \text{for} \quad z = 0 = L \\ \lim\limits_{r^2+z^2 \to \infty} \chi = 0 \end{cases}$$

with the condition :

$$K_r \frac{\partial \chi}{\partial r} = 0 \quad \text{for} \quad r = 0$$

Without considering a mixing layer, Berlyand-Kurenbin (1969) have given an analytical solution for this problem where a power law is taken for the vertical profile of the turbulent diffusivity and where the coefficient of the horizontal turbulent diffusivity is the product of the radial variable r by a power law in z. This latter choice is related to the assumption introduced about K_y in the former section. Without mixing height, the ground concentration coming from only one source is given by :

$$(12)\quad \chi = \frac{Q}{4\pi qHK_z(H)}\,\mu\left[\frac{4q^2K_z(H)}{K_r(H)}\right]^2 \left\{1 + \frac{4q^2K_z(H)}{K_r(H)}\,\frac{r}{H}\right\}^{-(1+\mu)}$$

where r : the source-receptor distance

$K_z=K_1z^n$: the profile of the turbulent diffusivity along the vertical. The numerical value of K_z for z equal H and L is respectively designated by $K_z(H)$ and $K_z(L)$.

$K_r=\beta^2rz^m$: the radial turbulent diffusivity. The value of K_r at r=H and z=H is $K_r(H)$ and $K_r(L)$ if r=z=L.

Parameters p,q,μ keep their values defined in (4). The coefficient in (12) which multiplies the whole parentheses, is the value of the ground concentration at the source location.

Here we will take into account a mixing layer which depth is L. Then the concentration on the ground is determined by :

$$(13)\quad \chi = \frac{Q}{4\pi q H K_z(H)}\,\mu\left[\frac{4q^2 \overset{\text{no } H}{\cancel{H}} K_z(H)}{K_r(H)}\right]^2 \{[1+(\alpha\eta^q)^{-2}]^{-(1+\mu)} +$$

$$\frac{(\alpha\eta^q)^{3+\mu}}{\underset{2^{\mu}\swarrow}{\boxed{2\mu}}\Gamma(1+\mu)}\int_0^{+\infty} s^{1+\mu} J_1(s)\,\frac{K_\mu(\alpha s)}{I_\mu(\alpha s)}\,I_{\mu-1}(\alpha\eta^q s)\,ds\ \}$$

with the parameters

$$(14)\ \left|\begin{array}{l} \alpha = \dfrac{1}{2q}\sqrt{\dfrac{K_r(L)}{K_z(L)}\,\dfrac{L}{r}} \\[2ex] \eta = \dfrac{H}{L} \end{array}\right.$$

From (13) the effect of the mixing height L on the concentration can be deduced. Indeed, if we note the following equivalence :

$$(15)\quad (\alpha\eta^q)^{-2} = \frac{4q^2K_z(H)}{K_r(H)}\,\frac{r}{H}$$

the first term in parentheses in (13) is the Berlyand's solution (L=∞). The second term in those parentheses is the perturbation function which is only dependant of the mixing height. In order to show the influence of L, we have compared numerically the value of the first term to the sum of two terms in parenthesis for three values of η : 0.2, 0.5 and 0.8, for α decreasing from 20 to 0.5 and for m=0.15 and n=1.

Figures 4, 5 and 6 show this comparison. The curves begin at the source (α=20), expand with r increasing or α decreasing and reach zero at a distance far away from the source. The curve (+) corresponding to a finite L, shows two important properties:

i) it is above the Berlyand's solution (*) for all η;

ii) it presents a maximum which increases with η. At this maximum, there is an increase of 18% to 77% when compared with Berlyand's solutions for η going from 0.5 to 0.8.

The application of solution (13) for Antwerpen is difficult because there is a lack of informations about the parameters which define the turbulent diffusivity profiles and the plume rise Δh. Berlyand in U.R.S.S. gives values from analysis of observation : in case where n equal one, the parameter β is related to parameter K_1 by the relation : $\beta \sim 2K_1$, with $K_1 = 0.15$. As a first approximation and before getting all required meteorological data of the boundary-layer in Antwerpen, we are planning to use this relation to estimate pollution by calm wind situation. Computation and meteorological observations are in progress.

4. CONCLUSIONS.

This model with oriented and calm wind allows to estimate long-term concentrations of nonreactive pollutants in sites where point and area sources are existing. The first results obtained for Antwerpen are encouraging if the approximations used in the model for this region are considered. We hope that a better knowledge of the boundary layer of the atmosphere will improve the relation between the theory and the observations.

ACKNOWLEDGEMENT

This study is part of the Air Project of the Belgian National Programme on the Environnement sponsered by the Ministry of Scientific Policy. The authors wish to express their gratitude for the financial assistance with the aid of which the work was carried out.

REFERENCES

BERGER A., DEMUTH Cl., JACQUART Y. (1976) : Long period average dispersion model. Technical Document 1/1976 M.P. 2.4 Principles of Multiple Source Air Quantity Modeling. NATO/CCMS Air Pollution Study Modeling Panel.

BERLYAND M. Ye, KURENBIN O.I. (1969) : "Atmospheric Diffusion of impurities during a calm" in American Institute of Crop Ecology Survey of USSR Air Pollution Literature, Vol. IV, edited by Nuttonson, 1970.

DEMUTH Cl., (1977a) : "A contribution to the analytical steady solution of the diffusion equation for line and point sources". (in preparation).

DEMUTH Cl. (1977b) : Evaluation de la pollution à l'aide d'un modèle à coefficients de diffusion variables. Programme National R-D environnement, projet air. Progress Report AL/4.1 - 1977/1, Dept. for Science Policy, Brussels, 8, rue de la Science.

GIFFORD F.A. - HANNA S.R. (1970) : "Urban air pollution modelling". Proceedings of the second International Clean Air Congress, held in Washington, D.C., December 6-11, 1970.

LEBEDEFF S.A. - HAMEED S. (1975) : "Study of Atmospheric transport over Area Sources by an Integral method". Atmospheric Environment, Vol. 9, pp. 333-338.

ROUNDS W. (1955) : Solutions of the two-dimensional diffusion equations. Transactions American Geophysical Union, 36, 395-405.

TSEYTIN G. Kh. (1963) : Propagation of an impurity from a high-altitude source, Trudy Leningr. Gidromet. In-ta, 15, 10-31.

VORONTSOV P.A. (1968) : "The structure of an airstream as a factor in the transport of products of atmospheric pollution" in American Institute of Crop Ecology Survey of USSR Air Pollution literature, Vol. 1, edited by Nuttonson, 1969.

POLLUTION ATMOSPHERIQUE, Bulletin mensuel edited by Meteorological Royal Institute of Belgium, January 1968 to december 1974 and I.H.E.

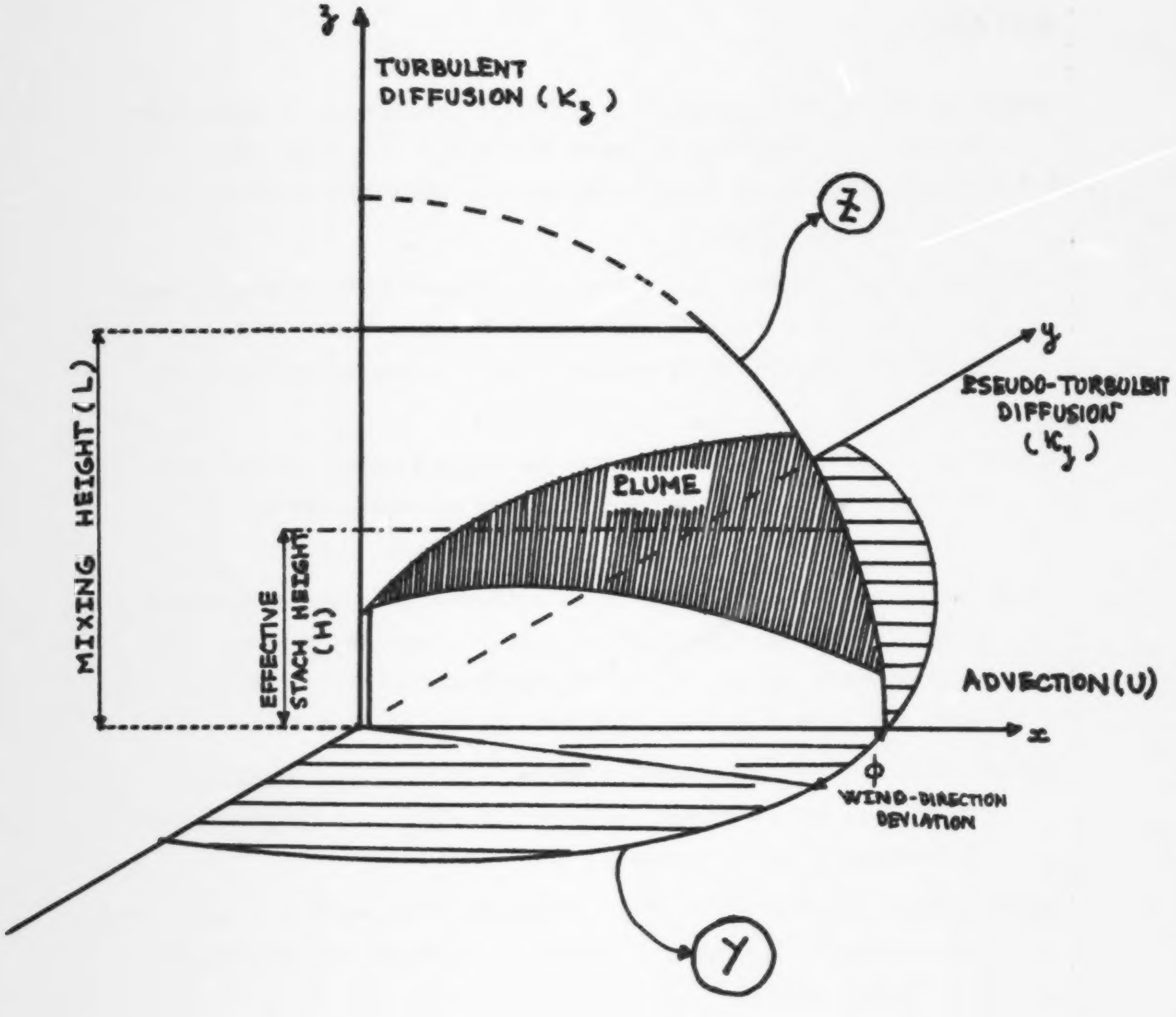
z
TURBULENT DIFFUSION (K_z)
Z
y
PSEUDO-TURBULENT DIFFUSION (K_y)
PLUME
MIXING HEIGHT (L)
EFFECTIVE STACH HEIGHT (H)
ADVECTION(U)
x
φ
WIND-DIRECTION DEVIATION
Y

Fig. 1 : Diagram for the diffusion of a pollutant emitted from a point source for an oriented wind.

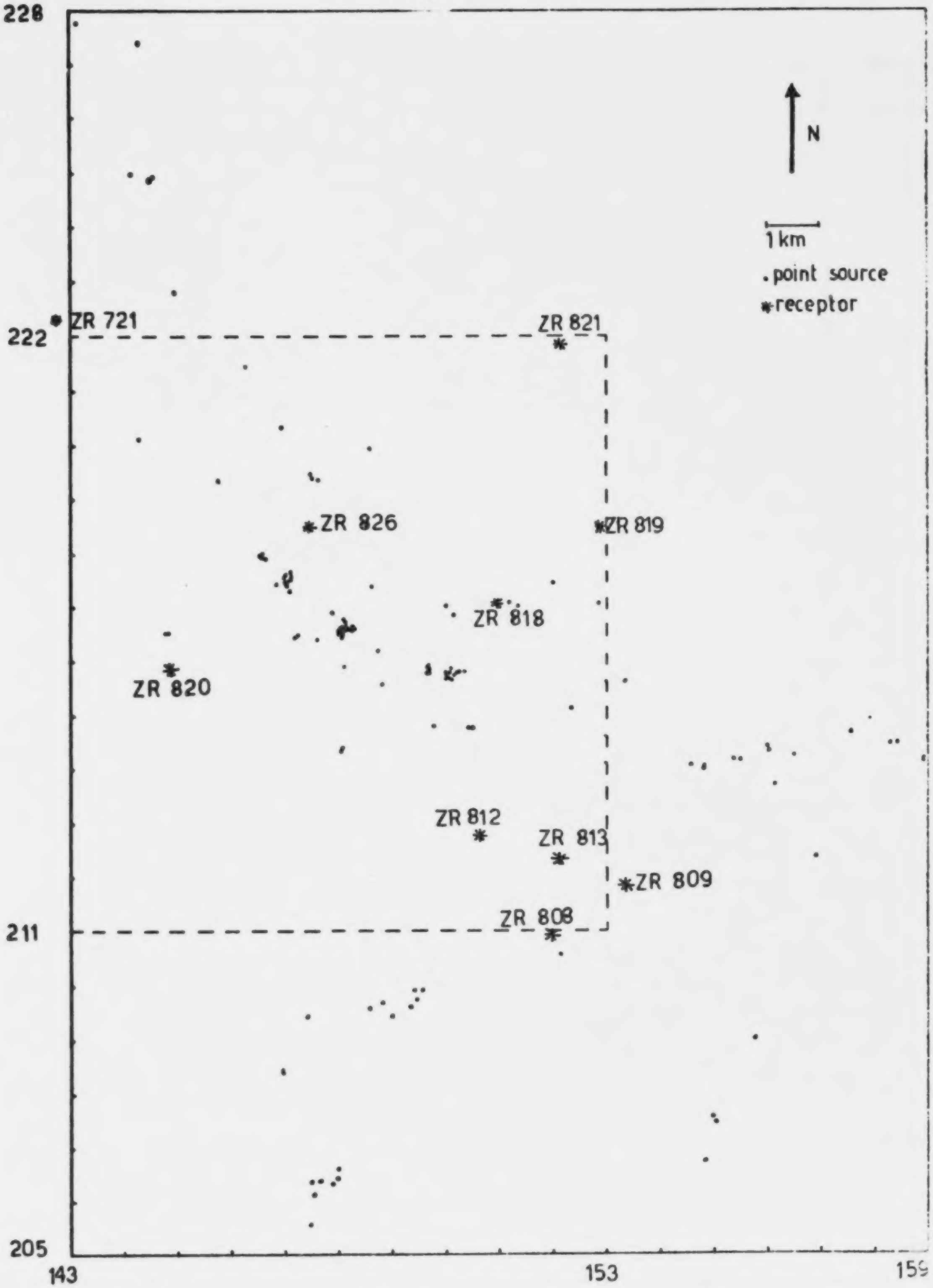
228
222
211
205
143
153
159
N
1 km
. point source
* receptor
ZR 721
ZR 821
ZR 826
ZR 819
ZR 818
ZR 820
ZR 812
ZR 813
ZR 809
ZR 808

Fig. 2 : Points sources and receptors for Antwerpen from 1 April to 30 September 1974.

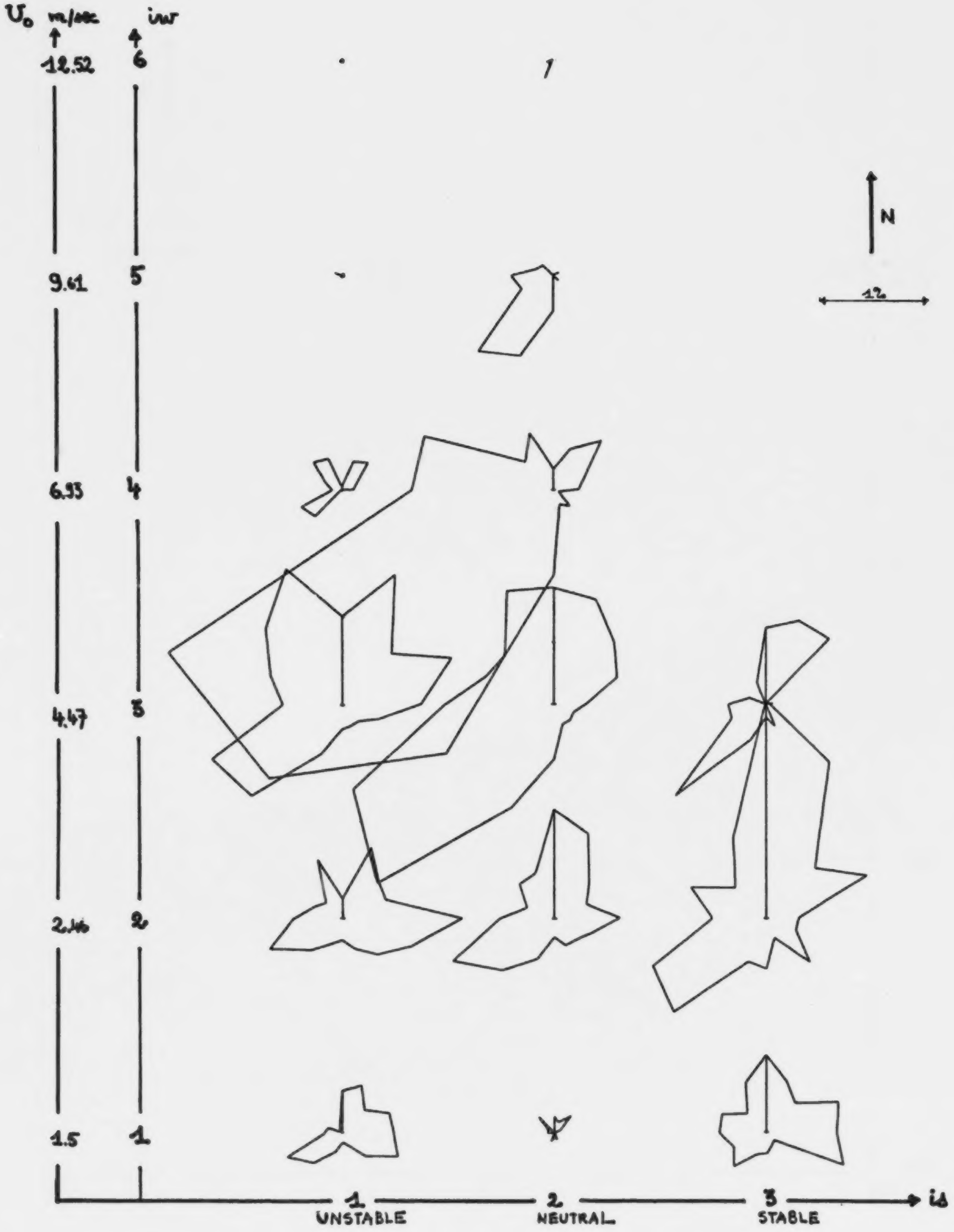

Fig. 3 : Wind-rose for Deurne as a function of stability class (is) and wind speed (iw) from 1 April to 30 September 1974.

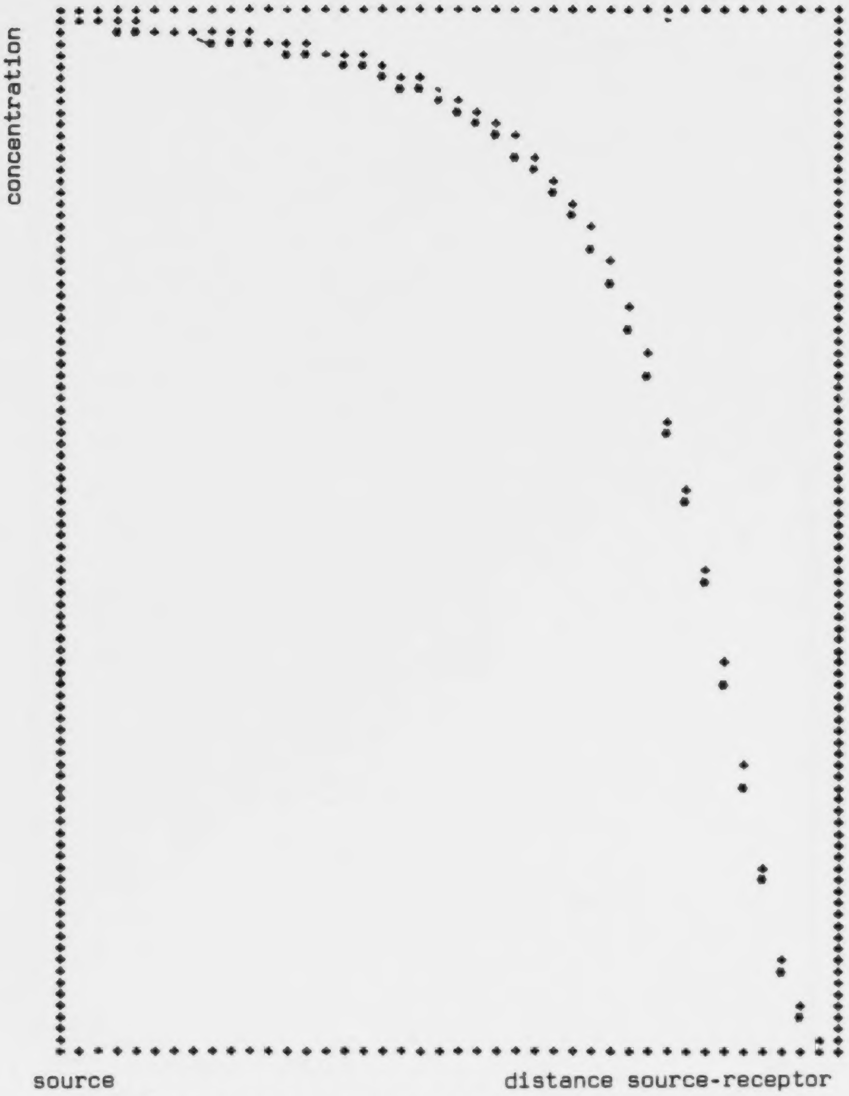

our solution ◆

```
XC= 0.971E 00
XC= 0.970E 00
XC= 0.969E 00
XC= 0.967E 00
XC= 0.966E 00
XC= 0.964E 00
XC= 0.962E 00
XC= 0.960E 00
XC= 0.958E 00
XC= 0.955E 00
XC= 0.953E 00
XC= 0.950E 00
XC= 0.946E 00
XC= 0.943E 00
XC= 0.939E 00
XC= 0.934E 00
XC= 0.928E 00
XC= 0.922E 00
XC= 0.915E 00
XC= 0.907E 00
XC= 0.898E 00
XC= 0.887E 00
XC= 0.875E 00
XC= 0.860E 00
XC= 0.843E 00
XC= 0.823E 00
XC= 0.800E 00
XC= 0.772E 00
XC= 0.739E 00
XC= 0.699E 00
XC= 0.652E 00
XC= 0.595E 00
XC= 0.528E 00
XC= 0.449E 00
XC= 0.359E 00
XC= 0.261E 00
XC= 0.163E 00
XC= 0.815E-01
XC= 0.289E-01
XC= 0.420E-02
```

Berlyand's solution ◆

```
X= 0.969E 00
X= 0.967E 00
X= 0.966E 00
X= 0.964E 00
X= 0.962E 00
X= 0.960E 00
X= 0.957E 00
X= 0.955E 00
X= 0.952E 00
X= 0.949E 00
X= 0.946E 00
X= 0.942E 00
X= 0.938E 00
X= 0.934E 00
X= 0.929E 00
X= 0.923E 00
X= 0.917E 00
X= 0.910E 00
X= 0.903E 00
X= 0.894E 00
X= 0.884E 00
X= 0.873E 00
X= 0.860E 00
X= 0.845E 00
X= 0.827E 00
X= 0.807E 00
X= 0.783E 00
X= 0.755E 00
X= 0.727E 00
X= 0.693E 00
X= 0.635E 00
X= 0.570E 00
X= 0.512E 00
X= 0.431E 00
X= 0.347E 00
X= 0.246E 00
X= 0.149E 00
X= 0.682E-01
X= 0.184E-01
X= 0.143E-02
```

Fig. 4 : Normalized concentration at the origin without and with mixing height fixed by $\eta=0.2$

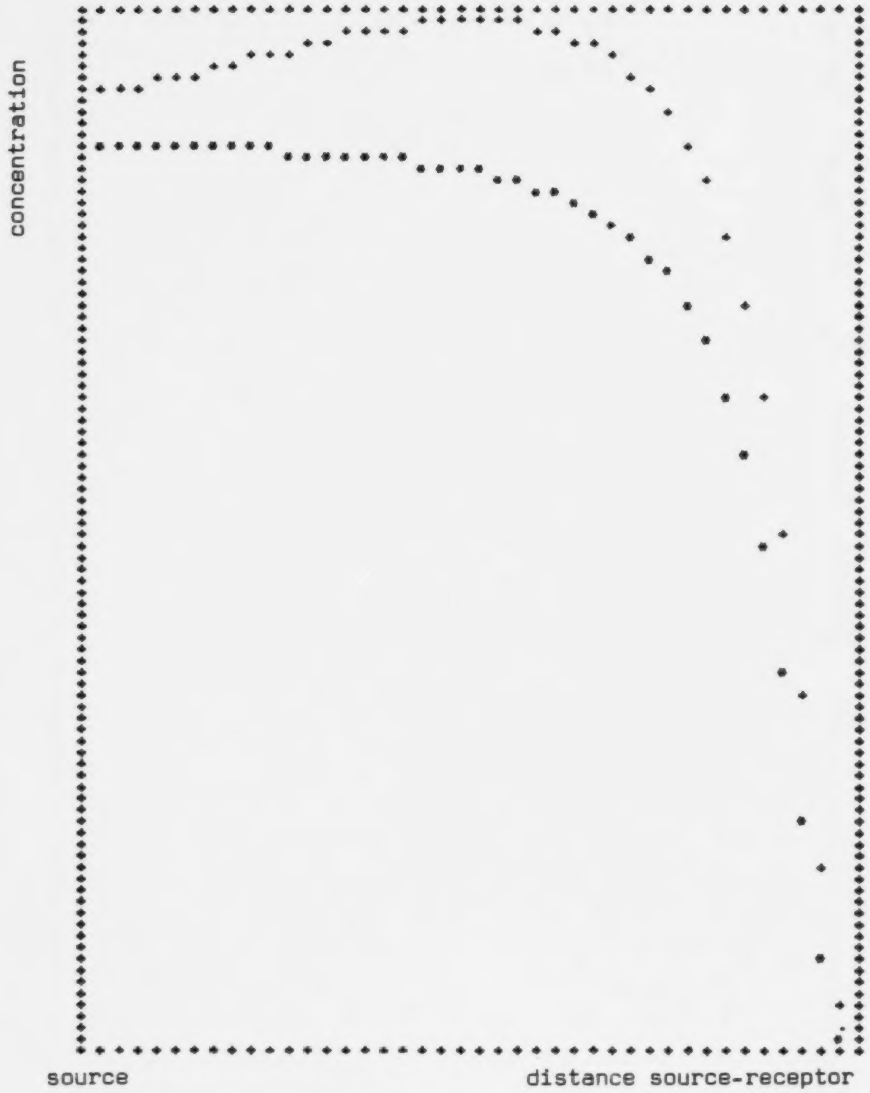

our solution ◆

```
XC=  0.105E 01
XC=  0.105E 01
XC=  0.105E 01
XC=  0.106E 01
XC=  0.106E 01
XC=  0.107E 01
XC=  0.107E 01
XC=  0.108E 01
XC=  0.108E 01
XC=  0.109E 01
XC=  0.109E 01
XC=  0.110E 01
XC=  0.110E 01
XC=  0.111E 01
XC=  0.111E 01
XC=  0.112E 01
XC=  0.112E 01
XC=  0.112E 01
XC=  0.112E 01
XC=  0.112E 01
XC=  0.113E 01
XC=  0.112E 01
XC=  0.112E 01
XC=  0.112E 01
XC=  0.111E 01
XC=  0.111E 01
XC=  0.110E 01
XC=  0.109E 01
XC=  0.107E 01
XC=  0.105E 01
XC=  0.102E 01
XC=  0.989E 00
XC=  0.944E 00
XC=  0.888E 00
XC=  0.811E 00
XC=  0.706E 00
XC=  0.565E 00
XC=  0.387E 00
XC=  0.195E 00
XC=  0.507E-01
```

Berlyand's solution ●

```
X=  0.989E 00
X=  0.988E 00
X=  0.988E 00
X=  0.987E 00
X=  0.986E 00
X=  0.986E 00
X=  0.985E 00
X=  0.984E 00
X=  0.983E 00
X=  0.982E 00
X=  0.981E 00
X=  0.979E 00
X=  0.978E 00
X=  0.976E 00
X=  0.974E 00
X=  0.972E 00
X=  0.970E 00
X=  0.967E 00
X=  0.964E 00
X=  0.961E 00
X=  0.957E 00
X=  0.953E 00
X=  0.947E 00
X=  0.941E 00
X=  0.934E 00
X=  0.926E 00
X=  0.915E 00
X=  0.903E 00
X=  0.887E 00
X=  0.869E 00
X=  0.844E 00
X=  0.812E 00
X=  0.771E 00
X=  0.717E 00
X=  0.644E 00
X=  0.545E 00
X=  0.414E 00
X=  0.253E 00
X=  0.965E-01
X=  0.103E-01
```

Fig. 5 : Normalized concentration at the origin without and with mixing height fixed by, $\eta=0.5$

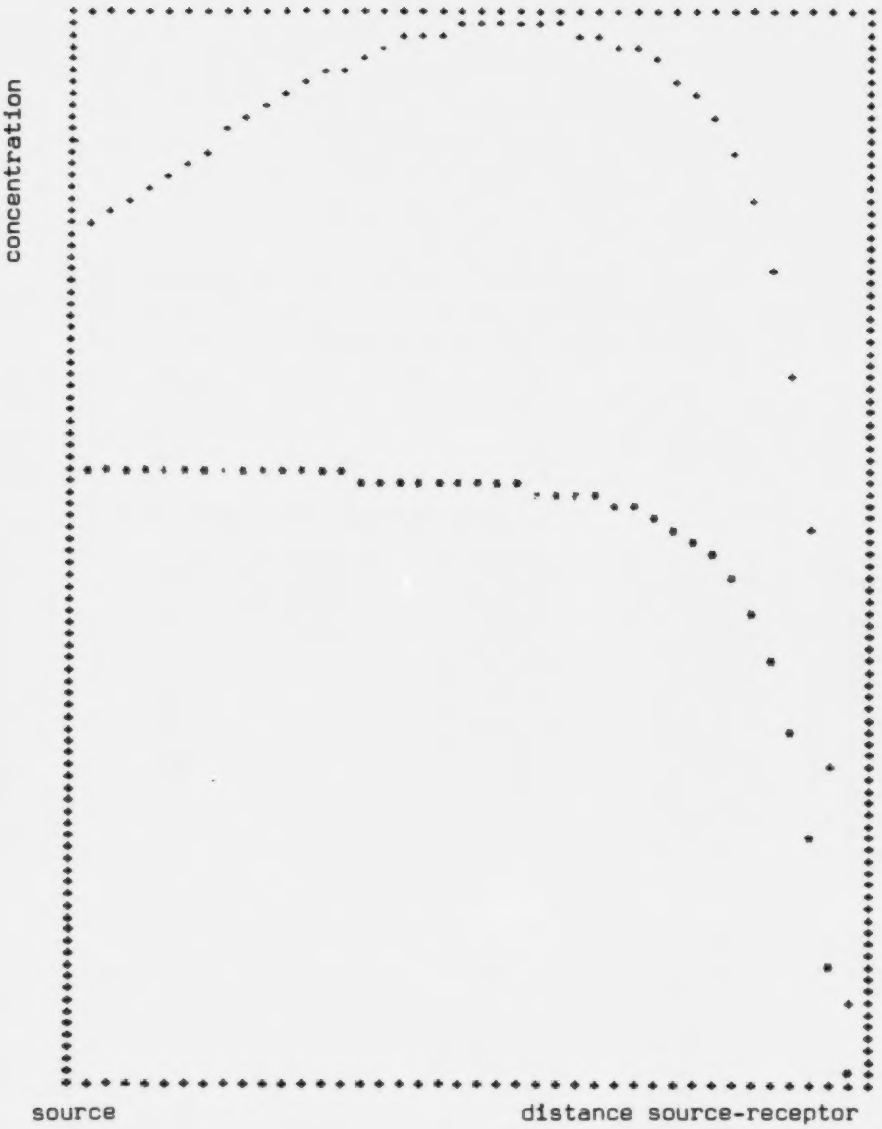

our solution ◆

```
XC= 0.139E 01
XC= 0.141E 01
XC= 0.143E 01
XC= 0.145E 01
XC= 0.147E 01
XC= 0.150E 01
XC= 0.152E 01
XC= 0.154E 01
XC= 0.156E 01
XC= 0.158E 01
XC= 0.160E 01
XC= 0.162E 01
XC= 0.163E 01
XC= 0.165E 01
XC= 0.167E 01
XC= 0.168E 01
XC= 0.169E 01
XC= 0.170E 01
XC= 0.171E 01
XC= 0.171E 01
XC= 0.172E 01
XC= 0.172E 01
XC= 0.172E 01
XC= 0.171E 01
XC= 0.171E 01
XC= 0.170E 01
XC= 0.169E 01
XC= 0.168E 01
XC= 0.167E 01
XC= 0.165E 01
XC= 0.163E 01
XC= 0.160E 01
XC= 0.156E 01
XC= 0.151E 01
XC= 0.143E 01
XC= 0.132E 01
XC= 0.115E 01
XC= 0.854E 00
XC= 0.126E 00
XC= 0.149E 00
```

Berlyand's solution ●

```
X= 0.994E 00
X= 0.993E 00
X= 0.993E 00
X= 0.992E 00
X= 0.992E 00
X= 0.992E 00
X= 0.991E 00
X= 0.991E 00
X= 0.990E 00
X= 0.989E 00
X= 0.989E 00
X= 0.988E 00
X= 0.987E 00
X= 0.986E 00
X= 0.985E 00
X= 0.984E 00
X= 0.982E 00
X= 0.981E 00
X= 0.979E 00
X= 0.977E 00
X= 0.975E 00
X= 0.972E 00
X= 0.969E 00
X= 0.965E 00
X= 0.961E 00
X= 0.956E 00
X= 0.949E 00
X= 0.942E 00
X= 0.932E 00
X= 0.923E 00
X= 0.904E 00
X= 0.884E 00
X= 0.856E 00
X= 0.818E 00
X= 0.765E 00
X= 0.687E 00
X= 0.571E 00
X= 0.403E 00
X= 0.190E 00
X= 0.263E-01
```

Fig. 6 : Normalized concentration at the origin without and with mixing height fixed by η =0.8

TABLE 3 : JOINT FREQUENCY FUNCTION FOR DEURNE FROM 1 APRIL TO 30 SEPTEMBER 1974 IF 96,5 PER CENT OF METEOROLOGICAL SITUATIONS ARE ENVISAGED (NO CALM WIND).

SECTOR	U1	U2	U3	U4	U5	U6
			FREQUENCY FUNCTION FOR STABILITY CLASS 1			
1	0.492110E-02	0.195450E-02	0.826050E-02	0.420000E-03	0.0	0.0
2	0.487230E-02	0.724130E-02	0.131328E-01	0.294330E-02	0.0	0.0
3	0.301300E-02	0.490030E-02	0.664760E-02	0.359820E-02	0.0	0.0
4	0.484150E-02	0.448310E-02	0.111979E-01	0.154290E-02	0.0	0.0
5	0.487510E-02	0.113407E-01	0.749330E-02	0.112850E-02	0.0	0.0
6	0.567040E-02	0.695280E-02	0.374940E-02	0.0	0.0	0.0
7	0.302980E-02	0.476310E-02	0.226810E-02	0.0	0.0	0.0
8	0.119570E-02	0.306620E-02	0.220650E-02	0.0	0.0	0.0
9	0.854100E-03	0.203850E-02	0.239420E-02	0.0	0.0	0.0
10	0.190130E-02	0.253980E-02	0.505990E-02	0.0	0.0	0.0
11	0.389220E-02	0.415270E-02	0.120968E-01	0.352920E-02	0.0	0.0
12	0.571520E-02	0.741770E-02	0.133232E-01	0.413870E-02	0.0	0.0
13	0.172210E-02	0.458670E-02	0.555550E-02	0.840100E-03	0.0	0.0
14	0.142810E-02	0.286460E-02	0.731130E-02	0.153450E-02	0.694400E-03	0.0
15	0.254800E-03	0.212250E-02	0.101702E-01	0.372140E-02	0.0	0.0
16	0.607600E-03	0.598680E-02	0.137293E-01	0.317260E-02	0.0	0.0
			FREQUENCY FUNCTION FOR STABILITY CLASS 2			
1	0.153450E-02	0.101926E-01	0.109151E-01	0.198250E-02	0.0	0.0
2	0.109210E-02	0.852930E-02	0.105595E-01	0.411910E-02	0.0	0.0
3	0.222890E-02	0.472390E-02	0.812890E-02	0.648240E-02	0.868000E-04	0.0
4	0.588000E-03	0.332380E-02	0.649360E-02	0.322300E-02	0.607600E-03	0.0
5	0.0	0.624160E-02	0.306060E-02	0.238860E-02	0.0	0.0
6	0.0	0.377460E-02	0.201610E-02	0.504000E-03	0.0	0.0
7	0.0	0.288420E-02	0.214770E-02	0.220930E-02	0.694400E-03	0.0
8	0.694400E-03	0.275540E-02	0.205250E-02	0.145610E-02	0.0	0.0
9	0.420000E-03	0.178650E-02	0.520270E-02	0.797210E-02	0.336300E-02	0.0
10	0.840100E-03	0.411630E-02	0.104727E-01	0.266745E-01	0.813730E-02	0.188730E-02
11	0.840000E-04	0.688000E-02	0.236027E-01	0.380628E-01	0.100246E-01	0.260400E-03
12	0.0	0.104139E-01	0.205477E-01	0.394517E-01	0.319500E-02	0.607600E-03
13	0.672000E-03	0.511310E-02	0.103019E-01	0.133316E-01	0.397070E-02	0.0
14	0.607600E-03	0.273020E-02	0.690240E-02	0.131768E-01	0.161850E-02	0.0
15	0.210290E-02	0.460630E-02	0.649640E-02	0.366820E-02	0.134410E-02	0.0
16	0.0	0.456710E-02	0.115115E-01	0.577400E-02	0.0	0.0
			FREQUENCY FUNCTION FOR STABILITY CLASS 3			
1	0.725530E-02	0.203593E-01	0.715450E-02	0.0	0.0	0.0
2	0.516070E-02	0.157286E-01	0.838930E-02	0.0	0.0	0.0
3	0.389780E-02	0.654960E-02	0.854990E-02	0.0	0.0	0.0
4	0.738690E-02	0.102850E-01	0.0	0.0	0.0	0.0
5	0.667560E-02	0.304660E-02	0.672000E-03	0.0	0.0	0.0
6	0.787970E-02	0.302420E-02	0.0	0.0	0.0	0.0
7	0.946500E-03	0.582160E-02	0.0	0.0	0.0	0.0
8	0.126010E-02	0.199650E-02	0.229890E-02	0.0	0.0	0.0
9	0.196010E-02	0.475190E-02	0.130210E-02	0.0	0.0	0.0
10	0.216170E-02	0.441310E-02	0.367380E-02	0.0	0.0	0.0
11	0.442150E-02	0.123936E-01	0.120912E-01	0.0	0.0	0.0
12	0.336580E-02	0.116291E-01	0.348900E-02	0.0	0.0	0.0
13	0.446350E-02	0.504310E-02	0.355060E-02	0.0	0.0	0.0
14	0.456430E-02	0.764730E-02	0.159610E-02	0.0	0.0	0.0
15	0.252300E-02	0.406310E-02	0.0	0.0	0.0	0.0
16	0.509630E-02	0.807290E-02	0.216170E-02	0.0	0.0	0.0

TABLE 1 : COEFFICIENT OF WIND PROFILE AS A FUNCTION OF WIND SPEED iw.

Wind speed classes		U_0
iw	speed interval (knots)	m sec^{-1}
1	0-3	1.50
2	4-6	2.46
3	7-10	4.47
4	11-16	6.93
5	17-21	9.61
6	> 21	12.52

TABLE 2 : MIXING HEIGHT AND THE PARAMETERS FOR U AND K_z AS A FUNCTION OF STABILITY CLASS is.

Stability class		L	m	K_1
is		m		m^{2-n} sec^{-1}
1	Unstable	1500	0.15	29.7
2	Neutral	1000	0.25	12.1
3	Stable	500	0.30	13.2

TABLE 4 : CONCENTRATION MEASURED AND CALCULATED FROM 1 APRIL TO 30 SEPTEMBER 1974.

RECEPTOR	CONCENTRATION			CONCENTRATION CALCULATED (μgr m^{-3})			
	MEASURED (μgr m^{-3})			GAUSSIAN MODEL	K-MODEL : 1974		
NAME	1972	1973	1974	LPADM : 1974	n=0	n=0.05	n=0.1
ZR721	46	44	42	18	18	17	16
ZR808	109	114	86	37	32	30	28
ZR809	119	126	118	37	34	32	30
ZR812	68	87	79	48	42	40	37
ZR813	101	115	94	39	34	32	30
ZR818	84	101	96	81	71	68	66
ZR819	84	116	91	57	50	48	45
ZR820	60	82	76	59	54	55	55
ZR821	76	89	91	49	51	49	46
ZR826	117	58	66	127	79	92	106

Rapporteur's Summary Report:

Prepared by: R. A. Porter

Papers covered by:
W. Kofler
J. Vanderborght
E. Runca
H. Schultz
A. Berger

Paper: The Austrian Alpes air pollution study
W. Kofler

Summary:

Measurements of sulfate, sulfur dioxide, and particulate were made throughout Austria in order to classify areas that would be suitable for recreation (little or no pollution) and areas that suffer moderate or significant air pollution. It is proposed that higher mixing heights during the winter allow more wide spread circulation of polluted air beyond the vallies.

Questions:

Slater: What was the relation of emissions in the winter and summer.

Answer: The emissions were higher in the winter.

Comment Slater: The higher emission rates could be the cause of higher observed concentrations in the winter instead of higher mixing heights.

Fischer: Were there any measurements of mixing height?

Answer: No.

Paper: Microscale Atmospheric Model
J. Vanderborght

A microscale model of the area around Liège, Belgium. The surface orography and thermal dishomogenity are found to be important factors. The surface studied ranges from 55 to 200 meters. The model considers 4 layers of equal pressure from the ground to 400 mb.

Initial efforts to solve the problem required too much computer time because of the calculation of high speed gravity waves. Adoption of a semiemperical model and a progressive grid scale system reduced computer time requirements to 2 hours.

Question Kwizak: Did you find problems with the boundary calculations.

Answer: Yes. We are not sure that the calculations at the boundaries.

Question Steenkist: How does the model calculations compare with observed wind fields.

Answer: We did not have enough observed data to make a comparison.

Question Padro: Has there been a scale analysis to validate the hydrostatic wind field assumptions.

Answer: The results show that on this small scale there is no problem.

Question Knox: Does your model generate artificial divergent and convergent winds that interfere with concentration calculations.

Answer: Only meteorology is considered with this model. Concentrations are not considered.

Paper: Air Pollution Studies using linked planetary boundary and K-models
E. Runca

Question Any validation?

Answer: No.

Question Williams: I would like your comments on the wind field exponent.

Answer: That is a worst case number, but even with this number we consider the performance very good.

Paper: Calculations of the Atmospheric Pollutant Dispersion by the Computer Program XPIC for instationary and inhomogeneous conditions
H. Schultz

Comment Knox:

The basic model has a mathematical error of 2 % when the source terms and key parameters are precisely known. The importance the wind field and other key parameters is illustrated by the fact that the model has validated within a factor of 2 65 % of the time with our best available wind field calculations.

Paper: A K-Analytical Model , including calm wind situations
A. Berger

Question Runca: I believe your analytical solution is inefficient in terms of computer time. What was the time required?

Answer: 6 minutes in the IBM 360.

Comment Berger: Our aim here was an academic investigation not development of a practical model, therefore, optimization of computer time usage was not considered.

8th NATO/CCMS INTERNATIONAL TECHNICAL MEETING ON AIR POLLUTION MODELING

TOPIC 8

TRANSNATIONAL AIR QUALITY MODELING

8th International Technical Meeting
on Air Pollution Modeling and its Application

PSEUDOSPECTRAL DISPERSION MODELING

Lars P.Prahm
Danish Air Quality Laboratory, Ministry of Environment
Risø National Laboratory
DK 4000,Roskilde,Denmark

Ruwim Berkowicz
Danish Meteorological Institute
Air Pollution Section,Lyngbyvej 100
DK 2100,Copenhagen,Denmark

September 2o-23 1977
Louvain-La-Neuve
Belgium

1. INTRODUCTION

Atmospheric dispersion modelling is applied in urban areas, local scale, in cross boundary studies, regional scale, and in studies of the whole troposphere and stratosphere, global scale. Real world is described in simplified models in one, two or three space dimensions. 1-D models describe all atmospheric dispersion by an artificial (vertical) diffusion, while 2-D and 3-D models include both advection and diffusion. Atmospheric chemistry might be included in all types of transport modelling. The meteorological model might be dynamic, i.e. based on solution of the equations of motion, or it can be non-dynamic operating on observed or computed winds. Both the dynamic and non-dynamic model is time-dependent. Further simplicity is obtained with stationary models such as the Gaussian plume model for local scale. Time-dependent models might be Eulerian referring to a fixed coordinate system in space, or they can be Lagrangian following a parcel of air. Also hybrid methods exist.

The Lagrangian type of model, i.e. a trajectory model, is often preferred treating single sources, resulting in a good spatial resolution especially close to the source. Eulerian models have advantages for a multiple source model, because most input information is referred to an Eulerian grid (coordinate system), and because interaction between different source areas and plumes can be treated without supplementary algorithms.

Transport and diffusion is in Eulerian models usually described by the dispersion equation giving the time and space variation of the concentration of a component c:

$$\frac{\partial c}{\partial t} = -\underset{\substack{\downarrow \\ \text{advec-} \\ \text{tive} \\ \text{flux}}}{\overline{\nabla}\cdot(\overline{v}c)} + \underset{\substack{\downarrow \\ \text{diffu-} \\ \text{sive} \\ \text{flux}}}{\overline{\nabla}(D\nabla c)} + \text{production} + \text{sink} \qquad (1)$$

where $\overline{v}$ is the wind velocity vector and D is the eddy diffusivity tensor.

Most numerical solutions of this equation ensures stability of the numerical scheme, however, the numerical errors are often considerable. Largest numerical errors are usually introduced by the advection term. A new numerical integration technique - the pseudospectral dispersion model - has recently been developed by Christensen & Prahm (1976). This model was compared with

18 other numerical methods and is found to be the most accurate applicable model presently available.

2. PSEUDOSPECTRAL, SPECTRAL AND FINITE DIFFERENCE METHODS

Numerical solution of eq. (1) is in most cases performed by the grid point method. In this method a set of points is introduced in the region of interest and dependent variables are initially defined and subsequently computed at these points. The set of points is called the grid. If the grid points are fixed in space, the system of equations is Eulerian and space and time coordinates are chosen as independent variables.

The most common way of solving the governing equations by grid point methods is to find approximate expressions for derivatives appearing in the equations. These approximate expressions are defined using only values of the dependent variables at the grid points and at discrete time intervals. Thus, they are formed using differences of dependent variables over finite space and time intervals. For that reason this approach is called the finite difference method. A number of various, more or less sophisticated finite difference methods have been developed in the last years. A review of such methods is recently given by Mesinger and Arakawa (1976).

Special effort has been directed towards the solution of the equation of motions. Such problems as numerical dispersion, pseudodiffusion or distortion of the energy spectrum inspired various researches to develop numerical schemes where the errors connected with the mentioned effects are minimized (Arakawa, 1966, 1972; Orszag,1971a). However, these methods are usually very difficult to treat and require much of computer time.

Another possible approach is to express the spatial dependence of the variables in terms of finite series of orthogonal functions, and then substitute this into the governing equations. In this way the equations reduce to a set of ordinary differential equations, and the coefficients of the series can be computed as function of time. This is the spectral method of solving the governing equations. The original idea of using truncated (finite) orthogonal series to solve differential equations was given by the Russian engineer Galerkin (1915). Orszag (1971b) adapted this method for solution of the hydrodynamic equations. Until recently the spectral method was considered to be inefficient compared with the grid point method. But the use of the fast Fourier transform has completely changed the situation and investigation of spectral methods is now the subject of intensive research.

Further development of the spectral methods is due to use of the pseudospectral approximation (Fox and Orszag, 1973; Christensen and Prahm, 1976). Here the expansion in the truncated Fourier series is used only to compute the space derivatives, whereas the local products and the time integration are evaluated on the grid points in the real space. The procedure used in the pseudospectral approximation is as follows:

The discrete set of values of the dependent variable (e.g. the concentration field c) is replaced by a continuous function given by the finite Fourier series,

$$c(x,t) = \sum_{k_n} \tilde{c}(k_n,t)e^{ik_n x} \qquad (2)$$

where $\tilde{c}(k_n,t)$ are the Fourier coefficients of $c(x,t)$ at the time t. The "wave vectors" k_n are given by

$$k_n = \frac{2\pi}{N\Delta x}n \qquad (3)$$

where n assumes integer values within limits

$$-\frac{N}{2} < n \leq \frac{N}{2} \qquad (3.a)$$

and N is the number of the grid points. Δx is the spacing of the grid points. Periodic boundary condition is assumed, i.e.

$$c(x + N\Delta x,t) = c(x,t) \qquad (4)$$

Fourier coefficients are computed by means of the Discrete Fourier Transform

$$\tilde{c}(k_n,t) = \frac{1}{N}\sum_{x_m} c(x_m,t)e^{-ik_n x_m} \qquad (5)$$

where values of the concentration field are taken at the grid points,

$$x_m = m\cdot\Delta x; \qquad m = 0,\ldots\ldots, N-1 \qquad (6)$$

The space derivatives can now be evaluated on grid points using (2) and (5),

$$\frac{\partial c}{\partial x}(x_m,t) = \sum_{k_n} ik_n\tilde{c}(k_n,t)e^{ik_nx_m} \tag{7}$$

If space derivatives in more than one dimension are required, the procedure described above can be repeated for each space dimension. All other calculations are provided on grid points only. The flow diagram illustrating the method is given in Fig.1. For time integration one of the standard linear integration procedures can be used. In the initial stage of the present work a second-order midpoint-rule integration (leap-frog) was used. The third-order linear multistep procedure (Adams-Bashforth), (Prahm and Christensen, 1977) was, however, found to be more economical and accurate. Expansion in the finite Fourier series (2) corresponds to an a priori assumption of the behaviour of the function between the grid points. The real behaviour is, however, not known. The solution obtained by the pseudospectral method corresponds thus to the hypothetical distribution given by eq. (2). In Fig.2 is shown the functional behaviour of a δ-like initial concentration field (e.g. an instantaneous point source) calculated by means of the finite Fourier expansion.

In the same figure is presented an one-dimensional cross-section of a Fourier expanded concentration field corresponding to a homogeneous source of a unit area. Fourier coefficients of this distribution are computed by means of a continuous Fourier Transformation but only components in the limits given by (3.a) are retained when the values on the grid points are computed (Berkowicz and Prahm, 1977b). The negative values appearing in the distribution obtained by means of the finite Fourier expansion seems to be physically unrealistic. However, the space derivatives calculated by means of (7) preserve the information about the single waves in the Fourier expansion. The numerical integration obtained by means of the pseudospectral method represents correctly the physical problem approximated by the finite Fourier series, because information on each single wave is conserved during the integration. This is not the case when a finite difference method is used. This subject is discussed further.

3. ADVECTION TEST

It is important to test the applicability of the pseudospectral method for advection computations. The usual test is a rotation of a conical distribution in a uniform circular velocity field. The analytical function describing the cone is a distribution $c(\bar{x},t)$

$$c(\bar{x},t=0) = \begin{cases} Q(1-\frac{|\bar{x}'|}{r}), & |\bar{x}'|\leq r \\ 0 & |\bar{x}'|>r \end{cases} \tag{8}$$

where $\bar{x}' = \bar{x}-\bar{x}^o$ is the position vector and r is the base radius of a cone with a maximum value Q at the cone center situated in $\bar{x}^o$. The uniform circular velocity field, centered at $\bar{x}^*$ is given by: $\bar{v} = \Omega(x_2-x_2^*,-x_1+x_1^*)$. The indices refer to the two spatial coordinates. Following values were used in the test (Christensen and Prahm, 1976): Q=1ooo, r=2, $\bar{x}^o=(5,9)$ and $\bar{x}^*=(9,9)$. The components of the vectors are given in grid point units. Fig. 3a shows the initial distribution and Fig.3b the cone after rotation of 2π through 8oo time steps. The maximum error introduced by the rotation is less than 2% of the center value.

Christensen and Prahm (1976) summarized the published results of similar tests and found that methods based on orthogonal functions have the highest accuracy and only slightly increased computation time compared with the higher order finite difference methods, if the same number of gridpoints is used. If a certain level of accuracy is required, the pseudospectral model is the most economical one with respect to computer time.

4. COMPUTATIONAL DISPERSION

The high accuracy of the pseudospectral approximation in solving the advection equation is, as mentioned above, due to absence of phase speed errors characteristic for finite difference schemes. To illustrate this, we consider an one dimensional linear advection equation,

$$\frac{\partial c(x,t)}{\partial t} = - v\frac{\partial c(x,t)}{\partial x} \tag{9}$$

where v is constant.

Equation (9) has a solution in form of a single harmonic wave,

$$c(x,t) = A(k,t)e^{ikx} + A^*(k,t)e^{-ikx} \tag{1o}$$

provided that

$$\frac{dA(k,t)}{dt} + ikvA(k,t) = 0 \tag{11}$$

Eqs. (lo) and (11) describe a single harmonic wave propagating with a phase speed $v_f=v$. It is seen that waves of all wave length are propagated with the same phase speed. There is no dispersion.

In the pseudospectral approximation the space derivative of (lo), where $A^*(k,t) = A(-k,t)$ is given by,

$$\frac{\partial c(x,t)}{\partial x} = ikA(k,t)e^{ikx} - ikA(-k,t)e^{-ikx} \tag{12}$$

Substitutions of (12) into (9) leads again to (11). In the pseudospectral approximation all waves propagate with constant phase speed $v_f=v$ and there is no dispersion. However, because the amplitudes of the wave components are computed, using a discrete grid point system, and from the periodicity condition, we have,

$$A(\pi/\Delta x,t) = A(-\pi/\Delta x,t) \tag{13}$$

where $\pi/\Delta x$ is the highest wave number in the finite Fourier expansion and Δx is the grid point spacing. Substitution of (13) into (12) yields,

$$\frac{dA(\pi/\Delta x,t)}{dt} = 0 \tag{14}$$

In the pseudospectral approximation the phase speed of the wave component with $k = \pi/\Delta x$ is zero. The highest Fourier component cannot be advected in the pseudospectral approximation. In the full spectral method where the time integration is outlined in the Fourier space the $A(\pi/\Delta x,t)$ component can be resolved from the $A(-\pi/\Delta x,t)$ component and in this case no phase speed errors exist.

If a finite difference scheme, e.g. the second order centered finite difference approximation is used to compute the space derivatives, we have

$$\frac{\partial c(x,t)}{\partial x} = \frac{c(x+\Delta x,t) - c(x-\Delta x,t)}{2\Delta x} \tag{15}$$

Substitution of (15) into (9), together with (lo) yields,

$$\frac{dA(k,t)}{dt} + ik\{v\frac{\sin k\Delta x}{k\Delta x}\}A(k,t) = 0 \tag{16}$$

Instead of the constant phase speed $v_f = v$, we see that waves now propagate with the phase speed

$$v_f = v\frac{\sin k\Delta x}{k\Delta x} \qquad (17)$$

This phase speed is a function of the wave number k, thus the finite differencing in space causes a dispersion of the waves, the so called computational dispersion. For $k = \pi/\Delta x$ we again obtain $v_f = 0$. The "slowing-down" of the short-wave components is characteristic for centered finite difference methods. Uncentered finite difference methods leads to a complex phase speed factor. Due to the imaginary part,the amplitudes of the single waves are attenuated during the integration. This effect is called pseudodiffusion, because the attenuation factor increases with increasing wave number as would be in the case of a non-zero diffusivity. Pseudodiffusion can often mask the real physical diffusion thereby distorting the solution of the advection-diffusion equation.

Comparison between the phase speed dependence on the wave number for the pseudospectral and second-order centered finite difference approximation is shown in Fig.4.

The present discussion explains the high accuracy of the pseudospectral method compared with finite difference methods.

5. ALIASING ERROR

In the pseudospectral approximation the functional behaviour of all variables is approximated by the finite Fourier series with the wave numbers in the limits

$$-K_{max} < k \leq K_{max} \qquad (18)$$

where

$$K_{max} = \pi/\Delta x \qquad (19)$$

Products of two space dependent variables in eq. (1) will in general contain Fourier components exciding the limits given by (18). As a simple example we consider the product p(x) of two functions a(x) and b(x) defined on the given grid point system. Fourier expantion of each of the two functions is,

$$a(x) = \sum_{-K_{max}<k\leq K_{max}} A(k)e^{ikx}$$

$$b(x) = \sum_{-K_{max}<k\leq K_{max}} B(k)e^{ikx} \tag{20}$$

The product $p(x) = a(x)\cdot b(x)$ will thus contain terms like

$$A(k_1)B(k_2)e^{i(k_1+k_2)x} \tag{21}$$

where in general

$$-2K_{max}<k_1+k_2\leq 2K_{max} \tag{22}$$

or using the solid state terminology, wave components outside the first Brillouin Zone (BZ). However, in the pseudospectral approximation the product $p(x)$ is also defined on the discrete grid point system. On the given grid point system the Fourier expansion of $p(x)$ is,

$$p(x) = \sum_{-K_{max}<k\leq K_{max}} P(k)e^{ikx} \tag{23}$$

where $P(k)$ will be given by,

$$P(k) = \sum_{-K_{max}<k_1\leq K_{max}} A(k_1)B(k-k_1) + \{\sum_{-K_{max}<k_1\leq K_{max}} A(k_1)\cdot(B(k-k_1+2K_{max})+B(k-k_1-2K_{max}))\} \tag{24}$$

where

$$-K_{max}<k,\ k-k_1,\ k-k_1\pm 2K_{max}\leq K_{max}$$

The term in the square brackets belongs in fact to wave components with the wave number $k\pm 2K_{max}$, thus outside the first BZ, but on the finite grid point system this component cannot be resolved from the component with the wave number k of the first BZ. This results in appearing of high wave components as low wave components inside the first BZ. This effect is called aliasing error. It leads e.g. to errors in space derivatives or can cause computational instabilities.

Orszag (1971b) developed a transform method which removes the aliasing terms. The product of two space dependent functions is computed on a twice as large grid point system what makes possible to resolve the aliasing Fourier components. Use of Orszag's transform method, however, usually increases computation time by factor of 3 - 4. Christensen and Prahm (1976) developed a method which at cost of some loss of accuracy can minimize the aliasing error without essential consumption of computation time. This approach is based on the assumption that one of the functions in the non-linear products (e.g. the velocity field or diffusion coefficient) is fairly slowly varying quantity on the grid. More specifically, it means that these quantities essentially can be represented by fairly longwave Fourier components. If now, the concentration field at each time step is "filtered" by a low-pass filter with respect to Fourier components, most of the aliasing terms will belong to the "cut-off" aliasing zone and the aliasing error is thereby minimized. Several tests (Christensen and Prahm, 1976) show that this method is quite effective in practical applications.

Aliasing error is characteristic for all grid point methods, also finite difference methods. In the full spectral method the aliasing terms can be removed because the products are computed in the Fourier space. However, the spectral method is known to be very time consuming and until now it was not used in practical applications for atmospheric dispersion computations.

6. BOUNDARY CONDITIONS

The use of Fourier series implies periodic boundary conditions. In the case of advection it means that a distribution $c(\overline{x},t)$ which is advected out over one boundary appears again on the opposite boundary. Physically it is not acceptable. Christensen and Prahm (1976) developed a method which makes it possible to avoid the effect connected with periodicity of the Fourier series. The method consists in adding a sink term at the boundary. The term is of the form

$$S = -\frac{c(\overline{x},t)}{\tau} \tag{25}$$

where τ is some appropriate decay time. When the sink term (25) is added to eq. (1), one can easy see that it results in an exponential decay of the concentration at the boundary, i.e.

$$c(x,t+\Delta t) = c(x,t)e^{-\frac{\Delta t}{\tau}} \tag{26}$$

at the boundary.

If the decay time τ is chosen properly, all mass transported to the boundary is removed at the boundary and is not appearing at the opposite boundary, as would be the case without the sink term. The value of τ can be found from the following considerations. The mass, that cross the boundary per unit area at an infinitesimally short time Δt is

$$\Delta M = c \cdot v_{\perp} \cdot \Delta t \tag{27}$$

where $v_{\perp}$ is the component of velocity perpendicular to the boundary. The rate at which the mass must be removed from the boundary is thus

$$\frac{\partial M}{\partial t} = - c \cdot v_{\perp} \tag{28}$$

Approximating M by $M \approx c \cdot \Delta x$, where Δx is the grid point spacing perpendicular to the boundary, we obtain

$$\frac{\partial c}{\partial t} = - c \frac{v_{\perp}}{\Delta x} \tag{29}$$

from (29) it follows that the appropriate choice of τ is

$$\tau = \frac{\Delta x}{v_{\perp}} \tag{3o}$$

Christensen and Prahm (1976) used two outermost rows and columns as boundary decay region. The decay length is thus equal to three grid point spacings. Substituting (3o) into (26) and with $t = 3 \cdot \Delta x / v$, we obtain that the decay factor is e^{-3}, thus only about 5% can be transported through the "boundary". In order to illustrate the discussed method we consider an one-dimensional linear advection equation with a continuous point source.

$$\frac{\partial c}{\partial t} = -v \frac{\partial c}{\partial x} + Q + S \tag{31}$$

where Q is the source strength and in our example we situate the source on the sixth grid point in the upstream direction. S represents the sink terms defined by (25) and the velocity v=1. 16 grid points are used in computations. In Fig.5 results are shown for the steady state case, i.e. $\frac{\partial c}{\partial t} = 0$, or no change in concentration distribution at the subsequent time steps.

In the case of a non-zero diffusivity, similar considerations give a sink term of the form

$$S = D \cdot \frac{\partial c}{\partial x} \cdot \frac{1}{\Delta x} \tag{32}$$

Non-periodic boundary conditions for diffusion are discussed by Berkowicz and Prahm (1977a). In this paper a pseudospectral, two-dimensional model for dispersion and dry deposition of atmospheric pollutants is developed. Dry deposition is usually treated as a boundary condition problem (Calder, 1961). In this formulation the vertical diffusive flux at the ground is assumed proportional to the concentration at the ground level,

$$F_d = \{D(z)\frac{\partial c}{\partial z}\}_{z=0} = V_d \cdot c(z=0) \tag{33}$$

The factor of proportionality, V_d is called the deposition velocity. In the case of $V_d=0$, the boundary condition to be satisfied is $\frac{\partial c}{\partial z} = 0$ at $z=0$. This condition is satisfied if the concentration is represented by cosine-Fourier series. In fact, it means, that Fourier series are used with the additional requirement,

$$c(z) = c(-z) \tag{34}$$

If the concentration field and other variables are defined on N+1 grid points 2N points are used to perform Fourier Transformations.

With the condition (34) the vertical diffusive flux is zero at the boundary. In order to account for the removal of the material by dry deposition, a sink term is introduced, which is acting only on the lower boundary (z=0) and which is defined as,

$$S(x,0) = -2 \cdot V_d \cdot c(x,0) \cdot \frac{1}{\Delta z} \tag{35}$$

The factor 2 in (35) appears because of the symmetric form of all source and sink terms as required by the condition (34). The sink term (35) accounts properly for the decrease of the total horizontal flux, in spite of $\frac{\partial c}{\partial z} = 0$ at the boundary. In Fig.6 are shown some vertical concentration profiles computed by the pseudospectral approximation in the case of constant diffusivity and wind velocity profiles. The deposition velocity $V_d = 0.01 \cdot V$. The numerical results are compared with the analytical solution given by Smith (1962). The agreement between the numerical and analytical solution is very good. The relative error is less than 5%, being somewhat larger only at the surface.

The pseudospectral model was also applied for simulation of dry deposition with diffusivity and wind velocity profiles corresponding to different atmospheric stability conditions (Berkowicz and Prahm,1977a). New, interesting results were obtained compared with other, less sophisticated deposition models.

The presented examples show, that the newly developed pseudospectral models, based on finite Fourier series can be used to solve practical dispersion problems with various, not necessary periodic boundary conditions.

7. REGIONAL TRANSPORT MODEL

The first practical application of the pseudospectral model (Prahm and Christensen, 1977) is here presented in summary.

The pseudospectral model is applied on the European area with the characteristic dimensions of 4000 x 4000 km^2 and grid point distances of about 100 km. A model simulation of sulphur oxide concentrations is performed for a three- and four-day episode in August and September 1974. Computed concentrations are compared with ground level and aircraft measurements. The influence of local sources is examined by correlating ground level measured concentrations with the surrounding emissions.

8. MODEL DESCRIPTION

The following two coupled partial differential equations gives a mathematical description of transport, diffusion, oxidation and deposition of the SO_2 - $SO_4^=$ system.

$$\frac{\partial C_1}{\partial t} = - \bar{v}\cdot\bar{\nabla}C_1 + D\nabla^2 C_1 + S_1 - \frac{C_1}{\tau_1} \qquad (36)$$

$$\frac{\partial C_2}{\partial t} = - \bar{v}\cdot\bar{\nabla}C_2 + D\nabla^2 C_2 + S_2 + \frac{3}{2}\frac{C_1}{\tau_3} - \frac{C_2}{\tau_2} \qquad (37)$$

All symbols are explained in Table 1. The rate of change in SO_2 and $SO_4^=$ concentrations is determined by advection, turbulent diffusion, sources and sinks.

a) Sulphur emission

The third term at the right-hand side of the equations, S_1 and S_2, represents the SO_2 and $SO_4^=$ emission per time and area unit. The pseudospectral model applies a detailed emission field based on a survey conducted by OECD as a part of the project: "Long Range Transport of Atmospheric Pollutants". Information on seasonal and daily variations showed a range of about ± 3o% in total emission in a country. In this study we have used a constant emission field equal to the yearly average emission. Errors on emission information are assumed not to be systematically biased but random.

b) Wind velocity fields

Wind fields are prepared by the Norwegian Institute for Air Research in cooperation with the Norwegian Meteorological Institute. Wind velocities are interpolated spatially in order to obtain values at all grid points. Linear time interpolation is applied for each time step in the numerical integration. Both ground level and 85o mb wind fields are used. The present model is 2-dimensional with one layer in the vertical direction. Instantaneous mixing is assumed through the whole mixing depth, which in the calculations is assumed to be 1ooo metres. Considerable errors are introduced by the loss of the vertical variation on wind and mixing height.

c) Decay and oxidation

The fourth and fifth term on the right-hand side of the equations describes decay of SO_2 and $SO_4^=$ and the production of $SO_4^=$ through oxidation of SO_2. The total sink of SO_2 is well described by a dry deposition rate, which using a mixing depth of 1ooo metres corresponds to an average lifetime of 18.5 hours. Sources within a grid cell create plumes which are not fully mixed up to the assumed mixing height of 1ooo metres. The ground level SO_2 concentration and the resulting dry deposition is therefore systematically underestimated. In order to correct this error, 15% of the total sulphur emission is deposited locally.

The dry deposition velocity for submicron particles during stable atmospheric conditions is roughly between o.1 and o.5 cm/sec over different surfaces (Slade, 1968). Recent experiments over the Atlantic gives about o.4 cm/sec (Prahm et al., 1976). An average $SO_4^=$ lifetime of 7o hours is used in this study. Wet deposition is not treated separately caused by lack of observations.

The rate of oxidation of SO_2 to $SO_4^=$ varies with the physical and chemical environment of the SO_2 - $SO_4^=$ system. Most data show a conversion rate of about 1% per hour, and in this regional model is used an equivalent transformation time of 14o hours. To take account of the more rapid oxidation in stacks, of plumes in the initial stages and of sources in the urban and industrial polluted atmospheres, 5% of the SO_2 is instantaneously oxidated to $SO_4^=$ expressed by the S_2 term in the second equation. The S_1 term in the first equation represents thus 8o% of the total sulphur emitted.

d) Diffusion

The second term at the right-hand side of equations (1) and (2) represents the horizontal turbulent diffusion. In the present computations a constant eddy diffusivity is assumed. Using values in the range from 3oo to 3oooo m^2/sec it was found that the diffusive term has only an influence of 2-3% on the regional concentration level. Most simple numerical methods introduce an uncontrolled numerical diffusion, and often this error is significantly larger than the physical diffusion. The pseudospectral model applied in this study completely avoids this important numerical error.

e) Numerical method

The numerical integration of the two coupled dispersion equations (1) and (2) is performed, using the 2-dimensional pseudospectral model developed by Christensen and Prahm (1976). The model makes use of a fast Fourier Transform (Cooley and Tukey, 1965), which requires the concentration to be complex. We take advantage of this feature by using the complex concentration $C = C_1 + iC_2$, where $i = \sqrt{-1}$. In this way the original pseudospectral model is used with very small changes for simultaneous integration of SO_2 and $SO_4^=$ concentrations. Since both C_1 and C_2 are real, it is always possible to separate the SO_2 and the $SO_4^=$- concentrations.

Time integration is undertaken using the third-order linear multistep (Adams-Bashforth)-procedure. This procedure and the stability considerations are discussed by Prahm & Christensen (1977). No special effect is taken to optimize the computational speed or storage requirements. For operational use the actual model might easily be improved saving about 1o% of present resources. About 5 minutes CPU time is used for a one-week computation on a

IBM 17o/165 computer, which is modest compared with the time resolution, space resolution and the geographical area covered. Storage requirements depend on the compiler used and on the organization of variables. About 16o K octahedral bytes are used for data allocation, and a total of about 25o K octahedral bytes are used running the present version of the model with a grid size of 32 x 32 mesh points.

9. MEASUREMENTS

As a part of the OECD LRTAP study 3o to 7o ground based measurement stations have been operated, distributed in all participating countries. SO_2 in gas phase and sulphur at aerosols ($SO_4^=$) were sampled as 24-hour mean values.

Daily data from about 3o stations operating in 1974 are used in this study. Detailed discussion of the network, sampling methods, chemical analyses and data quality is given by NILU (1976). Short time average concentrations with no influence from single local sources are measured by aircraft. During the OECD project a number of aircraft sampling measurements was arranged. The route ran along the Swedish west coast on August 26 1974. The aircraft sampling was performed by NILU (Gotaas, 1975), and the results are used in this work for comparison with computed concentrations. Both the ground level measurements and the aircraft sampling values are compared with computed concentrations during selected weather conditions.

1o. CASE STUDIES

During anti-cyclonic weather conditions a subsidence inversion is often created over a large part of Western Europe. Atmospheric dispersion of pollutants in the vertical direction is then confined to a well-defined mixing layer and relatively large concentrations occur especially due to distant sources. Such episodes are favourable situations for comparison between computed and measured concentrations. A three-day episode from August 25 - 27 1974 and a four-day episode from September 13 - 16 1974 is selected for comparison between measured and computed concentrations. The criterion for the selection is the relatively large variation in measured concentrations during these episodes.

11. RESULTS OF THE REGIONAL MODEL STUDY

Comparison between measured and computed values are described in detail by Prahm and Christensen (1977). The main results are:

- The pseudospectral dispersion model (Christensen and Prahm, 1976) of high numerical accuracy, avoiding numerical diffusion, is shown to be applicable for regional 2-dimensional simulations,

- computed concentration patterns over Europe reflect the variable meteorological conditions,

- correspondance between computed and measured concentrations is much better than correspondance between measured concentrations and local emissions, indicating that distant anthropogenic sources are of major importance for rural sulphur pollution,

- correlation between computed and measured 24-hour mean concentrations gives correlation coefficients (r) between o.4 and o.8, using more than 4oo measured values,

- correlation between ½-hour mean aircraft measurements and computations (8 samples) gives a correlation coefficient (r) larger than o.9,

- mean values of measured and computed concentrations averaged in time and space deviate less than 2o%.

Special information on the numerical simulation and on possible model improvements was obtained:

- A diffusivity describes the dispersion not accounted for by variation of the mean wind (time step = 15-3o minutes). This diffusivity is found only to change the maximum computed concentrations 2-3%, stressing the necessity of application of a numerical method, which avoids numerical diffusion,

- ground level winds are too slow to represent the average transport in the mixing layer,

- 85o mb winds are applicable for the dispersion model although winds from a height between ground level and the 85o mb surface represent a more accurate mean transport height for the mixing layer up to looo metres,

- application of detailed precipitation fields would improve model results,

- inclusion of a dry deposition velocity as function of surface characteristics and atmospheric stability would be an advantage,

- improved information on the vertical structure of the atmospheric boundary layer, giving a variable mixing height, would improve results of long term time series correlation and of correspondance between short term mean values, measured and computed.

Based on the experience from this research the regional pseudospectral dispersion model might be applied for forecasting of regional air pollution episodes, using prognostic meteorological data from weather forecasting models. The model might also be applied for study of the relative influence of regional pollution sources compared with local sources. Such studies are of special importance for assessment of the impact of both national and international emission regulation strategies.

ACKNOWLEDGEMENTS.

This study is partially based on interpretation of results published with participation of Ove Christensen.

The research is supported by the Danish National Technical Scientific Research Council.

REFERENCES

Arakawa, A., 1966: Computational design for long term numerical integration of the equations of fluid motion: Two dimensional incompressible flow. Part I. J.Comput. Phys., 1, 119-143.

Arakawa, A., 1972: Design of the UCLA general circulation model. Numerical Simulation of Weather and Climate. Dept. of Meteorology, Univ. of California, Los Angeles, Tech.Rept., 7, 116 pp.

Berkowicz, R., and L.P. Prahm, 1977a: Pseudospectral simulation of dry deposition from a point source. Presented at the international symposium on sulfur in the atmosphere, September 7-14, 1977, Dubrovnik, Yugoslavia. To be publ. Atmos.Env., 12, (1978), No. 1.

Berkowicz, R., and L.P. Prahm, 1977b: Sub-grid scale information in the pseudospectral model. Submitted to J.Atm.Sci.

Calder, K.L., 1961: Atmospheric diffusion of particulate matter, considered as a boundary value problem. J.Meteor., 18, 413-416.

Christensen, O., and L.P. Prahm, 1976: A pseudospectral model for dispersion of atmospheric pollutants. J.Appl.Meteor., 15, 1284-1294.

Cooley, J.W., and J.W. Tukey, 1965: An algorithm for the machine calculation of complex Fourier series. Math.Comp., 19, 297-3ol.

Fox, D.G., and S.A. Orszag, 1973: Pseudospectral approximation to two-dimensional turbulence. J.Comput.Phys., 11, 612-619.

Galerkin, B.G., 1915: Series occurring in some problems of elastic stability of rods and plates. Eng.Bull., 19, 897-9o8. (In Russian)

Gotaas, Y., 1975: Aircraft sampling of sulphur dioxide and sulphates. Norwegian Institute for Air research, Report LRTAP, No. 7/75.

Mesinger, F., and A. Arakawa, 1976: Numerical methods used in atmospheric models. GARP Publications Series. No. 17, Vol 1.

NILU, 1976: European Monitoring Programme, Manual for sampling and chemical analysis procedures. Norwegian Institute for Air Research, Lillestrøm, Norway. Report 1/76.

Orszag, S.A., 1971a: On the elimination of aliasing in finite-difference schemes by filtering high-wave number components. J.Atm.Sci., 28, 1o74.

Orszag, S.A., 1971b: Numerical simulation of incompressible flows within simple boundaries. I. Galerkin (spectral) representations. Stud. Appl.Math., 5o, 293-326.

Prahm, L.P., U. Torp and R.M.Stern, 1976: Deposition and transformation rates of sulphur oxides during atmospheric transport over the Atlantic. Tellus, 28, 355-372.

Prahm, L.P. and O. Christensen, 1977: Long range transmission of pollutants simulated by the 2-D pseudospectral dispersion model. To be publ. J.Appl.Meteor., Sept-1977.

Slade, D.H., 1968: Meteorology and Atomic Energy. TID 2419o.

Smith, F.B., 1962: The problem of deposition in atmospheric diffusion of particulate matter. J.Atmos.Sci., 19, 429-434.

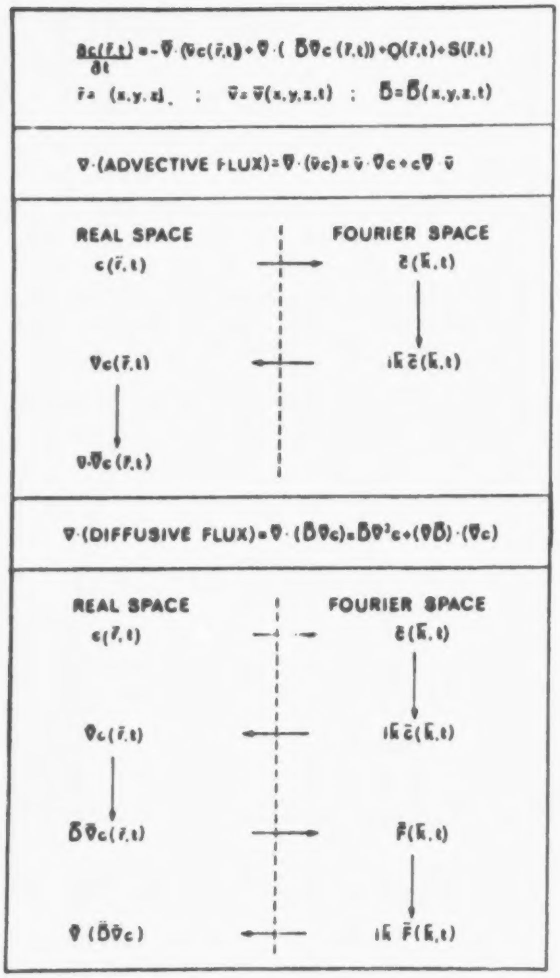
$\frac{\partial c(\vec{r},t)}{\partial t} = -\nabla\cdot(\vec{v}c(\vec{r},t)) + \nabla\cdot(\bar{\bar{D}}\nabla c(\vec{r},t)) + Q(\vec{r},t) + S(\vec{r},t)$
$\vec{r} = (x,y,z)$; $\vec{v} = \vec{v}(x,y,z,t)$; $\bar{\bar{D}} = \bar{\bar{D}}(x,y,z,t)$
$\nabla\cdot$(ADVECTIVE FLUX)$=\nabla\cdot(\vec{v}c) = \vec{v}\cdot\nabla c + c\nabla\cdot\vec{v}$
REAL SPACE
FOURIER SPACE
$c(\vec{r},t)$
$\tilde{c}(\vec{k},t)$
$\nabla c(\vec{r},t)$
$i\vec{k}\tilde{c}(\vec{k},t)$
$\vec{v}\cdot\nabla c(\vec{r},t)$
$\nabla\cdot$(DIFFUSIVE FLUX)$=\nabla\cdot(\bar{\bar{D}}\nabla c) = \bar{\bar{D}}\nabla^2 c + (\nabla\bar{\bar{D}})\cdot(\nabla c)$
REAL SPACE
FOURIER SPACE
$c(\vec{r},t)$
$\tilde{c}(\vec{k},t)$
$\nabla c(\vec{r},t)$
$i\vec{k}\tilde{c}(\vec{k},t)$
$\bar{\bar{D}}\nabla c(\vec{r},t)$
$\tilde{F}(\vec{k},t)$
$\nabla(\bar{\bar{D}}\nabla c)$
$i\vec{k}\,\tilde{F}(\vec{k},t)$

FIG. 1: FLOW DIAGRAM ILLUSTRATING PRINCIPLES OF THE PSEUDOSPECTRAL METHOD

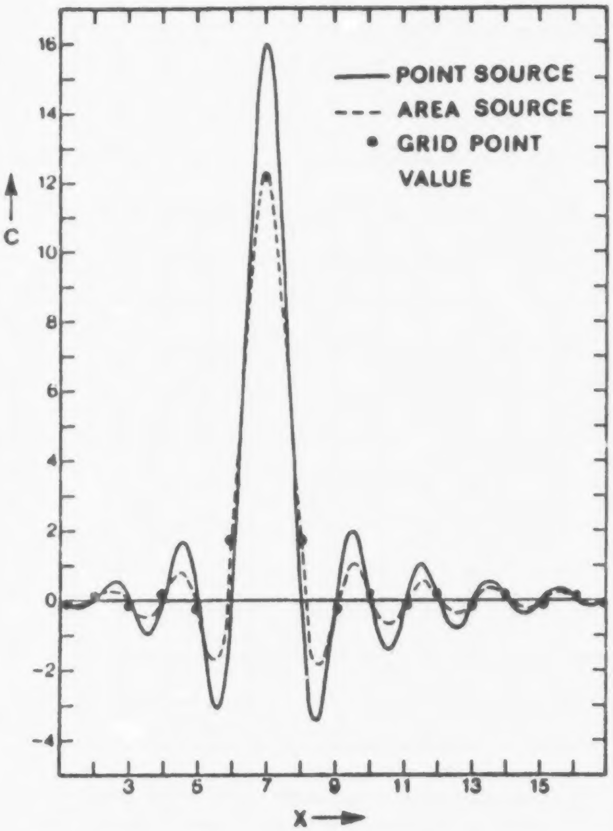

FIG. 2: CONCENTRATION FIELDS CORRESPONDING TO A POINT AND AN AREA SOURCE REPRESENTED BY FINITE FOURIER SERIES. THE TOTAL, INTEGRATED STRENGTH IS THE SAME FOR BOTH THE POINT AND AREA SOURCES

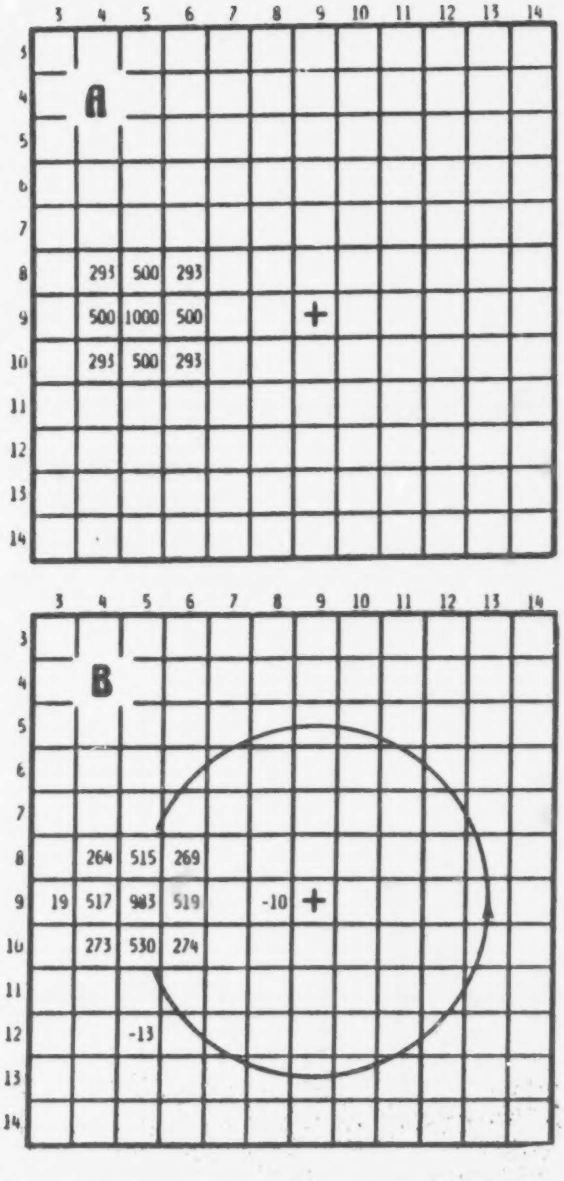
3
4
5
6
7
8
9
10
11
12
13
14
A
293
500
293
500
1000
500
293
500
293
B
264
515
269
19
517
983
519
-10
273
530
274
-13

FIG. 3: PSEUDOSPECTRAL SIMULATION OF ROTATION OF A CONICAL DISTRIBUTION IN A UNIFORM CIRCULAR VELOCITY FIELD. (A) INITIAL DISTRIBUTION. (B) AFTER ONE REVOLUTION. VALUES NUMERICALLY LESS THAN 10 HAVE BEEN SUPPRESSED. THE CENTER OF THE CIRCULAR VELOCITY FIELD IS INDICATED BY THE CROSS (CHRISTENSEN AND PRAHM, 1976)

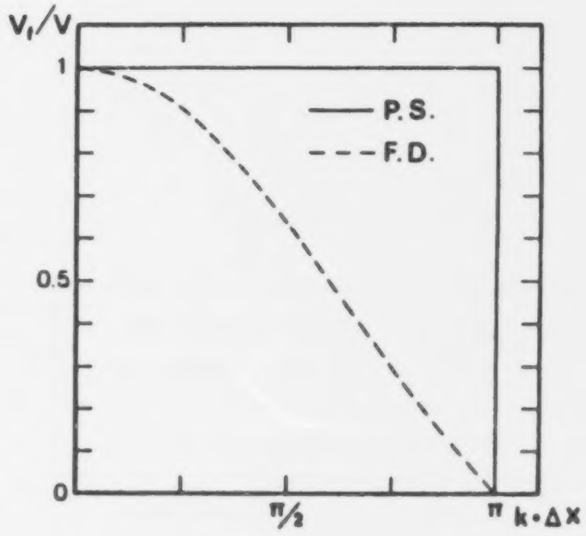

FIG. 4: PHASE SPEED FOR THE LINEAR ADVECTION EQUATION IN THE PSEUDOSPECTRAL APPROXIMATION (P.S.) AND THE SECOND ORDER CENTERED FINITE DIFFERENCE METHOD (F.D.)

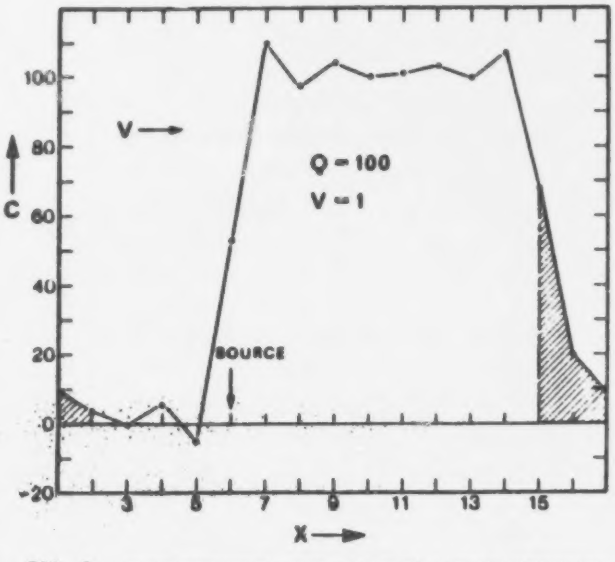

FIG. 5: PSEUDOSPECTRAL SIMULATION OF LINEAR ADVECTION FROM A CONTINUOUS POINT SOURCE. THE POSITION OF THE SOURCE IS INDICATED BY THE ARROW. THE BOUNDARY, DECAY REGION IS SHADOWED ON THE FIGURE

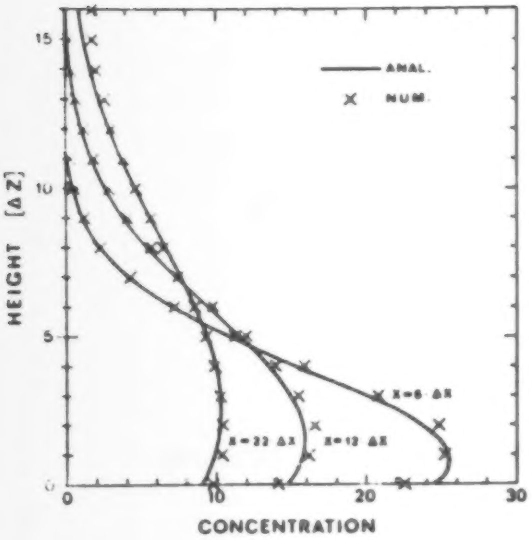

FIG. 6: VERTICAL PROFILES OF THE CONCENTRATION IN THE CASE OF DRY DEPOSITION (v_D=0.01v) COMPUTED BY THE PSEUDOSPECTRAL METHOD COMPARED WITH THE ANALYTICAL SOLUTION (SMITH, 1962) FOR CONSTANT WIND AND DIFFUSIVITY AND A SOURCE LOCATED AT GROUND LEVEL. THE HEIGHT AND THE DOWNWIND DISTANCE FROM THE SOURCE IS IN GRID POINT UNITS (BERKOWICZ AND PRAHM, 1977A)

TABLE 1

Symbol	unit	characteristic value	variable
C_1	$\mu g/m^3$	10	SO_2
C_2	$\mu g/m^3$	10	$SO_4^=$
$\bar{v}$	m/sec	10	Wind (two dimensions)
D	m^2/sec	10000	Diffusivity
S_1	$\mu g/m^3$ sec	4×10^{-4}	Emission of SO_2
S_2	$\mu g/m^3$ sec	3×10^{-5}	Emission of $SO_4^=$
τ_1	sec	18.5 x 3600	lifetime for SO_2 (dry deposition)
τ_2	sec	70 x 3600	lifetime for $SO_4^=$ (dry deposition)
τ_3	sec	140 x 3600	equivalent lifetime for $SO_2 \rightarrow SO_4$ oxidation
Δt	sec	30 x 60	time step
n		200	number of time steps
k	m^{-1}	2.5×10^{-5}	wave number
L	m	127×10^3	grid point spacing (32 x 32) points

8th International Technical Meeting
on Air Pollution Modeling and its Application

LONG-TERM REGIONAL DISTRIBUTIONS AND TRANSFRONTIER EXCHANGES OF AIRBORNE SULFUR POLLUTION IN EUROPE

Warren B. Johnson, Daniel E. Wolf, and Robert L. Mancuso
Atmospheric Sciences Laboratory
SRI International
Menlo Park, California 94303
U.S.A.

September 20-23, 1977
Louvain - La - Neuve
Belgium

I INTRODUCTION

There has been in recent years a growing awareness that air pollution can have significant effects on areas located long distances (thousands of km) away from source regions. The quality of the background air coming into a given country may be critically important in terms of the ability of that country to meet its air quality goals.

Thus there has developed a need to be able to more accurately identify source areas affecting air quality in a given region, and to quantify those effects. This need has prompted considerable efforts, particularly in Europe, for the development and evaluation of regional-scale air pollution simulation models. The most ambitious study has been the cooperative OECD-sponsored LRTAP* project, led by the Norwegian Institute for Air Research (Ottar, 1976, 1977). Other major efforts include the work of Prahm and Christensen (1977), Wendell et al. (1976), Fisher (1975), Bolin and Persson (1975), Rao et al. (1976), Smith and Jeffrey (1975), Renne and Elliott (1976), McMahon et al. (1976), and Sheih (1977), among others.

The work discussed in this report involves the development of an innovative trajectory-type regional air pollution model, called "EURMAP," which stands for "European Regional Model of Air Pollution." The overall objectives of this study are to develop, evaluate, and apply an accurate and practical quantitative technique for assessing the current and future effects of air pollution emissions in each country in central and western Europe on long-term air quality in each of the other countries. This report is intended to be an updating of our earlier progress report (Johnson et al., 1976) on this continuing project.+

The model developed for this purpose (EURMAP) has a number of distinctive features, among which are these:

---

* Long Range Transport of Air Pollutants

+ Sponsored by the Federal Environmental Office of the Federal Republic of Germany

- It uses as input long sequences of historical meteorological data at 6-hour intervals, and preserves all of the temporal and spatial detail inherent in these data.

- It calculates long-term (monthly, seasonal, and annual) SO_2 and $SO_4^=$ concentration and dry and wet deposition patterns and international exchanges resulting from SO_2 emissions in each of 13 countries in central and western Europe, taken both individually and jointly. These long-term values are obtained by totaling and/or averaging short-term values calculated at 3-hour time steps.

This approach is in contrast with a number of other models (e.g., Rao et al., 1976) which are not designed to obtain long-term values or interregional exchanges.

II DESCRIPTION OF EURMAP DESIGN AND APPLICATION

A. Model Rationale and Design Goals

In the design and development of any air quality simulation model, there are usually two conflicting goals: maximum realism and accuracy on the one hand, and minimum computing requirements on the other. The achievement of better realism and accuracy usually requires more detailed and sophisticated formulations, which in turn requires more computer time and memory capacity.

In designing EURMAP, it was clear from the outset that the computing requirements could become severe, for two reasons:

- The model must treat a very large geographical area (2100 km N-S by 2250 km E-W), and yet preserve acceptable spatial resolution (50 x 50 km).
- The model must compute monthly and annual mean concentration and deposition fields while preserving the original temporal resolution (6 hours) of standard meteorological data, and thus must make repetitive calculations for long sequences of input data.

Accordingly, as a first step, we set out to design a very simple model--one that would have minimum computing requirements (and thus be practical and economical to use), while at the same time offering acceptable realism in simulating the most important processes involved in the transfrontier air pollution problem. Our approach is to add sophistication only when it is proven to be needed. The result of this effort is the current basic version of EURMAP, which is described in the following sections.

B. Pollutant Emissions

The SO_2 emissions inventory used in this study was taken from that developed by Rystad et al. (1974) as part of the OECD-sponsored LRTAP project. As shown in Figure 1, annual total SO_2 emissions data for 1973 were available for an array of cells 0.5° in latitude by 1.0° in longitude

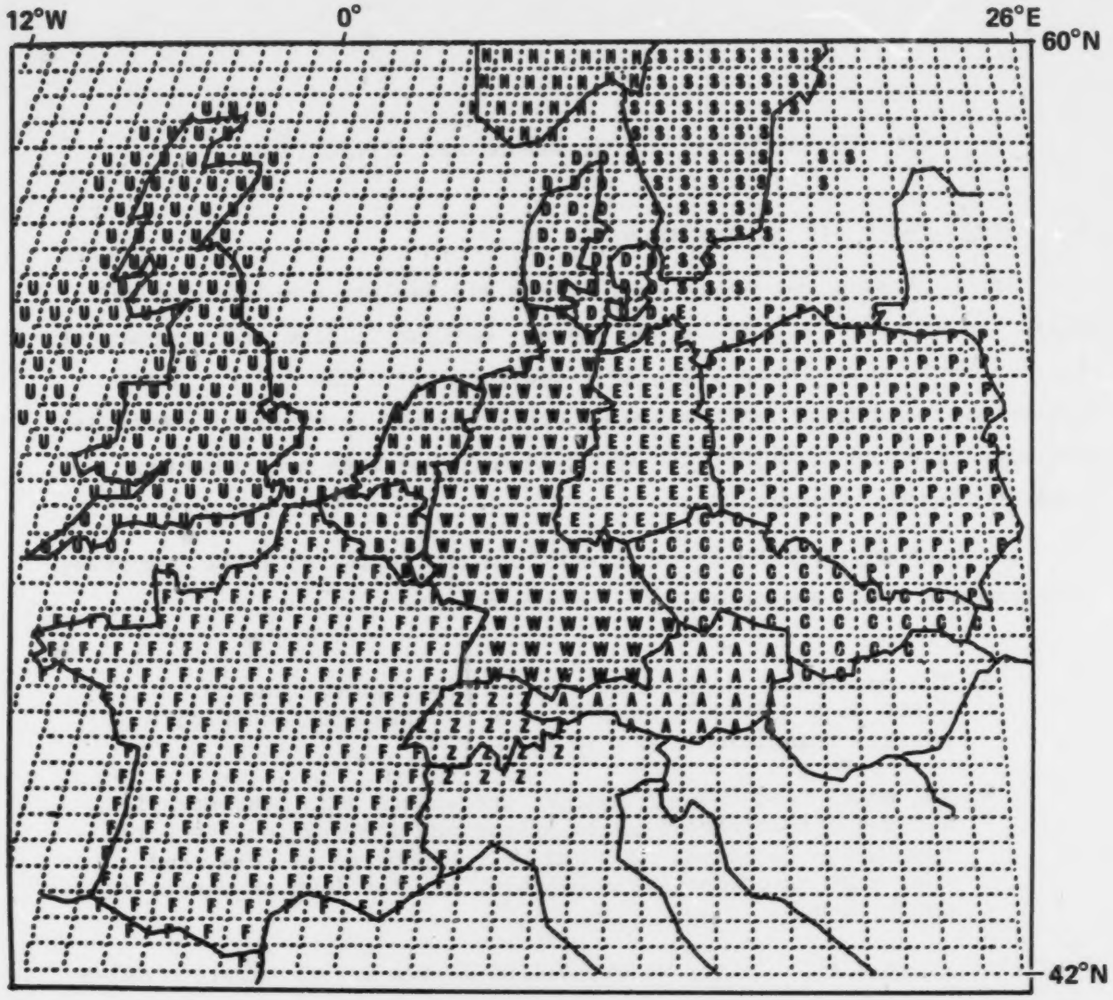

FIGURE 1 EMISSIONS DATA GRID USED IN THE MODEL RUNS; LETTERS REPRESENT COUNTRIES (SEE BELOW) FOR WHICH 1973 SO_2 DATA WERE AVAILABLE FROM RYSTAD ET AL. (1974)

A--Austria
B--Belgium/Luxembourg
C--Czechoslovakia
D--Denmark
E--East Germany (GDR)
F--France
H--The Netherlands (Holland)
N--Norway (South of 60°N)
P--Poland
S--Sweden (South of 60°N)
Z--Switzerland
U--United Kingdom
W--West Germany (FRG)

(approximately 55 km N-S by 70 km E-W), which includes most countries in central and western Europe. Letter identifiers are used in Figure 1 to designate those countires for which emissions data are available. Unfortunately, emissions data for Spain, Italy, Yugoslavia, Rumania, Bulgaria, and the USSR are not yet available for this detailed grid.

C. Pollutant Transport

Figure 2 illustrates the basic principles behind the operation of the model.* Normally the model is run separately for each country of interest. Thus only the array of emissions cells associated with the particular country of interest is used at any one time.

For each of these cells, the annual-average emissions are divided into discrete 12-hour-average emission increments, or "puffs," which are released at 12-hour intervals and tracked at 3-hour time steps until either they move outside the overall study region (see Figure 1) or their concentration drops to an insignificant level. The reason for selecting the 12-hour intervals is that these intervals correspond to the frequency at which most synoptic upper-air wind observations are available. Thus, 730 puffs/year, or 61 puffs/month, are released and tracked for each of the cells. The largest country, France, contains 146 emissions cells, while West Germany, an average-size country, contains 67 cells. Thus, during the course of a month 4,087 puffs from West Germany are tracked, and at an average of 28 tracking steps/puff, a total of 114,436 puff positions/month are calculated for this country alone. This indicates the magnitude of the computational requirements.

The individual puffs are transported according to the wind field applicable at that time, as interpolated objectively from the available upper-air wind observations at 850 mb (approximately 1500 m above sea level) from about 45 sounding stations for the year 1973. Although

---

* The basic concept is similar in principle to that developed by Start and Wendell (1974) in their MESODIF model, except that MESODIF was designed to be used with only one or a few point sources.

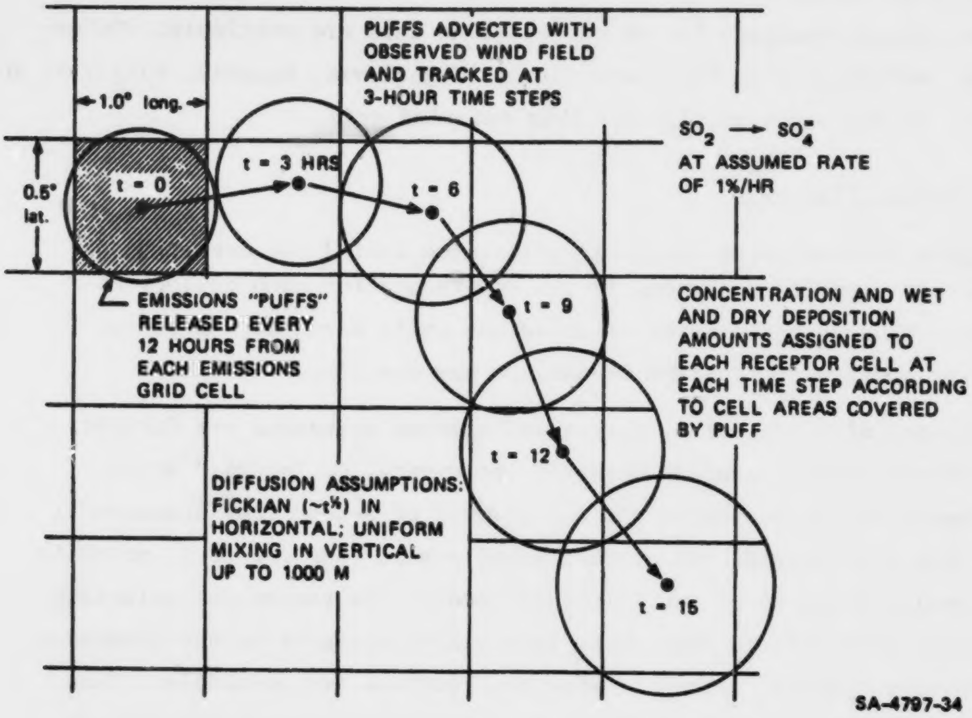
PUFFS ADVECTED WITH OBSERVED WIND FIELD AND TRACKED AT 3-HOUR TIME STEPS
1.0° long.
0.5° lat.
t = 0
t = 3 HRS
t = 6
t = 9
t = 12
t = 15
$SO_2 \longrightarrow SO_4^=$ AT ASSUMED RATE OF 1%/HR
EMISSIONS "PUFFS" RELEASED EVERY 12 HOURS FROM EACH EMISSIONS GRID CELL
CONCENTRATION AND WET AND DRY DEPOSITION AMOUNTS ASSIGNED TO EACH RECEPTOR CELL AT EACH TIME STEP ACCORDING TO CELL AREAS COVERED BY PUFF
DIFFUSION ASSUMPTIONS: FICKIAN (~$t^{1/2}$) IN HORIZONTAL; UNIFORM MIXING IN VERTICAL UP TO 1000 M
SA-4797-34

FIGURE 2 EMISSIONS PUFF ADVECTION AND DIFFUSION SCHEME USED IN EURMAP

we recognize that significant vertical wind shears occur between the surface and the 1500-m level, especially in winter and at night, we believe that the use of a single wind to represent the transport within this layer is justified as a first approximation.

To account in an approximate fashion for surface-friction effects that cause wind shear in the boundary layer, the 850-mb winds have been adjusted as follows to give a more representative layer average:

$$\overline{U} = 0.75\ U_{(850\ \text{mb})}$$

$$\overline{\theta} = \theta_{(850\ \text{mb})} - 15^{\circ}$$

where $\overline{U}$ and $\overline{\theta}$ are the assumed layer-average wind speed and direction, respectively.

D. Model Formulation

The model assumes that the pollutant concentration is always uniform throughout each puff at any given time. Accordingly, the SO_2 concentration (C_1) in a puff at any time (t) is determined as follows:

$$C_1 = M_1/V = (M_o - M_T - M_{d1} - M_{w1})/V \qquad (1)$$

where M_1 = mass of SO_2 in puff at time t
M_o = initial mass of SO_2 in puff
M_T = mass of SO_2 lost by transformation to $SO_4^=$ from t = 0 to t = t (0 → t)
M_{d1} = mass of SO_2 lost by dry deposition (0 → t)
M_{w1} = mass of SO_2 lost by wet deposition (0 → t)
V = volume of puff at time t

Similarly, the $SO_4^=$ concentration (C_2) becomes

$$C_2 = M_2/V = (3M_T/2 - M_{d2} - M_{w2})/V \qquad (2)$$

where the factor of 3/2 is the ratio of the molecular weight for $SO_4^=$ to that for SO_2.

Assuming that the rates of change of pollutant mass in a puff due to transformation and deposition processes are proportional to the pollutant mass, we have

$$(dM/dt)_{\text{transformation (T)}} = k_T M \tag{3}$$

$$(dM/dt)_{\text{wet deposition (d)}} = k_d M \tag{4}$$

$$(dM/dt)_{\text{wet deposition (w)}} = k_w M \tag{5}$$

where k_T = $SO_2 \rightarrow SO_4^=$ transformation coefficient (hr^{-1})

k_d = dry deposition coefficient (hr^{-1})

k_w = wet deposition coefficient (hr^{-1})

= $\lambda \cdot R(t)$

and λ = washout/rainout coefficient [$hr^{-1}(mm/hr)^{-1}$, or mm^{-1}]

$R(t)$ = precipitation rate (mm/hr of liquid water) at location of puff at time t.

The wet deposition is thus taken to be a function of precipitation rate, in accordance with findings by Bielke (1970) and others.

Converting pollutant mass in a puff to concentration times puff volume, Equations (3-(5) become

$$(dM/dt)_T = k_T \, C \, V \tag{6}$$

$$(dM/dt)_d = k_d \, C \, V \tag{7}$$

$$(dM/dt)_w = k_w \, C \, V \tag{8}$$

which can be integrated to obtain

$$M_T = \int_0^t k_T \, C \, V \, dt = k_T \int_0^t C \, V \, dt \tag{9}$$

$$M_d = \int_0^t k_d \, C \, V \, dt = k_d \int_0^t C \, V \, dt \tag{10}$$

$$M_w = \int_o^t k_w \, C \, V \, dt \tag{11}$$

Substituting these expressions into Equations (1) and (2), we have

$$C_1 = \frac{M_o}{V} - \frac{(k_T + k_d)}{V} \int_o^t C_1 \, V \, dt - \frac{1}{V} \int_o^t k_w C_1 V \, dt \tag{12}$$

$$C_2 = \frac{3k_T/2}{V} \int_o^t C_1 V \, dt - \frac{k_d}{V} \int_o^t C_2 V \, dt - \frac{1}{V} \int_o^t k_w C_2 V \, dt \tag{13}$$

E. Pollutant Diffusion

Since diffusion on the regional scale is less important than the transport and removal processes, a very simple treatment of diffusion is used in the current version of EURMAP. Upon release, each puff is assumed to immediately diffuse vertically to give a uniform concentration in the layer between the surface and the 1000-m level. Aircraft measurements reported by Jost (1973, 1974) indicate that an average mixing depth of 1000 m is reasonable for Central Europe. However, to be more realistic, the mixing depth should vary with latitude and with season. Incorporation of this refinement into EURMAP is planned, but a constant mixing depth has been used for the computer runs so far. Thus the seasonal variations in the results to be presented in the next section reflect only the seasonal changes in wind and precipitation patterns, rather than changes in mixing depth.

Horizontal diffusion is also treated very simply. The initial lateral extent of the puff is approximated by a disk whose diameter (about 60 km) is adjusted so that the cross-sectional area of the disk is the same as that of the emissions cell. Fickian diffusion is then assumed during the transport of the puff, so that the puff radius (r) at any time (t) is given by

$$r = (r_o{}^2 + Kt)^{1/2} \tag{14}$$

where r_o = initial puff radius
K = horizontal eddy diffusivity
$\equiv 10^8 \text{ cm}^2 \text{ sec}^{-1} = 36 \text{ km}^2 \text{ hr}^{-1}$

and the puff volume (V) is

$$V = \pi H (r_o^2 + Kt) \qquad (15)$$

where H = height of the mixed volume ≡ 1000 m.

The particular magnitude selected for K was based upon average values available from the literature [Heffter (1965), Hilst (1968)] for travel times of 10 to 100 hours.

The assumption of Fickian diffusion may lead to underestimates of the horizontal puff spread, since current evidence (Gifford, 1977) indicates that $r \sim t$ is a better descriptor of atmospheric diffusion than $r \sim t^{1/2}$. This change will be considered for incorporation into the next version of EURMAP. When this is done, however, the resulting concentration and deposition fields are unlikely to differ much from the current results. This is because the use of a faster horizontal diffusion rate will simply cause adjacent puffs to merge together faster, resulting only in a smoothing of the concentration and deposition fields.

F. Pollutant Transformation and Deposition

Recognizing that the processes of SO_2 conversion to sulfate aerosol and SO_2 removal by dry and wet deposition are particularly significant over the long transport distances involved in this study, we have included these effects in the model formulation (Equations 12 and 13), but in a relatively simplified manner. Clearly these processes are very complex, depending upon such variables as surface and vegetation types (Whelpdale and Shaw, 1974); meteorological conditions (humidity, clouds, rain, fog, atmospheric stability, sunlight intensity, etc.); and concentrations of other chemical species in the air, such as ammonia and metal catalysts (Weber, 1971). However, until these processes are better understood, the simple treatment used here seems reasonable for this type of model.

A review of recent field, laboratory, and theoretical studies was conducted to find the best values available for the transformation coefficient (k_T) and the wet and dry deposition coefficients for $SO_2(k_{w1}, k_{d1})$ and $SO_4^=$ (k_{w2}, k_{d2}). The values selected are compared in Table 1 with those used

Table 1

COMPARISON OF SELECTED TRANSFORMATION AND DEPOSITION COEFFICIENTS WITH THOSE USED BY OTHER INVESTIGATORS

	$SO_2 \rightarrow SO_4^=$ Transformation Rate (hr^{-1})	Deposition Coefficients (hr^{-1})			
		Dry		Wet+	
Investigator		SO_2	$SO_4^=$	SO_2	$SO_4^=$
Ottar et al. (1976)	0.007	0.036*	0.0144*	- - -	- - -
Renne and Elliott (1976)	0.050	0.036	0.0036	0.500	0.050
Rao et al. (1976)	0.015	- - -	- - -	- - -	- - -
McMahon et al. (1976)	0.010-0.020	0.054	0.0070	0.216	0.108
Johnson, Wolf, and Mancuso (1977)§	0.010	0.029	0.0070	0.216	0.070

* Includes wet deposition

+ Values shown are of washout coefficient λ, where $k_w = \lambda R$, and rainfall rate R is in mm hr^{-1}

§ Current paper

by other investigators. The value of 0.029 hr^{-1} selected for k_{d1} corresponds to a dry deposition velocity for SO_2 of 0.8 cm sec^{-1}, which is within the generally accepted range of values (cf. Eliassen and Saltbones, 1975)

Two important points should be noted here:

- Coefficient values used by various investigators show a wide scatter, reflecting the relative lack of reliable experimentally derived values.
- The outputs of all models (including EURMAP) which simulate $SO_2/SO_4^=$ transformation and deposition processes are highly dependent on the values of these coefficients.

Thus all model results, including those from EURMAP, should be treated with caution. Values of the transformation and deposition coefficients used in EURMAP are based upon best available information, but nevertheless these are uncertain, and accordingly the model results should be considered tentative at this time.

For the purpose of calculating the SO_2/sulfate removal by wet deposition, daily total precipitation observations during 1973 at a total of about 535 surface stations are input to the model. Interpolated precipitation values are used to calculate the mass of SO_2 and $SO_4^=$ removed from each puff at each location on the grid during each three-hour time step.

The computer program keeps track of each puff's location and duration of exposure to the variable precipitation intensity, calculates the pollutant mass removed during each time step based upon the assumed values of k_{w1} and k_{w2}, and assigns these amounts to the appropriate cell (geographical location) in the receptor grid. The precipitation rate is calculated by dividing the observed values of accumulated precipitation by the number of hours in the accumulation period. This infers an assumption that the precipitation was uniform during this period.

Dry deposition is handled in a similar but simpler manner. Based on the assumed values of k_{d1} and k_{d2}, the model removes appropriate fractions of the SO_2 and $SO_4^=$ mass in each puff at each time step, and assigns these amounts as dry deposition to the appropriate cell (geographical location) in the receptor grid.

G. Calculation of Monthly-Mean Concentration and Deposition Distributions

EURMAP is designed to calculate long-term (monthly, seasonal, and/or annual) mean distributions of SO_2 and $SO_4^=$ concentrations, dry deposition, and wet deposition over all of western and central Europe, resulting from SO_2 emissions from each of the 13 countries in this area taken individually. Accordingly, each computer run of EURMAP involves reading in long sequences of surface and upper-air meteorological data at 6-hourly intervals. Each of the SO_2 puffs released at 12-hourly intervals from each of the emissions cells for the country of interest is moved every three hours in accordance with the interpolated field of observed winds applicable for that time.

Values of concentration, dry deposition, and wet deposition are summed up at each 3-hourly time step over a 41 x 44 grid of receptor cells, each of which is 50 km on a side. This is carried out by adding the contributions of each of the puffs at each of the receptor cells.

Concentrations are assigned to cells around the location of the puff at the beginning of the time step. Deposition amounts are evenly divided between the cells at the starting location and those at the ending location of the puff for each time step. Both for concentration and deposition, pollutant amounts are assigned to the cell containing the center of the puff and to the eight surrounding cells in amounts proportional to the area of the puff relative to the area of the central cell.

Long-term mean concentration distributions are obtained simply by averaging the concentrations assigned to each cell at each time step over the total period (number of time steps) of interest. Corresponding deposition distributions are obtained by totalling all amounts deposited in each cell during the period of interest.

III RESULTS FROM EURMAP COMPUTER RUNS

A. Description of Results

For the purpose of developing a set of model results for evaluation against available observations, the basic model has been run for the months of January, April, July and October 1973 in the manner described in the last section, using detailed meteorological data at 6-hourly intervals. These particular months were selected in order to examine seasonal variations in the results. Separate runs have been made for each of the 13 countries for which emissions were available (Figure 1).* For each of the four months, maps of SO_2 and $SO_4^=$ concentrations, dry deposition, and wet deposition resulting from the SO_2 emissions in each of the 13 individual countries have been prepared.† Space limitations preclude the presentation of these results in this paper. However, Figure 3 gives an example of such results for Belgium for October 1973. The results from the individual runs have also been combined into maps for each month showing the total concentration, dry deposition, and wet deposition distributions resulting from SO_2 emissions from all 13 countries taken together (Figures 4-7).

Finally, assuming that the results for each of the four months are representative of seasonal values, annualized depositions have been estimated by totaling the four monthly deposition values and multiplying by three. Similarly, estimates of annual average concentrations have been obtained by averaging values for the four months. Annualized concentration and deposition patterns calculated in this way are presented in Figure 8. Note that the units of deposition in Figure 8 are 10 mg/m^2 (10^{-2} g/m^2), while those in Figures 3-7 are mg/m^2 (10^{-3} g/m^2).

Logarithmic contour intervals (2,4,8,16,32,...) are used in the maps shown in Figures 4-8, and only the open contours are labelled. The other numbers on the contour maps and the adjacent crosses (+) are the magnitudes and locations of maximum values in the concentration and deposition fields.

---

* For convenience, Luxembourg has been combined with Belgium and denoted simply as "Belgium."

† Seasonally dependent emission rates have not been included in these computations so that the effects of seasonal changes in wind patterns could be examined by themselves, but this refinement will be added in later computer runs

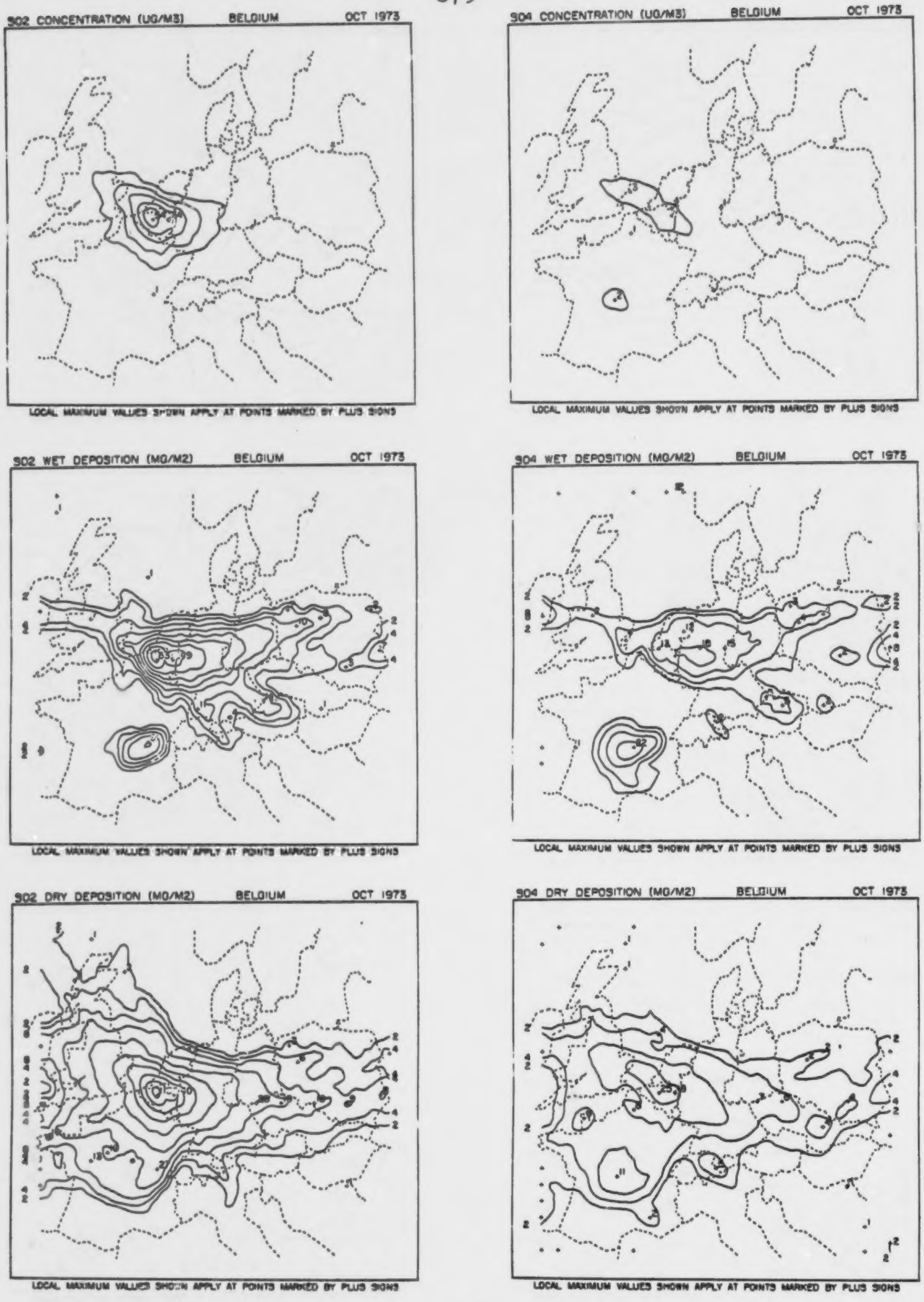
SO2 CONCENTRATION (UG/M3) BELGIUM OCT 1973
LOCAL MAXIMUM VALUES SHOWN APPLY AT POINTS MARKED BY PLUS SIGNS
SO4 CONCENTRATION (UG/M3) BELGIUM OCT 1973
LOCAL MAXIMUM VALUES SHOWN APPLY AT POINTS MARKED BY PLUS SIGNS
SO2 WET DEPOSITION (MG/M2) BELGIUM OCT 1973
LOCAL MAXIMUM VALUES SHOWN APPLY AT POINTS MARKED BY PLUS SIGNS
SO4 WET DEPOSITION (MG/M2) BELGIUM OCT 1973
LOCAL MAXIMUM VALUES SHOWN APPLY AT POINTS MARKED BY PLUS SIGNS
SO2 DRY DEPOSITION (MG/M2) BELGIUM OCT 1973
LOCAL MAXIMUM VALUES SHOWN APPLY AT POINTS MARKED BY PLUS SIGNS
SO4 DRY DEPOSITION (MG/M2) BELGIUM OCT 1973
LOCAL MAXIMUM VALUES SHOWN APPLY AT POINTS MARKED BY PLUS SIGNS

FIGURE 3 ESTIMATED SO_2 (LEFT) AND $SO_4^=$ (RIGHT) CONCENTRATIONS, WET DEPOSITION, AND DRY DEPOSITION (TOP TO BOTTOM) FROM EMISSIONS IN BELGIUM
(MONTHLY MEANS AND TOTALS FOR OCTOBER 1973)

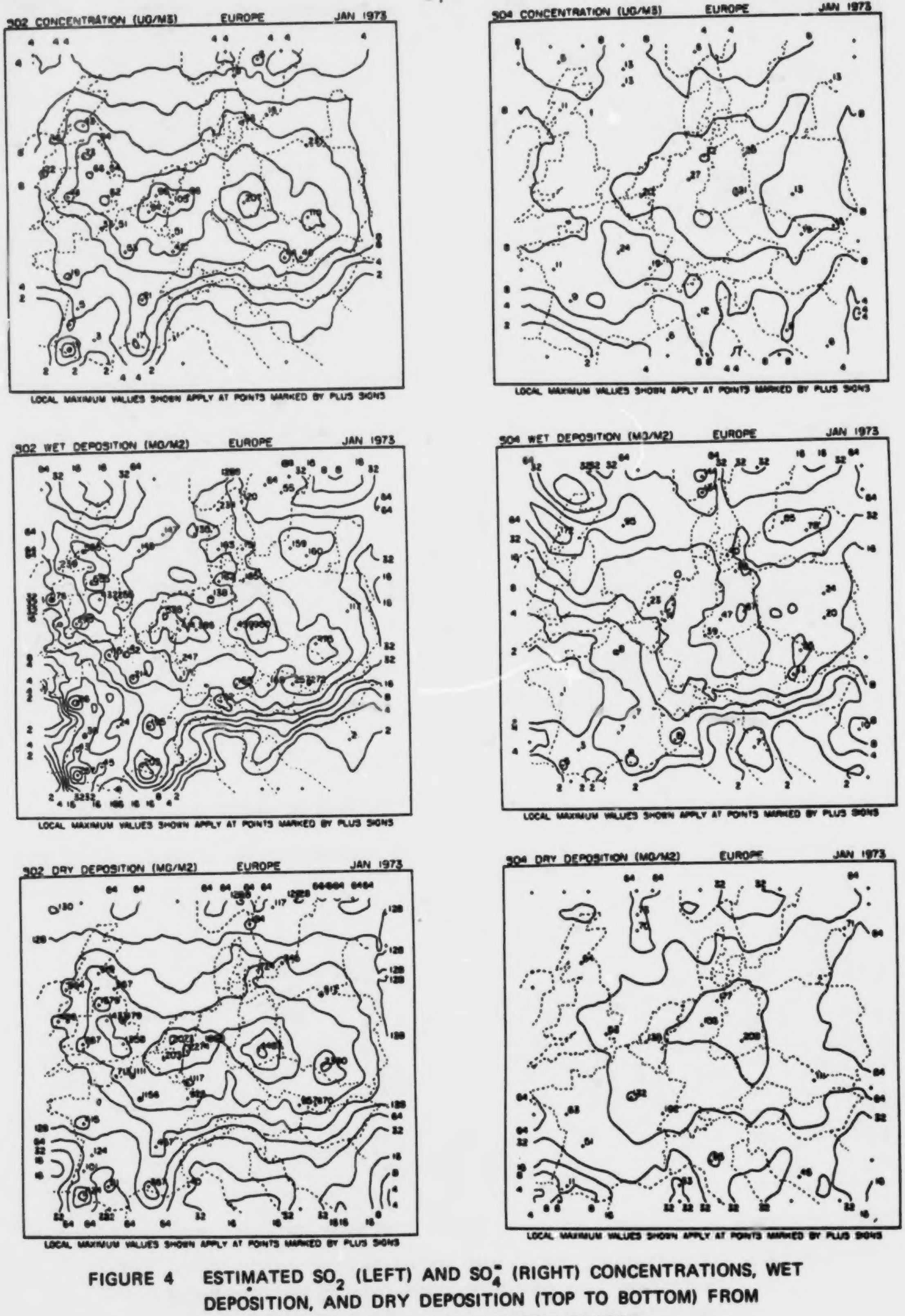
SO2 CONCENTRATION (UG/M3) EUROPE JAN 1973
LOCAL MAXIMUM VALUES SHOWN APPLY AT POINTS MARKED BY PLUS SIGNS
SO4 CONCENTRATION (UG/M3) EUROPE JAN 1973
LOCAL MAXIMUM VALUES SHOWN APPLY AT POINTS MARKED BY PLUS SIGNS
SO2 WET DEPOSITION (MG/M2) EUROPE JAN 1973
LOCAL MAXIMUM VALUES SHOWN APPLY AT POINTS MARKED BY PLUS SIGNS
SO4 WET DEPOSITION (MG/M2) EUROPE JAN 1973
LOCAL MAXIMUM VALUES SHOWN APPLY AT POINTS MARKED BY PLUS SIGNS
SO2 DRY DEPOSITION (MG/M2) EUROPE JAN 1973
LOCAL MAXIMUM VALUES SHOWN APPLY AT POINTS MARKED BY PLUS SIGNS
SO4 DRY DEPOSITION (MG/M2) EUROPE JAN 1973
LOCAL MAXIMUM VALUES SHOWN APPLY AT POINTS MARKED BY PLUS SIGNS

FIGURE 4 ESTIMATED SO$_2$ (LEFT) AND SO$_4^=$ (RIGHT) CONCENTRATIONS, WET DEPOSITION, AND DRY DEPOSITION (TOP TO BOTTOM) FROM EMISSIONS IN CENTRAL AND WESTERN EUROPE (MONTHLY MEANS AND TOTALS FOR JANUARY 1973)

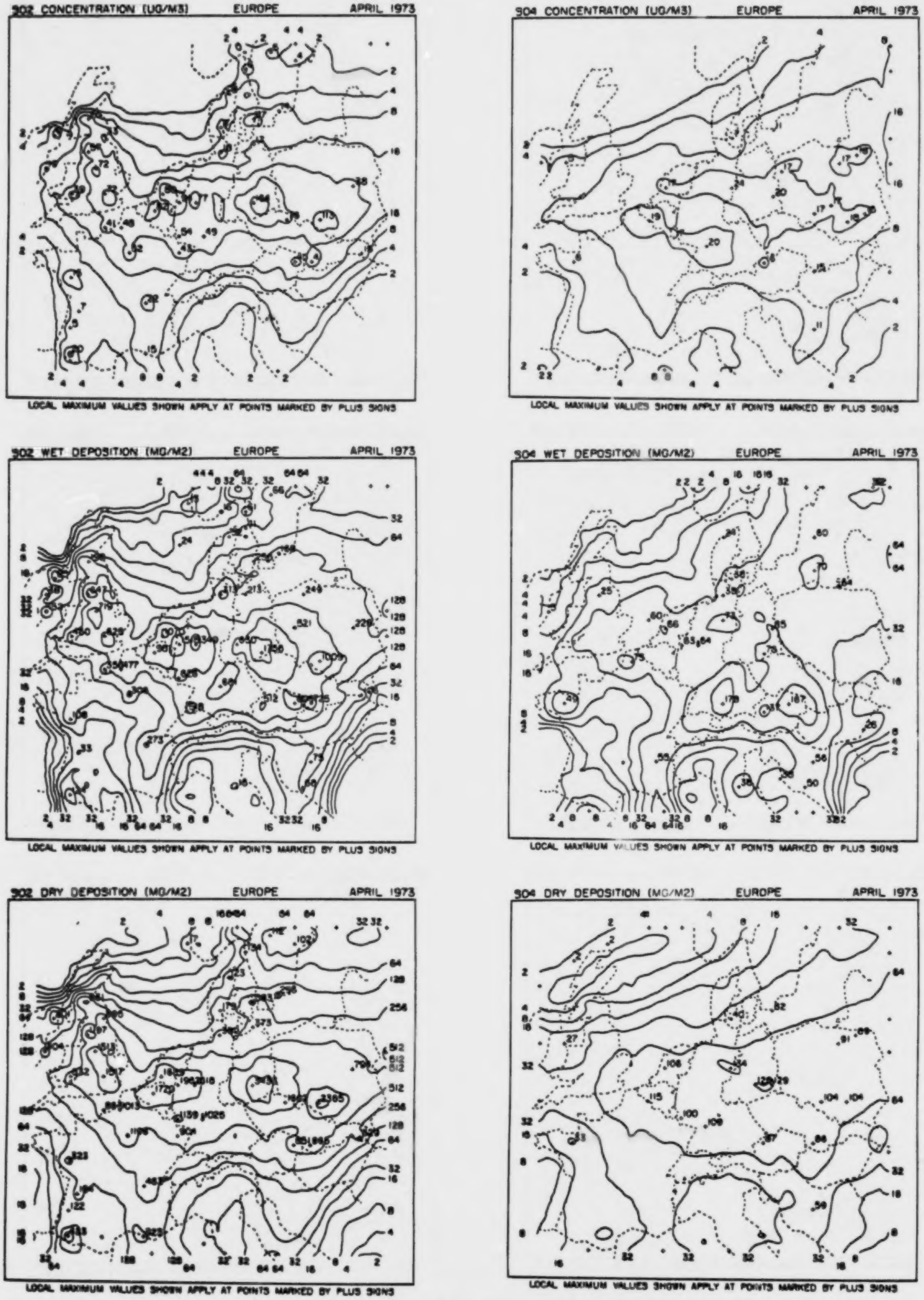
SO2 CONCENTRATION (UG/M3) EUROPE APRIL 1973
LOCAL MAXIMUM VALUES SHOWN APPLY AT POINTS MARKED BY PLUS SIGNS
SO4 CONCENTRATION (UG/M3) EUROPE APRIL 1973
LOCAL MAXIMUM VALUES SHOWN APPLY AT POINTS MARKED BY PLUS SIGNS
SO2 WET DEPOSITION (MG/M2) EUROPE APRIL 1973
LOCAL MAXIMUM VALUES SHOWN APPLY AT POINTS MARKED BY PLUS SIGNS
SO4 WET DEPOSITION (MG/M2) EUROPE APRIL 1973
LOCAL MAXIMUM VALUES SHOWN APPLY AT POINTS MARKED BY PLUS SIGNS
SO2 DRY DEPOSITION (MG/M2) EUROPE APRIL 1973
LOCAL MAXIMUM VALUES SHOWN APPLY AT POINTS MARKED BY PLUS SIGNS
SO4 DRY DEPOSITION (MG/M2) EUROPE APRIL 1973
LOCAL MAXIMUM VALUES SHOWN APPLY AT POINTS MARKED BY PLUS SIGNS

FIGURE 5 ESTIMATED SO_2 (LEFT) AND $SO_4^=$ (RIGHT) CONCENTRATIONS, WET DEPOSITION, AND DRY DEPOSITION (TOP TO BOTTOM) FROM EMISSIONS IN CENTRAL AND WESTERN EUROPE (MONTHLY MEANS AND TOTALS FOR APRIL 1973)

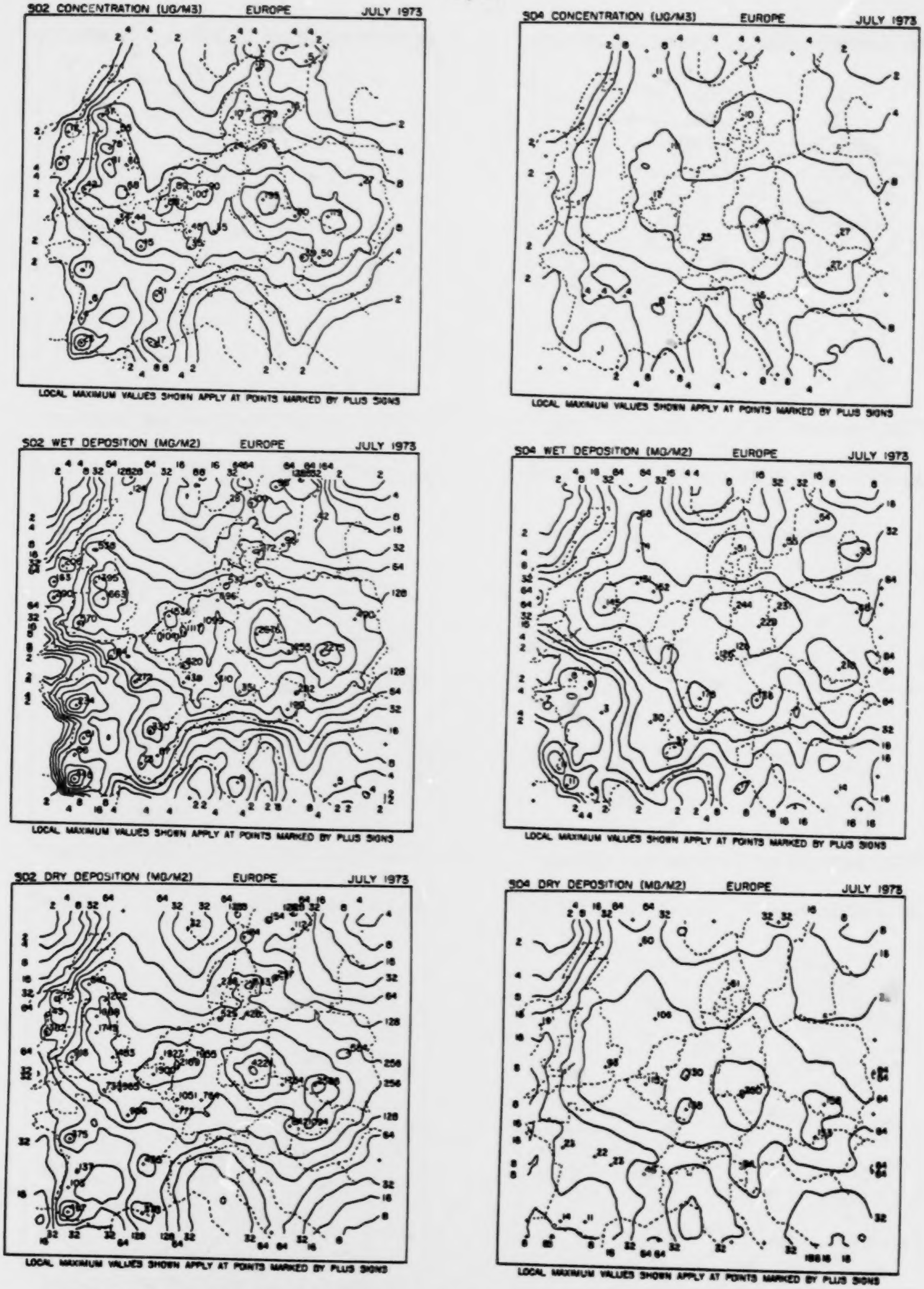
SO2 CONCENTRATION (UG/M3) EUROPE JULY 1973
LOCAL MAXIMUM VALUES SHOWN APPLY AT POINTS MARKED BY PLUS SIGNS
SO4 CONCENTRATION (UG/M3) EUROPE JULY 1973
LOCAL MAXIMUM VALUES SHOWN APPLY AT POINTS MARKED BY PLUS SIGNS
SO2 WET DEPOSITION (MG/M2) EUROPE JULY 1973
LOCAL MAXIMUM VALUES SHOWN APPLY AT POINTS MARKED BY PLUS SIGNS
SO4 WET DEPOSITION (MG/M2) EUROPE JULY 1973
LOCAL MAXIMUM VALUES SHOWN APPLY AT POINTS MARKED BY PLUS SIGNS
SO2 DRY DEPOSITION (MG/M2) EUROPE JULY 1973
LOCAL MAXIMUM VALUES SHOWN APPLY AT POINTS MARKED BY PLUS SIGNS
SO4 DRY DEPOSITION (MG/M2) EUROPE JULY 1973
LOCAL MAXIMUM VALUES SHOWN APPLY AT POINTS MARKED BY PLUS SIGNS

FIGURE 6 ESTIMATED SO_2 (LEFT) AND $SO_4^=$ (RIGHT) CONCENTRATIONS, WET DEPOSITION, AND DRY DEPOSITION (TOP TO BOTTOM) FROM EMISSIONS IN CENTRAL AND WESTERN EUROPE (MONTHLY MEANS AND TOTALS FOR JULY 1973)

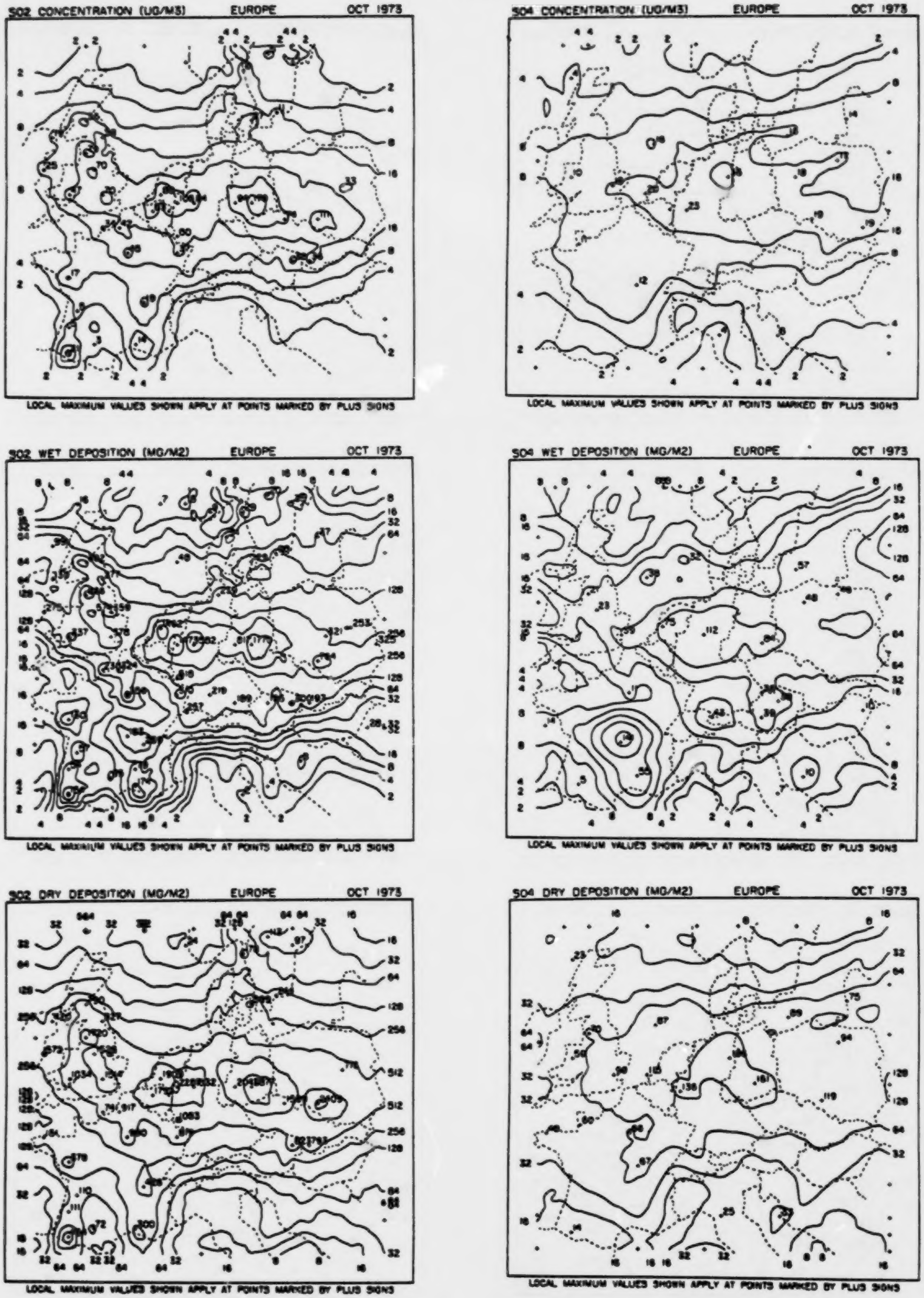

SO2 CONCENTRATION (UG/M3) EUROPE OCT 1973

LOCAL MAXIMUM VALUES SHOWN APPLY AT POINTS MARKED BY PLUS SIGNS

SO4 CONCENTRATION (UG/M3) EUROPE OCT 1973

LOCAL MAXIMUM VALUES SHOWN APPLY AT POINTS MARKED BY PLUS SIGNS

SO2 WET DEPOSITION (MG/M2) EUROPE OCT 1973

LOCAL MAXIMUM VALUES SHOWN APPLY AT POINTS MARKED BY PLUS SIGNS

SO4 WET DEPOSITION (MG/M2) EUROPE OCT 1973

LOCAL MAXIMUM VALUES SHOWN APPLY AT POINTS MARKED BY PLUS SIGNS

SO2 DRY DEPOSITION (MG/M2) EUROPE OCT 1973

LOCAL MAXIMUM VALUES SHOWN APPLY AT POINTS MARKED BY PLUS SIGNS

SO4 DRY DEPOSITION (MG/M2) EUROPE OCT 1973

LOCAL MAXIMUM VALUES SHOWN APPLY AT POINTS MARKED BY PLUS SIGNS

FIGURE 7 ESTIMATED SO_2 (LEFT) AND $SO_4^=$ (RIGHT) CONCENTRATIONS, WET DEPOSITION, AND DRY DEPOSITION (TOP TO BOTTOM) FROM EMISSIONS IN CENTRAL AND WESTERN EUROPE (MONTHLY MEANS AND TOTALS FOR OCTOBER 1973)

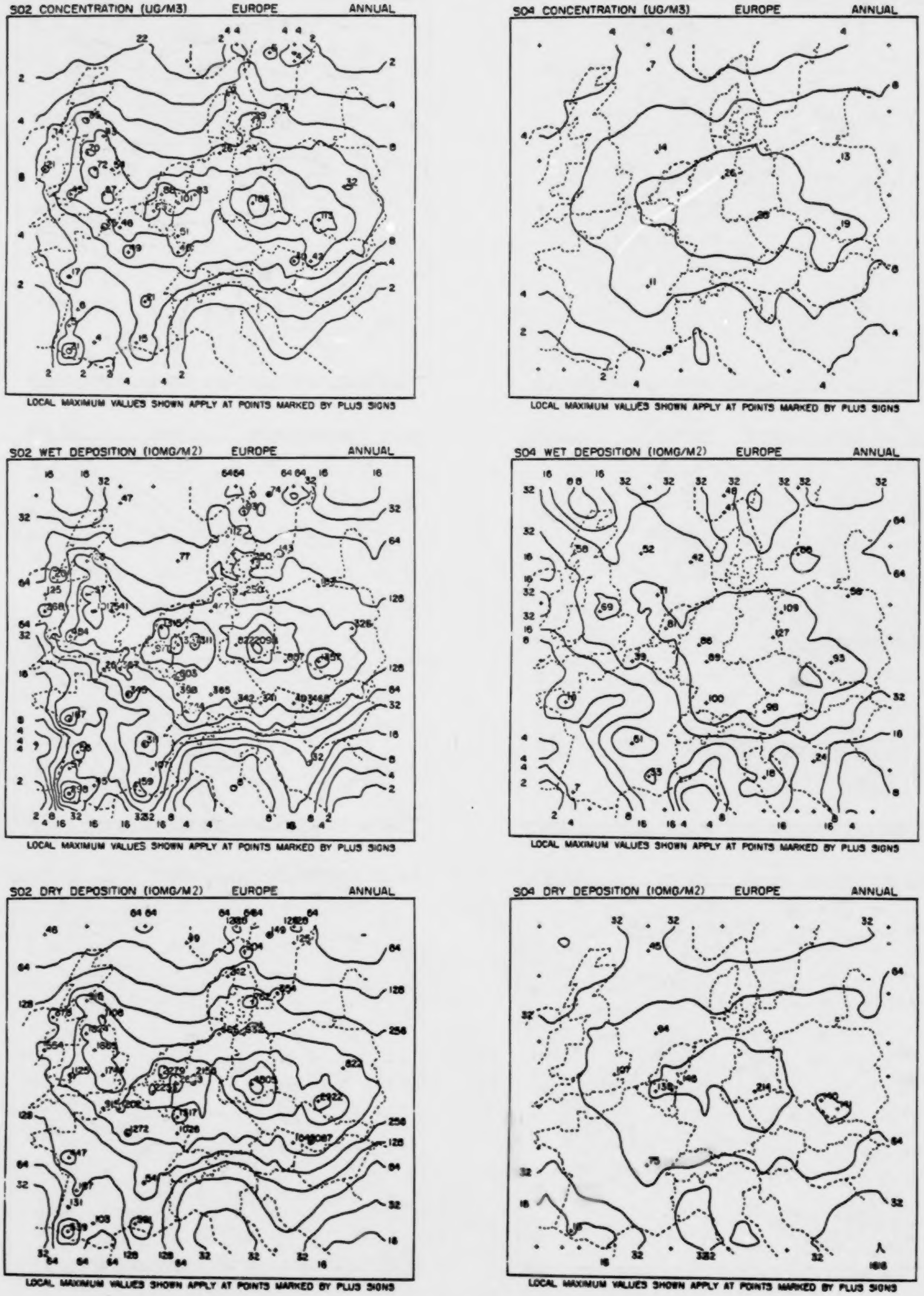

SO2 CONCENTRATION (UG/M3) EUROPE ANNUAL

LOCAL MAXIMUM VALUES SHOWN APPLY AT POINTS MARKED BY PLUS SIGNS

SO4 CONCENTRATION (UG/M3) EUROPE ANNUAL

LOCAL MAXIMUM VALUES SHOWN APPLY AT POINTS MARKED BY PLUS SIGNS

SO2 WET DEPOSITION (IOMG/M2) EUROPE ANNUAL

LOCAL MAXIMUM VALUES SHOWN APPLY AT POINTS MARKED BY PLUS SIGNS

SO4 WET DEPOSITION (IOMG/M2) EUROPE ANNUAL

LOCAL MAXIMUM VALUES SHOWN APPLY AT POINTS MARKED BY PLUS SIGNS

SO2 DRY DEPOSITION (IOMG/M2) EUROPE ANNUAL

LOCAL MAXIMUM VALUES SHOWN APPLY AT POINTS MARKED BY PLUS SIGNS

SO4 DRY DEPOSITION (IOMG/M2) EUROPE ANNUAL

LOCAL MAXIMUM VALUES SHOWN APPLY AT POINTS MARKED BY PLUS SIGNS

FIGURE 8 ESTIMATED SO_2 (LEFT) AND $SO_4^=$ (RIGHT) CONCENTRATIONS, WET DEPOSITION, AND DRY DEPOSITION (TOP TO BOTTOM) FROM EMISSIONS IN CENTRAL AND WESTERN EUROPE (ANNUAL MEANS AND TOTALS FOR 1973)

The results shown in Figures 3-8 are fairly self-explanatory, but a few general comments are in order:

- The patterns for concentration and dry deposition are similar, since dry deposition is taken to be proportional to concentration.
- The wet deposition patterns reflect the normal inhomogeneities in the spatial distribution of precipitation, and thus are less similar to the concentration patterns.
- Particularly for SO_2, the patterns are strongly influenced by the emissions distribution, with maxima generally corresponding to maxima in the emissions field. The patterns thus show a broad band of high values corresponding to the heavily industrialized region extending from central England east-southeastward to southern Poland.
- The occurrence of large horizontal gradients in the concentration and deposition fields in the southern and eastern portions of the maps is an artifact caused by the fact that emissions from Spain, Italy, Yugoslavia, Hungary, Rumania, and the USSR have not yet been included.
- The results for the individual countries (see Figure 3) are much more revealing of transport directions, etc., than are the combined results from all countries.
- The $SO_4^=$ concentration and deposition maxima are generally displaced to the eastward of SO_2 source areas (i.e., in the mean downwind direction), as would be expected considering the finite time required for transformation of SO_2 to $SO_4^=$.
- $SO_4^=$ wet deposition maxima frequently occur in regions far from source areas, such as the maximum in southern France from Belgium emissions (Figure 3), and the maxima from European emissions in January over the Baltic Sea and western Scotland (Figure 4), in April over eastern Austria (Figure 5), and in October over the northwestern USSR and southern France (Figure 7).
- Particularly for SO_2, the shapes and magnitudes of the concentration and deposition patterns for the four months are rather similar. More realistic seasonal variations will probably be obtained in later runs after the model has been revised to include seasonally-dependent mixing depths and emission rates. However, it is not expected that the annual-average results obtained with this revised model will differ substantially from those presented here.

Table 2 lists the calculated 1973 international exchanges of SO_2 and $SO_4^=$ wet and dry deposition among the 13 countries included in the model runs. Similar tables are also available for the months of January, April, July and October, but these do not differ greatly and are not presented here. The

Table 2

PERCENT CONTRIBUTIONS TO SO_2 AND $SO_4^=$ WET AND DRY DEPOSITION WITHIN RECEPTOR COUNTRIES FROM SO_2 EMISSIONS IN EMITTOR COUNTRIES

(Annual totals for 1973; totals for each receptor country are also given in metric kilotons)

(a) SO_2

ANNUAL (1973) EUROPE

PERCENT CONTRIBUTIONS TO SO2 WET DEPOSITIONS WITHIN RECEPTOR COUNTRIES

EMITTOR COUNTRY	FRG	GDR	FRANCE	POLAND	CZECH	DENMARK	HOLLAND	BELGIUM	U. K.	S.NORWAY	S.SWEDEN	AUSTRIA	SWITZ
W. GERMANY (FRG)	47.5	12.7	3.8	3.7	8.0	12.0	9.8	4.6	1.3	6.6	4.9	17.4	11.3
E. GERMANY (GDR)	8.9	73.3	.3	30.1	28.0	15.6	1.3	.1	.3	23.1	10.7	13.2	4.9
FRANCE	10.6	1.6	73.9	.7	1.3	1.0	3.5	20.7	4.3	.7	.4	7.0	34.5
POLAND	.3	1.5	.0	46.1	9.1	2.3	.0	.0	.0	7.1	8.1	2.7	.0
CZECHOSLOVAKIA	1.8	3.6	.1	15.8	46.5	2.2	.2	.0	.0	4.4	1.6	14.3	1.1
DENMARK	.2	.5	.0	.6	.1	45.3	.0	.0	.0	12.8	18.5	.0	.0
HOLLAND	12.1	2.5	1.4	.7	1.5	4.9	53.8	6.3	1.5	1.0	3.3	2.4	1.3
BELGIUM	8.9	1.9	4.4	.6	.6	1.0	16.4	50.4	1.7	.5	.5	3.9	3.7
U. K.	8.5	2.1	15.1	.7	1.1	14.6	14.9	17.8	90.7	11.9	6.4	5.0	10.3
S. NORWAY	.0	.0	.0	.0	.0	.2	.0	.0	.0	24.8	3.7	.0	0.0
S. SWEDEN	.0	.0	.0	.1	.0	1.1	.0	.0	.0	6.9	43.7	.0	.0
AUSTRIA	.5	.2	.0	.8	3.7	.1	.0	.0	.0	.3	.1	[illegible]	.8
SWITZERLAND	.7	.1	.9	.0	.1	.0	.0	.0	.0	.0	[illegible]	[illegible]	32.0
TOTAL (%)	100.0	100.0	100.0	100.0	100.0	100.0	100.0	100.0	100.0	100.0	[illegible]	[illegible]	100.0
TOTAL (KT)	1166	732	499	1080	559	76	254	179	742	31	85	101	54

PERCENT CONTRIBUTIONS TO SO2 DRY DEPOSITIONS WITHIN RECEPTOR COUNTRIES

EMITTOR COUNTRY	FRG	GDR	FRANCE	POLAND	CZECH	DENMARK	HOLLAND	BELGIUM	U. K.	S.NORWAY	S.SWEDEN	AUSTRIA	SWITZ
W. GERMANY (FRG)	48.9	9.8	7.6	3.1	5.1	9.8	17.9	12.3	1.5	5.6	3.6	11.1	14.7
E. GERMANY (GDR)	17.6	76.6	1.7	28.2	27.4	17.0	2.6	2.0	.3	8.4	8.9	13.6	4.2
FRANCE	7.4	.8	60.8	.5	.9	.6	2.8	15.3	3.4	.9	.2	2.6	29.8
POLAND	.6	2.1	.1	48.2	11.3	3.7	.1	.0	.0	4.0	6.4	4.7	1.0
CZECHOSLOVAKIA	4.0	5.6	.6	16.7	48.6	2.2	.3	.2	.0	1.2	1.2	21.8	2.8
DENMARK	.4	.9	.0	.6	.2	54.5	.1	.0	.1	16.8	21.5	.1	.0
HOLLAND	9.3	1.6	3.0	.6	.7	2.5	51.2	9.7	2.1	2.0	1.8	1.0	1.6
BELGIUM	6.0	1.0	8.0	.4	.5	.8	15.0	46.8	2.0	1.1	.4	1.4	3.5
U. K.	4.4	1.1	18.0	.4	.6	6.7	10.0	13.6	90.6	8.4	3.8	1.6	9.7
S. NORWAY	.0	.0	.0	.0	.0	.4	.0	.0	.0	41.1	5.4	.0	0.0
S. SWEDEN	.0	.1	.0	.2	.0	1.9	.0	.0	.0	10.4	46.8	.0	.0
AUSTRIA	.8	.4	.1	.9	4.6	.1	.0	.0	.0	.1	.1	40.6	2.1
SWITZERLAND	.5	.0	.9	.0	.1	.0	.0	.0	.0	.0	.0	1.3	30.5
TOTAL (%)	100.0	100.0	100.0	100.0	100.0	100.0	100.0	100.0	100.0	100.0	100.0	100.0	100.0
TOTAL (KT)	2325	1787	1730	2589	1388	196	523	449	1910	35	181	328	93

(b) $SO_4^=$

ANNUAL (1973) EUROPE

PERCENT CONTRIBUTIONS TO SO4 WET DEPOSITIONS WITHIN RECEPTOR COUNTRIES

EMITTOR COUNTRY	FRG	GDR	FRANCE	POLAND	CZECH	DENMARK	HOLLAND	BELGIUM	U. K.	S.NORWAY	S.SWEDEN	AUSTRIA	SWITZ
W. GERMANY (FRG)	19.0	10.8	11.8	9.9	12.8	9.3	15.4	7.5	11.8	7.3	10.6	13.9	12.9
E. GERMANY (GDR)	17.2	31.1	2.4	27.6	24.8	19.8	9.4	3.3	9.5	26.7	17.9	25.9	22.7
FRANCE	14.9	7.6	45.7	5.2	7.2	3.5	13.0	27.3	17.6	1.6	2.6	12.6	27.7
POLAND	1.8	5.9	.1	25.3	11.9	7.5	.2	.0	.9	21.8	12.0	3.6	.5
CZECHOSLOVAKIA	4.7	7.5	.6	17.1	20.7	5.9	2.4	.6	2.3	12.6	5.1	10.9	4.5
DENMARK	.4	.8	.1	1.6	.4	7.1	.2	.1	.4	5.2	6.3	.4	.2
HOLLAND	8.6	5.6	5.3	2.6	4.3	6.6	19.2	5.0	5.6	1.6	7.0	3.6	1.9
BELGIUM	8.6	8.2	6.3	2.6	3.0	2.7	11.9	18.7	6.8	.7	1.7	5.4	3.7
U. K.	22.7	12.6	25.8	5.3	10.1	35.8	27.8	36.9	44.2	16.7	28.9	17.5	17.0
S. NORWAY	.0	.0	.0	.1	.0	.2	.0	.0	.0	1.5	1.2	.0	0.0
S. SWEDEN	.1	.1	.0	.3	.1	.7	.0	.0	.1	2.7	5.6	.1	.0
AUSTRIA	1.2	1.4	.3	2.3	4.1	.8	.1	.1	.6	1.4	.8	4.9	3.1
SWITZERLAND	.7	.4	1.7	.3	.4	.2	.2	.6	.2	.2	.1	1.2	5.7
TOTAL (%)	100.0	100.0	100.0	100.0	100.0	100.0	100.0	100.0	100.0	100.0	100.0	100.0	100.0
TOTAL (KT)	204	103	102	203	86	24	24	14	110	19	44	61	17

PERCENT CONTRIBUTIONS TO SO4 DRY DEPOSITIONS WITHIN RECEPTOR COUNTRIES

EMITTOR COUNTRY	FRG	GDR	FRANCE	POLAND	CZECH	DENMARK	HOLLAND	BELGIUM	U. K.	S.NORWAY	S.SWEDEN	AUSTRIA	SWITZ
W. GERMANY (FRG)	23.9	16.6	13.3	9.5	10.5	10.8	20.6	15.5	10.1	14.0	10.8	12.6	17.2
E. GERMANY (GDR)	26.9	43.0	7.2	30.8	30.3	24.4	14.0	13.8	6.1	15.6	10.0	30.7	14.2
FRANCE	8.7	3.7	33.5	3.3	4.3	2.4	8.7	14.6	10.6	3.9	2.1	6.4	19.3
POLAND	2.9	6.8	.5	26.4	14.5	11.3	1.1	.5	.8	13.8	14.0	8.9	4.3
CZECHOSLOVAKIA	8.1	9.8	2.4	16.4	23.5	7.8	3.2	2.5	1.2	5.6	5.1	17.5	7.7
DENMARK	.9	1.9	.3	1.5	1.0	11.8	.4	.3	.9	11.9	9.7	.7	.5
HOLLAND	7.8	4.8	5.7	2.7	3.1	5.1	20.2	7.8	6.4	4.6	6.2	2.5	4.6
BELGIUM	6.2	3.5	8.1	2.1	2.2	1.9	10.3	19.4	6.0	3.1	1.9	3.0	4.8
U. K.	17.5	7.5	27.2	4.3	5.8	22.0	20.8	25.0	57.4	18.2	21.3	8.5	17.7
S. NORWAY	.0	.1	.0	.1	.0	.4	.0	.0	.0	3.6	2.0	.0	0.0
S. SWEDEN	.2	.6	.1	.5	.4	1.5	.1	.0	.1	4.7	8.1	.3	.1
AUSTRIA	1.4	1.7	.5	2.2	4.2	.5	.4	.5	.2	.7	.8	8.2	4.1
SWITZERLAND	.5	.3	1.1	.2	.3	.1	.2	.2	.1	.1	.1	.8	5.5
TOTAL (%)	100.0	100.0	100.0	100.0	100.0	100.0	100.0	100.0	100.0	100.0	100.0	100.0	100.0
TOTAL (KT)	324	161	295	315	154	38	44	36	168	12	50	67	25

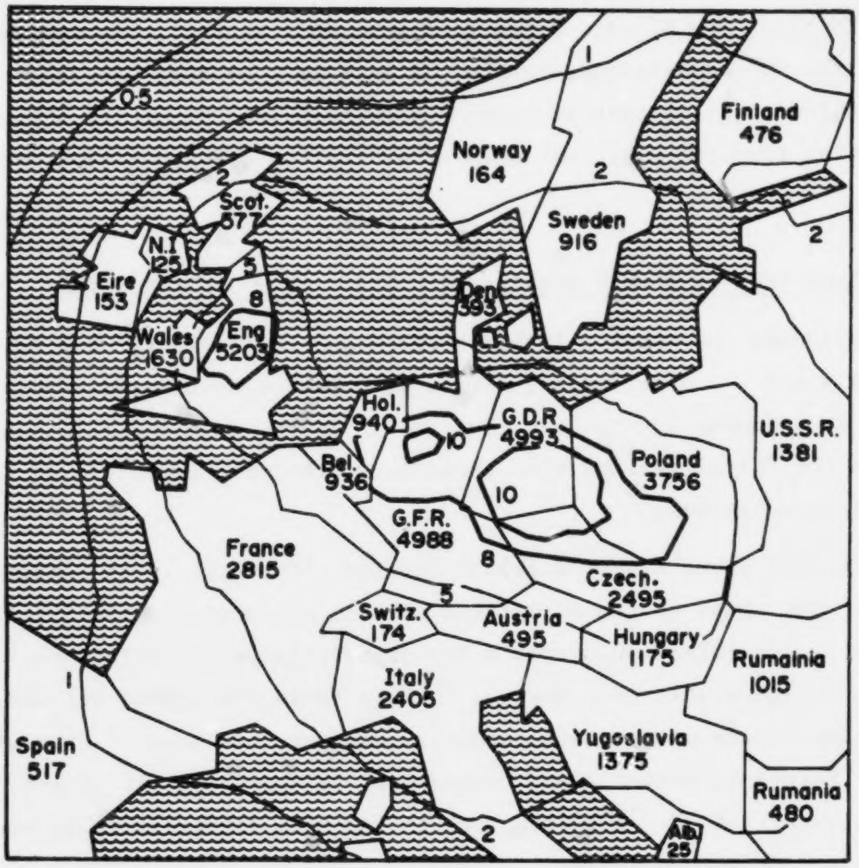
0.5
1
Finland
476
Norway
164
2
2
Scot.
577
Sweden
916
2
N.I
125
Eire
153
5
8
Den
393
Wales
1630
Eng
5203
Hol.
940
G.D.R
4993
10
U.S.S.R.
1381
Poland
3756
Bel.
936
10
G.F.R.
4988
France
2815
8
Czech.
2495
5
Switz.
174
Austria
495
Hungary
1175
Rumainia
1015
1
Italy
2405
Spain
517
Yugoslavia
1375
Rumania
480
2
Alb.
25

FIGURE 9 FISHER'S (1975) RESULTS FOR DRY PLUS WET DEPOSITION IN g m^{-2} SO_2 y^{-1} FROM ALL THE EUROPEAN SOURCES SHOWN

Diffusivity = 50 m^2 s^{-1}; deposition velocity = 5 mm s^{-1}; maximum mixing depths = 1000 and 2000 m. Scavenging coefficient = 10^{-4} s^{-1}. Emission strengths for each country are shown in units of kilotons SO_2 y^{-1}.

annualized SO_2 wet and dry deposition exchanges generally are similar, although some significant differences do occur (e.g., the results indicate that southern Norway receives 23% of its SO_2 wet deposition from East Germany, but only 8% of its SO_2 dry deposition from this source). In comparing the SO_2 to the $SO_4^=$ depositions, however, a different picture emerges. For example, the results indicate that southern Sweden receives 29% of its $SO_4^=$ wet deposition from the U.K., but only 6% of its SO_2 wet deposition from the same source.

B. Comparison of EURMAP Results with Those from Other Models

Obviously the results just described must be evaluated and verified against available observations before they can be considered credible. This effort is underway but not yet completed. In the meantime, it is useful to compare the EURMAP results with those from other models to get an idea of their reasonableness.

Figure 9 shows Fisher's (1975) results for annual total deposition in Europe. The shape of the deposition pattern calculated by Fisher is very similar to the EURMAP SO_2 wet and dry deposition patterns (Figure 8), and the magnitudes agree well over most of the map (when the EURMAP wet and dry deposition values are added together). However, the 10-g/m^2 contour in central Europe on Fisher's map corresponds to approximately 20 g/m^2 as calculated by EURMAP. Possible reasons for this disagreement between maximum values include the following:

- EURMAP has a basic temporal resolution, in terms of grid size, of 50 x 70 km (emissions grid) and 50 x 50 km (receptor grid), while Fisher's model uses a 127 x 127-km grid size for both emissions and receptor areas. Thus, the EURMAP calculations should contain more spatial detail (less areal smoothing), which accordingly should result in higher maximum values.
- Fisher used a dry deposition velocity of 0.5 cm/sec, compared with our value of 0.8 cm/sec.
- A value of 1000 m is used in EURMAP for the mixing depth, while Fisher used 1000 m for half the year, and 2000 m for the other half of the year.

A detailed comparison between the EURMAP results and the model results from the LRTAP Project (Ottar, 1976, 1977) has also been made. In general, the shapes of all concentration and deposition patterns are quite similar. In terms of magnitudes, the EURMAP dry depositions (SO_2 and $SO_4^=$) agree closely with the LRTAP values. The wet deposition results for EURMAP are lower than those from the LRTAP by about a factor of two near the boundaries of the modeled area, probably because the LRTAP model includes emissions from Italy, the USSR, and other countries near the boundaries. However, the EURMAP values are higher than those of the LRTAP model by about a factor of two in the regions of maximum values. For SO_2 and $SO_4^=$ concentrations, the EURMAP results are again approximately twice as high as the LRTAP values in the regions near maxima.

The reasons for this lack of agreement are not fully understood at this time, but again the differences in spatial resolution between the two models may be involved. The LRTAP model has the same 127 x 127 km resolution as Fisher's, and thus the point previously raised may also hold here. Another, but probably minor, factor may be the difference in years modeled: the EURMAP results apply for 1973, while those for the LRTAP are for 1974.

Finally, Table 3 presents a comparison of the international exchanges of sulfur deposition as calculated by the three models for various pairs of countries selected as examples. EURMAP appears to agree a bit better with Fisher's model than does LRTAP (except for the UK-to-UK value). LRTAP gives much lower values than does EURMAP for exchanges involving Holland. Again, the poorer spatial resolution of the LRTAP model may be the cause of this. In the LRTAP model, Holland is covered by only about 4 emissions grid cells, with several of these overlapping into high-emission regions of West Germany, while EURMAP uses 11 emissions cells and 15 receptor cells for Holland. If the Holland values are excluded, the LRTAP and EURMAP dry deposition exchanges are similar.

With regard to wet deposition exchanges, the LRTAP values on the average are considerably lower than those of EURMAP. Although the EURMAP results may be overestimates, some of the LRTAP values for wet deposition exchanges are surprisingly low relative to those for dry deposition: 0.24 g/m^2 (wet)

Table 3

COMPARISON OF EURMAP ESTIMATES OF SULFUR EXCHANGES BETWEEN VARIOUS EUROPEAN COUNTRIES WITH THOSE FROM FISHER (1975) AND THE LRTAP PROJECT (Ottar, 1976)

(Values are Annual Deposition in g m^{-2} as SO_2)*

		Dry Deposition			Wet Deposition			Total Deposition		
Emittor	Receptor	Fisher	LRTAP	EURMAP	Fisher	LRTAP	EURMAP	Fisher	LRTAP	EURMAP
UK	UK	4.0	4.31	5.28	---	0.24	2.08	5.0	4.55	7.36
Sweden	Sweden	0.3	1.67	0.61	---	0.24	0.27	0.4	1.91	0.88
Sweden	UK	---	0.00	0.00	---	0.00	0.00	---	0.00	0.00
UK	Sweden	0.2	0.15	0.10	---	0.58	0.10	0.2	0.73	0.20
FRG	Sweden	---	0.11	0.07	---	0.35	0.05	---	0.46	0.12
Denmark	Sweden	---	0.24	0.30	---	0.21	0.12	---	0.45	0.42
GDR	Sweden	---	0.27	0.16	---	0.44	0.10	---	0.71	0.26
Poland	Sweden	---	0.15	0.11	---	0.13	0.06	---	0.28	0.17
FRG	FRG	---	4.70	4.53	---	0.82	2.21	---	5.52	6.74
FRG	Holland	---	0.64	2.66	---	0.11	0.73	---	0.75	3.39
FRG	UK	---	0.05	0.12	---	0.02	0.05	---	0.07	0.17
FRG	GDR	---	---	1.79†	---	---	0.99†	---	---	2.78†
FRG	France	---	0.16	0.29	---	0.04	0.05	---	0.20	0.34
Holland	FRG	---	0.17	0.89	---	0.12	0.58	---	0.29	1.47
UK	FRG	---	0.27	0.50	---	0.55	0.50	---	0.82	1.00
GDR	FRG	---	0.50	1.78	---	0.14	0.48	---	0.64	2.26
France	FRG	---	0.34	0.72	---	0.38	0.55	---	0.72	1.27
Holland	Holland	---	3.20	7.31	---	0.22	3.73	---	3.42	11.04
Holland	UK	---	0.02	0.14	---	0.01	0.05	---	0.03	0.19
UK	Holland	---	0.69	1.57	---	0.64	1.13	---	1.33	2.70
France	France	---	1.90	2.05	---	0.24	0.74	---	2.14	2.79
France	UK	---	0.07	0.23	---	0.05	0.13	---	0.12	0.36
UK	France	---	0.26	0.68	---	0.20	0.17	---	0.46	0.85
Averages			0.90	1.34		0.26	0.63		1.13	2.00

---

* For convenience in obtaining sums, values are carried to three significant figures rather than rounded, but this does not imply a similar level of accuracy.

† Average does not include FRG to GDR amounts since LRTAP values are not available.

vs. 4.31 (dry) for UK-to-UK; 0.22 (wet) vs. 3.20 (dry) for Holland-to-Holland; 0.82 (wet) vs. 4.70 (dry) for FRG-to-FRG.

C. Conclusions

Results from the current version of EURMAP are generally similar to those from other comparable models, but significant differences do exist. In those cases, it is not clear at this time which model is more correct. An ongoing effort to evaluate EURMAP with available observations should yield more definitive information. Based upon the results of this evaluation, appropriate refinements will be incorporated into the model.

Ultimately, information in the form shown in Table 2 from a suitably validated version of EURMAP should be useful in the management of air quality on an international basis in western and central Europe. Using information on planned or potential future changes in the emissions distribution over the region, EURMAP could also be used at some later stage to prepare air quality projections for future years.

ACKNOWLEDGEMENTS

This study is being conducted under a contract from the Federal Environmental Office (Umweltbundesamt) of the Federal Republic of Germany (FRG), under the direction of Dr. J. Pankrath and Dr. D. Jost of that office and Dr. E. Weber of the Federal Ministry of the Interior (FRG). We wish to acknowledge with thanks the assistance of Dr. Pankrath, Dr. Jost, Dr. Weber, and Dr. B. Ottar of the Norwegian Institute of Air Research in offering useful suggestions and furnishing valuable technical information necessary for this project. We are also grateful for the assistance of Miss Joyce Kealoha, Mrs. Linda Jones, and Mrs. Evelyn Freisheim in the preparation of this report.

REFERENCES

Beilke, S., 1970: Laboratory investigations on washout of trace gases. Precipitation Scavenging (1970)--Proceedings of a Symposium Held at Richland, Washington, June 2-4, 1970. AEC Symposium Series 22, 1970.

Bolin, B., and C. Persson, 1975: Regional dispersion and deposition of atmospheric pollutants with particular application to sulfur pollution over Western Europe. Tellus, 27, No. 3, 281-310.

Eliassen, A., and J. Saltbones, 1975: Decay and transformation rates of SO_2, as estimated from emission data, trajectories and measured air concentrations. Atmospheric Environment, 9, 425-429.

Fisher, B.E.A., 1975: The long range transport of sulphur dioxide. Atmospheric Environment, 9, 1063-1070.

Gifford, F.A., 1976: Tropospheric relative diffusion observations. Unpublished paper, ATDL Contribution File No. 76/10, NOAA, Oak Ridge, Tennessee, May 1976.

Heffter, J.L., 1965: The variation of horizontal diffusion parameters with time for travel periods of one hour or longer. J. Appl. Meteor., 4, 153-156.

Hilst, G.R., 1968: Meteorological management of air pollution. Chapter 10, Air Pollution, Vol. 1, 2nd ed., 321-347. Ed. Arthur C. Stern, Academic Press, N.Y.

Johnson, W.B., D.E. Wolf, and R.L. Mancuso, 1976: The European Regional Model of Air Pollution (EURMAP) and its application to transfrontier air pollution. Proceedings of the 7th Int. Tech. Meeting on Air Pollution Modeling and Its Application, 7-10 Sept. 1976, Airlie House, VA, a report of the Air Pollution Pilot Study, NATO Committee on the Challenges to Modern Society.

Jost, D., 1973: Zue Husbreitung von Luftbeimengungen über Industriegebieten. Annalen der Meteorologie, 6, 151-156.

Jost, D., 1974: Aerological studies on the atmospheric sulfur budget. Tellus, 26, No. 1-2, 206-212.

McMahon, T.A., P.J. Denison, and R. Fleming, 1976: A long-distance air pollution transportation model incorporating washout and dry deposition components. Atmospheric Environment, 10, 751-761.

Ottar, B., 1976: The deposition and distribution in European countries of pollutants from distant and local sources. Draft final report for the OECD project, LRTAP, coordinated by the Norwegian Institute for Air Research.

Ottar, B., 1977: The OECD study on Long Range Transport of Air Pollutants (LRTAP). Proceedings of the International Symposium on Sulfur in the Atmosphere, 7-14 Sept. 1977, Dubrovnik, Yugoslavia.

Prahm, L.P., and O. Christensen, 1977: Long range transmission of pollutants simulated by the 2-D pseudospectral dispersion model. Danish Meteorological Institute Report 77/1, Denmark, Feb. 1977.

Rao, K.S., I. Thomson, and B.A. Egan, 1976: Regional transport model of atmospheric sulfates. Proc. of Annual Meeting of APCA, June 1976, Portland, OR, Paper No. 76-34.3.

Renne, D.S., and D.L. Elliott, 1976: Regional air quality assessment for northwest energy scenarios. Presented at the 69th Annual Meeting of the Air Pollution Control Association, June 27 - July 1, 1976, Portland, OR, Paper No. 76-23.5.

Rystad, B., S. Stromsoe, E. Amble, and T. Knudsen, 1974: The LTRAP emission survey. Norwegian Inst. for Air Research, Norway, 19p.

Sheih, C.M., 1977: Application of a statistical trajectory model to the simulation of sulfur pollution over northeastern United States. Atmospheric Environment, 11, 173-178.

Smith, F.B., and G.H. Jeffrey, 1975: Airborne transport of sulphur dioxide from the U.K. Atmospheric Environment, 9, 643-659.

Start, G.E., and L.L. Wendell, 1974: Regional effluent dispersion calculations considering spatial and temporal meteorological variations. NOAA Tech. Memo ERL ARL-44, Air Resources Laboratories, Idaho Falls, ID, 63p.

Weber, E., 1971: Removal of sulfur dioxide from the atmosphere. Proc. of the Second Meeting, NATO/CCMS Panel on Modeling, July 1971, Paris, France, Report No. 5, Chapter XII.

Wendell, L.L., D.C. Powell, and R.L. Drake, 1976: A regional scale model for computing deposition and ground level air concentration of SO_2 and sulfates from elevated and ground sources. Proc. of the Third Symposium on Atmospheric Turbulence, Diffusion and Air Quality, Oct. 19-22, 1976, Raleigh, NC, published by the AMS, Boston, MA. Also in Proceedings of the 7th Int. Tech. Meeting on Air Pollution Modeling and Its Application, 7-10 Sept. 1976, Airlie House, VA, a report of the Air Pollution Pilot Study, NATO Committee on the Challenges to Modern Society.

Whelpdale, D.H., and R.W. Shaw, 1974: Sulphur dioxide removal by turbulent transfer over grass, snow, and water surface. Tellus, 26, 196-205.

8th International Technical Meeting on
Air Pollution Modeling and its Application

TRANSNATIONAL AIR QUALITY: THE CASE FOR THE STRATOSPHERE

Joseph B. KNOX
Marvin H. DICKERSON
Rolf LANGE
Kendall R. PETERSON

September 2o - 23,1977
Louvaine-La-Neuve
Belgium

TRANSNATIONAL AIR QUALITY:
THE CASE FOR THE STRATOSPHERE*

Joseph B. Knox, Marvin H. Dickerson,
Rolf Lange and Kendall R. Peterson
Lawrence Livermore Laboratory, University of California,
Livermore, CA 94550

August 1977

1. INTRODUCTION

During the past decade the trend in commercial aircraft design has lead to increased use of flight corridors in the stratosphere. This tendency has been accelerated with the advent of the Concorde and the 747 SP commercial aircraft, and with modern Lear-type jets for corporate travel. Flight levels for these aircraft are nominally at 14 to 18 kilometres, depending on aircraft type. The FAA reports that North Atlantic corridors are now crowded and becoming more crowded with the passage of time.[1] It is anticipated that future flight levels will gradually increase in order to permit heavier travel over certain routes, thereby leading to increased use of the stratosphere as a flight medium.

Concern about cabin environments and the exposure of flight crews and passengers to ionizing radiation at stratospheric flight levels is not a new issue. Ionizing radiation within the aircraft cabin may come from two significant sources: cosmic rays whose intensity increases with height, and radionuclides from nuclear tests in the atmosphere when aircraft encounter the debris cloud. A high yield nuclear cloud stabilizes at levels of 15 to 25 kilometres, depending on yield and the thermal stratification of the stratosphere;[2] the cloud may remain relatively coherent for more than a week in a weak, turbulent diffusion environment of the stratosphere. Since our society places a high value on public safety and welfare, it is the intent of the FAA and ERDA, that modern environmental assessment methodology and existing capabilities of the U. S. government be applied to minimize exposure of passengers and crew to ionizing radiation during flight travel. A secondary but important issue is the possible contamination of the aircraft and the costs and problems attendant to its proper maintenance following contamination. This latter issue will, however, not be directly addressed in the development of SEAC, whose primary purpose is to provide useful information to minimize or avoid exposure of passengers and crew to ionizing radiation from nuclear debris clouds. In accomplishing this primary objective, the second issue can also be met to a very large extent.

Federal and public attention to this issue was recently renewed following the Chinese nuclear tests on September 26, 1976 and November 17, 1976. It is pertinent to summarize some of the events and effects arising in the U. S. during and following the passage of these nuclear debris clouds. The September 26 Chinese test had a yield of about 200 kt.[3] At this yield more than half of the debris stabilized in the upper troposphere.[2] The debris cloud passed over the U. S. from 6 to 10 days after the detonation; first over the Pacific Northwest and later over the mid-Atlantic states.[4] Precipitation scavenging lead to rapid deposition of the debris in the vicinity of the Peachbottom Nuclear Power Plant located near Philadelphia.[5] The reactor operators were apparently not informed of these wet deposition relative hotspots or their possibility, and initially interpreted the events as a possible malfunction of the reactor due to monitor readings and swipes from employee's automobiles. Lacking further information, as a conservative measure the managers sent their employees home, including contractor personnel working on the cooling towers, subsequent to washing down about 300 of their automobiles.[5] In retrospect, it is clear that sharing of proper information in an early warning sense of expected events and probable areas affected would have permitted this situation to be avoided. Following this event, LLL indicated that there was an existing capability that could have been, and could in the future, be used to forecast the wet or dry deposition radiation levels in similar circumstances.

The next Chinese test on November 17th had a yield of 4 MT[3] and created a coherent, stabilized stratospheric debris cloud centered at about 20 km.[2] Concern about the possible impacts and effects on SST passengers and crew became a matter of concern to the public and to operating [illegible] crews. ERDA and LLL were alerted to the need for estimates of the possible and expected radiation exposures from external gamma radiation in the event flights intersected the cloud. A synopsis of our response to this request is now described.

2. THE RESPONSE TO THE STRATOSPHERIC DEBRIS CLOUD OF NOVEMBER 1976

On the morning of November 17, the LLL was informed of the test and its yield. An early trajectory prediction was made in the afternoon. Subsequent cloud sampling information at the U. S.-Canadian border indicated a cloud center concentration of 10^8 pCi/SCM for gross beta fission products or a corresponding external gamma, whole body dose rate of about 200 mr/hr.[6] Estimates of cloud dilution by turbulent diffusion indicated that the stratosphere was relatively quiet and that subsequent dilution would occur slowly. Computer simulations of cloud dilution were performed with turbulent diffusion parameters selected to be consistent with the historical dilution of the cloud.* Based on these calculations, we advised ERDA and the FAA that our conservative estimate of the external whole body dose rate for possible Concorde interception with the cloud at 18 km was 10 mr/hr beneath the cloud center, and could in the remote case of cloud descent be as high at 100 mr/hr. Figure 1 shows the cloud concentrations as claculated with the LLL 2BPUFF code as compared to those actually measured at various times and altitudes by U. S. aircraft. Based on the coherence of the cloud and the relatively low levels of the expected radiation levels, operations were deemed safe.

However, as a conservative measure the LLL and EG & G, at the request of the FAA and ERDA, placed health physicists with portable gamma spectrometers on board trans-Atlantic Concorde flights during Thanksgiving weekend, when the planes were expected to intercept the lower part of the debris cloud. Spectra recorded during three flights were characteristic of fresh fission debris; these observations gave positive identification as well as in-cabin dose rates of 0.7 to 1.3 mr/hr.[7] These measurements are shown in Fig. 1 as the three symbols beyond 200 hours.* Figure 2 shows the 9 km (upper troposphere) and 20 km cloud center trajectories.

The in-flight measurements were made with several portable instruments. A Geiger counter was used to measure small variations in cosmic ray activity. A gas proportional chamber provided a continuous log of activity seen during the flights. Both LiF thermoluminescent dosimeters and whole air samples gave an integrated assessment of radiation exposure for each flight. Finally, a portable gamma spectrometer was used to identify fresh fission product debris. Lanthanum-140, a bomb-produced nuclide, was identified on some of the flights.

---

*The turbulent diffusion parameters used will be discussed at the end of the next section.

*The cosmic ray background dose rate, observed to be 0.6 mr/hr, has been subtracted from the measured values to make the observations compatible with previous aircraft filter samples.

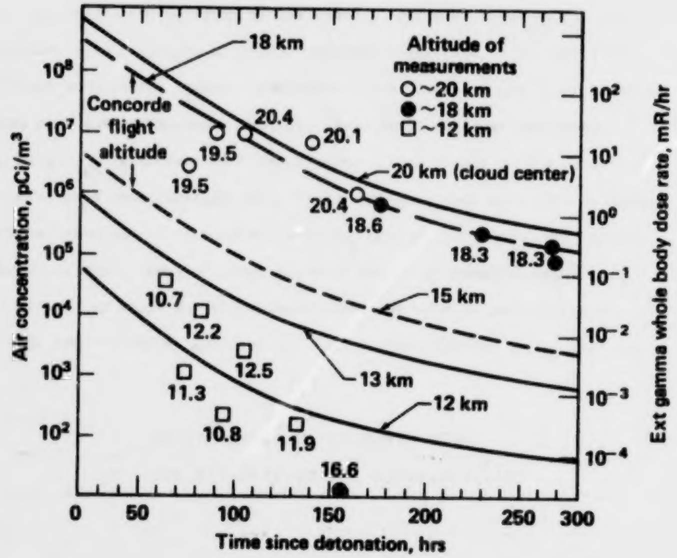

FIGURE 1. 2BPUFF predicted and observed air concentrations and dose rates vs. time. Number adjacent to symbol is altitude of measurement in kilometers.

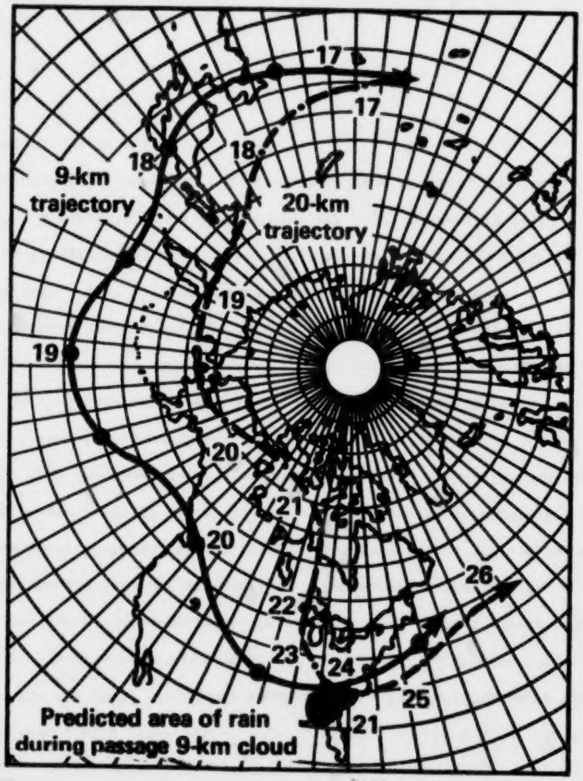
9-km trajectory
20-km trajectory
17
17
18
18
19
19
20
20
21
21
22
23
24
25
26
Predicted area of rain during passage 9-km cloud

FIGURE 2. Estimated cloud center trajectories at 9 and 20 km. Numbers along trajectory are day and position at 1200 GMT. Other dots are for 0000 GMT.

3. THE 2BPUFF LARGE CLOUD DIFFUSION CODE

It is pertinent to give a brief description of the 2BPUFF large cloud diffusion code used to prepare the assessment of the November 1976 debris cloud, and then proceed to present the recently developed techniques for treating transport and diffusion in three dimensions and to extended ranges.

2BPUFF

The 2BPUFF large cloud diffusion code[8-10] assumes the source is a vertical-axis right circular cylinder and uses a coordinate system fixed to the puff center. The scale dependent diffusion approach is used to calculate the horizontal dispersion, while the vertical diffusivity is a time-variable input parameter. Other code input includes initial puff radius and half-thickness, temperature inversion heights, precipitation rate, puff center wind speeds, topography under the trajectory of the puff center, and deposition velocity. In addition, for each nuclide, up to a maximum of 30, input is made for the initial number of picocuries, the radioactive half-life, and dose conversion factors for up to seven pathways to man. 2BPUFF calculates air concentrations and dose rates at altitudes from the top of the cloud to the surface and the surface deposition for both dry and wet (rainout) conditions. The assumptions and the physical equations of this model are shown in Table 1 with the definition of symbols in Table 2.

TABLE 1. Summary of 2BPUFF method for predicting the distribution of debris from a tropospheric cloud.

Initial Conditions

Volume Source: Depth and radius of a cylindrical cloud
Source strength: Q
Height: h

Governing Equations

$$\frac{d\chi}{dt} = K_h\left(\frac{\partial^2\chi}{\partial r^2} + \frac{1}{r}\frac{\partial\chi}{\partial r}\right) + \frac{\partial}{\partial z}\left(K_z\frac{\partial\chi}{\partial z}\right)$$

$\sigma^2 = \sigma_0{}^2 + 1.33\ C_1(\varepsilon\sigma_0)^{2/3}\ t^2$ and $K_h = 0.2\sigma^{4/3}$ (Early times)

Transition time: $t_1 = C_3\sigma_0{}^{2/3}\ \varepsilon^{-1/3}$

$\sigma^2 = \sigma_1{}^2 + \frac{C_2}{3}\varepsilon(t - t_1)^3$ and $K_h = 0.2\sigma^{4/3}$ (Intermediate times)

K_h = constant (Late times)

C_1, C_2 and C_3 are of order unity

Parameter Selection (General Guides)

$$\varepsilon = \frac{300}{z}\left|\frac{U}{5}\right|^3$$

z = height of cloud center above local terrain (m)
U = horizontal wind speed (m/sec)
K_z = a function of weather along the cloud path (cm^2/sec). Values range from 10^2 to 10^5 cm^2/sec
v_d = 1 cm/sec (most commonly used value)
Maximum value of K_h = 1 - 3 x 10^{10} cm^2/sec

Removal Mechanisms

Dry deposition: $\chi_s v_d$
Wet deposition: $e^{-\Lambda t}$
Radioactive decay
} Amounts removed from cloud are deposited on ground

Boundary Conditions

$$\chi_s v_d = K_z\frac{\partial\chi}{\partial z}$$

TABLE 2. Symbols used in the calculation.

h	Initial height
Q	Source strength
K_h	Horizontal diffusion coefficient
K_z	Vertical diffusion coefficient
r	Radius
t	Time
U	Mean speed of cloud
v_d	Deposition velocity
x	Distance cloud has traveled downwind
y	Distance crosswind
z	Height above surface
ϵ	Rate of dissipation
Λ	Washout coefficient
σ	Standard deviation of distribution of radioactivity in cloud.
σ_0	Initial value of σ (at time of cloud stabilization)
χ	Concentration of radioactive debris in cloud
χ_s	Concentration of radioactive debris at surface

In the late 1960's we used cloud concentration data from U. S. cratering tests to help verify 2BPUFF calculations. The Cabriolet nuclear cratering test occurred on January 26, 1968. Figure 3 depicts the main cloud center concentrations vs. time based on meteorological input from climatology, a forecast made about four hours before the experiment, and observed weather parameters (diagnostic) as the debris cloud moved downwind.[11] The open circles represent exposure rate measurements converted to concentrations, while the closed circles indicate filter samples.

Figure 4 is a similar diagram to Fig. 3, except that the curves and data points are for the cloud center concentrations for the Schooner cratering experiment on December 8, 1968. No forecast curve is shown; also in Fig. 4 the squares and circles represent exposure rate and filter sample measurements, respectively.

It is apparent from these figures that for those measurements made on the cloud centerline, 2BPUFF forecast concentrations are within a factor of three of the observations.[10] Diagnostic (post-detonation) calculations are within a factor of two. Similar accuracy is seen in the 2BPUFF estimates for the PRC test on November 17, 1976 (Fig. 1) when appropriate stratospheric values of ϵ and K_z are used. The stratospheric values of K_z and ϵ used for the PRC test of November 17, 1976 are shown in Fig. 5b. Figure 5a shows typical tropospheric diffusion parameters for comparison. Our experience with two-dimensional extended scale Lagrangian transport, diffusion, and deposition calculations indicates that:

1. There is significant advantage in using a Lagrangian expanding grid for cloud diffusion calculations;
2. The physically reasonable scale-dependent horizontal eddy diffusion prescription provided by similarity theory gives results consistent with measurements;

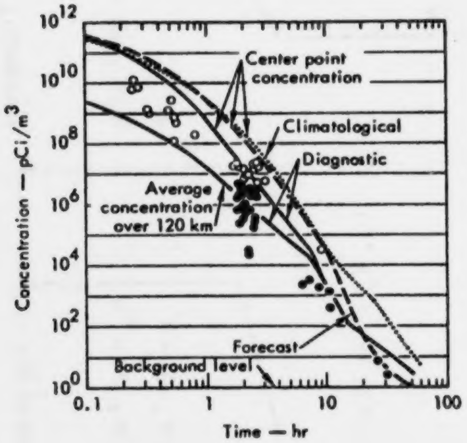

FIGURE 3. Calculated and measured airborne concentrations as a function of time for the Cabriolet event of January 26, 1968.

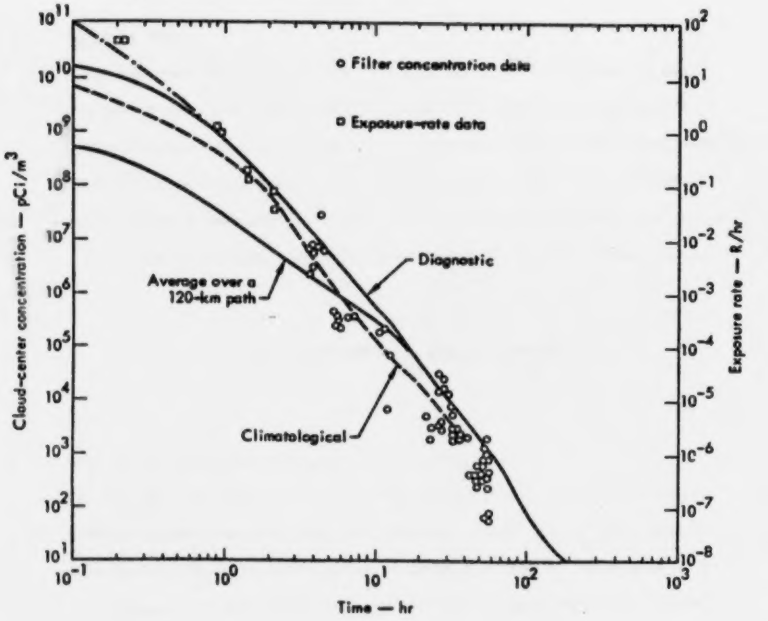

FIGURE 4. Schooner main cloud: cloud center total concentration as a function of time (the right hand ordinate should be used with the dot-dashed curve.)

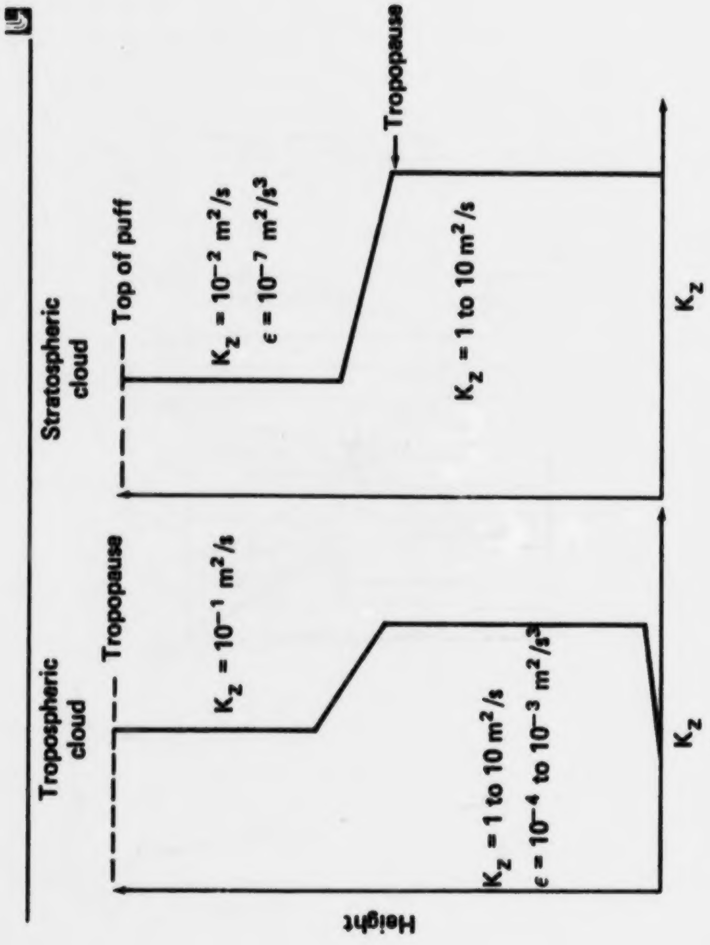
Tropospheric cloud
Tropopause
$K_z = 10^{-1}\ m^2/s$
Height
$K_z = 1$ to $10\ m^2/s$
$\epsilon = 10^{-4}$ to $10^{-3}\ m^2/s^3$
K_z
Stratospheric cloud
Top of puff
$K_z = 10^{-2}\ m^2/s$
$\epsilon = 10^{-7}\ m^2/s^3$
Tropopause
$K_z = 1$ to $10\ m^2/s$
K_z

5a

5b

FIGURE 5

3. The separation of the cloud diffusion calculation from the trajectory prediction problem permits practical calculations c· essential characteristics of the pollutant distribution.

Perhaps the most outstanding deficiency of this technique is the lack of estimation of cloud shape in three dimensions. Nonetheless, this research illustrates the verified state-of-the-art in the late 60's to the mid-70's for the treatment of puff diffusion to extended ranges as well as the feasibility of this type of approach.

4. THE ADPIC-PATRIC DIFFUSION MODELS

In the early 1970's we began investigating various methods for simulating three-dimensional transport and diffusion of radionuclides in the atmospheric boundary layer. As a result of this study the Atmospheric Diffusion Particle-In-Cell (ADPIC)[12] computer code has been developed and tested over the past 5 years. Recently, a simplified version of ADPIC has been developed in the form of a Particle Trajectory In Cell (PATRIC) code.

ADPIC

The ADPIC code is a numerical, three-dimensional, Cartesian, particle-diffusion code capable of calculating the time-dependent distribution of air pollutants under many conditions. These conditions include strongly distorted advection wind fields, calm conditions, surface roughness, wet and dry deposition, radioactive decay, and space- and time-variable diffusion parameters.

Basically, the code solves the three-dimensional advection-diffusion equation in its flux conservative form (pseudovelocity technique) for a given non-divergent advection field. The method is based on the particle-in-cell technique with the pollutant concentration represented by Lagrangian-marker particles inside a fixed Eulerian grid.[13-16] Most air pollution scenarios involve time- and space-varying advection fields (shear) and diffusion parameters. They involve topography, precipitation, and gravitational effects for a variety of active or inert source and are inherently three-dimensional in nature. ADPIC was developed to model these aspects of pollutant dispersal over short or long times for any specified source term with the exception, for the present, of photochemistry.

With the development of the three-dimensional non-divergent (mass-conservative) windfield model MATHEW,[17] which is used to provide the full three-dimensional space- and time-varying advection field to ADPIC, pollutant dispersion studies of any desired complexity can be undertaken.

The basic equations of ADPIC are shown in Table 3 together with a typical computational cycle. During the first half cycle a diffusivity velocity U_D is computed from the pollutant concentration χ at each grid point and the advection velocity U_A is added to get the pseudo velocity U_p. During the second half cycle the coordinates R for each particle are advanced in time, resulting in a new concentration distribution χ. ADPIC has undergone extensive validation tests against closed analytic solutions and regional tracer studies, and compares to within a 5% standard deviation error against selected analytic solutions.[16] Regional tracer

TABLE 3. Governing equations for ADPIC

Advection-diffusion equation:

$$\frac{\partial \chi}{\partial t} + \vec{U}_A \cdot \nabla \chi = \nabla \cdot K \nabla \chi$$

Assume:

$$\nabla \cdot \vec{U}_A = 0 \qquad \text{(incompressibility)}$$

Define:

$$\vec{U}_D = -K \frac{\nabla \chi}{\chi} \qquad \text{(diffusivity velocity)}$$

Pseudo-velocity form of diffusion-advection equation:

$$\frac{\partial \chi}{\partial t} + \nabla \cdot (\vec{U}_p \chi) = 0$$

$$\text{where} \quad \vec{U}_p = \vec{U}_A + \vec{U}_D$$

ADPIC computational cycle:

Eulerian part (at each grid point):

$$\vec{U}_D = -K \frac{\nabla \chi}{\chi}$$

$$\vec{U}_p = \vec{U}_A + \vec{U}_D$$

Lagrangian part (for each particle):

$$\vec{R}_{T+\Delta T} = \vec{R}_T + \vec{U}_p \cdot \Delta T$$

$\vec{U}_p$ is the pseudo velocity vector
$\vec{U}_A$ is the advection velocity vector
$\vec{U}_D$ is the diffusivity velocity vector
K is the diffusivity
χ is the concentration
$\vec{R}$ is a typical particle position
ΔT is a computational time step
T is time

studies using ^{131}I at Idaho Falls (Fig. 6) and ^{41}Ar plumes at Savannah River Plant (Fig. 7) were used to partially validate ADPIC against regional field data using fixed high-volume samplers, γ-detector-equipped cars, and helicopters.[12] Without tuning the model to any given regional site, type of source, or sampling method ADPIC was 60% of the time within a factor or 2 of field data while 96% of the time it agreed to within an order of magnitude.

PATRIC

Fully three-dimensional, time varying transport models like ADPIC are unsuitable for long time or synoptic scale assessment studies at the present time because of the high computational costs. However, ADPIC with its particle-in-cell pseudo-velocity approach lends itself to a number of simplifying approximations that lead to a significant reduction in computer time for such studies, while still retaining the capability to model the important basic features of the transport and dispersal processes in the atmosphere. This simplified particle trajectory-in-cell model (PATRIC) has recently been developed at LLL and is being used both as a regional annual assessment model and as a global fallout model for nuclear aerosol debris clouds.

The three major simplifications made in ADPIC to derive PATRIC are the following:

a. The wind field for PATRIC has no vertical velocities (w = 0). But, because the horizontal components U and V are functions of space and time, both, power, and directional shear can be modeled.

b. The topography is flat in PATRIC.

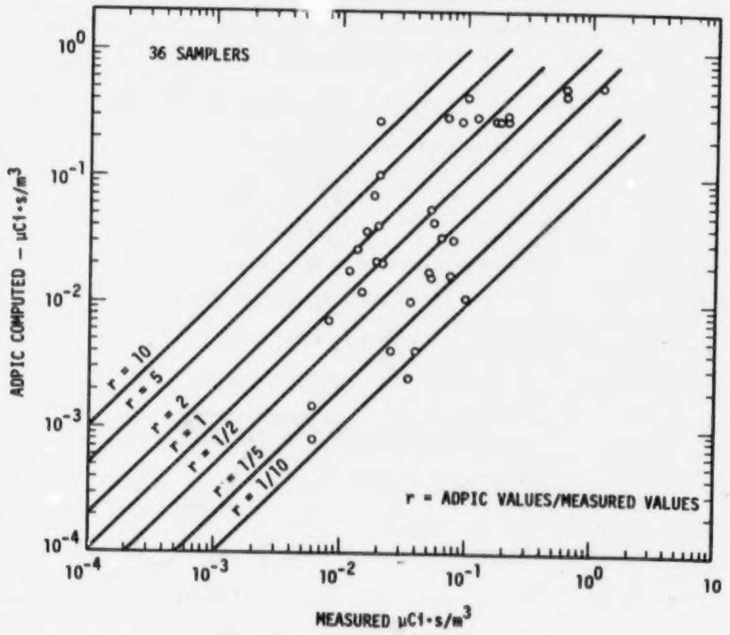

FIGURE 6. Measured and computed time integrated ^{131}I surface air concentrations for 36 samplers at Idaho Falls.

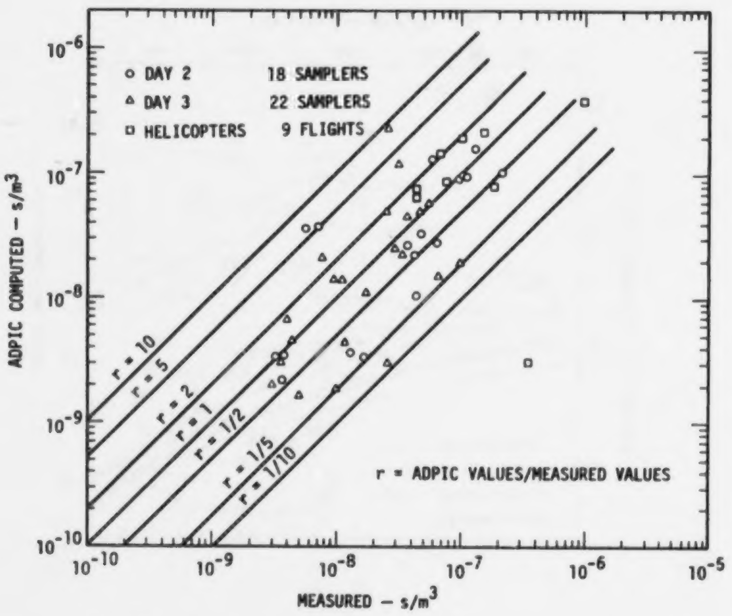

FIGURE 7. Measured and computed relative concentrations for three ^{41}Ar plumes at 49 samplers at SRP.

c. The assumption is made that diffusion is governed by a Gaussian distribution rather than by gradient transport between adjacent grid cells, as in ADPIC. This makes diffusion in PATRIC independent of a grid mesh and the PATRIC grid cells need only be small enough to resolve the features of the wind field but not those of the pollutant distribution. This results in a reduction in the number of Eulerian grid cells needed by one or two orders of magnitude over ADPIC.

Generally, PATRIC is the same as ADPIC and hence most of the options available for ADPIC, as discussed earlier, are also available in PATRIC.

5. PATRIC POST ANALYSIS OF STRATOSPHERIC DEBRIS CLOUD OF NOVEMBER 1976

A post analysis of the stratospheric debris cloud of November 1976 was made with PATRIC, both with and without speed and directional shear. All input parameters were held the same as for the 2BPUFF calculation for the same cloud as discussed in Sections 2 and 3. The PATRIC results are given in Fig. 8 against the same set of experimental measurements shown in Fig. 1 with the 2BPUFF comparison. A cloud center trajectory was assumed with a mean wind of 24 m/s as obtained from the trajectory estimation in Fig. 2. The stratospheric diffusion parameters used were $K_z = 10^{-2}\ m^2/s$ and $\varepsilon = 10^{-7}\ m^2/s^3$ as shown in Fig. 5b. The horizontal diffusivity K_H was related to ε and the standard deviation of the cloud σ_y by scale dependent diffusion[17] $K_H(t) = \varepsilon^{1/3}\ (\sigma_y(t))^{4/3}$.

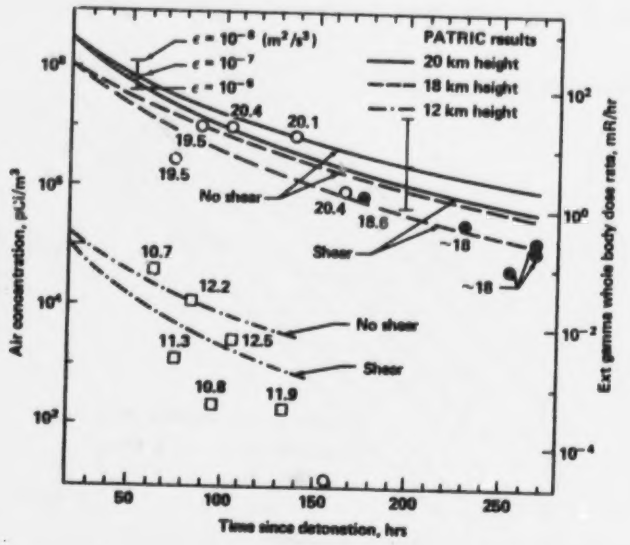

FIGURE 8. PATRIC predicted and observed air concentrations and dose rates vs. time. Numbers adjacent to symbols are altitudes of measurement in kilometres. Concorde flight altitude ∿ 18 km. Cloud center height ∿ 20 km. The error bar on the 20 km no-shear curve at 50 hrs and at 200 hrs indicates how this curve would be shifted if ϵ were increased or decreased by an order of magnitude.

Figure 8 indicates that the best fit obtainable with PATRIC to the 20 km and 18 km measurements appears to be with $\epsilon = 10^{-7}$ m^2/s^3 and some moderate shear. The shear chosen in this case was an average of radiosonde measurements obtained at Fairbanks, Alaska; Trout Lake, Canada; and Nashville, U.S.A. during the period of cloud passage over North America and corresponds to a vertical speed shear of 10^{-3} s^{-1} and a directional shear of 10^{-3} deg/m. The error bars on the no-shear 20 km PATRIC curve at 50 hrs and at 200 hrs indicate the expected change in the results if ϵ were changed by an order of magnitude higher or lower. Evidently, the PATRIC results corroborate the results from 2BPUFF that the stratosphere was extremely non-turbulent at the time as indicated by the very small dissipation rate ϵ needed in the models to match the measurements.

Comparison of PATRIC and 2BPUFF results between Fig. 8 and Fig. 1 show some differences despite the fact that both codes used the same input as closely as possible. These differences are to be expected and are not large when one considers the difference in the two approaches, code geometries, and the typical ensuing numerical and parameterization errors.

6. TRANSFERABLE EXPERIENCE TO TRANSNATIONAL AIR POLLUTION PROBLEMS

Our experience provides the following significant points for transnational air pollution studies:

a. The importance of the use of a unique tracer for positive identification of the pollutant cloud against an ambient background.

b. The essential role of ε in determining the accuracy of solutions at extended ranges.

c. The illustrative use of a "repro" model with the desirable characteristics of being a simulator of processes in a more complete, long-running code rather than simply as interpolator among solutions.

REFERENCES

1. Broderick, T., private communication, January 1977.
2. Peterson, K. R., "An Empirical Model for Estimating World-Wide Deposition from Atmospheric Nuclear Detonations," *Health Physics, 18*, pp. 357-278, 1970.
3. *New York Times*, November 18, 1976, p. 6.
4. Telegadas, K., private communication, November 1976.
5. *New York Times*, October 6, 1976, p. 1, 20.
6. Deal, L. J., private communication, November 1976.
7. Crites, T., private communication, December 1976.
8. Crawford, T. V., "A Computer Program for Calculating the Atmospheric Dispersion of Large Clouds," Lawrence Livermore Laboratory Report UCRL-50179, 1966.
9. Knox, J. B., T. V. Crawford, K. R. Peterson, and W. K. Crandall, "Comparison of U. S. and U.S.S.R. Methods of Calculating the Transport, Diffusion, and Deposition of Radioactivity," Lawrence Livermore Laboratory Report UCRL-51054, 1971.
10. Knox, J. B., "Numerical Modeling of the Transport Diffusion and Deposition of Pollutants for Regions and Extended Scales," *JAPCA, 24*(7), July 1974.
11. Crawford, T. V., "Atmospheric Transport, Diffusion and Deposition of Radioactivity," Lawrence Livermore Laboratory Report UCRL-71433, 1969.
12. Lange, R., "ADPIC - A Three-Dimensional Particle-in-Cell Model for the Dispersal of Atmospheric Pollutants and Its Comparison to Regional Tracer Studies," Lawrence Livermore Laboratory Report UCRL-76107, Rev. 2, 1976.
13. Welch, J. E., F. H. Harlow, J. P. Shannon, and B. J. Daly, "The MAC Method," Los Alamos Scientific Laboratory Report LA-3425, 1965.
14. Amsden, A. A., "The Particle-in-Cell Method for the Calculation of the Dynamics of Compressible Fluids," Los Alamos Scientific Laboratory Report LA-3466, 1966.

15. Sklarew, R. C., A. J. Fabrik, and J. E. Prager, "A Particle-in-Cell Method for Numerical Solution of the Atmospheric Diffusion Equation, and Application to Air Pollution Problems," Systems, Science and Software, La Jolla, CA, Report 3SR-844, 1971.

16. Lange, R., "A Three-Dimensional Computer Code for the Study of Pollutant Dispersal and Deposition Under Complex Conditions," Lawrence Livermore Laboratory Report UCRL-51462, 1973.

17. Sherman, C. A., "A Mass-Consistent Model for Wind Fields Over Complex Terrain," Lawrence Livermore Laboratory Report UCRL-76171, Rev. 2, 1976.

18. Walton, J. J., "Scale-Dependent Diffusion," *J. Appl. Meteoro.*, *12*(3), pp. 547-549, 1973.

NOTICE

"This report was prepared as an account of work sponsored by the United States Government. Neither the United States nor the United States Energy Research & Development Administration, nor any of their employees, nor any of their contractors, subcontractors, or their employees, makes any warranty, express or implied, or assumes any legal liability or responsibility for the accuracy, completeness or usefulness of any information, apparatus, product or process disclosed, or represents that its use would not infringe privately-owned rights."

"Reference to a company or product name does not imply approval or recommendation of the product by the University of California or the U.S. Energy Research & Development Administration to the exclusion of others that may be suitable."

Rapporteur's Summary Report:

Prepared by: Brubacker

Papers covered by: Berkowicz /Prahm
Johnson
Knox

Paper: Pseudospectral Dispersion Modeling
R. Berkowicz and L. P. Prahm

Question S.R. Hanna: Diffusion is treated by K-theory in this approach. How are the horizontal and vertical eddy diffusivities chosen?

Answer: In the long range application described the effects of using different horizontal diffusivity values were examined and the results were not too sensitive to the precise values. Those used by Heffter were used in this work. In the examination of the effects of dry deposition, the vertical eddy diffusivities of F.B. Smith were used directly.

Question F. Nieuwstadt: Should K-theory be used for elevated sources?

Answer: K-theory is useful in these cases and the discrepancies with statistical approaches are not significant.

Question R.T.Yamartino: What is the relationship between the pseudospectral methods and the turbulent energy spectrum?

Answer: The concentration field is Fourier transformed in the pseudospectral approach. No information regarding the energy spectrum is used; there is no close connection. The phase speed of each component in the spectrum of the concentration field is treated accurately.

Question T. Knox: You and your coworkers are providing significant new mathematical frameworks in which to treat atmospheric dispersion. This approach is much better than finite difference approaches for treating the problem of long range transport.

Question J. Padro: In the procedure used by you to test the accuracy of numerical schemes sufficiently good to imply that the scheme will be successful in a practical problem when the advective wind is assumed to vary in space?

Answer: In some cases, modifications must be made to the Fourier transformation algorithm.

Paper : Seasonal and Annual Patterns of SO_2 and $SO_4^=$ Concentration and Deposition in Europe as Simulated by the EURMAP Model.

by: B. Johnson

Question H.H. Slater: How are the trajectories determined?

Answer: Using only the 850 mb winds

Question Slater: According to Heffter, trajectories are hard to evaluate accurately. Better results are obtained in the U.S. using surface winds.

Answer: It is an important point. Surface winds by themselves are not adequate due to the existence of sources with substantial emission heights and to the effect of the diurnal variation in stability on the surface winds. In the OECD work, a two-level model was examined and no substantial improvement obtained. A one-level model is adequate especially for long term calculations.

Question J.G. Kretzschmar:

What is the meaning of the concentration values? They deviate substantially from observations.

Answer: The total estimated concentration is in agreement with observations.

Question K. Fischer: Is the dependence of the wet deposition removal coefficient on rainfall rate considered?

Answer: It is included.

Question B. Sivertsen: Why not take into account the nearest information on mixing height rather than assuming 1000 meters? This would affect the local deposition.

Answer: The local deposition seems to be estimated seasonably well already.

Question K. Fischer: How is gas-to-particle conversion handled? It is in general difficult to include.

Answer: Gas-to-particle conversion depends on many things, such as the pH of the rain and the UV light intensity. Treating it by a constant conversion rate is only an approximation and a range of values of this rate must be examined.

Fischer: SO_2 is also converted to ammonium sulfate.

Answer: The more detailed features of the relevant chemistry are currently being examined.

Question T. Schneider: The seasonal variations in the emission rate were not taken into account, and the transport of pollutant different levels is also important.

Answer: Including the seasonal variation of emission rates will be very easy to do. Regarding the transport, the use of only the 850 mb wind seems to be adequate. The transport is handled reasonably well.

Paper: Transnational Air Quality. The case for the stratosphere.
J. B. Knox

Question K. Fischer: How is the whole body dose rate calculated ?

Answer: The whole body dose rate is estimated using the conversion factor: 10^8 picocouries / m^3 is approximately 220 mv/hour.

Question K. Fischer Is no integration performed ?

Answer: It is not needed for a large cloud, although for a small cloud it would be.

Question H. H. Slater: What was the horizontal dimension of the nuclear cloud ?

Answer: Several hundred miles in diameter.

Question E. Voelz: How many time steps are needed ?

Answer: I cannot recall this number precisely, but the time steps are such that no particle moves further than about halfway across a cell in one time step.

Question	S. R. Hanna:	What pollutant was used in the ADPIC validations studies described ?
Answer:		Argon 41 at Savannah River, methyl iodide at Idaho Falls; sulfur hexafluoride and Krypton are also being used.
Question	S. R. Hanna:	He measured concentrations varied by about a factor of ten while the predictions ranged over a factor of 1000.
Answer:		Concentration ratios were displayed, not concentrations themselves. Also, it is easy to miss plumes in conducting the field measurements.

8th NATO/CCMS INTERNATIONAL TECHNICAL MEETING ON AIR POLLUTION MODELING

TOPIC 9

ESTIMATING THE COMBINED EFFECTS OF EMISSIONS FROM SEVERAL LARGE STACKS

8th International Technical Meeting on Air Pollution Modeling and its Application

MODELING OF COMBINED EFFECTS OF EMISSION FROM MULTIPLE SOURCES

D. Anfossi[✱], G. Bonino[●,✱], F. Bossa[✱,▲], R. Richiardone[✱]

[✱] Laboratorio di Cosmo-Geofisica del CNR , Torino, Italy

[●] Istituto di Fisica Generale dell'Università, Torino, Italy

[▲] T. G. T. Servizio Ricerche Misure Ambientali, Milano, Italy

September 20 - 23, 1977
Louvain-La-Neuve
Belgium

NOMENCLATURE

H_{max} = Maximum height of plume centerline (m)

F = Buoyancy parameter ($m^4 \, sec^{-3}$)

H_e^N = Effective height of merged plume produced by N stacks (m)

ΔH_1 = Maximum plume rise from a single stack (m)

D = Distance between chimneys (m)

d = Spacing between two contiguous chimneys (m)

ΔH_N = Maximum plume rise from N stacks above the chimneys mouth (m)

E_N = Enhancement factor

S_1, S_2, S_3 = Numerical coefficients appearing in 1974 Briggs' model

z = Height of plume centerline above the source (m)

H_1, H_2 = Stack heights (m)

H_i = Merging point height (m)

C = Variable containing all the meteorological parameters not directly related to source emission

ΔH_2 = Maximum single plume rise from lower stack H_2 (m)

Q = Emission rate (Kg/sec)

χ_{max} = m.g.l. concentration (Kg/m^3)

σ_z = Vertical standard deviation (m)

σ_y = Crosswind standard deviation (m)

$\bar{u}$ = Mean wind velocity (m/sec)

χ^N = m.g.l. concentration relative to N stacks (Kg/m^3)

1.) INTRODUCTION

A great deal has been written about the rise of plumes from single sources and thus a lot of models, able to fit experimental data or to forecast maximum plume rise in planning problems, have been proposed up to date (Slade, 1968; Briggs, 1969; Pasquill, 1974; Moore, 1974; Stern, 1976). The most widely used (those due to Briggs, 1969 and 1975 and Moore, 1974) constitute an important reference for people working in the modeling field.

On the contrary, the understanding of rise of plumes from multiple sources, that is from many stacks close to each other, whose plumes merge during the rise, has not been given so much attention. In Briggs opinion (1974), this problem is important mainly for arrays of cooling towers, in that for the common tall stacks the present trend of constructors is to combine as much effluents as possible into one stack, this configuration assuring the maximum possible plume rise.

Nowadays, two empirical models giving the maximum plume rise from multiple sources, both due to Briggs (1974 and 1975) and dealing with chimneys all of the same height and with the same buoyancy flux, are available; furthermore a new semiempirical model (Anfossi et al., in press) has recently been derived by us for computing maximum plume rise from many adjacent stacks of different heights and buoyancy fluxes. It is to be noted, as to this last point, that in our country we have many plants having three or four stacks of different heights connected to sections of different power. Of course, our general model, when reduced to the case of stacks all of the same height, leads to an alternative to Briggs' methods.

In the next sections all the three above models will be briefly presented and discussed and then a method for estimating m. g. l. concentrations in the multiple sources case will be shown.

2.) MULTIPLE SOURCES PLUME RISE MODELS

It seems intuitive that the main variables governing the rise from multiple sources will be the number of stacks N and the adimensional ratio $\Delta H_1 / D$ which takes into account all the meteorological and stack parameter, respectively influencing the rise (ΔH_1) and the distance D between the chimneys* (Briggs, 1974).

We should point out that using ΔH_1 does not imply any particular single source model, so it seems reasonable to utilize the best proven. This is the reason why Briggs' models for single sources will be used in the following.

Another point to be noted is that extending to the case of multiple sources the single source models without any adjunctive assumptions, means to assume no change in the entrainment rate even if plume dimensions are increased.

Briggs (1974) fitted data referring to multiple sources to a relation which is a monotonic function of $\Delta H_1/d$ and has the correct asymptotes, namely:

$$E_N = \frac{\Delta H^N}{\Delta H_1} = \left(\frac{N+S}{1+S}\right)^{\frac{1}{3}} \tag{1}$$

S being, in turn, expressed by:

$$S = S_1 \frac{d}{\Delta H_1} \; ; \quad S = S_2 N \left(\frac{d}{\Delta H_1}\right)^{3/2} ; \; S = S_3 \left[\frac{(N-1)\,d}{N^{1/3}\,\Delta H_1}\right]^{3/2}$$

The reason for these three different forms of S are of empirical origin and discussed in Briggs 1974 paper. The data considered by Briggs showed that the expression

$$S = 6\left[\frac{(N-1)\,d}{N^{1/3}\,\Delta H_1}\right]^{3/2} \tag{2}$$

gives the best fit. In particular, this relation, that can be easily applied both to a cluster or a line of stacks, has a very simple interpretation: it is the ratio of the total line width to the total possible rise if all the plumes combined.

---

* In the case of N stacks D will be equal to (N - 1) d, d being the spacing between two contiguous stacks.

One year later Briggs (1975), dealing with cooling tower. plumes, suggested a new simplified model assuming that a very simple model will suffice. He considered the plumes separated until they abruptly merge when the height of the plumes equals the spacing d; then multiplying all buoyancy fluxes by N and replacing z^2 with $z(z + (N - 1)\,d)$ in the expression for the effective volume flux, was able to obtain:

$$E_N = \left[\frac{N + \frac{1}{2}(N-1)\left(\frac{\Delta H_1}{d}\right)^{-3}}{1 + \frac{3}{2}(N-1)\left(\frac{\Delta H_1}{d}\right)^{-1}} \right]^{1/3} \qquad (3)$$

This second model is considered by Briggs more conservative.

We recall that both models (1 + 2) and (3) apply to stacks all of the same height H and buoyancy flux F.

We consider now our model which instead refers to stacks of different heights. It is based on the concept of a virtual stack which, from merging point H_i up, takes the place of the real stacks (this kind of concept, was also proposed by Briggs in his 1974 paper, even if not exactly alike and furthermore limited only to the case of buoyant plumes in calm conditions).

Let us write in the most general possible way the single plume rise formula as (Anfossi et al., in press):

$$H_{max} = H_1 + C\,F_1^{\,a} \qquad (4)$$

and look for a buoyancy flux F_i which, associated to a virtual stack of height H_i, gives the same H_{max} as the real stack H_1 does (see Fig. 1); we obtain

$$F_i = \left(F_1^{\,a} - \frac{H_i - H_1}{C} \right)^{1/a} \qquad (m^4\ sec^{-3})$$

Applying the same reasoning to the two stacks of heights H_1 and H_2 of Fig. 2, we obtain for the resultant buoyancy flux:

$$F_i = \left(F_1^{\,a} - \frac{H_i - H_1}{C} \right)^{1/a} + \left(F_2^{\,a} - \frac{H_i - H_2}{C} \right)^{1/a} \qquad (m^4\ sec^{-3}) \qquad (5)$$

In the general situation of N stacks, using eqs. (4) and (5) we can write

$$H_e^N = H_i + C\left\{\sum_{1}^{N}{}_{J}\left(F_J^{1/3} - \frac{H_i - H_J}{C}\right)^3\right\}^{1/3} \qquad \text{(m)} \qquad (6)$$

having assumed that merging point coincides for all the plumes under situations of windy conditions (a = 1/3). For calm stable conditions "a" equals 1/4.

An important feature of eq. (6) is that H_e^N is relatively insensitive to errors in H_i evaluation, and this fact let a simple empirical expression be drawn for H_i, namely:

$$H_i = H_1 + \frac{\Delta H_2 - (H_1 - H_2)}{1 + \frac{\Delta H_2 - (H_1 - H_2)}{D}} \qquad \text{(m)} \qquad (7)$$

In fact, with reference to Fig. 3, we can write:

$$H_i - H_1 = \frac{AB}{K} = \frac{\Delta H_2 - (H_1 - H_2)}{K} \qquad \text{(m)}$$

and express K as a function of AB/D (in the present problem similar to the previous mentioned $\Delta H_1/d$) in the following simple way: $K = 1 + \alpha AB/D$, where α was estimated to be 1.

Lastly, if we now consider Briggs' problem, i.e. chimneys of equal heights and emissions, eqs. (6) and (7) lead to:

$$E_N = \frac{\Delta H^N}{\Delta H_1} = \frac{1 - N^{1/3}}{1 + \frac{1}{N-1}\,\frac{\Delta H_1}{d}} + N^{1/3} \qquad (8)$$

3.) DISCUSSION OF THE ESTIMATES GIVEN BY THE THREE MODELS

First of all, let us compare the trends of E_N given by the three models (1 + 2), (3) and (8). Fig. 4, in which we plotted the enhancement factor E_N as a function of stacks number N having set $\Delta H_1/d = 10$, shows a quite similar trend of eqs. (1 + 2) and (8), while eq. (3) yields a lower estimate than the other two all over the range of N.

Fig. 5, in which E_N is instead plotted as a function of $\Delta H_1/d$, having set N = 3, shows a certain discrepancy between the two Briggs' models and ours, evidentiating a different bending, although the forecastings they give are similar.

It is also possible to compare the forecastings given by the three above models with a series of experimental data quoted by Briggs (1974) belonging partly to near neutral conditions, partly to stable conditions. We made such a comparison (Anfossi et al., in press) and found a good agreement for both stability condition, among data and either (1 +2) or (8), while (3) gave a substantially less accurate forecastings.

As far as our (6 + 7) model is concerned, only a few complete sets of data are available up to date confirming its goodness, and more numerous data coming from four Lidar experimental campaigns are in due course.

4.) EVALUATION OF χ_{max}

Since the final aim of any research on plume rise and dispersion is the evaluation of m. g. l. concentrations of pollutants, we can write down an expression giving such parameter in the particular case of multiple sources, namely:

$$\chi^N_{max} = \frac{2}{e\pi\bar{u}} \, \frac{\sigma_z}{\sigma_y} \, \frac{\sum_{1}^{N}{}_J Q_J}{(H_e^N)^2} \qquad (\mathrm{Kg/m^3})$$

and also to compare it to the expression giving m. g. l. concentrations for the single source case obtaining:

$$\frac{\chi^N_{max}}{\chi^1_{max}} = \frac{\sum_{1}^{N}{}_J Q_J}{Q} \, \frac{(H_1 + \Delta H_1)^2}{(H_e^N)^2} \qquad (9)$$

in which χ^1_{max} refers to the concentration expected by the emission from the stack of height H_1 and having made the hypothesis of independence of ratio $\frac{\sigma_z}{\sigma_y}$ from the number of combining plumes.

If we now consider the case of chimneys of equal heights, eq. (9) becomes:

$$\frac{\chi^N_{max}}{\chi^1_{max}} = N \frac{(H + \Delta H_1)^2}{(H + \Delta H^N)^2} \qquad (10)$$

Fig. 6 shows the comparison of trends obtained by means of eq. (10), in which eqs. (1 + 2) and (8) were introduced, with the following empirical expression due to Montgomery et al., (1973):

$$\frac{\chi^N}{\chi^1} = N^{0.8}$$

It can be noted that the two curves (Briggs 75 and our own model) practically coincide, both underestimating Montgomery et al. results.

For comparison, in Fig. 6, also the curve $\chi^N_{max} = N\,\chi^1_{max}$ was drawn, showing that any hypothesis of no effects on m.g.l. concentration of combining plumes must be refused: in fact, this last curve overestimates Montgomery et al. expression more than the other two underestimate (at least for N $\geqslant$ 4).

5.) CONCLUDING REMARKS

In this paper three models of combined effects of emissions from multiple sources are presented; they constitute a simple tool for workers involved in multiple source emission and dispersion modeling.

As to our model(6 + 7) in particular, further experimental work we are presently carrying on, will probably contribute to increase our confidence level about it, while its reduced form (eq. 8) already appeared (Anfossi et al., in press) as consistent with experimental data as Briggs' (1 + 2) model.

REFERENCES

Anfossi D., Bonino G., Bossa F., Richiardone R. Plume rise from multiple sources: a new model. In press on Atmospheric Environment

Briggs G. A. (1969) Plume rise. AEC Critical Review Series TID - 25075

Briggs G. A. (1974) Plume rise from multiple sources. Proceedings of cooling tower environment held at University of Maryland, pp 161 - 179

Briggs G. A. (1975) Plume rise predictions. Lectures on Air Pollution and Environmental Impact Analysis. pp 59 - 111

Montgomery T. L., Norris W. B., Thomas F. W., Carpenter S. B. (1973) A simplified technique used to evaluate atmospheric dispersion emissions from large plants. J. Air Poll. Control Ass., vol 23, N 5, pp 388 - 395

Moore D. J. (1974) Comparison of the trajectories of rising buoyant plumes with theoretical empirical models. Atmospheric Environment, vol 8, pp 441 - 457

Pasquill F. (1974) Atmospheric diffusion. Hellis Horwood Publ.

Slade D. H. (1968) Meteorology and Atomic Energy. USAEC

Stern A. C. (1976) Air Pollution. 3rd Edition, vol I, Academic Press

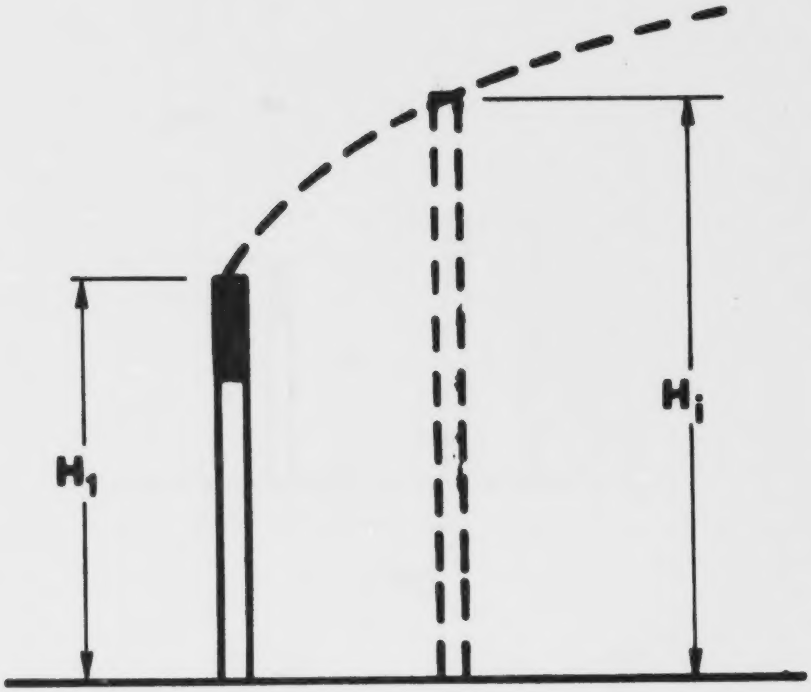

FIG. 1

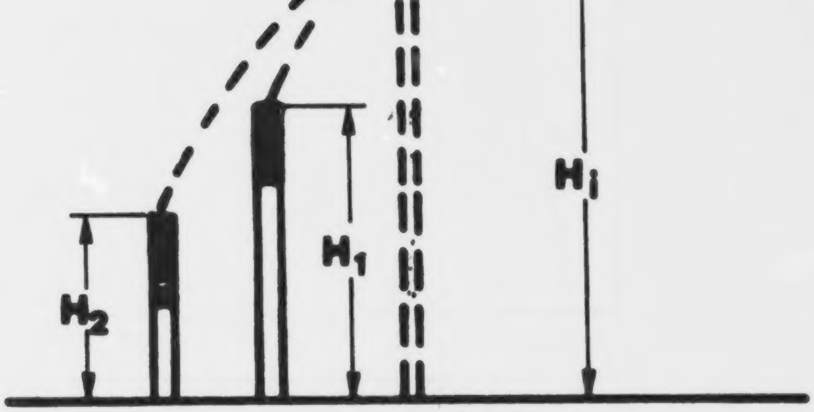

FIG. 2

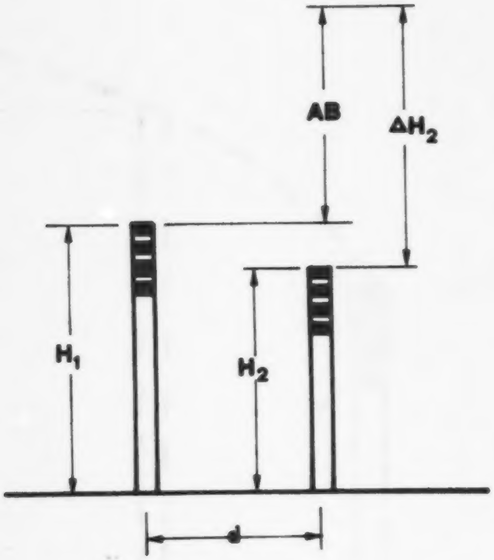
AB
ΔH_2
H_1
H_2
d

FIG. 3

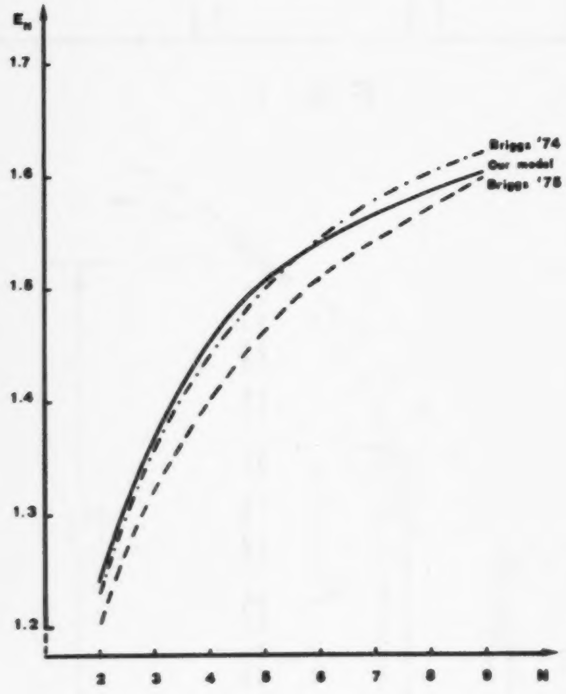

FIG. 4 - Plots of E_N after Briggs '74 Briggs '75 and our model as a function of N $\left(\frac{\Delta H_1}{d} = 10\right)$

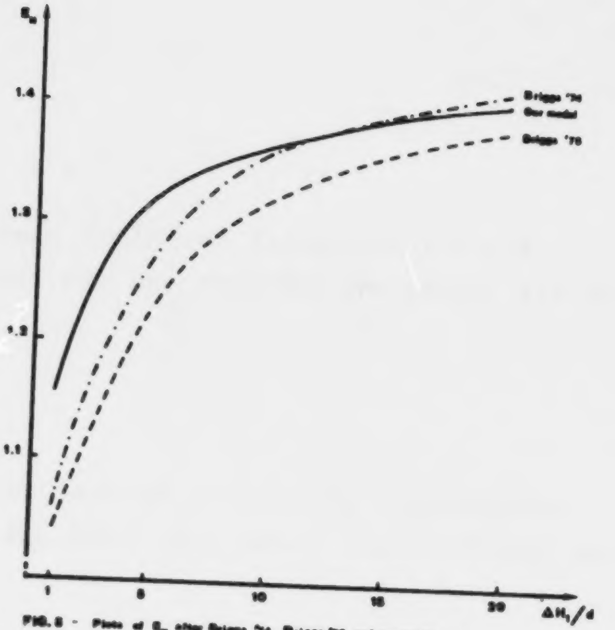

FIG. 5 - Plots of E_N after Briggs '74, Briggs '75 and our model as a function of $\frac{\Delta H_1}{d}$ $(N = 2)$

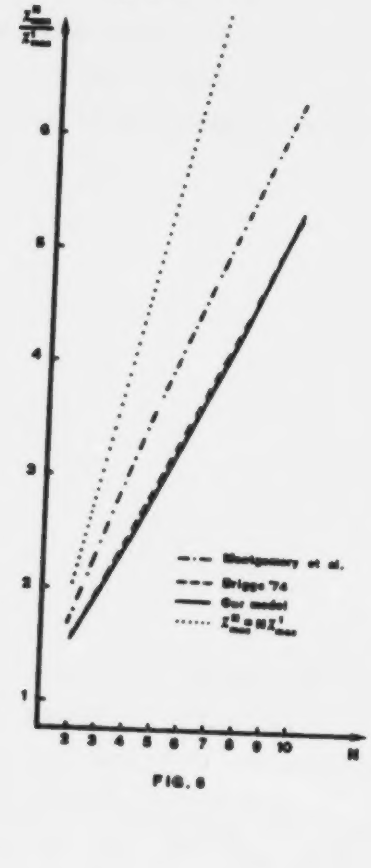

FIG. 6

8th International Technical Meeting
on Air Pollution Modeling and its Application

Aerodynamic effects of natural draught cooling towers on the local low level air pollution

K. Fischer
TÜV Bayern e. V., München, Germany
H. Ruscheweyh
Institut für Leichtbau, RWTH Aachen, Germany

September 20-23, 1977
Louvain-la-Neuve
Belgium

1. Introduction

This study was performed to investigate the aerodynamic effects of natural draught cooling towers on the local low level concentration of pollutants which are emitted from near-by located stacks. These investigations were aimed at the solution of special problems rather than intended as a matter of basic research. But, never-the-less, the results of the tests are most striking. Consequently the technical concept of emission of pollutants within the vicinity of natural draught cooling towers has to be submitted to new considerations. The problem of concern has come of the large capacity of modern power plants which are equipped with natural draught cooling towers. For the purpose of an effective natural vertical draught these types of cooling towers are of a height of at least 140 m. That means speaking in the terms of boundary-layer-meteorology: the field of flow within the atmospheric boundary layer that is generated by the effective aerodynamic surface roughness of the surroundings is heavily disturbed by aerodynamic interferences in the vicinity of natural draught cooling towers. Therefore, diffusion of effluents from stacks installed there and consequently the ground level concentration of pollutants must not commonly be calculated by using the GAUSS-model of dispersion. By performing experiments in a wind tunnel information on the local field of concentration can be obtained. However, to receive correct results it must be taken for granted that the essential conditions of the flow round cylindrically shaped bodies are realized along with the wind tunnel experiments.

2. Aerodynamic effects of cooling towers

The following remarks will be concerned with the phenomena generated by boundary layer flow around cooling towers. It should be noted that here aerodynamic effects are of concern, but not any effects of water vapor plumes of cooling towers. The flow field of the lower atmosphere has the structure of turbulent boundary layers. Because of the boundary conditions the velocity of the mean horizontal flow increases from zero at the ground to the value of the geostrophic wind at the upper boundary. It is known that such a vertical gradient within a flow field results in a vertical gradient of the static pressure in the wake of an obstacle. This can be explained by the fact that because of the vertical gradient of the mean horizontal flow its retardation in front of an obstacle and its accelaretion after an obstacle are functions with respect to the vertical.

The vertical pressure gradient in the wake is a function of the effective aerodynamic surface roughness which is involved in the boundary flow. In the case of an isolated cooling tower which is surrounded by a surface of homogeneous roughness the vertical pressure gradient is negative (L 1); that means: the subpressure is larger at higher levels than at ground level. The reverse case, i. e. a positive vertical pressure gradient, occurs, if the approaching boundary flow has been effected by near-by located obstacles like buildings and, of course, other cooling towers (Fig. 1) (L 2). The absolute value of the positive vertical gradient depends on the arrangement of buildings the surroundings are covered with. Therefore, at all power plants consisting of an aggregation of buildings and cooling towers a more or less intense positive vertical pressure gradient must be expected in the wake of cooling towers and buildings. A positive vertical pressure gradient results in a downward directed component of the field flow, as the subpressure increases with decreasing height. Consequently the emission of effluents into parts of the flow field, which pass the regions of downward directed flow in the wake of cooling towers, yields concentrations at ground level, which are higher in comparison to those due to undisturbed diffusion.

In general two kinds of eddies are characteristic of the flow around cylindrical obstacles (Fig. 2): there are vortices of vertical and of horizontal axis.

1. Vortices having a vertical axis are shed alternatively at either side of cylindrical obstacles. The location of the shedding point is a function of the Reynolds-number. It should be emphasized that the Reynolds-numbers occuring in the flow around natural draught cooling towers are far above the transcritical point. According to ROSHKO (L 3) the drag coefficient of a circular cylinder increases in the domain of transcritical Reynolds-numbers. This indicates that the flow in the wake is not chaotic, but there exists a certain periodicity in shedding vortices. Also, the position of the shedding point proceeds foreward by increasing the Reynolds-number beyond the transcritical point. Similar conditions are valid for the flow around cooling towers.

2. The second kind of vortices occuring in the flow field around cooling towers has a horizontal axis directed along the mean flow. These eddies are generated at the top of cooling towers at either side. The axis of rotation of the two eddies is opposite to each other. If taking the direction of the mean flow field as reference the vortex at the right-hand side is turning clockwise, whereas the vortex at the left-hand side is turning counter-clockwise. During operation of the natural draught cooling tower the intensity of these horizontal vortices at the collar is increased. The degree of reinforcement depends on the velocity of the air flowing out of the cooling tower. So, the pure aerodynamic effects of cooling towers discussed so far are added to by an enhancing effect caused by their operation.

Summing-up the features, discussed above, of the wake of cooling towers the ground level concentration within the range of the wake is dependent on

- the arrangement of the surrounding buildings,
- the effective stack height in relation to the height of the cooling tower,

- the distance between the stack emitting and the cooling tower,
- the velocity of the mean atmospheric flow,
- the direction of the mean atmospheric flow.
- the status of operation of the cooling tower

When considering the properties of the eddies mentioned above it is evident that a mean flow directed along the tangent to the cooling tower with respect to the stack will yield the most increasing effect on the concentration at ground level. It is also evident that there exists no analytical method for calculating ground level concentrations in the wake of cooling towers. Therefore, for instance to determine the necessary height of stacks with respect to limits of ground level air pollution wind tunnel experiments have to be made. Thus, by comparing the measured ground level concentration due to undisturbed diffusion to that determined within the region of the wake of the model a straightforward method can be applied to get sufficient information about the aerodynamic effect of cooling towers on the low level air pollution.

3. Experiment

A detailed description of the experiments performed is beyond the scope of this report. Two important facts have to be regarded when simulating the conditions of atmospheric flow round cooling towers. The first one concerns the spectrum of atmospheric turbulence, as the structure of the wake is a function of the properties of the mean flow field. Here, the atmospheric turbulent flow is simulated by generators of turbulence according to Counihan (L 4). The power spectrum of turbulence is in agreement with the power spectrum of neutral atmospheric conditions. The second, more important condition concerns the problem of simulating the status of the flow of the regime of transcritical Reynolds-numbers, for, as mentioned above, the location of the shedding point and consequently the pattern of eddies within the wake is a function of the Reynolds-number. Clearly, Reynolds-numbers of the order of magnitude of 10^8 cannot be realized in wind tunnels, but it is possible to simulate the status of flow of Reynolds-numbers beyond the transcritical point. By some full scale measurements the distribution of pressure along the circumference of cooling towers is known (L 5, 6, 7) and thereby the position of the shedding points, too. Thus, equipping the shell of the models of cooling towers with ribs of the right geometric shape and arrangement shedding of eddies can be forced at the correct position so that the status of the flow of Reynolds-numbers beyond the transcritical point can be generated in the wind tunnel without producing the high Reynolds-numbers themselves.

Smoke consisting of a suspension of condensed vapor of oil in CO_2 was used as tracer. The concentration of the tracer at ground level was determined through measuring the extinction. By this method variations of the concentration can be resolved down to 1 min with regard to the full time scale. For the purpose of determining air pollution mean values of 30 min referring to the full time scale were used.

4. Results

For a certain arrangement of cooling towers and buildings the ground level concentration is dependent on the direction of the mean flow, on the velocity of the flow, and on the effective stack height, which in turn is a function of the velocity of the mean flow.

Two examples of arrangements will be presented here to demonstrate the essential features. It will be seen that the aerodynamic influence of cooling towers strongly depends on the total arrangement of the plant so that it would be very difficult to assess the ground level concentration of effluents without any basis of experimental data.

The arrangement of the first example is shown in Fig. 3. The two cooling towers are of a height of 145 m. The distance between the cooling towers and the stack is about 250 m. The remaining buildings of the plant are of a height of up to 60 m. The velocity of emission of the effluent cold gases is about 9 m/s. In Fig. 4 there is shown the slope of the ground level concentration c versus the parameter u_∞/w_k that is involved in the effective stack height. u_∞ denotes the velocity of the mean undisturbed flow above the boundary layer, w_k is the vertical velocity of the flow out of the stack. The direction of the mean flow in Fig. 4 is about 120°, into which the strongest influence of the cooling towers was revealed, as will be shown below. The distance the curves are related to is 1000 m downwind of the stack. There the maximum ground level concentration is located. The ground level concentration is drawn for the following stack heights h: 100 m, 115 m and 160 m; also, the ground level concentration relating to diffusion from the isolated stack of h = 100 m is recorded in Fig. 4.

The maximum value of the ground level concentration is at $u_\infty/w_k = 1.6$ due to diffusion from the isolated stack; within the disturbed field of flow the maximum concentration is between $u_\infty/w_k = 1$ and $u_\infty/w_k = 1.4$ depending on the height of emission. Comparing the diffusion from the stack of 100 m the maximum ground level concentration is larger by 6-7 times within the disturbed flow field than within the undisturbed one. In the former case the same order of magnitude of the ground level concentration is not achieved till a stack height of 150 m - 160 m.

Fig. 5 is an illustration of the ground level concentration versus the direction of flow ß at the maximum value of the parameter u_∞/w_k. The distance related to is about 1000 m. Considering the two stack heights 100 m and 115 m six peaks of the concentration occur. These peaks are assigned to those directions of the mean flow, which are the tangents to the cooling towers with respect to the stack. The stack is situated downwind of the cooling towers at $50^{\circ} \leq \beta \leq 125^{\circ}$ and upwind at $235^{\circ} \leq \beta \leq 310^{\circ}$. At a stack height of 160 m the peaks of the ground level concentration are smoothed down, if the cooling towers are in operation. Note, that there are two maxima, respectively, if there is no operation of the cooling towers. These maxima are shifted on to the prolonged junction lines stack - cooling towers.

The arrangement and the results concerning the second example are shown in Fig. 6-10. Fig. 6 is an outline of the arrangement of the cooling towers, the buildings, and the stack. The height of the two natural draught cooling towers is 160 m. The buildings belonging to the power plant are of a height of about 40 m - 60 m. The distance between the cooling towers and the stack is 160 m and 250 m, resp. The height of the stack is limited to 170 m. Note, that the stack is not located symmetrically with respect to the centre line between the two cooling towers, so that there exists a particular direction of the mean flow, which is the tangent to both cooling towers with respect to the stack at the same time. Thus, a kind of tandem interference can be expected with strong effects on to the dispersion of effluents from the stack.

To begin with the just-mentioned case, the ground level concentration is shown versus the parameter u_{∞}/w_k' in Fig. 7. Here w_k' is kept constant at 4.1 m/s as reference. The direction of flow is 280°. The most striking feature is the difference of the values of the ground level concentration due to the isolated stack from those due to the simultaneous aerodynamic effects of both cooling towers. The ground level concentration is increased nearly by a factor of 30 caused by the tandem interference of the two cooling towers. Considering the effect of increasing momentum of flow out of the stack two facts can be stated from Fig. 7: 1. the ground level concentration is lowered, because the effluents jet through the regions of disturbance to an increasing extent. 2. The maximum value of the ground level concentration is shifted to higher values of the velocity of flow; that means: to speeds of wind, which occur less frequently at higher values, so far as usual meteorological statistics are concerned. So, in practice, increasing the velocity of flow out of the stack is an effective method to compensate for the aerodynamic interference of cooling towers; a stack of sufficient height must be provided, of course.

In Fig. 8-10 the ground level concentration at a distance from the stack of 1430 m is recorded versus the direction of flow. The velocity of the flow out of the stack is increased from 4.1 m/s to 30.75 m/s. Furthermore, there are illustrated cases of operation and non-operation of the cooling towers. Note, that at an angle of $\beta = 100^{\circ}$, that is the reverse direction of $\beta = 280^{\circ}$ discussed above, the ground level concentration is increased by nearly two orders of magnitude in comparison to the isolated stack! In detail, the peaks of the ground level concentration can be well assigned. There are six peaks according to the tangents to the cooling towers, if they are in operation. There are four peaks located on the prolonged junction lines between stack and cooling towers, if they are not operating. As can be stated from Fig. 10, the level of concentration due to emission from an isolated stack is not achieved till a velocity of emission of about 30 m/s.

Summing-up the results presented so far there is a vertical pressure gradient in the wake of cooling towers. This vertical pressure gradient depends on the arrangement and heights of the buildings surrounding. The aerodynamic effect of cooling towers can be investigated only by experiment. The ground level concentration of effluents emitted from near-by located stacks is most increased, if the mean flow is directed along the tangent to the cooling towers and the cooling towers are in operation. If the cooling towers are not operating the maxima of the ground level concentration are located on the prolonged junction line stack-cooling tower. As the ground level air pollution is increased considerably, the technical conditions of emission from stacks located near-by cooling towers have to be adapted by suitable means, for instance by increasing the effective stack height, as discussed above.

References

L 1 Ebner,H. & Ruscheweyh,H. 1974. Windlasten an hyperbolischen Kühlturmschalen. Forsch.-Bericht des Landes Nordrhein-Westfalen, Westdeutscher Verlag

L 2 Ruscheweyh,H. Untersuchung des Einflusses der Kraftwerksgebäude auf die Windbelastung eines Naturzugkühlturmes. Berichte des Instituts für Leichtbau, RWTH Aachen, 21/1968, 7/1969, 21/1969, 19/1970, 133/1975

L 3 Roshko,A. 1961. Experiments on the flow past a circular cylinder at very high Reynolds number. Fluid Mech. 10, 345

L 4 Counihan,J. 1969. An improved method of simulating an atmospheric boundary layer in a wind tunnel. Atmospheric Environment 3, 197

L 5 Scanlan,R.H. & Sonnenberger N.J. 1975. Pressure differences across the shell of a hyperbolic natural draught cooling tower. Proc. 1st Int. Conf. on wind effects on buildings and structures. London

L 6 Niemann, H.J. & Propper, H. 1975. The influence of surface roughness on the average wind pressures on cooling towers. Proc. 1st Int. Conf. on wind effects on buildings and structures. London.

L 7 Ruscheweyh,H. 1976. Wind loadings on the television tower at Hamburg, Germany. J. Industrial Aerodynamics 1, 315.

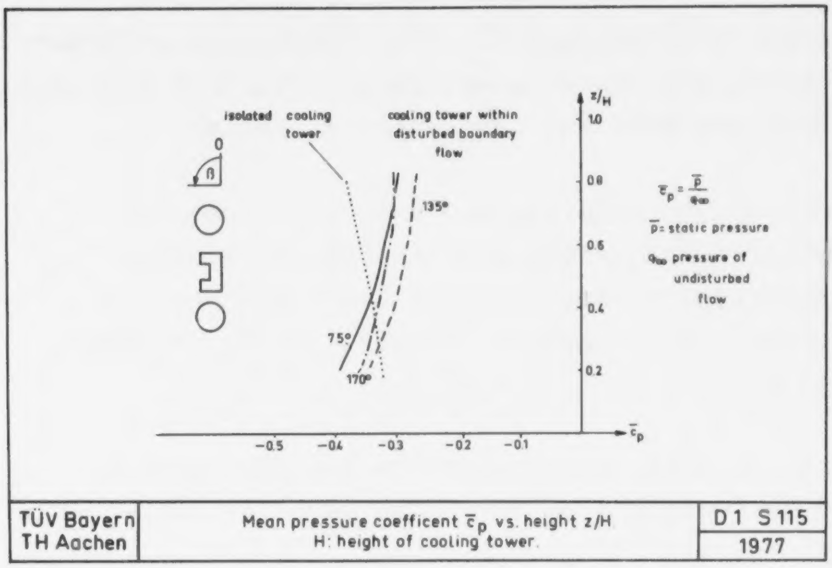

Fig. 1. Mean pressure coefficient $\bar{c}_p$ vs. height z/H downwind at the shell of a cooling tower. Isolated cooling tower within undisturbed shear flow ($\frac{dp}{dz}$ < o) and cooling tower within disturbed shear flow ($\frac{dp}{dz}$ > o); cooling tower located as outlined on the left.

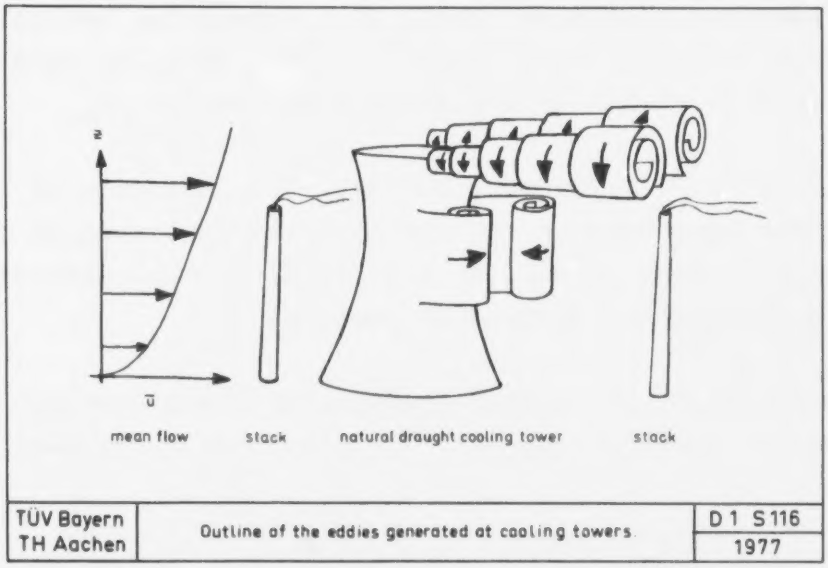
z
$\bar{u}$
mean flow
stack
natural draught cooling tower
stack
TÜV Bayern
TH Aachen
Outline of the eddies generated at cooling towers.
D 1 S 116
1977

Fig. 2. Outline of the eddies generated at cooling towers illustrating the aerodynamic effects on the dispersion from near-by located stacks.

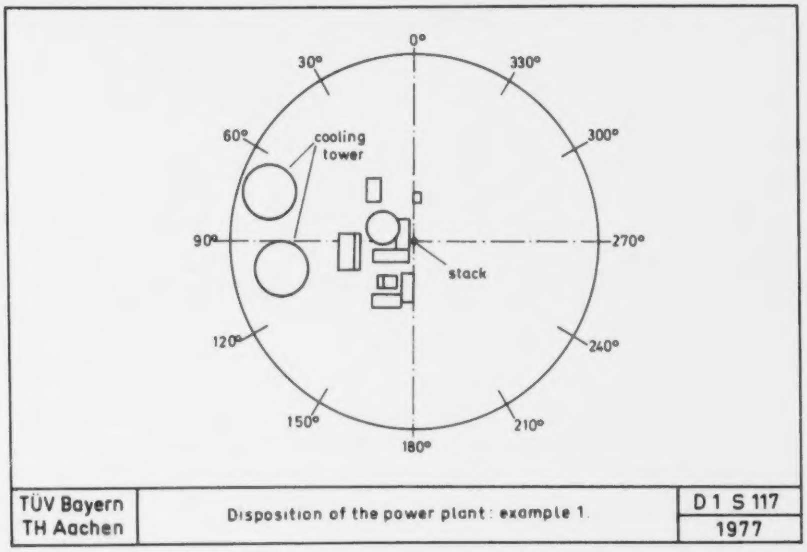
0°
30°
330°
60°
300°
cooling tower
90°
270°
stack
120°
240°
150°
210°
180°
TÜV Bayern
TH Aachen
Disposition of the power plant: example 1.
D 1 S 117
1977

Fig. 3. Arrangement of the first example as to the location of the buildings, the natural draught cooling towers, and the stack (cf. text).

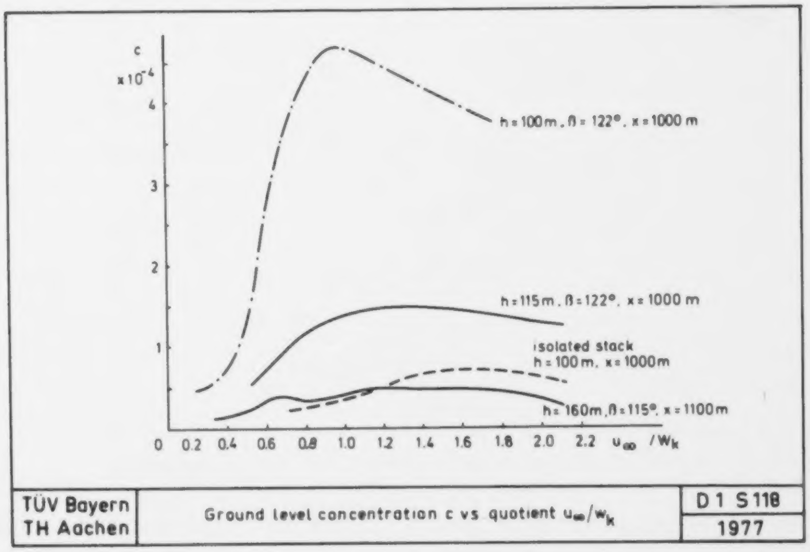

Fig. 4. Ground level concentration c (parts per 10^4) vs. quotient u_∞/w_k. u_∞ velocity of undisturbed flow; w_k velocity of emission from stack; h height of emission; arrangement of buildings as outlined in Fig. 3.

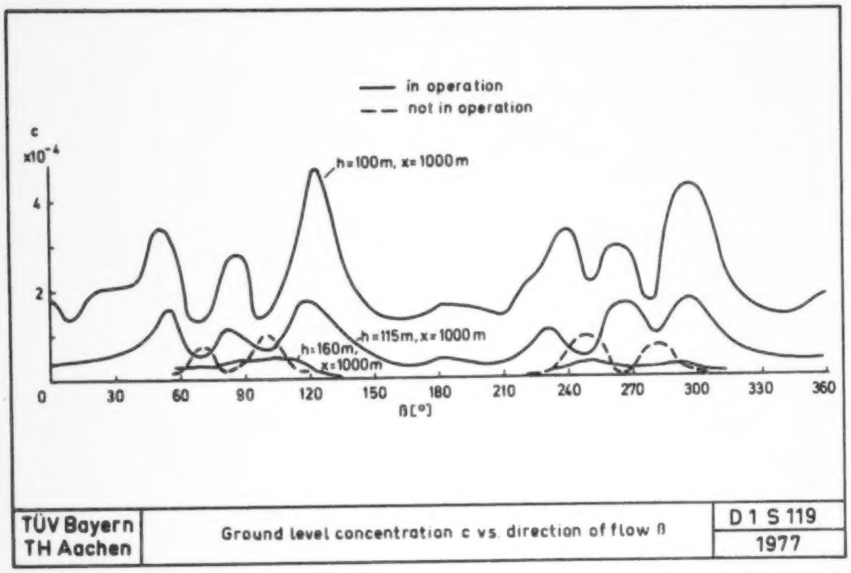

Fig. 5. Ground level concentration c (parts per 10^4) vs. direction of flow β referring to Fig. 3 (cf. text).

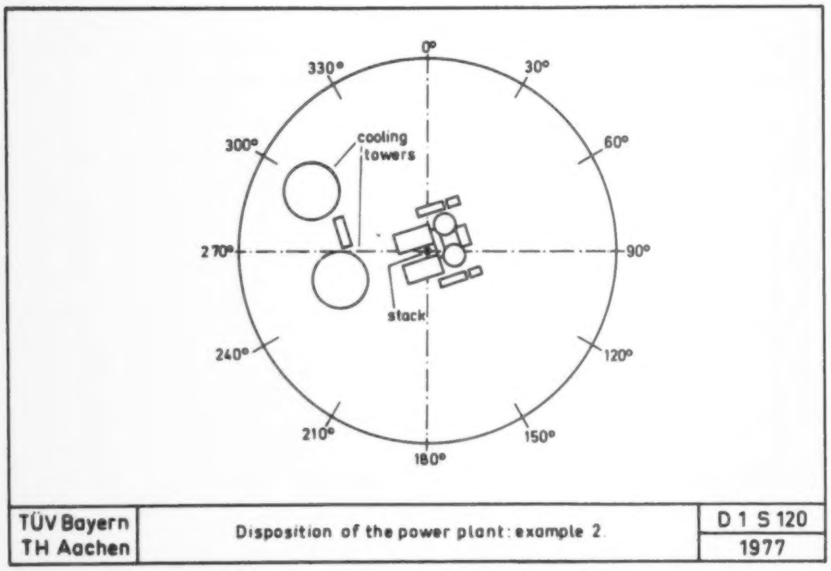
0°
30°
60°
90°
120°
150°
180°
210°
240°
270°
300°
330°
cooling towers
stack
TÜV Bayern
TH Aachen
Disposition of the power plant: example 2
D 1 S 120
1977

Fig. 6. Arrangement of the second example as to the location of the buildings, the natural draught cooling towers, and the stack (cf. text).

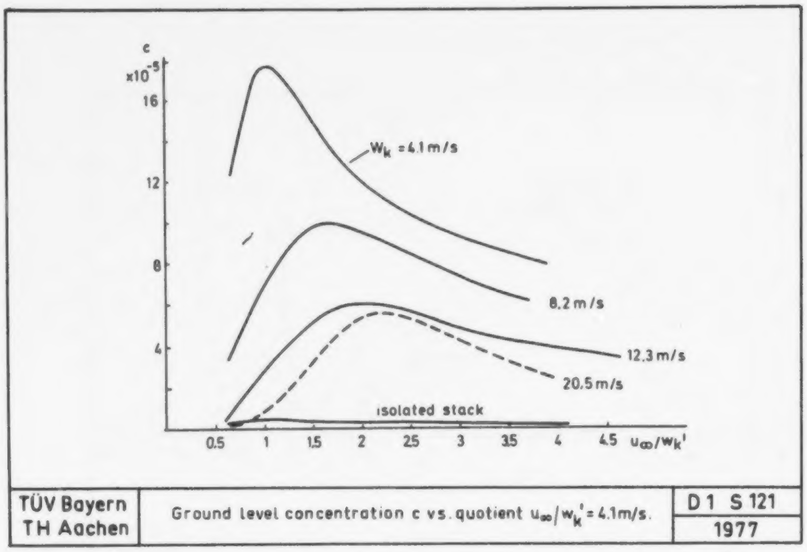

Fig. 7. Ground level concentration c (parts per 10^5) vs. quotient u_∞/w_k'. u_∞ velocity of undisturbed flow; w_k velocity of emission; w_k' = 4.1 m/s; arrangement of buildings according to Fig. 6. The ground level concentration due to the isolated stack is related to w_k' = 4.1 m/s.

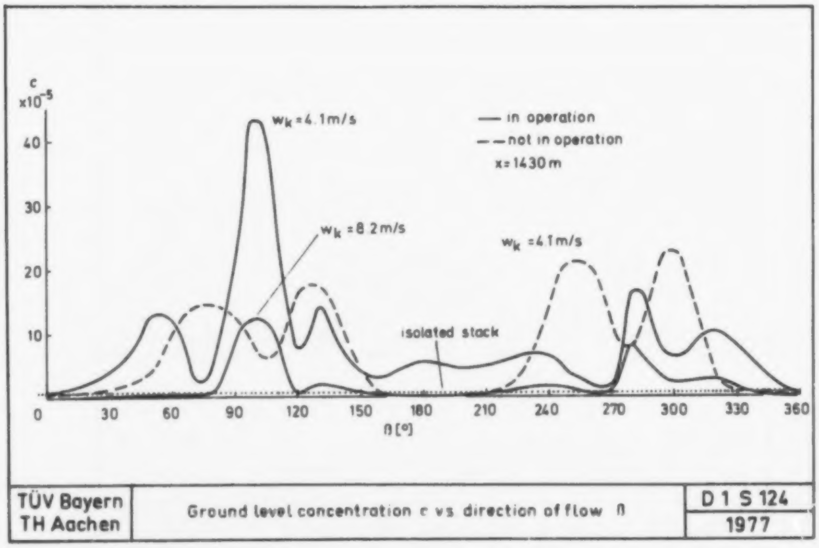

Fig. 8. Ground level concentration c (parts per 10^5) vs. direction of flow ß referring to Fig. 6 (cf. text).

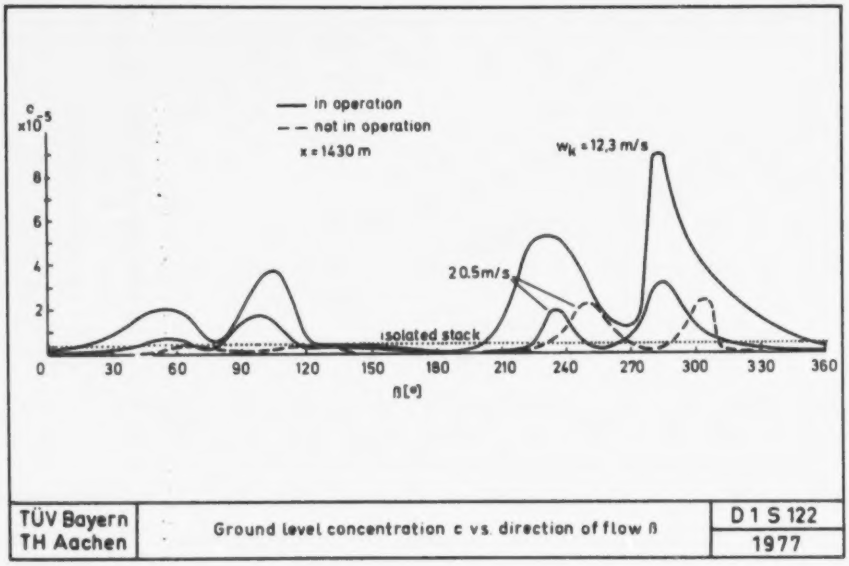

Fig. 9. Ground level concentration c (parts per 10^5) vs. direction of flow ß referring to Fig. 6 (cf. text).

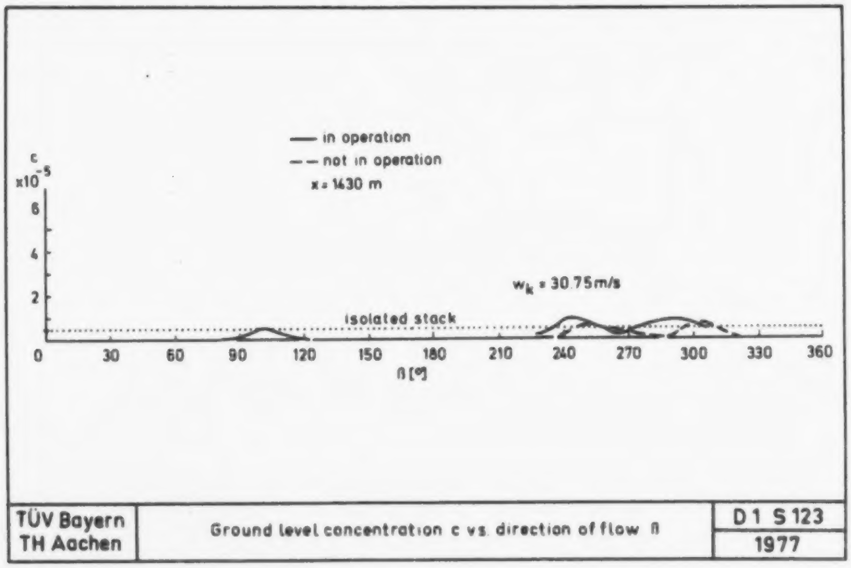

Fig. 10. Ground level concentration c (parts per 10^5) vs. direction of flow ß referring to Fig. 6 (cf. text).

8th NATO /CCMS
International Technical Meeting
on Air Pollution Modeling

AGENDA

LOUVAIN-LA-NEUVE
BELGIUM

Tuesday, September 20, 1977

Social Hour and Registration of Participants

Wednesday, September 21, 1977

Registration of Participants
Opening of the Meeting

Chairman: Dieter JOST

Presentation and Discussion of Topic 1:

Quantitative Application of Models to the Development of Control Strategy (Air Quality Management System)

Chairman: H. H. SLATER

Rapporteur: W. B. JOHNSON

1. J. G. Kretzschmar

   Some practical examples of the impact of individual sources upon the cumulative frequency distributions of the daily SO_2-concentrations in an urban and industrial area.

   (J. G. Kretzschmar, G. de Baere, J. Vandervee,
   G. Cosemans, J. Mertens
   SCK/CEN, Boeretang
   B - 2400 Mol, Belgium;

   J. Mertens, National R + D Programme - Air,
   Interministerial Commission for Science Policy
   Rue de la Science 8,
   B - Brussels, Belgium)

2. R. J. Yamartino, Jr.:

   A source finding algorithm: A novel approach for relating air quality data to dispersion models.

   (R. J. Yamartino, Jr.,
   EES Argonne National Laboratory
   9700 South Cass Avenue,
   Argonne, Illinois 60 439/ USA)

3. Y. Jacquart

   Dual Analysis in Air Pollution Modeling

   (Y. Jacquart,
   Institut d'Astronomie et de Géophysique,
   Université Catholique de Louvain,
   B - 1348 Louvain-la-Neuve, Belgium)

4. B. Gutsche,

   A unit construction system of dispersion models for air quality management

   (B. Gutsche, D. Jost
   Umweltbundesamt
   Bismarckplatz 1
   D - 1000 Berlin 33, Federal Republic of Germany

   Ch. Ludwig
   Freie Universität Berlin,
   Thielallee 49,
   D - 1000 Berlin 33, Federal Republic of Germany)

5. A. Joukoff,

   Development of an air pollution index

   (A. Joukoff
   Royal Meteorological Institute of Belgium
   Avenue Circulaire 3,
   B - 1180 Brussels, Belgium)

6. L. Van der Auwera,

   Forecasting the air pollution potential by means of a multiple regression model

   (L. van der Auwera,
   Royal Meteorological Institute of Belgium
   Avenue Circulaire 3,
   B - 1180 Brussels, Belgium)

7. J. P. Orfeuil,
   A purely statistical approach to the warning, alarm and emergency problem.

   (J. P. Orfeuil,
   École Nationale Supérieure des Mines de Paris,
   Centre de Géostatistique,
   35, Rue St. Honoré,
   F - 77305 Fontainebleau, France)

8. G. Finzi,

   Univariate stochastic models and real time predictors of daily SO_2 pollution in Milan.

   (G. Finzi, G. Fronza, A. Spirito
   Istituto di Elettrotecnica ed Elettronica -
   Centro Teoria dei Sistemi C. N. R.-Politecnico
   di Milano, Italy)

Presentation and Discussion of Topic 2:

Comparison of different diffusion models

Chairman: T. SCHNEIDER

Rapporteur: B. SIVERTSEN

1. K. L. Brubaker,

   A methodology for the comparision of air quality simulation models

   (K. L. Brubaker, A. E. Smith, D. M. Rote,
   EES-12 Argonne National Laboratory
   9700 South Cass Avenue
   Argonne, Illinois 60439, U S A

2. R. Porter

   Comparative study of four mathematical air dispersion models for a new urban industrial complex at Sines, Portugal

   (J. F. Conceicao, L. D. Canelas,
   Divisao Controle Ambiente Rua A. Tilharia
   Lisboa, Portugal;

   R. Porter, J. Christiansen, Texas Air Control Board;
   University of Texas and Dallas, Environmental
   Sciences Program (BE - 22) Box 688,
   Richardson, Texas 75080, U S A)

3. S. R. Hanna

   Application of the ATDL simple urban dispersion model to Frankfurt, West Germany,

   (S. R. Hanna, F. A. Gifford, Jr., Air Resources
   Atmospheric Turbulence and Diffusion Laboratory,
   National Oceanic and Atmospheric Administration,
   Post Office Box 4,
   Oak Ridge, Tennessee, 37830, U S A)

4. L. Kropp

   Comparision of dispersion calculations with measurements in the Cologne area.

   (L. Kropp,
   FB Umweltschutz, Luft,
   TÜV Rheinland,
   Postfach 10 17 50
   D - 5000 Köln 1, Federal Republic of Germany)

Presentation and Discussion of Topic 3:

Guidelines for the application of air quality simulation models in the NATO community.

Chairman: T. SCHNEIDER

Rapporteur: J. G. KRETZSCHMAR

1. L. Kropp

   Influence of meteorological data on the dispersion calculation results.

   (L. Kropp, W. Bahmann
   TÜV Rheinland
   Fachbereich Umweltschutz Luft
   Postfach 10 17 50
   D - 5000 Köln 1, Federal Republic of Germany)

2. D. B. Turner

   Experience with UNAMAP

   (D. B. Turner, United States Environmental
   Protection Agency, Environmental Sciences
   Research Laboratory, Environmental Applications
   Branch, Meteorology and Assessment Div.,
   Research Triangle Park
   North Carolina 27 711, U S A)

3. F. H. Fanaki

   Air pollution studies in Canada

   (F. H. Fanaki, M. Kwizak,
   Atmospheric Environment Service
   Environment Canada,
   4905 Dufferin Street
   Downsview, Ontario, M3H 5T4, Canada)

4. H. H. Slater

   The development of a guideline on air quality modeling by the US Environmental Protection Agency

   (H. H. Slater
   United States Environmental Protection Agency,
   MDAD (MD- 14)
   Research Triangle Park
   North Carolina 27711, U S A)

Thursday, September 22, 1977

Presentation and Discussion of Topic 4:

Influence and choice of meteorological inputs

Chairman: L. M. MALET

Rapporteur: C. A. VELDS

1. R. Santangelo

   Simulation of daily temperatures for environmental modelling

   (R. Cecchi, M. Marseguerra, S. Morelli,
   S. Pugnaghi, R. Santangelo
   Istituto di Fisica ed Osservatorio Geofisico
   Università di Modena, Italy)

2. F. Nieuwstadt
   The dispersion of pollutants over a water surface

   (F. Nieuwstadt,
   Royal Netherlands Meteorological Institute
   Utrechtseweg 297
   NL - De Bilt, Netherlands)

3. J. Padro

   A procedure for computing vertical wind profiles in the planetary boundary layer

   (J. Padro
   Atmospheric Environment Service
   4905 Dufferin Street
   Downsview, Ontario, M3H 5T4 /Canada)

Rapporteur: D. B. TURNER

1. A. Longhetto

   Assessment of stability categories as meteorological input of air pollution modeling

   (A. Longhetto, P. Bacci, L. Briatore,
   G. Elisei, L. Santomauro
   Laboratorio Ricerche Ambientali ENEL/CRTN,
   Milano, Istituto di Fisica Generale dell'
   Università di Torino, Osservatorio Meteorologico
   di Brera
   Via Brera 28,
   I - 20121 Milano, Italy)

2. A. Saab

   New technics of estimation of dispersion coefficients - Generalization of the diffusivity concept -

   (A. Saab, J. P. Granier
   Direction des Études et Recherches
   Electricité de France
   6, Quai Watier
   F - 78400 Chatou

3. G. Schayes

   Comparison between inversion observation and Modeling

   (G. Schayes
   Institut d'Astronomie et de Géophysique,
   Université Catholique de Louvain
   Chemin du Cyclotron 2
   B - 1348 Louvain-La-Neuve

Presentation and Discussion of Topic 5:

Considerations of transformation processes of air pollutants in models

Chairman: M. KWIZAK

Rapporteur: St. R. HANNA

1. N. V. Gillani

   Project MISTT: Plume modeling of the dispersion transformation and ground removal of SO_2 over the B-mesoscale range (25 - 250 km)

   (N. V. Gillani, R. B. Husar

   Air Pollution Research Laboratory
   Washington University
   Saint Louis, Missouri 6330 /U S A

2. J. Giebel

   An improved source depletion model for deposition from a GAUSSian Plume

   (J. Giebel
   Landesanstalt für Immissionsschutz des Landes
   Nordrhein-Westfalen
   Wallneyer Str. 6
   D - 4300 Essen 1, Federal Republic of Germany)

3. K. H. Müller

On the dispersion of chemically reacting pollutants

(K. H. Müller
EURATOM, Kommission der EG
21020 Centro Euratom di Ispra
I - Varese, Italy)

Presentation and Discussion of Topic 6

Modelin in complex terrain

Chairman: L. M. MALET

Rapporteur: R. A. PORTER

1. W. Kofler

The Austrian Alps air pollution study

(W. Kofler
Institut für Hygiene der Universität Innsbruck
Fritz-Pregl-Str. 3
A - 6010 Inssbruck, Austria)

2. J. Vanderborght

Microscale atmospheric model

(Josette Vanderborght

Institut Royal Météorologique de Belgique
Avenue Circulaire 3,
B - Brussels, Belgium)

3. M. Schorling

Calculation of carbon monoxide caused by traffic

(M. Schorling
IABG/SZA
D - 8012 Ottobrunn, Federal Republic of Germany)

Presentation and Discussion of Topic 7:

Novel Approaches in air quality modeling

Chairman: L. M. MALET

Rapporteur: R. PORTER

1. E. Runca

   Air pollution studies using planetary boundary layer and K-models

   (E. Runca
   IBM Italia, Centro Scientifico
   Dorsoduro 3228
   I - 30 123 Venezia, Italy

   R. D. Bornstein
   Department of Meteorology
   San José State University
   San José, California 95193, U S A)

2. H. Schultz

   Calculation of the atmospheric pollutant dispersion by the computer program XPIC for instationary and inhomogeneous conditions

   (H. Schultz, E. Voelz, C. D. Wüneke
   Arbeitsgruppe für Technischen Strahlenschutz
   der TU Hannover
   Callinstr. 15
   D - 3000 Hannover, Federal Republic of Germany)

3. A. Berger

   A K-analytical model, including calm wind situations

   (C. Demuth, A. Berger, Y. Jacquart,
   G. Schayes
   Institut d'Astronomie et de Géophysique
   Université Catholique de Louvain
   B - 1348 Louvain-la-Neuve, Belgium)

Friday, September 23, 1977

Presentation and Discussion of Topic 8:

Transnational air quality modeling

Chairman: A. KEDDIE

Rapporteur: K. L. BRUBAKER

1. R. Berkowicz

   Pseudospectral dispersion modeling

   (R. Berkowicz, L. P. Prahm
   Danish Air Quality Laboratory
   Ministry of Environment
   Meteorological Institute
   Lyngbyvej 100
   DK - 2100 Copenhagen, Danmark)

2. W. B. Johnson
   Long-term regional distributions and transfrontier exchanges of airborne sulfur pollution in Europe

   (W. B. Johnson
   Stanford Research Institute
   Atmospheric Sciences Laboratory
   333 Ravenswood Ave, Menlo Park
   California 94025, U S A)

3. J. B. Knox

   Transnational air quality: The case for the stratosphere

   (J. B. Knox, M. H. Dickerson, R. Lange,
   R. Peterson
   Lawrence Livermore Laboratory
   University of California
   P. O. Box 808
   Livermore, California 94550/ U S A)

Presentation and Discussion of Topic 9:

Estimating the combined effects of emissions from several large stacks

Chairman: A. KEDDIE

Rapporteur: F. H. FANAKI

1. D. Anfossi

   Modeling of combined effects of emissions from multiple sources

   (D. Anfossi, F. Bossa, R. Richiardone
   Laboratorio di Cosmo-Geofisica del CNR
   Corso Fiume 4
   I - Torino;

   G. Bonino
   Istituto di Fisica Generale dell'Università
   I - Torino, Italy)

2. K. Fischer

   Aerodynamic effects of natural drought cooling towers on the local low level air pollution

   (K. Fischer
   TÜV Bayern, e. V.
   Kerntechnik + Strahlenschutz
   Rüdesheimer Str. 11
   D - 8000 München 21, Federal Republic of Germany

   H. Ruscheweyh
   Institut für Leichtbau der Rheinisch-Westfälischen TH
   D - 5100 Aachen, Federal Republic of Germany)

8th NATO/CCMS INTERNATIONAL TECHNICAL MEETING ON AIR POLLUTION MODELING

ATTENDEES

LOUVAIN-LA-NEUVE

BELGIUM

Dr. Omar Tabouli ABULKASEM
Cultural Comf. Department
Garyounis University

Benghazi /LIBYE

Dott. Domenico ANFOSSI
Laboratorio di Cosmo-Geofisica
Del C N R
Corso Fiume 4

I - 10133 Torino

Stamatia ARAVANTINOU
Environmental Control Project
Athens
147, Portissian Street

GR - Athenes

W. BAHMAN
TÜV Rheinland e.V.
Postfach 101750

D - 5000 Köln 1

Prof. A. BERGER
U. C. I.
Institut Astronomie et Géophysique
Chemin du Cyclotron 2

B - 1348 Louvain-la-Neuve

Dr. Giuseppe BONINO
Istituto di Fisica Generale
dell'Università
Massimo d'Azeglio, 46

I - lol25 Torino

BOSCH
Energy Strategy Branch
US Environmental Protection Agency
MD - 12
Research Triangle Park

North Carolina 27711 /USA

Simon BREMER
R. I. V.
Postbus 1

NL - Bilthoven

Kenneth L. BRUBAKER
Energy and Environmental Systems
Div.
Argonne National Laboratory
9700 S. Cass Ave.

Argonne, Ill. 60439 /USA

Dr. Mathias BUCHEN
Hessische Landesanstalt f. Umwelt
Aarstr. 1

D - 6200 Wiesbaden

BULTINCK
C. E. N.
Boeretang 2oo

B - 2400 Mol (DONK)

G. J. CATS
Koninklijk Nederlands
Meteorologisch Instituut
Utrechtseweg 297

NL-Debilt

J. von CHAMIER
VDI-Kommission Reinhaltung d.Luft

D - 4000 Düsseldorf

CHINES
Centre de Géostatistique
35, Rue Saint-Honoré

F - 77305 Fontainbleau

Dr. G. COSEMANS
C. E. N.
Boeretang 2oo

B - 2400 Mol (DONK)

Dr. Giovanni Angezo DALU
Atmosphéric Physics Group
Imperial College
Queen's Gate

GB - London SW

Dr. IR. Cl. DEMUTH
O. C. L.
Inst. Astronomie et Géophysique
Chemin du cyclotron, 2

B - 1348 Louvain-la-Neuve

D. DUBOIS
ULG
Institut de Mathematiques
Av. Tilleuls, 15

B - 4000 Liège

IR. F. ENGELS
Commission des Communautes Europeennes
DG XIII A 4

L - Bâtiment J. Monnet

Dr. Klaus FISCHER
TÜV Bayern e. V.
Kerntechnik und Strahlenschutz
Rüdesheimer Str. 11

D - 8000 München 21

Ing. André FOUSSAT
Institut von Karman
Dynamique des Fluides
Chaussee de Waterloo, 72

B - 1640 Rhode-St.-Genese

Prof. Giorgio FRONZA
Istituto di Elettrotecnica
Centro Teoria dei Sistemi
Via Ponzio, 34/5

I - Milano

Engineer Philippe GAILLARD
METRAFLU
Chemin des Mouilles, 24 Bis

F - 69130 ECULLY

H. GEISS
Kernforschungsanlage Jülich
Zentralabteilung Strahlenschutz

D 5170 Jülich

Josef GIEBEL
Wallneyer Str. 6

D - 43oo Essen, LIS

Dr. Noor V. GILLANI
Department of Mechanical Engineering
Washington University
Box 1135

St. Louis 63130, Missouri /USA

Prof. O. GODART
UCI
Inst. Astronomie et Géophysique
Chemin du Cyclotron, 2

B - 1348 Louvain-la-Neuve

J. P. GRANIER
Electricité de France
Direction des Et. et Recherches
6, Quai Watier

F - 784oo Chatou

Dr. Steven Rogers HANNA
Atmosph. Turbulence and Diff.Lab.
National Oceanic and Atmospheric
Administration
P.O. Box E

Oak Ridge, Tennessee 37880 /USA

Gisela N. HARP
Regionale Planungsgemeinschaft
Untermain
Zeil 127

D - 6ooo Frankfurt / Main

Gunter HERBERG
Abteilung für Praktische Math.
Hoechst AG
Postfach 800320

D - 623o Frankfurt/Main 80

Peter HESS
Battelle-Institut e. V.
Am Roemerhof 35

D - 6000 Frankfurt/Main

IR. Y. JACQUART
UCL
Inst. Astronomie et Géophysique
Chemin du Cyclotron, 2

B - 1348 Louvain-la-Neuve

Dipl.-Phys. Pierre JEANNET
Institut Suisse de Meteorologie
Sec. de la Protection de l'Air
Station Aerologique

CH - Payerne 153o

Dr. W. B. JOHNSON
Atmospheric Sciences Laboratory
SRI International

Menlo Park, California 94025/USA

Dr. D. JOST
Umweltbundesamt
Bismarckplatz 1

D - 1000 Berlin 33

Dr. Alexandre JOUKOFF
Inst. Royal Météorologique
Avenue Circulaire, 3

B - 1180 Bruxelles

Univ. Doz. Walter KOFLER
Inst. für Hygiene u. Mikrobiologie
Universität Innsbruck
Fritz Preglsstr. 3

A - 6010 Innsbruck

Dr. H. KOLB
Institut f. Meteorologie und
Geophysik der Universität Wien
Hohe Warte 38

A - 1190 Wien

Dr. Joseph KNOX
Phys. Depart. Atmosph.
Geophys. Sciences
Lawrence Livermore Laboratory
P.O. Box 808

Livermore, Ca. 94526 /USA

Dr. IR. J. G. KRETZSCHMAR
CEN
Boeretang 2oo

B - 2400 Mol (DONK)

Dr. KUMMER
Lab. Medecine du Travail
Hygiène du Milieu
Rue Belliard 100

B - 1040 Bruxelles

Dir. M. KUIZAK
Air Quality and Inter-Environmental
Atmospheric Environment Service
4905 Dufferin Street

Downsview, Ontario M3H 5T4/CANADA

C. LEGROS
Avenue des Sarcelles, 35

B - 1410 Waterloo

Dr. A. LEVY
Tecneco

I - S. Ippolito (PS)

Dott. Arnaldo LONGHETTO
ENEL - CRIN
Bastioni Porta Volta, 10

I - Milano

Fernand L. MAGDONELLE
Service Environnement
Protection des Consommateurs
Commission des Communautes Europeennes
200, Rue de la Loi

B - 1040 Bruxelles

IR. MALENGRAUX
UNERG
Bd. E. de Laveleye

B - 4020 Liège

Dr. L. M. MALET
Inst. Royal Météorologique
Avenue Circulaire, 3

B - 1180 Bruxelles

Dr. I. MERTENS
C. E. N.
Boeretang 200

B - 2400 Mol (DONK)

K. H. MULLER
EC - FRC

I - Ispra

F. Th. M. NIEUWSTADT
Koninklijk Nederlands
Meteorologisch Instituut
Utrechtseweg 297

NL - De Bilt

Prof. J.C.J. NIHOUL
Méchanique Fluides Géophys.
Université de Liège
Sart Tilman Par. Liège 1

B - 4000 Liège

J. P. ORFEUIL
Centre de Géostatistique
35, Rue Saint Honoré

F - 77305 Fontainebleau

Dr. Jacob PADRO
Atmospheric Environment Service
Department of the Environment
4905 Dufferin Street

Downsview, Ont., M3H 5T4/Canada

Richard A. PORTER
907 Park Village Cave

Austin, Texas 78758 /USA

Lars P. PRAHM
Research Establishment
Danish Air Quality
Lab. Min. of Environment

DK - 4000 Roskilde

Claude RONNEAU
Charge de Cours - Chimie Nucléaire
Université Catholique de Louvain
Chemin du Cyclotron, 2

B - 1348 Louvain-la-Neuve

Dr. Donald M. ROTE
Energy, Environmental Syst. Div.
Argonne National Laboratory

Argonne, Illinois 60439 /USA

Dott. Elidoro RUNCA
IBM
Dorsoduro 3228

I - 30100 Venezia

A. E. SAAB
Electricité de France
Direction des Et. et Recherches
6, Quai Watier

F - 78400 Chatou

Prof. Renato SANTANGELO
Istituto di Fisica
Via Università, 4

I - 41100 Modena

Prof. Luigi SANTOMAURO
Osservatorio Meteorologico
di Brera
Via Brera, 28

I - 20121 Milano

Dr. G. SCHAYES
U. C. L.
Inst. Astronomie et Géophysique
Chemin du Cyclotron, 2

B - 1348 Louvain-la-Neuve

Dr. T. SCHNEIDER
National Inst. of Public Health
P.O. Box 1

NL - 3720 Bilthoven

Dr. Michael SCHORLING
c/o. Industrieanlagen-Betriebsges.
Einsteinstr.

D - 8022 Ottobrunn

Prof. Heinrich SCHULTZ
Arbeitsgruppe f. Techn. Strahlenschutz - TU Hannover
Appelstr. 9A

D - 3000 Hannover

R. H. SCHULZE
Trinity Consultants
P.O. Box 31481

Dallas, Tex. 75231 /USA

SERRES
METRAFLU
24 Bis, Chemin des Meuilles

F - 69130 Ecully

Dr. Farhat Saleh SHERNANNA
Cultural Conf. Dept.
Garyounis University

Benghazi /LIBYE

Bjarne SIVERTSEN
Research Sc.
P.O. Box 130

N - 2001 Lillestrom

Herschel H. SLATER
Monitoring and Data Analysis Div.
OAQPS - EPA
Research Triangle Park

North Carolina 27711, /USA

J. S. SMITZ
Institut de Mathématique - ULG
15, Av. Tilleuls

B - 4000 Liège

Ing. Aldo SPIRITO
Istituto di Elettrotecnica
Centro Teoria dei Sistemi
Via Ponzio 34/5

I - Milano

IR. R. STEENKIST
KEMA
Utrechtseweg 310

NL - Arnheim

Bruce TURNER, Chief
Environmental Applications Branch
Meteorology and Assessment Div.
Mail Drop 80, EPA
Research Triangle Park,

North Carolina 27711 / USA

H. E. A. VAN DEN AKKER
Koninklijke Shell-Lab.
Postbus 3003

NL - Amsterdam-Noord

L. VAN DER AUWERA
K M I
Ringlaan, 3

B - 1180 Bruxelles

Dr. Josette VANDERBORGHT
Inst. Royal Météorologique
Avenue Circulaire, 3

B - 1180 Bruxelles

Dr. IR. Jan Willem VAN HEUVEN
CTI INO
POB 342

NL - Apeldoorn

C. A. VELDS
Koninklijk Nederlands Met. Inst.
Utrechtseweg 297

NL - De Bilt

Erich WEBER
Bundesministerium des Innern
Rheindorfer Str. 198

D - 5300 Bonn 7

Dr. M. WILLIAMS
Warren Spring Laboratory
Department of Trace and Industry
Gunnels Wood Road

GB - Stevenage SG1 2BX

Robert J. YAMARTINO, Assistant
Energy, Environmental System Div.
Argonne National Laboratory
9700 S. Cass Avenue

Argonne, Ill. 60439 /USA
